UNIVERSITY OF SOUTHAMPTON

FACULTY OF ENGINEERING AND APPLIED SCIENCE

A STUDY OF HELICOPTER ROTOR NOISE WITH PARTICULAR REFERENCE TO TRANSIENT EFFECTS

by

JOHN W LEVERTON. B.Tech., M.Sc(Eng), C.Eng., M.RAeS

Thesis submitted for the degree of Doctor of Philosophy

in the Institute of Sound and Vibration Research

November 1977

CONTENTS

UNIVERSITY OF SOUTHAMPTON

ABSTRACT

FACULTY OF ENGINEERING AND APPLIED SCIENCE
INSTITUTE OF SOUND AND VIBRATION RESEARCH

Doctor of Philosophy

A STUDY OF HELICOPTER ROTOR NOISE WITH PARTICULAR REFERENCE TO TRANSIENT EFFECTS

by John William Leverton

The noise generated by a helicopter is essentially a function of the sound emitted by the rotors. Rotor noise is complex in nature since it is a combination of the sound produced by several individual sources, each of which generates acoustic energy by more than one mechanism.

The general characteristics of helicopter noise and rotor noise have been established with the aid of results from real helicopters, full scale rotor tests and model rotor studies. Rotational (discrete frequency) noise is very sensitive to the inflow conditions while broadband noise appears to be solely dependent on the rotor geometry and operating conditions.

Transient effects, arising from the interaction between the rotor and any flow disturbance, give rise to a marked increase in rotor rotational noise and is subjectively annoying because of its impulsive characteristic. Emphasis has been placed on studying the main sources associated with a helicopter responsible for such effects. These are blade slap, attributed in most cases to an interaction between the main rotor blade and a tip vortex shed by a previous blade, blade/gust interaction and blade/fuselage interaction. These sources have been simulated experimentally and, following a study of the mechanism involved, the corresponding theory developed. For these transient noise sources, and by implication others where the rotor is subjected to a well defined disturbance, it has been shown that the excess noise associated with the interaction can be predicted and that the results agree well with those obtained experimentally.

Blade slap has been studied in depth both from the theoretical and practical point of view. It has been shown that it is necessary to apply a subjective correction to standard measurements to account for its impulsive characteristics. A design criterion in the form of a blade slap factor has been developed and general design guidelines established.

/

ACKNOWLEDGEMENT

The author expresses his sincere thanks to the supervisors of the various phases of the investigation, and in particular to Professor P.E. Doak, for all their help, guidance and interest shown throughout the study reported in this thesis. The supervisors were:

Professor E J Richards, OBE, M.A., D.Sc., Hon D.Sc., Hon.LLD, Hon D.Tech, C.Eng, F.RAeS, F.I.Mech E. (1966-1967)

Dr. C L Morfey, B.A., M.Sc.(Eng) (1967-1970)

Professor P E Doak, B.S., B.A., M.S. (1970-1975)

The author is also grateful to Dr H K Tanna for his help with the development of the rotational noise programs and the numerous other members of the ISVR staff who freely gave advice and assistance.

The financial support for the work outlined in this thesis was provided by the following:

US National Aeronautics and Space Administration (Langley Research Centre)

UK Ministry of Technology, London

UK Ministry of Defence, London

Westland Helicopters Ltd, Yeovil

The author is also grateful to the members of staff of Westland Helicopters Ltd, in particular Mr O L L Fitzwilliams, Chief Engineer (Research), for their assistance and for supplying test data during the initial phases of the investigation reported in this thesis.

The author also wishes to thank the following companies for making available flight test data and/or conducting special flight tests:

Bell Helicopter Company, Fort Worth, Texas, USA.

British Hovercraft Corporation, Cowes, I.o.W.

Boeing Helicopters, Vertol Division, Morton, Penn., USA

Sikorsky Aircraft, Stratford, Conn. USA.

Westland Helicopters Ltd, Yeovil, Somerset, England.

LIST OF TABLES

LIST OF PLATES

LIST OF FIGURES

CHAPTER 7

APPENDIX 1

NOMENCLATURE

Note: The notation used in some instances in the Appendices is different from that given below; in these cases the symbols are defined in the appropriate section.

ABBREVIATIONS

AM	Amplitude Modulation (as applied to tape recorders)
AUW	All up weight
B&K	Bruel and Kjaer (Denmark - Equipment Manufacturers)
BSF(E)	blade slap factor based on energy of impulse
BSF(P)	blade slap factor based on power of impulse
CRO	(Cathode Ray) Oscilloscope
dB	decibel
dB(A)	A weighted SPL
dB LIN	Linear (unweighted) SPL
FM	Frequency modulation (as applied to tape recorders)
F.S/N	Filter signal-to-noise ratio
'FLAT' SPL	Maximum sound pressure level of broadband noise on analysis
GW	gross weight
HP	Horsepower
ISVR	Institute of Sound and Vibration Research, University of Southampton
K_f	Kussner's function
MOD	Ministry of Defence, London
NASA	National Aeronautics and Space Administration, Washington DC, USA
NPL	National Physical Laboratory, Teddington
OASPL	Overall sound pressure level
rms	root mean square
rpm(RPM)	revolutions per minute (rotational speed)
Re	Reynolds number
S/N	Signal-to-noise ratio
S.F.	filter shape factor
SPL	Sound pressure level
SPL(mB)	Sound pressure level of the mB^{th} harmonic
St	Strouhal Number
PNL	Perceived noise level
EPNL	Effective perceived noise level
PNdB	perceived noise decibel

PWL	sound power level
UV	Ultra-Violet (trace)
WHL	Westland Helicopters Ltd
WR	Working Range

SYMBOLS

a	radius of fuselage (cylinder)
a_1	radius of cylinder which transforms into a flat plate of chord $4a_1$
a_o	lift curve slope
A_B	effective blade area
Ao	distance blade to cylinder centre
An	Fourier coefficient of impulse
b	half chord of blade (c/2)
B	number of blades
B^1, B_w	filter bandwidth.
Bn	Fourier coefficient of impulse
c	blade chord
c_o	speed of sound
C_D } C_{Do} }	profile drag coefficient
C_L	blade lift coefficient
$\bar{C}_L$	mean blade lift coefficient (=3 C_{LT})
C_{LT}	blade lift coefficient referred to tip (= $T/\frac{1}{2}\rho V_T^2.S$)
d	distance from beginning of gust
d^1	vertical distance from blade to point on cylinder
D	width of vortex filament; distance from source point to rotor disc field point.
E_B	blade slap impulse 'bang' energy
f	frequency
f_B	broadnoise centre frequency
f_{BP}	'break point' frequency
fc	cancellation frequency.
fe	end correction factor
f(z)	complex potential of flow field
f1, f2, f3	correction terms
g	= 0.13 (constant)
Fi	fluctuating force
h	microphone height; dipole separation

H	distance from blade to centre of cylinder
H'	true distance blade to centre of cylinder (H + coning effect)
I	acoustic intensity
k	wave number
$\hat{k}$	inverse power law of blade loading
k, k', k''	constants
k_L	lift function correction factor
k_m	$= 2\pi bm/Y$
K	vortex strength
Ko	mean (steady) vortex strength
K_1	$= (\pi/d)^2$
K_2	$= \left[\frac{\pi}{d-b}\right]^2$
L	lift
L_{BS}	blade span loading
L_m	loading at point due to m^{th} harmonic of input
Lo	mean (steady lift)
$L(s)$	blade loading at point s
Ls	blade loading per unit span
L_T	transient blade loading (transient lift)
L_{TM}	maximum transient lift (ΔL_{TM} max. transient lift per unit span)
m	harmonic order (i.e. 1, 2, 3 etc)
M	blade Mach number ($= V_T/co$)
n	harmonic order (i.e. 1, 2, 3 etc)
$(p-po)$	Acoustic pressure
p_{im}	imaginary component of sound pressure
po, Po	atmosphere pressure
p_{re}	real component of sound pressure
P1, P2, P3,	terms in cylinder pressure equations
r	distance; radius
r^1	gust radial width = $(r_o - r_1)$
$\bar{r}$	distance from observer to midpoint of 'area' under consideration
r_c	blade radius at cuff (root); radius of tip vortex core
r_1	inner radius of gust
r_o	outer radius of gust
r_p	radius in tip vortex at which motion changes from rigid body to potential flow.
r_v	radial distance from tip vortex centre

R	rotor radius
R^1	rotor radius at which blade twist starts
$\mathcal{R}_e$	real part of equation
R_f	distance from centre of rotor head to field point
R_T	rotor radius (radius of blade tip)
s	non-dimensional distance measured from beginning of gust
S	blade plan area; rotor/cylinder separation distance
S^1	constant depending on spanwise loading distribution
$SPL(mB)$	sound pressure level of mB^{th} harmonic
t	time
tp	project blade thickness
T	thrust; total blade thrust
T_B	thrust per blade
U	induced flow velocity
V	velocity; blade velocity
V^1	flow speed relative to the blade
V_M	maximum tangential velocity in a tip vortex
Vr	blade velocity at radius r
Vt	tip vortex tangential velocity
V_T	rotor tip speed
$V_{0.7}$	blade velocity at 0.7 radius
w	disc loading
$w(\sigma)$	velocity of gust at σ
w_r	inflow velocity at radius r
W_1	'peak' (maximum) velocity amplitude of gust
W_B	total 'bang' power
W_E	total 'bang' energy
W_m	velocity amplitude of m^{th} harmonic of gust
W_1	acoustic power of a single dipole
W_2	total acoustic power of two point dipoles
x_i	co-ordinates of any point
x_n	co-ordinate measured in direction normal to blade chord
$\overline{x_n}$	co-ordinate normal to blade span at mid-point of blade area under consideration
yi	co-ordinates of any point
Y	actual (true) length of gust
X_1	$\frac{1}{2}\pi Vca_o$ 0.065 (Note in Appendix 8 this value is denoted as B)
X_2	$\frac{1}{2}\pi Vca_o$ 0.5 (Note in Appendix 8 this value is denoted as A)

α	angle of attack
β	angle between tip located dipole axis and the observer (microphone)
γ	d^1/R_T
Γ	strength of circulation
$\delta; \delta_o$	angle on cylinder (vertical given by δ , $\delta_o = 90^o$)
Δ	incremental or small change
ϵ	r/R_T
ζ	complex co-ordinates in the transformed plane
η	$\tan^{-1}$ km
θ	pitch angle; angle
θ_c	pitch angle at blade cuff (blade root)
θ_r	pitch angle at radius r
θ_T	pitch angle at blade tip
ν	kinematic viscosity
ν	induced angle at blade section
ν_o	collective blade pitch
$\rho; \rho_o$	density
σ	non-dimensional point at which load is considered to act; angle between rotor plane and field point
τ	blade passing interval
ϕ	$\tan^{-1}$ km/0.13
ϕ	inflow angle
ϕ_r	inflow angle at radius r
Φ	angle of observer (microphone) relative to vertical
ψ	blade azimuth angle
ω	angular velocity, rotor rotational speed (rad/s)
Ω	angular frequency
ϕ	angle subtended between dipole axis and source - observer (source/ microphone) line.

REFERENCE LEVELS

SOUND PRESSURE LEVEL

All sound pressure level (SPL) values are quoted to the same reference pressure; the convention for quoting this has changed over the period of the investigation and the following forms are used in this thesis,

Pref. = 0.0002 dynes/sq cm; 0.0002 dynes/cm^2; 20 μ N/m^2

On some of the figures the SPL values are quoted simply as SPL ~dB or SPL and, although it is not stated, the values are in dB relative to the standard reference pressure mentioned above.

ACOUSTIC SOURCE POWER

The power level (PWL) values are quoted in dB rel. 10^{-12} watt.

CHAPTER 1: SCOPE OF INVESTIGATION

1.1. INTRODUCTION

The sound of a rotorcraft is very complex in nature since it is a combination of the sound produced by several individual sources, each of which in turn may generate acoustic energy by more than one mechanism. Externally the important sources are the rotor(s) and to a lesser extent the engine; while internally the transmission system (gearbox) is the main additional source. Main rotor noise consists principally of two components, rotational (or discrete frequency) noise and broadband noise, while tail rotor noise is dominated by its rotational components.

With the exception of some light weight helicopters, the majority are powered by gas-turbine engines and thus inlet (compressor whine) and exhaust noise are of interest. On existing helicopters the exhaust noise is lower in level than the broadband rotor noise and is no real problem, and the inlet noise, although sometimes troublesome, can be effectively controlled by the use of 'inlet silencing treatments'.

It is worth noting that in a piston-engined helicopter, the engine itself is the main noise generator with the primary source being the exhaust noise emanating from the periodic expulsion of hot gases of combustion. This produces harmonics at the engine firing frequency and in addition to being of relatively high amplitude is annoying because of its impulsive character.

For a gas-turbined engined helicopter, however, even when engine noise is taken into consideration the sound is characterised by the noise produced by the rotors. The most objectionable sound generated by a helicopter is 'blade slap', which is a banging/impulsive noise which emanates from the main rotor. When this is not present tail rotor noise is of major importance, particularly because of its pronounced 'whine' characteristics. It is very noticeable during manoeuvres in hover and low speed flight, as well as in many cases during high speed cruise. The helicopter is also prone to generating a number of other transient type noises and like 'blade slap' and tail rotor noise they tend to enhance the annoyance.

It follows, therefore, that helicopter noise is controlled, on modern gas-turbined engine helicopters, essentially by the level of main rotor noise and tail rotor noise and at the start of this investigation in 1966 these were still relatively little understood.

A preliminary study of 'blade slap', in addition to giving an understanding of the basic mechanisms involved, had indicated that a significant proportion of rotor noise (and hence helicopter noise) could be attributed to non-steady or transient blade loading effects. A long term research programme was therefore formulated with the view of explaining these transient effects and deriving information on the basic mechanisms involved. At this time certain blade slap aspects needed further clarification and the influence of asymmetric flows, gust effects and the fuselage/tail pylon on rotor noise clearly needed to be established. The programme was planned to some extent as a number of individual self-contained entities in order to make them viable research studies, although in the wider sense they were interrelated and inter-dependent. The main programme was linked around a 9 ft (2.74 m) diameter model rotor at the University of Southampton, Institute of Sound and Vibration Research (ISVR), although use was made of full scale rotor and helicopter flight test data where appropriate. To provide a background to this investigation a review type study was made of the general characteristics of helicopter noise. In the initial phases consideration was also given to defining the nature of the 'steady state' (hover) noise, since the characteristics were not well understood and it also seemed essential that the 'base noise' should be established as a reference for the study of the transient effects which give rise to additional noise. The main results of the complete programme are reported in this thesis and although for clarity the studies of the various aspects are to some extent treated as separate investigations, they were often carried out in parallel with other investigations.

1.2. AIMS OF THE RESEARCH PROGRAMME

The principal aims of the research programme were as follows:-

(i) to define the mechanism involved and provide a basic understanding of the following three sources of impulsive noise:
   (a) blade slap (blade/tip vortex interaction);
   (b) transient blade stall - blade/gust interaction;
   (c) blade fuselage interaction;

(ii) to high-light the general characteristics of helicopter noise and rotor noise.

Implicit in these aims was the need to develop appropriate theoretical models and where possible prediction methods (theoretical or empirical) which could be used by helicopter manufacturers and others to estimate the

noise of a particular source or the complete helicopter. This naturally included taking into account the subjective aspects related to impulsive noise as well as the mechanisms involved.

1.3. STUDY PERIOD

The complete study covered the period 1966-1975 ($8\frac{1}{2}$ years); the general study of helicopter and rotor noise and the application of the 'blade slap' results to the real helicopter case was carried out during the period 1966/68 (3 years) under a National Aeronautics and Space Administration (NASA) contract (NGR 52-025-002) and then later detailed investigations of transient effects were supported by Westland Helicopters Ltd (WHL) and the UK Ministry of Defence (MOD) (Contracts AT/2040/039/SRA and AT/2040/085/SRA). A small WHL/ISVR experiment into the influence of tip shape changes on rotor noise was also funded by the MOD (Contract K25A/523/CB.25A-M).

1.4. THESIS FORMAT

The complete programme, as can be gauged from the brief outline in section 1.1, covered a relatively wide range and individual topics were in some cases investigated over a number of years. To avoid confusion, however, each of the main aspects is treated in this thesis as a separate study and all the work relating to specific topics included in one chapter. For this reason, and in order that an overall view of the programme may be obtained, an extended summary of the complete research programme is given in section 1.7. This lists the complete range of topics covered in as near as possible chronological order. Also, largely because of the nature of the investigation, a relatively large number of individuals assisted with the work outlined. These included Technical Assistants, M.Sc. Students and Research Assistants and in one or two cases other research workers. In each case the work conducted by these individuals was under the author's direct supervision. Thus, except for the three years in the period between 1966/69 while the author was in full time residence at the ISVR, many of the results of individual investigations were reported by the individual concerned in ISVR reports and/or M.Sc. theses, etc. To avoid the necessity of repeatedly making reference to the individual concerned, the involvement of those mainly concerned is summarised in section 1.5, together with the formal status of the author during the period of the complete investigation.

1.5. FORMAL STATUS OF AUTHOR AND RESEARCH STAFF

The whole study covered an $8\frac{1}{2}$ year period, during which the author's affiliations were as follows: 1966 Research Assistant, ISVR, 1967/68 Research Fellow, ISVR; 1968/70 Senior Noise Engineer, WHL; 1968/73 Visiting Lecturer, ISVR; 1970/75 Head of Applied Acoustics, WHL and 1973/75 Visiting Lecturer, ISVR. During the investigation joint papers on helicopter noise generation and the instrumentation aspects were prepared with S.E. Wright, Research Fellow, ISVR, and T.R. Ives, Research Experimental Engineer, WHL, respectively.

Measurements for the preliminary study of transient noise and rotor configuration studies were carried out by A.R. Whatmore and A.D. Dodson respectively as ISVR M.Sc. projects under the author's supervision. Phase I of the Transient Rotor Noise Study was conducted by C.B. Amor and Phase II by S.H. Devani as Research Assistants/Junior Research Fellow at the ISVR on MOD contracts supervised by the author.

Assistance with the theoretical rotational noise studies conducted during the various phases of the investigation was obtained from H.K. Tanna, Research Fellow ISVR. The 'tip shape' study and the re-evaluation of the model/full scale rotor result comparison was made with the help of J.S. Pollard, Senior Research Engineer (Acoustics), WHL.

1.6. TRANSIENT ROTOR NOISE SOURCES

On a helicopter, apart from the small scale lift fluctuations arising from the interaction of a blade with the turbulence in the (inlet) flow and the wake shed by the previous blades, the main sources of impulsive noise (in order of priority) were considered to be the following (at the outset of the research programme):

(a) blade/discrete tip vortex interaction;

(b) transient blade stall (influence of large scale flow disturbances).

(c) blade fuselage interaction.

The most important of these was considered to be blade/tip vortex interaction and, although a number of other mechanisms had been proposed for the generation of very impulsive main rotor noise (see Chapter 5, section 5.3) it was postulated that this was the most likely source of blade slap. This had been investigated in general terms as a part of an M.Sc. project by the author and basic understanding established. It was decided to extend the theoretical model which had been developed [1] to the real helicopter case and conduct a number of flight tests (in conjunction with WHL) to establish if the position at which blade/tip

vortex interaction occurred could be predicted. This is discussed in Chapter 5, together with the corresponding studies aimed at giving an insight into the problems of measuring and (subjectively) rating impulsive/blade slap noise.

The position regarding 'transient blade stall' was very confused. Some authors had used it to explain blade slap, while others had stated that it could not occur in the traditional sense on a helicopter rotor blade in flight or a hovering rotor unless the 'distance of influence' was large. An experiment was, therefore, tailored to enable this aspect to be examined in detail. A review of the real helicopter case suggested that if stall occurred it would be over a relatively small portion of the rotor blade. For this reason, and since there was equal interest in the influence on rotor noise of 'discrete gusts', the programme was formulated in a manner such that only a small portion of the rotor blade would be subjected to 'stall'. This had numerous advantages from the experimental and theoretical point of view and although it was initially anticipated that the effect of 'stalling' larger portions of the rotor blade would have been established in due course, this was not the case. This curtailment was a combined result of the fact that the 'discrete gusts' had given information from which the influence of 'stalling' large sections of the rotor disc could be estimated, and of the non-availability of funding.

The 'blade fuselage' interaction case was of interest from both main rotor/main fuselage and tail rotor/tail pylon considerations. It was known from helicopter noise recordings that the magnitude of the main rotor noise is higher at the rear (tail on) of the helicopter where it passes over the fuselage and it was believed that the impulsiveness of tail rotor noise is dependent on the distortions in the flow caused by the tail pylon or tail fin. As far as could be determined, except for one study related to the aerodynamic interference, this aspect had never been investigated, although it was obviously important if the noise generated by a helicopter is to be fully understood. With use of the ISVR model rotor facility a programme aimed at clarifying this position was therefore developed. The fuselage/tail pylon case was simulated by use of a cylinder which was mounted under the model rotor. A cylinder was chosen, in preference to any other shape, to ease the complexities of the theoretical model and it was 'sized' so that the rotor diameter/cylinder diameter was comparable with the ratio of the rotor-fuselage (and tail rotor-tail pylon) dimensions on a real helicopter. The details of this programme, together with the theoretical and experimental results, are discussed in Chapter 7.

1.7. SUMMARY OF PROGRAMME

The blade slap work initiated in the author's M.Sc. investigation [1] which had shown that blade/tip vortex interaction was the main mechanism for blade slap noise during the early part of the study, was extended to cover real helicopter aspects in greater depth. The theoretical analysis was refined to enable the dependency of blade slap on design factors to be assessed, a review of other possible mechanisms was made and further flight tests (which enabled the blade/tip vortex interaction to be determined) were conducted with the help of WHL. Some preliminary subjective assessments of blade slap were made. The results of all this work were subsequently published as NASA Contract Reports [2,3]. An investigation into the New York Pan-Am Building operation was also conducted [4].

With the award of the NASA contract in 1966 the study was broadened to cover the investigation of general helicopter and rotor noise. This work showed, for the first time, the importance of high frequency rotational noise and the relative levels of broadband and rotational noise. It soon became clear that the analysis facilities at ISVR and WHL were inadequate for detailed rotor analysis and a survey of available analysis systems was made. This resulted in the development of a system based on a Spectral Dynamics Analyzer; funding for such a system was subsequently obtained and a unit set up within ISVR [5]. This was the forerunner of similar systems at WHL [6] and other groups involved with detailed narrowband analysis.

Detailed model rotor noise tests were conducted at ISVR and analysis of full scale WHL/MOD rotor recordings made. This highlighted again the importance of rotational noise and indicated that many of the then existing concepts on the generation of rotor noise were not applicable. Controlled hover flight tests were also performed (at WHL); these showed the variable nature of the rotational noise in nominally 'steady state hovers' and that the general characteristics of the model results were representative of those on a real helicopter. Detailed theoretical investigations were subsequently initiated at ISVR (by Wright and Tanna) in an attempt to explain and develop appropriate rotational noise theories. From the model rotor, full scale rotor and helicopter tests, generalized practical prediction methods for rotational noise, broadband noise and overall helicopter noise were developed by the author [7]. These have been used, and are still being used, by a number of helicopter

manufacturers including WHL for estimating helicopter noise. This work also enabled the detailed characteristics of rotor noise to be established [8].

At the time of these investigations doubt was expressed on the applicability of model rotor noise results; a detailed comparison was therefore made between full scale and model tests. This confirmed that the model could be used for detailed investigations of transient effects where the 'source' could be readily controlled and defined and, providing care was taken in the interpretation of results, this could be used with confidence for studying full scale rotor noise. This data was subsequently re-evaluated at a later date and a paper published [9].

In addition to noise studies the aerodynamic aspects of rotor noise were reviewed and a model for calculating lift developed. This was checked on a full scale rotor and a good agreement obtained. More recently 'thrust' results for the actual rig were obtained and these confirmed the applicability of the aerodynamic model.

Following the interest in the USA into the use of 'tip shapes' for the control of rotor noise a small study was carried out in conjunction with an aerodynamic investigation of the influence of changes in blade tip planform by Noak [10]. The ISVR model rotor was fitted with several different 'tips' and simultaneous noise and aerodynamic measurements made. Difficulties were unfortunately experienced with the aerodynamic evaluation and the noise aspects had to be studied in isolation. This analysis [11] clearly illustrated that the rotor noise was dependent on tip shape and that a full scale experiment was warranted.

Since the 'blade slap' study and the general investigations of rotor/helicopter noise showed clearly the importance of transient effects, a preliminary study of these aspects was undertaken in order to assess the suitability of conducting such investigations on the ISVR model rotor. The study [12] was essentially experimental in nature and only limited correlations with theoretical trends were made. The importance of 'gust effects' was, however, clearly established. A qualitative study of blade slap type impulses was also made; this indicated that problems existed in the measurement, analysis and rating of such signals if conventional instrumentation/analysis methods were used. These aspects were investigated by the author in some depth and a number of papers subsequently issued [13, 14, 15].

During the same period as that of the preliminary transient study, an investigation into the influence of rotor configuration/layout on 'tandem rotor' noise was conducted. The main emphasis was placed on rotational noise, and the importance of blade separation, blade overlap and the influence of the wake of one rotor on another was established [16].

Theoretical methods for predicting main rotor noise were being developed at ISVR and, although they could not be used for detailed prediction, two specific studies were conducted. The first involved the use of measured S58 (Wessex) blade lift data and a comparison with experimental data. This showed relatively good agreement for the first few harmonics but at the same time high-lighted the weakness of such a method in that the aerodynamic data was inadequate. Theoretical studies on the influence of blade chordwise lift fluctuation were also made. The results of these studies were included in a major review paper - outlining both the experimental and the theoretical state of the art - presented to the Royal Aeronautical Society and subsequently published in the Society's Journal [17].

Following the completion of the preliminary transient and rotor configuration studies, a detailed programme aimed at fully understanding the two main sources of 'transient noise' was established. This programme was divided into two phases: Phase 1 was aimed at the study of the influence of discrete gusts (with gust lengths up to 24 chords) and Phase 2 at the effect of blade/fuselage interaction (which is equally applicable to the tail rotor/tail pylon case) on rotor noise.

Phase 1 covered both theoretical and experimental aspects, the theory being based on a 'blade loading' method developed in connection with the previous blade slap study [1] and the rotational noise prediction method developed by Tanna [18]. Good agreement between theory and experiment was obtained [19] and a paper covering the main aspects published [20].

Phase 1 also included a further review of the measurement/analysis problems involved with impulsive signals and confirmed that standard instrumentation, even if it included IMPULSE settings, could not be used for quantifying impulsive noise. A number of other aspects, including the effect on noise of stalling of the blade and the variation of overall noise and broadband noise with gust length were established. A method for simulating blade slap was developed [19]. (This approach has recently been used by NASA, the National Physical Laboratory (NPL) and WHL for subjective studies of blade slap.)

Phase 2 of this programme included the development of a test rig as well as a theoretical and experimental evaluation of the influence of an idealized fuselage on the generated rotor noise. The blade/fuselage interaction aerodynamic theory was based on the work of Bramwell and Johnston [21]; restrictions in this theory were removed and the output modified to enable the 'acoustic signature' as well as the noise spectrum characteristics to be obtained. 'Up wash' and 'down wash' cases were studied and the limitations of the theory evaluated. General trends likely to influence the noise on a real helicopter were established, but it was clear that further work is necessary before the method could be applied directly to the main rotor/fuselage or tail rotor/tail pylon problems on a real helicopter [22].

In parallel with the transient rotor noise study, a review was made of the results of full scale tests conducted at WHL. A joint ISVR/WHL paper on this has been published [23]. Recently additional studies have been conducted at WHL and this work - based largely on the results of previous ISVR model tests - has shown clearly that many of the trends classically associated with rotor noise do not apply and that rotor thrust, which has often been assumed to be an important parameter, does not have a marked effect on rotor noise [24, 25].

CHAPTER 2: INSTRUMENTATION AND TEST FACILITIES

2.1. INSTRUMENTATION

Except for the development of the analyzer system described in section 2.2, standard instrumentation was used throughout this investigation. The laboratory data collection system was based on Brüel and Kjaer (B&K) equipment and data was normally recorded on magnetic tape for subsequent analysis. The 'standard' data collection system consisted of a B&K $\frac{1}{2}$" condenser microphone (type 4133), B&K cathode follower (type 2615), a B&K microphone amplifier (type 2603) and a Nagra III AM-Direct Tape Recorder. Where low frequency recordings were required the tape recorder was replaced with a Leevers-Rich (Twin Track-Special Model) FM tape recorder and (when they became available) B&K FET low frequency units (type 4145 & 2619) were used. During the latter investigations the Nagra IIIB tape recorder was replaced by a Nagra IVD.

Normal calibration procedures were employed and followed the pattern detailed in reference (1). Since these methods are effectively standard there are no specific references to techniques employed in this thesis unless the individual investigation required a departure from the norm.

Analysis was performed in the main by using the narrowband system discussed in section 2.2, although this was supplemented where necessary with $\frac{1}{3}$ octave band, 1/1 octave band, dB(A) and dBLIN values obtained by using a B&K Audio Frequency Spectrometer (Type 2113). Data playback was made in the conventional manner, with 'tape loops' being made for use with the narrowband analyzer.

A similar data collection system was employed for the full scale/flight tests, but in this case a B&K 1" Microphone (type 4131), B&K Battery Cathode Follower (Type 2630) and B&K Precision Sound Level Meter (Type 2205) were normally used with the Nagra tape recorder. Full scale rotor noise data was collected by WHL by means of a similar system, but in this case a Muirhead K-348-A amplifier was used instead of the B&K amplifier and data was collected on an Ampex FR-1300 FM tape recorder as well as on a Nagra III (or Nagra IV) tape recorder; this sytem is described in reference (6).

2.2. DEVELOPMENT OF ANALYZER SYSTEM

2.2.1. Introduction

When the original 'blade slap' study was commenced at ISVR there were no narrowband analyzers available and digital analysis was in the early stages of development. After some initial analysis in terms of $\frac{1}{3}$ octave bands (29%) and 6% on a B&K Frequency Analyzer Type 2107, it soon became clear that a much narrower bandwidth was required. At that time Westland Aircraft Ltd (Yeovil) had a Muirhead K-101-A Automatic Wave Analyzer which had been used successfully for helicopter noise analysis over a period of years. This was made available to the author for the blade slap study and the majority of the analysis was carried out on this analyzer. During the later stages of the blade slap study and the initial rotor/helicopter investigations the limitations of the Muirhead K-101-A Automatic Wave Analyzer became apparent. It was also fairly clear that the understanding of rotor noise was being restricted and spectra often classified as 'broadband' in nature consisted of discrete frequencies. Thus an improved narrowband analyzer facility was required.

The use of narrowband analyzers for acoustic analysis in 1966 was somewhat limited and information on the various types on the market, particularly in the USA, was not readily available. It was decided therefore to carry out a survey to determine the most suitable for rotor/helicopter noise studies. In this context it should be remembered that at this time, except for the B&K 2107, there was no narrowband analyzer available at ISVR. Thus the survey was conducted in a manner such that other research groups could use the data obtained to evaluate suitable systems to meet their particular requirements.

2.2.2. Survey

The survey (reported in reference(5)) covered 16 analyzers, 14 of which were considered in detail. Since the Muirhead K-101-A Analyzer had previously been used for helicopter noise analysis, this was used as a reference for comparing the other systems. Many aspects were considered and the survey was conducted on the pattern which is now often used by the consumer magazine "Which". Particular emphasis was placed on the filter bandwidth characteristics and hence the 'skirt characteristics' as well as the quoted (3dB down point) bandwidth were of importance. Also since it was anticipated that the analyses of a large number of conditions would be required, it was considered essential that the analyzer was automatic in operation. In the context of this survey it should be

remembered that at the time of evaluation in 1966/67 digital systems were not available and hence the study concentrated on analogue analyzers only. This is not to imply that from the point of view of rotor noise analogue systems are now obsolete since, although digital analyzers (and mini computers) are now readily available, analogue analyzers are still used extensively in many research establishments.

2.2.3. Analyzer Requirements

2.2.3.1. General characteristics

With the points mentioned above taken into consideration, a tentative specification was drawn up. This took the form of a statement (in addition to standard electrical requirements relating to input/output voltages, etc) that "the analyzer had to be capable of effectively resolving the first 40 or so harmonics of blade passing noise of a rotor which had a fundamental frequency between 5-40 Hz." Implicit in the statement was a frequency range of 5 Hz to 2kHz, although at that time, since it was not clear if the lower frequency range could be obtained, analyzers with a 20 Hz lower limit were included in the survey.

It is interesting to note that although 22 major manufacturers were contacted, 8 were immediately rejected since the minimum bandwidth they offered was 1/6 or 1/3 octave band. This is not surprising since in 1965/7 this was the standard 'narrowband analyzer' for acoustic studies. Consideration at this stage was also given to price and two units rejected since, although they appeared to offer the desired features, they were part of complex integrated systems and hence very costly.

The analyzers fell into two main classes: constant percentage (%) bandwidth or constant bandwidth. The former has the advantage that it provides constant resolution through its complete frequency range and enables a wide frequency range to be covered with ease if the data is presented in the form of a 'log frequency plot'. This is useful in analyzing some signals, such as from structures, where the resonant bandwidth and spectral components tend to become broader and further apart at high frequencies. Thus this type of analyzer provides optimum resolution and speed of analysis for signals of this nature.

The main problem with constant percentage bandwidth analyzers is the relatively poor filter characteristic, particularly when the 'skirt' or attenuation at 'off tune' frequencies is taken into account. This basically results from the fact that the components making up the filter have to be continually altered to provide the necessary change in centre frequency and bandwidth as the filter is swept through its

frequency range. It is of interest to note that at the time of the survey - and even today - this aspect tends to lead to confusion and there is a general feeling that if the bandwidth (at the quoted 3 dB down point) is small this automatically implies good discrimination. This, of course, is not the case and both aspects had to be taken into account, as illustrated in Figure 2.1 which shows a comparison of the 'skirt characteristics' for a 1.5% filter and a 2 Hz filter. From the data made available from the manufacturers it soon became clear, therefore, that there were no 'percentage analyzers' available to meet the need for separating the individual rotor noise harmonics.

The constant bandwidth analyzers were all based on the heterodyne principle. The input, regardless of the actual frequency, is translated in frequency so as to fall within the fixed pass band of a fixed centre frequency filter. Since in effect only one filter is used the filter can be of higher quality and the filter characteristic can be better controlled with the result that the filter 'skirts' are steeper than those on a tunable type filter. Heterodyne constant bandwidth filters are of two basic types, one which is tuned by the use of a high frequency local oscillation and the other in which an external audio sine wave source is used. The tuning of the first type is usually mechanical, being driven by a motor arrangement and hence it appears similar to many of the constant percentage analyzers. The second approach is more flexible, particularly in terms of sweep rates etc, since it uses an electrical tuning signal from an audio oscillator.

2.2.3.2. Filter bandwidth

The filter bandwidth necessary to provide adequate discrimination of the rotational harmonics is a function of both the '3 dB down point bandwidth' and the skirt characteristic which is defined in terms of the 'shape factor'. Also, in determining the appropriate value, consideration has to be given to the dynamic range or signal-to-noise ratio of the analyzer. This is discussed in detail in Appendix 1 and from the study described there it was clear that a 'maximum bandwidth' of 2 Hz with a 'shape factor' of 4 was acceptable. In this brief review the influence of the 'sweep rate' on the filter output was assumed to be negligible. This was considered a viable approach since the 'sweep rate' would be chosen to enable the filter to reach 99% of its final value and the output suitably averaged. The maximum sweep rate for a filter of 3 dB down bandwidth B_w is $B_w^2/4$, on the assumption of zero averaging. It is difficult

to estimate the value necessary to give a 'true rms level' since this depends on the variation of the signal under examination. Some tests were conducted at ISVR and these showed that as a rough guide the sweep rate had to be set at $B^2/8$ (i.e. half the ideal value). The normal procedure, however, was to set the value by inspection of the final trace and comparison of the values obtained, respectively, from a 'swept signal' and when the analyzer was stopped (fixed) at a particular frequency. It followed, therefore, that the filter bandwidth/shape factor could be selected purely on the steady state condition evaluated as outlined in Appendix 1.

2.2.3.3. Signal-to noise ratio

In addition to the points outlined above a number of other aspects had to be taken into account in selecting an analyzer for rotor/helicopter noise analysis. The most important of these was signal-to-noise ratio (S/N), which is often referred to in general terms as dynamic range although technically this is not the case. Considerable difficulty was experienced since practically every manufacturer quoted the signal-to-noise ratio/dynamic range in a different form so as to give, of course, the highest possible figure. Often the values were quoted at the most favourable input/output setting and thus it was necessary to establish the value at other settings and in particular at those likely to be required for the analysis envisaged. Also on the analyzer there is more than one S/N ratio value which is of importance: for example, the 'filtered signal S/N ratio' will be higher than that for the 'output signal' and, although it is the overall system signal-to-noise ratio which is important, the former value was often quoted. Thus it was vital to determine the true nature of the S/N ratio, particularly since each operation in the system naturally tends to decrease its value. In selecting the appropriate value, consideration was also given to the fact that for rotor/helicopter noise the majority of the data would be obtained from tape recordings. Direct (AM) recording systems have quoted S/N values of 55/60 dB, while on typical FM tape recorders the values are usually limited to 40/45 dB. These figures are again somewhat arbitrary and cannot be used except for suggesting that the S/N ratio of the analyzer (based on the same form of measurement) should have a value in the order of 55/60 dB. Also the S/N ratio and the dynamic range of the microphone/cathode/conditioning amplifier - which for the rotor/helicopter noise programme was based on Brüel and

Kjaer equipment - had to be taken into account. At this time difficulties were being experienced with 'equipment noise' in analysis of rotor noise by the use of available systems, even though the quoted signal-to-noise values appeared adequate.

In the rotor/helicopter noise situation the position appeared to be further complicated by the impulsive nature of signals, which unfortunately was not fully appreciated by a number of investigators. It soon became clear that, although standard electrical terminology could be used to some extent, the detailed requirements of the analyzer system could not be finalised unless a new format was devised. This led to the development of two terms -filtered signal-to-noise ratio (F.S/N) and working range (WR) - which proved invaluable in clarifying the position relating to the true S/N ratio and the levels of 'equipment noise' expected on any analyzers.

The definition of filtered signal-to-noise ratio is illustrated diagrammatically in Figure 2.2 and is simply the difference between the peak level of the signal and the level of 'equipment noise' when frequency analyzed (i.e. filtered). As would be expected this is a function of frequency and thus the value has to be quoted at various frequencies or, as in the case under consideration, the least favourable result for two frequency ranges. These were 5-150 Hz, which covered the region dominated by low frequency rotational noise, and 160 Hz - 20 kHz which is appropriate to high harmonic rotational noise and the broadband noise.

The 'peak level' indicated on the figure is the absolute magnitude at the system (or analyzer) input as determined from a time history. For this measurement an ultra-violet trace recorder and/or oscilloscope was used. The peak dB value of the impulsive signal is defined as follows: a signal with a peak level of, say, 123 dB is one where the maximum impulsive amplitude (+ ve or - ve) is the same as the peak level of a sine wave with an rms sound pressure level (SPL) of 120 dB. In other words (see Figure 2.2) the peak level Y = (X+3)dB where X is the rms value of the equivalent sine wave.

It follows that, providing the 'peak level' when measured in voltage terms does not overload the system, the F.S/N can be used to assess the relative merits of a number of analyzer systems. This was achieved by analyzing on the available systems a specimen tape (from a Nagra III tape recorder) containing a sine wave and then repeating the analysis at the same setting with a 'dead input'. Also, where possible,

values were obtained at a range of input settings. In many cases analysis of this form was not possible and the values had to be estimated from available data supplied by the manufacturer or other users.

It was appreciated at this time, however, that it was pointless to obtain equipment with a high signal-to-noise ratio if, when on subsequent analysis, the levels of the rotor noise in the mid-frequency range were so low that they would be influenced by internal tape recorder noise. In this context it is worth noting that early measurements had indicated that rotor noise often had crest factors of up to 20 dB. The term working range (WR) was therefore devised; this is illustrated in Figure 2.3 and is defined as the difference in dB between the maximum rms signal level which occurs on any spectrum analysis and the maximum rms level of the 'equipment noise + 6 dB', when both are analyzed on the same system. Again the whole frequency spectrum and individual frequency ranges were considered.

2.2.3.4. Other requirements

Other requirements considered in the selection of the analyzer included facilities for 'overall' (or 'Straight Through') analysis, range of sweep rates/frequency scanning times, frequency range and range of filters/filter bandwidth available. In this context consideration was given to the fact that the analyzer, in addition to meeting the requirements for rotational noise analysis, should if at all possible be suitable for broadband rotor noise analysis and more general work. Integral with this study was a review of the best method of presenting the data and the selection of the most suitable level recorder. In each case, in addition to the technical specification, consideration was given to cost and the ease of operation.

The need for broadband noise analysis indicated that in addition to very narrowband filters (or bandwidths in the range 1 to 2 Hz), filters of 20 Hz to 100 Hz bandwidth would be required. Also, since rotor noise is commonly measured in terms of rms values, a good quasi-rms detector incorporating a log amplitude (dB) output with adequate signal-to-noise ratio was required. Since optimization of 'effective integration time' is extremely difficult it was also considered essential that the system should contain an output device capable of providing a wide range of time constants (or 'pen writing speeds'). Also since the main objective was to provide good harmonic discrimination it was clear that fairly long trace lengths were necessary. This may seem at first glance an obvious requirement, but many narrowband systems present data in a form such that

much of the advantages of the small bandwidth is nullified by the 'blurring' together of the individual peaks on the final trace. The detailed analysis of rotational noise is shown best on a linear frequency trace, particularly since the frequency range of interest is usually limited. For more general work, however, and in order to cover the complete range, use of a 'linear frequency' trace presents a number of difficulties. In practice spectra contain far more 'peaks' in the low and mid frequency range than at high frequency and hence the trace would either be so long that it was unmanageable or the low frequencies would be effectively unreadable. A more useful trace can therefore be obtained if a 'log frequency' presentation is used.

A number of other factors were also taken into account; included in these were control layout, automatic bandwidth switching, unit or single system layout, possibilities of extending the capability of the system with 'add on' units and the detail control/operation sequence.

2.2.4. Analyzer System

The Spectral Dynamics SD-101A system appeared to meet best the required characteristics discussed in the preceding sections. The system as purchased is illustrated in block diagram form in Figure 2.4 and, as will be noted, was extended to include, in addition to the facilities for straight forward narrowband analysis (Figure 2.4(a)), the ability for 'tracking mode' analysis (Figure 2.4(b)) and 'signature ratio mode' analysis (Figure 2.4(c)). The 'tracking mode' enables the level of, say, an individual harmonic to be followed as the rotor speed is varied and the 'signature ratio mode' allows a 'harmonic scale' independent of rotor speed or rotor speed variations to be plotted. It will also be noted from Figure 2.4 that a General Radio Type 1521 Level Recorder was selected as the plotter. This was suitably modified at ISVR to enable the output voltage ramp, from the sweep oscillation (or tracking frequency multiplier) to drive and control the paper trace. A number of options were developed which enable any linear range and 1, 2 or 3 'log decades' to be plotted on a trace 20 inches long.

The Brüel & Kjaer Type 2305 chart level recorder had similar characteristics to the General Radio Level Recorder and the final selection was based solely on ease of installation of the modification. A second Spectral Dynamics system was subsequently developed at WHL [6] for similar rotor/helicopter noise analysis and in this case a B&K Level Recorder with a stepping digital servo system which operated from the voltage output ramp was employed. This system proved, like the ISVR

system, very useful and at WHL a second unit based on the Spectral Dynamics SD-101B was subsequently added. The WHL systems, as well as that of ISVR, were used for the analysis of rotor/helicopter noise during this investigation.

2.3. ISVR TEST FACILITIES

2.3.1. Single Rotor Rig

The main experimental part of the overall investigation was carried out by using the ISVR 9 ft (2.74m) diameter hover rig which in helicopter terms is commonly referred to as a 'whirl tower'. This rig is shown in Plate 2.1 and was driven by an electric motor, via a Ward-Leonard set. The blades were of a rectangular plan form without twist, having a radius of 54 inches, a chord of 4 inches and a NACA 0012 aerofoil section. The main spar and leading edge were made of 'folded' aluminium and the trailing edge constructed from expanded polystyrene. The tips were made of wood and painted different colours for identification purposes. These blades were used up until the time of the blade/fuselage interaction study (Chapter 7), when the trailing edge sections were replaced with a balsa wood construction. In all six blades were available but one was subsequently damaged beyond repair.

A number of rotor heads were available or constructed during the period of the investigation. These included a '4 bladed' rotor head (which could also be used with 2 blades) which had 'flapping' hinges, but no lead/lag arrangement. A similar 3 bladed rotor head and single bladed (with balance weight) rotor head were available. A set of 'rigid' rotor heads were manufactured; these consisted of a 4 bladed version (which could be used for 2 blade and 1 blade work) and a 3 bladed rotor head. During the original investigation the rotor heads with 'flapping hinges' were used, but later in the studies of blade stall (blade/gust interaction) and blade/fuselage interaction the rigid rotor version was employed. From tests conducted the choice of the type of rotor head did not have any influence on the level of rotor noise and the 'rigid' rotor heads were simply used since they allow more control of the rotor blade positions particularly when the rig was being 'run up' or 'shut down'.

The pitch of the blades could be adjusted on the rotor head prior to running to angles between $\pm 15^{\circ}$ in $\frac{1}{2}^{\circ}$ increments by means of a screw arrangement at the cuff. Since the stall angle for the blades employed is 14°, the rotor was rarely used at a pitch angle above 12°.

The maximum rpm of the rotor was in the order of 1200 rpm, although for blade stress reasons it was normally limited to 900 rpm (corresponding to a tip speed of 425 ft/s). Power limitations prevented the high speeds being obtained at the higher pitch settings and the upper limit for the 3 bladed rotor at 12° pitch was 660 rpm which corresponds to a tip speed of 312 ft/s.

The ISVR 'hover rig' is situated in the Sir George Edwards Laboratory which is semi-reverberant and contains a considerable number of other rigs and equipment. The area close to the rig was, however, clear and although initially concern was expressed at the suitability of taking measurements in such an environment, tests confirmed that provided care was taken in selecting the microphone position, meaningful results could be obtained and the rig was particularly well suited to studying transient effects where the 'source' was effective only over a small portion of the rotor disc area. For safety reasons the rig was enclosed in a large wire mesh guard; this can be seen in Plate 2.1. The rotor disc plane is 7.75 ft (2.36 m) above the floor and there is a 12.25 ft (3.73 m) clearance (approx 1.4 rotor diameters) above. To reduce the re-circulation effects and general flow interference it was normal procedure to operate the rotor with 'negative pitch' (downwash upwards). Also measurements were normally curtailed if the re-circulation effects were noticed to have any subjective effect on the rotor noise.

2.3.2. Tandem Rotor Rig

The tandem rotor rig was originally obtained from NPL where it had been used for aerodynamic wind experiments [26]. It was subsequently redesigned at the ISVR in order to reduce the gearbox noise and used by Stainer for a preliminary study of tandem rotor rotational noise [27]. The rig was capable of running either one or two 3 bladed 51 inch diameter rotors. The blades were of rectangular planform without twist having a chord of 1.5 inches and an NACA 0012 blade section. The main spar and leading edge were made of spheroidized steel and the trailing edge of wood. The rotor heads had both lead/lag and 'flapping' hinges, with the former having cork friction dampers. The collective pitch was adjusted by a screw arrangement at the cuff.

The maximum speed of the rotor was in the order of 1800 rpm which gave a tip speed of 400 ft/s. In the tandem configuration percentage blade overlaps of 51%, 31.4% and zero were obtainable. In addition the rotor disc height separation could be set at 8 inches, 5 inches or zero.

The phase angle between the two rotors could also be varied from 0 to 90 degrees.

The 'fuselage' was originally of cylindrical shape; this was, however, substantially modified to reduce the gearbox noise and final arrangement is illustrated in diagrammatic form in Figure 2.5. As can be seen a single drive motor is used and the rotor drive is via 'notched belts'. For the investigation conducted by Stainer [27], in which the author took an active part, the tandem rotor rig was mounted in the ISVR large anechoic chamber; the same arrangement was used and the subsequent investigation made under the supervision of the author.

2.4. OTHER TEST FACILITIES

2.4.1. Rotor Rigs/Whirl Towers

In addition to the ISVR results, data obtained by WHL was included in this investigation. The WHL data was derived from a 'whirl tower' at Yeovil fitted with a 3 bladed S55 rotor and a 'whirl tower' at Weston-super-Mare fitted with a single (1) bladed S55 rotor. Later this data was supplemented with data derived from tests at Weston-super-Mare where the rotor was run 'upside down' with 1, 2 and 4 blades. The basic characteristics of this rotor system are outlined in section 3.4.

2.4.2. Helicopters

Flight test measurements were made on a variety of helicopters; these are discussed in the appropriate sections of this thesis and their general characteristics are defined in Table 2.1 together with an indication of the study in which they were involved. For the flight experiments conducted under the direct supervision of the author by WHL in connection with the blade slap source location study (section 5.7) the helicopters used were the Wessex (British built Sikorsky S58) and the Sycamore. The Wessex was also used for the detailed hover tests, designed to enable the precise nature of hover noise to be assessed, conducted by WHL for the author (section 4.10). In other cases the tests were performed by the manufacturers to a programme requested by ISVR or data already available in the form of tape recordings was supplied to the author for analysis.

2.5. ISVR SINGLE ROTOR RIG - THRUST MEASUREMENTS

2.5.1. Introduction

There was no direct thrust measurement facility on the ISVR rotor rig when used for the initial rotor noise, blade slap and blade stall (blade/gust interactions) experiments. Consideration was given to incorporating such a device at a number of stages during the

investigation, but this was rejected on the grounds of complexity, cost and the fact that for the main body of experiments precise details of the thrust were not essential. In this context it is worth noting that a theoretical model for calculating the thrust had been developed and when checked against full scale measurements on a whirl tower gave good agreement. Even so it was found that when the study of the influence of 'tip shapes' on noise was completed (section 3.12) the validity of the results was questionable due to the non-availability of precise thrust measurements. Also when the blade/fuselage interaction study (Chapter 7) was being formulated, it was clear that it would be advantageous if direct thrust measurements could be made. It was decided therefore at this stage (in 1972) to modify the rig to enable thrust measurements to be obtained.

2.5.2. Thrust Measuring Device

A review of the 'off-the-shelf' load cells revealed that there was no available design which would meet the specifications required and/or the rig dimension and other mechanical considerations. A special unit had therefore to be designed and built. This device consisted of four 2 inch long horizontal beams of $\frac{3}{4}$" x 0.1" cross-section: the inner ends of the beams were fixed at 90° spacing to the rotor shaft via a thrust bearing and the other ends were fastened via an arrangement of spacer blocks to the top plate of the rig. The design is illustrated in Figure 2.6 and, as shown, strain gauges were bonded to the beams to provide a means of detecting the load. The gauges (one on top and one on the bottom of each of the beams) were connected to form two Wheatstone bridges with the connections being such that the output from all the gauges were 'summed'. The outputs of the two bridges were then added together electrically by using an operational amplifier.

2.5.3. Special Coupling

It was necessary to ensure that the motor drive system did not influence the thrust measuring device. This presented a major problem and a commercial unit which in principle allowed free axial movement of the input/output shafts resulted in a non-linear response and a significant loss in sensitivity. To overcome this difficulty a special coupling was designed and built at ISVR. This consisted of the 'cup and boss' arrangement illustrated in Figure 2.7. The circular cup has four oblong slots at 90° intervals which act as bearing surfaces for four small roller bearings mounted on the edges of two 'torque-pins' which are attached rigidly to the boss as shown in Figure 2.7. This device proved very satisfactory and was installed as a permanent feature of the rotor rig.

2.5.4. Calibration

The thrust measuring device was calibrated by applying loads, in situ, to the rotor shaft. A typical calibration curve is shown in Figure 2.8 and it was found that the accuracy was within 1% over the full test range of ± 100 lb. It was assumed that the static calibration was equally applicable to the rotating (dynamic) load case. There was no adequate method of checking this, although it was verified by adding a weight to the rotor head at a known rotor speed and comparing the value with the normal reading for that speed. This confirmed the assumption (within ± 3%) for the case when the rotor was loaded, but it could not be checked for the 'negative lift case'.

2.6. BLADE LOADING MODEL

The ISVR model rotor rig initially had no facilities for the measurement of thrust. Since it was considered vital to have an estimate of the total, a blade element (strip momentum) theory was used to calculate the 'ideal' spanwise load distribution and an allowance for the tip effect was then made empirically. This approach is outlined in Appendix 2, together with a general description of the calculation process. Although this method had obvious limitations it was considered to be sufficiently accurate for this particular noise investigation.

A similar approach was subsequently applied to the single bladed full scale rotor where actual thrust measurements were available. Figure 2.9 shows a comparison of the estimated and measured thrust value. The 'theory' tended to over-estimate the measured value in all cases except the high pitch (15° cuff) and high speed conditions at 11° and 13° cuff pitch settings. The 5° and 7° cuff pitch measurements shown on the figure are suspect and it would appear that the load cell was incorrectly zerded at the commencement of the tests, with the result that the indicator 'bottomed' at 500 lbs. In general, however, the agreement is relatively good, with the biggest error being in the order of 13%, which is the same order as would be obtained by more complex theories.

During the blade/fuselage interaction study (Chapter 7) a thrust measurement device was installed and this enabled for the first time a direct comparison between the theory and measurements to be made. This is illustrated in diagrammatic form in Figure 2.10 which shows thrust as a function of blade pitch, for rotor speeds from 400 to 800 rpm. Again it will be observed there is generally good agreement particularly at

the higher pitch settings. The largest error occurred at high speed/low pitch where the predicted value was 35% above that measured. Over the majority of the test range the values were, however, within 15% with the theoretical values normally being high.

The blade loading model mentioned above was used to derive the relationship between angle of attack (α) and pitch angle (θ), and Thrust (T) and pitch angle (θ). Results for the ISVR 9 ft diameter fitted with 3 blades is shown in Figures 2.11 and 2.12 respectively. Figure 2.11 shows the solution for α at 95%R but since the changes of α with radius over the outer portion of the blade is small (see Figure A2.2), it is equally applicable to radial sections from 85%R to the tip if tip effects are ignored. This relationship is independent of rotor speed and as can be seen results in $\theta = 2.6\,\alpha^{0.774}$ or $\alpha = 0.385\,\theta^{1.29}$. As a rough guide over the main range of interest (2° to 10°) the angle of attack α is simply half the pitch value; i.e. the approximate solution is $\alpha = 0.5\theta$.

The corresponding T/θ relationship is illustrated in Figure 2.12. The lift/thrust term, which is independent of rotor speed, is plotted as a function of log blade pitch. Over the range of interest it will be noted that T varies approximately as $\theta^{4/3}$. On the figure results are indicated for the 'total lift' and the value at 90%R (rotor radius r ≙ 4.1 ft). The lift/thrust term ($r^2 k_L(\theta-\phi) \equiv r^2 k_L \alpha$, ϕ being the inflow angle) is presented in a generalized form and it is necessary to use the following relationship to obtain the lift/thrust:-

$$L = \tfrac{1}{2}\rho c a_0 B \times \omega^2 \int_0^R r^2 k_L(\theta-\phi)\,dr \qquad (2.1)$$

where ρ = density, c = blade chord, a_0 = lift curve slope

ω = rotor rotational speed = rpm/60 x 2π , B = number of blades and k_L = lift function correction factor.

This solution is outlined in Appendix 2 and as can be seen from equation 2.1, the lift/thrust varies as ω^2 or in other words as blade velocity V^2.

A similar approach (see Appendix 2) was used to derive the basic torque characteristics. In this case both the profile drag (C_{D_0}) and the induced drag are important. A typical set of results which illustrate the general characteristics is reproduced in Figure 2.13. This shows the generalized torque term as a function of pitch angle; the influence of both drag terms is indicated together with the calculated total torque (drag) and some experimental results. In a similar manner to that discussed above for the lift/thrust, the actual torque was

obtained by use of the following expression:

$$\text{Torque} = \tfrac{1}{2}\rho c \; B \times \omega^2 \int_0^R r^3 \left[k_L a_o (\theta - \phi)\phi + C_{D_o} \right] dr \qquad (2.2)$$

This is outlined further in Appendix 2. It will be noted from Figure 2.13 that there are some differences between the theoretical and experimental results with the measured values rising at a more rapid rate with pitch than predicted. This effect is well known and as discussed in Appendix 2 (section A2.4.2) it is necessary to use a modified solution for C_{D_o}. Some work along these lines was carried out (see Appendix 2) and resulted in the 'dashed curve' indicated on Figure 2.13. This shows better agreement with the experimental results but tended to over-estimate the torque at the higher pitch setting. It was considered that a further refinement to the theory could have been made, but this was considered outside the scope of the rotor noise investigation.

TABLE 2.1: HELICOPTER CHARACTERISTICS

			MAIN ROTOR					TAIL ROTOR					STUDY
			NO.OF BLADES	ROTOR RADIUS	BLADE CHORD	ROTOR SPEED	TIP SPEED	NO.OF BLADES	ROTOR RADIUS	BLADE CHORD	ROTOR SPEED	TIP FT/S	
		lbs		ft.	ins.	rpm	ft/s		ft.	ins.	rpm	ft/s	
Aerospatiale	Gazelle	3900	3	17.25	10.6	378	683	13 °	1.14	1.53	5770	689	2
Bell	UH-1B	8500	2	22	21	324	745	2	4.25	*	1662	740	1,2,4,10
	UH-1D	9000	2	24	21	324	814	2	4.25	11.5	1662	740	1,4,7
Boeing Vertol	V107	19550	2x3	25	18	264	690	-	-	-	-	-	1,4,7
	Chinook(CH-47)	33000	2x3	30	25.3	230	720	-	-	-	-	-	1,4,7
Milhail	MIL 10	95790	5	57.4	39	120	720	4	10.4	*	661	720	2,4
Sikorsky	S61	19000	5	31	18.25	203	660	5	5.17	5.7	1133	614	1.
Westland	Widgeon	5900	3	24.5	16.4	202	518	3	4.1	6	1458	625	1,2
	Whirlwind	8000	3	26.5	16.4	218	605	2	4.47	6+	1524	713	2.
	Sycamore	5600	3	24.3	9.5+	260	660	3	4.8	3	1314	660	5,6
	Belvedere	19000	2x4	24.5	15.5	250	640	-	-	-	-	-	2,4
	Scout	5500	4	16	10.5+	400	670	2	3.75	8+	1923	755	2,9
	Wessex 1	11000	4	28	16.4	221	650	4	4.75	7.3	1318	656	1,3,8
	Wessex 3	13500	4	28	16.4	228	669	4	4.75	7.3	1352	673	2,3,6,7,10
	Wessex 2 & 5	12600	4	28	16.4	230	674	4	4.75	7.3	1376	684	2.
	Lynx	9000	4	21	15.5	326	717	4	3.63	7.1	1887	717	2.
	Sea-King	20500	5	31	18.2	209	678	5	5.17	7.3	1281	694	2,5,8
	Westminster	33000	5	36	21.5	171	645	4	7.5	13.5	821	645	5.

*Data not available. ° 'FAN-IN-FIN' ('FENESTRON' TAIL ROTOR). + Tapered Blades - values quoted @ 0.9 Radius.

STUDY
1. GENERAL NOISE INVESTIGATION
2. DEVELOPMENT OF PREDICTION FORMULA
3. CONTROLLED FLIGHT TESTS
4. BLADE SLAP - GENERAL INVESTIGATION
5. BLADE SLAP - STUDY OF TIP VORTEX PATHS
6. BLADE SLAP - LOCATION OF TIP VORTICES
7. BLADE SLAP - SUBJECTIVE EVALUATION
8. THEORETICAL INVESTIGATION
9. TAIL ROTOR NOISE
10. CABIN NOISE

PLATE 2.1. ISVR 9 FT MODEL ROTOR RIG

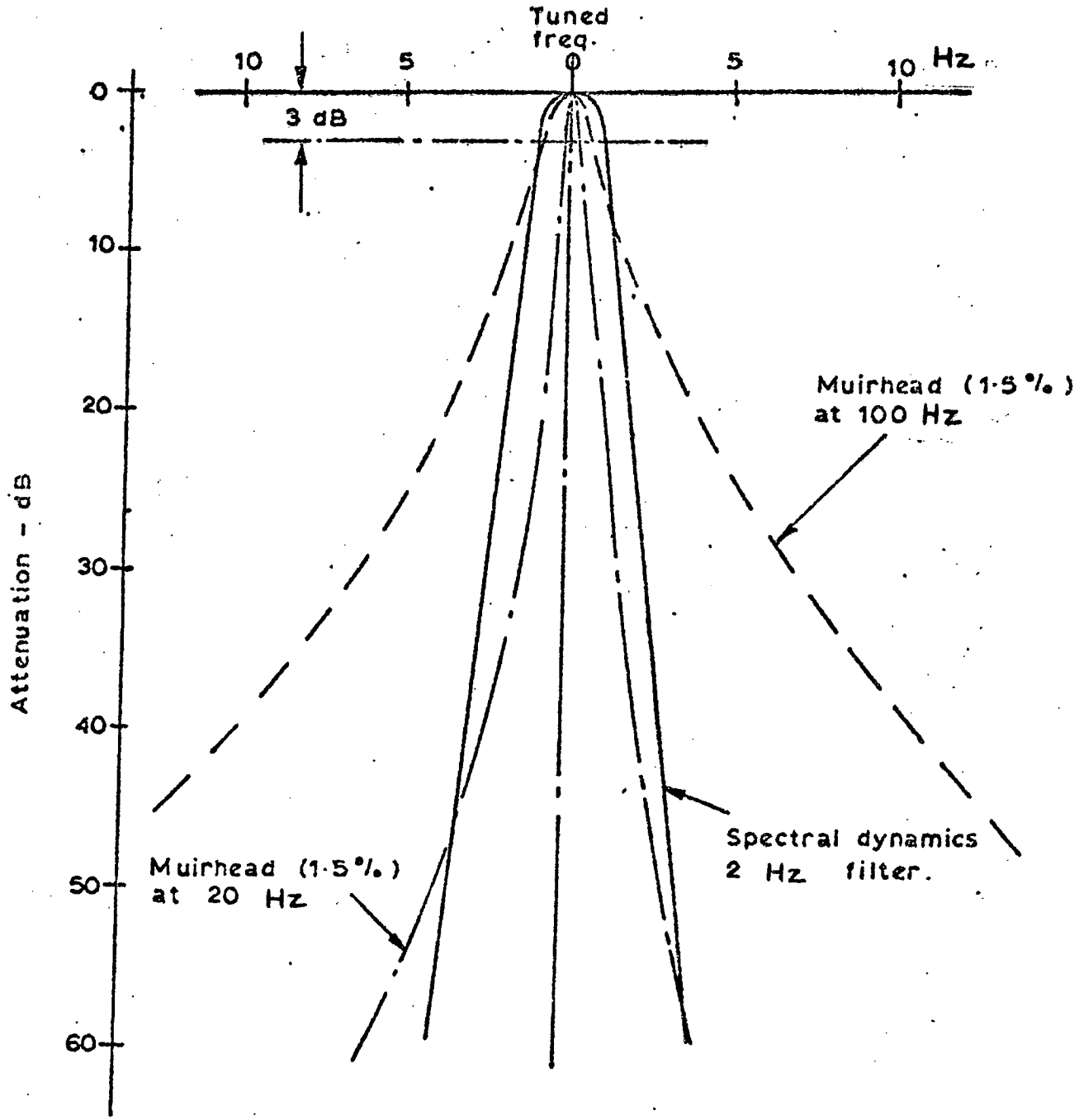

FIGURE 2.1 FILTER CHARACTERISTICS

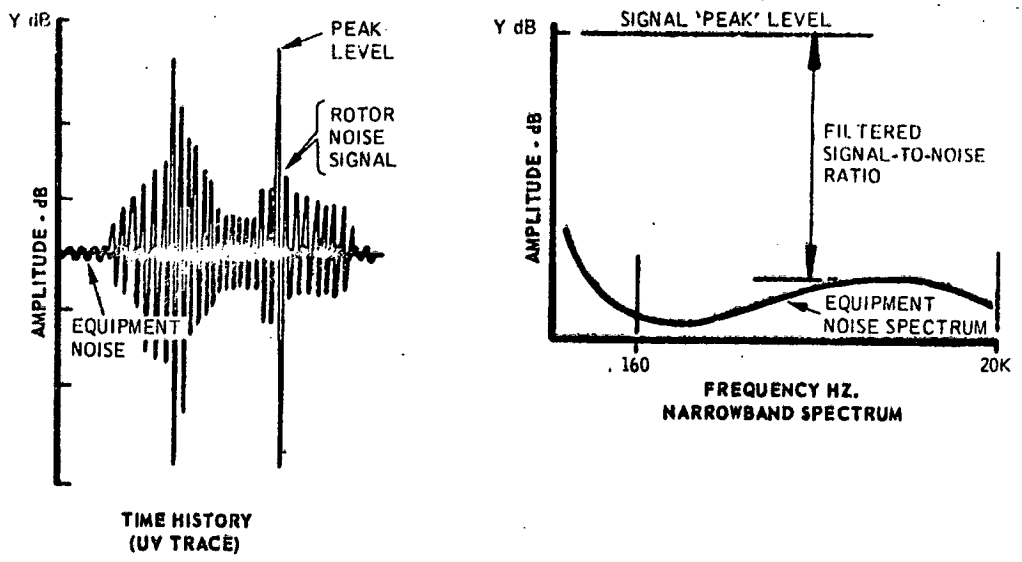

FIGURE 2.2 DEFINITION OF FILTERED SIGNAL-TO-NOISE RATIO

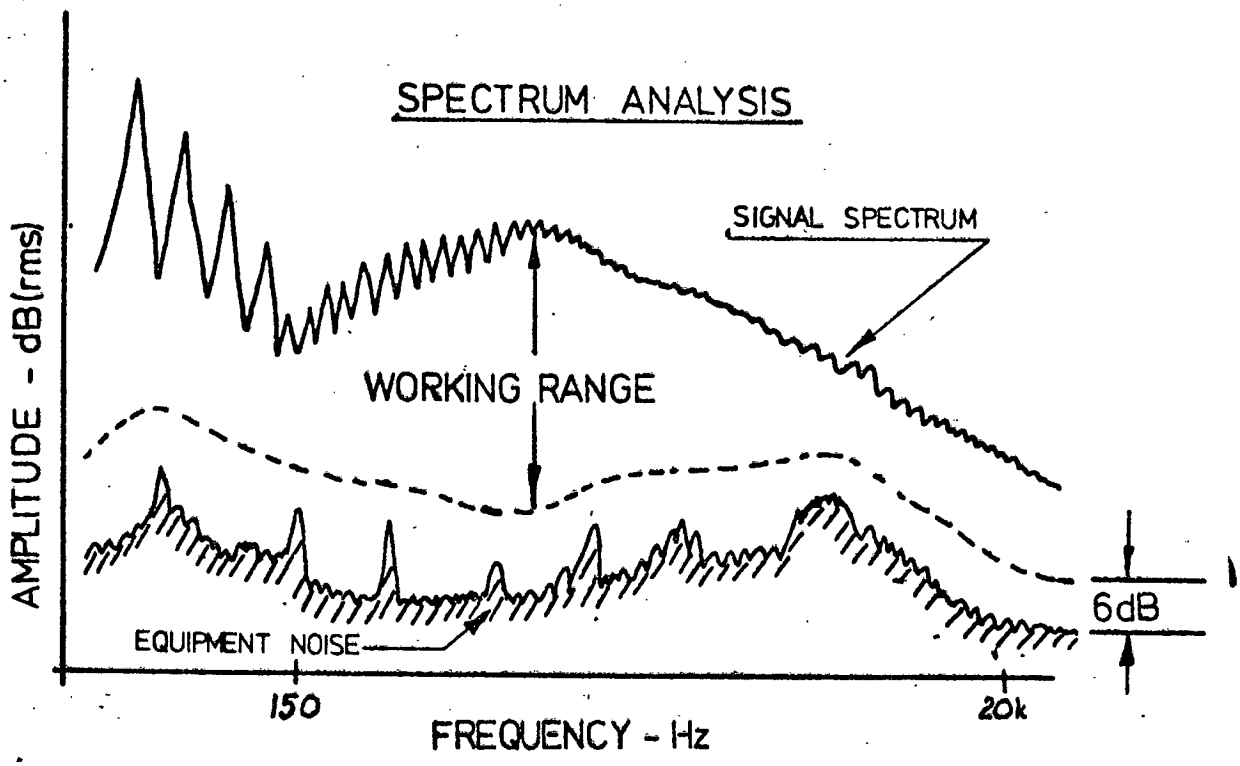

FIGURE 2.3 DEFINITION OF WORKING RANGE

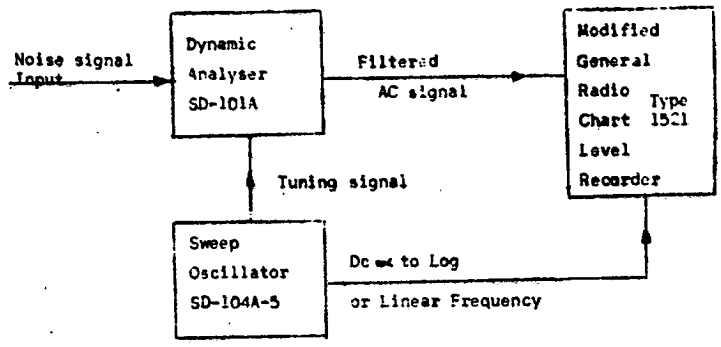

(a) Sweep Frequency (Narrowband Analysis) Mode

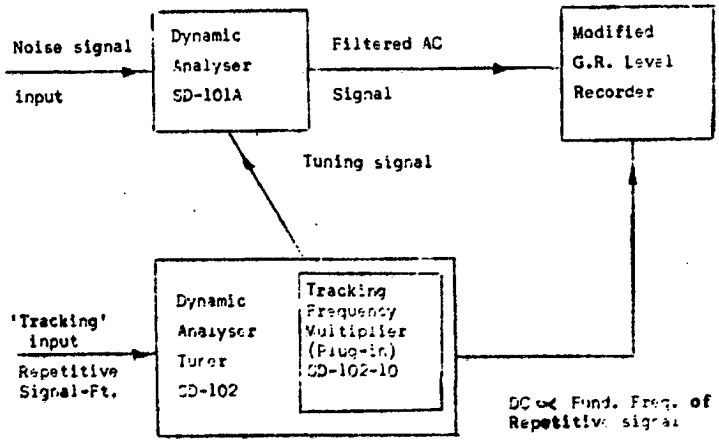

(b) Tracking Mode

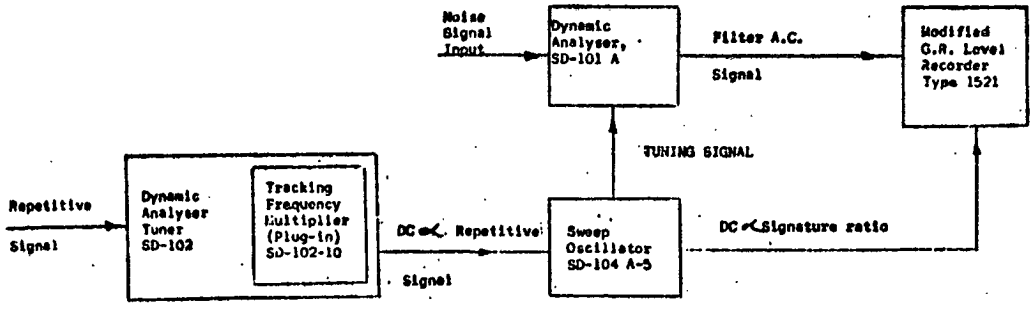

(c) Signature Ratio Mode

FIGURE 2.4 BLOCK DIAGRAM OF SPECTRAL DYNAMICS ANALYZER SYSTEM

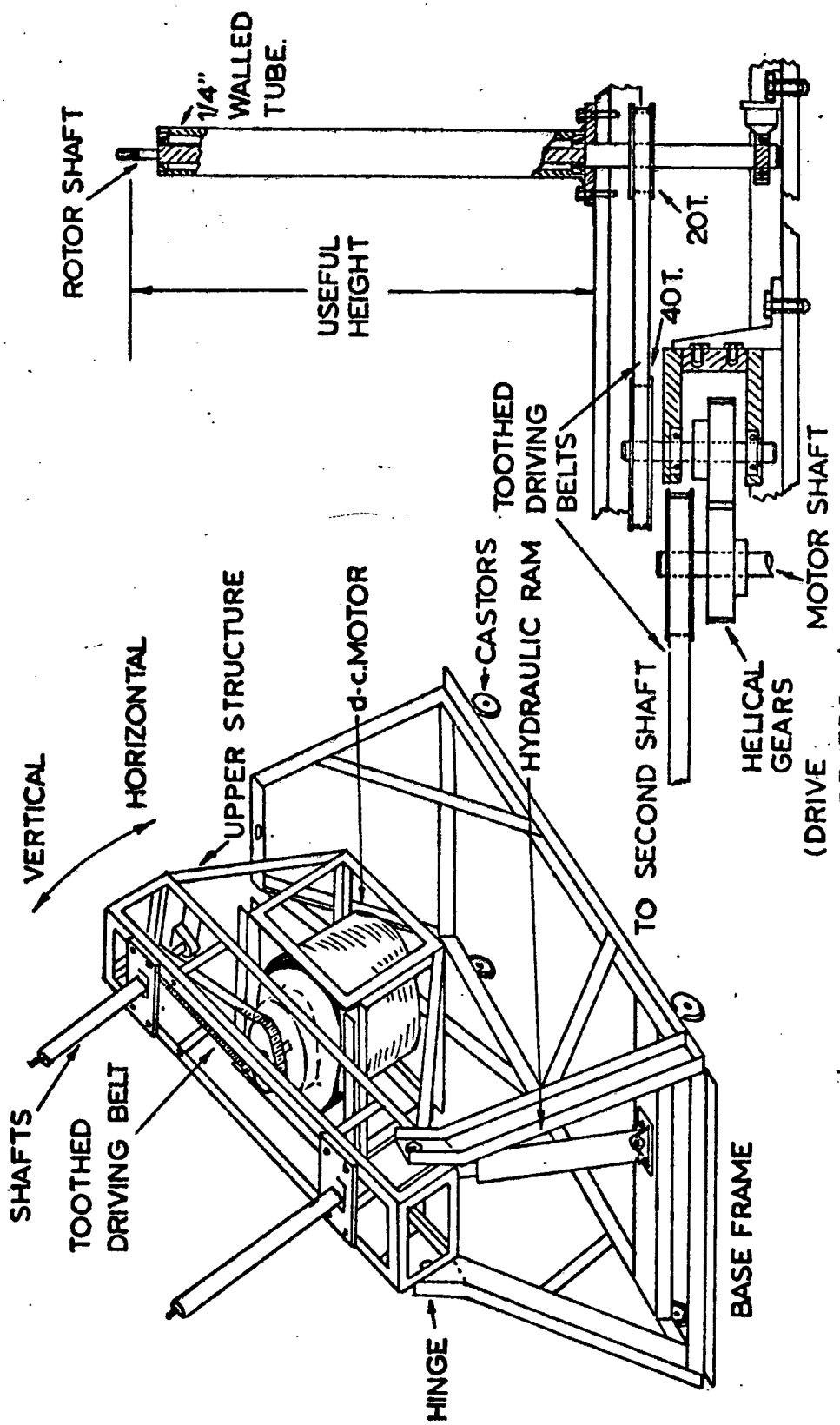

FIGURE 2.5 TANDEM ROTOR RIG DRIVE SYSTEM

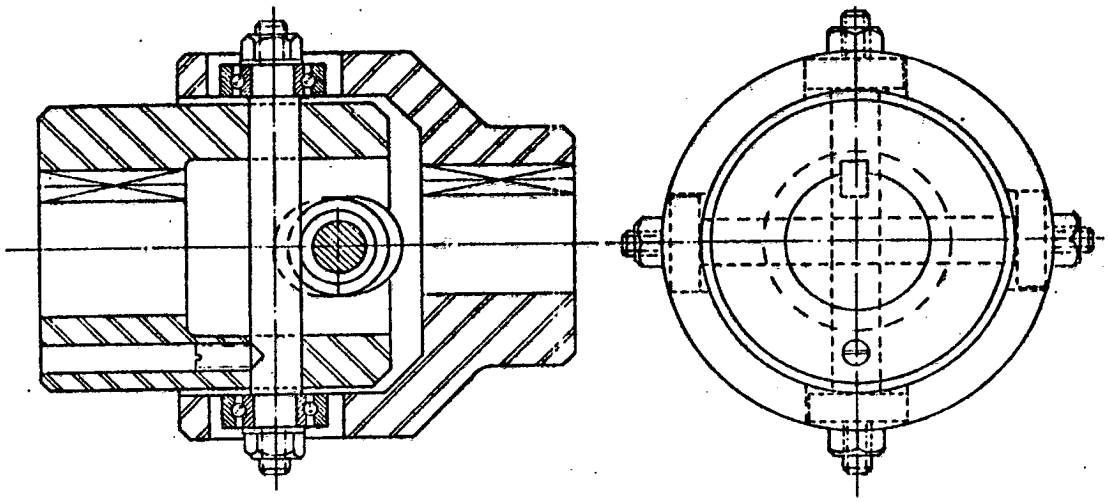

FIGURE 2:7 ROTOR SHAFT COUPLING

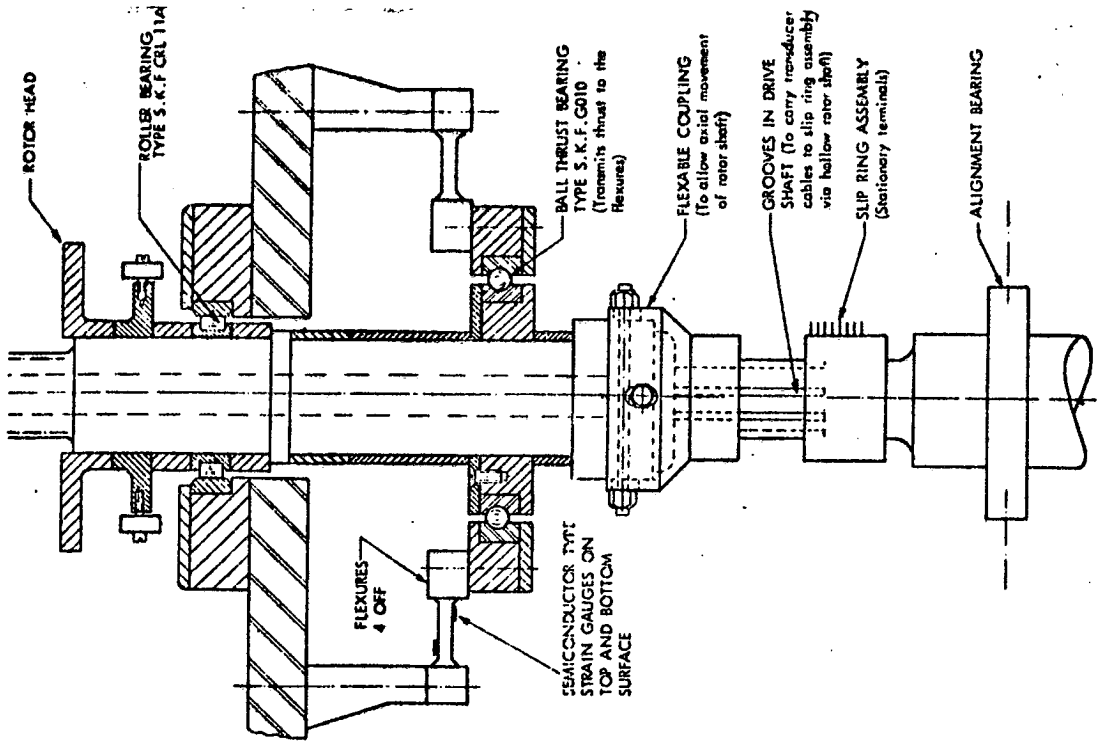

FIGURE 2:6 THRUST MEASURING DEVICE

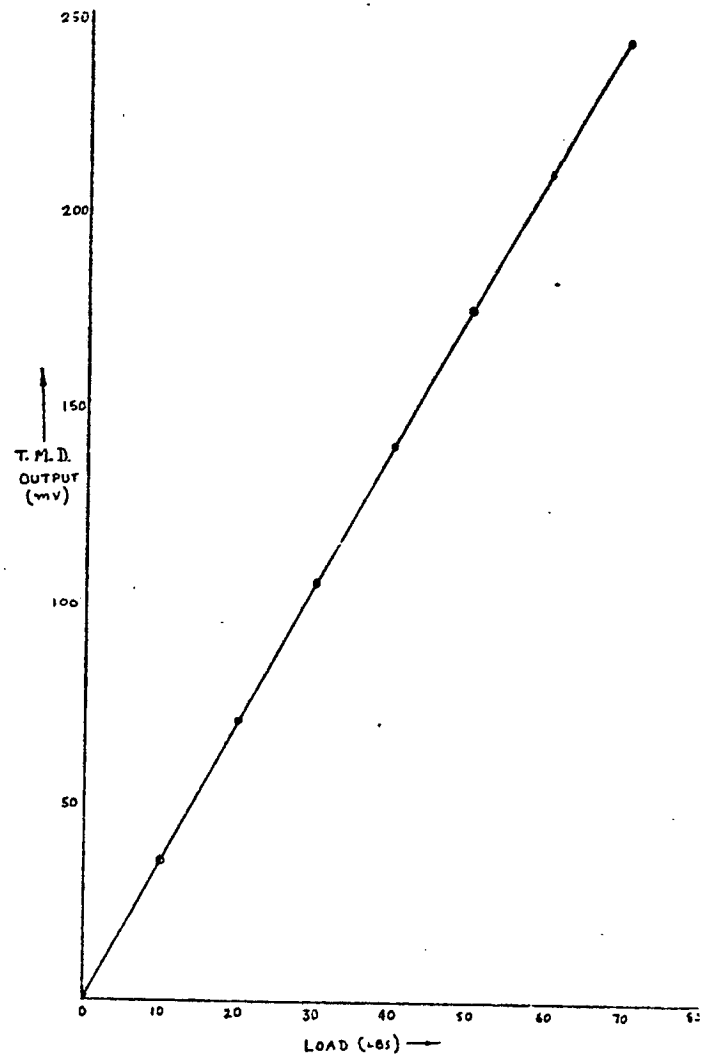

FIGURE 2.8 CALIBRATION FOR THRUST MEASURING DEVICE

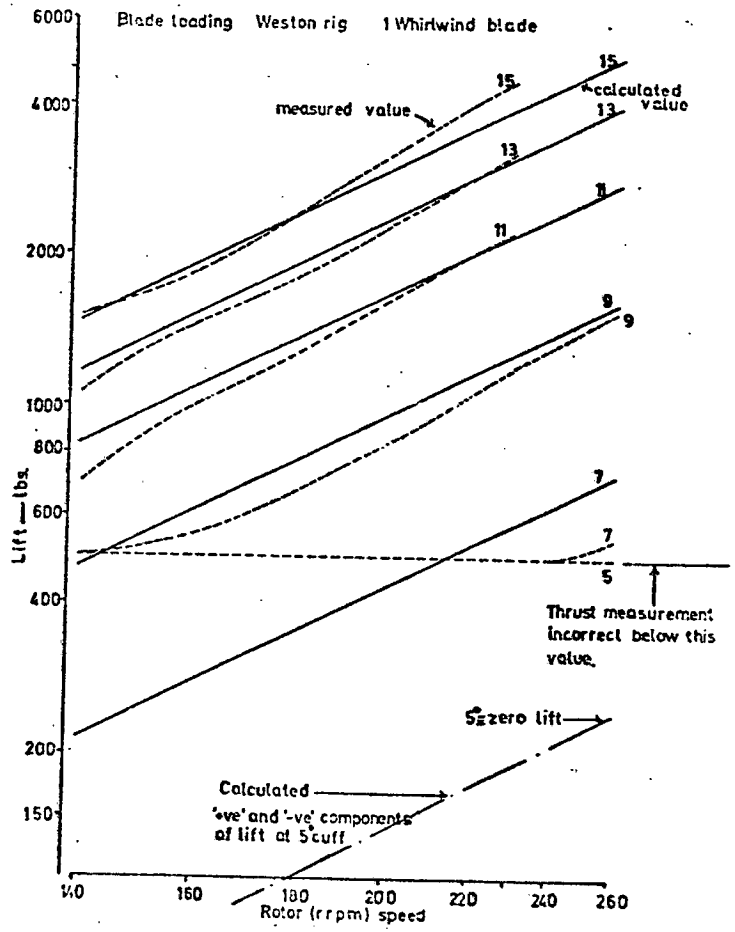

FIGURE 2.9 COMPARISON OF CALCULATED AND MEASURED LIFT (1 BLADED FULL SCALE ROTOR)

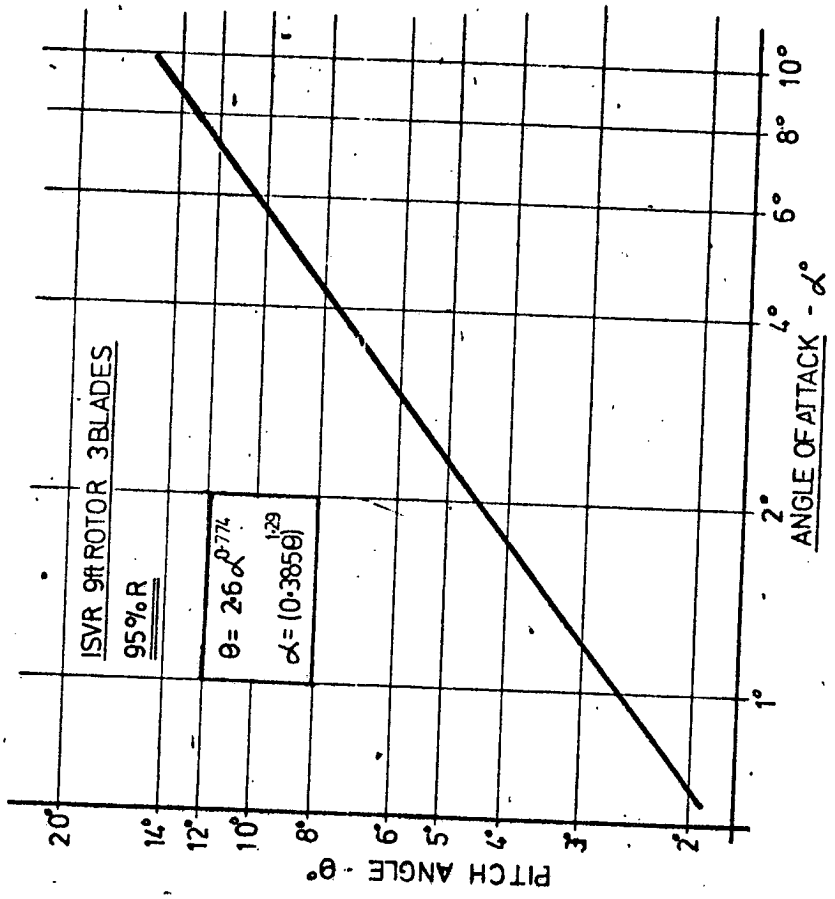

FIGURE 2.11 PITCH ANGLE vs ANGLE OF ATTACK

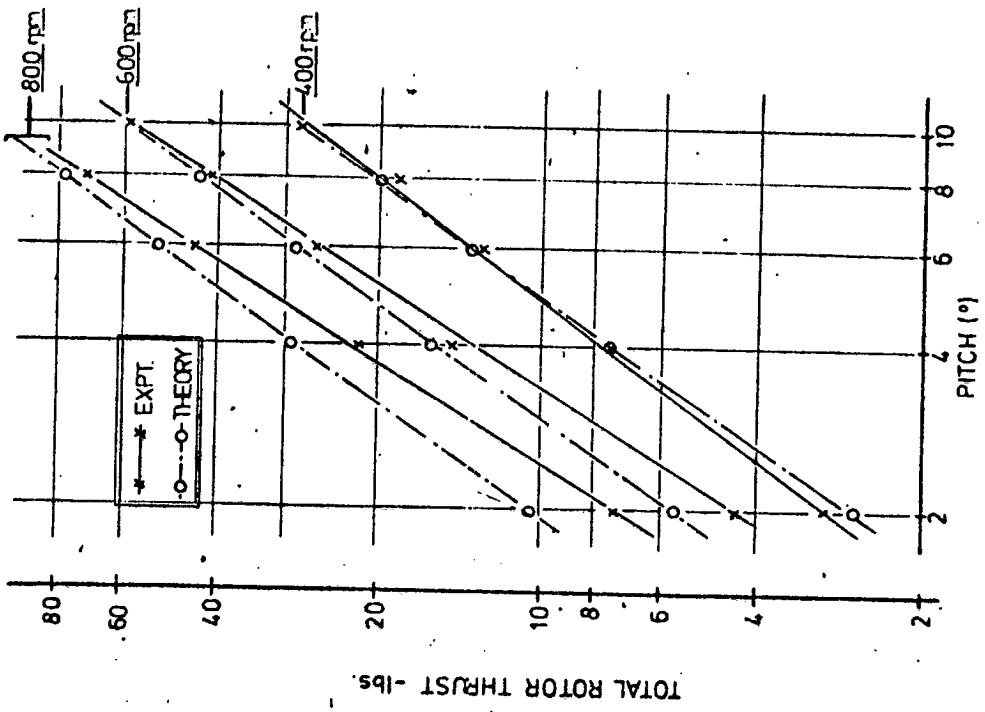

FIGURE 2.10 COMPARISON OF CALCULATED AND MEASURED THRUST (ISVR 9FT MODEL ROTOR)

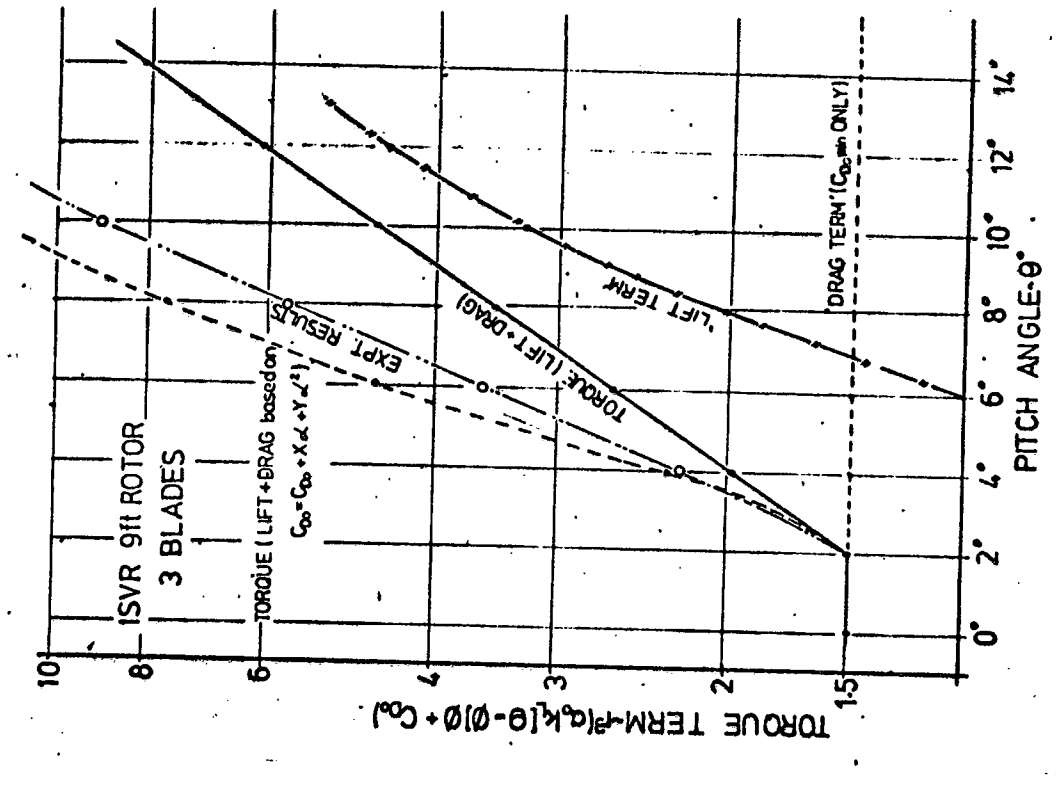

FIGURE 2.13 VARIATION OF TORQUE WITH PITCH ANGLE

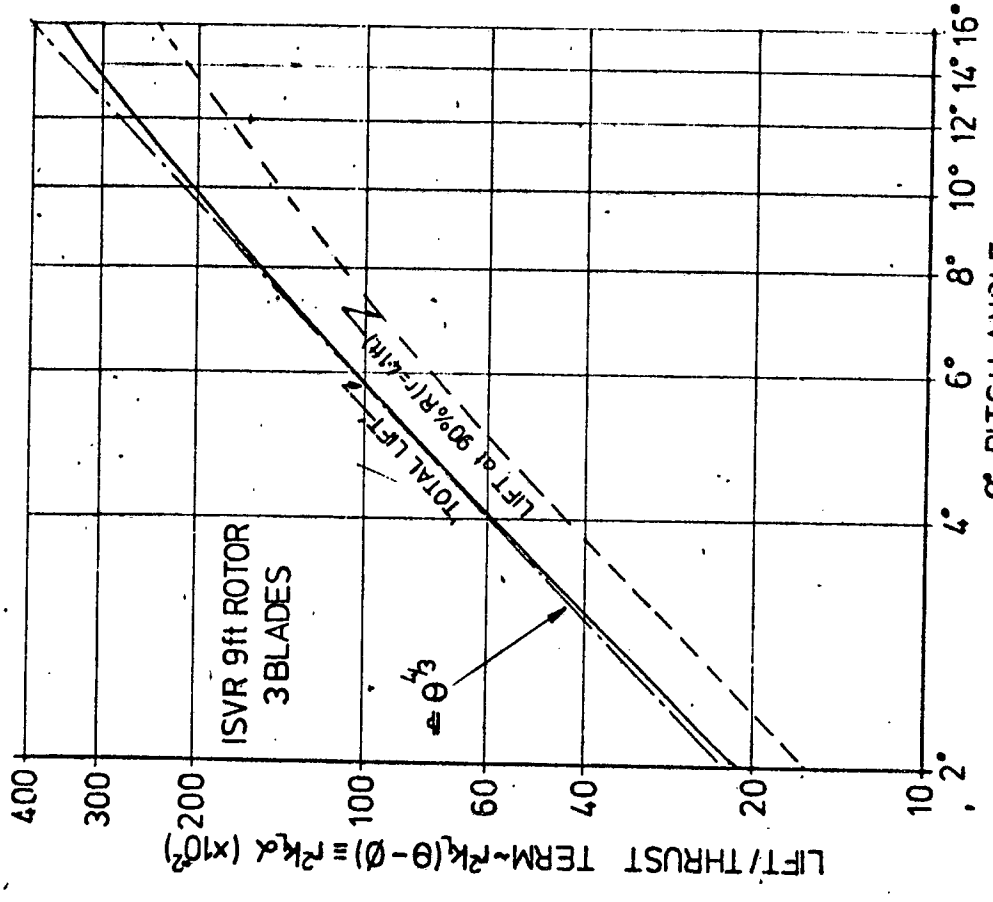

FIGURE 2.12 VARIATION OF LIFT/THRUST WITH PITCH ANGLE

CHAPTER 3: ROTOR NOISE

3.1. INTRODUCTION

Numerous investigations were conducted at ISVR and a large number of the recordings obtained by WHL and on a joint basis by WHL/ISVR were analyzed at ISVR. As can be imagined this yielded a vast amount of data, much of which was used simply to obtain the general characteristics of rotor noise. It is not proposed in this thesis to outline these results in full but rather to concentrate on aspects which are of general interest and which were used to guide other investigators engaged in the study of rotor noise. It was also necessary to know the basic characteristics of normal rotor noise when formulating the main impulsive noise studies reported in Chapters 5, 6 and 7. This work also formed the basis for study of overall helicopter noise outlined in Chapter 4.

3.2. NOISE SOURCES

It is not possible to consider the noise produced by a rotor as one entity since it is a combination of the sound generated by a number of individual mechanisms. Loosely the sound can be grouped in three categories, namely rotational or discrete frequency noise, broadband noise, often termed 'vortex' noise, and blade slap or blade bang. Theoretically blade slap can be considered under the heading of rotational noise, but since it is an isolated disturbance which occurs only over a small proportion of the rotor disc it is usually more convenient to consider it as a separate source. This topic is discussed in depth in Chapter 5.

Rotational noise consists of individual frequencies or tones which show up as harmonically related discrete frequencies or 'peaks' on a narrowband analysis: With the exception of the fundamental and first few harmonics which are a function of the steady (mean) parameters of the rotor, at moderate speeds this type of noise is generated by the fluctuating forces exerted by the blade. In this context the high order force (lift and drag) fluctuations are very important. At high speeds 'thickness' noise, which is dependent on the physical size of the blade, also becomes important giving rise to an impulsive type noise.

Broadband noise, which during the period of the early phases of this investigation was often referred to as 'vortex noise', shows up on analysis as a band or 'hump' of random noise spread over a relatively wide frequency range. Unlike rotational noise which can be defined in

specific terms, broadband noise does not have well defined spectral characteristics and the precise details of the frequency range associated with it is still at the present time somewhat vague.

Several mechanisms for the generation of broadband noise are possible and have been proposed by various investigators. It would appear that random lift fluctuations are the most likely generators of this type of sound. Initially it was postulated that this resulted from the interaction of the blade with a tip vortex of a previous blade and/or the wake shed by the previous blade. Recently, however, partly as an outcome of ISVR test results, doubt has been shed on the actual mechanism, since the measured levels appear to correlate with the blade geometric parameters and tip speed only; this is also true when measured on an actual helicopter as discussed in section 4.5. It would appear, therefore, that this self generated noise is in some way associated with the boundary layer on the blade itself but a full explanation has not yet been found.

It is difficult to distinguish between higher harmonic rotational noise and broadband noise and the following definition was therefore adopted by the author. Experimentally all the acoustic energy which did not show up as a 'peak' on a very narrowband spectrum analysis (where the filter bandwidth was much less than the blade passing frequency) was considered to be broadband noise.

On an actual rotor the broadband noise travels with the blade and is responsible for the characteristic 'swishing' sound heard by an observer when relatively close to a rotor. At the time of the commencement of the ISVR study broadband noise over the complete audio frequency range of 20 Hz - 2 kHz was simply treated as one source. An outcome of the ISVR model tests - later confirmed by full scale tests conducted at WHL - was that there were at least two distinct broadband noise regions which exhibit relatively well defined and repeatable characteristics. This view is now shared by a number of other investigators and, following the notation adopted by the author, commonly referred to as 'low frequency broadband noise' and 'high frequency broadband noise'. The former is the source discussed above and the latter, which occurs at a frequency region which is in the order of 10/20 times the low frequency noise, is considered to be associated with the shed wake/boundary layer of the blade.

It would also appear logical that the broadband noise should be dependent on the Reynolds number - in other words different characteristics would be expected to occur on a low speed rotor (with laminar boundary

layer) and a high speed rotor (turbulent boundary layer). Although detailed studies have revealed differences, there appears to be no dramatic change in the characteristics of broadband noise as the rotor speed is increased such that the boundary layer would be expected to change from laminar to turbulent and model results (low Reynolds number) and full scale results (high Reynolds number) show the same basic general trends. It would appear therefore that the influence of Reynolds number effects (and hence the classic boundary layer concept) is much less than originally postulated.

3.3. TEST ANALYSIS PROGRAMME

Tests were conducted on the ISVR rotor facility (section 2.2) with 1, 2, 3 and 4 bladed rotors. It was originally anticipated that the experimental data would have compared with, or at least correlated with the aid of, theoretical models which were initiated at ISVR. The development of the theoretical models, by Wright [28] and later Wright and Tanna [29] proved more complex than originally envisaged. It also became clear that even when this work was completed it could not be readily used to correlate the noise characteristics of the model rotor rig. As a natural consequence the model results were treated solely from an experimental point of view, linked where possible with similar full scale test results. In this context the situation has changed little since, although theories by Ollerhead and Lowson [30], Wright [31], etc, are available, they cannot be directly compared to experimental results since they require knowledge of the appropriate blade loading data. Once such experimental data is available, however, the theories can be used to explain the observed trends as indicated by Wright in reference(31). It follows, therefore, that the data included in this chapter is presented largely to illustrate the change in the noise characteristics with operating conditions and is solely of an experimental nature. The ISVR model data was also supplemented by full scale results supplied by WHL, analysis of recordings supplied by WHL and analyzed by the author [32] and more recently tests conducted at WHL under the direction of the author [33].

Recently correlation of full scale data within WHL by the author has suggested a dependency of broadband and rotational noise on the projected thickness (tp) based on the angle of attack α [34]. The data from the ISVR model has not yet been examined in this format; even so it is worth noting that the work conducted at the ISVR was used as a basis

for formulating both the WHL test and analysis programme. Also the data presented in this thesis has been essentially limited to that which illustrates the basic characteristics of rotor noise used as a reference for the impulsive noise studies or results directly relative to the understanding of impulsive noise. The model and full scale analysis did, of course, give results which were of a wider interest and although reported in a number of general papers (some of which were purely working papers) by the author, they have not been included in this thesis.

3.4. TEST CONDITIONS

The test conditions associated with the ISVR model and the full-scale (WHL) rotor are summarized in Tables 3.1 and 3.2 respectively. It will be noted that the ISVR model tests were conducted at a range of rotor speeds and pitch angle (θ) settings, while in the case of the full scale tests measurements were taken at a range of rotor and thrust conditions. In the full scale tests reported in reference(32), the same basic rotor was used but instead of varying thrust, measurements were taken at cuff pitch angles ranging from 7° to 15°.

In Tables 3.1 and 3.2 the corresponding C_{LT} (and in the case of the model rotor estimated total thrust) values are given. The main analysis was conducted with the rotor configuration indicated, although the model tests were also carried out with 4 bladed, 2 bladed and 1 bladed rotors and full scales with 4 and 1 bladed rotors. The main measurement positions are also given in the tables.

Also given are the Reynolds number range associated with the two rotors and as can be seen these are significantly different. The value corresponding to a change from laminar flow to turbulent flow is normally taken to 1×10^6 and thus based on classical aerodynamics it seems reasonable to assume that while on the model rotor it is laminar it is turbulent on the full scale rotor. It could, however, be argued that the high speed conditions on the model rotor (Reynolds number 0.9×10^6) would also be turbulent and thus if the changeover in flow conditions had a marked effect on the noise it should be observable in the model rotor results.

The model rotor blades had zero twist and thus at zero pitch the blades were travelling in their own shed wake. At 2° pitch there is a small lift and the wake is 'pushed down' thus giving a 'cleaner inflow' over the blade. As the pitch is further increased these effects are increased and the magnitude of the tip vortex, which is directly proportional to blade loading, and hence pitch, is increased. On the real

rotor with twist, used for the full scale tests, the case corresponding to zero pitch on the model never occurs since at zero thrust part of the blade is generating positive thrust and part is generating negative thrust. It is estimated for the rotor tested that the magnitude of this lift at the higher tip speeds is in the order of ± 70 lb. It follows that except for a small region on the blade where the angle of attack (not blade pitch) is zero there is always a flow away from the blade path and hence the next blade should be passing into relatively 'clean air'. As pitch and/or thrust is initially increased the negative component of lift is decreased, the positive lift component increased and the 'zero angle of attack' position moves towards the tip. Again as further lift is applied all the thrust becomes positive and the tip vortex strength increased.

The above is a relatively simple visualization since three dimensional effect near the tip has a major influence on the local flow field and it is difficult to estimate the precise position of the 'zero of angle of attack point'. Also as the pitch or thrust is increased it would be intuitively expected that since the mean flow is increased, the tip vortex would move further away from the blade. Flow visualization studies* have shown this is not the case and that the tip vortex remains in, or close to, the rotor tip path plane until the next blade passes when it moves rapidly down with the general downwash. This is equally applicable to the model and full-scale rotor and must, of course, be taken into account when studying the influence of rotor operating parameter on the noise.

3.5. TEST RESULTS

Test results for the rotational noise components, broadband noise levels, overall (dB LIN) noise as well as blade lift and torque (HP) values were obtained for the ISVR 9 ft diameter rotor fitted with 1, 2, 3 and 4 blades with the main emphasis being placed on 3 bladed results. In addition similar data was obtained for the tandem rotor rig and the two sets of full scale WHL S55 rotor tests. Some of this data has been reproduced in ISVR technical and contract reports, although the majority is stored in the author's files. It is not proposed to reproduce any of these tables (which as can be imagined are numerous) in detail but rather to limit the results to the points of general interest and graphical representation. Reports in which fairly extensive coverage of the data in tabular form is reproduced are reference(32)(full scale single bladed

*A general discussion of tip vortices, and their trajectories, is presented in section 5.8.

tests), reference[35] (4 bladed ISVR rotor tests), reference[36] (3, 4 blade ISVR rotor tests) and reference[37] (full scale - 1, 2, 4 blades).

The data presented in this thesis was obtained in the case of the ISVR model mainly from a microphone positioned at an angle 9° below the rotor disc and 25 ft from the rotor centre which corresponds to a distance of 2.8 rotor diameters. The full scale single rotor whirl tower results [32] were obtained at a similar position, 5° below the ideal rotor disc plane at 3.2 rotor diameters (177 ft ~ rotor diameter 48 ft) and the other full-scale rotor data [37] at -11.5° and 250 ft (4.46 rotor diameters).

3.6. ROTOR NOISE - GENERAL CHARACTERISTICS

Typical narrowband analysis traces are presented in Figures 3.1 and 3.2 for the ISVR and S55 full scale rotors respectively; also indicated on these figures are the three sources of interest. These traces are from a 'quick look' analysis and although the filter bandwidth is changed at 200 Hz and 1.5 kHz this does not imply that the three sources are defined within these frequency limits since, as can be seen from the traces, the sources blend from one to another.

It will also be noted from these figures that, except for the differences in frequency range of each noise source for each rotor, the spectrum shapes are very similar in character.

As explained previously the low frequency region for both rotors is dominated by rotational noise, while the mid-frequency region consists of a combination of rotational noise and low frequency broadband noise with the relative levels depending on the blade operating conditions. It will be observed from Figures 3.1 and 3.2 that although the full scale results exhibit, particularly at the low speed conditions, a well defined high frequency broadband noise (at 3.5 kHz) the corresponding characteristics associated with the model results are less clear.

3.7. ROTATIONAL NOISE

3.7.1. Spectrum Characteristics

Typical narrowband analysis results for the model rotor and the full scale rotor are reproduced in Figures 3.3, 3.4 and 3.5. Figure 3.3 is for the model rotor fitted with 3 blades and at the higher speeds well over 20 harmonics can be detected. Figures 3.4* and 3.5 show results derived from the initial full scale rotor tests [32] and the more recent WHL full scale tests [37] respectively. Again it will be observed that many blade passing harmonics can be detected. In cases where very narrowband analysis (1 Hz) was performed and extra care taken, up to

*The vertical lines, 'kicks', on Figure 3.4 were due to an instrumentation problem associated with the ISVR analyzer system - these should be ignored.

50 harmonics could be detected: Figure 3.5 shows such an example for the full scale measurements. It was found from an examination of the traces that the full scale results tended to give 'cleaner' more well-defined peaks (discrete frequencies) than the model and when real helicopter recordings were examined it was found that these gave a further improvement in the quality/appearance of the traces (see Figures 4.3 and 4.4). It appears that, as would be expected, the higher the tip speed and blade loading the more well defined the discrete frequencies.

3.7.2. Variation with Tip Speed

The general trend with speed is illustrated in Figure 3.6 which shows results for three different rotors. These are the ISVR model rig (fitted with 4 blades), the WHL full scale rotor fitted with 1 S55 blade and a 19 ft diameter hovercraft propeller. In the case of the latter two, both rotors were operating at their designed load. It will be observed that to a first order the noise levels follow a V^{10} relationship.

If model results are examined in greater detail it can be seen that in fact different results occur at different pitch settings. Figure 3.7 shows results for 8° pitch; here again the majority of the harmonics approximate V^{10} although there is an indication of a more rapid increase in level with velocity (approaching V^{18}) between 700 and 800 rpm. At 2° pitch (which for all practical purposes gives results identical to the zero pitch/zero thrust case) the higher harmonics tend to be independent of tip speed as shown in Figure 3.8.

On the full scale rotor, however, all harmonics appear to follow similar characteristics as indicated for the '1 Whirlwind Blade' in Figure 3.6 although the power law dependency appears to decrease at the low tip speeds. This is illustrated in Figure 3.9 which shows 'full scale' results for the 1st, 5th, 10th, 20th and 30th harmonics. In this case, however, the results are quoted for constant thrust settings of the rotor. As the rotor speed is increased the effective pitch will be decreased (to maintain constant thrust) and this has to be taken into account when comparing this figure with the results shown in Figures 3.6 to 3.8. The data in Figure 3.9 supports the earlier finding that all harmonics follow very similar trends, although as will be observed the fundamental (1st harmonic) departs from this general trend varying as V^{6} to V^{8} (depending on the thrust setting) over the complete test range. It can also be seen whereas the harmonics follow a V^{12} dependency at high tip speeds (758 ft/s) it is nearer V^{3} at low tip speed (466 ft/s). Over the normal operating range - 650/700 ft/s - however the results follow closely V^{10} mentioned previously.

The fundamentals(1st harmonic) associated with the full scale results in Figure 3.6 (1 Whirlwind Blade) were examined and compared with the Gutin solution [38] as indicated in Figure 3.10. It will be noted that except for an overestimation, typically by 6 dB, the measurements and predictions correlate reasonably well. Part of this discrepancy could be due to choice of the effective radius for the Gutin calculation (0.8 x tip radius) since if a smaller value had been used a lower noise level would have been predicted.

3.7.3. Variation with Pitch/Thrust

Model and full scale results showing SPL as a function of blade pitch are shown in Figures 3.11 to 3.14. At low tip speeds the model results show little increase in SPL with pitch (Figure 3.11, 500 rpm; 236 ft/s), while at higher tip speeds (Figure 3.12, 900 and 1000 rpm; 424 and 471 ft/s) it will be observed that although the first harmonic is effectively independent of pitch (and hence thrust) the higher harmonics show a marked increase as the pitch is applied. The trends associated with the fundamental (1st harmonic - '1' on the figures), and the 2nd harmonic, is understandable since at angles close to the rotor disc (as used for these tests) the steady forces which control these harmonics are dependent on the torque or drag term which will not vary to any great extent for pitch angles up to 6°.

The full scale results show very different characteristics as indicated in Figure 3.13 which shows results for the '1 Whirlwind S55 blade' and the first harmonic for 3 similar (Wessex - S58) blades obtained from reference(39). It will be noted that, with the exception of the first harmonic associated with the 1 blade rotor, the harmonics are relatively insensitive to pitch, and hence to thrust, although there is an increase at the higher pitch settings. These variations have been studied in greater depth from the 2 blade S55 data and a typical set of results is reproduced in Figure 3.14. In this case, however, the data is plotted as a function of rotor thrust and influence of pitch changes discussed in section 3.7.1 must be taken into account. At the higher tip speeds (230 rpm, 670 ft/s which is the same as used for the data given in Figure 3.10) the levels are independent of thrust (T), although in the case of the 5th to 15th harmonics there is an indication of T^2 dependency at the higher thrust settings. This agrees well with the data presented in Figure 3.13. At low speed (160 rpm, 466 ft/s), however, there is a marked difference and with the exception of the

fundamental (1st harmonic) the levels increase over most of the range according to a T^2 relationship. It will be noted, however, that initially there is a decrease in level at low tip speed for all harmonics except the first (fundamental) which appears insensitive to thrust. This is very similar to the model results reproduced in Figure 3.12 which correspond to tip speeds of 424 ft/s (900 rpm) and 471 ft/s (1000 rpm). It appears, therefore, that the resulting trend is a function of the absolute tip speed. It could be argued that it is a Reynolds number effect, but the model results appear to 'blend' into the full scale and there is no sudden or dramatic change in the character of the noise as would be expected if it were associated with a change in the boundary layer from laminar to turbulent.

The trends shown on Figure 3.14 have (since completion of this work) been shown to correlate well with a tp^4 term where tp is the projected blade thickness based on the angle of attack [25]. It is not clear if this could also be applied to the model results.

The main emphasis of this work has been in determining the variation with thrust and/or pitch and there has been no attempt to correlate the data on an absolute level basis. It is of interest to note in the case of the 'three-bladed' results indicated on Figure 3.13 that the fundamental follows the same trends as the 2nd/3rd harmonics of the single blade tests and that there is no correlation with the 'Gutin value' except at the high pitch setting. This is unlike the behaviour of the fundamental in the case of single blade tests which agrees relatively well with the Gutin solution as shown in Figure 3.10.

3.8. LOW FREQUENCY BROADBAND NOISE

3.8.1. Spectrum Characteristics

As indicated previously the low frequency broadband noise region is often a combination of broadband noise and rotational (discrete frequency) noise and it is necessary to select a filter bandwidth which gives a fairly accurate measure of the broadband energy, while at the same time allowing the spectrum characteristics to be determined. It was found that a 20 Hz filter was most suitable for both the analysis of model and full scale results.

Typical 20 Hz bandwidth analysis results are presented in Figures 3.15 and 3.16 for the model and full scale rotors respectively. A study of these results, and the 5 Hz bandwidth analysis shown in Figure 3.1 and 3.2, showed that although there was some indication of a

'hump' in the broadband region the 'peak' was not well defined. This was in direct conflict with some earlier analysis carried out by the author (for a three blade rotor) which is summarized in Figure 3.17. The more recent broadband noise analysis suggested an 'analysis model' for the low frequency broadband noise of the form illustrated in Figure 3.18. This is based on a log frequency scale and the SPL variations have a 'FLAT level' and a constant dB/octave 'fall-off' portion with the latter extending over a range of two octaves. Due to difficulties of defining the low frequency this was ignored and since a centre frequency could not be readily located, the 'break point' frequency (see Figure 3.18) was used as a reference.

At first glance the spectrum shape illustrated in Figure 3.17 seems completely different from the analysis model reproduced in Figure 3.18. This is, however, not the case. The early analysis was based on $\frac{1}{3}$ octave band analysis and the discrepancy largely arose from use of such an analyzer. This can be best explained with reference to Figure 3.19 which shows the $\frac{1}{3}$ octave band spectra corresponding to the 'analysis model' for three different 'breakpoint frequencies' set at the lower limit, the centre frequency and upper limit of a $\frac{1}{3}$ octave band respectively. It will be noted that the 'flat topped' analysis model from a constant bandwidth analysis is transformed to the traditional 'hump' spectrum by use of $\frac{1}{3}$ octave bands and that an apparent 'peak frequency' is created at a value corresponding closely to the 'break point frequency'. The influence of the use of a low frequency rejection filter is also illustrated on Figure 3.19.

On figure 3.17 the 'dashed line' illustrates the results obtained originally from $\frac{1}{3}$ octave band analysis, the continuous line is an estimate of the results likely from a narrowband percentage bandwidth analysis and the 'dotted line' an estimate of the spectral shape as would be obtained from a narrowband constant bandwidth analyzer. It is clear now that the width of the peak (a $\frac{1}{3}$ octave band) was solely a function of the analyzer. The high frequency 'fall-off' rate indicated of 7/10 dB agrees, however, well with the more recent results. The low frequency characteristics are, however, difficult to quantify and although there is a clear indication of a 'fall-off' in level of the order indicated in Figure 3.17 it is difficult to determine any precise figures. It follows, therefore, that the difference between the original analysis and the more recent results is essentially due to the fact that $\frac{1}{3}$ octave band analysis

was used. At the time this was, of course, the standard method and this problem is not only applicable to the work by the author but also to that of many other investigators who also used similar analysis techniques to define the characteristics of (low frequency) broadband noise.

The 'analysis model' (Figure 3.18) is shown superimposed on both the model and full scale results in Figures 3.15 and 3.16 respectively. As can be seen there is very good agreement, although in the case of the model results it is more difficult to locate the 'FLAT SPL' because of the influence of the higher harmonic (rotational) noise. If, however, a wider bandwidth analyzer had been used, the spectral details would have been lost. It could be argued that the original spectrum shape illustrated in Figure 3.17 could be equally applied to the full scale results, but this is not the case since the signal below 150 Hz has been in effect 'cut off' by filtering prior to recording.

3.8.2. Variation with Tip Speed

Figures 3.20 and 3.21 show the low frequency broadband noise variations with blade tip speed (V) at constant pitch from the model (Figure 3.20) and at constant thrust for the full scale rotor (Figure 3.21). The model results suggest that, except at very low speeds, the noise follows a V^4 law at zero pitch and a V^6 law at high pitch. Thrust (at constant pitch) is proportional to V^2; it could be argued therefore that the relationship at high pitch is also a V^4 law at constant thrust. It will also be noted that there is a dramatic drop in the level at the very low speed of 236 ft/s (500 rpm) - this was observed on all the tests. The full scale results show typically a V^6 to V^8 variation at constant thrust while at angles nearer the rotor axis the dependency is less than V^6, particularly at the high thrust condition. Since this analysis it has been shown that this noise is proportional to the fourth power of the projected blade thickness (tp based on the angle of attack at 0.9R) and if this is taken into account then the broadband noise correlates well with V^6 tp^4 [25].

Even with this latter finding taken into account there is still some slight difference between the model and full scale results. If the full scale results are studied in detail (Figure 3.21) it will be observed that the velocity law at the lower rotor speeds is lower than that at high tip speed. In other words, rather than a single velocity law, the dependency varies with the absolute tip speed. In this context

it is of interest to note that the velocity law associated with the maximum test speed of the model (900 rpm, 424 ft/s) is for all practical purposes identical to that associated with the full scale rotor operating at the minimum test speed (140 rpm, 408 ft/s). Thus it would appear that as the speed is increased the dependency on tip speed also increases. Even so these values are considerably different from those found by other investigators who have suggested that when thrust is held constant the broadband noise varies as V^2 [40, 41] or $V^{2.7}$ [39].

3.8.3. Variation with Pitch/Thrust

Figures 3.22 and 3.23 show the variations in SPL with pitch for the model rotor and thrust for the full scale rotor respectively. It will be noted that both the pitch (θ) and the thrust (T) scales are presented on a log base and that the zero pitch/thrust values have also been added for completeness. The model result (Figure 3.22) varies as $\theta^{8/3}$ at high pitch settings, which corresponds to T^2, and shows a 'minimum' level at a pitch angle of 2 to 3°. The measurements of the power absorbed by the rotor also show similar characteristics. This is considered to be due to the fact that at zero pitch the blades are travelling in their own wake, while at 2° pitch the wake is 'pushed down', giving a cleaner inflow over the blades and hence lower noise levels.

The results for the full scale rotor (Figure 3.23) show that the noise exhibits two trends, one which decreases slightly with thrust and the other which increases at a rate of approximately T^2. The 'change over point' corresponds to a zero angle of attack α near the tip. Since α is dependent on the tip speed, different trends occur at high and low tip speeds and as shown at high tip speed (260 rpm, 758 ft/s) the level is for all practical purposes independent of thrust. The T^2 variation occurs over the normal rotor operating range for such a rotor and agrees with that usually associated with broadband noise [39, 40]. It is also of interest to note that the variation with thrust shows very similar trends to the results compiled by Widnall [42], but in this case a curve was used instead of the 'two law' approach of Figure 3.23. As mentioned previously it has been shown that data of the form shown in Figure 3.23 can be collapsed according to a $V^6\ tp^4$ relationship, where tp is the projected blade thickness based on the angle of attack at 0.9R, such that the standard deviation is 1.5 dB [25]. To date it has not been possible to link this with a physical mechanism and no attempt has been made to see if the model rotor data could be reduced according

to the same relationship. It is likely, however, that due to differences in the velocity dependency discussed in section 3.7.1 that a formula of the form $V^x tp^4$, where x is a function of the absolute velocity would have to be used.

3.8.4. Frequency Characteristics

Although the low frequency broadband noise 'peak' is normally associated with a Strouhal number relationship, it was not really possible to detect a 'peak' frequency on either the full scale or model results. There was, however, an indication of a 'hump' shape as illustrated in Figures 3.15 and 3.16. In an attempt to overcome this problem the 'break-point' frequency (defined in Figure 3.18) was determined and plotted as a function of rotor for both the model and full scale rotors as shown in Figures 3.24 and 3.25 respectively.

It is clear from the model rotor results that the break-point frequency, and by implication the 'peak' centre frequency, is a function of tip speed. On the model results (Figure 3.24) the continuous line represents the best straight line through the data points and the dotted line corresponds to a Strouhal type relationship of

$$f_{BP} = 0{\cdot}18 V_T / tp \qquad (3.1)$$

where V_T = the tip speed (ft/s) and tp = projected thickness (ft)

On the full scale rotor, however, the 'break-point frequency' near the rotor disc plane is for all practical purposes independent of the rotor speed (upper set of results in Figure 3.25). A plot of data measured at 75° to the rotor disc gives similar results, except at high thrust where the frequency appears vaguely to be a function of tip velocity as indicated by the lower set of results on Figure 3.25.

This variation from the expected Strouhal number relationship could be associated with errors in determining the break-point frequency and/or a significant change in the broadband spectrum with tip speed. Even if these aspects were taken into account, however, it appears that the full-scale rotor results would still not follow a Strouhal number relationship. Wilkes [43] also found that the broadband noise peak was insensitive to tip speed on a full scale rotor.

The conventional Strouhal relationship for the centre frequency, f_B, used for helicopters is

$$f_B = St.V_{0.7}/tp \qquad (3.2)$$

where St = Strouhal number - normally taken as 0.28, $V_{0.7}$ = velocity at 0.7 radius, tp = projected blade thickness = t Cos α + c Sin α, t = blade thickness, α = angle of attack and c = blade chord.

Alternatively this can be written as (approximately)

$f_B = 0.2\ V_T/tp$ where V_T is the tip speed. (3.3)

The value for α is taken at 0.7%R (where R is the rotor radius) by some investigators and at 0.9%R by others. In this context it is of interest to note that if such solutions were used for the full scale rotor, the predicted value for 'f_B' would lie in the majority of cases even above the measured 'break-point' frequency. When compared with $\frac{1}{3}$ octave band analysis of the full scale results, however, a relatively good agreement is obtained for the lower tip speed conditions, partly because of the upward shift in frequency associated with this type of analysis as discussed in section 3.8.1.

Goddard and Stuckey in their full scale rotor work [39] showed that the 'peak frequency' was given by:-

$f_B = 0.18\ V_T/0.4c = 0.45\ V_T/c$, (3.4)

where c = blade chord. This gives a value for the 'peak' frequency considerably lower than the conventional Strouhal relationship (equation (3.2)) with the difference being of the order of a factor of 2 to 3. Even so the predicted value appears to agree relatively well with full scale data (correct order for frequency range), while underestimating the value for the model rotor.

When 'hovering helicopter' data was examined, however, it was found that equation (3.3) gave relatively good agreement with the (apparent) centre frequency. This can be seen by reference to Figures 4.2 and 4.3 on which the frequency 'f_B' is marked (520 Hz). Also indicated on Figure 4.2 is the predicted value (750 Hz) for the model. This apparent difference between a full scale rotor (on a whirl tower/hover rig) and the same rotor on a 'hovering helicopter' cannot be explained and obviously requires further investigation when one bears in mind the results of Goddard and Stuckey [39] and Wilkes [43]. At the present time, however, it would appear that as a general rule for real helicopters equation (3.3) can be used.

Details on the spectrum shape are even more limited and since the 'analysis model' (Figure 3.18) did not give any low frequency dependency, it is necessary to make some approximation if the complete spectrum is to be considered. Goddard and Stuckey [39] suggested a $7\frac{1}{2}$ dB/octave 'fall-off' either side of a peak of a $\frac{1}{3}$ octave bandwidth. This is in general agreement with the high frequency 'fall-off' rates of 7/10 dB discussed in section 3.8.1. With this and the results from real helicopters taken into account it would appear at the present time that a

spectrum with a 'fall-off' of 8 dB/octave either side of 'peak' is a reasonable assumption. It is suggested that this could be applied from $f_B/2$ to $4f_B$ (where f_B is the peak frequency) and that the accuracy would be sufficient for most prediction purposes. A check with a number of helicopter 'hovering records' confirmed this approach although it is, as mentioned previously, difficult to determine the true spectral shape.

3.9. HIGH FREQUENCY BROADBAND NOISE

For the high frequency broadband noise study 20 Hz bandwidth analysis was used for the model rotor (Figure 3.15) and 100 Hz for the full scale rotor (Figure 3.16). In this context it is worth noting that when analyzing high frequency noise these filters are essentially narrowband filters.

From the traces illustrated in Figure 3.16 it is clear that there is a 'hump' of high frequency noise at 4 to 5 kHz on the full scale rotor. The prominence of this noise source is very dependent on tip speed and the angle relative to the rotor disc. This can be seen by comparing the results in Figure 3.2 and 3.16. Near the rotor disc plane (Figure 3.2) the 'hump' is practically non-existent at high speed, while at angles near the rotor axis (Figure 3.16) it can be detected at all test conditions.

On the model rotor results illustrated in Figures 3.1 and 3.15 the 'hump' or peak is not so well defined and only really exists at low speeds and small pitch angles. At other measurement angles to the rotor disc the 'hump' is, however, more predominant but again becomes insignificant as the pitch and/or tip speed is increased. On the model it has only been possible, therefore, to study the noise source in detail at low tip speeds. It is not clear from the results available if the 'hump' disappears or if other broadband energy in the region rises to a level above the 'hump' when the rotor conditions are changed.

It has not been possible to determine a velocity law on the model rotor, but as the pitch (θ) was increased the SPL increased according to $\theta^{1/2}$ which corresponds approximately to a $T^{3/8}$ law. This is illustrated in Figure 3.26. In the case of the full scale rotor it follows a V^4 law at constant thrust and $T^{-1/6}$ law at constant velocity as shown in Figures 3.27 and 3.28 respectively. Thus on both rotors the level of the high frequency broadband noise is for all practical purposes independent of thrust.

The full scale rotor shows that the frequency of the 'hump' is a function of tip speed (i.e. a Strouhal type relationship) as illustrated in Figure 3.29. This could not be studied in detail on the model but there was some indication of a similar trend. An attempt was made to scale the noise source between the two rotors but this failed. This is not surprising since, if the high frequency broadband noise source is due to some characteristic 'wake shedding' process, then it will be greatly influenced by the boundary layer/wake thickness and whether the flow is laminar or turbulent. From the model tests with blade tip shapes (see section 3.12) it was also clear that other high frequency broadband noise 'humps' can be present in the spectrum when the thickness of the blade trailing edge is increased. Lowson et al [44] also showed similar results on a model with 'cropped' tip shapes.

3.10 OVERALL NOISE

3.10.1. General Characteristics

As stated previously the overall noise (OASPL) generated by a rotor is a function of the three individual noise sources. On both model rotors and full scale rotors the high frequency broadband noise is generally relatively unimportant in terms of the overall noise level. This does not imply that it is also subjectively insignificant, but the overall noise is effectively controlled by the levels of rotational and low frequency broadband noise.

As can be seen from Figures 3.1 and 3.2 the rotational noise is higher in level relative to the broadband noise on a model rotor than on a full scale rotor. At angles near the rotor disc plane the broadband noise is significantly reduced (relative to the rotational noise) such that, even on a full scale rotor, the overall noise is essentially dependent on the level of the rotational noise. To obtain the desired tip speeds on a model rotor, the rotational frequencies are significantly higher (typically by a factor of 3 to 5) than on a full scale rotor. Thus the model rotor has a greater part of the spectrum dependent on the rotational noise than has the full scale rotor. The rotational noise also becomes more predominant as the number of blades and the physical size of the rotor are decreased and on some small model rotors the noise is effectively all rotational in character.

It follows, therefore, that on the full scale rotor the OASPL follows (for all practical purposes) the same trends as the low frequency broadband noise, except at angles very near to the rotor disc plane where

the rotational noise dominates. On the other hand the overall noise for a model rotor is linked essentially to the rotational noise characteristics or a combination of rotational and low frequency broadband noise.

3.10.2. Effect of Number of Blades

The effect of changing the number of blades was not studied to any great extent. A brief review was, however, made of the model rotor data and a typical set of results which illustrates the general trends is reproduced as Figures 3.30 and 3.31. These results show the OASPL values plotted as a function of tip speed (at 6° pitch) and pitch (at 600 rpm) respectively. As mentioned previously the OASPL is essentially a function of the rotational noise components except at very low speed when it is controlled by a combination of rotational and low frequency broadband noise. In a similar manner to that discussed previously in sections 3.7.2 and 3.8.2, it will be noted that the 'rate of increase' for all the rotor increases with the absolute speed, varying from approximately V^3 to V^{10}. As expected there was an increase in level with the number of blades, although the difference between 1 and 2 blades is relatively small. This can be seen in the cross plot against number of blades given in Figure 3.32.

In Figure 3.31 with the OASPL as a function of pitch it can be seen whereas on the 3 and 4 bladed rotors the noise decreased as the pitch was initially applied, in the case of the 1 blade rotor it increased. This is considered to be due to the fact that on the 4 bladed rotor the contribution from the broadband noise is higher than the rotational noise - and as mentioned previously this shows a decrease as pitch is varied from 0° to 2° - while in the case of the 1 blade rotor the reverse is true.

No attempt was made to correlate data on a thrust basis, but the 4 bladed rotor operating at 475 rpm/6° would produce the same order of lift as the 1 blade rotor running at 800 rpm/6°. These 'values' are indicated on Figure 3.30 and this suggests that the 4 bladed rotor would be 2.6 dB quieter than the 1 bladed rotor giving the same lift. The practical case would, however, be more complex since it is necessary to change other parameters as well as tip speed. It does, however, agree with the general concept that it is advantageous from the noise control point of view to use as many rotor blades as practical.

3.11. DIRECTIVITY

Very little direct measurements of the directivity characteristics have been made, largely because of the complications of making such measurements. Stainer [27] using the 51 inch (130 cm) diameter model rotor in an anechoic room obtained some rotational noise data for the author and a typical plot is reproduced in Figure 3.33. This shows a general 'figure of 8' appearance for the higher harmonic rotational noise and a reduction of sound in the rotor disc plane as predicted in reference (30). Similar analysis of the broadband noise was not possible due to the fact the noise generated on this rotor was dominated by rotational noise.

Some full scale results derived from the WHL full scale investigation are reproduced as Figures 3.34 and 3.35 for broadband noise and rotational noise respectively. For the high lift/high tip speed condition shown in Figure 3.24, the broadband noise is a minimum in the rotor disc and shows a 'dip' directly below the rotor. This dip of 5 dB, which checks confirm is not a function of any cancellation effects, is for all practical purposes independent of blade tip speed and occurs only at high blade loading 'thrust'. The dB(A) and OASPL levels follow the same general shape as the broadband noise except near the plane of the rotor disc, where the low frequency rotational noise dominates the sound (see Figure 3.35).

The rotational noise showed considerable variation in harmonic content with operating conditions and angle and the scatter about a mean was large. Thus directivity plots of individual harmonics failed to reveal any clear trend. To overcome this difficulty the measurements were averaged over successive bands of harmonics to give the results shown in Figure 3.35. The 'shape' of the harmonics gradually departs, with increasing frequency, from the directivity of the low frequency noise until the high harmonics (15th to 20th) take on a distribution very similar to the broadband noise. Again there is a 'dip' under the rotor at high thrust, but as with the broadband noise it disappears at lower thrust.

3.12. TIP SHAPE STUDY

3.12.1. Scope of Investigation

The use of special tip shapes to control the noise generated by rotors had been suggested by many investigators and Bell Helicopters [45], Sikorsky Aircraft [46] and the Boeing-Vertol Company [47] had all made claims of significant noise reductions by modification of the tip shape.

It was extremely difficult, however, from the available data to evaluate in detail the effectiveness of such methods since the tests conducted were usually of a comparative nature and the prevailing aerodynamic conditions before and after making tip modifications were not known. It was decided, therefore, to conduct a small pilot study to establish the magnitude of the changes associated with different 'tip shapes'.. It was originally intended that this would be a joint aerodynamic/acoustic study with aerodynamic aspects being carried out by an investigator in the University of Southampton Department of Aeronautics and Astronautics. Unfortunately the aerodynamic study was never completed and thus the acoustic aspects had to be considered in isolation. As a consequence there was no thrust measurement information which meant that it was only possible to correlate the data on a blade pitch, tip speed and power basis.

3.12.2. Test Rotor

The basic 9 ft diameter model was fitted with the range of tip shapes illustrated in Figure 3.36. In order to ensure that the available rotor blades were not damaged the tips were simply fitted to the existing rotor blades after removal of the standard tip cap. Each tip was 6 inches in length and hence the overall diameter of the rotor was increased to 10 ft.

The 'Sikorsky tip' was based on information given in reference (41) and in addition to being trapezoidal in shape it was later learnt that a '2° twist down' was associated with this tip. In these tests, however, only planform changes were considered.

3.12.3. Test/Analysis Programme

Noise levels were measured at a distance of 25 ft (2.5 rotor diameters) and at an angle of approximately 10° below the rotor disc plane.

Measurements were made over a range of rotor speeds 500 to 800 rpm, corresponding to tip speeds of 262 to 418 ft/s and of blade pitch angles from 0° to 10°. Information on the power absorbed by the various rotor was noted for each condition.

Analysis was made in terms of OASPL, dB(A) and $\frac{1}{3}$ octave bands supplemented by 1.5% bandwidth narrowband analysis - full details are given in reference (48).

3.12.4. Results

A selection of results are shown in the following figures:

Figure 3.37 : dB(A) vs rotor speed ~ pitch 6°;

Figure 3.38 : dB(A) vs blade pitch ~ rotor speed 700 rpm (366 ft/s);

Figure 3.39 : Power absorbed vs rotor speed ~ pitch 6°; and

Figure 3.40 : Power absorbed vs blade ~ rotor speed 700 rpm.

From these results, and other analyses, the general noise and power characteristics of each tip were determined and compared. From this it was possible to rank in order of descending 'noisiness' and 'power absorbed' the various tips tested as indicated in the lists given below. These lists and the corresponding comments must, of course, only be taken as a general guide to characteristics associated with each tip.

Noise

(i) 60° blunt trailing edge tip: noisy at all speed/pitch conditions, large rotational and broadband contributions; very dominant noise hump at high speed/pitch conditions in 2.5k-3.5k Hz frequency region,

(ii) 45° blunt trailing edge tip: noisy at all conditions; large rotational and broadband contributions.

(iii) Sikorsky tip: noisy at low pitch but quiet at high pitch; large rotational noise contribution at low pitch.

(iv) Standard tip: falls in middle of noise range at all conditions; low rotational noise content.

(v) 45° faired trailing edge tip/60° faired leading edge tip: both tips give similar noise levels; generally quiet at low pitch but noisy at high pitch.

(vi) 45° faired leading edge tip: fairly quiet at all conditions; low rotational noise contribution.

(vii) Square tip: noisy at zero pitch, but at 2° and above it was consistently the quietest tip, small broadband noise contribution over 100 Hz - 400 Hz frequency region.

Power (Data for 60° faired edge tip not available)

(i) 60° blunt trailing edge tip: absorbed the most power at all conditions.

(ii) 45° blunt trailing edge tip: absorbed less power than (i), but more power than all other tips at all conditions.

(iii) Sikorsky tip/45° faired trailing edge tip: both tips absorbed approximately the same power, the 45° tip with the faired trailing edge fell in the middle power range at most conditions, while the Sikorsky tip absorbed less power at low pitch.

(iv) Standard tip: lower end of power range for all conditions.

(v) Square tip/45° faired leading edge tip: at 2° pitch and above the square tip absorbed the least power of all tested, the 45° faired leading edge tip absorbed the least power at 0° and slightly more power than the square tip at high pitch.

It will be observed that to a first order there was a direct correlation between the noise generated and power absorbed. This is in agreement with the suggestion that in many cases the 'tip shape' development within the USA was aimed at improving the aerodynamics and that noise was simply an indirect benefit. The blunt trailing edge tips (as intuitively expected) consistently generated the highest noise and absorbed the most power, while both the square tip and the 45° faired leading edge tip were the quietest absorbing minimum power.

The square tip, as indicated above, was better both from the noise and power absorbed point of view than the standard tip. Similar trends have been found by Spirey and Morehouse [49] at low tip speeds, but at higher tip speeds corresponding to those on a real helicopter they found the reverse was true. Thus it is, most likely, unwise to read across the model noise results to a full scale rotor. Even so this study illustrated clearly that noise was dependent on the tip shape and that significant noise reductions should be possible. With regard to real helicopters it may not be possible to lower the noise level below a certain minimum, but at least it should be possible to ensure that unnecessary high levels are not produced. In this context it is of interest to note that the standard tip, which is fitted to a wide range of helicopters including the majority manufactured by WHL, was well down the list both as regards noise and power absorbed. An interesting exception to the general trend was the Sikorsky tip which was relatively noisy at low pitch, even though it absorbed less power than expected under these conditions.

3.13. Tandem Rotor Investigation

3.13.1. Test programme

A general investigation of the noise characteristics associated with a tandem rotor configuration was conducted using the rig described in section 2.3.2. The rig was located in the large anechoic chamber at ISVR which was designed to give free-field conditions down to a frequency of 70 Hz. Some preliminary calibration checks using the rotor rig and a loudspeaker as a 'source' confirmed this figure. Tests were conducted with 3 height (rotor) separations (0, 5" and 8"), 3 rotor overlap

settings (0, 31.5% and 51% based on rotor radius) and 3 rotor phase relationships (normal 60°, 45° and 30°). Recordings were taken for three rotational speeds, (23.33 rps, 26.66 rps and 30 rps corresponding to tip speeds of 311 ft/s, 356 ft/s and 400 ft/s) and four pitch settings (0, 4°, 8° and 12°).

In addition to the tests conducted with the tandem rotor configuration, measurements were made with only one rotor fitted (i.e. single rotor case). Noise measurements were taken with the aid of a rotating boom and thus, in addition to data at fixed positions, polar (directivity) plots were obtâined. All measurements were taken at 8.5 ft (2 rotor diameters) from the centre of the lower rotor.

3.13.2. Noise Characteristics

The noise characteristics of the tandem rotor were, as expected, very similar to that of the single rotor and because of the small size of the rotor (51 inch diameter) mainly rotational in character. A typical narrowband spectrum is presented in Figure 3.41 and is similar to the single rotor results presented in reference(27). The main difference on the tandem rotor was that rotor rotational harmonics (designated 1R, 2R etc.) were detected as well as the more usual blade passing harmonics 1B, 2B etc. where for the 3 blade rotor nB = 3nR, or in other words 1B = 3R, 2B = 6R etc. The levels of these rotor rotational harmonics were, however, well below the level of the blade passing harmonics (see Figure 3.41).

3.13.3. Results

3.13.3.1. Effect of rotor (height) separation

Figure 3.42 shows the effect of varying the rotor separation on the harmonic content and as can be seen the 'fall-off' is in the order of 4 dB/octave with the 'scatter' about the mean being $\pm$ 5 dB. This general decay rate was observed in all tests, irrespective of the rotor speed or blade pitch.

It will be observed from Figure 3.42 that with 5 inches (2.5 chords) separation the noise levels were on average 6 dB above the 'zero separation' case. This was as expected since the lower rotor was running in the downwash produced by the upper rotor and this would be more pronounced as the separation distance was increased from zero. Intuitively a further increase was expected as the separation was increased to 8 inches (4 chords) but as can be seen from Figure 3.42 the levels were 4 dB below the 'zero separation' results. Thus it would appear that the 'flow distortion' experienced by the lower rotor decreased. This is under-

standable since as the distance from the upper rotor is increased the flow will become more uniform and the area of interference decreased due to vena-contracta created by the flow through the upper disc. It follows, providing the overlap is not too great, that if the separation distance was increased even further the situation would be approached where the two rotors would act as two separate rotors and hence the noise would be akin to that associated to a single rotor.

3.13.3.2. Effect of blade overlap

The effect of varying the overlap is illustrated in Figure 3.43 which shows the generalized 'fall-off' curves obtained from the narrowband analyses for the three conditions evaluated. The 'fall-off' rate is again 4 dB/octave and the results apply to a '5 inch rotor separation'. It will be noted that, as expected, the rotational noise increased in level as the overlap, and hence area of flow interference, was increased.

3.13.3.3. Effect of the 'phase' between rotors

'Phase' in this context is defined as the azimuthal displacement between one rotor and another when viewed from above as illustrated in Figure 3.44. Tests were conducted at three settings; these showed that a reduction in angle from the normal 60° to 45° resulted in 3 dB increase in all harmonics and a further 2/3 dB as it was decreased to 30°. This increase was considered to be due to a strengthening of the interaction between the flow from the upper rotor and the lower blades.

3.13.3.4. Comparison of single and tandem rotor configurations

A typical set of results are reproduced in Figure 3.45 which shows results for the '8 inches separation' tandem rotor case (30 rps, 8° pitch, 31.4% overlap) and the corresponding single rotor result. It will be noted that the levels for the tandem rotor are typically 7/8 dB higher than those for the single rotor, even though the '8 inch separation' gives the lowest level of interaction noise as mentioned in section 3.13.3.1. The thrust of the tandem rotor would, however, be in the order of 1.5 times that of the single rotor. The reason for a factor of 1.5 rather than 2 is that the thrust is lost in the tandem rotor configuration when the lower rotor interacts with the downwash created by the upper rotor. It is difficult to take this into account, but a crude approximation suggests that the single rotor would generate a noise level as indicated by the 'dotted' line on Figure 3.45. Thus it follows that the tandem configuration would be in the order of 3/4 dB noisier than the corresponding single rotor.

The measured levels of the tandem rotor with zero separation and zero overlap are slightly above the corresponding single rotor levels. Making an allowance for the thrust difference, however, it is suggested that for all practical purposes the levels were identical. As the overlap was increased the level associated with the tandem rotor also indicated an increase and, taking into account the thrust difference, it was concluded that the tandem configuration was 2 dB noisier. It follows, therefore, that a tandem configuration is always louder than the corresponding single rotor when operating under identical thrust conditions. The differences were, however, extremely small particularly when the overlap was small and rotor separation large. It seems reasonable to assume therefore that on a real helicopter, when an allowance is made for the fact that on a single rotor helicopter a tail rotor has to be used to counteract the main rotor torque, the tandem configuration has obvious advantages from the noise point of view.

3.13.3.5. Directivity - polar elevation plots

Directivity plots of the type illustrated in Figure 3.33 for the single rotor were obtained for the tandem rotor; two typical sets of results are reproduced in Figure 3.46. These show that, like the single rotor results, the fundamental blade passing frequency exhibited a different shape from the higher harmonics. This was assumed to arise from the fact that the fundamental is controlled over certain angles by the steady forces on the blade, while the higher harmonics are dependent on the fluctuating forces. In the case of the single rotor results the fundamental agreed well with the Gutin prediction [38] over an angle of $\pm$ 45° while in the case of the tandem rotor it is more like $\pm$ 25°. Outside these ranges the fundamental is also controlled by the fluctuating forces and the difference between the two rotors is associated with the fact that on the tandem rotor the fluctuating forces, relative to the steady forces, are higher. On the single rotor (Figure 3.33) there was a clear indication of 'dip' in the rotor disc plane but in the case of the tandem rotor these local 'dips' were either missing or greatly reduced. The main difference, however, was in the overall shape; on the single rotor they tended for all conditions to be symmetrical within $\pm$ 2 dB about the rotor axis (shaft) while in the tandem rotor the directivity patterns showed large differences (up to 10 dB) from side to side (see Figure 3.46). These effects varied considerably with conditions and are most likely due to cancellation effects between the two rotors. These effects could not, however, be explained since the directivity patterns appear to display a random preference for direction.

3.14. INFLUENCE OF INFLOW DISTORTIONS

The initial blade slap study [1] had shown that a sharp gust had a major effect on the higher harmonic rotational noise and it was considered of interest to determine the influence of a general flow disturbance. At the same time there was from the study of helicopter noise a need to determine the impact of wind and re-circulation effects on rotor noise. A simple experiment was conducted in which air from a 15 inch diameter fan was blown across the ISVR 9 ft diameter model. No attempt was made to quantify the magnitude of the 'wind' which covered approximately $\frac{1}{3}$ of the rotor disc area, but its direction was chosen such that it appeared to have the maximum influence on the noise generated. Measurements were made at a relatively close distance of 9 ft (1 rotor diameter) at 45° to the rotor disc, with the rotor pitch at 10° to give as high as possible 'steady forces'. The results are summarized in Figure 3.41 which shows the influence on the first 10 harmonics for two rotor speeds. As can be seen there was a marked increase in the level of the higher harmonics, and, of more interest in this study, in the level of the 2nd and 3rd harmonics. In the mid-frequency range the increase was up to 25 dB and overall the results agreed well with the findings of Hicks and Hubbard [50] which showed that measurements taken on propellers in a 20 mph wind were up to 15 dB higher than those obtained on 'low wind' days. There did not appear to be any significant increase in the level of the broadband noise, but this could not be studied in detail because of the 'wind noise' from the fan. These results confirmed the importance of wind when studying helicopter noise and in particular the sensitivity of rotational noise to changes of inflow conditions. This aspect was later investigated, to some extent, in connection with the blade/gust interaction study reported in Chapter 7.

3.15. THEORETICAL CONSIDERATIONS

3.15.1. Rotational Noise

It was clear from the initial 'blade slap' investigation [1] that lift fluctuations were important from the point of view of the generation of noise and that small disturbances could result in a marked increase in rotational noise. A theoretical study was, therefore, commenced by Tanna and Wright in parallel with author's experimental study. Prior to these studies, and similar studies in the States by Ollerhead and Lowson [30], Schlegel *et al* [41], Loewy and Sutton [51] etc., rotational theories were essentially limited to those based on the work of Gutin [38] which took into account only the steady lift and drag

(torque) forces. Thickness noise components had, however, been included by a number of investigators including Noad [52] who had developed a programme for calculating helicopter rotor noise based on the steady thrust, drag and thickness forces: this was based on work conducted at the RAE on propeller noise [53, 54]. With the development of the theories based on fluctuating forces (lift and drag) the thickness effect was ignored. Recently there has been a renewed interest in thickness effects [55, 56] and it is of interest to note that these theories are essentially the same as the thickness component used by Noad in the early 1960's. It is also worth noting that although the theories developed by Wright [31], Ollerhead and Lowson [30], etc., consider both spanwise and chordwise loading effect, the fundamental fluctuating lift relationship is the same as that outlined in connection with the prediction of noise from blade slap and blade/gust interaction detailed in Chapters 5 and 6 of this thesis.

Although the significance of fluctuating forces on rotors has been established it is not possible to compare precise theoretical predictions for a real rotor (or helicopter) with experimental results or use the theories in the design stage because the detailed aerodynamic information required cannot be predicted. There is also still some disagreement on the relative importance of spanwise and chordwise pressure fluctuations. Schlegel et al [41] have stated that chord and span variations in lift are important while other investigators [28, 30] have implied that this is of secondary importance. Tanna [57] suggested that both aspects must be considered and Wright [31] has now also taken up this view. Intuitively it would be expected that both spanwise and chordwise fluctuations are significant. It also seems reasonable to assume the latter is more important since rapid chordwise pressure fluctuations are easy to visualize, while lift (pressure) changes along the span of the blade would most likely be of a magnitude slower.

The theories are complex and are, therefore, difficult to summarize in terms of a real rotor or helicopter. Wright in reference [31] has attempted this but it is not clear if the trends he has suggested occur in practice. A number of points are, however, of particular interest. To predict m noise harmonics on a B bladed rotor operating at tip Mach number M, it is necessary to know at least (1 + M) mB blade loading harmonics. Thus to predict 30 rotational noise components on a four bladed rotor operating with a tip speed of 650 ft/s (200 m/s)

190 blade loading harmonics are required. This is impossible and will be for many years - if not for always. It also raises the important question of the physical measuring of such very high harmonic lift fluctuations.

The relationship between the sound and blade loading is also complicated but the 'point loading' solution can be used as a general guide, that is,

$$SPL(mB) \propto (1-K)\ 20 \log mB, \qquad (3.1)$$

where K is the inverse power law associated with the blade loading. Thus if K is zero (flat blade load spectrum) the noise will increase with frequency at a rate corresponding to 6 dB/octave. Ollerhead and Lowson [30] stated that this type of solution is applicable to the real helicopter, while Wright [31] indicated that span and chord distribution of loading on a large rotor is of considerable assistance in reducing the high frequency sound radiation particularly at angles away from the rotor axis. Wright suggested originally that this additional attenuation was, for typical helicopter rotors, equivalent to 6 dB/octave in the mB range 10 to 100. Thus a flat blade loading spectrum, on a four blade rotor would give a flat noise spectrum, above the second blade passing harmonic. Recently Wright [31] has re-assessed these aspects and concludes that up to 9 dB/octave is accounted for by the distributive loading effects across the blade chord.

3.15.2. Broadband Noise

The generation of broadband noise is normally taken to be due to the unsteady random fluctuating forces exerted by the blades on the air during vortex shedding from the trailing edges. From fundamental consideration in reference(58) it has been shown that the intensity I was dependent upon the following:-

$$I = k.(Re)^{-0.4}.S.V_T^{\,6}. \qquad (3.2)$$

where Re = Reynolds number (based on tip speed), V_T = tip speed and S = blade area. Yudin [59] stated that, providing the Reynolds number was high enough to ensure that the flow had a fixed 'breakaway' (fixed rear separation point), the sound power (W) was given by an expression which took the form:-

$$W = k.C_D^{\,2}.S.V^6. \qquad (3.3)$$

where C_D = blade profile drag coefficient, S = blade area, V = typical blade velocity and k = constant. This work of Yudin was subsequently used by Hubbard [60] for the derivation of a formula for the prediction

of 'vortex noise' on a propeller. From test data [61] Hubbard obtained the constant of proportionality and derived the following relationship:-

$$I = 10 \log_{10} \left[k A_B (V_{0.7})^6 / 10^{-16} \right] \quad (3.4)$$

where $V_{0.7}$ = blade velocity at 70% radius, k = constant (3.8×10^{-27} for propellers tested) and A_B = effective blade area, the effective blade being defined as:-

$$A_B = 2T/\rho \, C_L (V_{0.7})^2 \quad (3.5)$$

where T = total rotor thrust and C_L = blade lift coefficient.

Schlegel et al [41] later used Hubbard's solution as the base for developing a formula for helicopter rotors. To account for differences they added a 20 log $C_L/0.4$ since 0.4 was the coefficient of lift used by Hubbard in deriving his basic equation (equation 3.4), Schlegel also replaced A_B by the actual blade area S and derived a new value for the constant k from test data. This resulted in a formula of the form:-

$$SPL = 10 \log \left[k^1 S (V_{0.7})^6 / 10^{-16} \right] + 20 \log \left[C_L / 0.4 \right] \quad (3.6)$$

which was re-written in more general terms as

$$SPL = 10 \log \left[k^{11} (V_{0.7})^2 . T^2 / S \right], \quad (3.7)$$

where k^{11} = constant.

Davidson and Hargest [40] also used the work of Yudin as the basis for developing a formula for predicting broadband noise. They argued that use of the C_D^2 term (in equation 3.3) was doubtful and replaced it with C_L^2, partly as a result of work by Goddard and Stuckey [39] which had indicated that the SPL varied very closely with C_L^2. Their solution therefore took the form:

$$SPL = 10 \log k . V_T^6 . C_{LT}^2 . S \quad (3.8)$$

where V_T = tip speed, C_{LT} = a tip speed referred lift coefficient = $T/\frac{1}{2}\rho V_T^2 S$ and S = total blade plan area.

This formula can be re-written as

$$SPL = 10 \log \left[k . T^2 V_T^2 / S \right] \quad (3.9)$$

Goddard and Stuckey [39] stated that they based the analysis on the work of Yudin and private communications from Professor Lilley (University of Southampton). From these considerations they assumed that the parameters appropriate to broadband noise were blade velocity

(V_T) and a blade tip referred lift coefficient (C_{LT}). They then showed (contrary to the statement given in reference (40)) that the broadband (vortex) noise was given by an expression of the form

$$SPL = 10 \log\left[k.V_T^{2}.C_L^{1.66}\right] \qquad (3.10)$$

and this was reduced to $SPL = 10 \log\left[k.T_B^{1.66}.V_T^{2.68}\right]$ (3.11)

where T_B = thrust per blade. The full derivation of the formula developed by Hubbard, Schlegel et al, Davidson and Hargest, and Goddard and Stuckey is discussed in section 4.8.3 and outlined in more detail in Appendix 3.

3.15.3. Comparison with Experimental Results

As can be seen from the selection of results presented in this chapter the position relating to rotational noise is still far from clear and even if it is accepted that the noise is a direct result of the fluctuating forces it is difficult to understand the difference between the full scale and model results. This is likely to be due to the sensitivity of rotational noise, particularly the higher harmonics, to the input flow conditions/test environment. Intuitively it was expected that the fluctuating loads, under controlled test conditions, would have been to some extent (at least on one rotor) dependent on the steady thrust and torque conditions of the rotor. This is obviously not the case and thus it would seem prudent to ask if there is another mechanism at the lower tip speeds in addition to 'fluctuating lift' involved in the generation of discrete rotor noise. To date it is impossible to answer this question although the theoretical developments of Ollerhead and Lowson [30], Wright [31] and Wright and Tanna [29] can all be used to explain, by applying various arbitrary blade loading spectra, the general trends observed. It is, however, difficult to use these theories to explain the velocity dependencies observed. It seems fair to conclude, therefore, that although there is now a good understanding of fluctuating force rotational noise, there is still a number of points which need clarification before the development reaches a satisfactory stage from the designer/user point of view. Also the importance, or otherwise, of thickness effects on low and moderate tip speed rotors needs to be positively established.

The position relating to broadband noise is also far from clear and there is still considerable doubt on the controlling parameters, although it does appear that a V_T^6 dependency is realistic. It is interesting to note, however, that whereas the original solutions

(equations 3.2 and 3.3) contain blade area and velocity terms the C_L and/or Thrust (T) dependencies have been introduced by investigators largely on an intuitive basis. Yudin's formula (equation 3.3) contains a C_D^2 term while the solution derived from reference(58)has only a Reynolds number dependency. It would appear that these original solutions are more in keeping with the experimental data, since as explained in section 3.8.3 the low frequency broadband noise appears to correlate well with a thickness term which by implication could equally be interpreted in the form of profile drag. Over the normal operating ranges of most rotors the noise would, however, still be expected to be dependent on the thrust even if the basic term was considered to be drag dependent. This is because the total drag at such conditions is dominated by the 'lift drag' or induced drag term which is a function of the absolute lift (thrust) generated by the rotor. It does appear, however, that as in the case of rotational noise, further understanding is required before a satisfactory solution is obtained.

3.16. CONCLUSIONS

1. Rotor noise can be considered to consist of three sources - rotational (discrete frequency) noise, low frequency broadband noise and high frequency broadband noise.
2. On a model rotor 20 rotational noise harmonics can normally be detected, while on a full scale rotor up to 50 harmonics can often be seen on narrowband analysis.
3. Scale effects result in the level of rotational noise on a model rotor being higher, relative to the low frequency broadband noise, than on a full scale rotor.
4. The high frequency broadband 'hump' can be clearly observed on full scale results - on model results the 'hump' is far less clear and often not detectable.
5. The rotational noise content increases rapidly with tip speed and at the high speeds the 'discrete frequencies' are more well defined than at low speed.
6. Rotational noise for a wide range of rotors operating with lift appears to follow a V^{10} law, although there is normally an indication of a more rapid increase at the higher test speeds and a lower value at low tip speed. Variations from V^3 to V^{18} were observed.
7. On a lightly loaded model rotor the higher harmonics appear independent of tip speed.

8. On a full scale rotor all harmonics follow similar trends with increases in tip speed and thrust.
9. The fundamental for the full scale single (1) bladed rotor followed closely the Gutin value, while in the case of a similar three bladed rotor there was not real agreement except at high lift/high speed.
10. The model and full scale rotors show very different trends as blade pitch and/or thrust is varied. On the model the higher harmonics show a marked increase with pitch, while in the case of the full scale rotor they are independent of thrust except at low speed when they vary approximately as T^2.
11. The rotational noise trends observed appear to be a function of absolute tip speed, since the high speed model rotor results (470 ft/s) show similar characteristics to the low speed full scale tests which were conducted at similar speeds.
12. Recent analysis of the full scale rotational noise results suggest that the noise is a function of tp^4 where tp is the projected blade thickness (based on α, angle of attack, at 0.9R). The model results have not been examined in this manner.
13. The 'hump' characteristics (and its frequency) traditionally associated with the low frequency broadband noise appears to be a direct result of the $\frac{1}{3}$ octave band analysis used originally.
14. An 'analysis model' has been developed for the broadband noise - this has a 'Flat SPL' and high frequency 'fall-off'. The low frequency characteristics could not be established.
15. On the model rotor the low frequency broadband noise varies typically as V^4 to V^6 and on a full scale rotor as V^6 to V^8. Detailed studies suggest that the dependency varies with the absolute tip speed varying from V^2 at low (model rotor) tip speed to V^{12} at the high (full scale rotor) tip speeds.
16. Values for low frequency broadband noise (approximately proportional to V^6) are considerably different from those of the V^2 proportionality proposed by other investigators.
17. Broadband noise varies as T^2 on the model rotor and on the full scale rotor at the lower tip speeds while at high tip speed the full scale rotor results show a slight decrease in level with increasing thrust.
18. Further analysis of the full scale results indicates that the broadband noise varies as $V^6 tp^4$ where tp is the projected blade thickness (based on α, angle of attack at 0.9R). Similar correlation has not been attempted on the model rotor results.

19. On the model rotor the frequency associated with broadband noise correlates with a Strouhal type relationship - there is no such agreement on the full scale rotor.
20. The Strouhal formula traditionally applied to calculate the centre frequency of the broadband noise 'over predicts' for a full scale rotor - it gives, however, relatively good correlation with the (false) $\frac{1}{3}$ octave band spectrum.
21. High frequency broadband noise is practically independent of thrust and from the full scale tests appears to vary as V^4. The 'frequency' on the full scale rotor is a function of rotor tip speed (a Strouhal type relationship) - it could not be studied on the model rotor.
22. Overall noise on the model rotor follows the rotational noise characteristics and on the full scale rotor is essentially a function of the broadband noise. Rotational noise becomes more predominant at high speed.
23. Broadband and high harmonic rotational noise exhibits typically a 'figure of 8' directivity with a minimum in the rotor disc plane. The fundamental, and in the case of the full scale rotor the lower harmonics, show a maximum in the rotor disc plane.
24. Tip shapes have dramatic effect on the noise generated by a rotor - the 'standard tip' is relatively quiet. The 'square tip' was the quietest tested and absorbed the lowest power. The maximum test tip speed was 418 ft/s and available evidence suggested the observed trends may be different at high tip speeds.
25. On a tandem rotor configuration noise is increased by the blade overlap, reduction in the 'phase' between the rotors and by the initial increase in rotor separation. At large separations (if the overlap is small) the two rotors act as 'separate' rotors and the noise approaches that for two single rotors.
26. The tandem rotor configuration is generally noisier (by a few dB) than the single rotor for equivalent thrust rating.
27. If the rotor blade overlap is small and the rotor (height) separation large then a tandem rotor configuration acts as two single rotors. Taking into account the noise contribution from a tail rotor on a single (main) rotor helicopter it is concluded that a tandem configuration would be quieter than the equivalent single rotor helicopter.
28. Wind effects can cause a dramatic increase in rotational noise, affecting even the low rotational noise harmonics (3rd).

29. Rotational noise and broadband noise theories currently available do not correlate particularly well with the observed noise results. Although tip speed is obviously an important parameter, blade thrust does not appear to have as marked an effect on the level of the noise generated as theories would suggest.

TABLE 3.1: ISVR MODEL ROTOR

(a) Blade parameters

Number of blades (B):	3
Radius (R):	4·5 ft
Chord (c):	4 in
Area (BcR):	4·5 ft²
Section:	NACA 0012
Twist:	0

(b) Test conditions

Rotor speed (rev/min)	Tip speed (V_T) (ft/s)	Pitch angle (θ) (degrees)					
		0	2	4	6	8	10
		Estimated total thrust (lb)					
500	236	0	4·76	11·7	20·22	29·43	39·15
600	283	0	6·84	16·3	29·22	42·45	56·43
700	330	0	9·4	22·9	39·5	—	—
800	377	0	12·15	29·79	51·6	—	—
900	424	0	15·42	37·8	65·4	—	—
C_{LT} value		0	0·016	0·039	0·068	0·098	0·131

Reynolds number range: 0·503 to 0·904 × 10^6.

(c) Measurement position

Microphone at 9° below the disc and 25 ft radius

TABLE 3.2: S55 FULL SCALE ROTOR

(a) Blade parameters

Number of blades (B):	2
Radius (R):	27·85 ft
Chord (c):	16·4 in
Area (BcR):	76·2 ft²
Section:	NACA 0012
Twist:	8°

(b) Test conditions

Rotor speed (rev/min)	Tip speed (V_T) (ft/s)	Total thrust (T) (lb)										
		0	700	875	1125	1450	1850	2375	3050	3900	5000	
140	408	0	0·046		0·075	0·096	0·123					
160	466	0	0·036	0·045	0·057	0·074	0·094	0·121	0·155	0·20		
180	525	0	0·028		0·047		0·077	0·095	0·126			C_{LT} values
205	598	0	0·022	0·027	0·035	0·045	0·057	0·074	0·094	0·121	0·154	
230	670	0	0·017		0·028		0·046		0·075	0·096	0·123	
260	758	0	0·014	0·017	0·022	0·028	0·036	0·046	0·059	0·075	0·096	

Reynolds number range: 3·57 to 6·62 × 10^6.

(c) Measurement position

Microphone at F7 (11·5° below disc) at 250 ft radius

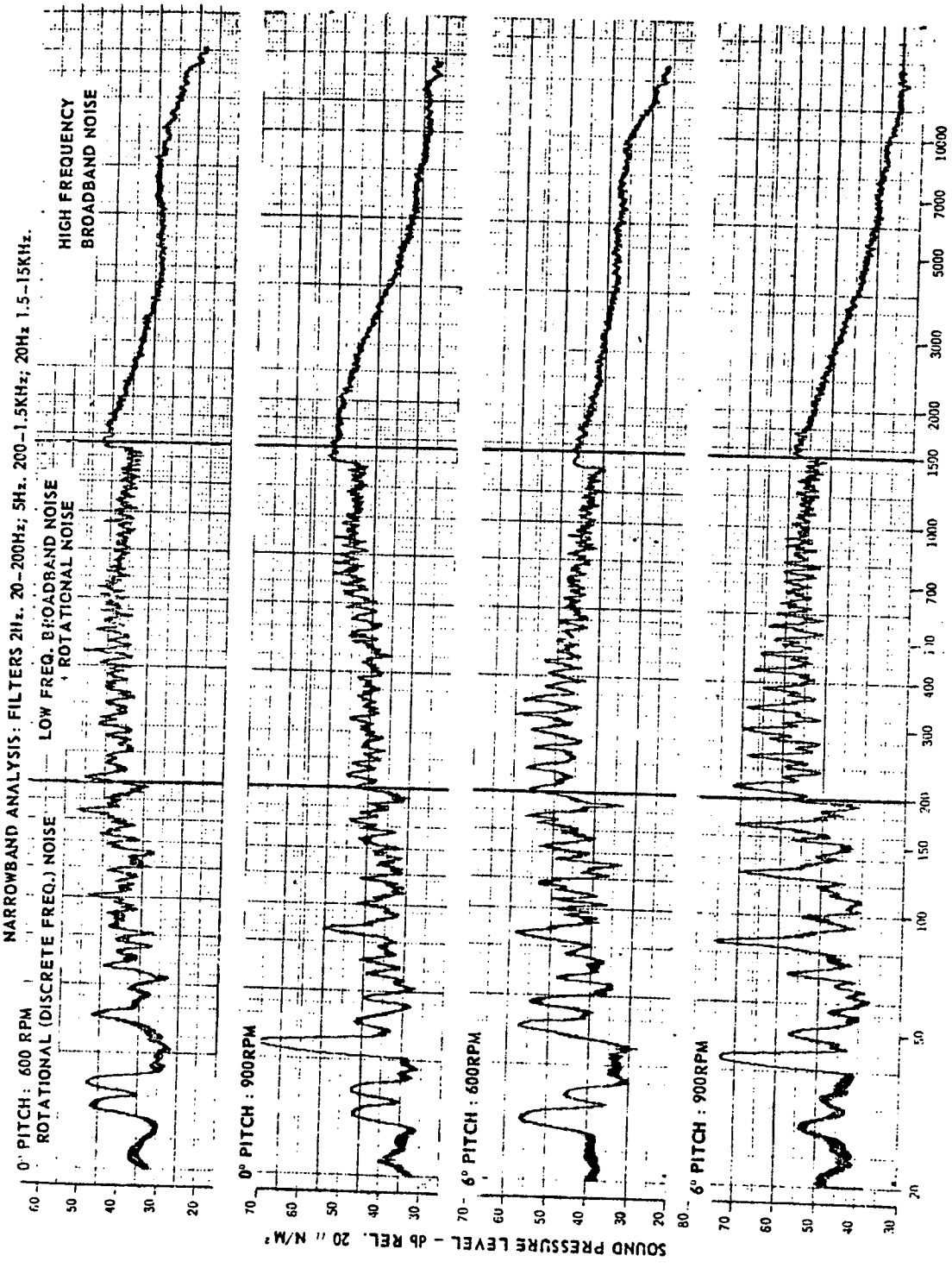

FIGURE 3.1 ROTOR NOISE SPECTRA - MODEL ROTOR

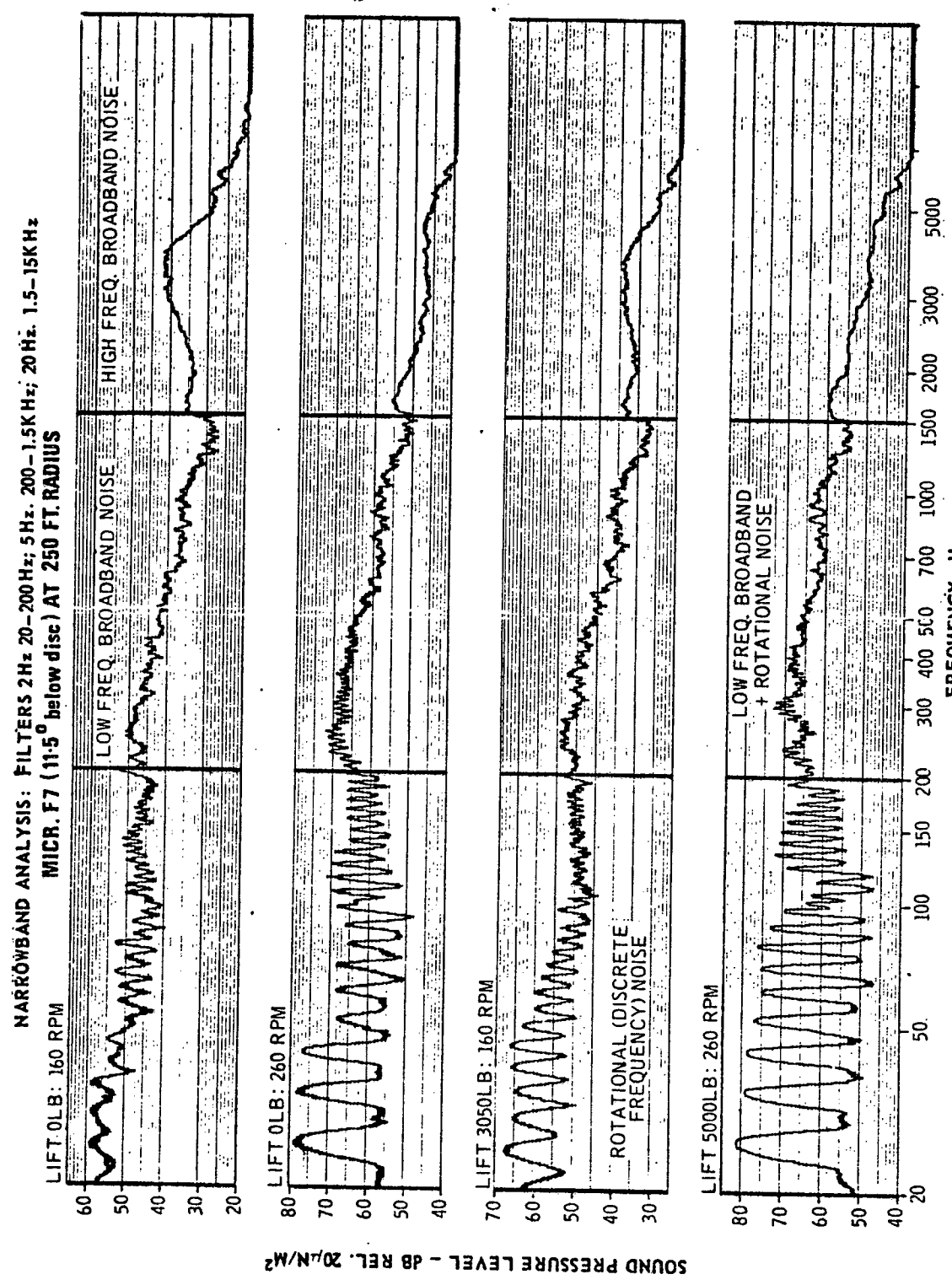

FIGURE 3.2 ROTOR NOISE SPECTRA - FULL SCALE ROTOR

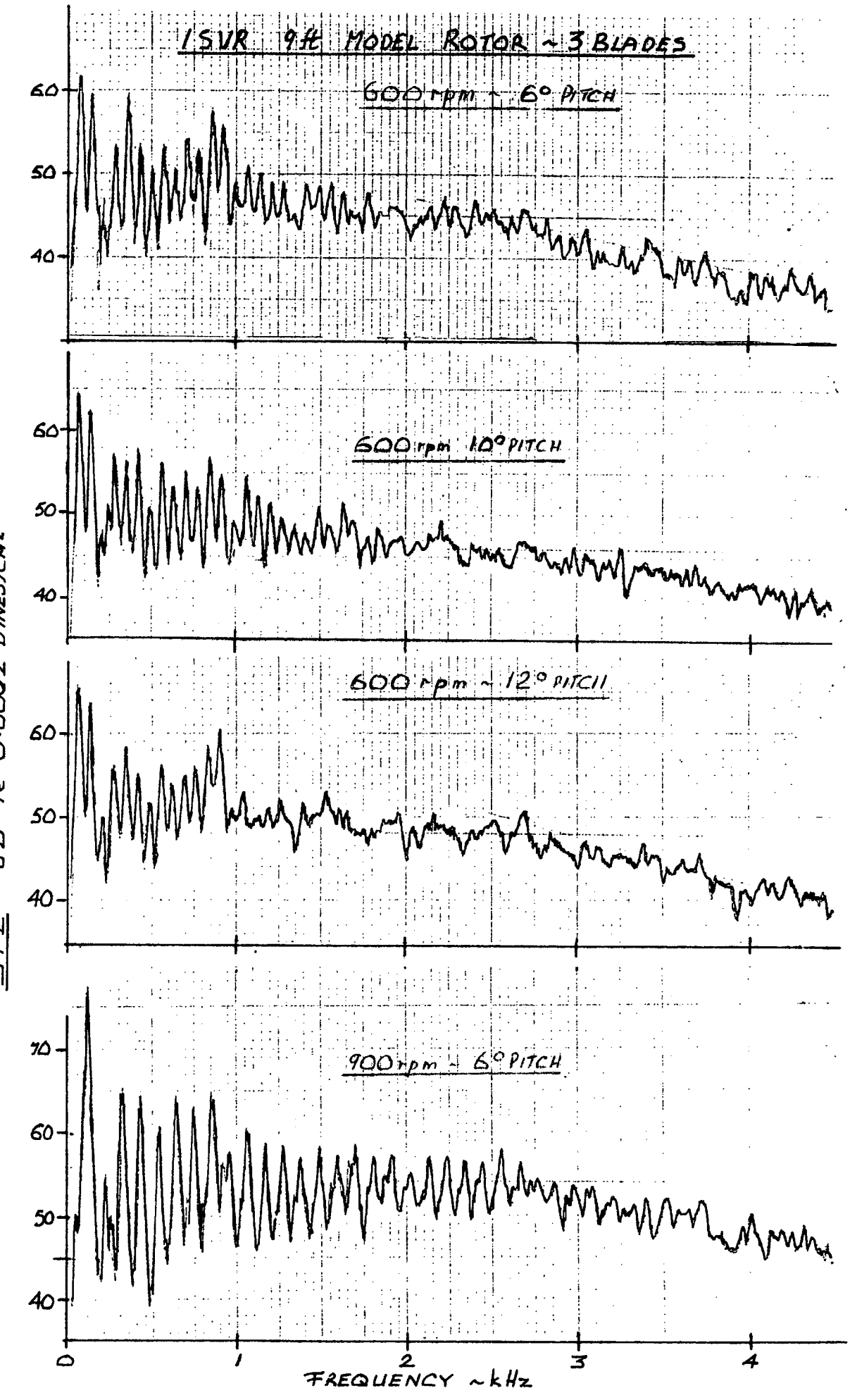

FIGURE 3.3 NARROWBAND ANALYSIS (3 Hz) - MODEL ROTOR

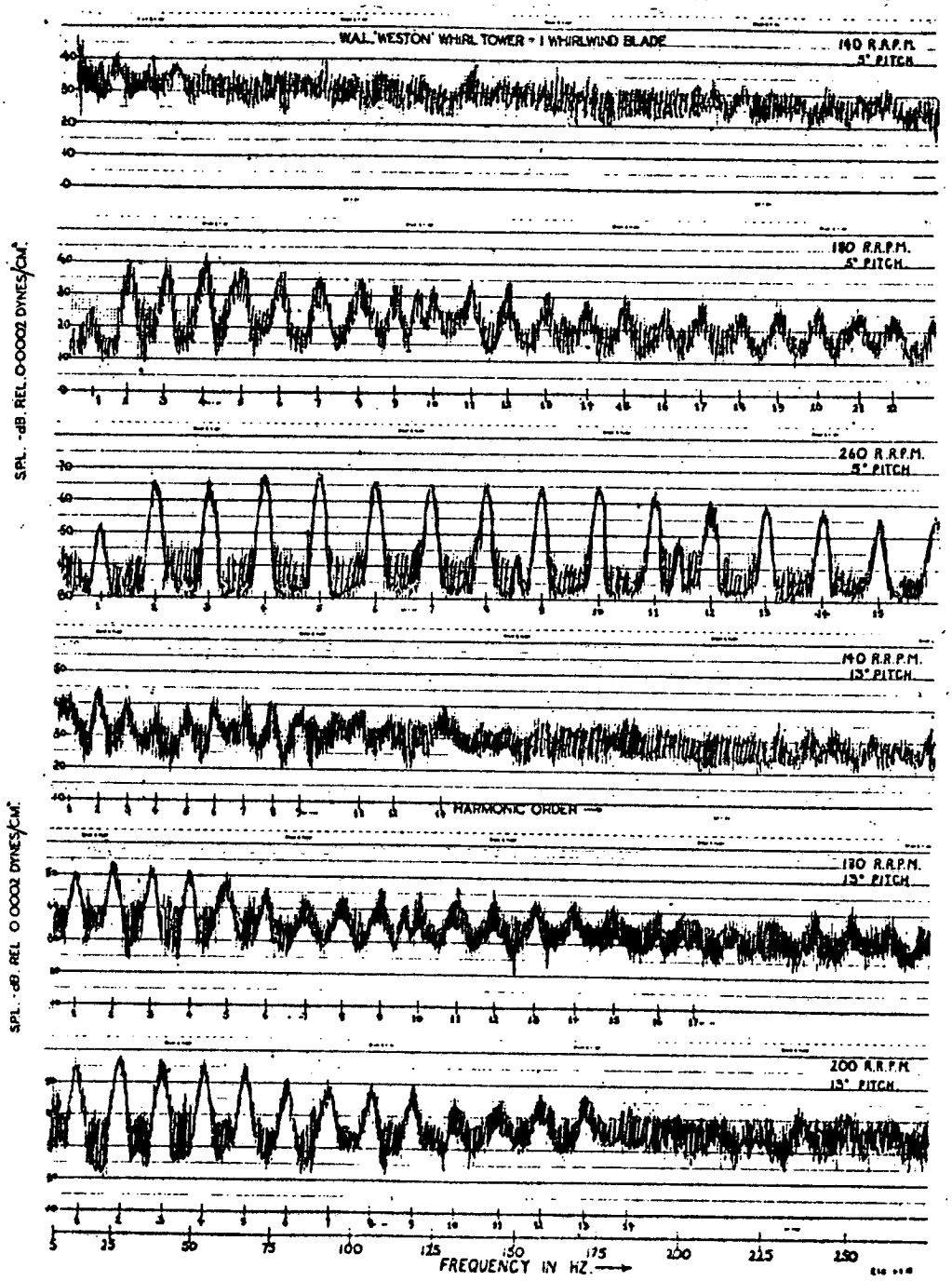

FIGURE 3.4 NARROWBAND ANALYSIS (2 Hz) - FULL SCALE ROTOR

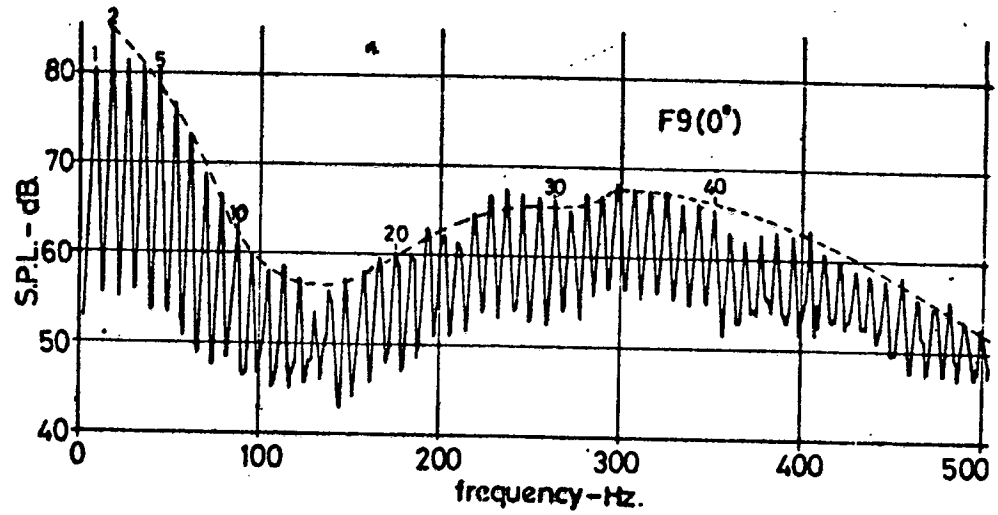

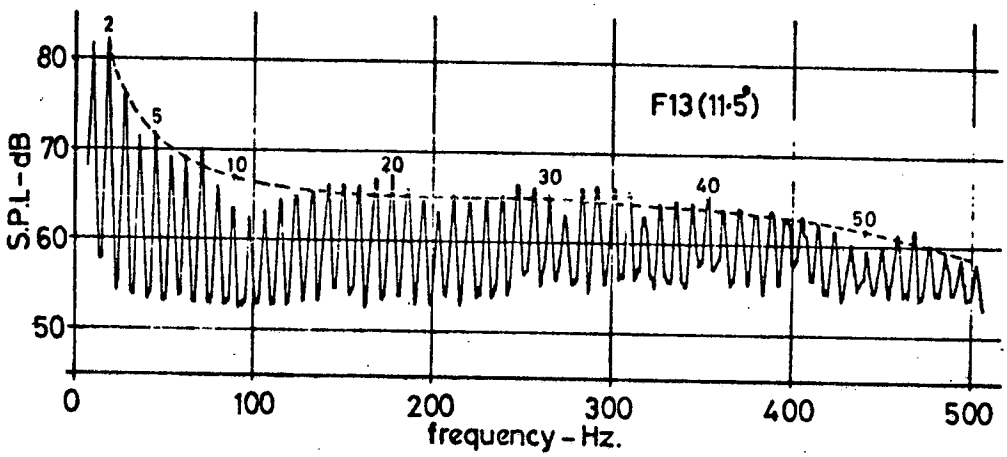

2 BLADED 555 ROTOR

MIC. 250 ft ≙ 5 DIA.

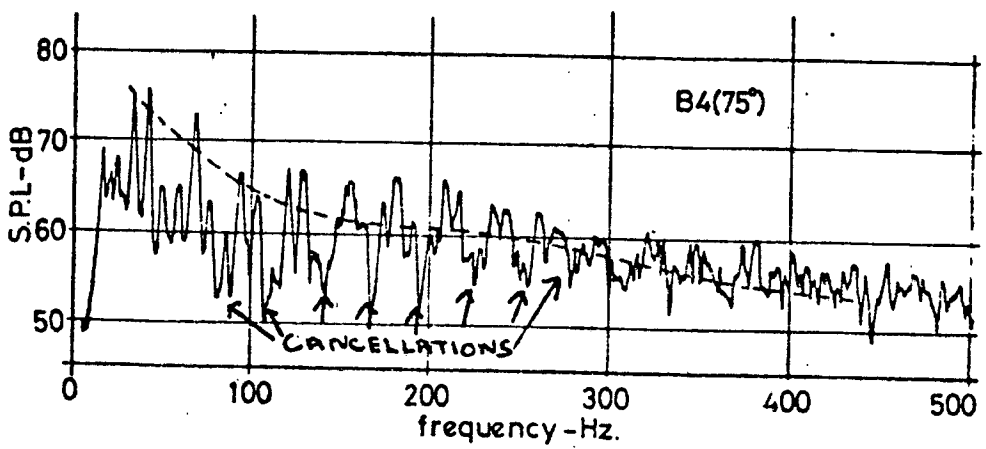

OLBS - 260RPM (758ft/sec)
Analysis Bandwidth = 1.5Hz.

FIGURE 3.5 NARROWBAND ANALYSIS - FULL SCALE ROTOR

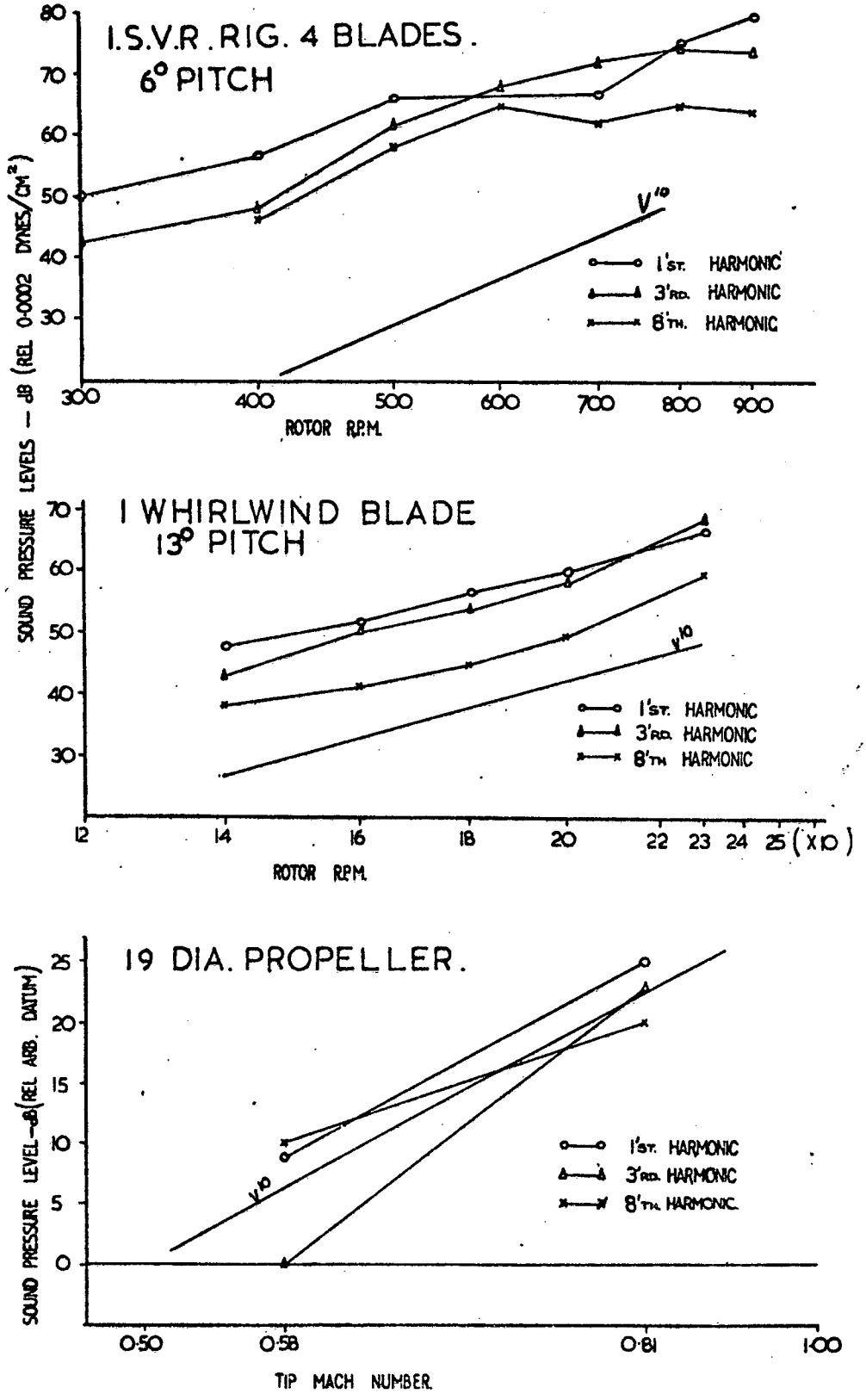

FIGURE 3.6 ROTATIONAL NOISE: SPL vs ROTOR SPEED

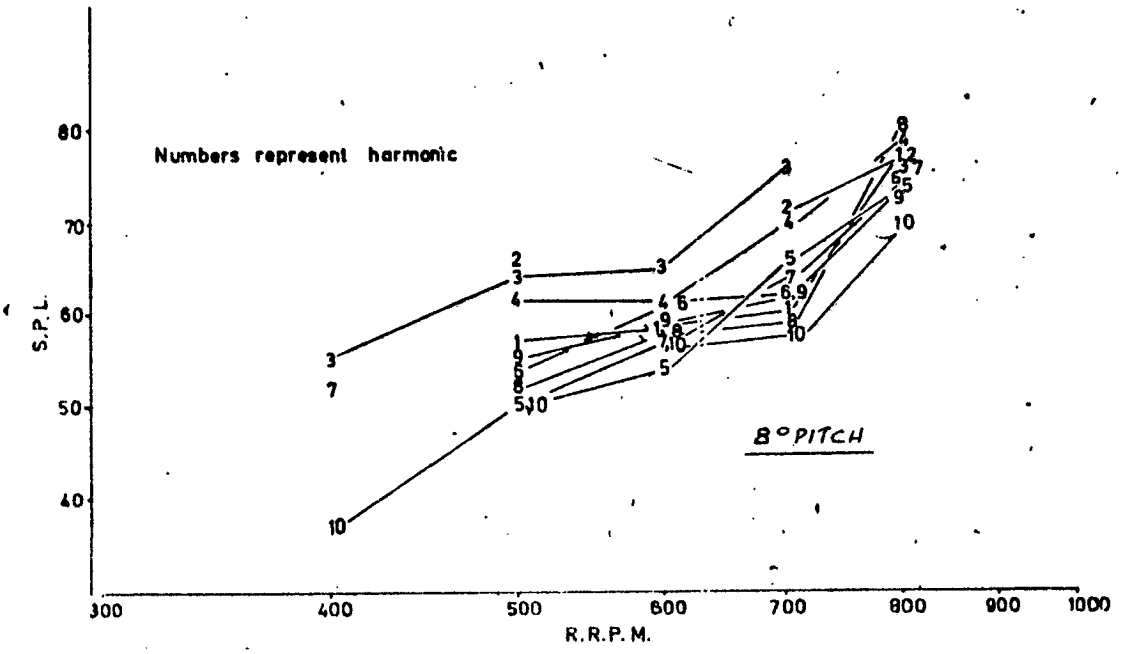

FIGURE 3.7 ROTATIONAL NOISE: SPL vs ROTOR SPEED - MODEL ROTOR (8° PITCH)

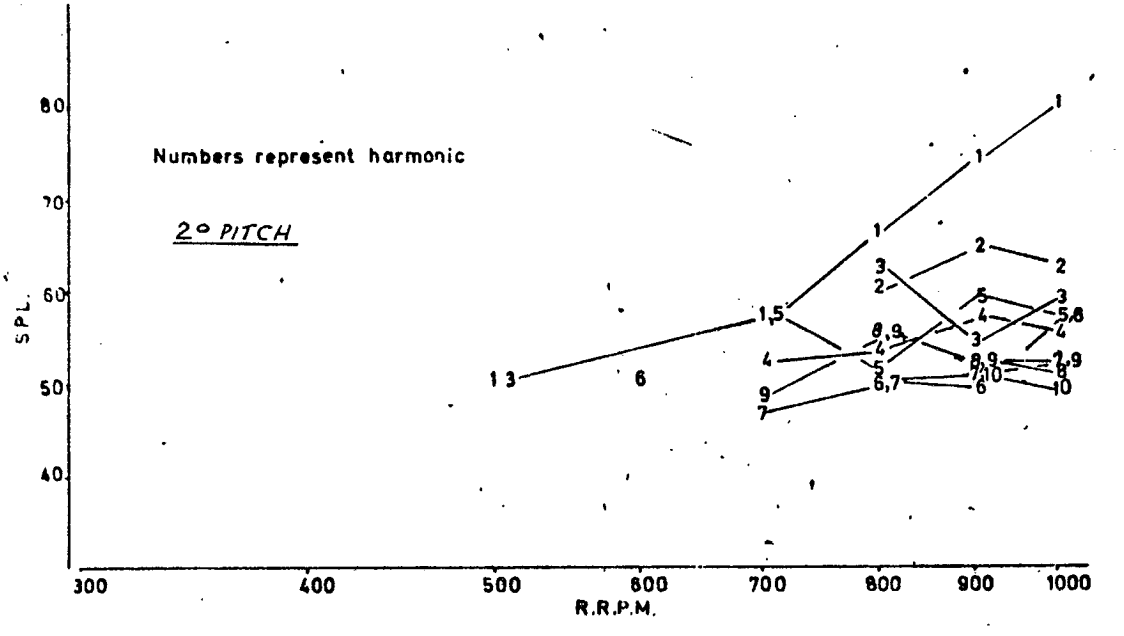

FIGURE 3.8 ROTATIONAL NOISE: SPL vs ROTOR SPEED - MODEL ROTOR (2°PITCH)

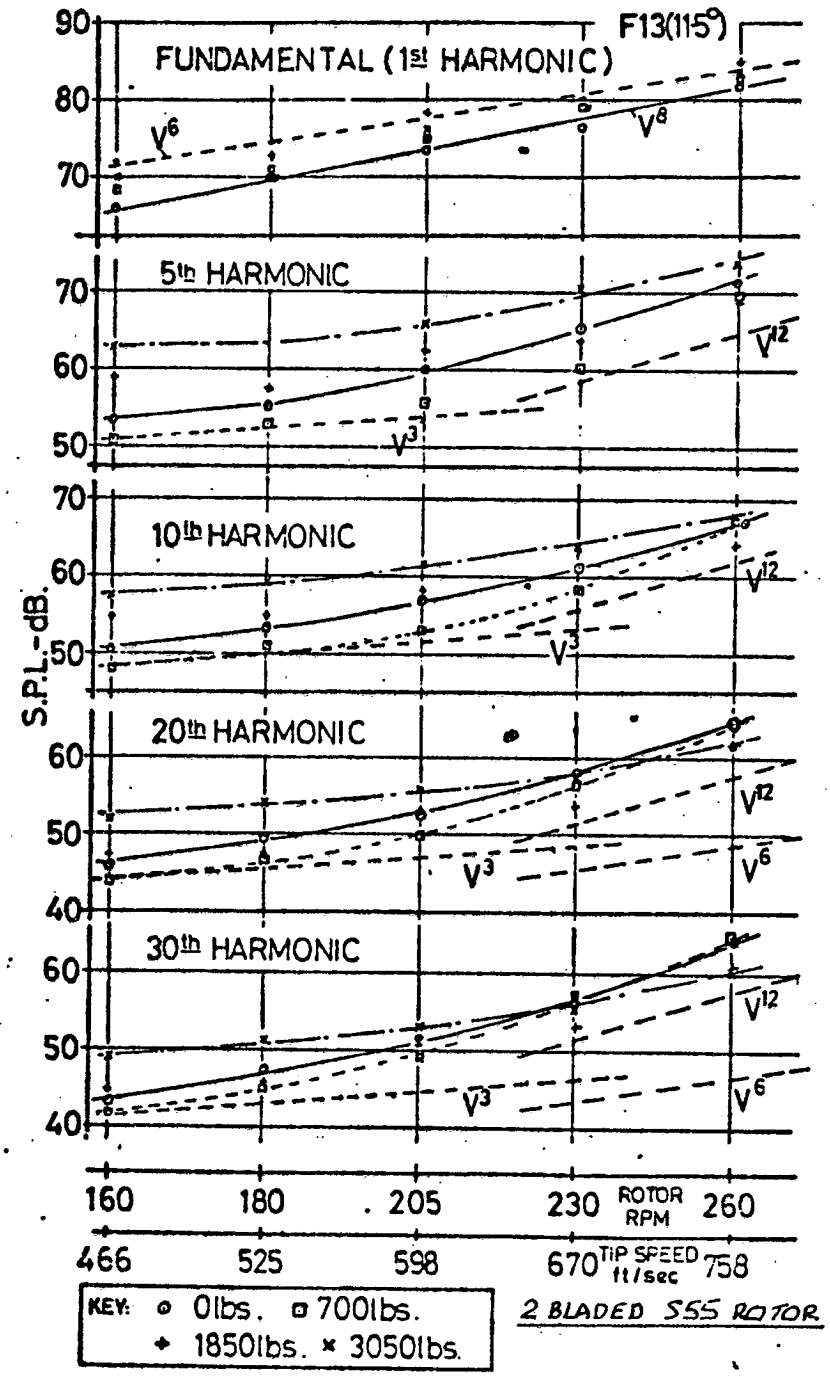

FIGURE 3.9 ROTATIONAL NOISE: SPL vs ROTOR SPEED - FULL SCALE ROTOR

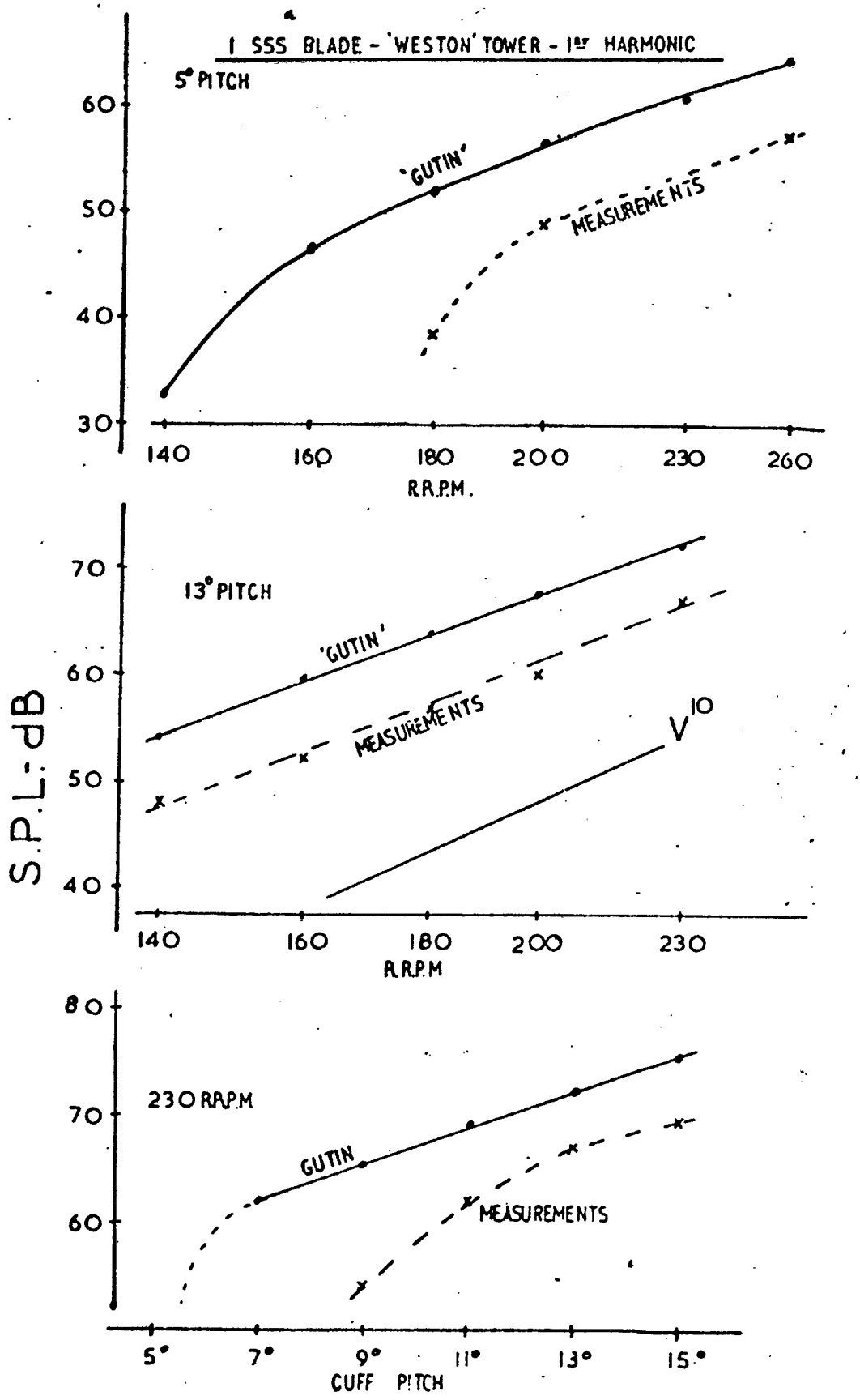

FIGURE 3.10 ROTATIONAL NOISE: SPL vs ROTOR SPEED - EXPERIMENTAL AND THEORETICAL RESULTS

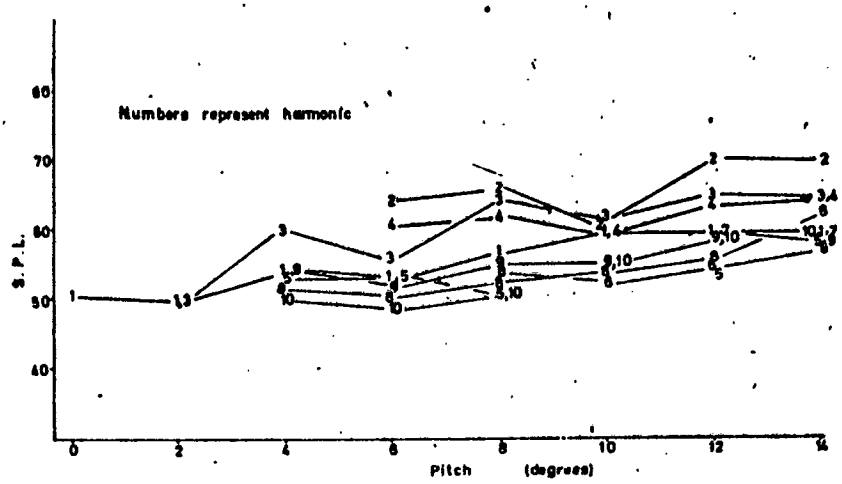

FIGURE 3.11 ROTATIONAL NOISE: SPL vs PITCH ANGLE - MODEL ROTOR (500 RPM)

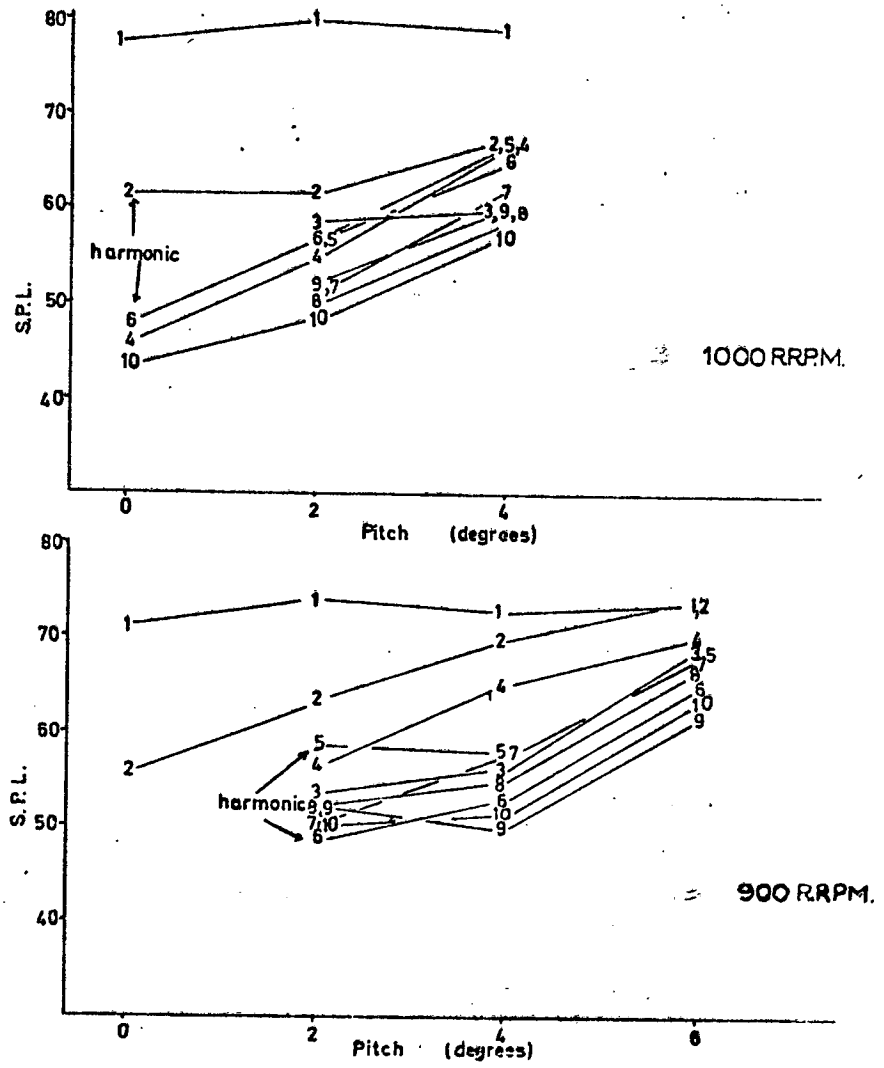

FIGURE 3.12 ROTATIONAL NOISE: SPL vs PITCH ANGLE - MODEL ROTOR (900 RPM, 1000 RPM)

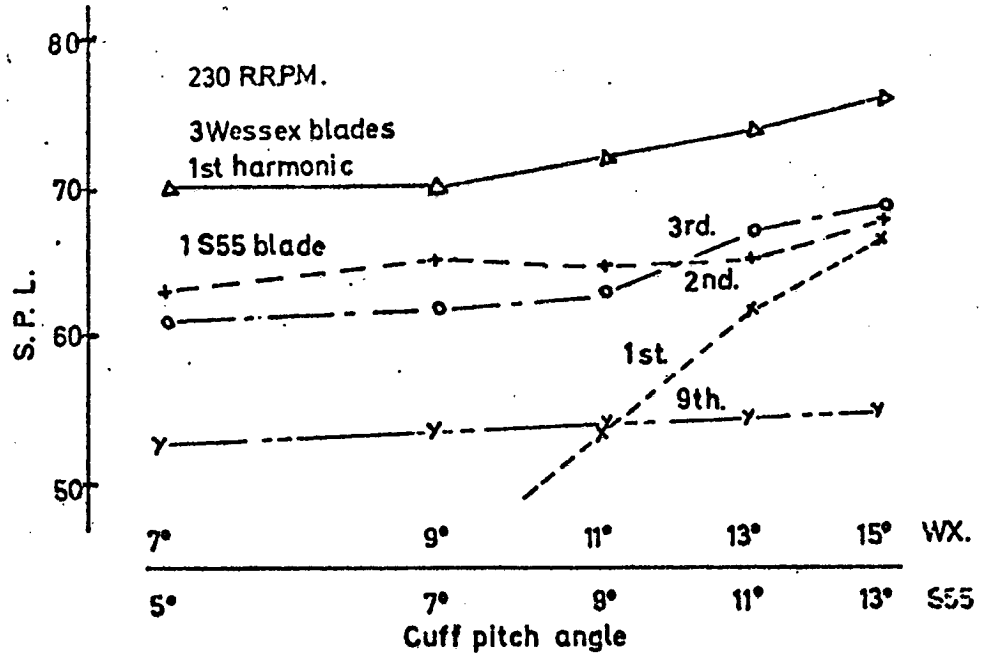

FIGURE 3.13 VARIATION OF SPL WITH PITCH ANGLE - S55 FULL SCALE ROTOR

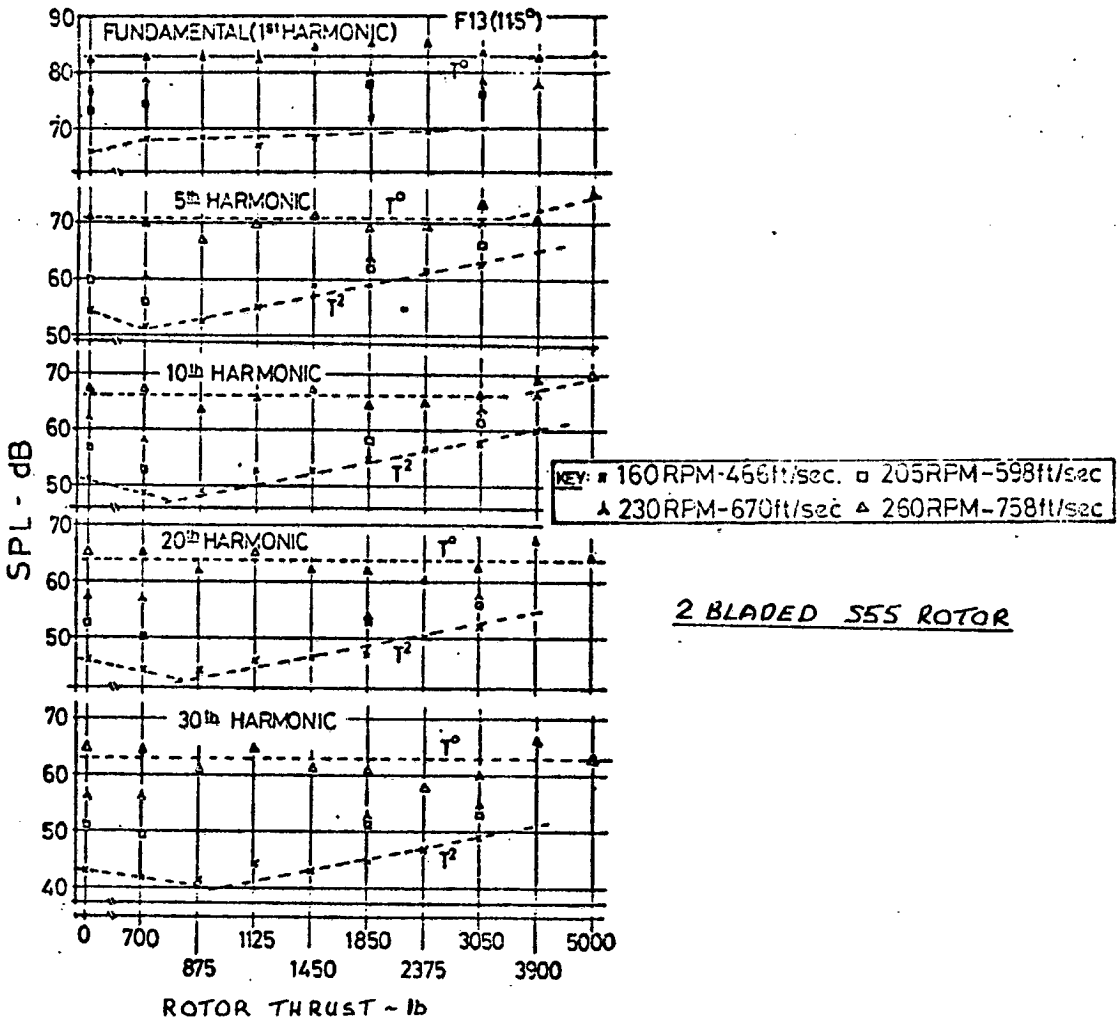

FIGURE 3.14 VARIATION OF SPL WITH ROTOR THRUST - FULL SCALE ROTOR

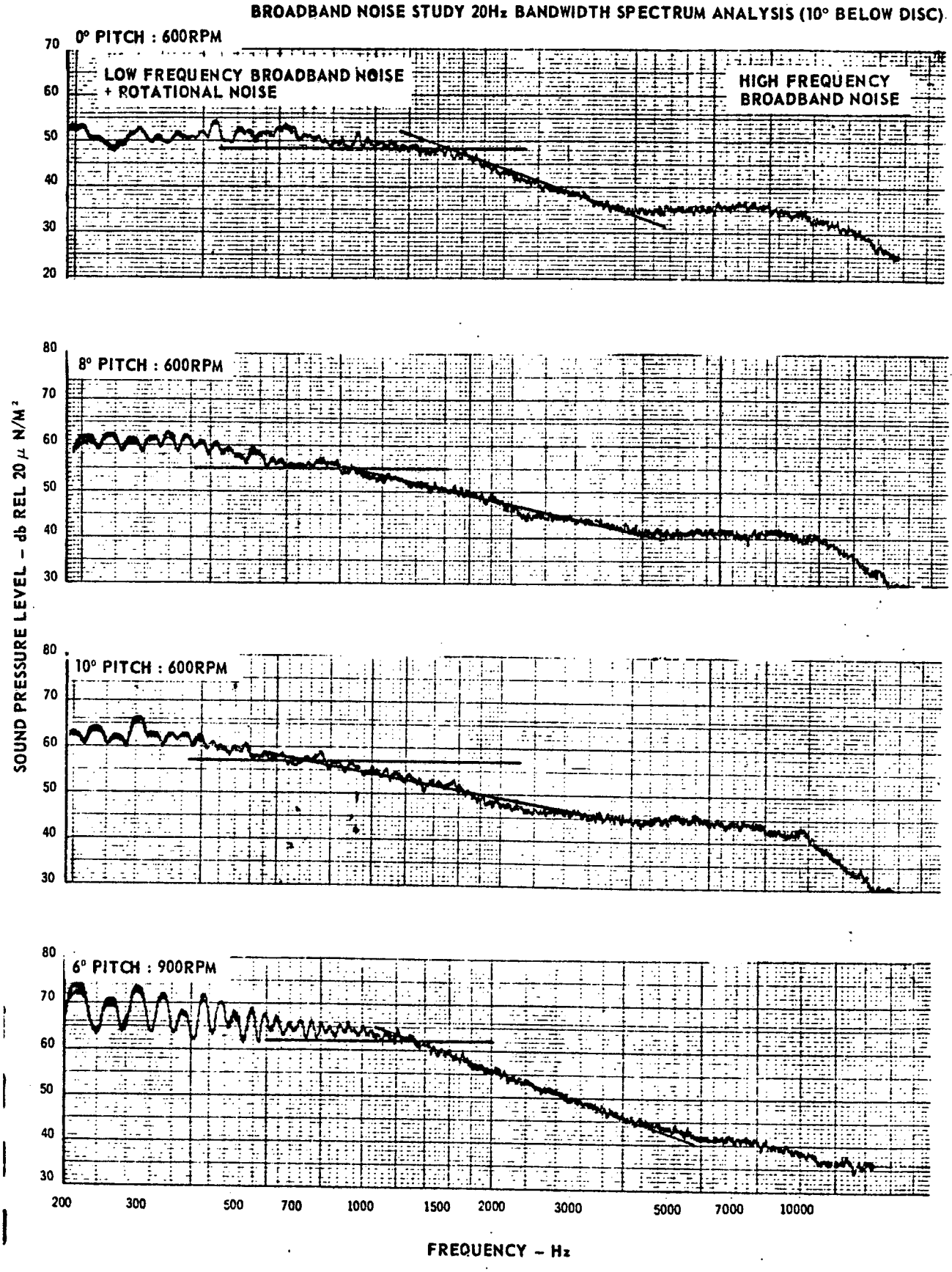

FIGURE 3.15 BROADBAND NOISE SPECTRA - MODEL ROTOR

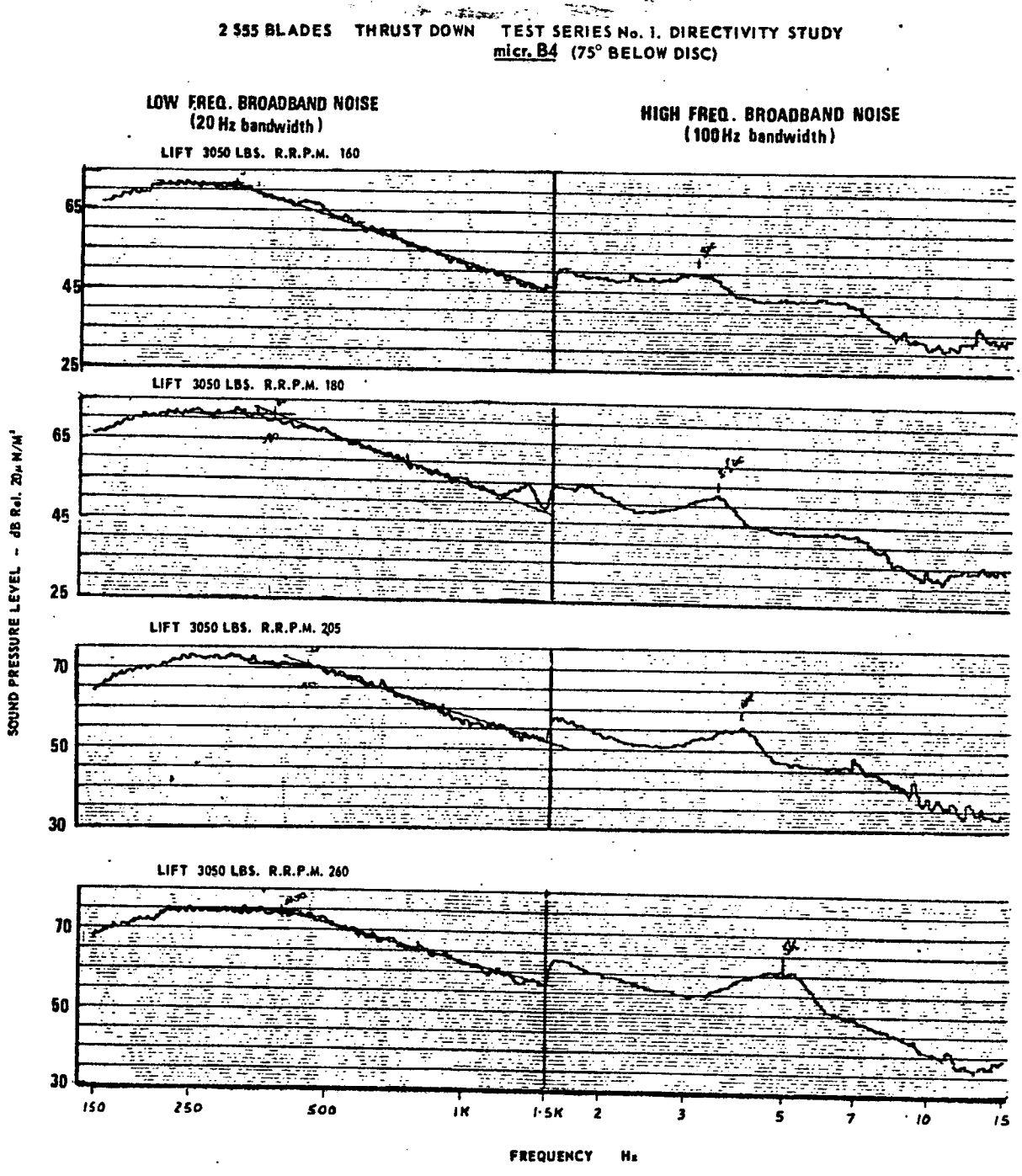

FIGURE 3.16 BROADBAND NOISE SPECTRA - FULL SCALE ROTOR

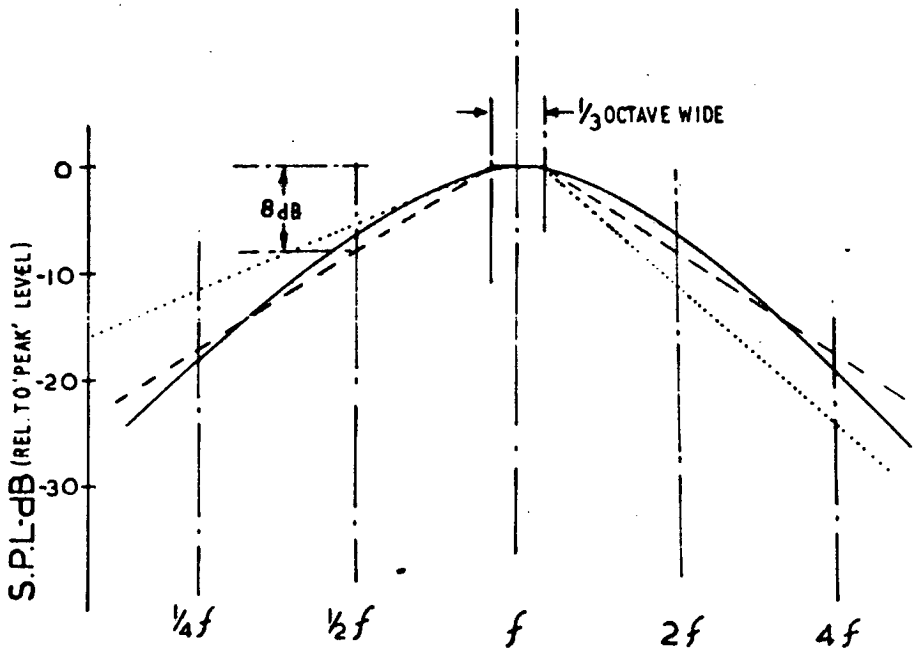

FIGURE 3.17 LOW FREQUENCY BROADBAND NOISE - SPECTRUM SHAPE

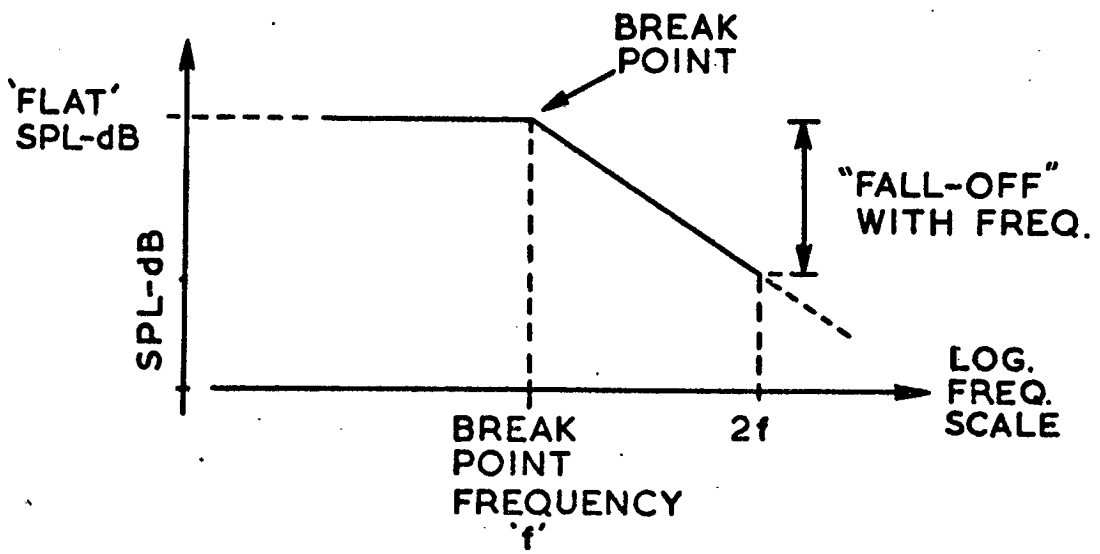

FIGURE 3.18 LOW FREQUENCY BROADBAND NOISE ANALYSIS MODEL

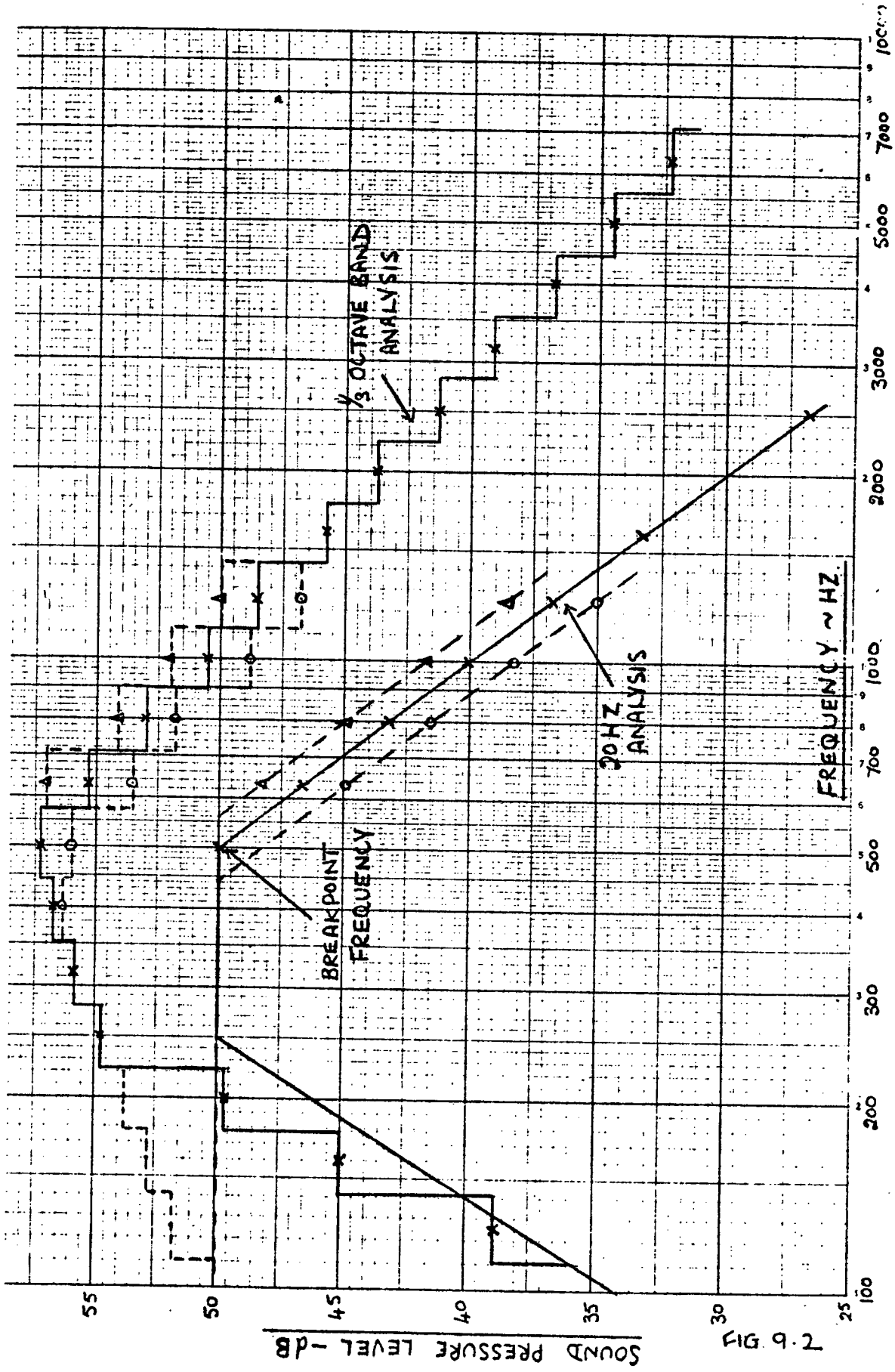

FIGURE 3.19 EFFECT OF ANALYSIS BANDWIDTH ON LOW FREQUENCY BROADBAND NOISE.

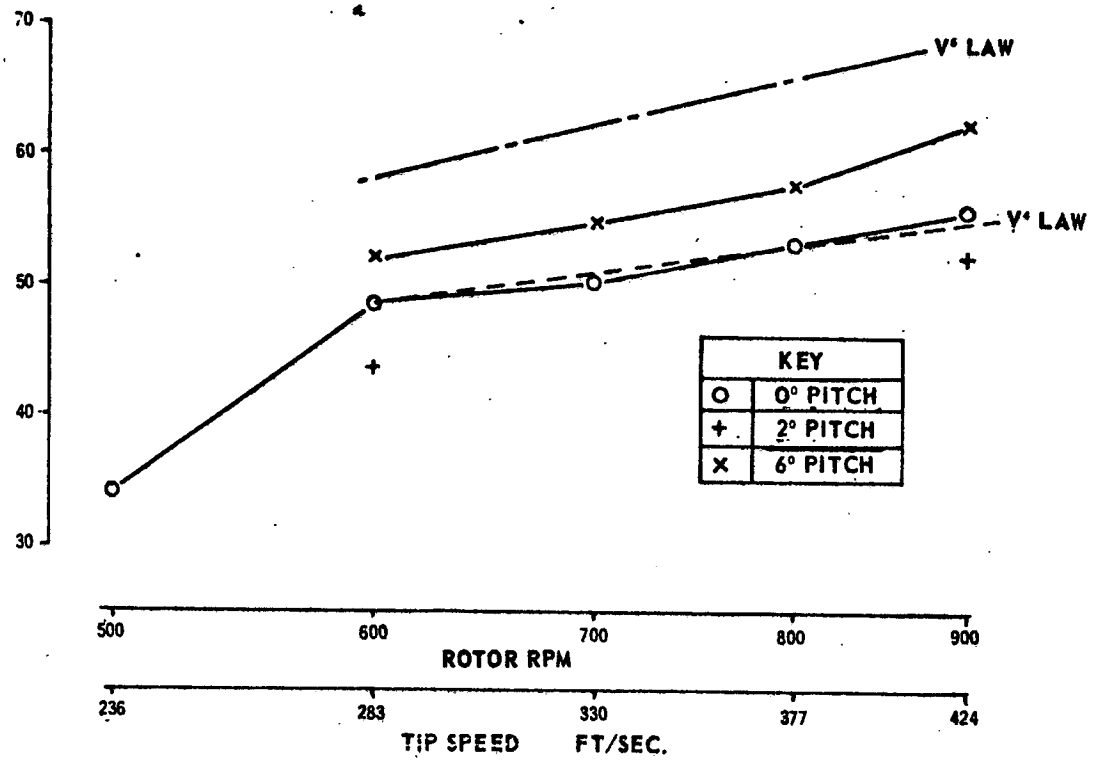

FIGURE 3.20 'FLAT' SPL vs TIP SPEED - MODEL ROTOR

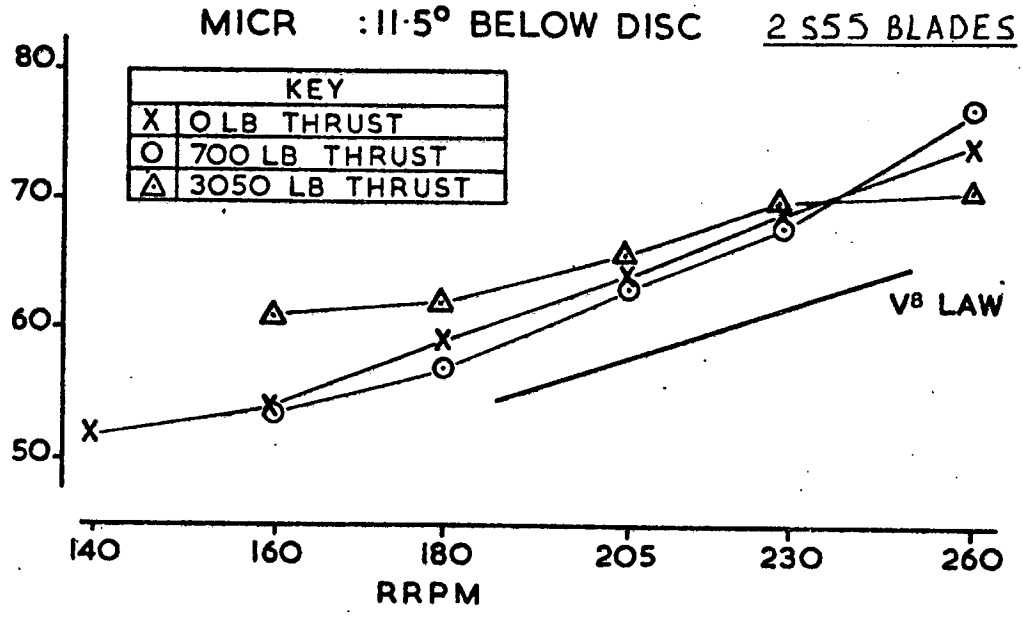

FIGURE 3.21 'FLAT' SPL vs TIP SPEED - FULL SCALE ROTOR

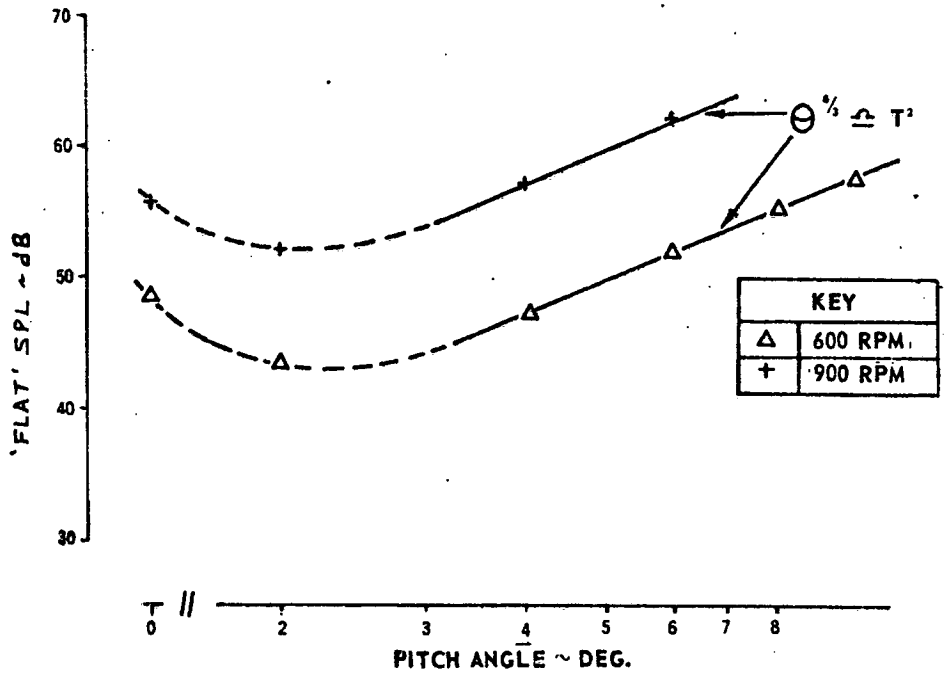

FIGURE 3.22 'FLAT' SPL vs PITCH ANGLE - MODEL ROTOR

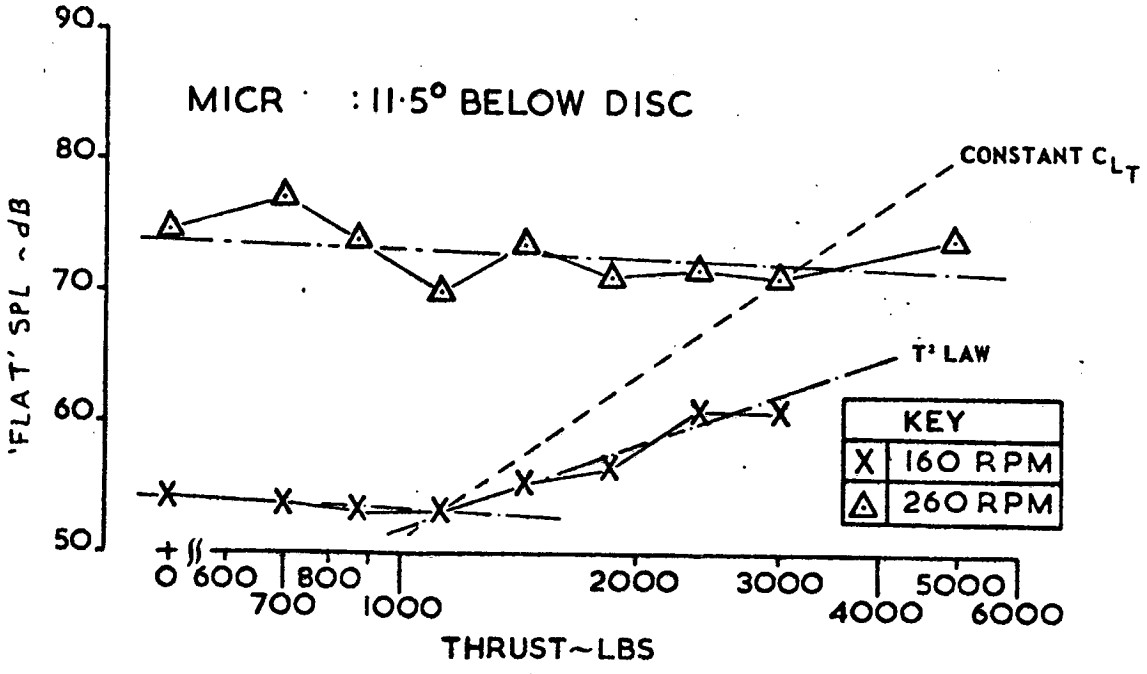

FIGURE 3.23 'FLAT' SPL vs THRUST - FULL SCALE ROTOR

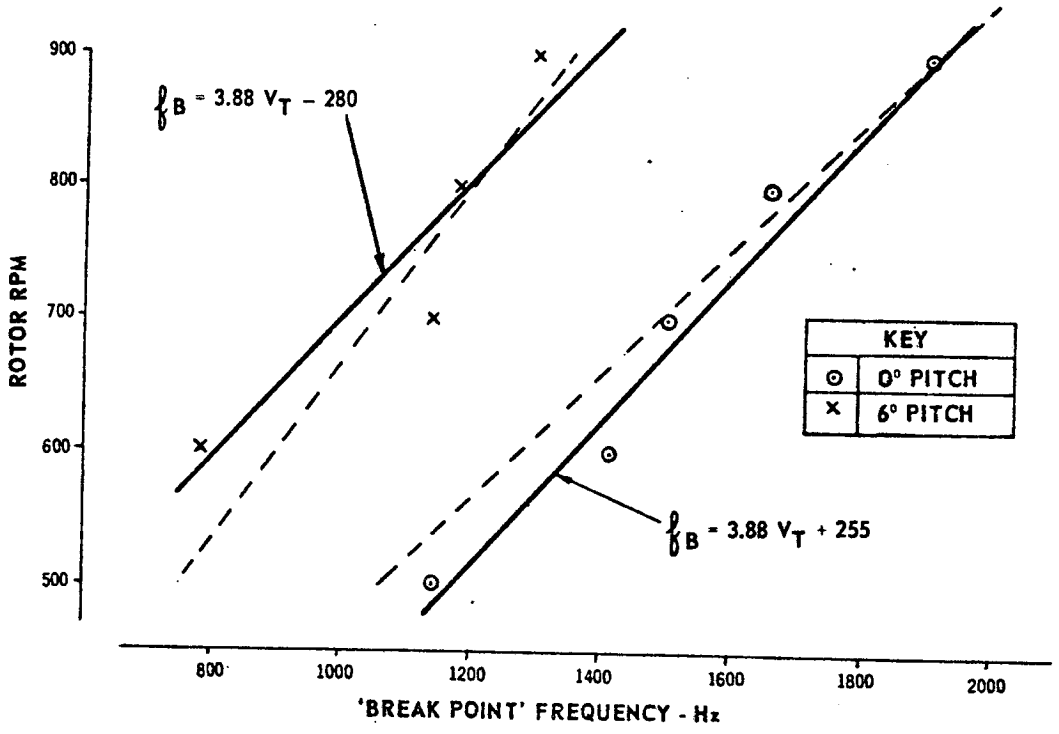

FIGURE 3.24 'BREAK POINT' FREQUENCY vs ROTOR SPEED - MODEL ROTOR

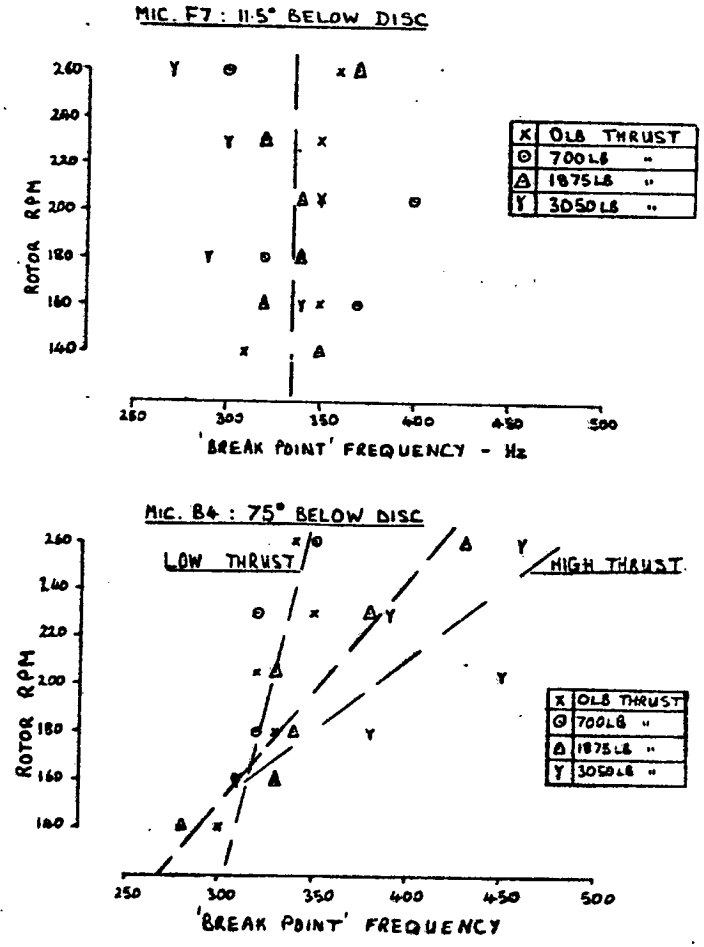

FIGURE 3.25 'BREAK POINT' FREQUENCY vs ROTOR SPEED - FULL SCALE ROTOR

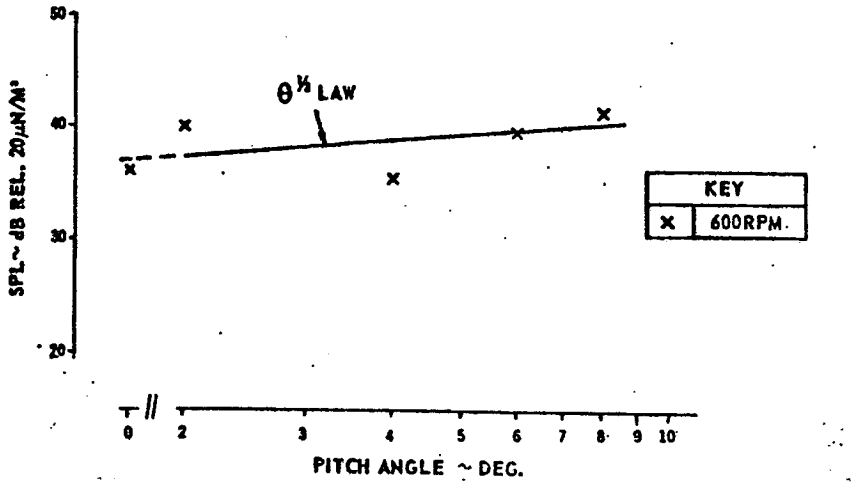

FIGURE 3.26 HIGH FREQUENCY BROADBAND NOISE: SPL vs PITCH ANGLE - MODEL ROTOR

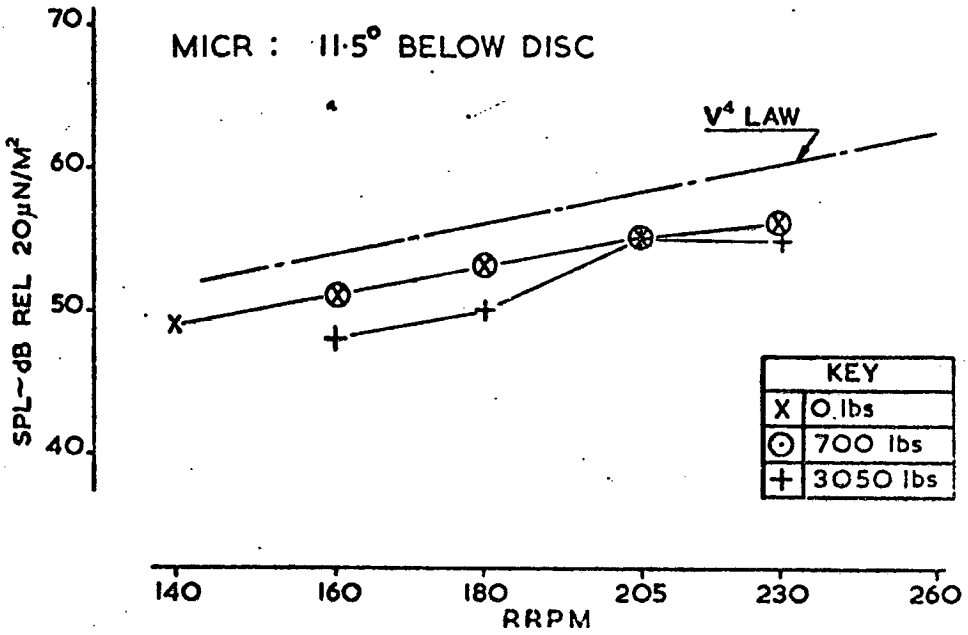

FIGURE 3.27 HIGH FREQUENCY BROADBAND NOISE: SPL vs ROTOR SPEED - FULL SCALE ROTOR

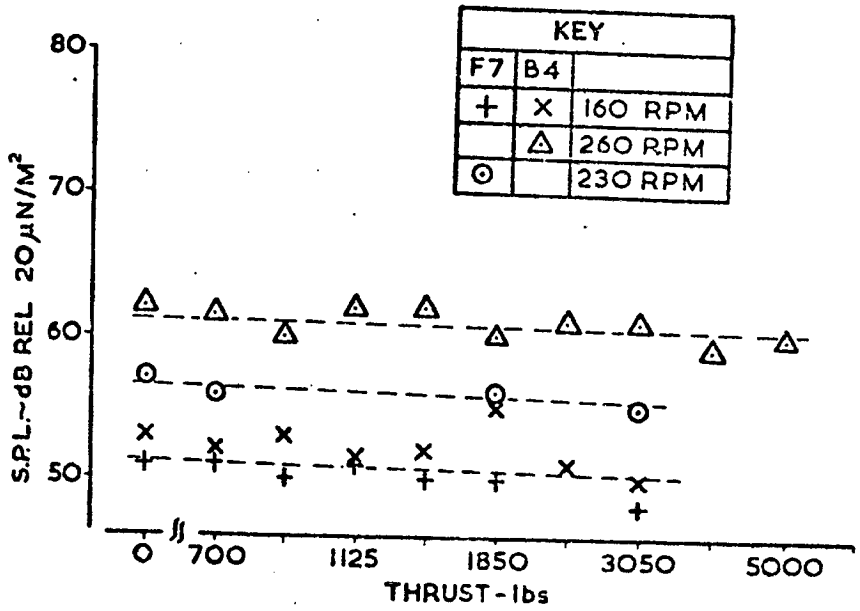

FIGURE 3.28 HIGH FREQUENCY BROADBAND NOISE: SPL vs THRUST - FULL SCALE ROTOR

HIGH FREQUENCY BROADBAND NOISE
'HUMP' FREQ. 'v' RRPM

TEST SERIES 14

MIC. F7 : 11·5° BELOW ROTOR DISC

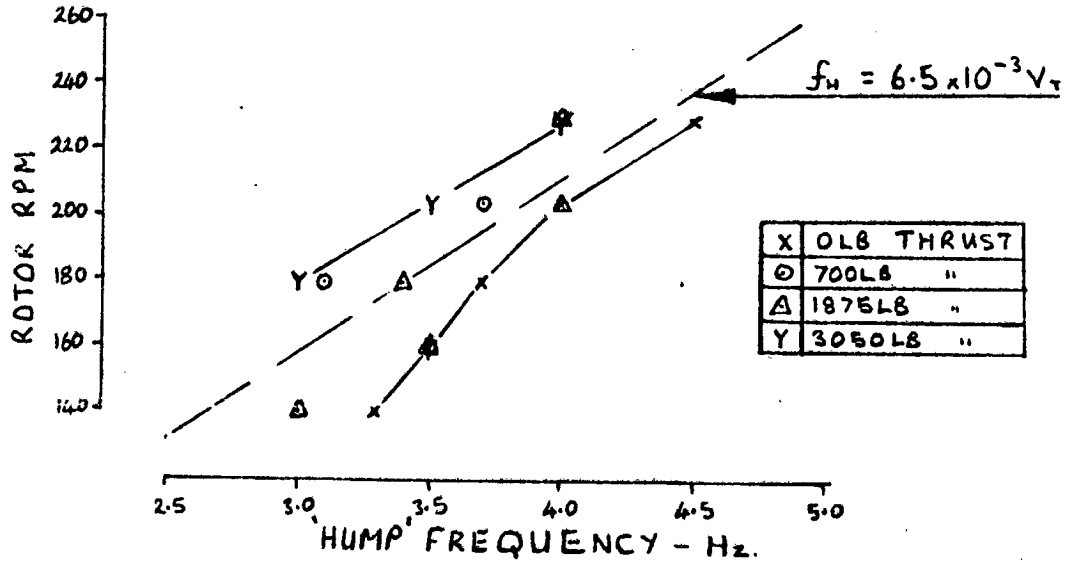

MIC. B4 : 75° BELOW ROTOR DISC

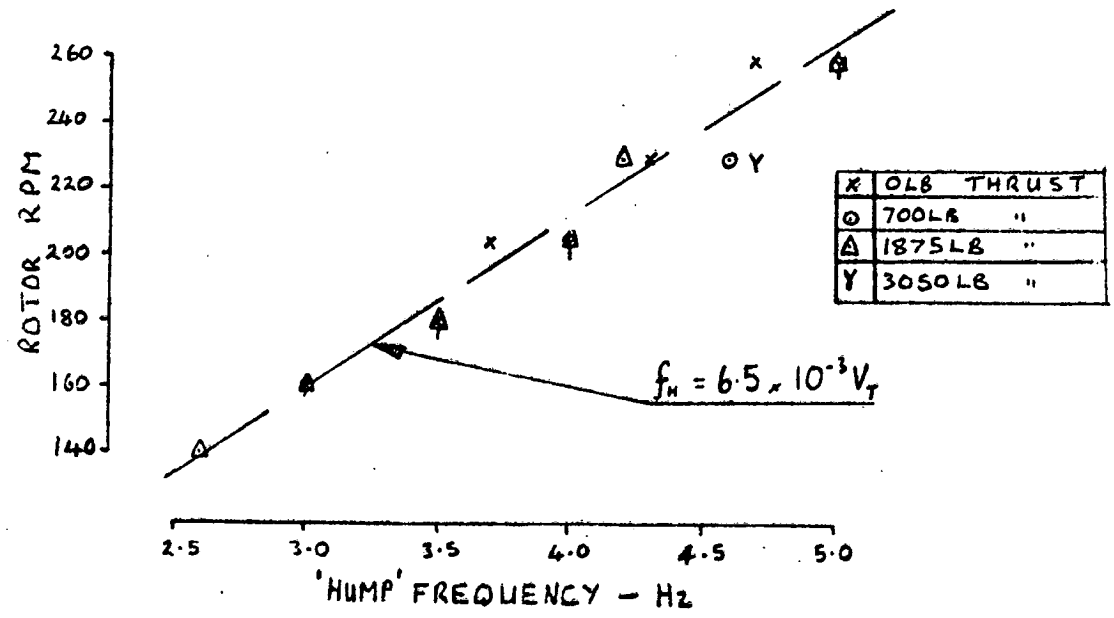

FIG 10·1

FIGURE 3.29 HIGH FREQUENCY BROADBAND NOISE: 'HUMP' FREQUENCY vs ROTOR SPEED - FULL SCALE ROTOR

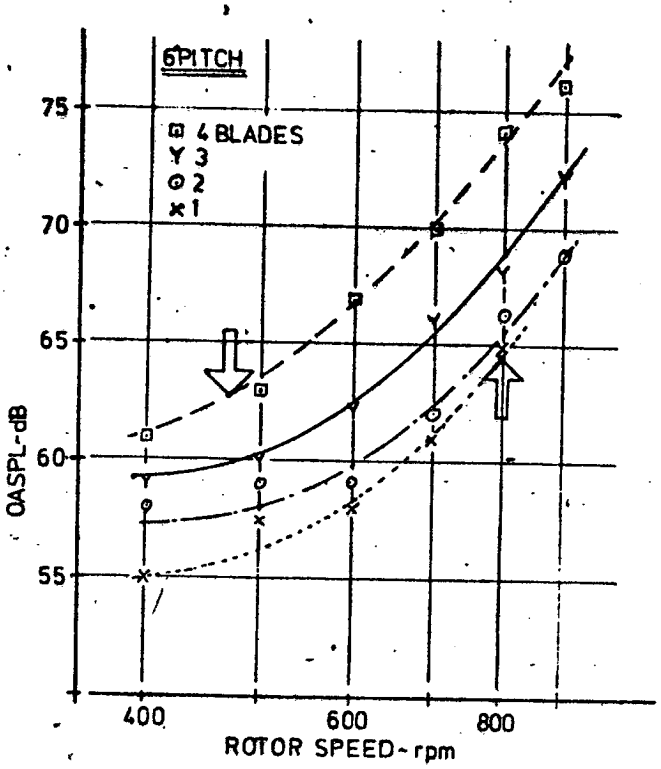

FIGURE 3.30 OASPL vs ROTOR SPEED - MODEL ROTOR

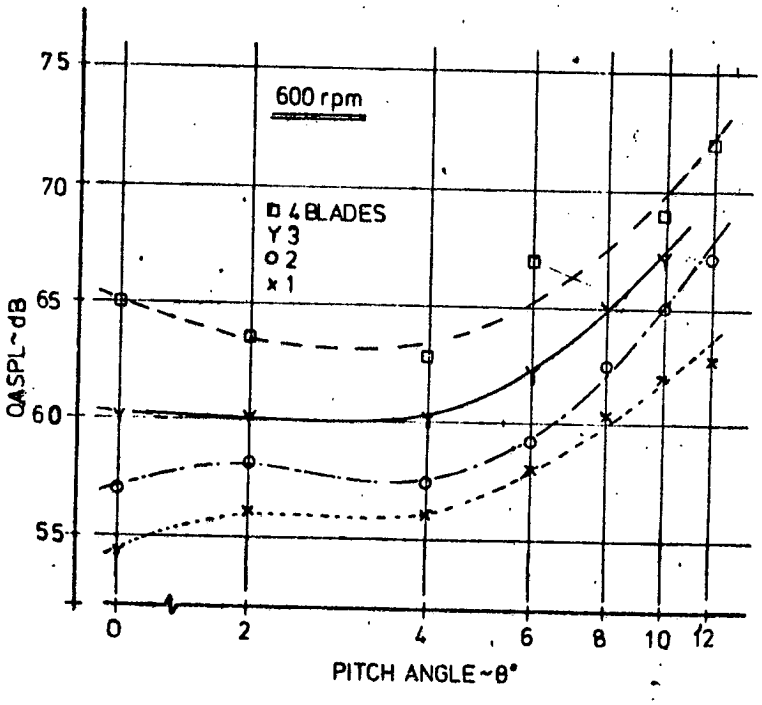

FIGURE 3.31 OASPL vs PITCH ANGLE - MODEL ROTOR

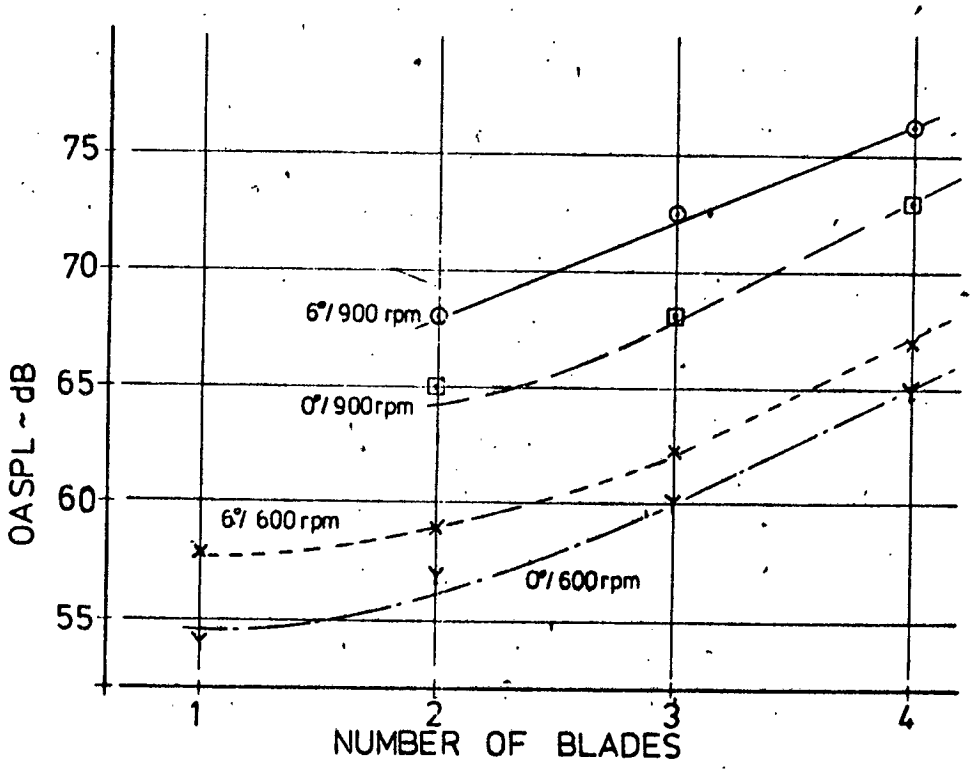

FIGURE 3.32 OASPL vs NUMBER OF BLADES - MODEL ROTOR

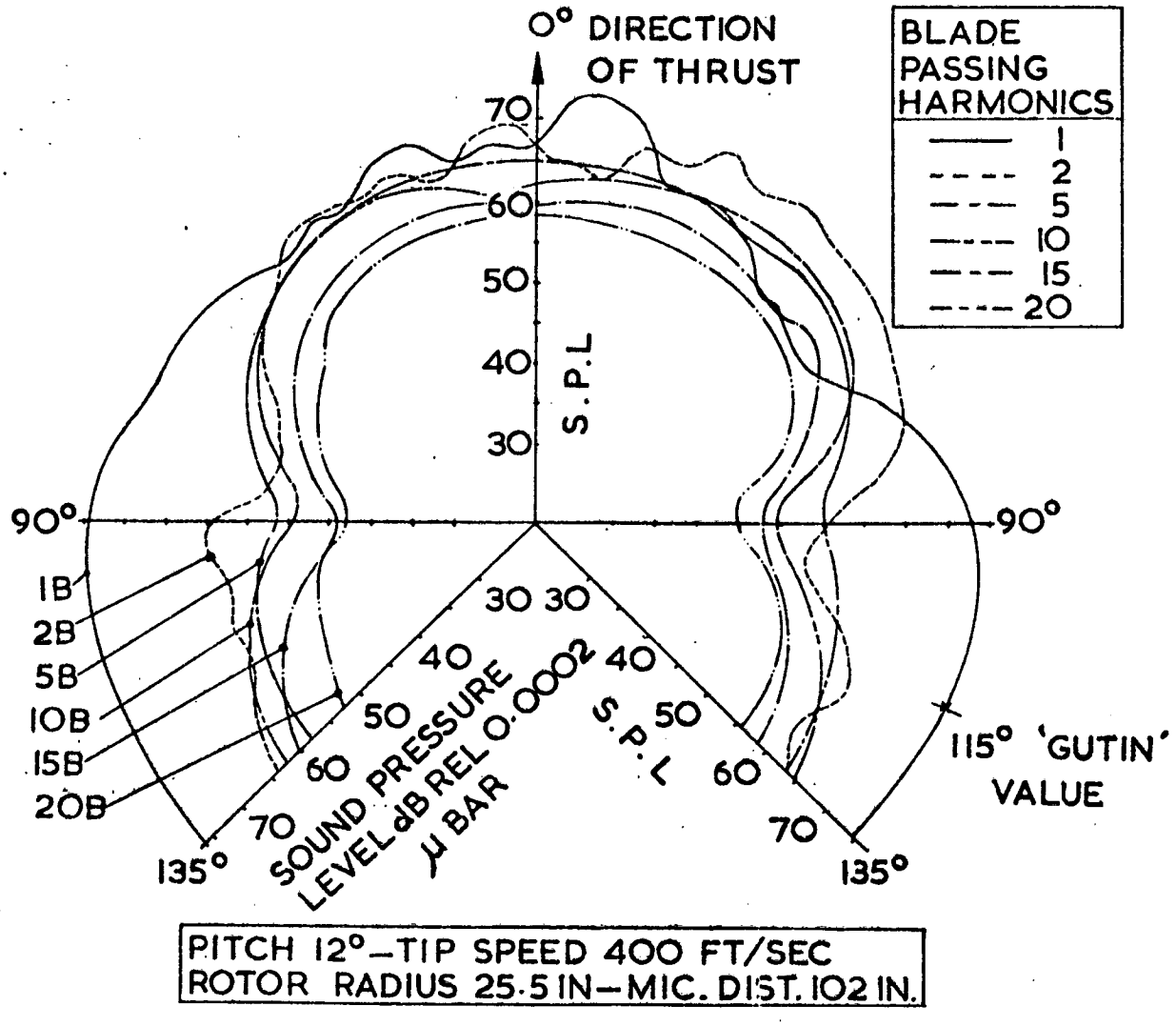

FIGURE 3.33 POLAR PLOT OF ROTATIONAL NOISE - MODEL ROTOR

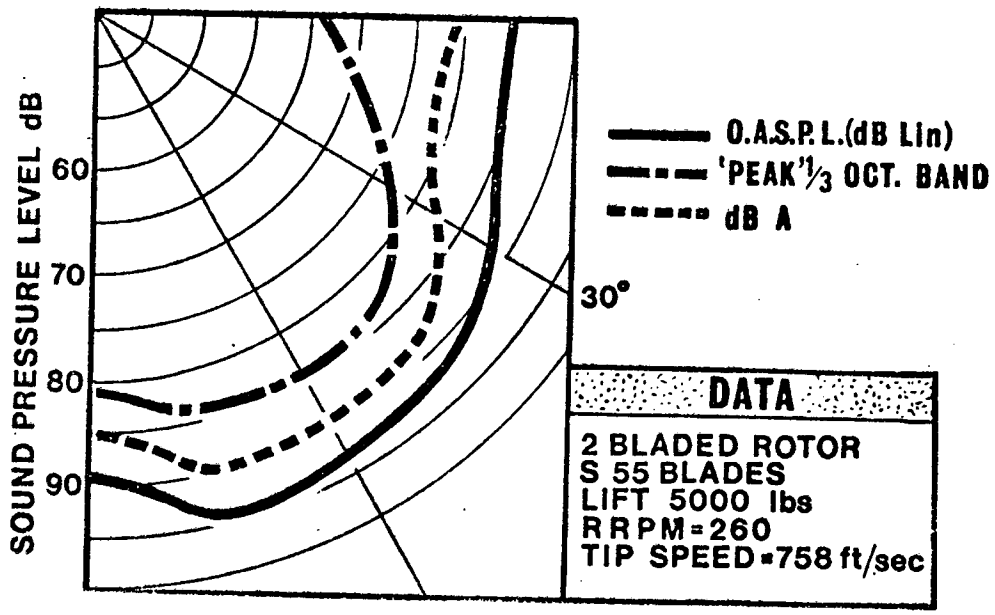

FIGURE 3.34 BROADBAND NOISE/OASPL - DIRECTIVITY

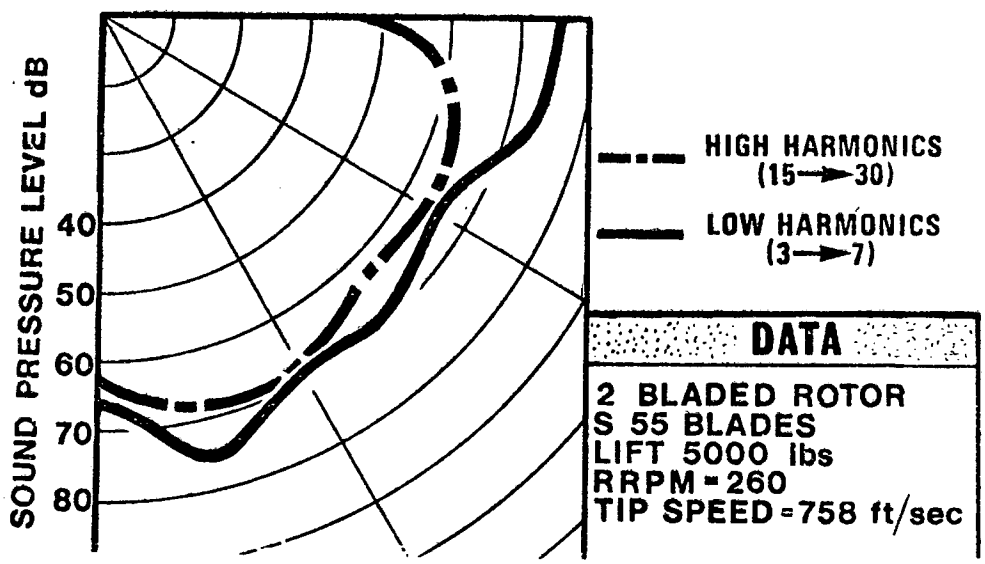

FIGURE 3.35 ROTATIONAL NOISE - DIRECTIVITY

RADIUS R = 5 FT. CHORD C = 4 IN. SECTION = NACA 0012

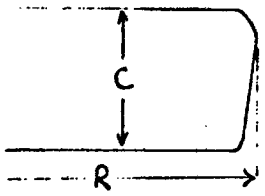

(a) STANDARD

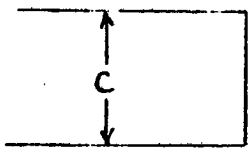

(b) SQUARE

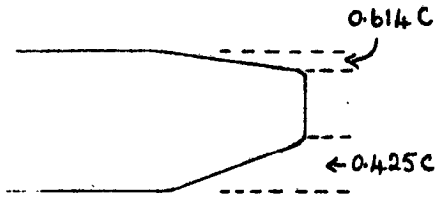

(c) SIKORSKY

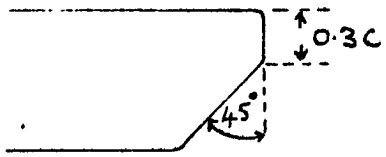

(d) 45° BLUNT TRAILING EDGE CUT OUT

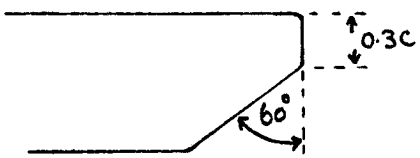

(e) 60° BLUNT TRAILING EDGE CUT OUT

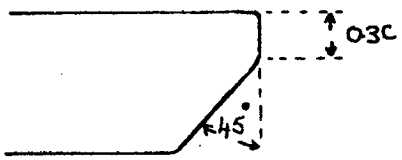

(f) 45° FAIRED TRAILING EDGE CUT OUT

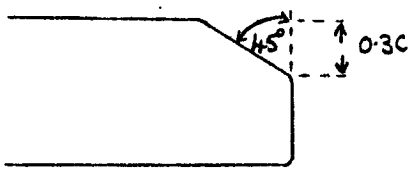

(g) 45° FAIRED LEADING EDGE CUT OUT

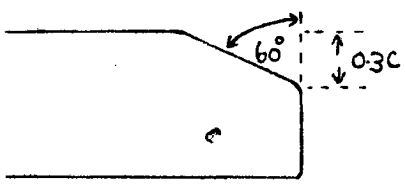

(h) 60° FAIRED LEADING EDGE CUT OUT

FIGURE 3.36 TIP SHAPE PLANFORMS

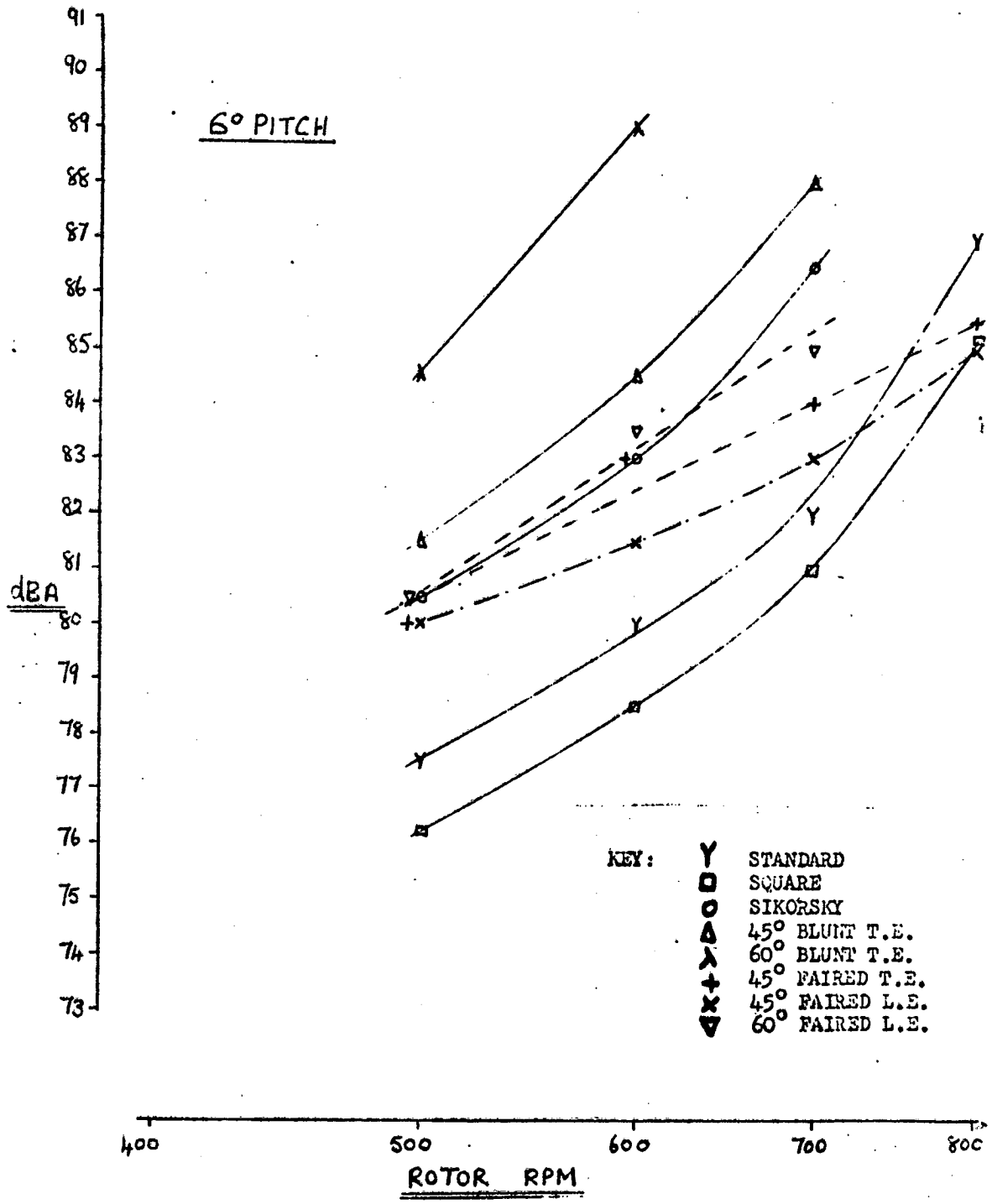

FIGURE 3.37 dB(A) vs ROTOR SPEED - MODEL ROTOR

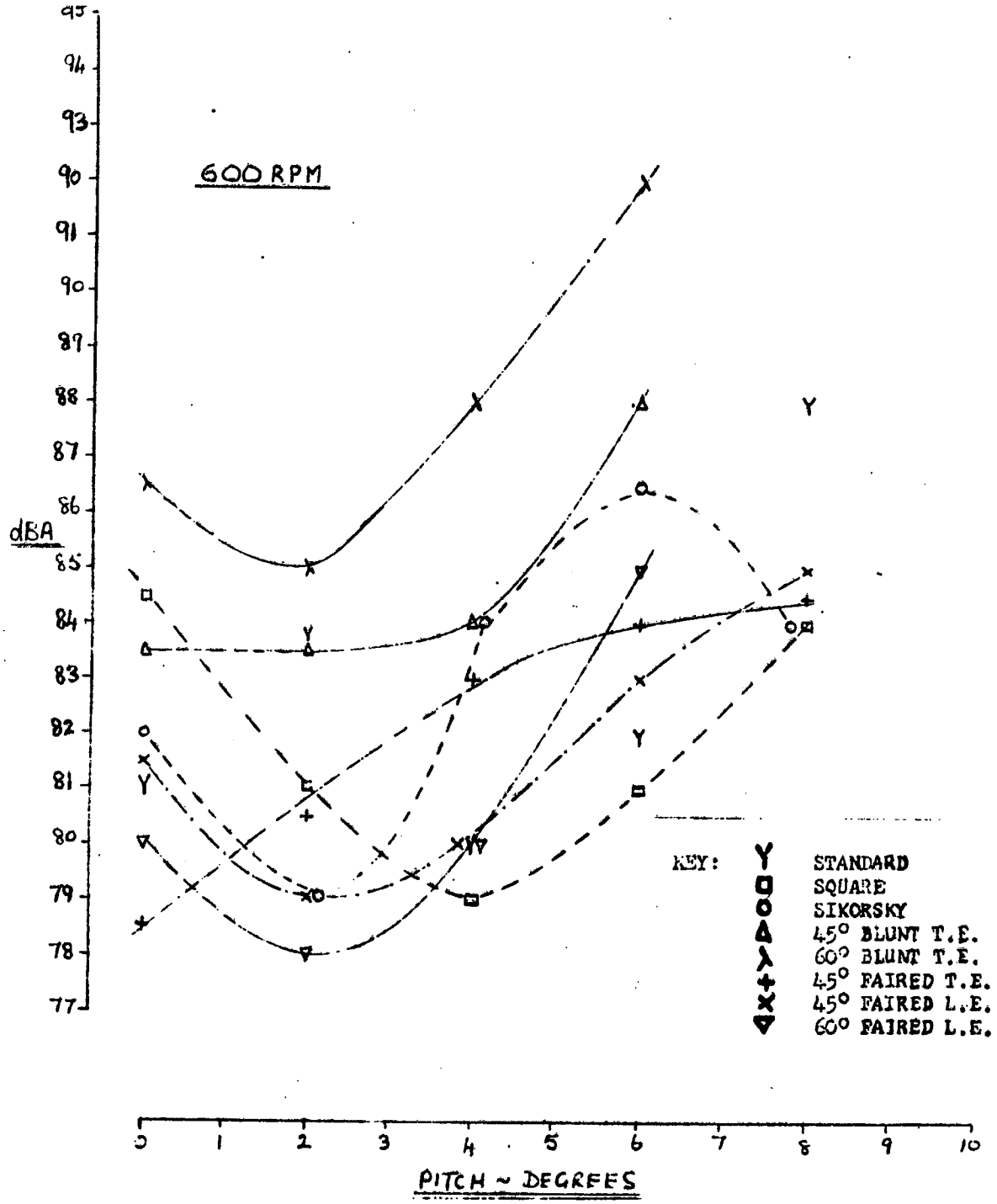

FIGURE 3.38 dB(A) vs PITCH ANGLE - MODEL ROTOR

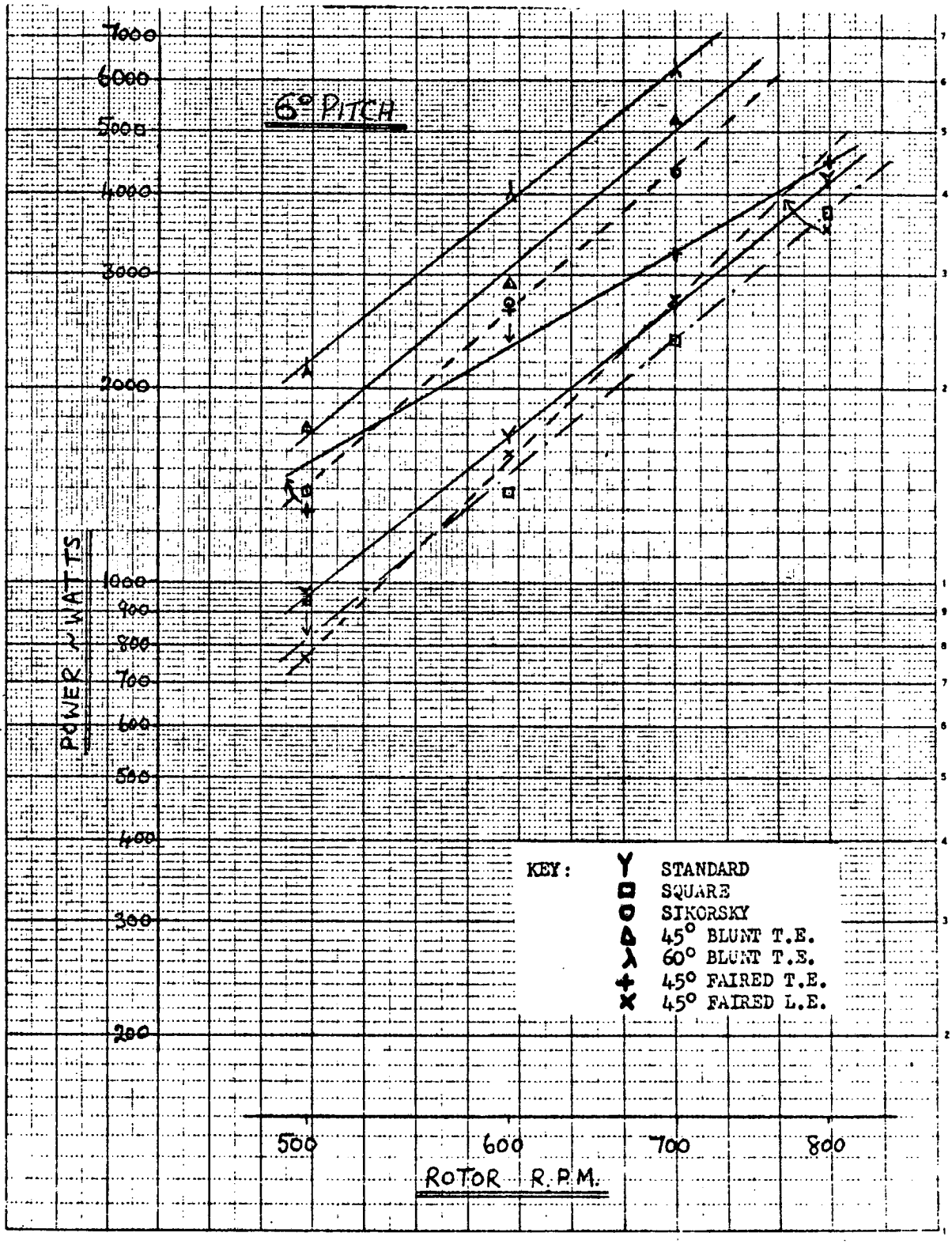

FIGURE 3.39 POWER vs ROTOR SPEED - MODEL ROTOR

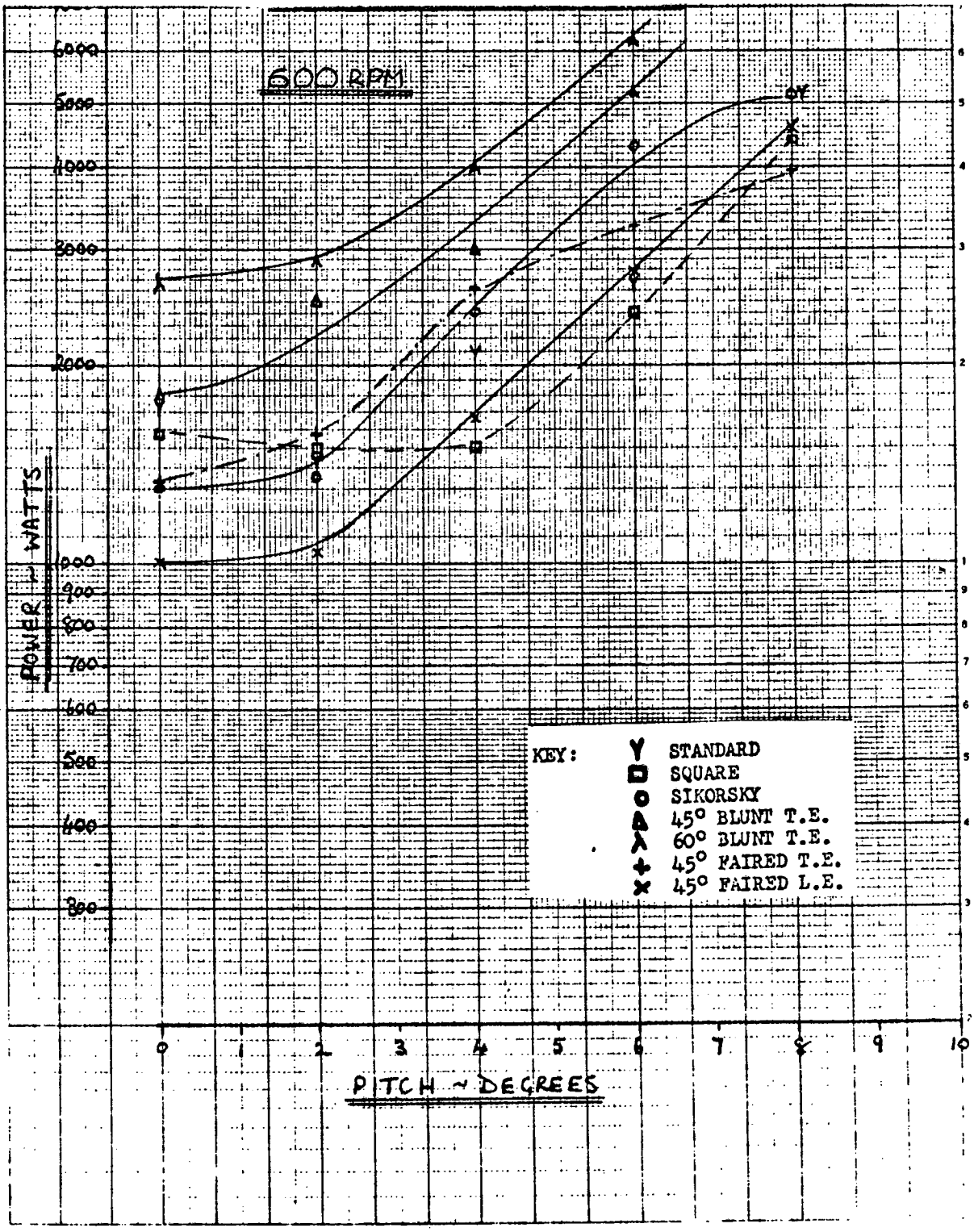

FIGURE 3.40 POWER vs PITCH ANGLE - MODEL ROTOR

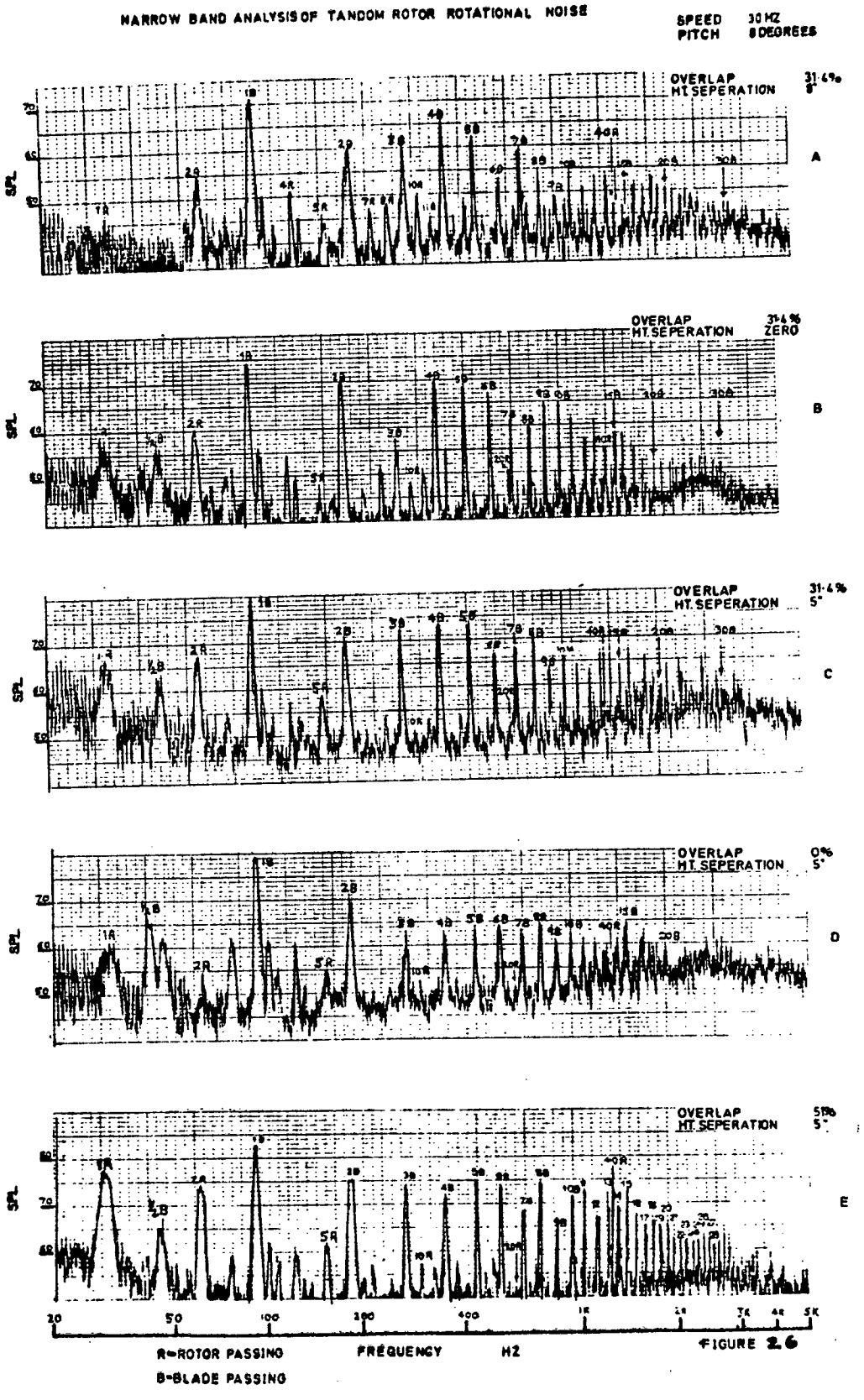

FIGURE 3.41 NARROWBAND ANALYSIS OF TANDEM ROTOR NOISE

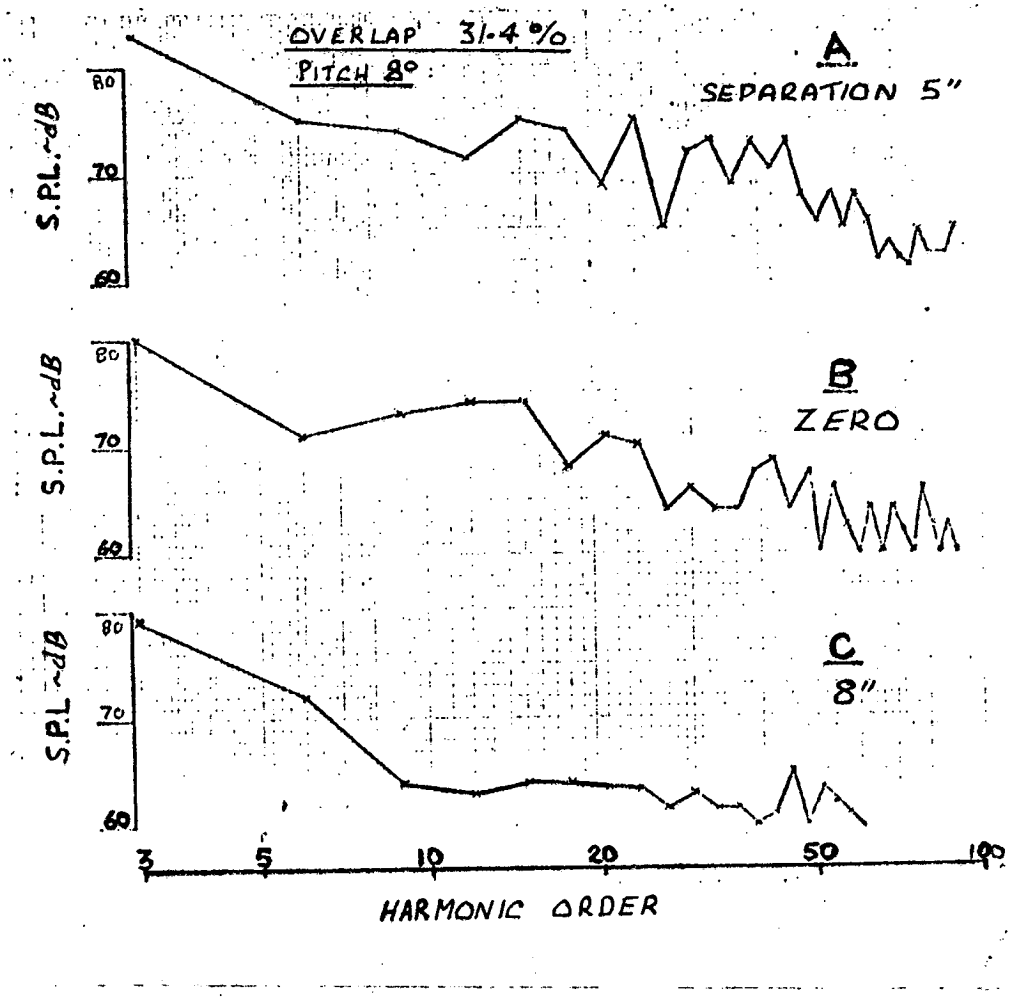

(a) Spectra

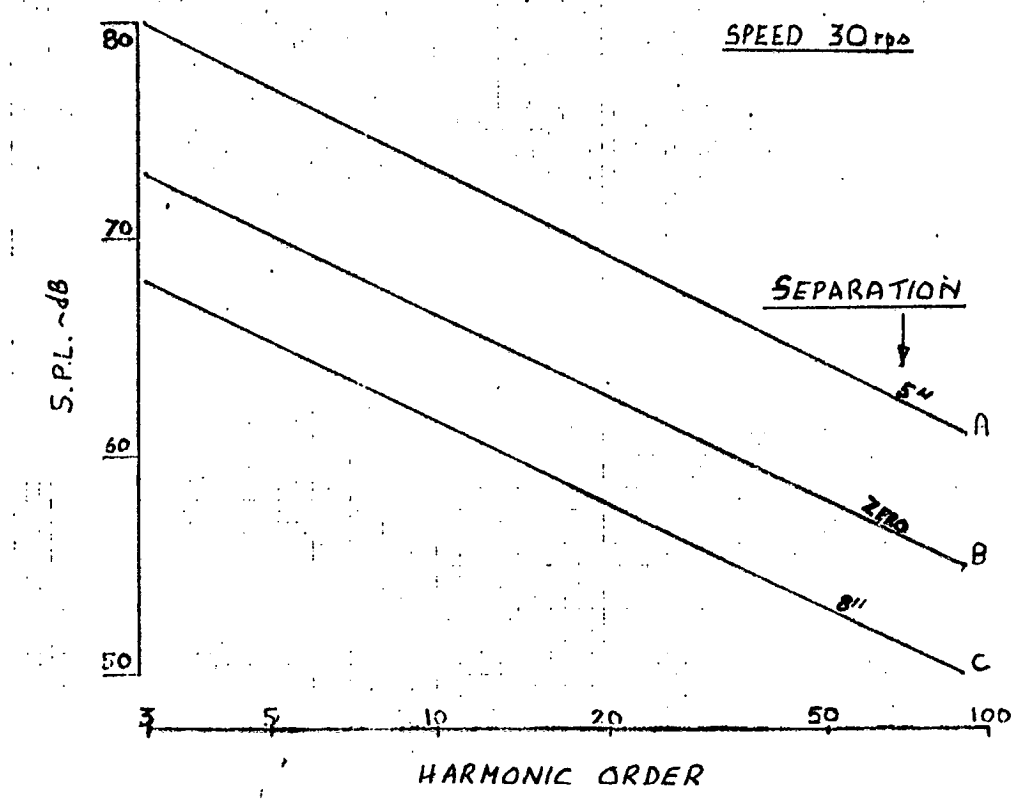

(b) Generalized fall-off Characteristics.

FIGURE 3.42 EFFECT OF HEIGHT SEPARATION ON TANDEM ROTOR NOISE

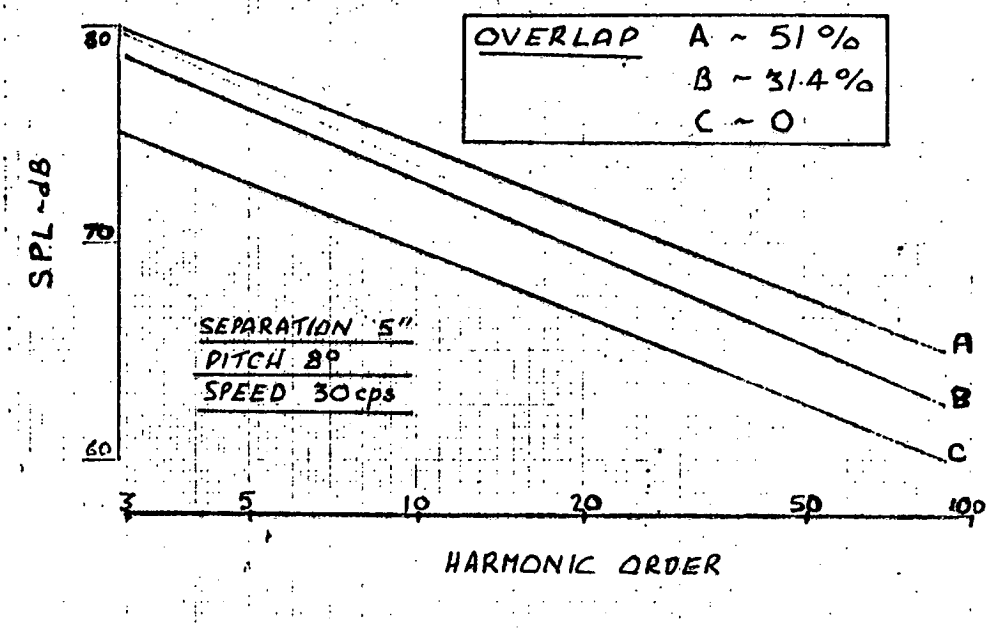

FIGURE 3.43 VARIATION OF TANDEM ROTOR NOISE WITH ROTOR OVERLAP

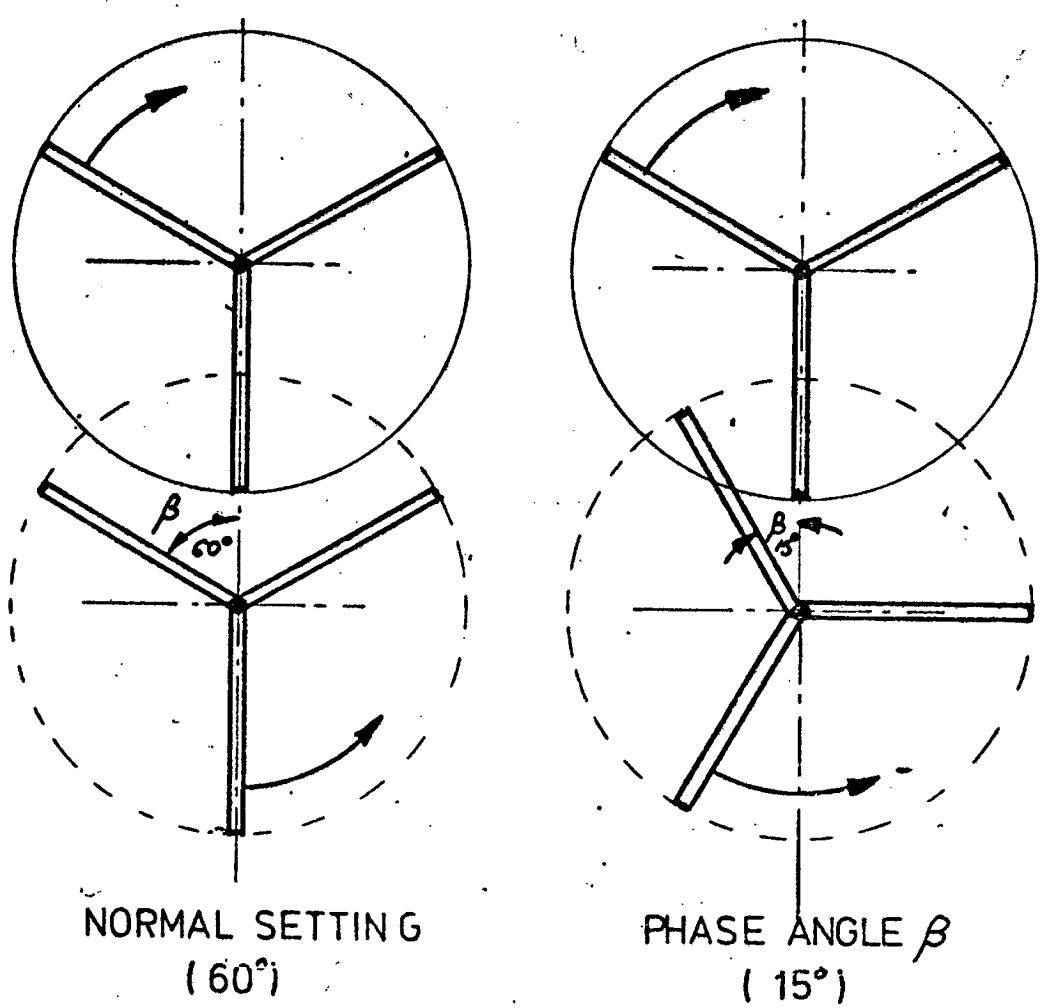

FIGURE 3.44 DEFINITION OF 'PHASE ANGLE' ON A TANDEM ROTOR

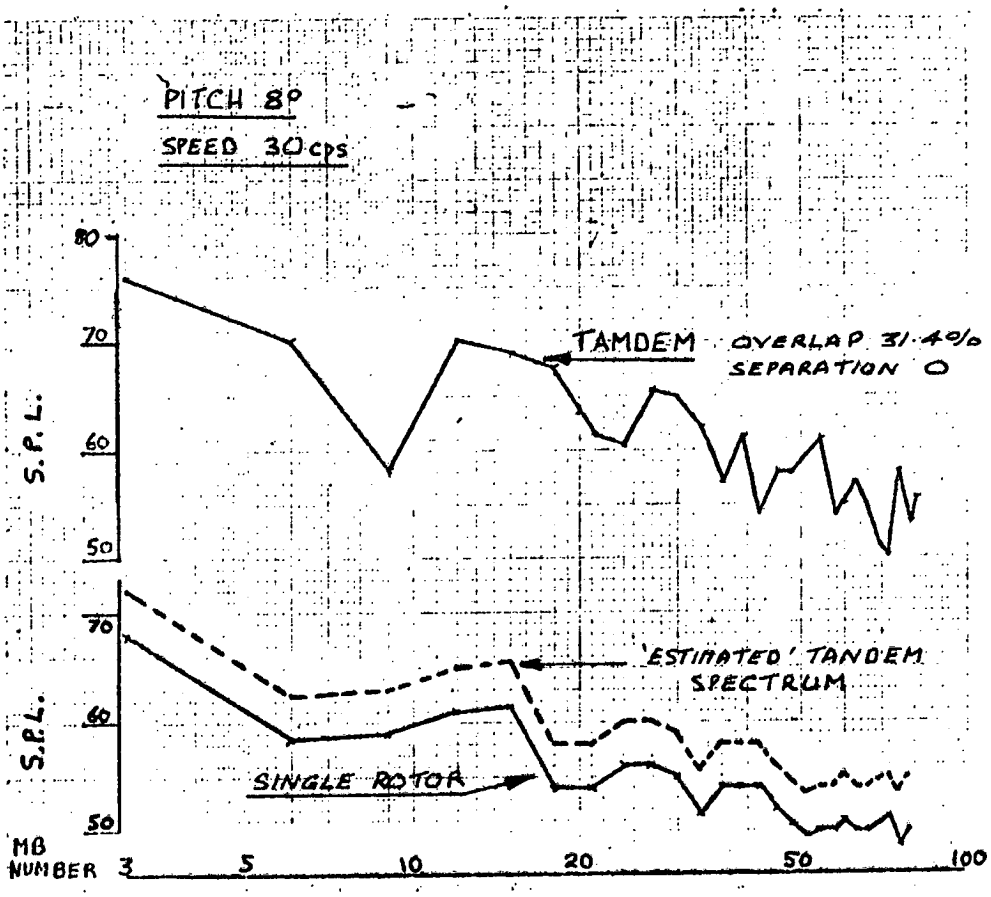

FIGURE 3.45 COMPARISON OF TANDEM ROTOR AND SINGLE ROTOR NOISE LEVELS

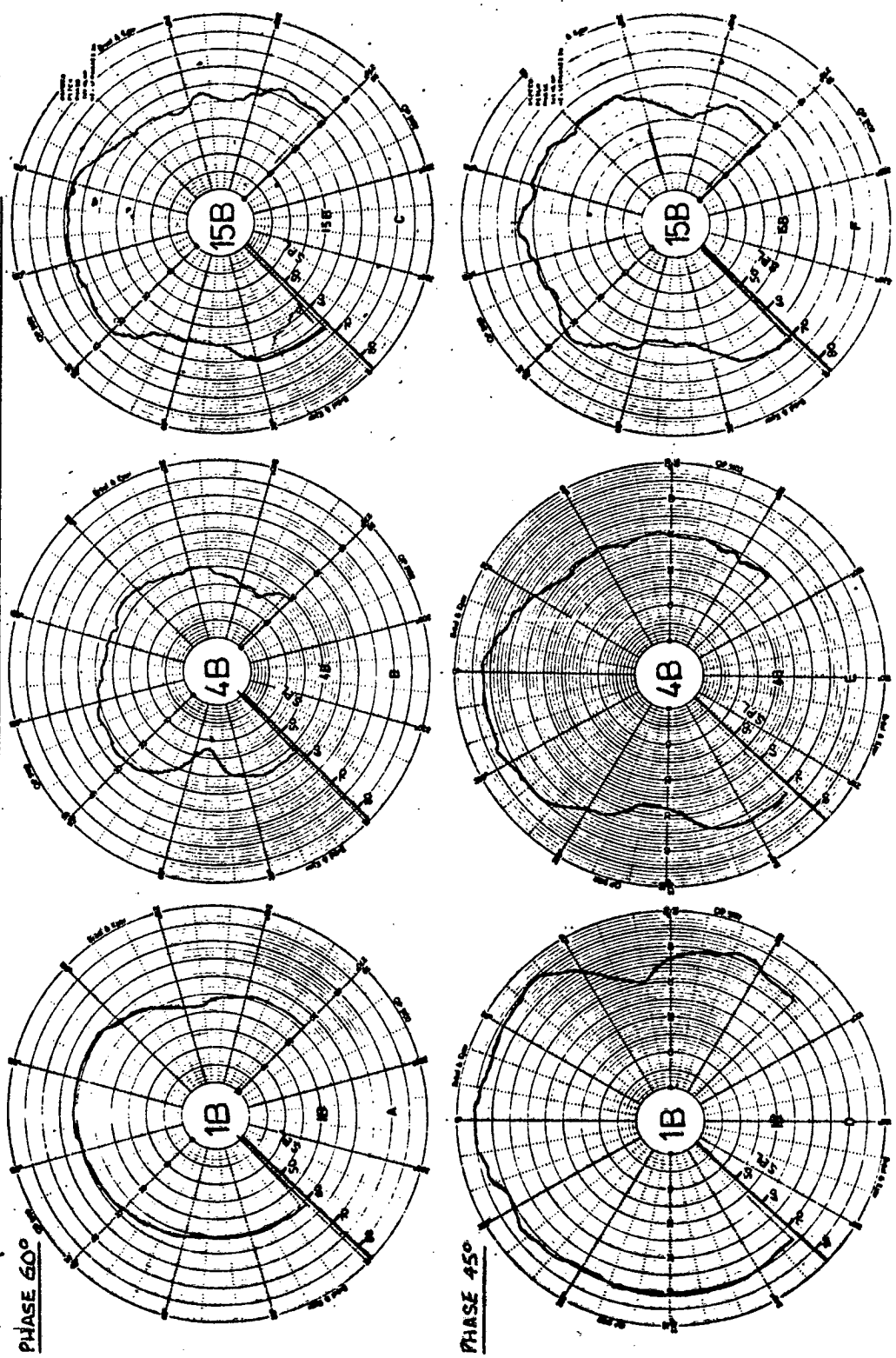

FIGURE 3.46 DIRECTIVITY PLOTS FOR TANDEM ROTOR

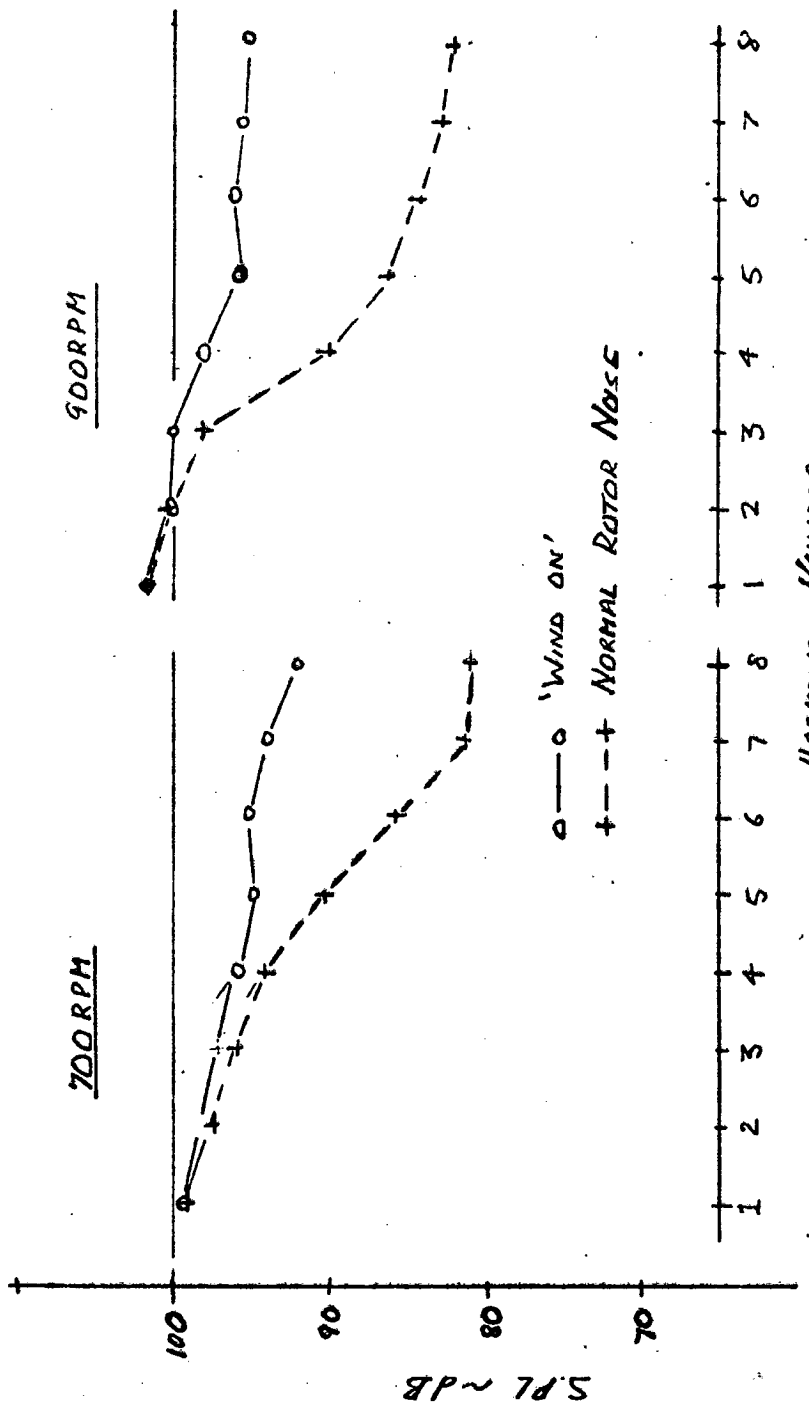

FIGURE 3.47 EFFECT OF 'WIND' ON ROTATIONAL NOISE - MODEL ROTOR

CHAPTER 4: HELICOPTER NOISE

4.1. INTRODUCTION

Considerable data on the noise produced by real helicopters was collected and analyzed during the initial phases of the investigation. This varied from the results of ad hoc measurements taken of a single flight to a series of controlled tests on specific helicopters. In some cases the data was used for the study of a particular aspect, while in other instances it was used solely as back up material. It is not possible, or desirable, to present this data in full in this thesis, but the conclusions drawn from such analyses are obviously of interest and relevant. Thus in this chapter the aspects of main importance are outlined together with appropriate examples of the test data. The one exception to this is in the case of the helicopter noise tests conducted in connection with the blade slap study which are discussed and reported in Chapter 5 (Blade Slap). Also where the data was used in the study of rotor noise, as distinct from helicopter noise, this has been included in Chapter 3 (Rotor Noise) and emphasis in this chapter is limited solely to studies directly related to the noise generated by the complete helicopter. A general review of basic helicopter noise characteristics is also given and, although the majority of the investigation was related to external noise, internal (cabin) noise is briefly outlined.

In the context of this chapter it is worth noting that when the initial studies were carried out in 1966/7, there had been very few detailed investigations of helicopter noise although two general reviews had been completed by Bell Helicopters [45] and Davidson and Hargest [40] and a number of theoretical papers published [30, 51]. Thus to a large extent the data examined was aimed at giving guidance to the general programme being formulated at ISVR. A number of general results were obtained and these are presented in this chapter; similar results were obtained in many cases by the helicopter manufacturers and, although they were discussed with the author, they have in the majority of cases not been published. Thus reference to other work of a nature similar to that conducted by the author is not included in this chapter.

4.2. TEST DATA

Noise analysis was carried out on the following helicopters, the general parameters of which are outlined in Table 2.1:

WHL (UK) : Wessex Mk.1, Wessex Mk.2, Wessex Mk.3 (2 series), Wessex Mk.5, Whirlwind, Widgeon, Wasp, Scout

Boeing Vertol (USA) : V107 (CH-46)

Bell Helicopters (USA) : UH-1B

Milhail (USSR) : MIL 10

In addition measurements were made of the noise of the SRN 4 hovercraft 19 ft diameter propeller.

In the evaluation of the data account has to be taken, of course, of the cancellation/reinforcement effects which are superimposed on the signal. This is much more critical in the case of external noise measurements on real helicopters where the microphone is usually mounted 4 ft (1.2m) above the ground (reflecting surface), than in laboratory experiments where the microphone positions are usually chosen to minimise the reflection effects. These acoustic interference effects can be readily detected on a narrowband analysis trace by a series of 'dips' which occur at f_c, $3f_c$, $5f_c$, etc., where f_c is the fundamental cancellation frequency. If the helicopter is assumed to be a point source then the cancellation frequency 'f_c' can be readily calculated from the geometry of the layout. This is discussed further in section 4.10.4. Theoretically the reinforcement can increase the sound pressure level by 6 dB (doubling of the intensity) and perfect cancellation would give a zero sound pressure. In practice, however, since the ground is not an ideal reflector and the signals arise from a finite rather than a point source, the typical difference between the maximum (reinforcement) and minimum (cancellation) rarely exceeds 10 to 15 dB and often it is as low as 6 to 8 dB.

Analyzer bandwidth and the analysis time or 'sweep time' employed can also influence the apparent spectrum and hence care had to be taken in the selection of the most appropriate parameters. In the case of the latter it was found by the author that the minimum acceptable analysis time was equivalent to 10 blade passing intervals (typically 1s) and that ideally it should be double this value. These aspects were particularly important in the case of evaluating data prepared by other investigators/manufacturers, since many did not at the time of the initial investigations in 1967 appreciate the influence on the result of the analyzer and analyzer settings used. It is also fair to say that even today the importance of this aspect is often overlooked.

4.3. GENERAL CHARACTERISTICS

As mentioned in section 1.1 the important sources externally are rotor noise and engine noise and internally there is transmission (gear) noise as an additional source. The frequency ranges associated with the various sources are illustrated on Figure 4.1 which shows in diagrammatic form a composite narrowband spectrum.

On a piston engine helicopter the noise is dominated by the engine exhaust noise (at engine firing harmonics) which extends over a frequency range 100 Hz to 1000 Hz (see Figure 4.1). Such engines are only used on small light-weight helicopters and the main interest is therefore in gas turbine engined helicopters.

On gas-turbine engined helicopters inlet (compressor whine) and exhaust noise are of significance. The high frequency compressor noise is centred around 8 to 10 kHz, while the exhaust noise (not indicated on Figure 4.1) produces considerable energy in the 250 to 500 Hz region. On all the helicopters examined this noise was lower in level than the broadband rotor noise and hence no real problem and the inlet noise, although troublesome,can, according to available information, be effectively reduced by using existing methods.

Even when engine noise is taken into account, the sound is characterized by the noise produced by the rotors. On a tandem helicopter this is obviously solely main rotor noise, while on a 'Sikorsky type' helicopter both main and tail rotor noise are important. As will be noted from Figure 4.1, main rotor noise is treated as two separate entities, rotational (or discrete frequency) noise and broadband noise, while tail rotor noise is dominated by its rotational components. As explained previously rotational noise shows up on a narrowband analysis as a series of peaks or discrete frequencies at the blade passing frequency and its harmonics. The fundamental frequency associated with the main rotor and tail rotor typically lies within the frequency ranges 10 to 20 Hz and 80 to 120 Hz respectively. 10 to 20 harmonics are usually detectable as indicated on the figure and by detailed analysis 30 to 40 or more can sometimes be detected. The 'harmonic fall-off' for both rotors vary considerably although initially for the first 10 or so harmonics the rate for the main rotor is in the order of 1 dB/harmonic. Since the fundamental frequency of the main rotor is low it cannot be heard and subjectively only the higher harmonics are of interest. This results (if blade slap is not present) in a periodic 'throbbing' or 'thudding'

sound. The tail rotor on the other hand produces subjectively the characteristic rotor whine which is similar to those associated with aircraft propellers. When blade slap is present this 'banging' produces a dramatic increase in the rotational (discrete frequency) components by 10 to 20 dB in the 150 to 400 Hz range. Theoretically, therefore, blade slap could be treated simply as a severe form of rotational noise. Subjectively, however, it is easily detectable and can be readily distinguished from impulsive main rotor rotational noise. The 'source' is usually well defined in space and for all practical purposes can be considered as to be generated at a 'point'; rotational noise on the other hand is the result of the 'noise' generated by the complete rotor. For these reasons it is usual to consider 'blade slap' as a separate entity (see Chapter 5).

Broadband noise, commonly termed 'vortex' noise, shows on analysis, as outlined in Chapter 3, as a band or 'hump' of random 'broadbandish' noise spread over a relatively wide frequency range (see Figure 4.1) with the maximum level typical in the region 250 to 500 Hz. The source of this noise travels with the blade and is responsible for the characteristic 'swishing' heard by an observer when relatively close to a helicopter. There is still some confusion about the precise nature of the broadband noise and, as discussed in section 4.5, what is often termed broadband noise contains both broadband and rotational noise components. Also when examined in detail the low frequency broadband noise (150 Hz to 1.5 kHz) and the high frequency broadband noise (2 to 5 kHz) exhibit different trends and hence these two regions have to be considered separately. The 'high frequency' broadband noise may also have a 'hump', but it is narrower in bandwidth than the low frequency broadband noise and subjectively sounds like a high frequency 'broadish' whistle. It is detected on many helicopters during ground running or just prior to the application of lift. When the rotor is fully loaded or in flight it is either non-existent or below the level of the other sources.

The above aspects relating to the general topic of rotor noise are discussed in greater depth in Chapter 3.

The above comments apply to the external noise field and are to some extent relevant internally. In this case, however, the main noise source is from the transmission system. It is not uncommon for the gearbox meshing frequencies to be 20 to 30 dB above the broadband spectrum level in the cabin and since these occur at frequencies around 1 kHz

gearbox noise is subjectively very loud. This noise is subjectively described as a high pitch whine or screech and on some helicopters, particularly on the smaller designs with an open gearbox arrangement, it can be heard externally. Drive shaft noise associated with the tail rotor drive, or in the case of a tandem rotor helicopter the 'synchronisation shaft', is also often a significant problem. A brief review of internal noise is presented in section 4.14 and some trends with flight speed in section 4.11.2.

4.4. NOISE SOURCES - ORDER OF IMPORTANCE

A brief outline of the main noise sources has been given in section 4.3. From a study of the available data these have been ranked in order of importance from the subjective point of view and typically are as follows:

A. Helicopters with 2 bladed main and tail rotors:	B. Helicopters with 3 or more bladed main and/or tail rotors (including tandem configurations):
1. blade slap,	1. blade slap (if it occurs),
2. tail rotor rotation noise,	2. main rotor broadband noise,
3. main rotor rotation noise,	3. tail rotor rotational noise (if applicable),
4. main rotor broadband noise,	4. main rotor rotational noise,
5. engine noise,	5. engine noise.

It will be noted that it has been necessary to sub-divide the helicopters into two main groups - those with 2 bladed rotors and those with multi-bladed rotors (3 or more blades). The above classifications are, of course, only a general guide since they are based on taking the complete helicopter flight profile into account. In other words the relative order may change in a particular manoeuvre; for example even on a multi-blade helicopter tail rotor rotational noise could dominate during slow speed turns. Also engine noise is more important on some helicopters than others. In this context it is worth noting that the rotational components become more pronounced at high speed and thus tail rotor noise is often the main source during high speed cruise flight. It also follows that on a multi-blade main rotor helicopter, main rotor rotational noise ($\dot{B}$, item 4) will on a very high speed military design become significantly more important than the main rotor broadband noise (B, item 2). Also in this case if both the main and tail rotors are of a multi-bladed configuration it is likely that the contributions from the main rotor and tail rotor will be of a similar order.

4.5. THE BROADBAND 'HUMP'

While reviewing other investigators' work and analyzing some ISVR model rotor and real helicopter recordings it was observed that under certain conditions the 'broadband' noise (or vortex noise) appeared to depart significantly from the expected V^6 type relationship and spectrum characteristics. At this time the standard form of spectrum analysis (considered to be narrowband) was $\frac{1}{3}$ octave band or in some cases 6% bandwidth. A detailed investigation was, therefore, conducted in which the Spectral Dynamics System (section 2.2) fitted with a 2 Hz filter was used. Initially analysis was performed on data available for the ISVR 9 ft diameter model rig and a hovering Wessex. A typical result is reproduced in Figure 4.2 and it will be noted that the 'broadband' region consisted of a large number of discrete frequencies which are rotational noise harmonic orders.

These results were produced at ISVR in 1966 and were the first to show that a large number of discrete components could occur in the region traditionally considered to be broadband. This discovery had a significant effect on the approach subsequently adopted in the analysis of rotor noise and helped to stimulate many of the subsequent theoretical studies.

It was known from the tests on the ISVR single rotor rig that broadband noise free from discrete components could be obtained provided the turbulence and/or the recirculation around the rotor was small. Since it was also desirable to know if these 'peaks' also occurred in the broadband-vortex region on a real helicopter operating under design loading conditions, a carefully controlled test was carried out with a Wessex helicopter. First a survey was made of the noise around the helicopter and it was found that the minimum influence from rotational noise components occurs directly in front of the helicopter (nose on). Recordings of the Wessex, hovering at 40 ft altitude and 200 ft from the microphone, were made in normal wind conditions (wind speed about 8 knots) and again with a very low wind environment (less than 2 knots). The narrowband analysis results are shown in Figure 4.3; trace (a) shows a typical 1.5% narrowband analysis while (b) and (c) are $\frac{1}{2}$ Hz bandwidth analysis of the 'less than 2 knot' and '8 knot' wind conditions respectively. The upper trace (a) was obtained from a Muirhead K-100-A analyzer at WHL and traces (b) and (c) on the ISVR Spectral Dynamic Analyzer System with the effective $\frac{1}{2}$ Hz bandwidth being obtained by using a 2 Hz filter

and lowering the playback tape speed by a factor of 4. It will be noted there are many discrete components in the light wind case, trace (c), and that the broadband noise is practically the same for both conditions.

Further tests were carried out and these showed that similar differences could be produced with the use of different helicopters and/or pilots. The two results illustrated in Figure 4.3 do, however, tend to show the minimum and maximum discrete frequency noise content in the broadband region for this particular helicopter under controlled hover tests. It was postulated from this type of data that the high frequency rotational noise was sensitive to changes in any parameter likely to influence the transient blade loading; these could include either wind or minor inputs by a pilot to control the helicopter. This data (and that from the model rotor) also strongly suggested that to a first order broadband noise was independent of the inflow conditions (turbulence, wind, re-circulation effects etc.). This was in opposition to the generally held view that both broadband and rotational noise were a direct function of the input and operating environment. Credibility was, however, later given to the view that broadband helicopter noise was normally independent of the rotor environment following the development of generalized broadband noise formula by the author (section 4.8) and others [39, 40, 41] based solely on rotor geometry and tip speed parameters. More recently Wright [31] has come to the same conclusion and developed formulae which cover a significantly wider range than attempted by the other investigators (and the author) who were interested only in helicopter noise. This is not to imply that the level of inflow turbulence always has no effect on the level of broadband noise, since there is experimental evidence which suggests that relative to a 'clean rotor', levels up to 6 dB higher can be generated if the recirculation/turbulent effects are very large. Wright [31] also supports this view.

When the occurrence of rotational (discrete frequency) noise in the broadband region was first appreciated, many investigators changed their views on the importance of the relative contributions of the two sources and implied that broadband noise was no longer a significant factor. This is not so on the majority of helicopters, except in the case of those with 2 bladed main rotors, since if the energy is summed over a wide band the contribution to it will be greater from the broadband noise than from the rotational components when the subjective weighting is taken into account. On the other hand if a semi-narrowband analyzer (6 to 23%) is

used to measure the broadband noise the maximum level detected may be due to the discrete components. This can explain many of the apparent anomalies in the broadband velocity laws which have been found in certain helicopters. This aspect is discussed further in section 3.6 in connection with the analysis of rotor noise.

4.6. ROTATIONAL vs BROADBAND NOISE

The relative levels of rotational and broadband noise generated by a helicopter rotor, if no blade slap is present, characterise the sound. It is, of course, not simply the relative magnitude of the two classes of noise since the subjective response of the ear must also be taken into account. It is generally recognised that the lower the rotational noise relative to the broadband noise (within limits) the lower the annoyance value of the sound. In addition, as the rotational content is increased the impulsive nature of the sound increases and the loudness and annoyance rise rapidly.

From the wide range of helicopter recordings obtained by the author it was possible to assess the relative impact of the blading design parameters on both the main rotor rotational and broadband noise and determine the relative importance of the two sources. Analysis of the helicopter recordings shows that the rotational is higher relative to the broadband noise on a 2 bladed rotor helicopter than on a multi-bladed design.

The influence of the number of blades on the relative levels of the two sources can be best appreciated by considering a simplified model. If the thrust and other operating conditions are fixed then to a first order as the number of blades are increased the rotational noise will decrease by 4 to 5 dB for each blade added. This is on the assumption that the harmonic 'fall-off' profile is fixed, that the level of the fundamental is given by the Gutin steady force relationship [38] and that the tip speed is typical of that used on helicopters (600 to 700 ft/s). The broadband noise on the other hand would be expected to increase with the number of blades (according to 10 log B_2/B_1 where B_1 and B_2 are the number of blades 'before' and 'after, respectively). In practice, however, the blade radius or chord would be decreased to offset the increase in number of blades and thus to a first order the total blade area would remain constant. The broadband noise appears essentially to be dependent on the total blade area and hence would remain constant. It follows that in changing from a 2 bladed to, say, a five bladed rotor there is a 12 to 15 dB change in the relative level of the rotational and broadband noise. This effect can be clearly seen in Figure 4.4 which compares the spectra for a 2 bladed Bell helicopter and a 5 bladed Sea King helicopter.

There is, as explained in Chapter 3, large variation in the rotational noise characteristics as a function of speed. If the pitch is held constant then on a real rotor it would appear that typically the levels vary as V^{10}. A similar review of broadband noise suggests V^{6}. Thus rotational noise becomes more pronounced as the speed of the rotor is increased.

From the test data it would appear that, as a rough guide, rotational and broadband noise are of equal importance on a four bladed rotor operating at a tip speed of about 680 ft/s. The sound of a two bladed rotor is always dominated by its rotational noise at tip speeds above 450 ft/s, while a six bladed rotor can operate up to about 800 ft/s before rotational noise is really noticeable.

The above are general guidelines and not specific rules and must be treated as such. They do, however, provide a useful method of quickly assessing the general noise characteristics of a particular rotorcraft design.

4.7. ROTATIONAL NOISE

4.7.1. Main Rotor

As already mentioned up to 40 (or more) blade passing harmonics could be detected by detailed analysis. An attempt was made to correlate the harmonic fall-off with various rotor parameters, but without success. A large number of helicopter and full scale whirl tower results were, however, available and it was found that in general the first 20 harmonics lay within the range illustrated on Figure 4.5. According to theoretical considerations the results should have been studied as a function of mB (where m = 1, 2, 3, etc, and B is the number of blades), rather than in terms of blade passing harmonic number m as indicated on Figure 4.5. This was attempted but gave far inferior results to that shown.

The envelope of the results (Figure 4.5) is limited to the first 20 harmonics, since above this frequency there was a large scatter and in many cases on the real helicopter well defined rotational noise components could not be detected. In the main the data used was from multi-bladed helicopters (single and tandem rotor) although results from the Bell UH-1B and UH-1D (2 bladed main rotor), a full scale single rotor [32] and the 19 ft diameter hovercraft propeller were included [62]. The envelope up to the 10th harmonic is 'flat' for the upper limit and drops off at 1 dB/harmonic as shown on the figure.

Measurements for this study were in general made at angles corresponding to 10° to 20° below the rotor disc. Directivity effects could not be evaluated but it seemed reasonable to a first order to consider that the trends applied around the complete rotor, at least to the accuracy required for project studies.

4.7.2. Tail Rotor

Tail rotor harmonics appeared to fall off more rapidly than the corresponding main rotor harmonics. In this there was insufficient data to enable a general trend to be derived, but it did appear that the typical 'fall off' was of the order of 3/4 dB per harmonic although in some cases the fundamental and second harmonic were of a similar level.

4.8. BROADBAND NOISE - EMPIRICAL FORMULA

4.8.1. ISVR Relationships

From the analysis of a wide range of 'hover data' available at ISVR an empirical broadband prediction formula was developed. The approach adopted was somewhat different than used by other investigators in that, rather than assuming the noise was of broadband origin depending on the type of relationship developed by Yudin [59] and subsequently proposed for propellers by Hubbard [60], correlation of the data was made on the basis that the noise was dependent on the physical blade parameters, the total thrust and the tip speed only. In other words it took the form of

$$SPL_{B/B} \propto V_T^a.R^b.c^c.t^d.B^e T^f, \qquad (4.1)$$

where V_T = tip speed, R = rotor radius, c = blade chord, t = blade thickness, B = number of blades and T = Total thrust.

The data was to some extent inadequate for the study envisaged; also the range of parameters was limited. Even so a somewhat surprising result was obtained in that the dependency on thrust vanished and 'R.c.B' was replaced by the total blade area S. The final relation obtained was:

$$SPL_{(500)} = 60 \log V_T + 10 \log S - 100 \text{ dB} \qquad (4.2)$$

The $SPL_{(500)}$ refers to the level at a distance of 500 ft from the rotor at angles, relative to the vertical rotor axis, of 70° to 80°. This $V_T^6.S$ dependency agrees well with the equation 3.2, derived from reference(58), and the original work of Yudin [59], (see section 3.15.2). It was not possible to determine any directivity term since the majority of the data had been derived from measurements made at positions typically 10° to 20° below the rotor disc plane. Even so it did appear that the influence of directivity was small, although there was some evidence to suggest that the noise level decreased in the plane of the rotor.

Results obtained by using equation (4.2) are compared with measurements for a number of helicopters in Table 4.1. It will be observed that relatively good agreement is obtained; this is however not surprising since all the data except for the Lynx and Sea King was used in the derivation of the relationship. Boeing-Vertol has also used equation (4.2) to predict the noise level associated with a large 3 bladed rotor and found it agreed within 2 dB with the measured results [63].

In the context of the formula (equation (4.2)) it is worth noting that since the blade loading of the majority of helicopters is to a first order similar (typically 60 to 90 lb/ft^2) differences in total thrust are essentially taken into account by the blade area term S.

Subsequent to the development of equation (4.2), a second review was made of the helicopter data in the light of the formulae developed by other investigators: namely Goddard and Stuckey [39], Davidson and Hargest [40] and Schlegel et al [41], all of whom suggested that thrust (T) was an important parameter. By this time additional helicopter and whirl tower data was available and this led, with a T^2 relationship assumed in the data reduction, to

$$SPL_{(500)} = 20 \log V_T + 20 \log T - 49 \text{ dB} \qquad (4.3)$$

This at first glance may seem radically different from equation (4.2), but if it is remember that

$$T = \tfrac{1}{2}\rho c V_T^2 S.C_{LT} \qquad (4.4)$$

and that for a typical helicopter operating in the hover $C_{LT} = 0.18$*, then it can be shown that for all practical purposes the two solutions are identical at realistic tip speeds/thrust values for Sikorsky type helicopters, the main difference being that instead of a '10 log S' term as in equation (4.2), it is effectively a 20 log S term in equation (4.3).

A comparison between equation (4.2), equation (4.3) and test data is given in Table 4.1. It will be observed that although the difference between the two solutions is typically only 3 to 4 dB, in the case of the Bell UH-1B and Gazelle there are 5 dB and 9 dB discrepancies respectively. A comparison by the author on a complete range of helicopters has indicated that differences up to 12 dB can result and that when the differences are large the test data tends to be above the value given by equation (4.3).

*$C_L = 3C_{LT}$ 0.5 to 0.6 for a typical helicopter

The scatter between either equation and the test data is typically ±5 dB and thus it is difficult to determine which is more appropriate. The author, however, favours the former (equation (4.2)), since there is some theoretical justification for it and although a number of investigators have implied a thrust (T) relationship, this does not appear to be supported by the test data. In this context it is of interest to note that the formulae recently proposed by Wright [31] although more complex in that a larger number of parameters are taken into account, supports the case that the broadband noise does not contain a direct thrust (T) term. Recent work by the author at WHL has suggested that the blade thickness and/or angle of attack are more important than the absolute thrust value [34]. Thus the author would propose use of equation (4.2) for prediction of helicopter noise (within ±5 dB) although the final value would normally tend to be slightly on the high side.

4.8.2. Other Formulae

The hover noise generated by a multi-blade helicopter is, as mentioned in section 4.4, controlled essentially by the level of the broadband noise. This is particularly true when the subjective response is taken into account since even if the level associated with the main rotor blade passing frequency and its first few harmonics is relatively high, it will effectively be ignored in the calculation since it occurs at low frequency. Also the influence of the tail rotor, even if the noise is pronounced, on the overall noise level is extremely small (see section 4.12.4). It follows, therefore, that in practical terms the total noise or overall noise will be equal to the total broadband noise. This was particularly true at the time that the semi-empirical predictions were being developed since the tip speed of the typical main rotor was only 650 to 670 ft/s. Over the years there has been a tendency to increase the main rotor tip speed and now values of 700 ft/s and above are common. Thus the rotational noise has tended to increase, relative to the broadband noise, and the original assumption is not now so valid as it was originally. It follows that although in various papers the predictions were stated as being applicable to overall noise, they are now normally taken to refer to the broadband noise content only. In this context it is also worth noting that in the main studies of interest the empirical formulae were based on either Sikorsky type helicopters or Sikorsky designed rotor blades on test stands [39, 40, 41].

4.8.3. Comparison of Prediction Methods

The four broadband (overall) noise formulae examined by the author were those developed by Davidson and Hargest [40], Goddard and Stuckey [39], Hubbard [60] and Schlegel et al (Sikorsky Aircraft) [41]. The general characteristics of these are outlined in Appendix 3 and where appropriate the formulae are quoted for values at 500 ft (152m) distance at (a) an angle of 15° below the rotor disc and (b) directly under the rotor disc.

The Hubbard formula [60], and equation (4.2) devised by the author, take a similar form in that the SPL is assumed to be proportional to $V_T^6 S$ and independent of angle to the rotor. The author's formula (equation (4.2)), however, gives a solution which is 15.8 dB higher in absolute terms than that obtained by using Hubbard's relationship.

The Davidson and Hargest relation [40], which is generally considered to be the most appropriate of all those available, gives a $V_T^2.T^2.S^{-1}$ relationship. In the Sikorsky solution [41] the noise is assumed to have the same dependency as the Davidson and Hargest relationship but the result is given for one angle (75° to rotor axis) only at 300 ft. If an appropriate allowance is given for distance according to the inverse square law then it can be shown that at this angle the Sikorsky result is 6 dB below that given by the Davidson and Hargest formulae. In this context it is worth noting that whereas Sikorsky obtained their results from a relatively high whirl tower, the Davidson and Hargest data was obtained from real helicopter measurements supplemented with data from a low level whirl tower [39]. Intuitively the Davidson and Hargest data would be expected to be higher and, although every effort was obviously taken by the authors to remove the influence of other sources in the helicopter case and recirculation effects from the tower tests, this is extremely difficult and complex and could account for the difference.

The Goddard and Stuckey solution [39] suggests that the noise followed a $V_T^{2.60}.T_B^{1.66}$ law; in their paper, however, T_B is defined as the thrust per blade (and not total rotor thrust). There appeared, however, to be some general confusion on the precise details of their formula and for this reason it was not examined by the author in any depth. They did, however, propose a $\sec^2\Phi$ relationship in a manner similar to that of Davidson and Hargest. A comparison was made between the various methods for a wide range of helicopters by the author and a summary of some of the results is presented in Table 4.1. Values for the Davidson and Hargest formula are quoted at $\Phi = 0°$ (directly under the rotor) and $\Phi = 75°$ which corresponds to the angle at which the test data has been typically obtained.

It is not proposed to discuss these comparisons in depth, but a number of points are of general interest. Firstly the Hubbard solution gives a value which is extremely low and would appear inappropriate for the prediction of helicopter noise. The author's formula (equation (4.2)) agrees well with those of Davidson and Hargest at the $\Phi = 0^{\circ}$ position (directly under the rotor). At $\Phi = 75^{\circ}$ there is, however, a 10 to 15 dB difference with the Davidson and Hargest solution being lowest and below the test data. It would appear, therefore, that the error lies in the directivity term. It may, however, equally be in the test data since there is a tendency for the decay of the rotor noise in the rotor disc plane to be 'filled in' by other sources. Overall the accuracy of these methods, particularly that proposed by the author which can only be described as 'crude', is ± 5 dB. They can, however, be used to give an estimate of the likely 'hover' noise levels and general trend characteristics to be obtained. It will also be observed from the test data that the noise level is essentially independent of size of the helicopter.

4.9. EMPIRICAL PREDICTION METHOD

An empirical prediction method based on the rotational noise (discrete frequency) characteristics outlined in section 4.7.1, the (low frequency) broadband noise spectrum discussed in section 3.8.4 and the broadband (ISVR) formula (equation (4.2)) reviewed in section 4.8 was devised. This excluded engine noise and tail rotor noise. This was considered acceptable since on a helicopter the engine noise in the low and mid frequency regions (below 1 kHz) was generally below the level of main rotor noise and if engine noise was to be 'added' into the spectrum it usually took the form of simple addition of a measured octave spectrum. In the case of tail rotor noise ignoring its contribution was not really justified, but since it had been established that the level of the tail rotor noise had little effect on the overall spectrum it was considered acceptable to base the calculations solely on the main rotor parameters. At a later stage at WHL [64] tail rotor rotational noise was added by using a modification of the method devised by Ollerhead and Lowson [30] but this procedure did not significantly affect the accuracy when studied in terms of broadband, octave band or dB(A) noise levels.

Using the broadband formula given by equation (4.2) and the general spectrum shape discussed in section 3.8.4, use was made of the relationship SPL (band) = (Spectral level) + 10 log Δf_w, where Δf_w is the bandwidth

in Hz, to convert the broadband levels into the corresponding spectral values. From knowledge of this and the corresponding rotational noise content (based on the Gutin value and the harmonic content envelope) the complete spectrum was compiled. An example for the Wessex is shown in Figure 4.6. Once such a complete spectrum had been obtained it could be simply 'weighted' as required and an estimate of the dB(A) or PNdB level obtained. This method was later applied at WHL to a wide range of helicopters and an SRN4 (hovercraft) propeller and it was found that the results were typically within ± 3 dB(A) of the 'hover' values. It is fair to point out, however, that in some cases differences up to 10 dB were found between the predicted and measured results. This usually occurred in the case of helicopters with vastly different parameters than used in derivation of the original formula: a helicopter with a high tip speed rotor or an exceptionally large chord, for example. This is not surprising when it is remembered that all the prediction methods contained a constant term derived from measurements. Even Wright's latest refinement [31] - which gives good agreement for a wider range of rotor - still suffers from the limitation of an empirical constant.

4.10. FLIGHT TESTS - EFFECT OF HOVER HEIGHT

A number of flight tests were carried out in conjunction with WHL in order to enable the various differences in noise levels with hover height, distance, etc, to be determined. The test work was funded by the MOD and carried out with a Wessex Mk.3 (XT 255) helicopter operating over a grass airfield. Measurements were made with standard instrumentation and in the case of the ground measurements the microphone mounted at a height of 3 ft (0.9 m).

4.10.1. Variation of Noise with Distance under Helicopter

With the helicopter hover at 1000 ft (305m) altitude (to reduce any ground effects) measurements were made with a microphone suspended at 7 ft (2.1m), 17 ft (5.2m), 27 ft (8.2m), 37 ft (11.3m) and 77 ft (23.5m) below the wheel level. The wheel-to-rotor distance on the Wessex is 14 ft (4.1m) and hence the corresponding distance rotor clearance is the 'quoted value + 14 ft (4.1m)'. The general characteristics for the main rotor and tail rotor harmonics are indicated on Figure 4.7. It can be observed, except for 8R (2nd main rotor blade passing harmonic), that above a clearance of 17 ft (5.2m) the fall-off rate follows closely the inverse square law.

The equivalent octave band spectra are shown in Figure 4.8; here only when the clearance is about 37 ft (11.3m) is there any real indication of the inverse square law. It can also be noted that the spectrum shape is independent of helicopter/microphone clearance.

4.10.2. Variation of Noise with Altitude

In the second series of tests the helicopter was hovered over a microphone (mounted at a height of 3 ft ~0.9m) and with wheel clearance altitude 10 ft (3m), 20 ft (6m), 30 ft (9m), 40 ft (12m), 80 ft (24.4m), 160 ft (49m), 320 ft (97.5m) and 640 ft (195m). The variations of the main rotor and tail rotor harmonics with height are indicated in Figure 4.9; the 640 ft (195m) values are not quoted because of the difficulties in reading the results from the narrowband traces. It will be noted that above a height of 40 ft (12m), which is approximately a rotor diameter (56 ft, 17m) ground-rotor head clearance, the noise levels decrease approximately according to the inverse square law. The corresponding octave band results are presented in Figure 4.10 and it can be noted that in this case the inverse square is not applicable until the altitude is 160 ft (49m), approximately 3 rotor diameters. There is a larger influence on the high frequency components; this is considered to be due to changes to the directional characteristics of the engine, rather than the impact of atmospheric absorption.

4.10.3. Comparison of 'Free Field' and Ground Microphone Results

There are some differences between the two sets of results, as can be seen by comparing Figures 4.7 and 4.9 and Figures 4.8 and 4.10. The 'free field' results are considerably lower; this can be best seen on the octave band plots where it will be observed that the '77 ft' (23.5m) value on Figure 4.8, which in theory corresponds to the '80 ft' (24.4m) result on Figure 4.10, is nearer the levels associated with a distance somewhere between 160 ft (49m) and 320 ft (97.5m). Even when taking into account possible ground reflection and the possible enhancement of the levels due to thrust reinforcement due to 'ground effect', this large difference cannot be explained. It would appear, however, that ground effect is significantly larger than anticipated. It can also be observed that the low frequency part of the spectrum - the main rotor rotational noise and to some extent tail rotor noise - is absent on the measurements made at height (free field case) while being clearly detectable on the straight forward hover tests. This can also be seen from the main rotor and tail rotor rotational results Figure 4.7 and 4.9.

This could be the influence of nearfield effects, unlikely since inverse square law is followed at the larger distances, or fuselage shielding effects. This is again unlikely since the main rotor is 56 ft (17m) diameter compared to 8 to 10 ft (2.4/3m) of the airframe and there is no shielding between the tail rotor and the micopphone. It is, however, more likely to be associated with the fact that in the high altitude tests the microphone was directly under the rotor axis, while in the case of the hover tests the helicopter was possibly to one side of the 'true datum'. This aspect was, unfortunately, not investigated in detail.

4.10.4. Microphone Cancellation Effects

During these tests the opportunity was also taken to quantify microphone cancellation effects, since there appeared to be general confusion on this topic. Corresponding measurements were made with the microphone at 3 ft (0.9m) and 5 ft (1.5m) ground clearance. Analysis was performed on the 1.5% Muirhead analyzer at WHL and the results are shown in Figure 4.11 for the frequency range 100-2000 Hz. The results are shown as a function of helicopter hover height and, as can be seen, cancellation effects are not clearly detectable until the altitude reached is 40 ft (12m) and also as the height is increased and the helicopter becomes more of a point source, the cancellation effects become more pronounced. The cancellation 'troughs', denoted as $1f_c$, $2f_c$, etc, are caused by phase cancellation due to the microphone height above the ground, with the height being $\frac{1}{4}$ of the cancellation frequency. In other words

$$(2n + 1)f_c = c/4h \qquad (4.5)$$

where n = 0, 1, 2, 3 etc, f_c = cancellation frequency Hz, h = microphone height and c = velocity of sound = 1120 ft/s.

It follows that for 3 ft (0.9m) and 5 ft (1.5m), the corresponding cancellation frequencies are 93 Hz and 56 Hz respectively. The figures show the cancellation frequencies at (2n+1)97 Hz (h=2.89 ft) and (2n+1)58.5 Hz (h=4.78 ft) which is either due to inaccuracies in setting up of the microphone height or more likely 'ground effects'; it is possible that the weight of the microphone/tripod caused it to sink into the ground after initial set-up.

4.11. FLIGHT TESTS - INFLUENCE OF FLIGHT SPEED

4.11.1. Main Rotor/Tail Rotor Rotational Noise

The variations of the main and tail rotor rotational (discrete frequency) harmonics over an I.A.S. from 20 to 100 knots are illustrated in Figure 4.12. These measurements were taken in the mid-cabin area on

a Wessex Mk.3 helicopter. It will be observed that although there is a slight indication of an increase in level with forward speed, the scatter is such as to prohibit any definite conclusions. 8R and 12R (where R is the rotational frequency on this 4 bladed rotor) both show a significant decrease in level as the speed is increased from 20 to 40 knots. 16R also exhibits a sudden decrease in level between 60 and 80 knots: these trends cannot be explained. In the context of these results it should be remembered that the microphone was directly under the main rotor axis inside the cabin and only 7 ft (2.1m, approximately 0.15 rotor diameters) below the rotor centre. There is, therefore, extreme difficulty in interpretation of these near field results. Also if it is argued that the noise is generated at the tip region, then the changes in speed over the test ranges are less than would appear at first glance. Considering the Wessex Mk.3 with a main rotor tip speed of 670 ft/s, then at 100 knots the combined speed is only 840 ft/s. Assuming, say, a V^{10} relationship for the rotational noise would in this case suggest a 7.6 dB increase over the speed range 20 to 100 knots. On average it would appear that the results show this order of difference, although as can be seen on Figure 4.12 there are significant departures from the general trend.

4.11.2. Cabin Noise Levels

The corresponding cabin noise, measured in terms of 1/1 octave bands on a Wessex Mk.5 helicopter, for the range of speeds examined, is shown in Figure 4.13. It will be noted that to a first order (within $\pm$ 2dB) the levels are identical for all flight speeds tested (hover to 100 knots). There is, however, some increase in main rotor rotational noise which controls the 31.5 Hz octave band. Data recorded on other helicopters was examined in a simpler manner and although in general the results were less precise, it is generally clear that the levels are independent of flight speed. The main exception to these general trends appears to be in the case of helicopters where the 'engine noise' propagates into the cockpit area and dominates the spectrum - typically, in the 8 kHz octave band. This is particularly true in the case of Sikorsky S61 and Sea King designs where the engine inlets are directly above the Perspex canopy of the cockpit. In this case the directivity characteristics of the compressor note appear to be very dependent on inflow conditions. The levels in the cockpit associated with the engine show large variation between hover and 20 knots, after which they remain constant with increases in speed.

Rotor speed variations normally have little effect on the cabin noise level as illustrated for the Wessex Mk.3 in Figure 4.14. This is not surprising since both the gearbox response and the cabin structure response would not be expected to vary significantly for the small changes in rotor speed possible.

4.12. RATING HELICOPTER NOISE

4.12.1. Rating Methods

Helicopter noise has been traditionally rated in terms of either the Perceived Noise Level - originally designated as PNdB but now more commonly abbreviated as PNL - or the dB(A) value. The former is based on the method developed for aircraft noise and is used extensively within the aircraft industry. When comparing helicopter noise with traffic and /or community noise levels it is more usual to adopt the dB(A) unit. There is a fairly well established relationship between the two units for a wide range of 'noises' including helicopter noise and thus there is little to choose between the PNL (PNdB) and dB(A) methods for general use. The PNL is, however, more sensitive to changes in spectrum shape and the recent Effective Perceived Noise Level (EPNL) methods allow 'tone' and 'duration' corrections to be applied. Also if temperature, humidity and distance corrections have to be applied, the $\frac{1}{3}$ octave band spectra levels have to be used and hence there is an obvious advantage in using the PNL method which is based on such analysis. In this context it is worth noting that during the early phases of this helicopter study octave band (often written as 1/1 octave band) results were the norm covering the range from 63 Hz to 8 kHz (centre frequency values); emphasis was subsequently placed on $\frac{1}{3}$ octave band analysis over the range 50 Hz to 10 kHz. This covers the same effective frequency range but instead of 8 octave bands, 24 $\frac{1}{3}$ octave bands are used.

In this section the applicability of use of the PNL and dB(A) methods for rating helicopter noise is discussed. No mention is made of the severe impulsive noise/blade slap case, however, since this is discussed in general in Chapter 5 and in particular in section 5.10.7. It should also be noted that since PNL and dB(A) give for all practical purposes identical results, the conclusions and general observations are equally applicable to both forms of analysis.

4.12.2. Non-Impulsive and Minimum Tail Rotor Noise Case

The time history of a non-impulsive helicopter noise is essentially random in character, taking the form indicated in Figure 4.15 which shows a result for a Wessex (S.58) helicopter. If the tail rotor noise

is low then on $\frac{1}{3}$ octave band analysis the spectrum is fairly 'uniform' in the mid-frequency region and shows a 'fall-off' in level at the higher frequencies as indicated in Figure 4.16. In the low frequency bands, the spectrum tends to be 'peaky' due to the influence of the main rotor (and to a lesser extent tail rotor) rotational noise components and at high frequency (8 to 10 kHz) the engine compressor whine gives rise to a 'peak' as indicated on Figure 4.16. When the 'engine peak' is ignored it is fairly clear that the PNL value is a fair representation of the complete spectrum, particularly when it is remembered that the PNL (or PNdB) unit was originally based on broadband jet engine noise. In this context it is worth noting that the 'peaky' low frequency region has little or no effect on the computed PNL value.

The engine compressor 'whine' is identical to that associated with conventional aircraft engines and thus the PNL concept, particularly if the 'tone correction' of the EPNL method is taken into account, can be expected to give an accurate rating of its annoyance. It seems fair to conclude, therefore, that providing the helicopter noise is of the type described above the PNL method - and by implication the dB(A) - is a good estimation of the overall annoyance/loudness.

4.12.3. Blade Slap - Impulsive Noise Case

This is discussed in section 5.10.7.

4.12.4. Tail Rotor Noise

During the various analyses it was clear that even if the helicopter noise exhibited a high content of tail rotor noise which showed up on narrowband analysis, it did not appear to influence to any great extent the overall or dB(A) level. The situation appeared to be somewhat similar to that connected with 'blade slap' which had little influence on the dB(A) or PNL value (section 5.10.7). A small study was, therefore, undertaken to evaluate this aspect.

Tail rotor noise, as explained previously, shows up on narrowband analysis as a series of discrete frequencies at the blade passing frequency and its harmonics. It is usual to be able to detect 10 harmonics and often in forward flight - and to a lesser extent during low speed 'on the spot' turns - it is often this noise which dominates. This is particularly true on small helicopters where two blade rotors are normally used. The tail produced, as discussed earlier, a characteristic whine which is akin to that generated by a propeller and hence is subjectively very noticeable.

A dB(A) time history for a Scout helicopter which exhibits a high level of tail rotor noise is reproduced in Figure 4.17. Also shown on this figure is the corresponding trace for a Wessex (S.58) helicopter which generates little tail rotor noise. For comparison purposes the two recordings were adjusted so that in each case the maximum level reached was 90 dB(A). 'Real time' narrowband analyses were performed on both recordings at the positions ('times') indicated on Figure 4.17: these are reproduced in Figure 4.18. It will be observed that on approach the tail rotor harmonics dominate the Scout recording while in the case of the Wessex the spectrum consists of main rotor and tail rotor rotational and broadband noise arising from the main rotor, engine exhaust etc. Although subjective studies were not made, as can be imagined the two helicopters sound very different; tail rotor noise on the Scout gives rise to complaints and is readily noticeable on approach, while the Wessex (which in practice generates higher levels than the Scout at a similar distance) does not give rise to any adverse comment.

The $\frac{1}{3}$ octave band spectra corresponding to the results presented in Figure 4.18 are reproduced in Figure 4.19. The corresponding PNL values are also indicated on the figures as are the $\frac{1}{3}$ octave bands controlled by the tail rotor noise. When compared in terms of EPNL, in which the noise level within the 'maximum -10 dB band' is considered, the Scout gives a value which is 2 PNdB higher than that for the Wessex and part of this (approximately 1 PNdB) is due to the difference in the duration correction arising from the slightly different flight speeds of the two helicopters. This, in the opinion of the author, is an underestimate of the relative differences.

This was further examined by taking the $\frac{1}{3}$ octave band for a condition with the maximum contribution of tail rotor noise; this is illustrated in Figure 4.20. The corresponding spectrum was then estimated for the case if the tail rotor noise was removed: in this case only two $\frac{1}{3}$ octave bands are affected to any extent as indicated on the figures. The PNL values for the two cases were then calculated and the difference is only 1.3 PNdB. When the tone correction procedure of the EPNL method was applied the difference was increased by 1.7 PNdB to give a 3 PNdB difference between the 'tail rotor' and 'non-tail rotor' conditions. These differences are extremely small when compared to the subjective difference. It must also be remembered that in many cases tail rotor noise, even when it can be clearly detected, has little or no effect on

the ⅓ octave band spectrum. There is no real evidence available on the subjective effect of the rotor noise but it is worth noting that in the recommendations in the Wilson Report [65], later incorporated in BS.4142 [66], a correction of 5 dB(A) is added to the measured value to take account of the tonal character of a noise which has a definite distinguishable continuous note such as a whine. It would appear therefore that a similar correction is required in this case if the noise is dominated by that from the tail rotor.

4.13. MAGNITUDE OF FLUCTUATING FORCES

The importance of fluctuating force on the generation of rotational noise has already been outlined in section 3.15.1. A review was, therefore, made to determine the levels likely to occur in practice, but the study had to be of a limited nature because of the lack of data. Even so there were a number of clear trends as summarized in Figure 4.21. As can be seen, results from the UH-1 and the H-34 (S.58) helicopters [67, 68] show the same general characteristics with the 1st blade loading harmonic being of the order of 1/10th of the steady state loading. Thereafter the harmonic context decays with what is for all practical purposes an inverse first power law. It should be emphasized, however, that the experimental aerodynamic data shows considerable scatter, with the amplitude of individual harmonics having variations from the 'mean' well in excess of ± 50%. The NH-3A (S61-F) data [69] gave similar decay rates in the hover, and at measurement positions near the tip for most forward flight regimes, to those on the UH-1 and H-34. At high forward speed (190 kts) and the 'inboard stations' for other flight cases the mean 'fall-off' was nearer an inverse square law. This first harmonic for this helicopter as indicated on Figure 4.21 often exceeded the steady state. This could not be explained but a review of the data suggested that the steady state values were in error.

If the inverse first power law is taken as a fair representation of the aerodynamic harmonic blade loading, then the predicted noise spectrum will be essentially 'flat' if a point loading concept is considered. Applying Wright's attenuation factor [70] suggests a 6 dB/octave fall-off rate above an mB of 10 and thus for a four-bladed rotor, the rotational noise would decay at this rate above the 2nd blade passing harmonic. Measurements (section 4.7) indicate the noise fall-off rate on many helicopters lies between these two values.

4.14. ROTATIONAL NOISE STUDIES

Even though the aerodynamic information was limited, some studies were carried out in an attempt to highlight some of the important points connected with the prediction of rotational noise.

4.14.1. Wessex/S.58 Helicopter

Calculations were made using the H-34 (S.58) flight data [68] for the hover condition with the aid of a Sikorsky Program [41] modified to run on the Atlas computer by Tanna and the results compared with Wessex (S.58) measurements. The aerodynamic data was restricted to 10 harmonics which implied that for a four bladed helicopter such as the S.58 the levels would not be expected to be correct above the 2nd rotational noise harmonic; even so it was expected that the general trends would apply.

Figure 4.22 compares results for 'Starboard (St'bd) On' and predicted levels for hover (steady load only), hover (steady + fluctuating loads) and an 11 knot flight condition. Also shown for reference is the Gutin (steady force) prediction. As expected the levels are vastly under-estimated at the higher harmonics and even the predicted 2nd harmonic is 10 dB or so low. It will also be noted that the predicted levels for the slow forward speed condition are slightly lower than the hover results. The dramatic impact of using the fluctuating forces in preference to just the steady values is also illustrated.

A more detailed comparison was made and this is shown in Figure 4.23. There is again a similar difference between the measured and predicted values and although the 15 dB variation in the level of the rotational noise components measured around the helicopter is predicted, the measured and calculated values are 90° displaced. Main rotor discrete frequency noise is usually a maximum in line with the tail (Tail ON), while calculations suggest it occurs on the port side. This was examined but a satisfactory explanation could not be found. The directivity associated with this investigation is shown in Figure 4.24 together with some measured values. It is of interest to note the dip in the first harmonic at 10° to 15° above the disc and the general circular nature.

4.14.2. Trailing Edge Lift Fluctuations

Measurements made in the hover and slow forward speed flight conditions give similar results and to a first order they are similar to rotor noise measurements made on a whirl tower in 'dirty flow' conditions. In the hover the span loading variations would be expected to be at a

minimum and it was postulated that the trailing edge (chord) fluctuations might be significant. This aspect was evaluated by considering the three conditions illustrated in Figure 4.25 which shows an ideal hover profile and the two ranges of lift fluctuations considered. Figure 4.26 shows the form of the assumed pressure variations at the two chord stations considered (70% and 90%). Since it is not possible to calculate the effects of small non-uniform flow in the hover, this was extracted from forward flight data prepared by WHL in connection with a particular project study. The corresponding rotational noise predictions obtained by using a point span program are given in Figure 4.27. The effect of the small amplitude trailing edge lift fluctuations is clearly shown. The minimum blade lift calculation increment of 5° prevented estimations above the 9th noise harmonic for the four blade rotor considered. It will be observed that the noise levels at the 8th harmonic are 40 dB above the steady loading (ideal hover) value. The levels of the two fluctuating cases are approximately the same and this is due to the common phase relationship inherent in the values used. The importance of trailing edge lift fluctuations is clearly illustrated.

4.14.3. Lynx Study

A similar study to that described above was made with the lift variations predicted for the 0.93R (93%R) station on the main rotor of the Lynx at 160 kts being used. In the estimations the helicopter was assumed to be fixed relative to the observer and hence the additional acoustic 'distortions' due to the forward speed were ignored. The spectrum at 15° below the rotor at a distance of 200 ft (61m) is given by the 'dashed line' on Figure 4.27 and the directivity around the rotor at 200 ft (61m) distance is shown in Figure 4.28. The calculations were again based on a point span model and take no account of the possible 'attenuation' (cancellation) of the higher harmonics proposed by Wright [28]. The aerodynamic data included the effect of shock wave formation on the advancing blade, and the 'rising' spectrum indicated that, as confirmed on the real helicopter, the main rotor noise would be fairly impulsive at 160 kts flight speed. The directivity plots show a large number of lobes due to the phase relationship in the input data: if a random phasing had been assumed between the various loading harmonics then the patterns would have been smoother and more like those presented in reference(30).

4.14.4. Azimuth/Elevation Variations

In an attempt to shed light on the difference between the Wessex (S.58) measured and predicted results mentioned in section 4.14.1, a series of calculations based on the WHL Lynx (WG-13) aerodynamic loads were made for azimuth angle of 0° (Tail ON), 90°, 180° (Nose ON) and 270° for 0° (in rotor disc plane) and -15° elevation. The results are reproduced in Figures 4.29 and 4.30. It will be noted that in the case of the 0° (in rotor disc) results the minimum value corresponds to the 'Tail ON' (0°) position and the highest levels at 90°. This is more akin to the Wessex 'hover' measurements (Figure 4.23). At -15° elevation, however, the results exhibit considerable variation with the minimum and maximum value at azimuth angles of 90° and 180° respectively. These results do not in themselves indicate any clear trends; they do, however, show the sensitivity and variation both with azimuth and elevation angles. Similar calculations were made for 180° azimuth position (Nose ON) at elevation angles of 0° (in rotor disc plane), -15° and -90° (along rotor axis ; under rotor) and the results are illustrated in Figure 4.31. These suggest that highest levels occur under the rotor: this is not substantiated in practice, but the increase at -15° (relative to 0°) is supported by test results.

These results are presented to illustrate the general trends and although no particular emphasis can be placed on the actual levels, the importance of lift fluctuation on the harmonic content and the sensitivity to azimuth and elevation angles is clearly illustrated.

4.15. INTERNAL NOISE

Although the topic of internal noise was outside the main scope of the research programme a general review was made during the various Wessex noise tests conducted in conjunction with WHL. The results of these exercises are discussed below.

A narrowband analysis which illustrates the internal noise content of a helicopter is reproduced in Figure 4.32. Although this is based on measurements made in the Wessex (S.58) it is representative of all helicopters with a separate cabin area. In small helicopters where the cockpit and cabin are effectively one, then higher levels of main rotor noise, engine noise (particularly if the inlets are situated above and aft of the cockpit) and sometimes tail rotor noise are detected. As can be seen the spectrum is dominated by gearbox noise and often the

2nd and 3rd harmonic of the 'gear meshing' noise is predominant. This is not surprising since in most helicopters the transmission system is mounted on the cabin roof and hence in close proximity to the area occupied by the passengers. Also to allow 'control runs' etc, there is nearly always a number of large 'holes' in the roof area. Even so in addition to the airborne noise, it is clear that a considerable amount of the noise is structure-borne. Thus the solution is basically one of engineering where vibration isolation, structural damping and 'sound proofing' must be incorporated in the original design. Except for the latter of these techniques this is, however, not a simple matter, since on many helicopters a 'soft mounting' between the gearbox and airframe is not acceptable because of control and airframe response and damping materials, although effective, introduce a severe weight penalty. An alternative approach which has been adopted by some manufacturers is to use a sealed isolated 'inner cabin' when low noise levels are required [71, 72]. Considerable effort into the reduction of gear noise and airframe response has taken place over the years and although it is outside the scope of this report, it is fair to conclude that it has to date not been very successful. Thus 'quiet helicopters' have usually only been obtained when bulk sound proofing or separate isolated 'inner cabin' schemes have been installed.

4.16. CONCLUSIONS

1. Helicopter noise is complex in nature since it is a combination of several sources which generate sound by more than one mechanism.
2. The dominant source on a 'piston engined' helicopter is the engine exhaust: on a helicopter with a gas turbine engine the engine noise is of secondary importance although the compressor whine can be clearly detected.
3. Blade slap is the most dominant source on any helicopter - on a helicopter with a 2 bladed main rotor it can occur during all regions of flight. (This is discussed in detail in Chapter 5.)
4. On small helicopters which traditionally have 2 bladed tail rotors, the tail rotor is the second most annoying source - on larger helicopters which traditionally have tail rotors with 3/4 blades, main rotor noise is the loudest noise.
5. On a two bladed main rotor, rotational noise is the most important mechanism, while on a multi-bladed rotor operating at conventional tip speeds (in the order of 650 ft/s) broadband noise mainly controls the total acoustic output.

6. The higher the rotor blade tip speed (and the lower the number of blades) the more impulsive and annoying the overall helicopter noise.
7. Broadband noise is a major source, although a significant portion of the energy previously described as broadband noise or 'vortex noise' is higher rotational harmonic noise.
8. Discovery of the high rotational harmonics in the broadband noise region had a significant impact on the understanding and theoretical development of rotor noise.
9. Broadband noise is for all practical purposes independent of the inflow environment and controlled solely by the blade physical dimensions and tip speed.
10. Rotational noise appears to be influenced to a large degree by the input flow field: on real helicopters, however, the decay rate for the first 20 main rotor rotational harmonics is fairly well defined and a 'fall-off' characteristic has been established.
11. The 'harmonic decay rate' for tail rotor rotational noise is higher than that for the main rotor: tail rotor noise is solely rotational (discrete frequency) in character.
12. A simple 'broadband' noise model based on blade tip speed and blade area was developed from the data available at ISVR. Further refinements based on the assumption that the noise should vary as $(\text{thrust})^2$ did not give any better correlation with test data.
13. An empirical prediction method based on simple parameters available in the design stage has been developed. This gives in general good agreement (± 3 dB), but large errors can result if used for non-conventional design.
14. In 'free field' (at high altitude) the rotor noise falls off in accordance with inverse square law at distances greater than 1 rotor diameter.
15. When hovering above the ground a microphone/helicopter separation of 1 rotor diameter is required before the 'fall-off rate' approaches the inverse square law.
16. 'Free field' noises are considerably lower (by up to 10 dB) than those derived from ground measurements even when taking into account rotor ground effect and acoustic reinforcement/cancellation effects.
17. Microphone cancellation effects can be clearly detected when making measurements of a hovering helicopter on the ground; thus correction of test data is possible.

18. Rotational noise (main rotor and tail rotor) only shows a slight increase in level with flight speed when measured in the cabin. (Tests were, however, only conducted over a limited flight speed range.)
19. Cabin noise levels are to a first order independent of flight speed and remain within $\pm$ 2 dB the same as those measured in the hover, except in the low frequency band (31.5 octave band) which shows a slight increase.
20. Standard PNL and dB(A) rating methods do not appear applicable if high levels of tail rotor noise are present on the helicopter. (Similar results occur in the case of blade slap: this is discussed in Chapter 5.)
21. Fluctuating forces, which are important from the point of view of generation of rotational noise, decay at a rate which approximates the inverse square law. This gives (from Wright's theory [28]) acoustic fall-off rates consistent with measurements.
22. Calculations of the rotational noise show good agreement for the first two harmonics (as expected), but the trends for higher harmonics do not follow those observed on a real helicopter.
23. Blade chord trailing edge fluctuations can have a significant influence on the generated rotational noise levels.
24. Available data indicates that rotational noise is very sensitive to minor changes in input condition and large variation with azimuth and elevation can be expected.
25. High speed helicopters (Lynx) would be expected to generate very impulsive main rotor noise.
26. Internal noise is controlled essentially by the meshing frequencies (components) of the main input gears in the gearbox and high level discrete frequencies are obtained.
27. Cabin noise levels are essentially independent of minor changes in rotor rotational speed.

TABLE 4.1 : NOISE LEVELS @ 500 FT (150 M)

Helicopter	Author's Equation (4.2) dB	Author's Equation (4.3) dB	Davidson & Hargest [40]		Test Data =70/80° dB
			Φ =0° dB	Φ =75° dB	
Mil 10 (USSR)	101.5	104	97	86	99.5
Bell UH-1B	92	87	91	80	89
Wessex Mk.3	91	89	91	80	91/93
Wessex Mk.5	91.5	90	91.5	80	96
Wasp/Scout	88	83	87	76	89.5
Whirlwind Mk.10	87	85	87	76	87.5
Belvedere	92	93	92	80.5	84/89
Sea King	93	94	93.5	82	98
Gazelle	88	79	83.5	72	83.5
Lynx	92	86	90	78.5	88

NOTE: Sikorsky [41] = 'Davidson & Hargest @ 75°' - 6 . dB

Hubbard [60] = Equation(4.3) - 15.8 . dB

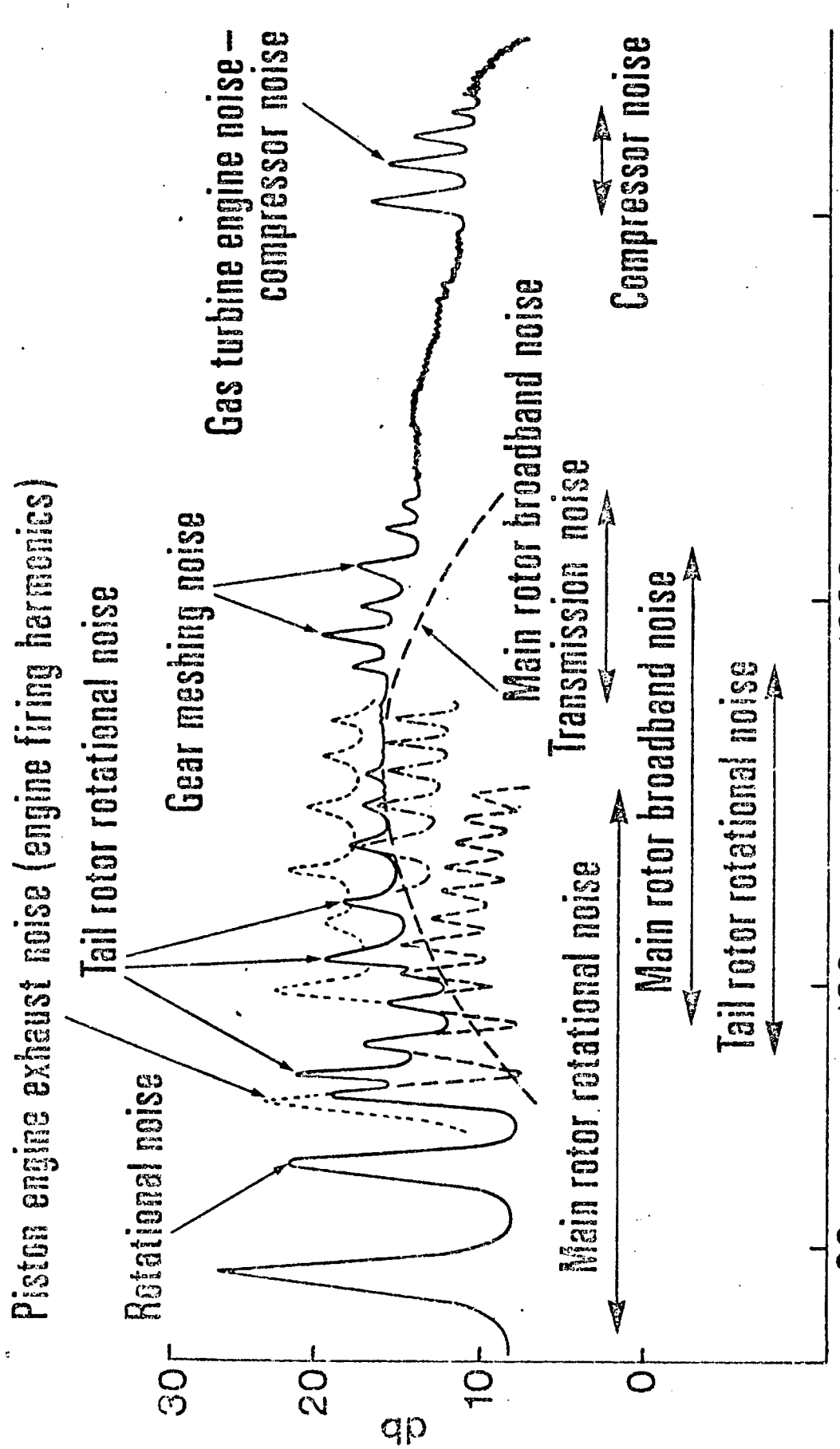

FIGURE 4.1. HELICOPTER NOISE - NARROWBAND SPECTRUM

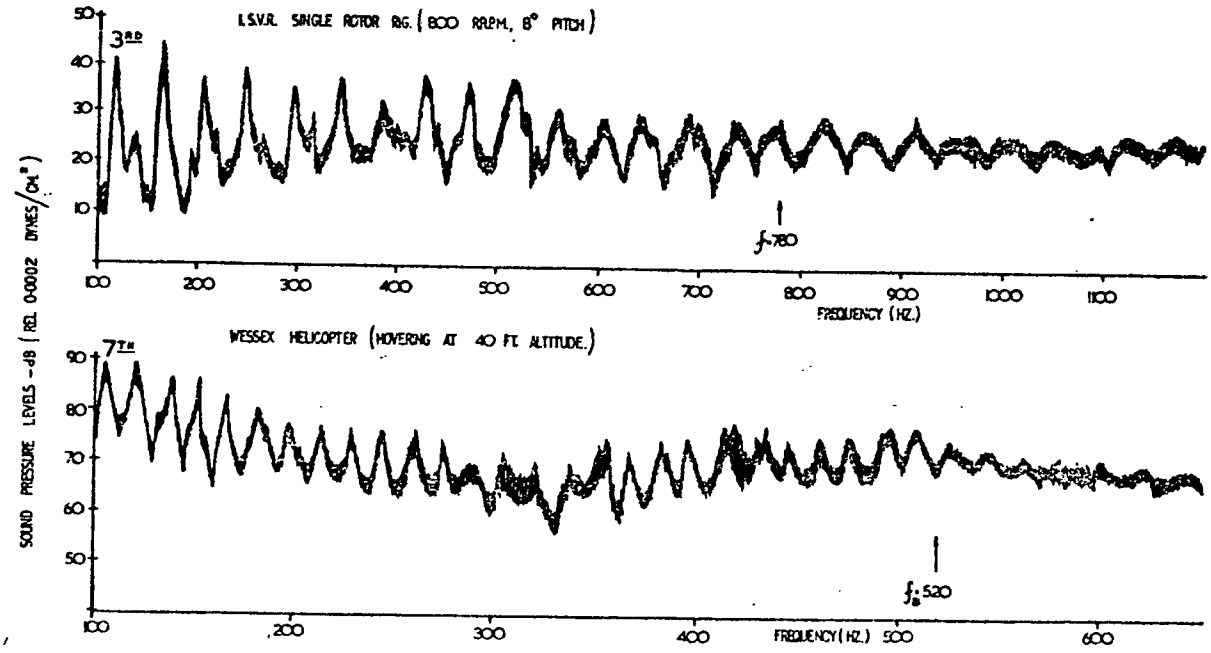

FIGURE 4.2. NARROWBAND ANALYSIS (3 Hz): WESSEX AND MODEL ROTOR

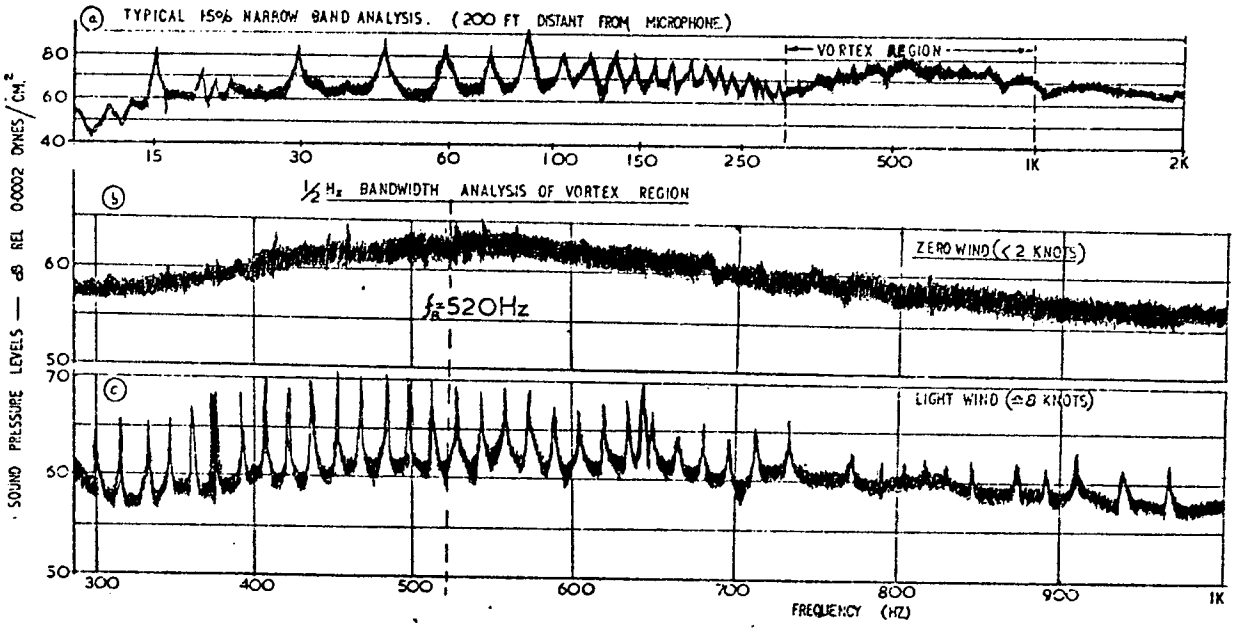

FIGURE 4.3. HOVERING WESSEX - NARROWBAND ANALYSIS

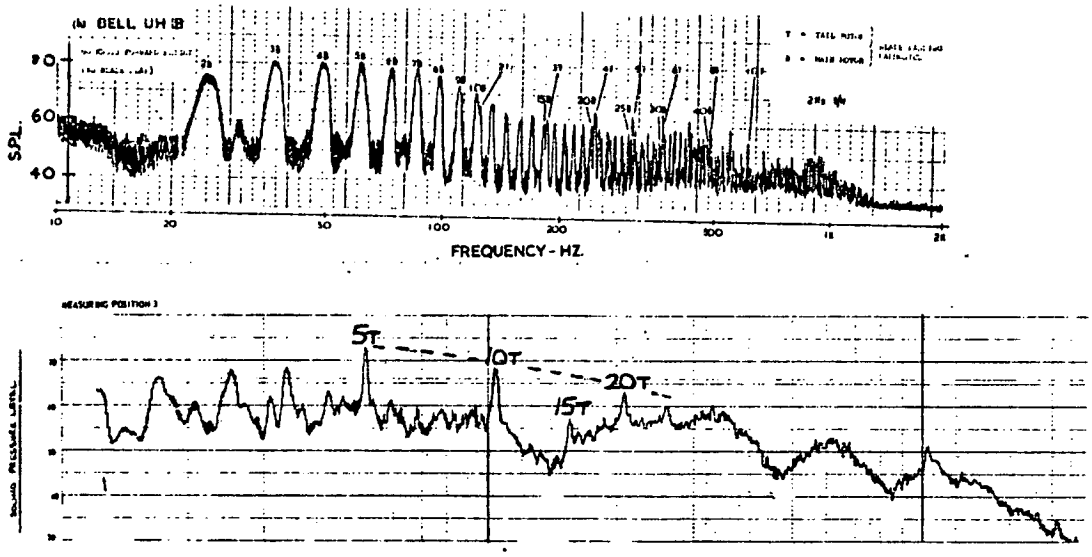

FIGURE 4.4. NARROWBAND ANALYSIS: UH-1B AND SEA KING

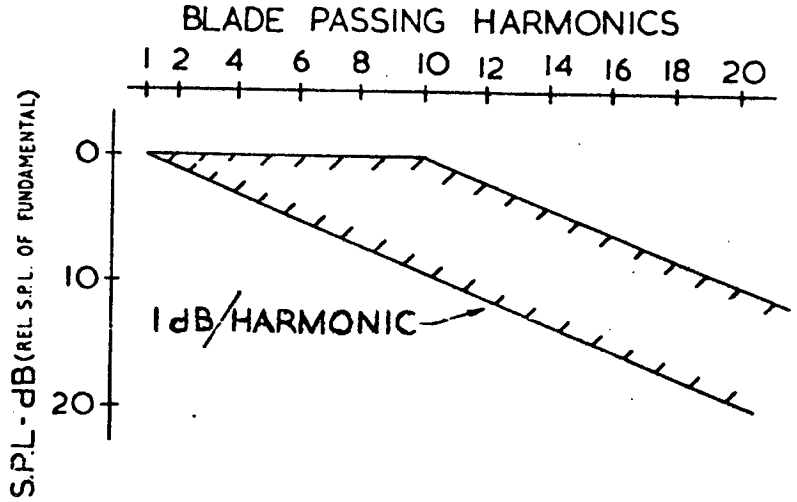

FIGURE 4.5. MAIN ROTOR ROTATIONAL NOISE - HARMONIC 'FALL-OFF'

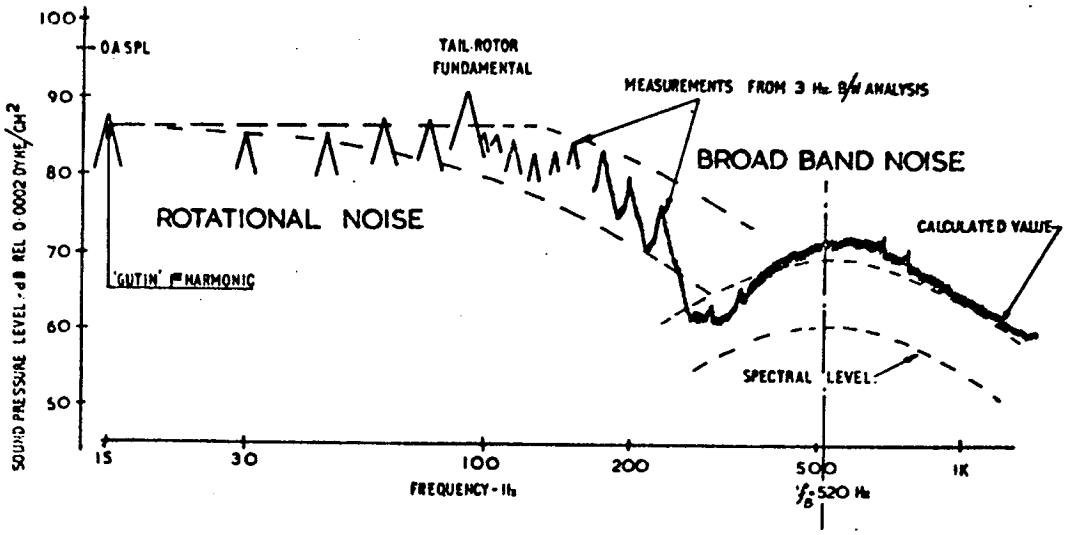

FIGURE 4.6. MEASURED AND CALCULATED EXTERNAL NOISE SPECTRUM (WESSEX)

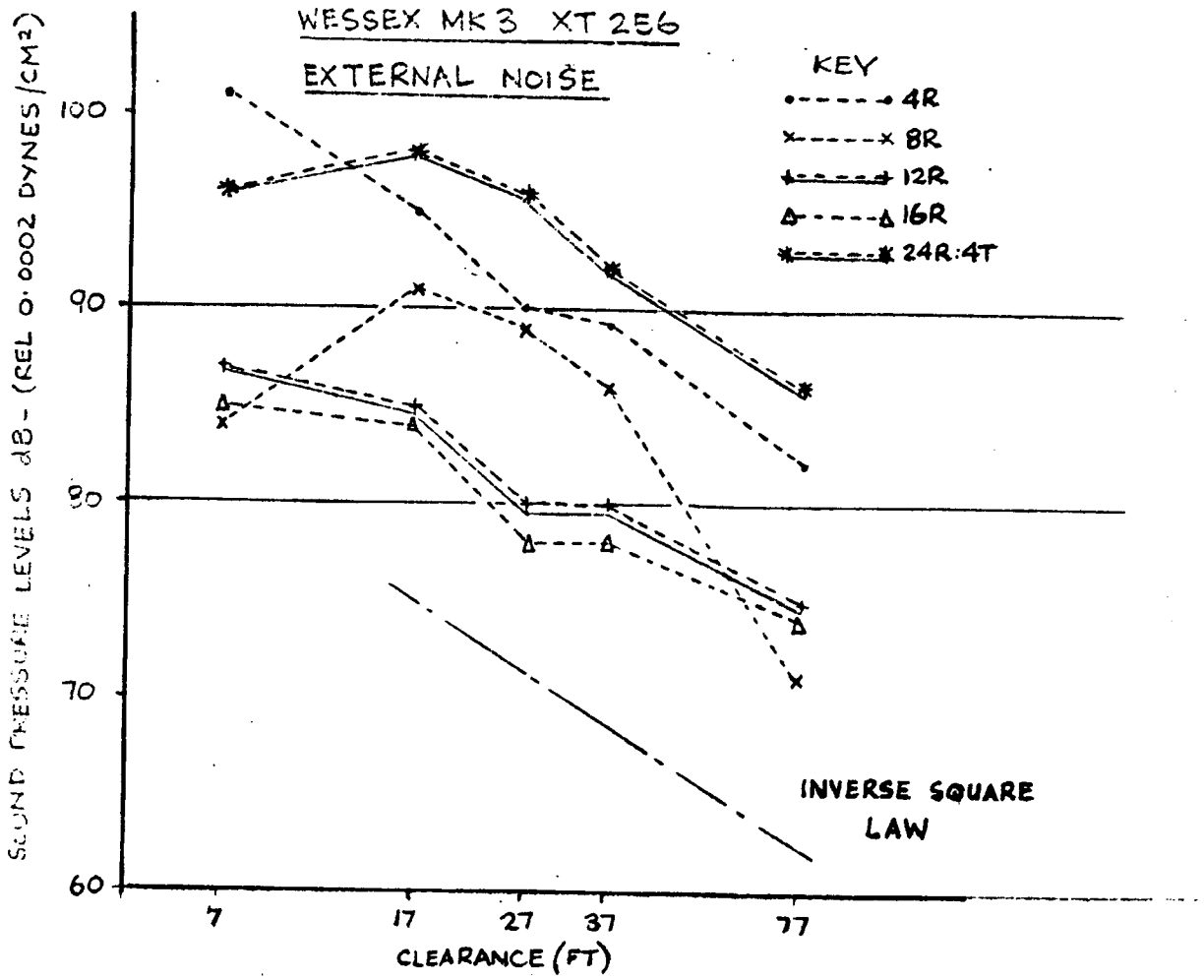

FIGURE 4.7. VARIATION IN ROTATIONAL NOISE WITH DISTANCE (WESSEX)

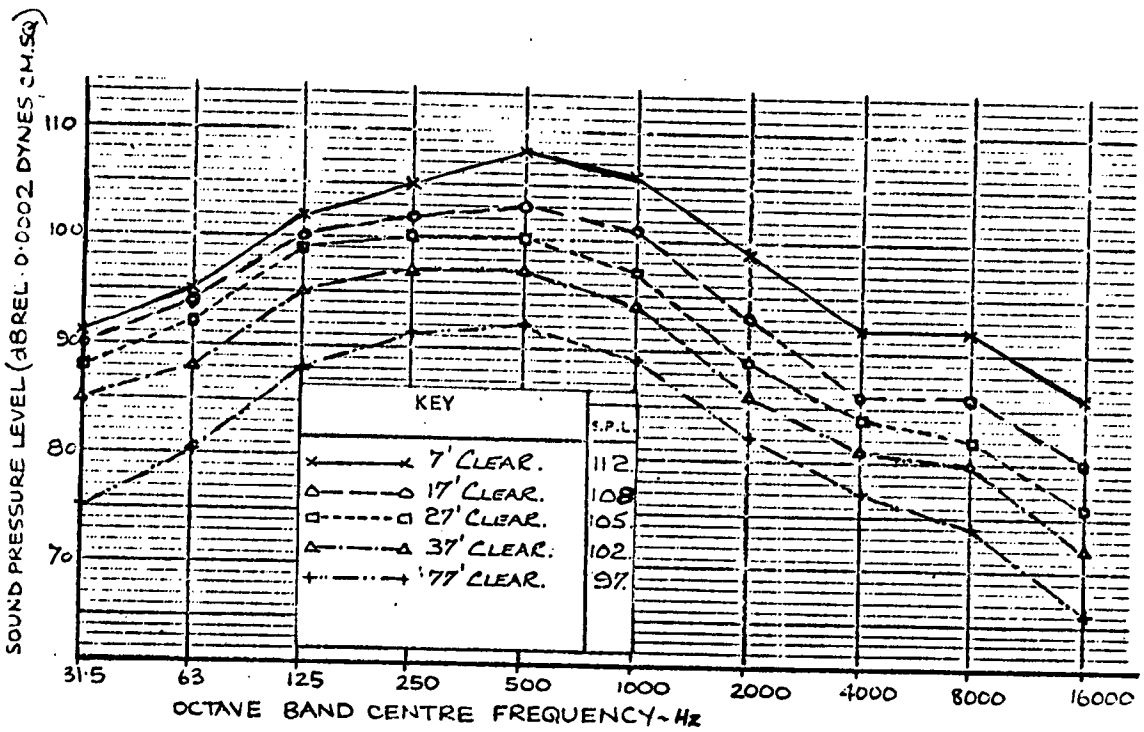

FIGURE 4.8. VARIATION IN SPL WITH DISTANCE (WESSEX): OCTAVE BAND PLOT

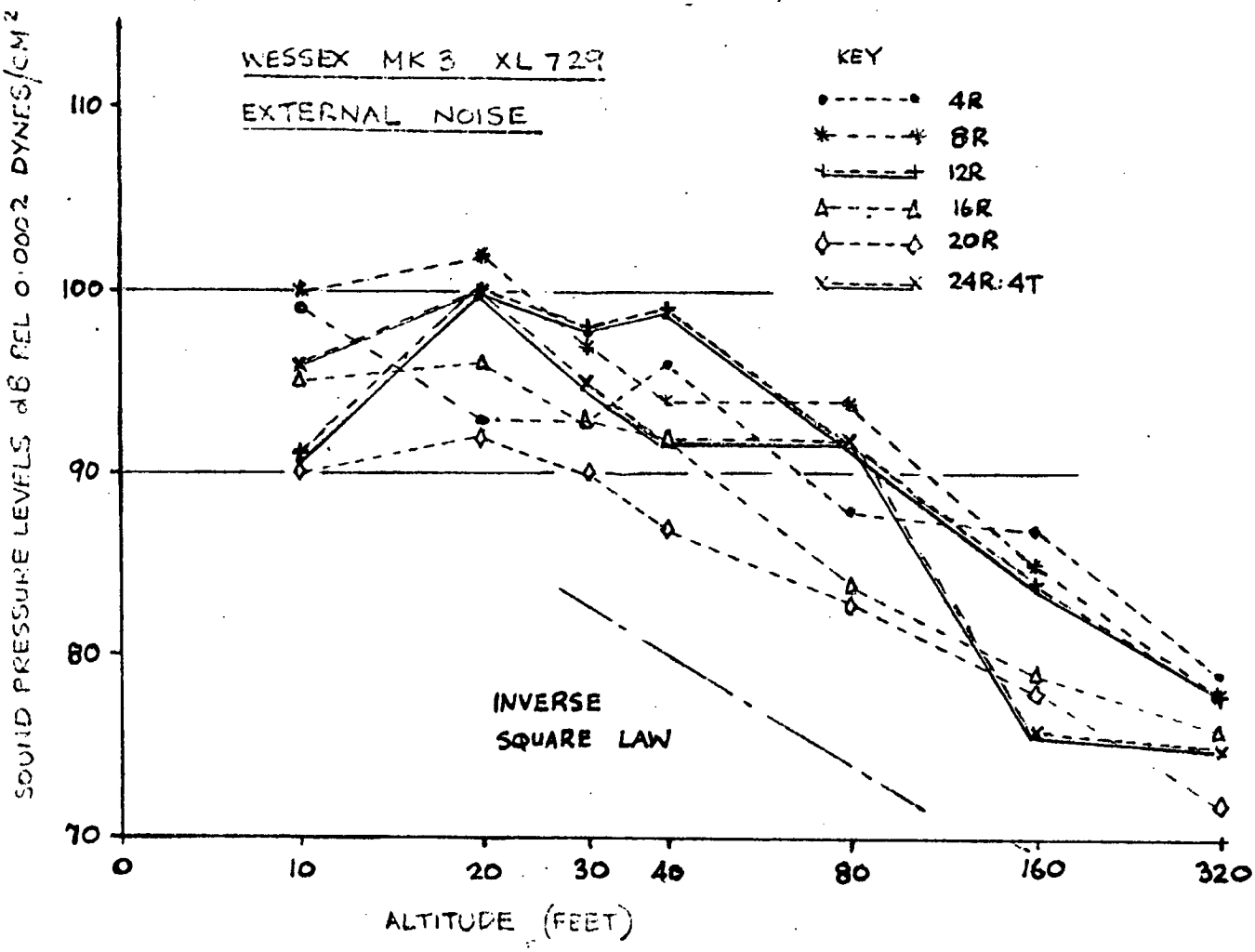

FIGURE 4.9. EFFECT OF HOVER HEIGHT ON ROTATIONAL NOISE MEASURED ON GROUND

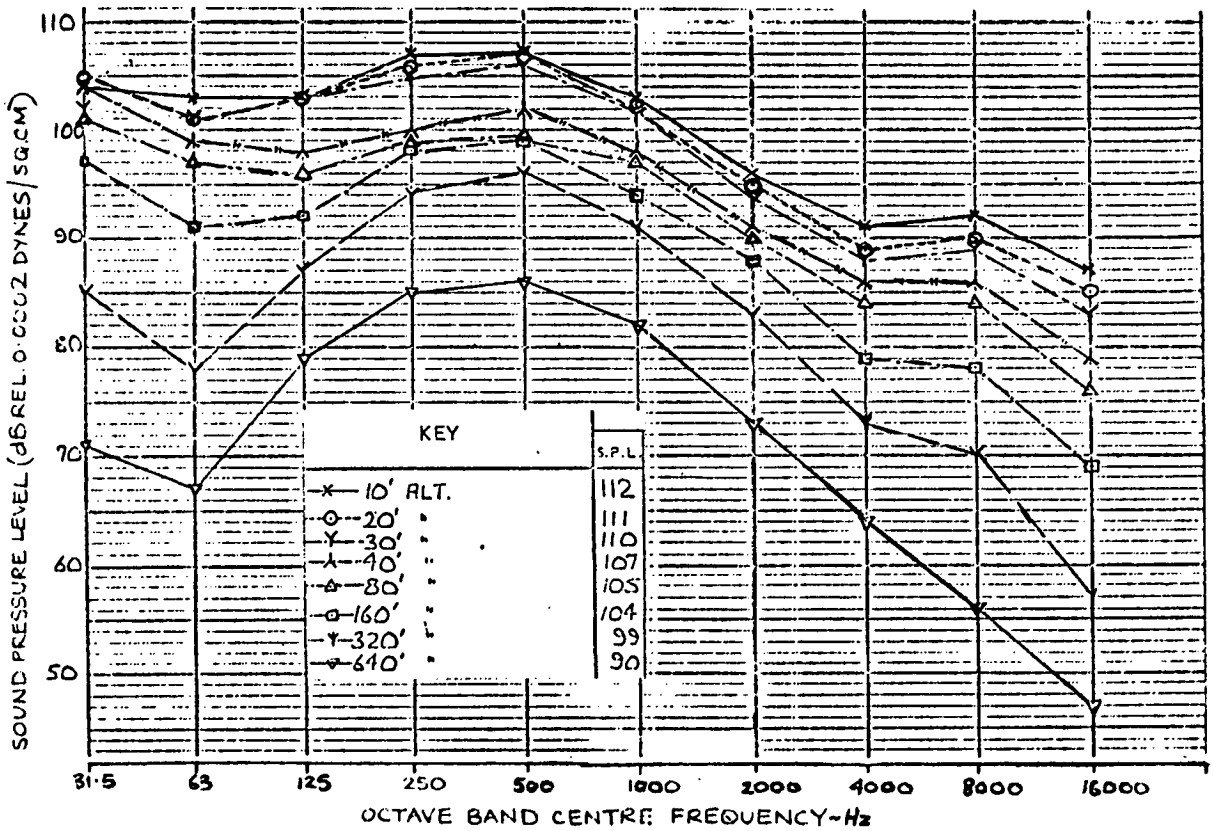

FIGURE 4.10. EFFECT OF HOVER HEIGHT ON SPL MEASURED ON GROUND: OCTAVE BAND PLOT

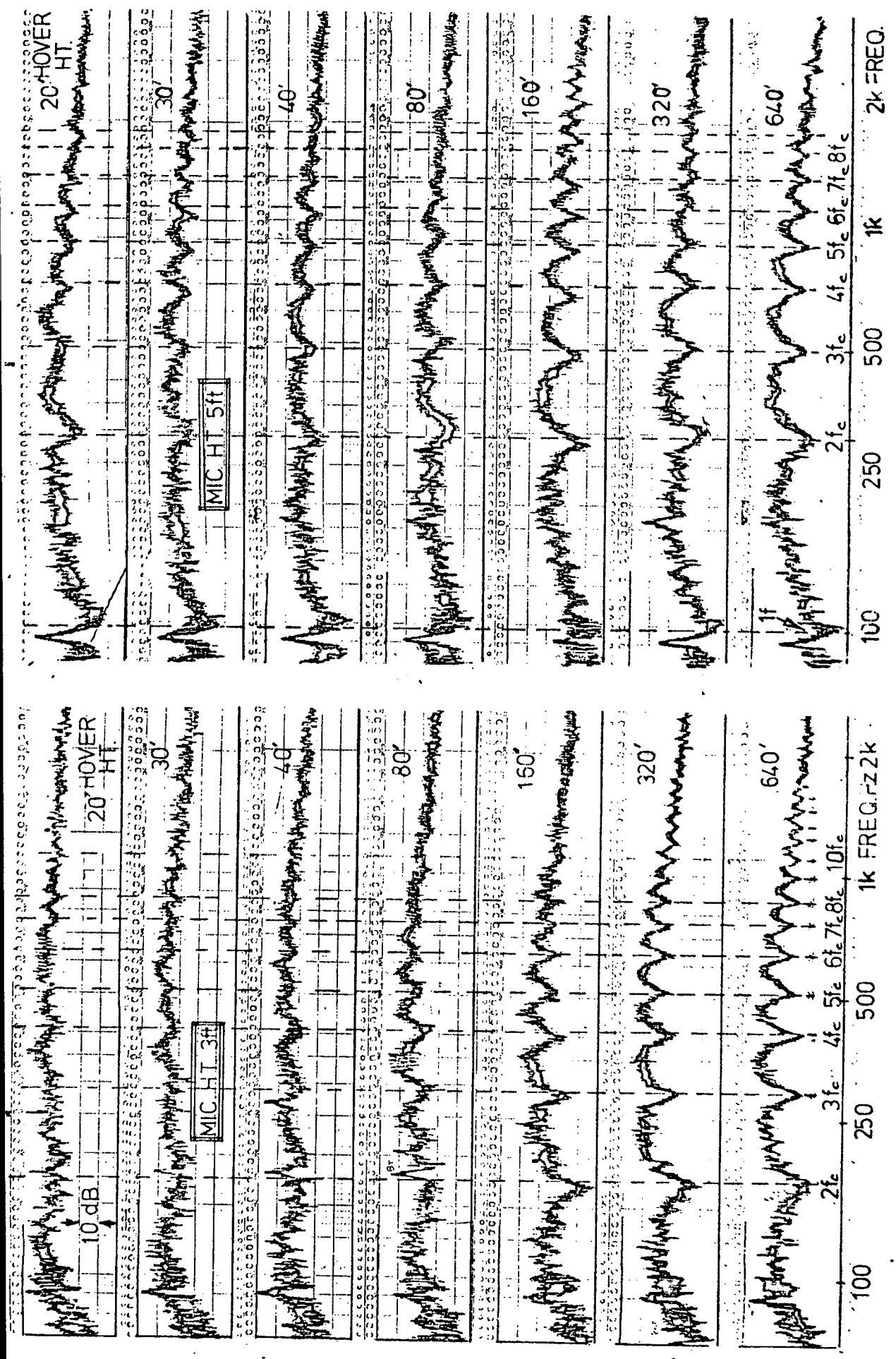

FIGURE 4.11. NARROWBAND ANALYSIS: EFFECT OF ALTITUDE ON GROUND LEVELS

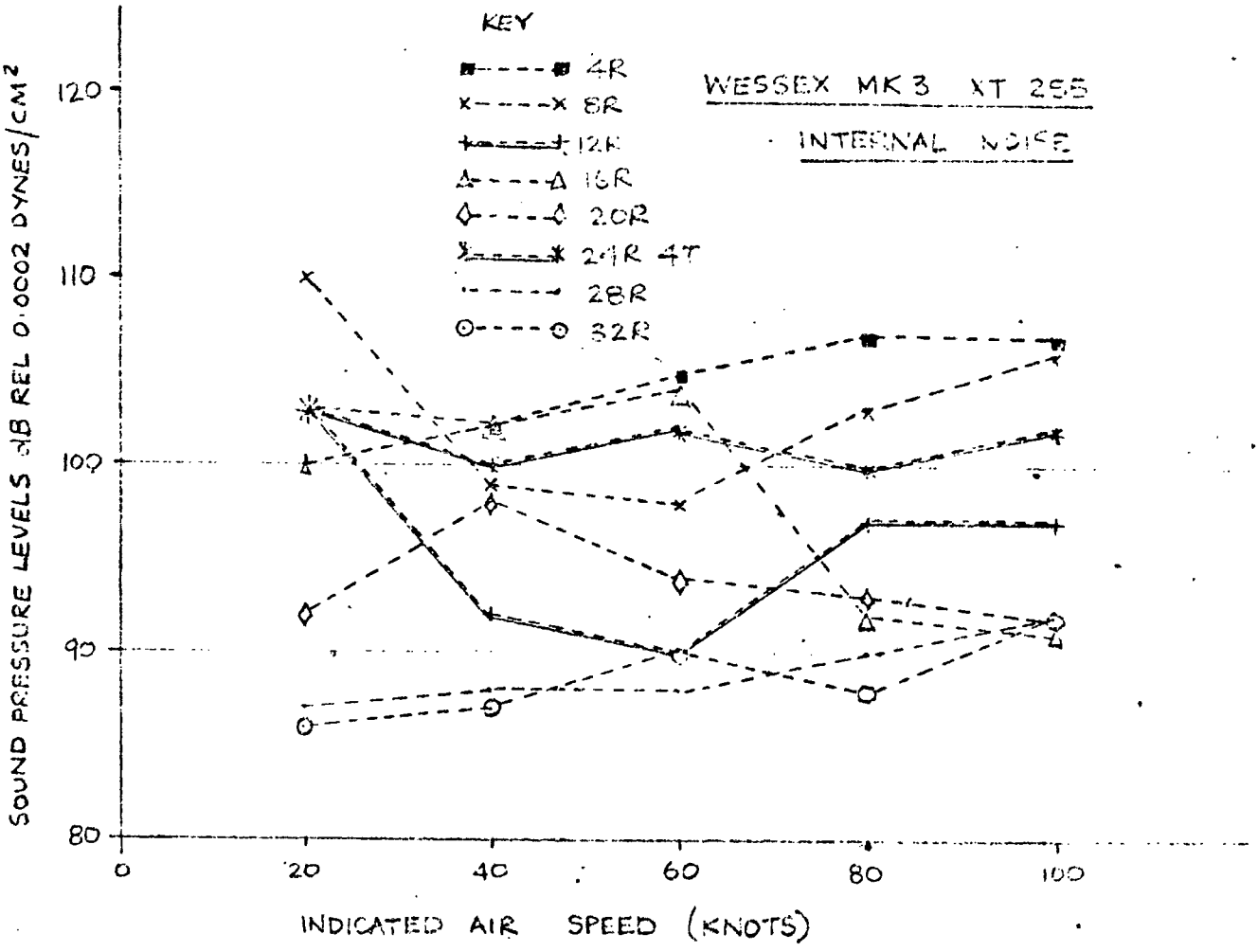

FIGURE 4.12. VARIATION OF ROTATIONAL NOISE LEVELS WITH FORWARD SPEED.

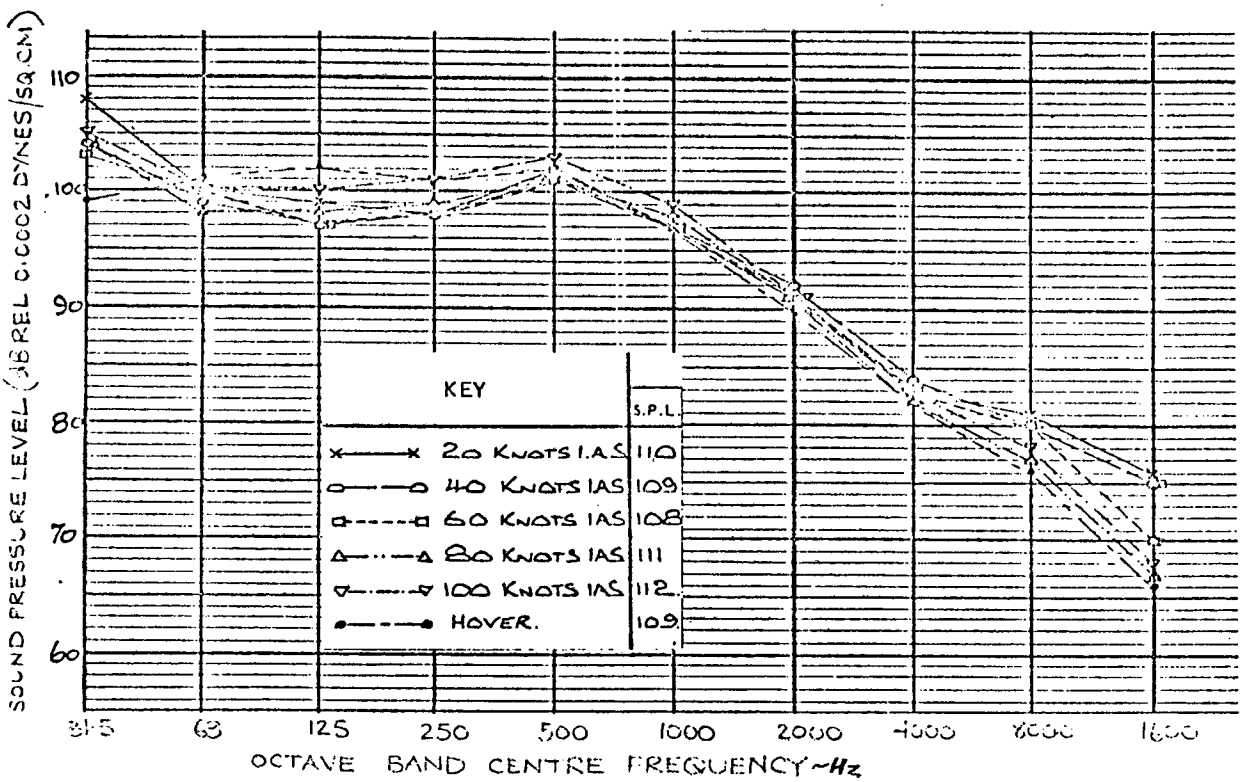

FIGURE 4.13. VARIATION OF CABIN NOISE WITH FLIGHT SPEED: OCTAVE BAND PLOT

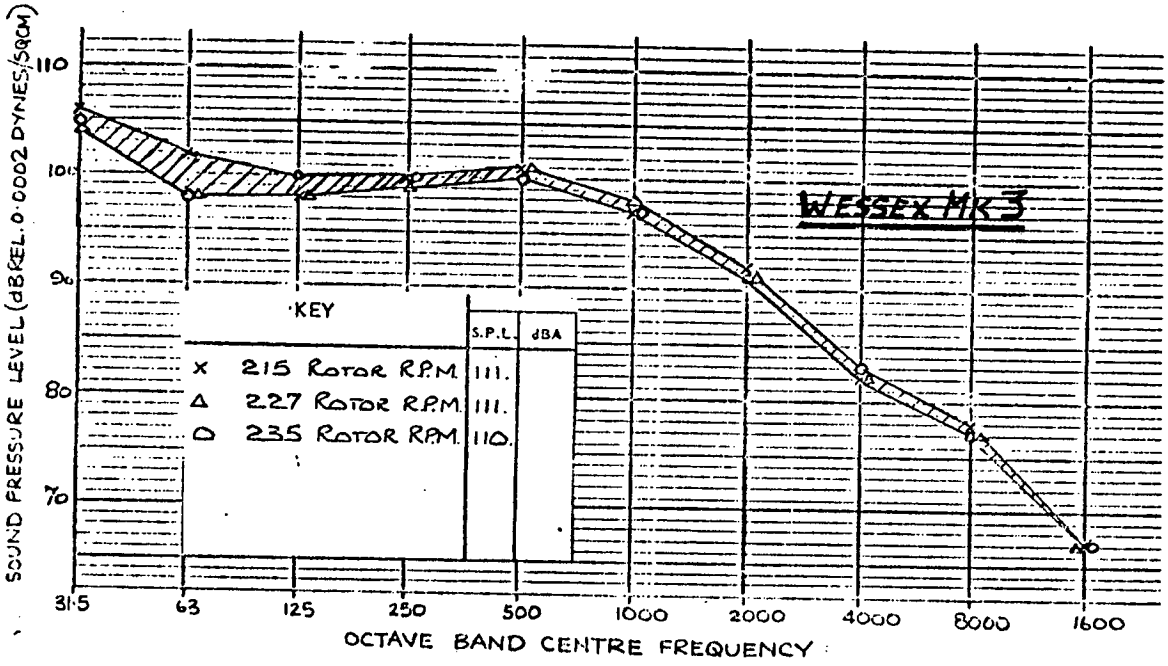

FIGURE 4.14. EFFECT OF ROTOR SPEED ON CABIN NOISE LEVELS

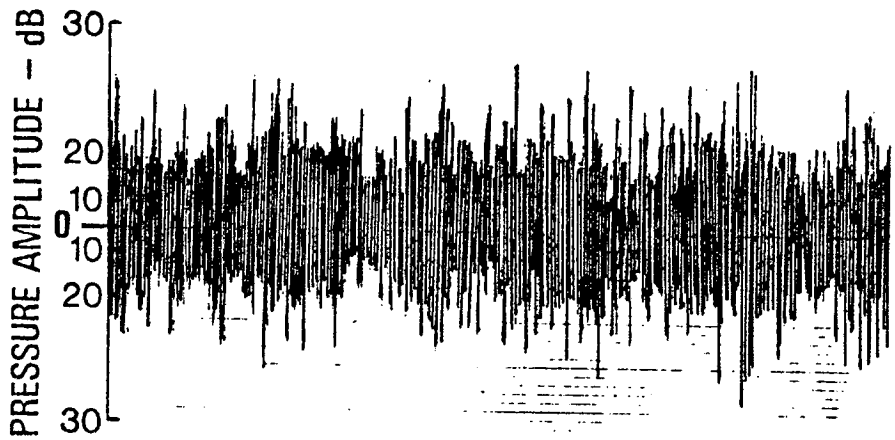

FIGURE 4.15. PRESSURE - TIME PLOT: HOVERING WESSEX

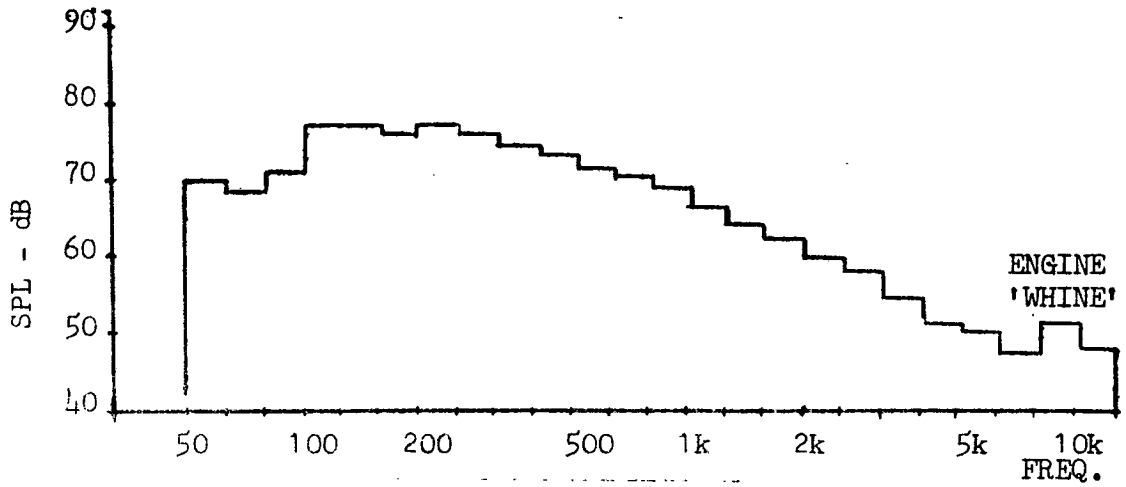

FIGURE 4.16. 1/3 OCTAVE BAND SPECTRUM: HOVERING WESSEX

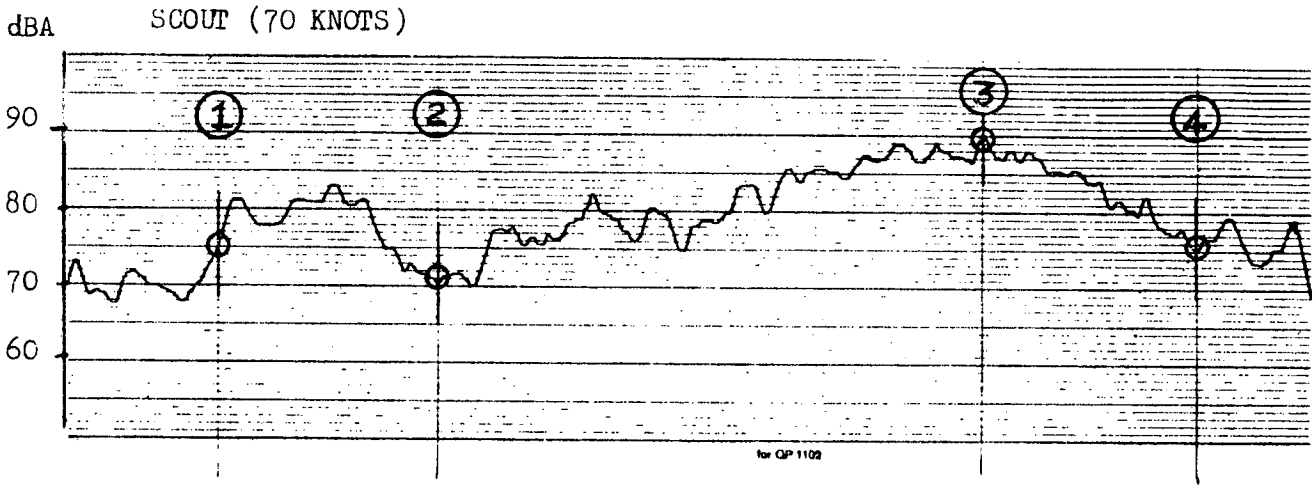

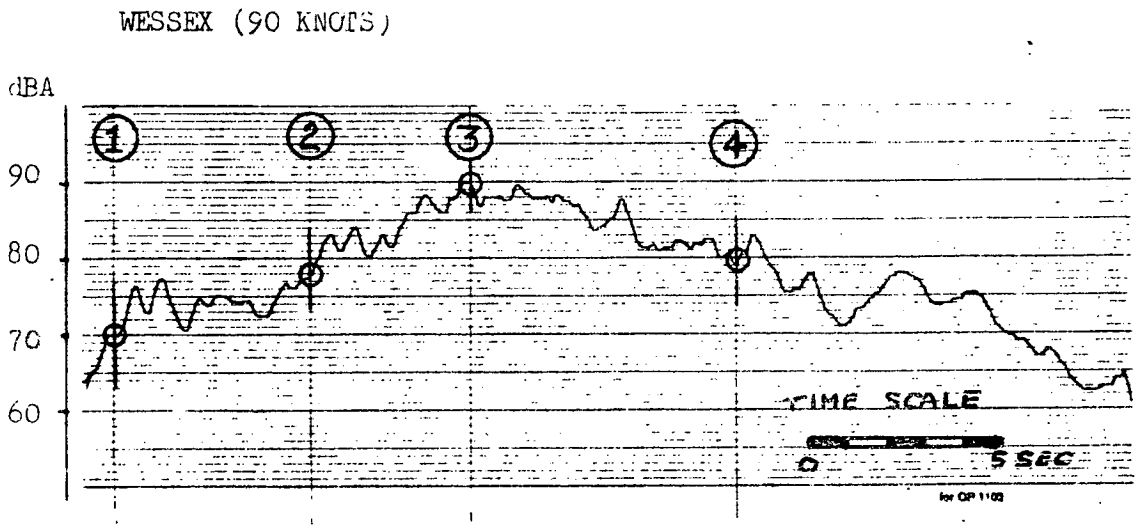

FIGURE 4.17. dB(A) TIME HISTORIES - SCOUT AND WESSEX FLYOVER

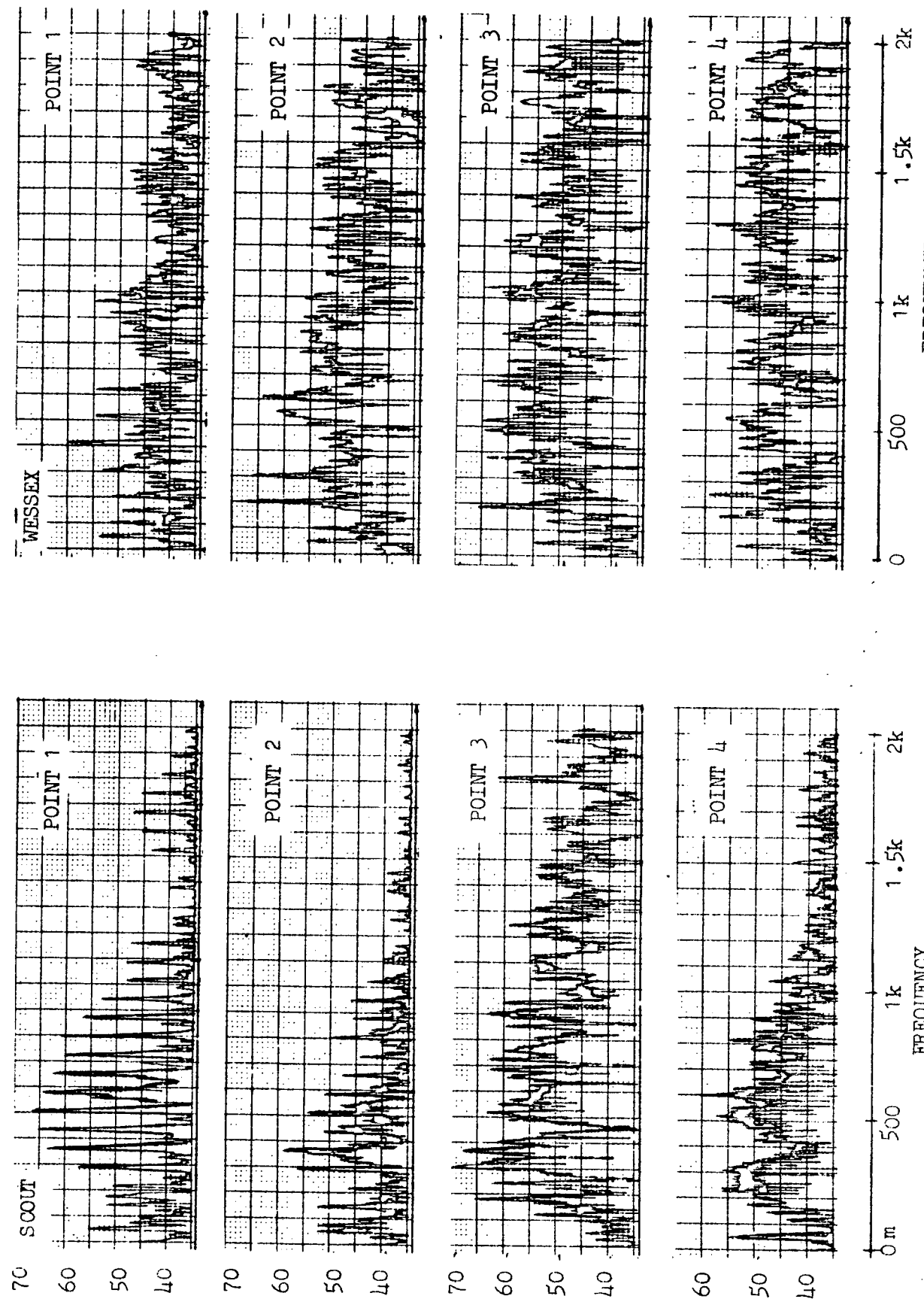

FIGURE 4.18. NARROWBAND ANALYSES - SCOUT AND WESSEX FLYOVER

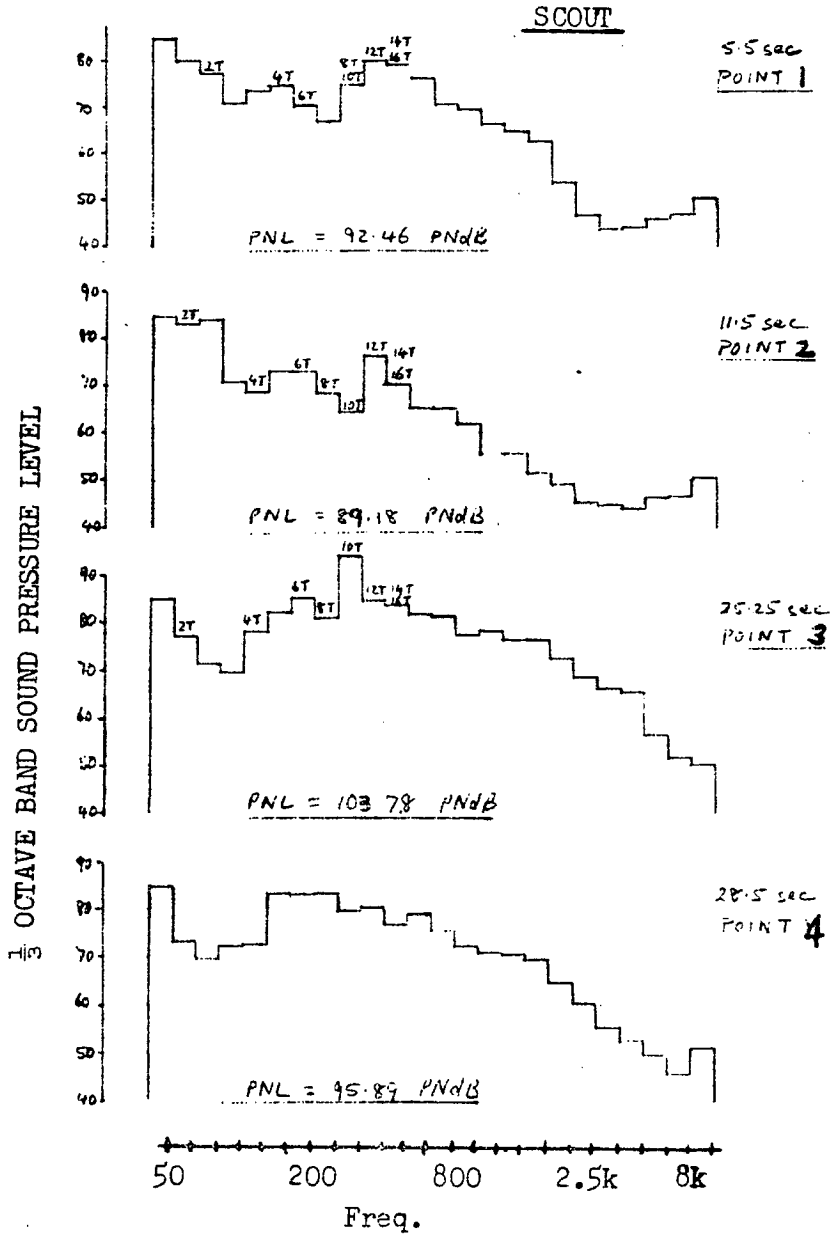

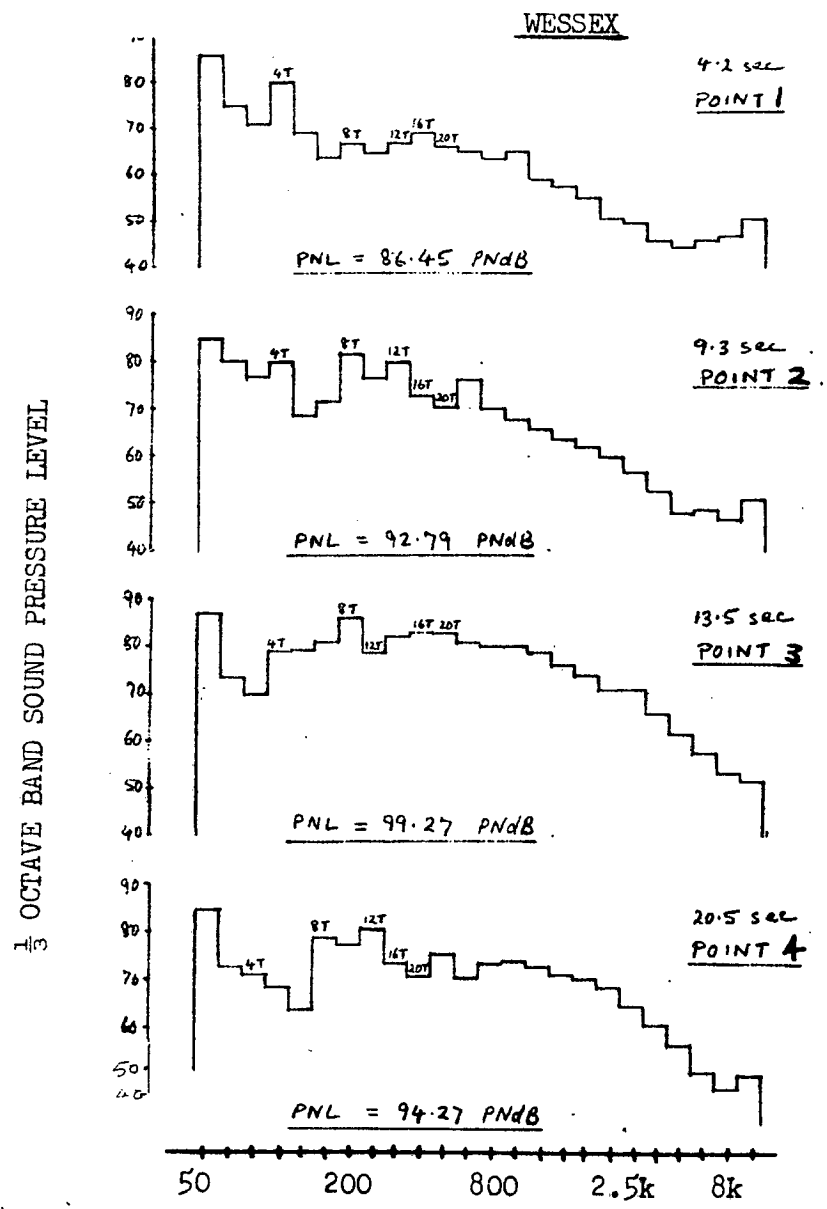

FIGURE 4.19. 1/3 OCTAVE BAND SPECTRA - SCOUT AND WESSEX FLYOVER

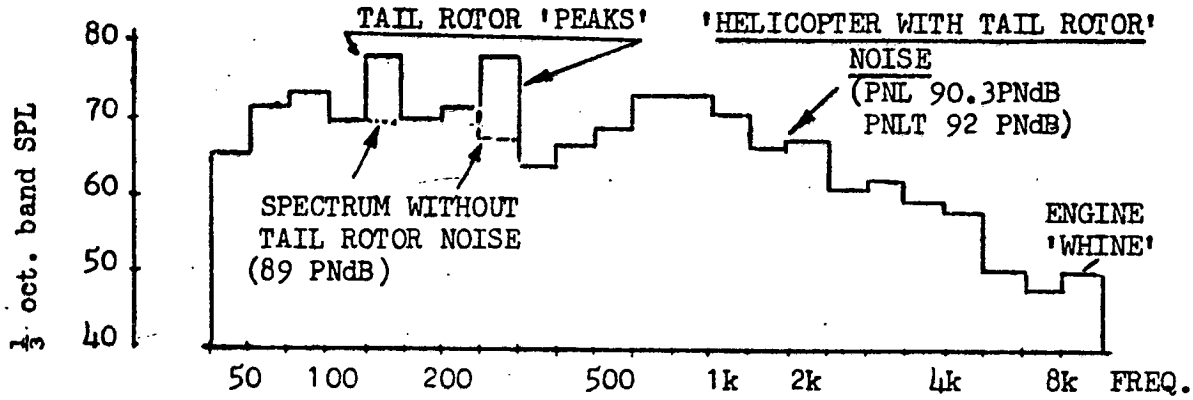

FIGURE 4.20. 1/3 OCTAVE BAND SPECTRUM - HELICOPTER WITH HIGH LEVEL OF TAIL ROTOR NOISE

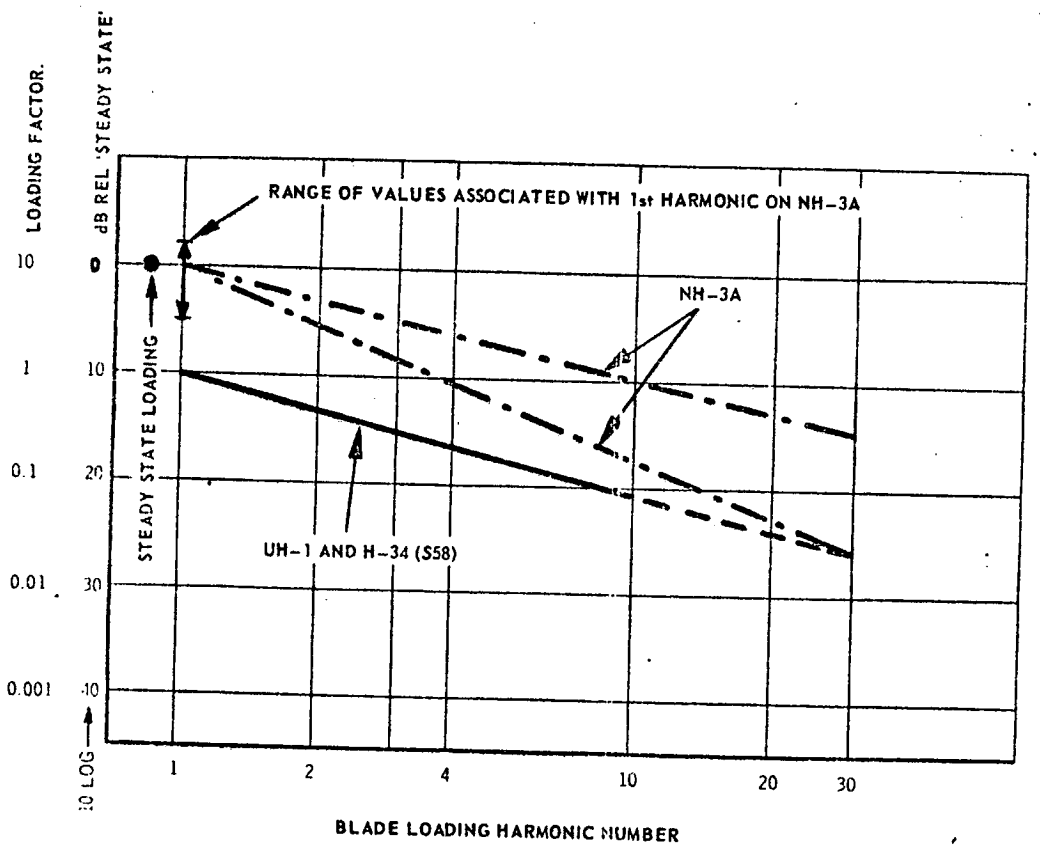

FIGURE 4.21. ROTOR BLADE LOADING - HARMONIC CONTENT

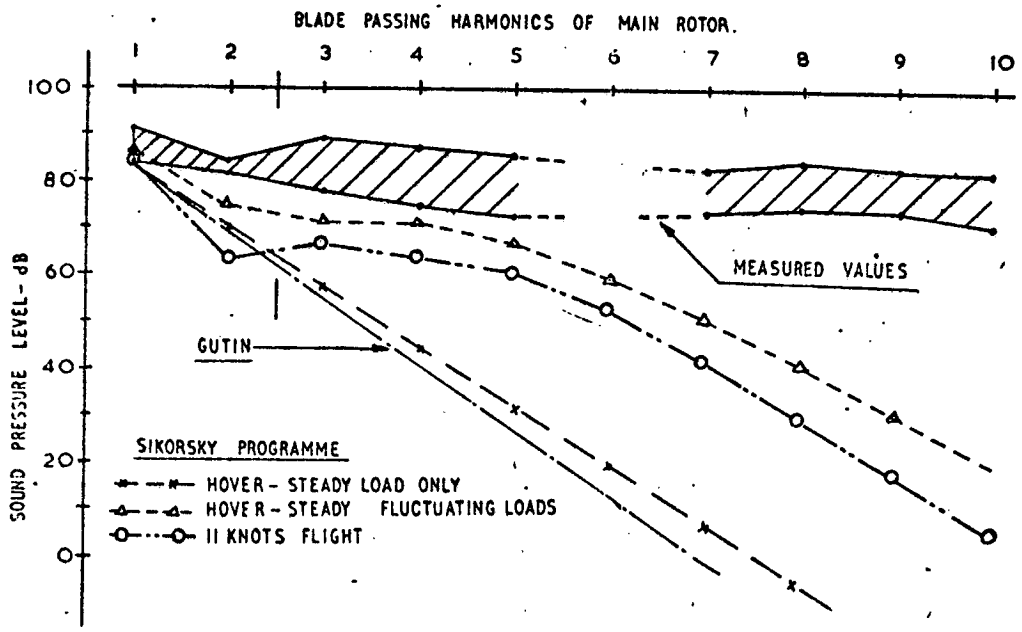

FIGURE 4.22. ROTATIONAL NOISE: COMPARISON OF MEASURED AND PREDICTED LEVELS

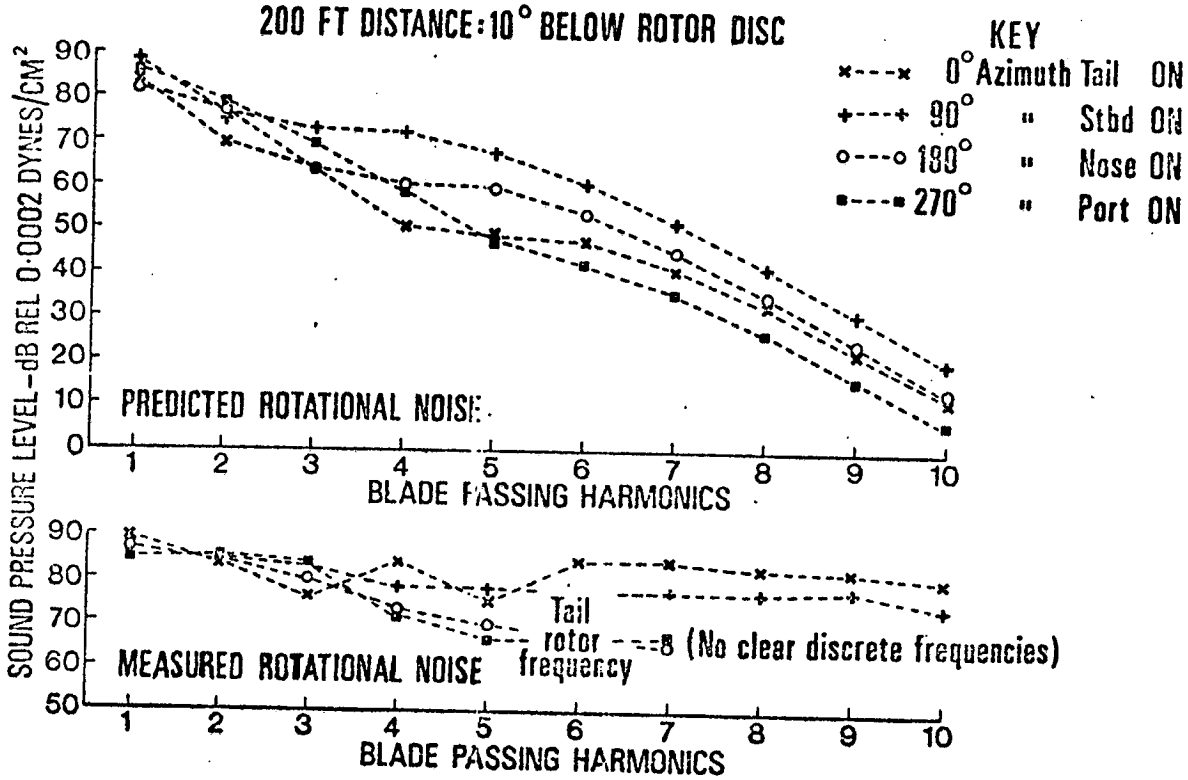

FIGURE 4.23. MEASURED AND PREDICTED ROTATIONAL NOISE LEVEL FOR HOVERING WESSEX

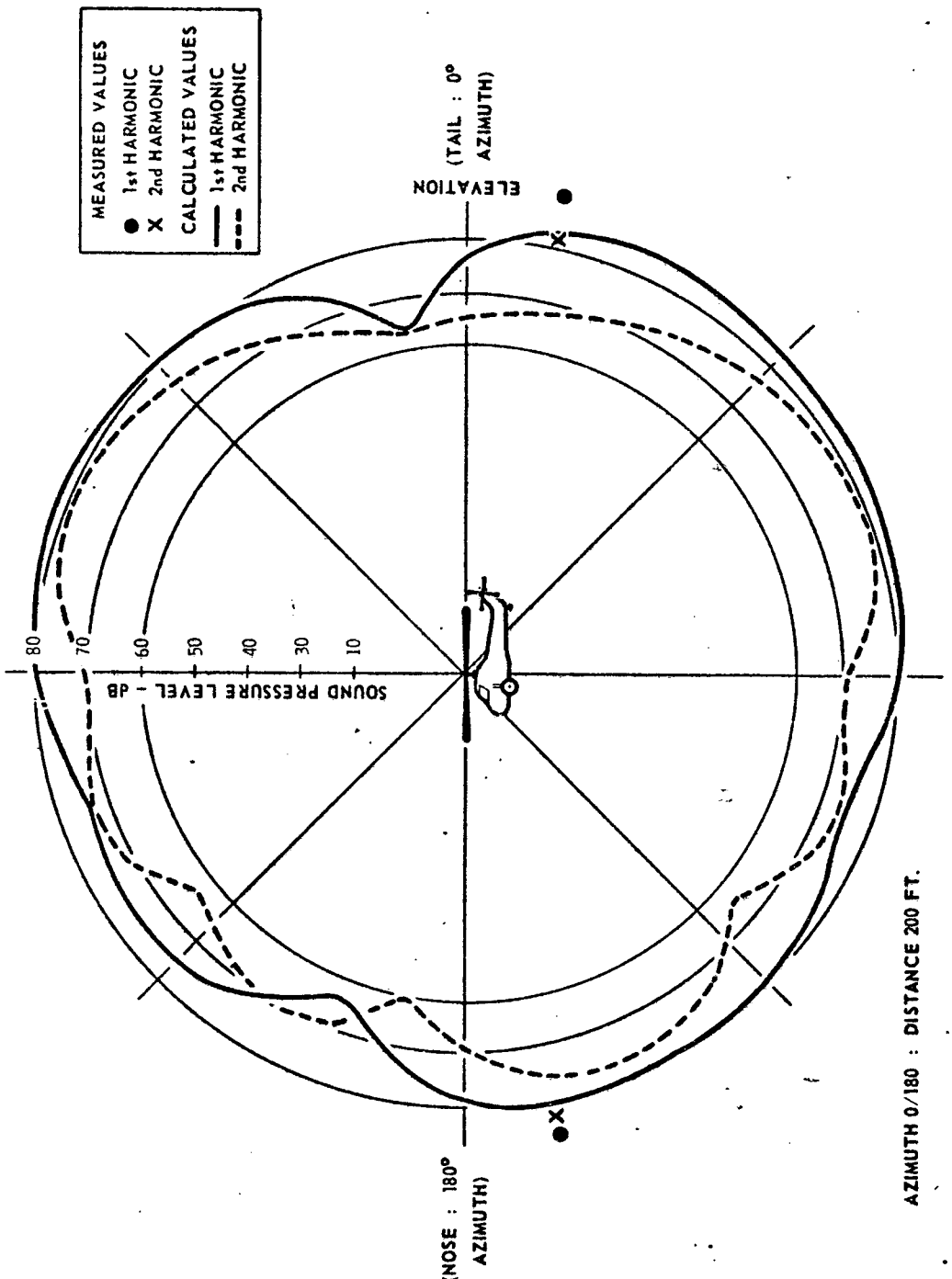

FIGURE 4.24. PREDICTED ROTATIONAL NOISE DIRECTIVITY FOR HOVERING WESSEX

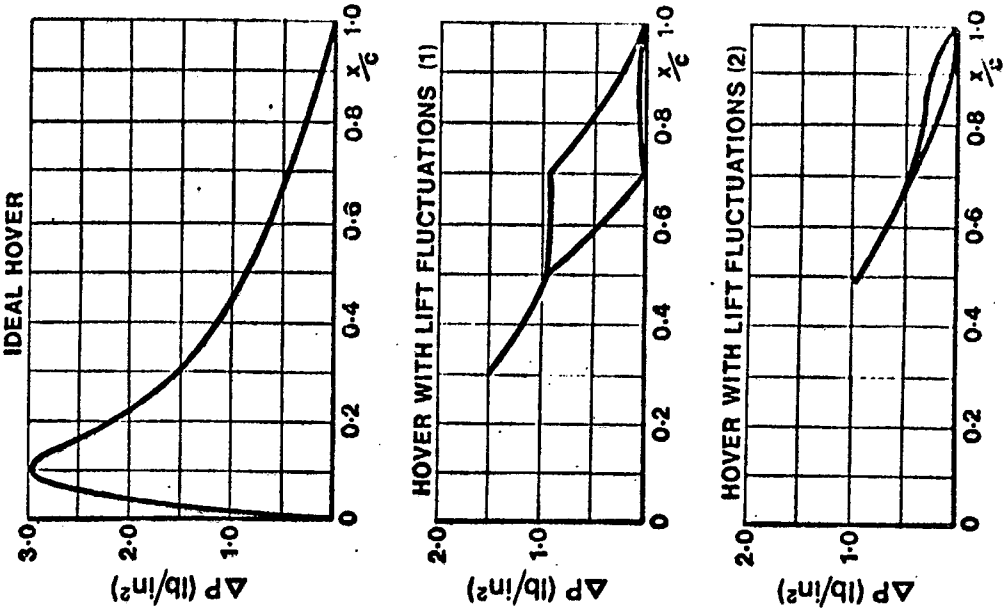

FIGURE 4.25. CHORDWISE BLADE LOADING (0.932 R)

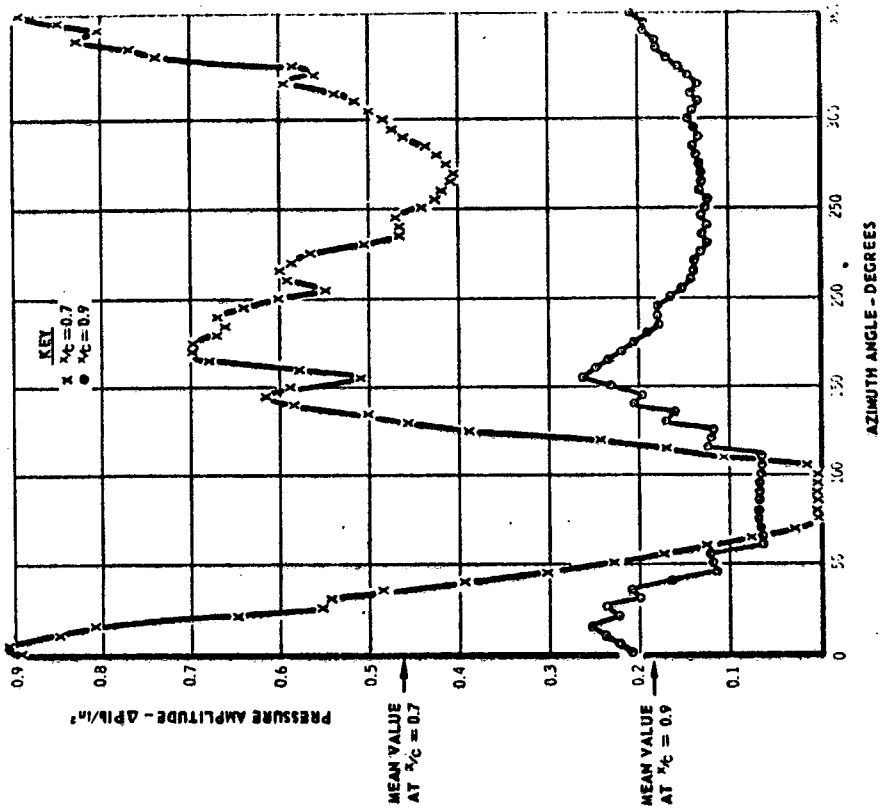

FIGURE 4.26. TRAILING EDGE PRESSURE FLUCTUATIONS

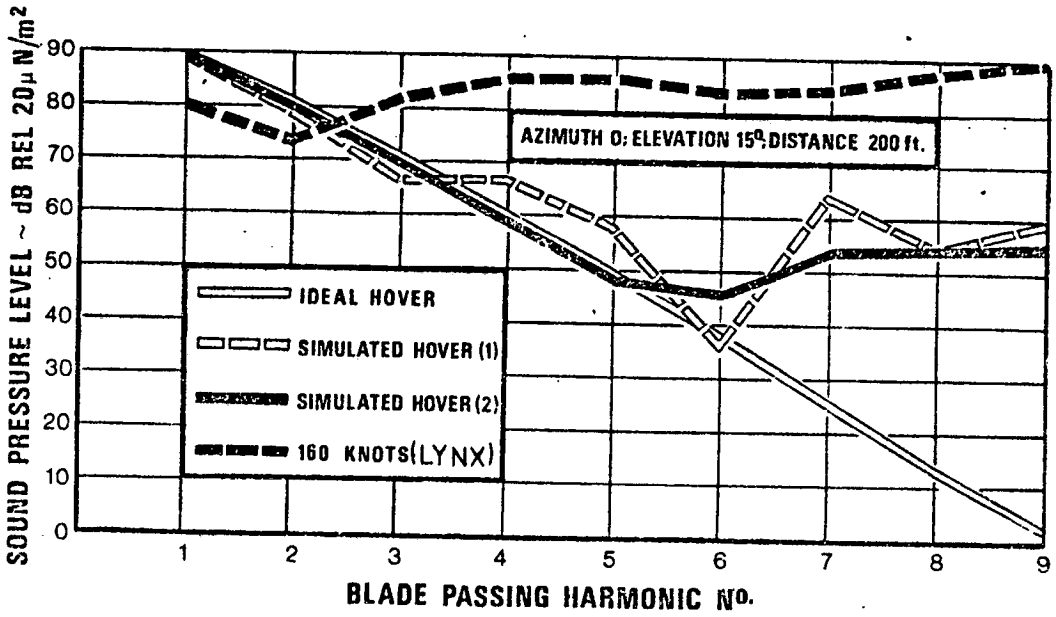

FIGURE 4.27. ROTATION NOISE - PREDICTED LEVELS

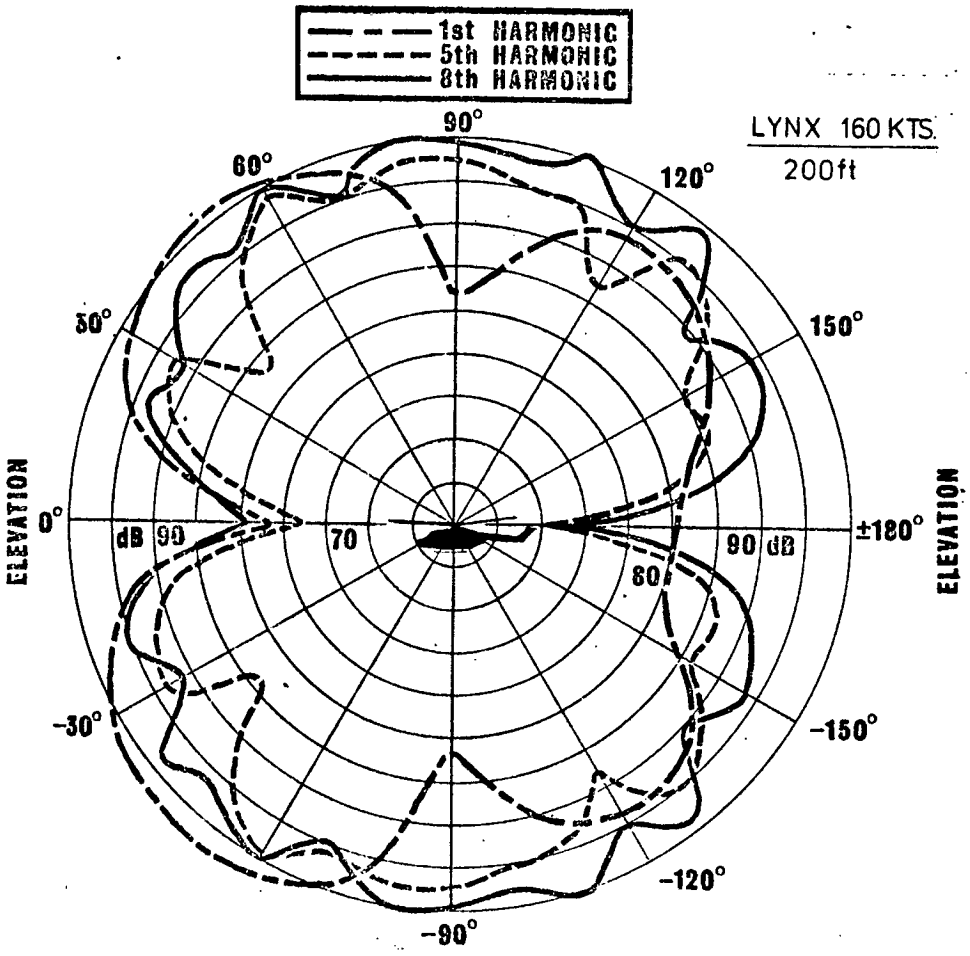

FIGURE 4.28. CALCULATED ROTATIONAL NOISE DIRECTIVITY

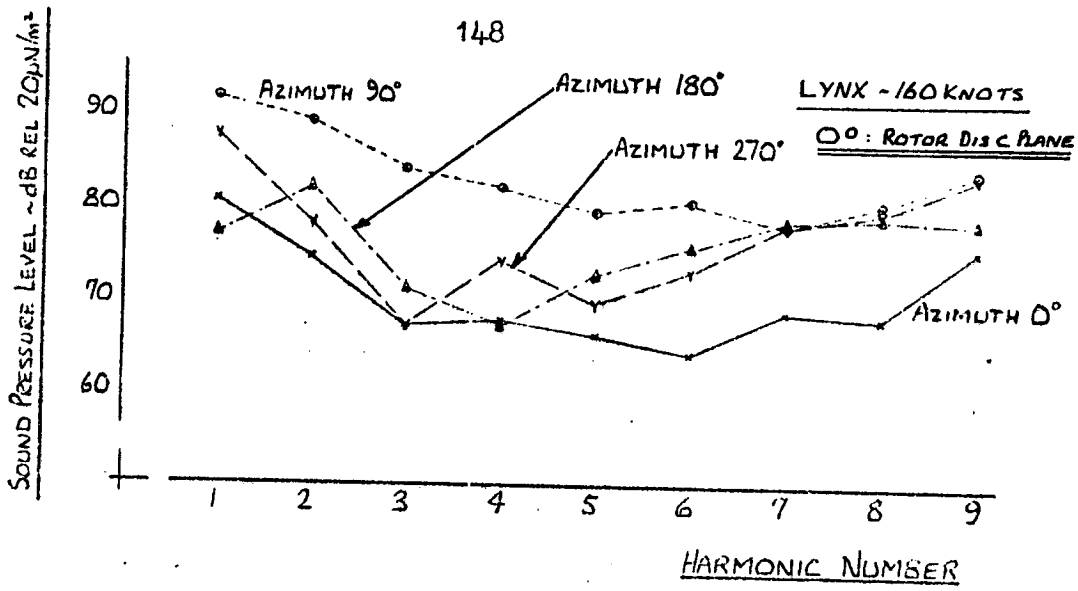

FIGURE 4.29. VARIATION OF ROTATIONAL NOISE WITH AZIMUTH IN ROTOR DISC PLANE

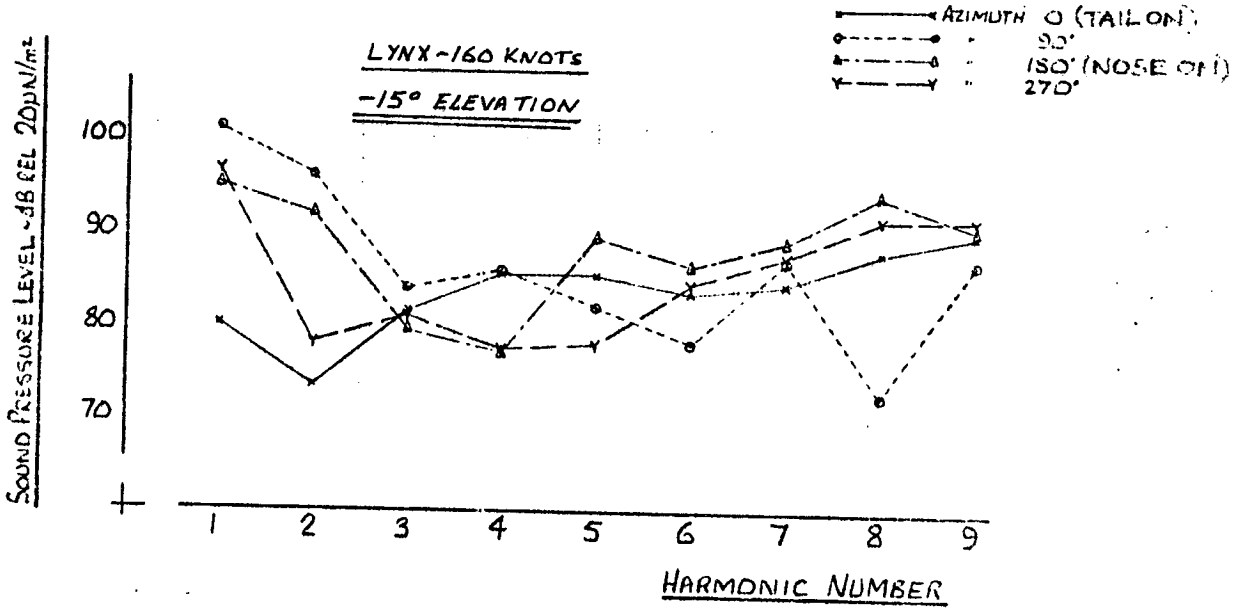

FIGURE 4.30. VARIATION OF ROTATIONAL NOISE WITH AZIMUTH AT -15° ELEVATION

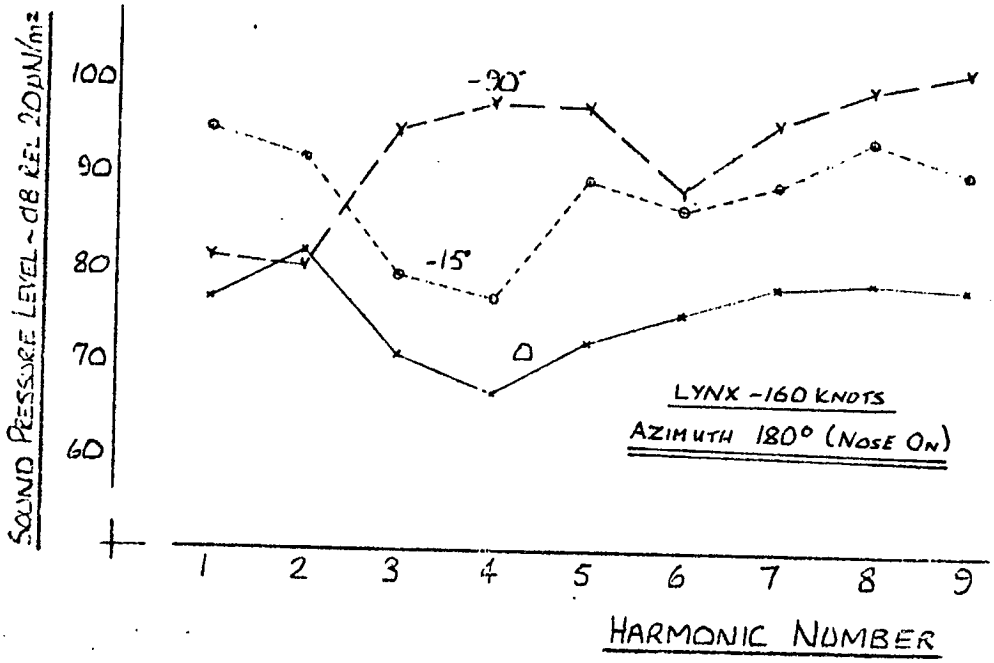

FIGURE 4.31. VARIATION OF ROTATIONAL NOISE WITH ELEVATION DIRECTLY IN FRONT OF ROTOR

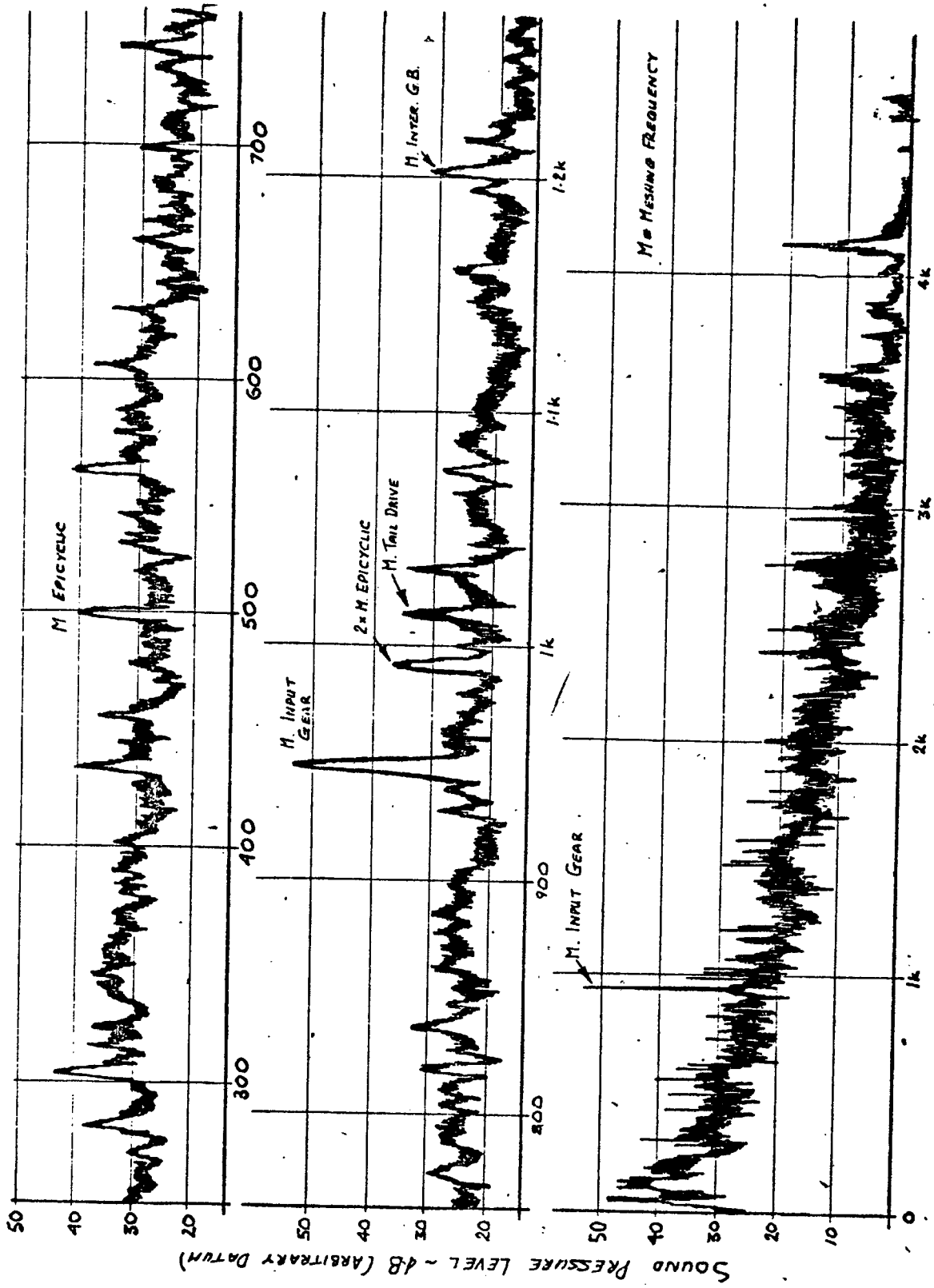

FIGURE 4.32. NARROWBAND ANALYSIS - CABIN NOISE (WESSEX)

CHAPTER 5: BLADE SLAP

5.1. INTRODUCTION

'Blade slap' is a colloquialism which has been applied to the sharp cracking or banging sound associated with helicopter rotors. It varies considerably in intensity and quality with the type of helicopter and flight condition. When blade slap occurs not only is it the predominant noise source on the helicopter but because of its impulsive characteristics it is the most objectionable. Blade slap can occur on any helicopter, but particular attention was focussed on this noise source in 1963/64 with the introduction into wide use of the Bell UH-1 range of helicopters, with its highly loaded two bladed main rotor, and the Boeing-Vertol V107 and Chinook range of tandem rotor helicopters. There had been little work on this topic in 1964 and only one paper [73] treated the subject in any detail. Thus the programme initiated at the ISVR as a part of M.Sc. studies by F.W. Taylor (U.S.Army) and the author was the first investigation to give serious attention to this topic. F.W. Taylor concentrated on the operational aspects, including a questionnaire to establish the magnitude of the problem, while the author was responsible for theoretical development and the planning of an experimental programme which was carried out on a joint basis. This investigation showed that blade/tip vortex interaction was most likely the main source responsible for blade slap and that based on this hypothesis the acoustic characteristics observed on real helicopters could be explained. The programme included the simulation of blade slap on a model rig by use of an air jet arrangement and it was shown that in this case the measured noise levels could be predicted, by using a simple model, from knowledge of blade and air-jet velocity characteristics. This work was reported in Taylor's and the author's M.Sc. Project Reports [74, 1] and subsequently the main conclusions were issued as joint papers [75, 76]. It was clear, however, that the work could be extended to the case of a real helicopter and that there were a number of aspects which could be resolved with the aid of further flight tests. A programme embodying these main points was therefore formulated; also, since during the M.Sc. projects only a brief review had been made of other possible mechanisms for the generation of blade slap, a more detailed examination was made. It soon became clear that in addition to the need for a further understanding

of the details of the mechanism involved, the subjective rating was an area which warranted further consideration. This aspect was subsequently investigated and eventually formed a major part of the overall programme.

The details of the various studies conducted in connection with the blade slap investigation are outlined in the following sections. A summary of the main results from the author's M.Sc. programme is also included in order to provide a background to the main programme.

5.2. SUMMARY OF M.SC. PROJECT STUDY [1]

From a review of the available data in 1964 it appeared that blade/tip vortex interaction was one of the most likely mechanisms for the generation of blade slap. This was simulated on a model by using an air jet arrangement as illustrated diagrammatically in Figure 5.1. The results obtained were compared, on a frequency spectrum and time history basis as shown in Figures 5.2 and 5.3 respectively, with data obtained from flight tests with a Belvedere (tandem rotor helicopter). As can be seen the simulated blade slap gave the same acoustic signature as that associated with the real helicopter. It was concluded therefore that blade/tip vortex interaction was the main mechanism responsible for the generation of blade slap.

A theory based on a point dipole acoustic concept and a blade loading model of the form suggested by Kussner's function [77] showed good agreement with the results obtained from the test rig, both in amplitude and characteristic as illustrated in Figure 5.4. This study showed that the noise produced by a blade passing through a fixed gust (tip vortex) varied like V^4, where V was the velocity of the blade, and was a function of Γ^2 where Γ represents the vortex strength or size. This was a most important result since it implied that helicopters with highly loaded blades are more likely to produce loud blade slap than those with low blade loading.

Experimentally it was shown that the 'blade slap' signal was independent of the pitch of the blade; thus blade pitch on a real helicopter is only important in that it affects the blade loading and, therefore, vortex size.

5.3. REVIEW OF POSSIBLE MECHANISMS

Originally three main mechanisms were postulated for blade slap; these were as follows:

(1) fluctuating forces caused by blade/tip vortex interaction;

(2) fluctuating forces resulting from stalling and un-stalling of the blade;

(3) shock wave formation due to local supersonic flow; it was suggested that this was either (a) a direct result of operating a blade at high tip speed or (b) caused by blade/vortex interaction.

It was subsequently proposed, particularly by research workers at Bell Helocopters, that 'blade slap' was linked to compressibility effects and/or drag divergence, but the precise details of the impulsive noise generation were not defined. Later a view was expressed that the impulsive noise was a result of shock waves which became detached from the blades and radiated into the far field. Again the precise details of the proposed basic mechanism involved were far from clear. More recently a 'thickness noise' model has been developed and this would appear to account for the generation of impulsive noise of the blade slap type on a rotor operating with a high blade velocity.

The above mechanisms are discussed in further detail in the following section and the latest position relating to blade slap is summarized in Section 5.4.

5.3.1. Blade/Vortex Interaction

Blade/vortex interaction is represented in idealized form in Figure 5.5; this shows possible interactions when the core is parallel to the spar of the blade. If an interaction as given by path 'A' occurs, fluctuating forces will clearly be produced. In this case the blade is subjected first to a 'down velocity' change and then to an 'up velocity' change, which produces a rapid change in angle of attack and subsequent impulsive loading. If path 'B' is followed a similar loading fluctuation occurs, but, of course, at a much smaller magnitude. In addition to this, however, it is possible that the velocity of the blade is such that when combined with the tangential velocity of the tip vortex, it exceeds the sonic velocity and produces a local shock wave. Path 'C' would produce a similar fluctuating force variation to that experienced by a blade travelling along path 'B', but in this case there is very little chance of sonic flow being produced. Thus the fluctuating force noise could result from interactions of the form indicated by paths 'A', 'B' and 'C', and local supersonic flow from a blade/vortex interaction of the type indicated by path 'B' only.

In the type of interaction described above, large changes in the angles of attack occur and it is suggested that the blade would stall. This fluctuation takes place, however, very quickly and it is unlikely that stall would occur in this instance (see the discussion in section 5.3.2 on stall).

5.3.2. Blade Stall

The 'stall' hypothesis is much more difficult to visualise. It is well known from fan and propellor studies that there is an increase in the broadband type of noise when a blade section is stalled. Even if the blade could be stalled and unstalled to produce a burst of broadband noise, this would not have the impulsive nature of blade slap. The impulse is of a short duration and must therefore be a direct result of a rapid load (lift) or force fluctuation. Since typical impulses on a single rotor helicopter are of durations of the order of 1-5 ms, the stall sequence or change in lift must therefore occur in an azimuthal blade movement of a few degrees. A study of papers concerned with stall [78 - 81] illustrates the complexity of the problem and suggests that it is impossible at the present time to obtain the necessary details required on stall to make even an elementary estimate of the impulsive type of noise (if any) associated with occurrence of stall. There is, however, a general feeling that the occurrence of stall is a relatively slow process. Ham [78] for example, showed that when a blade is taken rapidly above the 'stall angle' the high values of lift are sustained for a time equivalent to something of the order of that for 1/8th of a blade revolution. The delay in occurrence of stall is thought to be a function of the rate of change of angle of attack and the sustained upper surface suction associated with the chordwise passage of vorticity shed during the stall process. It is, of course, a well known fact that the onset of dynamic stall occurs at much higher angles of attack than those associated with the static stall. Thus there is very little chance of a blade stalling as it passes through, or close to, a tip vortex. Work at Southampton [1] showed that induced angles of $\pm$ 25° could be tolerated without any apparent stall, provided the time scale was small.

On an actual helicopter it is, however, true that blade slap is often associated with flight conditions in which stall can easily occur: i.e., high speed and large all up weight (A.U.W.) cases. It appears that this is the main reason for associating blade slap with the onset of stall. A closer study shows that stall can occur without blade slap being detected, and often the blade slap occurs when stall is unlikely. It was shown by using a Wessex [82] that 45/50° bank turns to port and starboard respectively produced identical blade slap, both in amplitude and characteristic. It is difficult to explain this in

terms of the 'stall theory' since a steady bank turn would not be expected to affect the stall characteristics to any great extent. It also appears that the 'stall' conditions of the majority of single rotor helicopter configurations are approximately the same, yet their blade slap characteristics are completely different, varying from no slap to extremely loud slap. Also during the Wessex tests it was found that in level flight blade slap could be induced by decreasing as well as increasing collective pitch: it is difficult to see how this can be explained in terms of the stall phenomenon.

A typical angle-of-attack contour for a single rotor helicopter is shown in Figure 5.6. If stall produces a 'bang', then as the blade rotates it would be expected that a continuous series of impulses would be produced as more of the blade became stalled. Experimental results, however, indicated that the main 'bang' on a single rotor helicopter is a single impulse of short duration. A typical bang duration in terms of blade azimuth movement is also shown on this figure. It will be noted that there is very little correlation between this and the stall duration.

A further point against the stall idea is the observation of the effect of very low wind on a hovering helicopter [82] and a whirl tower [83]; although stall is very unlikely in these cases, blade slap was produced in both. Distortion of the vortex filament path and blade/vortex interaction is, of course, much more likely in these circumstances.

The above discussion has been based on the traditional and classical concepts of stall. Studies, however, suggest that this form of stall does not occur on rotor blades.

To summarize, it would appear that although the 'stall blade slap' hypothesis cannot be completely disproved, the above points indicate the unlikelihood of blade slap being the result of such a mechanism.

5.3.3. Shock Wave Formation

The formation of shock waves on any aerofoil is very complex. It is suggested that on a single rotor helicopter a shock is formed when the local flow becomes supersonic, while on a tandem helicopter it is postulated that shock formation is a result of blade/vortex interaction as already outlined. Information of the details of shock wave formation is very sparse and there is practically no work on rotating systems such as the helicopter rotor.

Before considering the possible production of a shock wave on a rotor, it is worth noting that a blade travelling at an overall subsonic speed with a small local shock wave on it due to local supersonic flow, will itself not produce any noise. There is no comparison between this case and the sonic boom produced on supersonic aircraft. The noise source would, if it occurred, be a result of the fluctuation, or change, in lift caused by the formation of a discrete shock wave unless the shock became detached (see section 5.3.4).

Although shock wave formation is discussed in detail in references (84-86), there still appears to be a general lack of understanding of the topic.

The present position appears to be that the actual Mach number at which shock waves occur can be found accurately only by experiment; but this is complicated by the fact that weak shock waves which form owing to localised sonic flow are extremely difficult to detect. In fact on many aerofoils local regions can become supersonic without the formation of extensive shock waves.

Since the local flow is dependent on the conditions of the flow across the aerofoil section, the formation of the shock wave would be expected to be more random than indicated by the measurements, which suggest that it occurs (within the measuring accuracy) at blade passing frequency.

5.3.4. 'Shock Wave'/Thickness Noise

It followed from the above review that although local shock formation may be indicative of a 'high noise' condition, it was not considered a predominant mechanism from the blade slap point of view. The situation was, however, further confused in 1968/69 when research workers from the Bell Helicopter Company presented at a number of specialist meetings some unpublished Schlieren photographs taken of a model rotor blade which appeared to show a detached shock wave propagating into the far field. Reported theoretical efforts seemed, however, to discount this possibility because the advancing blade tip Mach number was less than unity. Also it appeared from aerodynamicists' point of view that although local shock waves could be present on the airfoil they should be locally fixed and hence should not radiate into the acoustic far field. Recently it appeared that this source could be explained in terms of 'blade thickness' [55, 56]. These theories showed that at a high blade speed (advancing blade Mach number of the order of 0.8 and above) the acoustic field is

dominated by the blade thickness noise. Good correlation between theory and experiment both in terms of the absolute 'peak' pressure level and pressure-time history characteristics was obtained for the Lynx and the UH-1H (US Army data from reference (87)) by Hawkings [55 and 88]. It appeared, therefore, that a satisfactory explanation for the high speed impulsive (blade slap) noise had been obtained. In the experiments conducted by the US Army on the UH-1H [87] and the subsequent wind tunnel experiments [89] it was shown that in addition to 'blade thickness noise' and blade/vortex interaction noise, there was a third pressure 'peak'. These three separate sources are illustrated in Figure 5.7 reproduced from reference (87). The positive pressure pulses '1' are associated by the authors to blade/vortex interaction, the negative pressure pulse '2' with the 'blade thickness' and positive pressure spike '3' to 'shock wave' effects. It will be observed that pulse '3' is larger in magnitude than pulse '1' although the 'blade thickness' peak pulse '2' clearly dominates the signals. From the model studies [89] it was concluded that at a blade azimuth angle between 85° and 110° a continuous shock develops off the tip of the blade and that as the azimuth angle increased the 'shock' moves forward ahead of the leading edge of the blade and propagates in the direction of forward flight. It could, of course, be argued that this is not a shock in the classic sense with a large pressure discontinuity but rather simply a strong compression wave with a high pressure gradient. In this context it is worth noting that as far as can be determined this would give the same appearance on a Schlieren photograph and such an approach would not be capable of separating the individual components of the pressure pulse. Also according to Hawkings any compression wave will tend to 'steepen up' as it is propagated from the advancing blade. It is obvious that there are still differences of opinion on the details of this source. The practical situation is further complicated by the fact that all the sources considered would radiate predominantly in the plane of the rotor. It is also worth noting that as far as can be determined the 'shock wave' source (peak '3' on Figure 5.7) has only been clearly identified on recordings of the UH-1H.

Another reason for the general confusion on this topic is that if parameters relating to a particular rotor are examined it can be shown that 'blade thickness' becomes important (relative to fluctuation

force noise) at an advancing blade tip speed which corresponds very closely to that associated with drag divergence and the onset of compressibility effects. This is in the region of an 0.7/0.8 Mach number and is also the blade tip speed where the local flow can become supersonic and local shock waves thus can form. It is not difficult to see therefore why each of these mechanisms have been associated with the generation of high speed blade slap, since it only becomes a significant source which can be easily identified at such advancing blade speeds.

5.4. BLADE SLAP GENERATION

From the review of the possible mechanisms, it appeared at the commencement of the study that blade/vortex interaction was one of the most important mechanisms from the point of view of the generation of blade slap noise on a real helicopter. This conclusion was given further credibility by the results of a full scale investigation conducted by the Boeing Vertol Company [90]. This confirmed that the 'blade slap' on their tandem helicopters was a direct result of blade/vortex interaction; this result was of particular interest since, according to available information, the programme was to some extent conducted to disprove the blade/vortex interaction concept. Thus, in the main, from the blade slap investigation reported in this document it was assumed that the 'impulse' was a direct result of the fluctuation in lift caused by the interaction of a blade and a tip vortex filament. On a real helicopter this can be either an actual interaction where a blade cuts right through a vortex filament or a 'near-interaction' where a blade passes very close to a vortex filament.

Such an assumption was not intended to imply that other mechanisms did not exist and in fact a brief study of recordings of the Bell UH-1D in 1965 suggested another mechanism at high speed. This could not, however, be correlated with the appearance of shock waves on the blade or compressibility effects. Thus at the time of commencement of the study none of these aspects could be pursued. This situation is still confused at present, as discussed in section 5.3.4, but even if 'blade thickness' noise is taken into account blade/vortex interaction is still undoubtedly an important noise source since it is responsible for the predominant 'blade slap' noise generation on all helicopters. The main exception is on the Bell UH range of helicopters during high speed flight, but even on these helicopters blade/vortex interaction is important at

moderate flight speeds and during landings and manoeuvres. Even so, if the significance of 'blade thickness' had been appreciated earlier, it would have been studied in parallel to blade/vortex interaction. From the subjective point of view, however, it is of interest to note that the results obtained in the author's studies are applicable to all forms of impulsive/blade slap type noise since the acoustic signatures of the pulses are very similar in all cases.

5.5. HELICOPTER TESTS

Flight tests were carried out at WHL; in addition tape recordings were supplied to ISVR by Bell Helicopter Company, the Boeing Vertol Company and the Sikorsky Aircraft Company. Narrowband analysis and time history traces were produced from these tapes and used, together with overall levels and dBA levels, to determine the general characteristics associated with blade slap. A representative selection of these results is reproduced in Figures 5.8 to 5.15 inclusive. The typical narrowband analysis results shown are as follows:

Figure 5.8, Belvedere (internal); V107 (external) and Wessex (internal);
Figures 5.9(a), 5.9(b), CH-46A (external);
Figure 5.10 UH-1B (external).

The Belvedere analyses are also shown in a slightly different format in Figure 5.2.

Time histories (UV traces) are reproduced as follows:

Figure 5.11(a) and (b), Wessex Mk.5 (internal);
Figure 5.12(a) and (b), Sycamore (internal);
Figure 5.13(a) and (b), UH-1B (internal);
Figures 5.14 and 5.15, CH-46A (external).

Traces for other helicopters have not been included since they are reproduced in the general literature and/or readily available in company reports.

The tape recordings made for hovering helicopters (tandem) and those obtained in the cabins are fairly constant in level and frequency content, and this produces a 'clean' trace on analysis. The external forward flight results show, as expected, considerable variation with time and hence are more difficult to analyse and interpret. When making the comparison discussed below, as near as possible identical non-slapping and blade slap conditions were examined.

5.5.1. Accuracy of Recordings

An examination was made of all the data available at ISVR to determine if the recordings contained a true representation of the blade slap impulse. The results of this study indicated that in the majority of cases some 'overload' or 'peak clipping'had most likely occurred. In many of the cases, however, it appeared to be only the intermittent 'peak' which was affected and that the recordings were a fair representation of the true levels.

The difficulty which occurs during recording is a direct result of the very impulsive signals produced when blade slap occurs. Typically the peak level of the impulse is 15 to 20 dB above the rms level. Thus when recording, an 'rms meter' will look effectively 'dead' when the attenuator controls are set at the correct level for recording blade slap. The conventional semi-impulse or 'peak' meter improves the situation; but even so, it is very difficult without the aid of an oscilloscope, or special peak level detector, to obtain a true recording of blade slap noise.

It is also possible that the 'peaks' may have been limited to some extent in rise-time by the transient response of the microphone and/or tape recorder. Even when allowing for these possible limitations, it was thought that the data was sufficiently acceptable for the particular investigations described in this report. The rise time of the impulse can also be modified by the recording equipment technique used.

5.5.2. Narrowband Analysis Results

Narrowband analysis was performed with a constant bandwidth analyzer system; the appropriate bandwidths and frequency ranges used are shown on the figures. As will be seen, typically a 2 Hz filter was used up to a frequency of 150 Hz, and a 5 Hz filter beyond this frequency. Although analysis was usually made over the frequency range 10 Hz to 10 kHz, blade slap analysis was usually curtailed at 3 to 5 kHz depending on the helicopter being studied. The amplitude scales are either in SPL re 0.0002 dynes/cm^2, or dB relative to an arbitrary datum.

In general, when blade slap occurs, the corresponding narrowband analysis shows an increase, relative to the non blade slap conditions, in the region equivalent to the 10th to 20th blade passing harmonic. Typically, this is in the range 150 to 400 Hz. Analysis shows that the maximum level of the peak envelope corresponds to the main frequency component of the impulse.

In addition to the increase of the 'impulse harmonics', the tandem helicopter recordings show an increase in the lower (4th to 10th) blade passing harmonics. This is considered to be an increase in the rotational rotor noise caused by the blade operating in a generally rougher flow environment. This is discussed in section 3.13 in connection with the results obtained on the ISVR 9 ft diameter single rotor hover model. This effect is further illustrated in the work described in section 5.10. There is also some indication of this effect during the 'high speed' blade slap on the UH-1B (Figure 5.10). In this case it is, however, very much more difficult to correlate the results because of the high levels of low frequency rotational noise present on this helicopter.

5.5.3. Time Histories - Oscillograms

It is clear from the traces that the blade slap 'bang' occurs at blade passing frequency; this applied to all the helicopters studied. On the Wessex, Sycamore and Belvedere helicopters the 'bang' approximates very closely to a single impulse (Figures 5.11 and 5.12). On the UH-1B (Figure 5.13) and the CH-46 (Figures 5.14 and 5.15) however the 'bang' consisted of two or three main 'impulses'. This could be the result of blade/vortex interaction occurring over a considerable portion of the blade span at slightly different instants or separate interactions occurring at practically the same time. A study of the traces shows that although the 'bang' sometimes contains several discrete impulses, there is, in general, one impulse which is larger than the others.

To obtain the filtered traces, the recordings were passed through a band pass filter and the signal studied on a CRO and/or UV recorder. The filter pass band limits were adjusted so that the blade slap impulses were not significantly affected while the other noise was reduced to a minimum. The signals were also evaluated subjectively and in each case the characteristic of the 'bang' was found to be unaffected by the filter settings chosen. It is worth noting in this context, however, that the subjective evaluation was made by the helicopter team and a jury was not used. Using the filter reduced the low frequency rotor rotational noise and the high frequency noise which was mainly from the gearbox and/or engines. This, of course, had the effect of making the 'bang' more readily detected both on analysis and subjectively.

The filtered frequency range associated with the helicopters examined was 50 Hz to 1 kHz. It is these frequency limits that were used to obtain the 'filtered' time histories shown in Figures 5.11 to

5.13. 'Non-filtered' refers to unweighted recordings which typically cover the frequency range 20 Hz to 15 kHz.

The filter ranges were further reduced to isolate, as nearly as possible, the blade slap 'bang'. Although this reduced the amplitude of the impulse, it allowed the main frequency content of the 'bang' to be determined. These frequency ranges are given in Table 5.1, together with the envelope peak obtained from the narrowband spectra (Figures 5.8 - 5.10). It seems fair to assume that the centre of this frequency band corresponds very closely with the main frequency component of the 'bang'. A review of the results shows that in general this is the case. The envelope peak frequencies quoted in Table 5.1 were obtained from the average of several narrowband spectra, and not just those reproduced in this report. In the case of the Bell UH-1B, CH-46 and V107, it is a little difficult to locate the peak frequency because of the general increase in the rotational rotor noise.

A study of the time history traces also reveals that on both single and tandem rotor helicopters the maximum peak-to-peak levels are increased by approximately 10 dB when blade slap occurs.

In the case of the UH-1B, however, the blade slap impulse is not so clearly defined and appears to be superimposed on top of the already impulsive rotor noise (Figure 5.13). For this helicopter the peak-to-peak difference between the banging and non-banging modes varied between 10 dB and zero for the various flight conditions studied.

The amplitude scale used on the oscillograms is SPL-dB relative to the standard reference level of 0.0002 dynes/cm^2. The scale is so chosen that a sine wave having an SPL of X dB would produce a sine wave on analysis having an amplitude of $\pm$ X dB.

5.5.4. Overall and dB(A) Levels

A review of available data was also made to determine the overall noise level difference between a banging and non-banging helicopter operating as far as possible under similar conditions. The results were rather interesting in that, in general, the addition of blade slap increased the OASPL (dB Lin) and dB(A) levels by only 2 to 3 dB. In one particular case for a tandem helicopter the difference was as large as 6 dB, but for other cases examined it was as little as 1 dB. However, in the most significant octave band, 250 Hz for most helicopters, larger differences were measured, with the average being of the order of 6 dB. On a narrowband analysis, the level difference at the envelope peak

frequency is typically 10 to 15 dB, although in the case of the Sycamore it was only 2 to 3 dB. These differences can be seen on Figures 5.8 - 5.10.

These general studies have clearly shown that it is not possible to determine the severity of blade slap by considering overall noise levels or octave plots. Even narrowband analysis can give a misleading impression if the general level of rotational noise is high. If results are correlated on a PNdB basis, then it is unlikely that the addition of blade slap will even affect the results. These aspects are discussed further in section 5.10.

5.5.5. Discussion of Results

5.5.5.1. Tandem helicopters (Belvedere, V107 and CH-46A)

On the V107 and CH-46A blade slap occurs in all flight regimes including hover, while on the Belvedere it is limited to forward flight conditions. On the Belvedere, blade slap is usually intermittent and of low level, except in banked turns and mild 'pull-outs' when continuous loud slap occurs. The blade overlap on this helicopter is extremely small and, in general, it displays blade slap of very similar characteristics to that of a four bladed single rotor helicopter. For all practical purposes it would appear, therefore, that the Belvedere can be considered as a four bladed single rotor helicopter with two isolated rotors. Although it is not documented, the author has been given to understand that at high forward speed the V107 acts in a similar manner. This is equally understandable since the wake at the 'front' of the rear rotor will either go above, or be at an acute angle to, the rotor disc at high speed, and thus not interact with the lower forward rotor.

The V107/CH-46A has a relatively large area of overlap and produces very loud blade slap. The V107 studied at ISVR was equipped with a longitudinal trim device that allowed the 'longitudinal cyclic' of the rear rotor, and in effect the blade separation, to be varied. In a steady state flight condition, including hover, the actuation of this trim device substantially strengthened or reduced the severity of blade slap. At moderate forward speeds trimming the V107 helicopter to its most nose down condition increased blade separation and practically eliminated blade slap. In this configuration it is suggested that the rotors are both acting like single rotors and the interaction between the wake of the rear and forward rotor is non-existent. This is very similar to the high speed conditions discussed previously. Figure 5.14

clearly illustrates the above effect on the CH-46A where the 'trim settings' have been adjusted for maximum and minimum blade slap noise. On the CH-46A, the gains which can be obtained from adjusting the trim settings are dependent on the forward speed and at higher speeds the reduction in blade slap is somewhat smaller. This is shown in Figure 5.9(a), which shows the 100 knot flight conditions.

A similar situation to that outlined above for the V107/CH-46A also exists on the U.S. Army Chinook Helicopter (CH-47).

5.5.5.2. Single rotor helicopters (UH-1B, UH-1D, Sycamore, Scout, Wessex and S.61)

Single rotor helicopters can be grouped into the two categories of 'two-bladed rotor helicopters' and 'multi-bladed' (3 or more) rotor helicopters. These are discussed separately below.

5.5.5.2.1. Multi-bladed rotor helicopters

A Wessex helicopter was flown in its standard configuration and blade slap was found to occur during the following flight conditions.

(a) low power descent

(b) port and starboard banked turns of 40° or more, at 60-80 knots.

The blade slap was identical for both the port and starboard banked turns. Intermittent blade slap was also found to occur when any sudden manoeuvre was made and when positive or negative collective pitch was applied. As far as could be determined, when blade slap occurred it could always be heard simultaneously in the cabin and externally. Similar characteristics are also associated with all the other helicopters studied, except on the Sycamore where a more severely banked turn was often necessary to produce continuous blade slap.

5.5.5.2.2. Two bladed rotor helicopters

A flight test programme carried out for ISVR by the Bell Helicopter Company using the UH-1B gave some interesting results. Firstly, at low speeds (up to 100 knots) blade slap of the type associated with the multi-bladed single rotor helicopter occurred. Thus banked turns and low power descent produced blade slap. A test in London with a Jet Ranger also gave similar results and very loud blade slap was produced during descent.

Very loud blade slap is also produced during straight and level flight at forward speeds around 120 knots. At 90 knots there is no indication of blade slap either internally or externally, while at 120 knots very loud blade slap is detectable externally. At this higher speed condition, however, blade slap could not be heard in the cabin. An

examination of recordings revealed practically identical characteristics in the cabin at 90 (no blade slap) and 120 knots (external blade slap), although overall noise levels were a few dB higher. Externally, the noise showed a considerable change both in level and characteristics. Bell researchers [91] associate this 'high speed blade slap' with the onset of compressibility effects on the advancing blade and the occurrence of local supersonic flow. The details of the noise generating mechanisms are not known, but the Bell researchers do not think it is the blade/vortex interaction type of noise which occurs at low speeds and during low power descents. A detailed examination of recordings of both blade slap conditions has not shown any characteristic difference, but this is not surprising since any impulsive mechanism would produce a similar acoustic signature.

5.6. BLADE/VORTEX INTERACTION ON HELICOPTERS

Although it is easy to imagine a blade and a tip vortex interacting it is extremely difficult to visualise the details of such an encounter and practically impossible to describe it mathematically.

Consider in the first instance the single rotor case. It was initially thought that the tip vortex took a considerable time after it was shed to form into a discrete filament, and that it moved away rapidly from the rotor plane after it had been shed. Experimental evidence has shown that the converse is often true. The photograph (Plate 5.1) of the Westland Westminster taken in high humidity condition shows the tip vortex filaments as condensation trails. The vortex trailed behind the blade in the port quarter is shown very clearly. Also shown, but much more faintly, is the vortex trailed by the previous blade (at approximately the 300° position) which can be traced to the forward position; it will be noted that this appears to go above the following blade. Although the blades are not cutting any vortex filament in this particular case, they are obviously passing very close to the vortex filament. Some equally interesting photographs were obtained on a Sea King (British-built Sikorsky SH-3D). Two of these photographs are reproduced in Plates 5.2 and 5.3. The helicopter was hovering in a light wind, estimated to be 10 to 15 knots, and the photographs were taken from above and to the side. In each case the trailing filaments pass above the following blade before descending below the rotor disc. In the flight mode shown the Sea King does not produce any blade slap, but the general rotor noise is more impulsive in nature than that produced by the other Westland

helicopters. Although other helicopters, including a Wessex 60 (partly shown in the photographs), were flying at the same time as the Sea King, condensation trails were not seen. To date it has not been possible to explain this phenomenon. It was initially thought that it might be correlated with blade loading or ideal vortex strength but this proved negative. The only parameter having a significant difference was the loading per blade which was greatest for the Sea King but it is difficult to see how this can offer an explanation. It is tentatively suggested that the spanwise loading distribution, and hence the 'true vortex strength' may be different on the Sea King and account for the appearance of the vortex filament.

Smoke tests on a model two bladed rotor rig situated in the wind tunnel at Southampton [92] showed that at the front of the disc there is a strong upwash with the result that the tip vortex after formation rises above the rotor disc. A typical trajectory of the cross-section of a vortex at the 180° position (i.e. at the front of the rotor) is reproduced in Figure 5.16. This is in general agreement with calculations and blade pressure measurements made by Ham [93]. In addition to this upwash at the front of the rotor considerable distortion in the flow pattern occurs around the disc, particularly in the 45° and 315° regions. This is shown clearly in Taraine's study [94] of the local flow around a rotor disc and was observed during the Southampton tests. Computations by Crimi [95] and White [96] for a two bladed rotor, and by Scully [97] have all demonstrated this trend.

The investigations mentioned above also confirmed that the basic tip vortex forms very rapidly. This is substantiated in the propeller research by Adams [98] and the study of the flow behind an aircraft wing by McCormick and Tangler [99]. Simons *et al* [100] concluded that the rolling-up is completed in about the time taken to travel a distance equivalent to one blade radius, which is in general agreement with that found for the vortex rolling-up process on wings. Thus the tip vortex would be practically in its final form by the time any blade vortex interaction could occur.

Flight tests are limited, although differential blade pressure measurements at the Bell Helicopter Company [73] have shown clearly that rapid changes of pressure of the type expected if a blade/vortex interaction occurs are indeed present when blade slap is being produced. If it is accepted that vortices can pass above or near the rotor disc, then

it is clear that blade vortex interaction can occur and it is very likely that a blade can actually cut a vortex filament. For the practical case the situation will be more complicated than the model tests indicate since turbulence, the helicopter fuselage and the general non-symmetrical nature of blade loading will cause even further distortion of the flow patterns.

On a tandem rotor helicopter, particularly if the blade overlap is large, it is easy to imagine a blade cutting a vortex filament since one rotor will be passing through the downwash of the other. This obviously accounts for the fact that blade slap is much more severe on tandem rotor helicopters. The Boeing Vertol Company [83] carried out a detailed experimental programme in which smoke was generated at the blade tips of a tandem helicopter. This showed clearly blade vortex interaction and that the position at which it occurred could be computed by using a relatively simple analytical model. It is worth noting that although on a tandem the rear rotor is above the front rotor in hover, the position can be reversed in forward flight due to the tilting of the rotor discs. Thus, as shown by the Boeing Vertol report [83], the rear rotor blades can cut the tip vortex filament shed by the front rotor system.

The flow visualisation technique reported in reference (92) was applied by Simons to a preliminary study of the 'tandem rotor' flow patterns. To date this work has not been published, but a selection of the photographs taken are reproduced in Plate 5.4. The photographs show clearly how the isolated tip vortex passes through the lower rotor and, since the vortices are in the form of a continuous filament, it is obvious that an interaction can occur under certain conditions. The bottom photograph illustrates the 'unwinding' of the vortex filament which appears to take place after the interaction.

The details of any interaction are extremely complicated and estimation of the actual fluctuation in load is not possible at the present time. An insight into the problem can, however, be obtained by considering the types of idealised interactions likely on helicopters. Figure 5.17 shows some typical cases where the vortex filament is represented by a rotating cylinder. Even an elementary study of this simplified situation will reveal the complex nature of determining the appropriate velocity profiles 'seen' by the blade. In practice the position will

be further complicated since the circulation of the blade and the vortex will affect one another and cause severe distortion of the filament when the blade and vortex are close together. On a single rotor helicopter the blade will most likely either pass close to the vortex filament, Figure 5.17(a), or cut through the filament, Figure 5.17(b). On a tandem helicopter it is more likely that one rotor will cut the vortex filament from the other rotor as illustrated in Figure 5.17(c). Although the details are not known it is clear that the velocity profile in the direction of motion will be similar in each case, and takes the form given by the interaction of a blade and an isolated vortex with its axis parallel to the span. The fact that large fluctuations in lift occur when a blade passes close to a vortex filament are obvious, as illustrated by Simons [101].

The 'peak' velocity amplitude encountered by the blade will be practically independent of the type of interaction and thus noise from any interaction, to a first approximation, will be dependent only on the vortex size and blade parameter. The theoretical development (see section 5.9) is based on this assumption and thus will predict the less favourable result, since any of the type of interaction illustrated in Figure 5.17 will tend to reduce slightly the peak amplitude and, more important, the rate of change of loading.

5.7. BLADE SLAP SOURCE LOCATION - FLIGHT TESTS

In an attempt to locate the rotor azimuth positions when the blade slap 'bang' occurred, a series of flight tests were carried out by WHL. The single rotor helicopters used were a Sycamore (3 bladed rotor) and a Wessex (4 bladed rotor).

A forward flight speed of 65 knots (approximately 110 ft/s) was selected for these tests since, with the helicopters used, blade slap could be conveniently generated at this speed. On the Wessex it was necessary to fly in a $40/45^{\circ}$ banked turn before continuous blade slap of a relatively loud level was produced, while on the Sycamore an even larger bank angle was required.

Simultaneous recordings of the noise in the cabin, at a known position, and a signal from a blade azimuth marker on the rotor head were made on a twin track tape recorder. The recordings were subsequently played back through a UV recorder and traces of blade slap and azimuth position obtained. Since blade slap occurs at blade passing frequency, four and three blade slap impulses were obtained per rotor revolution for

the Wessex and Sycamore, respectively. The rotor head orientation at the instant the 'bang' was measured acoustically could be fixed from these traces. To determine the blade position at the moment of blade slap it was necessary to take into account (a) the time taken for the impulse to reach the microphone, and (b) the blade lag relative to the rotor hub.

It seemed reasonable to assume that the 'bang' occurred near the tip. Initially this was assumed to be at 0.95R (where R is the blade tip radius) in which case the blades would have moved on the Wessex a further 34° before the signal reached the microphone. The blade lag of 5° was obtained from standard flight data for the condition flown. These angles are illustrated for the case of the Wessex in Figure 5.18, together with the estimated position of the blades when the 'bang' occurred. The 33° increment, equivalent to the interval between the azimuth marker 'blip' and the recorded blade slap signal, was the average of 10 rotor revolutions. The results were, as expected, very consistent, and within the measuring accuracy (better than $\pm$ 1%) the blade slap impulse occurred at blade passing frequency. As obtained by the approach outlined above, the blade positions when the 'bang' occurred for the Wessex and Sycamore are those shown diagrammatically in Figures 5.19(a) and 5.20(a), respectively. Although the rotor rotation on a Sycamore is clockwise (as viewed from above), the result has been converted to an anti-clockwise convention for comparison with the Wessex.

The theoretical blade bang azimuth position was calculated by using a simple rigid wake model, even though work on the wake patterns associated with single rotors has shown that the wake shapes are likely to be much more complex [95, 102].

The experimentally measured results were correlated with the predicted 'bang' positions obtained by using the following approach. When the trailing wake leaves the rotor tip it combines into a strong 'tip vortex' which moves inboard. Hover results show that the tip vortex can quickly move into a position which is equivalent to the 0.9 R station. In forward flight the contraction is considered to be less, and the tip vortex is more likely to take up a position just after leaving the blade which corresponds to 0.95 R. Limited experimental evidence to date does, however, suggest that the contraction of the wake is greater at the sides (90° and 270° regions) than at the front and rear of the rotor. Because of the lack of precise knowledge on this point, for this

particular study predictions were made for a range of values between 0.9 R and 0.95 R.

The results for the Wessex and Sycamore are shown on Figures 5.19(b) and 5.20(b) respectively. As can be seen, the 'bang' is assumed to occur at the position where the tip of a blade intersects the trailing vortex wake left by the preceding blade. A comparison of the measurements and predictions shown on Figures 5.19 and 5.20 show that there is good correlation, particularly in the case of the Wessex. Even in the case of the Sycamore the difference between the 0.9 R predicted position and the measured position is only 12°, which is surprisingly good when all the variables in estimating the rotor blade position and the limitations of the simple rigid wake model are taken into consideration. In this context it should be remembered that it is not possible to take into account the fact that the helicopters were banked to obtain blade slap. On the other hand it is well known that the vortex filament stays in or near the rotor disc until the next blade approaches (see section 5.6), when vortex distortion effects become significant. Thus a simple wake approach can be expected to give at least an indication of the blade position when the 'bang' occurs, if this is produced by the first blade/vortex interaction.

After the above tests were performed, the Boeing Vertol Company [83] reported an extensive blade slap flight programme carried out on a tandem rotor helicopter. They showed clearly that the 'bang' occurs when a blade intersects a tip vortex and that a simple rigid wake could be used for estimating the magnitude of the bang and the blade azimuth position at which it occurs. It is also of interest to note that these experimental results did not in any way agree with Sikorsky findings [103] that the 'bang' occurs on the retreating blade at the 270° position.

On the Wessex, identical results were obtained for both starboard and port bank turns, but this aspect was not examined on the Sycamore.

5.8. TIP VORTICES

5.8.1. Generation of Tip Vortices

Any aerofoil or lifting surface produces a system of trailing vortices as a result of the lift or circulation variation across the span. This trailing sheet of free vortices, which represents a surface of discontinuity, is unstable and cannot persist in this form. Instead the sheet tends to roll up rapidly behind the wing to form a pair of discrete vortex filaments. Thus the trailing wake some distance behind

the wing or rotor blade will consist only of a root and tip vortex, in opposite sense to each other. Since the tip vortex is very concentrated and the root vortex very diffuse, it is usual to consider only the tip vortex.

5.8.2. Theoretical Model

Theoretically it is very difficult to estimate the tangential velocity of a vortex. For two-dimensional potential flow the circumferential velocity varies inversely with the radius according to the relationship:

$$V_t = \Gamma / 2\pi r_v \qquad (5.1)$$

where V_t is the tangential component of induced velocity, r_v is the radius from the vortex centre and Γ is the circulation.

This results in a distribution as illustrated by the 'dotted' line in Figure 5.21, with the velocity at the centre being infinite. In a real fluid this could not occur and V_t would take the form shown by the 'solid' line. In this case the velocity departs from the potential theory value as the vortex is traversed, and reaches a maximum before decreasing to zero at the vortex centre. This centre region is known as the core, within which the fluid motion approaches that of a solid body in rotation. If in fact the core is simplified to a rigid body, then the velocity distribution in the core would take the form indicated by the 'dashed' line in Figure 5.21, i.e.

$$V_t = \left[\Gamma / 2\pi r_p^2\right] r_v \qquad (5.2)$$

where r_p is the radius at which the motion is considered to change from that of rigid body to potential flow (see Figure 5.21).

As already mentioned, a real fluid has a somewhat different profile, a good approximation to which is given by Lamb's solution for a viscous fluid [104].

$$V_t = \Gamma / 2\pi r_v \left(1 - e^{-r_v^2/4\nu\tau}\right) \qquad (5.3)$$

where ν is the kinematic viscosity and τ is the time (decay interval). This illustrates another property of a vortex, namely that the core diffuses with time due to viscous effects. It also follows that the maximum tangential velocity, V_M is dependent on the lift produced by the blade since Γ is directly related to the bound circulation on the aerofoil and the vortex structure.

In addition to the maximum tangential velocity, another important parameter is the core diameter. This is not a well defined dimension since the actual velocity distribution approaches asymptotically the

potential distribution. For convenience of this work, the core diameter has been taken as the diameter of a circle bounded by the maximum tangential velocity.

Since Γ , the circulation can be calculated for a helicopter blade, it is only necessary to know the core size to obtain V_M and an estimation of the velocity distribution.

Equation (5.3), Lamb's solution, defines the radial distribution of the velocity through the vortex as a function of time. From this it follows that the maximum velocity is at a radius given by:

$$r = \sqrt{1{\cdot}26(4\nu\tau)} \qquad (5.4)$$

Thus the maximum velocity V_M is

$$V_M = 0{\cdot}638\Gamma/2\pi\sqrt{1/4\nu\tau} \qquad (5.5)$$

These equations suggest that the core diameter increases as a function of $\tau^{\frac{1}{2}}$, while the maximum velocity decays as a function of $\tau^{-\frac{1}{2}}$.

Simons et al [93] suggested a modified relationship for the core radius where the time 'τ' was replaced by $(\tau + \tau_o)$. This implies that at $\tau = 0$, when the vortex is assumed to leave the blade, the vortex core is of finite size. This illustrates clearly the problem encountered, namely what to consider as zero time (i.e., $\tau = 0$). Since there are indications of a well formed vortex core soon after the vortex leaves the blade, it would appear that the time must be assumed to start from a datum in advance of this time. Alternately a solution of the form outlined by Simon et al [93] must be used. Thus to generalise, it would appear that although Lamb's solution can be used to predict the shape of the velocity distribution through an isolated vortex core and the indications of changes in vortex structure likely with time, it cannot be used to predict absolute values since 'zero time' cannot be defined. Equations (5.4) and 5.5) are, therefore, not general working solutions. For the particular case under consideration, however, the time between the vortex leaving the blade and a likely blade vortex interaction is fairly small and thus, if it is assumed that change of dimensions is of the form indicated by Lamb's solution, the change in vortex core size and peak velocity would not be expected to be large.

5.8.3. Measurements

At the commencement of the blade slap study in 1966 a review was made of the available data and as far as could be determined there had been no measurements of the characteristics of tip vortices shed from

real helicopter blades. A number of investigators had, however, made estimations for the tip vortices shed by wings. Piercy's [105] results, for example, indicate that the core radius is approximately 1/12 of the span while Spreiter and Sacks [106] gave a core radius equivalent to0.155 times the semi-span for an elliptically loaded wing. If a helicopter rotor is considered to be a wing with an aspect ratio of 20, then these results suggest a core diameter of about 3 chords (i.e. 3c).

Although only a few investigators have actually attempted to measure the profile of a tip vortex, their results indicate a much smaller core. An early study by Piercy (5.42) suggested a core diameter of 0.2c, with the maximum tangential velocity, being equivalent to an induced angle of $\pm 17\frac{1}{2}^{o}$. In a study on the V107 helicopter rotor [107] McCormick approximated the outer portion of the rotor blade by a wing and measured some velocity profiles about 6 chords behind it. This gave core diameters of the order of 0.25c and maximum induced angles of $\pm 18^{o}$.

Simons, Pacifico and Jones [100] carried out some experiments in a wind tunnel using a model helicopter rotor and measured the vortex profile with a 'hot wire anemometer'. This gave a core diameter of the order of 0.1c (where c is the blade chord) with a 4 inch chord blade. McCormick and Tangler [99] studied the vortex sheet behind a wing of an actual aircraft (U.S. Army Cessna L-19) and compared the results with a one-twelfth scale semi-wing in the wind tunnel. These wind tunnel results also suggested a core diameter of 0.1c, while the flight results indicated a value of half this value. Maximum induced angle in both cases was of the order of $\pm 22^{o}$.

Although the 'core diameter' has a major effect on the noise produced by any vortex/blade interaction the remainder of the vortex cannot be neglected when estimating the noise. The information on overall size of a tip vortex is even more limited than the details on the vortex core dimensions given above. An examination of the available information tends to suggest that the complete profile takes the form shown in Figures 5.22 with an 'overall width' of 0.75c. Although the 'peak' amplitude, V_M, is a function of blade speed and the blade chord, the experimental results already discussed indicate that the maximum induced angles are of the order of $\pm 20^{o}$ as presented in the figure.

More recently Rorke and Moffitt [108] simulated full scale vortices in a wind tunnel with the aid of wing. They showed that the tip vortex size was a function of the (wing) lift coefficient and elapse time

(age of vortex) and that the core diameter at an elapse time corresponding to a typical blade passing interval was in the order of 3/4% (0.035c) of the blade chord. The 'peak' velocities varied from 0.40 to 0.76 of the free stream velocity which in terms of the induced angle notation is 22° to 37°. Thus the 'core diameter' was less than, and the 'peak velocity' greater than, found by the other investigators mentioned above.

The only full scale helicopter rotor tests to have been carried out appear to be those conducted at WHL and reported by Cook [109]. In these tests a 'hot wire' anemometer was used to obtain the details of the vortex and flow visualization (smoke) to study the general tip vortex paths. The tests were carried out during a noise investigation directed by the author [110] in which a single (one) bladed rotor was run in an inverted (upside down) mode. At the rotor design thrust a 'peak' velocity equivalent to an induced angle of ± 18° was obtained, which is for all practical purposes identical to the data illustrated in Figure 5.22. The diameter of the vortex core was, however, found by Cook to be only 0.01c (1%) which is almost a factor of 10 times smaller than those found by other investigators. The vortex core size was independent of the 'age' of the vortex over an azimuthal test range from 70° to 200°. When the thrust was increased to a value where the tip was considered to be stalled, a core radius of the order of 0.12c (12%) was detected. It was also observed from this study that the rolling up process could be considered to be complete at the first measurement position (70° of rotor rotation) and that the total circulation in the tip vortex remained substantially constant over the age range considered. A comparison was also made by Cook with theory but due to the small viscous core size, and the 'fuller' overall velocity profile which was observed, it was not possible to correlate the experimental results with any theoretical model.

The 'peak' velocity results of Cook are in keeping with those of Simon et al [100] and McCormick and Tangler [99] but the 'core' is considerably smaller, and even smaller than reported in reference (108). From the available evidence it is difficult to generalise on the size of the tip vortex and it would appear from a general review of the literature that the consensus is that a core diameter of the order of 10% of the blade chord is considered reasonable. Thus it would appear that without further evidence the characteristics indicated in Figure 5.22 can still be considered representative of a real tip vortex. In an attempt to clarify the position relating to the size of the vortex core,

a study of the flow visualization photographs available was made by the author. This showed that the 'hole' of the vortex - which can be clearly seen in Plate 5.4 for the ISVR tandem rotor rig - correlates well with the blade chord. This is true in the case of the tandem rotor rig with a 1.5" blade chord, the rotor used by Simons et al [100] with a 4" blade chord and the full scale rotor of Cook with a 16" blade chord. If it is assumed that the 'hole' is a direct function of the vortex size, then it would be expected that the 'hot wire' results of Simons et al and Cook should have given better agreement. It could, however, be argued that the 'hole' size is controlled by the absolute swirl velocity, which would be higher (relatively) on a full scale rotor, or the velocity gradient within the vortex. In this case no correlation between the visual 'hole' and the core size would be expected. This type of study and review does, however, suggest that the position relating to the size of tip vortices is still far from clear and that further aerodynamic studies are warranted.

5.8.4. Real Helicopter Case

As can be gauged from the discussion presented in section 5.8.3 it is not possible to define precisely the tip vortex, and it is necessary therefore to make a number of assumptions before the real helicopter case can be defined. From the theoretical consideration outlined in section 5.8.2 and a general review of the aerodynamic aspects it seems reasonable to assume that the 'peak' or maximum velocity, V_M, is directly proportional to the vortex strength Γ, i.e.

$V_M \propto \Gamma$ (the circulation strength of the vortex).

The circulation strength of a vortex, Γ, is equal to the maximum bound circulation on the rotor blades. Consider the case of a helicopter in ideal hovering conditions with constant circulation.

The lift on an element dr at radius r is $dL = V\rho\Gamma dr$ and $V = \omega r$; thus $dL = \rho\Gamma\omega r\,dr$, and hence the total lift for 1 blade is

$$L = \int_0^R \frac{dL}{dr}.dr = \frac{\rho\Gamma\omega R^2}{2} \qquad (5.6)$$

Now the total lift is equal to the gross weight of the helicopter and hence the total thrust:

$$B.L = (AUW) = T,$$

where B is the number of blades. Thus the ideal vortex strength is

given by

$$\Gamma = 2T/V_T BR \tag{5.7}$$

Hence from equation (5.6) (5.8)

$$V_M \propto T/V_T BR$$

It should be remembered that the above is based on a two dimensional analysis for a perfect fluid containing isolated vortices.

When the blade cuts a vortex filament the blade can be considered to pass through a cylinder of vorticity as illustrated in Figure 5.17. In estimating the noise from any interaction it is necessary to know the span width affected by the vortex and the details of the 'gust length' in the direction of blade motion. These, as shown in Figure 5.17, are obviously functions of the width of the vortex filament, D.

The experimental work on the vortex size, already discussed, appears to suggest that the vortex width, or more precisely the vortex core, is a function of the blade chord. Correlation between various experimental results is poor and it is likely that measurements of the vortex size are given in terms of the blade chord simply because this is a convenient method of quoting the results. The theory on the other hand suggests that the vortex size is independent of all parameters except viscosity and time.

It is far more likely, however, that the core size is directly related to the span loading of the blade and in particular to the loading near the tip [111]. If this is assumed to be correct then, since the blade loading characteristics of the majority of helicopters are similar, it would appear reasonable to assume (at least until further information is available) that the span width effected by the vortex is a constant. Since the overall vortex filament is considered to be of the same order as the blade chord, the 'gust' or vortex filament width in the direction of blade motion can also be assumed constant for any of the isolated interactions illustrated in Figure 5.17.

The difficulties of predicting vortex paths have already been outlined. If, however, the tip vortex path just after leaving the blade is determined by simply assuming it to follow the blade tip path an estimation of where the interaction is likely to occur can be obtained. There is some justification in this since relative to the skew-helical wake configuration, the wake distortion appears to occur in the vertical plane [94, 95, 97]. Also since any interaction is likely to be caused by the preceding blade the distortion in the rotor disc plane can be

expected to be minimum since the time involved is small. The author used this approach for predicting the blade slap in location on the Wessex and Sycamore as discussed in section 5.7 and, as already mentioned, the Boeing Vertol Company [83] used this approach successfully on their tandem rotor helicopter. From this type of study it is clear that for the majority of helicopters the interaction is likely to occur over the outer portion of the blade. In estimating the noise the velocity of the blade at the intersection point is required. Unless a particular rotor configuration and flight condition is being investigated it would appear reasonable to take the less favourable case and assume the intersection velocity to be the same as the blade tip velocity, V_T.

5.9. THEORETICAL STUDY

5.9.1. Blade/Vortex Interaction Model

In the theoretical development initiated as part of the M.Sc. project [1] it was assumed that the blade passed directly through the centre of a discrete tip vortex. The axis of the tip vortex could be either parallel to the blade span or in the direction of rotation. It was further assumed that as the blade passed through the tip vortex it was subjected to a rapid change in lift, which in turn applied a fluctuating force on the surrounding air and thus generated noise. From the aerodynamic point of view the tip vortex was simply treated as a 'gust' with a velocity profile corresponding to that of an idealised tip vortex. The acoustic generation was considered to be dipole in nature with the dipole axis being in the same direction as the line of action of the fluctuating force. Since the rotor operates at zero or very low blade pitch angles the dipole axis was taken to be parallel to the main rotor axis (i.e., vertical).

5.9.1.1. Blade loading

The blade loading was calculated by using an approach incorporating Kussner's function [77] which is based on the two-dimension lifting line aerofoil theory. This is outlined in Appendix 4 and results in two expressions, one for the lift while the blade is inside the tip vortex (gust) and the other when the loading decays as the blade passes out of its zone of influence.

5.9.1.2. Acoustic theories

A simple point dipole theory was developed to compute the acoustic spectrum of the noise generated during the passage of the blade through the tip vortex. Use of a point source model was considered

adequate since the blade/tip vortex interaction occurs over a relatively small area and is effectively fixed in space.

The theory was developed for convenience in two different forms; the first allowed the total sound energy radiated (per unit time) into the far field to be calculated and the second enabled the 'nth harmonic' of the sound pressure level to be derived. These were based on the same Lighthill relationship [112] and are summarised in Appendices 5 and 6, respectively.

5.9.1.3. Accuracy of theoretical model

The two extreme profile distributions for an isolated blade/tip vortex interaction are illustrated in Figure 5.23. Figure 5.23.1(a) and (b) shows the velocity profiles along the span and in the direction of motion, respectively, for a blade passing through a vortex with the core axis parallel to the span.

Figure 5.23.2 shows similar results when the axis of the vortex core is parallel to the direction of motion. The theory has been developed for the case shown in Figure 5.23.1. The vortex is treated as a gust with a velocity profile equivalent to the velocity distribution that would be experienced by a blade if it passed through the centre of the vortex. The blade is assumed to be moving as a wing at a velocity equal to that of the blade section at the centre of the gust.

Since it is the blade loading fluctuation in the direction of blade motion which is important, the theory can also be modified to the case illustrated in Figure 5.23.2. For this the gust is treated as two separate gusts, one acting upwards and one downwards as shown in Figure 5.23.3. The 'power' from each of these is numerically equal and it is, therefore, only necessary to calculate it for one of these and modify the solution to give the total power. If it is assumed that the two parts of the gust act as separate and isolated dipole sources then there is no cancellation effect and the total power is just double that for one part of the gust. It has been shown by Morfey [113] by considering two point dipoles that the ratio of the total power, W_2, to the power in the far field for the single dipole, W_1, takes the following form:

$$W_2/W_1 = 2\left[1 + 3\cos kh/(kh)^2 - 3\sin kh/(kh)^3\right] \qquad (5.9)$$

where h is the separation of the point dipoles, $k = 2\pi f/c_o$ and f is the frequency (c_o is the speed of sound).

W_2/W_1 versus 'kh' is shown in Figure 5.24 and it follows that

as $kh \to 0, W_2/W_1 \to (kh)^2/5$; (5.10)

as $kh \to \infty, W_2/W_1 \to 2$ (isolated dipole case) (5.11)

It also follows that if details of the interaction are known, the total power can be easily found. It would also be necessary to modify the equations developed for the case shown in Figure 5.23.1, to take account of the different spanwise loading: this effect is, however, small and can for all practical purposes be neglected. As discussed in section 5.6 the 'peak amplitude' and the rate of change of the 'velocity' profile will be approximately the same for both the cases illustrated. Thus power and energy predictions will be equally applicable to either type of interaction, within the accuracy limits already outlined.

Although the treatment of the source as two separate dipoles is not exact, the theory based on two point dipoles can be used to give an estimate of the accuracy of the approach. If it is assumed that (1) the extremes of the vortex core diameter are the dipole centres (i.e., h = core diameter); (2) the core diameter is in the order of 0.2 of the blade chord, c, (see section 5.6 on experimental results) and (3) the typical frequency of the sound is given by $f = \frac{V'}{c}$ where V' = flow speed relative to blade, then

$kh = 2\pi fh/c_o = 2\pi Mh/c$ ($M = V/c_o$, Mach number of blade)

and taking a typical Mach number of 0.75 at the blade tip gives kh = 1.2 in which case W_2/W_1 is approximately 0.3 as shown in Figure 5.24. Thus the final solution obtained by using the acoustic theories outlined in section 5.9.1.2 could be up to the order of 8 dB above the exact solution.

5.9.2. Calculation of Blade Slap 'Power' and 'Energy'

5.9.2.1. Rating blade slap

Although the loudness of a single impulsive sound such as a sonic boom has been evaluated [114, 115] there is practically no information available on estimating the loudness of repeating impulses, except in connection with recommendations for damage risk criteria [116, 117]. For the single impulse, the loudness is determined by considering the sound energy in the impulse and applying appropriate weighting functions. For continuous sounds it is more usual to work in terms of the source power since this is directly related to the loudness and sound pressure level measurements. At the present time it is not clear which method of evaluation is best suited in estimating the loudness of repetitive type of noises like blade slap. Before new material becomes available, however, it would appear that the evaluation of the power of the impulse is the most applicable [118] but since it is not definite both forms are given in the following theoretical development.

5.9.2.2. Acoustic model

It has been shown that when a blade is subjected to a fluctuating load L_s per unit span, the total sound energy per unit time radiated into the far field is given by

$$W_s = 1/12\,\pi\rho\, c_o^3 \left[\partial L_s/\partial t\right]^2 (r_o - r_1)^2 \qquad (5.12)$$

where $(r_o - r_1)$ is the span width subjected to the disturbance. This derivation (which is reproduced in Appendix 5) assumes that both the blade chord and the region affected by the fluctuating load are small compared with the acoustic wavelength.

It was also assumed in developing equation (5.12) that the blade loading is constant over the span width $(r_o - r_1)$. A more representative spanwise loading for the type of blade/gust interaction under consideration is illustrated below:

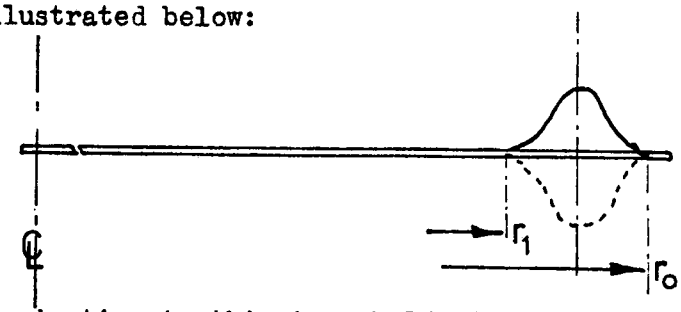

A good approximation to this is a half sine wave. If this is used then equation (5.12) is modified to

$$W_s = 1/3\,\pi^3\rho\, c_o^3 \left[\partial L_s/\partial t\right]^2 (r_o - r_1)^2 \qquad (5.13)$$

In the original blade slap study [1] a frequency analysis of the measured sound was made in terms of the blade passing frequency as fundamental, and for this reason the subsequent theory was developed in terms of harmonics of this frequency. This form does not, however, lend itself readily to working relationships for use with real helicopters. The following theory therefore treats the blade loading impulse as an isolated event; the total radiated energy from each impulse or 'bang' will be given, rather than the average power over a complete blade passing cycle. Work on impulsive noise and the subjective assessment of blade slap on actual helicopters also seems to suggest that this approach is more appropriate for loudness prediction.

Equation (5.13) can be used to calculate the acoustic power or energy radiated from the blade following a single gust or impulse. This simply involves an integration over the duration of the impulse, and leads to the following expressions for 'bang power', W_B, and 'bang energy', E_B, respectively.

$$W_B = \frac{(r_o - r_1)^2}{3\pi^3 \rho c_o^3} \cdot \frac{1}{\text{bang duration}} \cdot \int_{\text{bang}} \left[\frac{\partial L_s}{\partial t}\right]^2 dt \qquad (5.14)$$

$$E_B = \frac{(r_o - r_1)^2}{3\pi^3 \rho c_o^3} \cdot \int_{\text{bang}} \left[\frac{\partial L_s}{\partial t}\right]^2 dt \quad \text{since } E_B = (\text{bang duration}) \times W_B \qquad (5.15)$$

5.9.2.3. Blade loading

To calculate W_B and E_B accurately it would, of course, be necessary to know the variation of blade loading as it passes through or over the tip vortex filament. Thus an exact gust velocity profile in the direction of blade motion would be required. The time history of the blade loading is very important, since W_B and E_B are dependent on the rate of change of loading and not just the amplitude. The spanwise distribution normal to the direction of motion is not so important, although for an absolute estimate of noise it would be needed.

A study of the tip vortex paths associated with even a simple rotor system shows that it is practically impossible to estimate the gust profile experienced by the blade: this is discussed in section 5.6. It is therefore impossible at the present time to develop the theory in terms of absolute values for an actual helicopter.

It is possible, however, by considering an ideal blade/vortex interaction and making various simplifications, to obtain a relationship which shows both the important parameters for an actual helicopter, and indicates the severity of blade slap likely on any helicopter.

When blade/vortex interaction occurs, the blade effectively passes through a gust of known dimensions. The resulting lift can be calculated using the method outlined in Appendix 4. It is convenient to represent the gust as a series of harmonics based on the gust width as the fundamental length.

When this approach is used, the loading is obtained in the form of two separate expressions, one when the blade is experiencing the gust (equation 5.16) and the other when the loading decays as the blade passes out of its effect (equation 5.17):

$$L_m = \tfrac{1}{2}\rho V c a_o W_m \left[\frac{0.065}{\sqrt{k_m^2 + (0.13)^2}} \left(\sin(k_m s - \phi) + e^{-0.13s} \cdot \frac{k_m}{\sqrt{k_m^2 + (0.13)^2}} \right) \right.$$

$$\left. + \frac{0.5}{\sqrt{k_m^2 + 1}} \left(\sin(k_m s - \eta) + e^{-s} \cdot \frac{k_m}{\sqrt{k_m^2 + 1}} \right) \right], \qquad (5.16)$$

$$L_m = \tfrac{1}{2}\rho V c a_o W_m \left[\frac{0.065e^{-0.13s}}{\sqrt{k_m+(0.13)^2}} \left(e^{0.13x} \cdot \sin(k_m x - \phi) + \frac{k_m}{\sqrt{k^2_m+(013)^2}} \right) \right.$$

$$\left. + \frac{0.5e^{-s}}{\sqrt{k^2_m+1}} \left(e^{x} \sin(k_m x - \eta) + \frac{k_m}{\sqrt{k^2_m+1}} \right) \right] . \qquad (5.17)$$

In the above relationships, m = harmonic order of gust, $k_m = 2\pi b\, m/Y$, s = non-dimensional distance measured from beginning of gust given by s = d/b where d is actual distance, b = half chord = c/2, Y = total length of gust, x = non-dimension length of gust = Y/b, $\eta = \tan^{-1} k_m$ and $\phi = \tan^{-1} k_m/0.13$.

These expressions could be evaluated numerically for each case. The effort involved is not, however, justified unless the details of the gust profiles are accurately known. As already discussed this is not the case, and it is more useful to obtain a simplified solution which gives an estimate of W_B in terms of overall features of the gust.

Since the harmonics of a typical tip vortex profile as shown in Figure 5.25.1 fall off rapidly (Figure 5.25.2) it is not necessary to consider more than, say, the first three harmonics. The total loading (based on the first three gust harmonics) is shown by the continuous line in Figure 5.26. If the calculation is limited to the first harmonic alone, then the blade loading shown by the broken line on Figure 5.26 is obtained. The two curves are very similar in shape, suggesting that it is the first harmonic that largely determines the shape of the loading curve. It should be noted that the blade loading equations depend on the rate of change of loading ($\partial L/\partial t$) and the shape is important as well as the amplitude.

Thus a good estimate of W_B and E_B can be expected if the calculation is based on the first harmonic (i.e., m = 1). It will be noted that the blade loading equation is made up of two terms, with an amplitude ratio of approximately 1:8. These two terms are shown on Figure 5.27. The smaller term is of a similar shape to the larger, with the result that although it affects the amplitude it has very little effect on the shape. Since this term is small compared with the other it seems reasonable to neglect it, in which case the loading is given by a much simplified equation.

It is still theoretically necessary to harmonically analyze the velocity profile of the gust. If, however, the calculation is made by

using the peak amplitude W instead of W_1, then the resulting loading is increased in amplitude and now approximates closely the overall amplitude, as well as the shape, originally obtained by using the first three harmonics. This is, of course, due to the fact that the idealised tip vortex or gust profile approximates a sine wave and that the ratio of its width to the blade chord approaches unity. The agreement is shown in Figure 5.28, which compares the loading based on the first three harmonics (continuous line) with that obtained for only the first harmonic (m = 1) when W_1 is taken as the peak amplitude W and the first term is omitted as described above (broken line).

Since it is the rate of change of loading which is important, the main contribution to the 'bang' power and energy is expected to come while the blade leading edge is within the tip vortex (equation (5.16)) rather than from the exponential decay of loading after the leading edge emerges from the tip vortex (equation (5.17)). Part of equation (5.16) has been discarded already; the remaining terms of the sine term and an exponential term are compared in Figure 5.29.

If the exponential decay term can be neglected, the loading is given by the following simplified relationship:

$$L_s = \tfrac{1}{4}\rho V c W a_o \cdot 1/\sqrt{k_1^2+1} \cdot \sin(k_1 s - \eta) \qquad 0<s<x \qquad (5.18)$$

This is valid, within the limits already outlined, provided the width of the tip vortex is of the same order as the blade chord. It may appear that the simplifications made to obtain this equation are extremely severe. To obtain an indication of the difference between the exact solution (based on the first three harmonics of the gust) and equation (5.18), the time variation of $(\partial L/\partial t)$ has been computed by using both methods. The results are compared in Figure 5.30, and from this it can be seen that the 'peak levels' are under-estimated by a factor of 2.

5.9.2.4. W_B and E_B - general relationships

W_B and E_B depend on the time integrals of the 'squares of the curves' given in Figure 5.30; this has been computed and shows that the value calculated by using the exact solutions is 1.7 times as great as that given by the simplified solution. The comparison is illustrated in Figure 5.31.

Differentiation of equation (5.18) with respect to t = cs/2V, and squaring, gives

$$\left[\frac{\partial L_s}{\partial t}\right]^2 = \tfrac{1}{4}a_o^2\rho^2V^4W^2 \cdot \frac{k_1^2}{k_1^2+1} \cdot \cos^2(k_1 s - \eta) \cdot \qquad (5.19)$$

This expression is to be integrated over the duration of the impulse, which in the present approximation is from $k_1 s = 0$ to 2. Approximating $k_1^2/(k_1^2+1)$ by 1 (on the grounds that $Y \triangleq c$, so $k_1 \triangleq \pi$) leads to the result

$$\int_{\text{bang}} \left[\frac{\delta L_s}{\delta t}\right]^2 dt \triangleq \tfrac{1}{8} a_o^2 \rho^2 Y V^3 W^2 \qquad (5.20)$$

Substitution in equations (5.14) and (5.15) give the bang power and energy as

$$W_B = a_o^2/24\pi^3 c_o^3 \rho V^4 W^2 (r_o - r_1)^2 \qquad (5.21)$$

$$E_B = a_o^2/24\pi^3 c_o^3 \rho Y V^3 W^2 (r_o - r_1)^2 \qquad (5.22)$$

5.9.2.5. 'Bang' power and energy in terms of helicopter parameters.

$(r_o - r_1)$ is the span length subjected to the idealised tip vortex, or in the case of a real helicopter the blade length affected by the tip vortex filament. This is discussed in section 5.8.4 and it would appear reasonable to assume that $(r_o - r_1)$ is a constant.

The study of possible tip vortex paths has already shown that blade/vortex interaction is most likely to occur near the blade tip. Thus V can be replaced in the above equations by the blade tip velocity V_T.

It has also been shown in section 5.8 that although an exact solution for the maximum tangential velocity of a tip vortex is not possible V_M is connected to the parameters of a helicopter by the following proportionality

$$V_M \propto T/V_T BR \qquad \text{(equation 5.8)}$$

In this particular application $W \equiv V_M$ and hence

$$W_B \propto V_T^2 T^2/B^2 R^2, \qquad (5.23)$$

$$E_B \propto Y V_T T^2/B^2 R^2. \qquad (5.24)$$

Since it was assumed in the derivation of the blade loading that the 'gust length' is of the same order as the blade chord and since any blade/vortex interaction is likely to be a function of a blade chord (section 5.6), Y in equation (5.24) can be replaced by c, whence

$$E_B \propto V_T T^2 c/B^2 R^2. \qquad (5.25)$$

5.9.2.6. Blade slap factor

Equations (5.23) and (5.25) which give the 'bang power' and 'bang energy', respectively, can be used to compare the relative levels of blade slap likely from any helicopter. For convenience these equations have been termed the Blade Slap Factors and are referred to as BSF(P) and BSF(E) for the estimation based on power and energy respectively

$$BSF(P) = (V_T T/RB)^2; \quad BSF(E) = (T/BR)^2 cV_T \tag{5.26}$$

or in terms of the disc loading, w,

$$BSF(P) = (V_T wR/B)^2; \quad BSF(E) = (wR/B)^2 cV_T \tag{5.27}$$

The above equation can be used to illustrate the most important parameter on an actual helicopter. Consider in the first instance one particular helicopter; then c, R and B will be fixed, in which case

$$BSF(P) \propto V_T^2 T^2 \; ; \; BSF(E) \propto V_T T^2. \tag{5.28}$$

If now the 'pitch' is assumed constant, it follows that the vortex size or strength is directly proportional to the velocity of the blade, hence $T \propto V_T^2$ and

$$BSF(P) \propto V_T^6 \; ; \quad BSF(E) \propto V_T^5 \tag{5.29}$$

This is on the assumption, of course, that all other conditions and parameters are constant and is the typical law for the dipole type of radiation.

Consider next the case when the tip velocity is fixed; the thrust is to a first order proportional to the pitch angle, θ, and thus

$$BSF(P) \text{ and } BSF(E) \propto \theta^2 \tag{5.30}$$

5.10 BLADE SLAP ASSESSMENT.

5.10.1. Programme

Blade slap is characterised by its sharp impulse, which repeats typically at a blade passing frequency which varies between 10 Hz and 25 Hz depending on the helicopter design. It is heard as a series of 'bangs' at a fixed repetition rate and in the extreme case sounds very similar to rapid gun fire. Blade slap readily draws attention to the helicopter and it was fairly clear even in the initial studies that the subjective impression was underrated by conventional rating methods which were normally made in terms of either dB(A) or PNdB measurements. As a part of the blade slap investigation a number of individual studies into aspects related to the subjective assessment were made. These ranged from a theoretical determination of the effect of impulse shape

and duration on loudness to an examination of the problems of measuring impulsive signals with conventional instrumentation. These experiments are reported in this section and although they are treated as separate entities they were carried out in order that the overall impact of blade slap could be assessed. A vital part of this study included the (electrical) simulation of blade slap without which many of the more detailed studies would not have been possible.

5.10.2. Loudness/Annoyance of a 'Banging' and 'Non Banging' Helicopter

In order to gain information on the subjective effects of blade slap a limited series of tests were carried out at ISVR. For this study it was assumed that the data supplied by some helicopter manufacturers was a true representation of the blade slap 'bang'.

The main object of this study was to determine the increase in loudness and annoyance associated with the occurrence of blade slap on a helicopter.

A small jury of trained listeners was asked to compare the loudness of a 'banging' and 'non-banging' helicopter (as recorded out of doors) in the following environments: (a) in the open, well away from walls, (b) in a semi-reverberant room, equivalent to a large well-furnished lounge, and (c) in a small reverberant office (size 12 ft x 9 ft x 10 ft high). The measured difference between the 'banging' and 'non-banging' helicopter was 5 to 6 dB(A).

In the above tests the 'banging' helicopter sounded louder than the 'non-banging' one by 6 dB(A), 7 dB(A) and 8 dB(A) in locations (a), (b) and (c) respectively.

In the second part of the experiment to determine the annoyance, light music was played simultaneously with the helicopter recordings. The tests were carried out in a semi-reverberant room (location (b)) with the music at a level of 77 dB(A) and the helicopter recordings set initially at a level of 63 dB(A): i.e., 14 dB(A) below that of the music. In the light of a previous survey the levels chosen for these tests were considered to be representative of the noise levels experienced in a house near, or under, helicopter flight paths. A jury and individuals were asked to adjust the 'non-banging' helicopter to a level where it was, relative to the music, equally as annoying as the 'banging' recording. On average, the 'non-banging' case was adjusted to a level 6 dB(A) above that of the 'banging' case for equal annoyance. There was a large variation in results with one person stating that the 'banging' case

was not at all distracting, while another rated the difference at 14 dB(A). 60% were, however, in the range 4-8 dB(A). It is of interest to note that this type of variation in results is usual when judgements depend on individual interpretation of annoyance.

The results indicated that the 'banging' helicopter would have to be four times as far away as the 'non-banging' helicopter, in order to sound equally annoying. This corresponds to a 12 dB reduction in level, 5-6 dB to equalise the dB(A) ratings and a further 6 dB as indicated by the annoyance experiment.

5.10.3. Effect of Impulse Shape and Duration on Loudness

In developing the BSF's in section 5.9.2.5, a generalised form of the blade loading curve was used and it was shown that (1) in terms of the 'power' and 'energy' of the impulse sound only the first harmonic of the gust (a single sine wave) was important; and (2) the amplitude W_1, of the first harmonic could be taken as equivalent to the peak amplitude W of the gust velocity. This approach resulted in the approximate solution for the BSF being of the order of 1.7 less than that which would be obtained by using the exact solution (see Figure 5.31). The form of the exact (curve B) and the approximate (curve A) impulses is shown in Figure 5.32. The points used in the computation, described in the following sections, are indicated on the figure by an 'x'.

At the time of this particular investigation, and to the author's knowledge even at the present time, it is not possible to calculate the loudness of a series of impulses. Thus the study was limited to estimating the loudness associated with a single blade slap impulse. It was considered, however, that the general trends of the single impulse are equally applicable to the repetitive impulse case and thus worth investigating.

The time scale for the impulse was chosen such that it was typical of blade slap, with the total pulse duration (3 time units of the time scale shown on Figure 5.32) being equal to 2.4 ms. The loudness in terms of Phons was computed for the case when (a) amplitude scale of curve B ≡ amplitude scale of curve A and (b) amplitude scale of curve B ≡ 2 x amplitude scale of curve A.

In the prediction process, described in reference (115), it is necessary to fix the amplitude of the impulse in absolute units. A 100 dB level (phon curve) was used: this level was chosen as being representative of the levels experienced by personnel in the vicinity

of helicopters producing blade slap. The results were as follows:

	Loudness (Approx. Impulse; curve A)	Loudness (Exact Impulse; curve B)
Condition (a)	108 Phon	104 Phon
Condition (b)	108 Phon	109 Phon

The results for condition (b) correspond very closely to the results of the method used in the derivation of the BSF. From this it can be seen that the simplified approach gives a solution very close to the exact value. It is also of interest to note that this agrees well with the simple energy correlation discussed in section 5.9.2.3.

The second part of this study involved using the exact solution and determining the effect of pulse duration on the loudness. A range of pulse durations from 0.9 ms to 6 ms were used and the results are summarised on Figure 5.33. It will be observed that as the pulse duration is initially increased there is an increase in loudness. When the pulse duration exceeds the order of 3 ms, however, the loudness becomes practically independent of pulse duration.

A study of the time histories associated with blade slap revealed that typical bang durations vary from 3 to 6 ms. It would be reasonable to assume, therefore, that for all practical purposes the loudness is independent of the type (pulse duration) of the impulse.

If, however, the slap duration is dependent on the blade chord, as suggested by the BSF(E) – impulse energy approach, there may be some advantages in having small chord rotor blades.

5.10.4. Electrical Simulation

It was difficult to conduct detailed investigations by using the available helicopters and model rig recordings and it was decided therefore to simulate 'blade slap' electrically. It had already been shown that for a wide range of helicopters the main energy of the blade slap pulse lay in the frequency range 200 to 300 Hz. (see section 5.5.3, Table 5.1). A number of the available 'blade slap' recordings were examined in detail, with particular reference being given to the recordings obtained when using a Wessex since these contained both 'blade slap' and 'non-blade slap' conditions. From this study of the data it was evident that the 'blade slap impulse' for the Wessex could be represented by a single sine wave of 200 Hz (0.005 s.duration) pulsed at a repetitive rate of 15 per second (0.065 s.duration) which corresponds to the 'blade passing frequency'. The review of the other recordings indicated that

this approach could be applied to any helicopter, although in some cases a slightly more complex 'impulse' would be required. Even so, the difference between use of a single sine wave and the 'true impulse' would be expected to be small.

The electrical signal of the form indicated was obtained by use of a specially designed 'gating device' which enabled sine waves of any frequency from 100 to 500 Hz to be generated at repetition rates from 10 to 30 Hz.

The simulated 'blade slap' impulse was superimposed on to a cabin noise recording of a Wessex helicopter operating without blade slap. Standard instrumentation was used for this and the system was set up so that the relative level of the 'blade slap' impulse and the reference helicopter (Wessex) recording could be varied at will. The Wessex recording selected for use as the 'reference' was 'broadbandish' in character and contained no noticeable levels of impulsive main rotor noise, tail rotor noise, gear noise or engine noise. Consideration was given to the use of a 'white noise' and a 'weighted white noise' but when combined with the simulated blade impulse the final signal did not have the physical or subjective characteristics of a real helicopter.

For analysis purposes the combined signals were recorded on tape and one point of interest which emerged during this investigation was that it is impossible to record a single 200 Hz sine wave repeated at a typical blade passing interval on to a Nagra (direct record) tape recorder without obtaining severe distortion. The distortion was, in fact, so bad that on an oscilloscope the signal was unrecognizable. This is a significant factor since Nagra tape recorders are commonly used to record blade slap. The situation in practice is, however, unlikely to be quite as serious since the 'bang' impulse is added to an already existing noise signal which contains similar frequencies. This problem was overcome during this experiment by use of an FM (Lockheed) Tape Recorder.

The validity of the approach was checked by comparing the 'simulated blade slap' signal with recordings made of the Wessex during a 'bank turn' manoeuvre when it generates continuous blade slap. A subjective evaluation by a small jury indicated good agreement and as can be seen from Figure 5.34 the 'simulated blade slap' gave a narrowband spectrum very similar to that for the real blade slap case. Also shown on the figure for reference is the analysis of the basic cabin noise and the impulse.

At a later stage during the study the simulated signal was adjusted to give the characteristics associated with the Boeing Vertol Chinook. For this a single sine wave of 250 Hz and repetition frequency of 14 Hz was used and since it is impossible to obtain a 'non banging' recording, a 'nose on' Wessex external noise recording was used as the reference. This recording was selected since it had the same general characteristics as the 'cabin noise condition', but the gear (transmission) noise was non-existent. Subjectively this recording sounded more representative of a real helicopter since the 'swishing'/blade passing effect of the helicopter could be detected. Subjective evaluation at ISVR which was later repeated at WHL, and more recently at NPL, confirmed that blade slap on the Chinook could be successfully simulated by using this method.

The approach outlined above was subsequently used for a number of investigations, and although initially the cabin noise Wessex recording was used as the 'reference signal' this was subsequently replaced by the external Wessex 'nose on' noise condition recorded 200 ft directly in front of the helicopter when hovering at 40 ft ground/rotor clearance.

If the traces presented in Figure 5.34 are examined in detail it will be observed that, although as mentioned previously they show general agreement, there are some differences. The simulated blade analysis (trace C) contains more high level harmonics in the region 120 to 160 Hz than the real blade slap analysis (trace B). This cannot be accounted for in detail, but it is considered that the dip in the spectrum of the real helicopter recording is most likely due to signal cancellation at the microphone.

5.10.5. Subjective/Analysis Detection

Since it was fairly clear from the initial subjective evaluations that the impact of 'blade slap' was underrated by conventional analysis methods, it was considered essential to determine if 'blade slap' could be detected on narrowband analysis when it was audible. A simple experiment was, therefore, performed using the simulated blade slap signal based on the Wessex cabin noise recording.

A small jury of six individuals (4 familiar with helicopter noise) listened to the recordings via a high quality headset and adjusted the level of the simulated 'impulse' (which could be varied relative to the fixed level of the reference signal) so that it was just audible above the Wessex cabin noise. The variation between the individuals was surprisingly small (3 dB in terms of the 'peak' levels) and thus there

was general agreement on the level of the impulses when it could be just heard. Time history analysis (using an Ultra Violet Recorder) and narrowband analysis were performed on the signal at this setting and similar analysis was made for the setting when the impulse could not be heard and when it subjectively dominated the signal. The results are reproduced in Figure 5.35 (time history traces) and Figure 5.36 (narrowband results). As will be observed when 'just audible' the blade slap could be detected on the narrowband analysis and seen on the time history. If a recording of a helicopter with basically more impulsive characteristics had been used and the mid frequency region had been composed of discrete frequency components, it is possible that detection of the 'just audible' condition may have been more difficult. Even so this small study reconfirmed that 'blade slap' could be simulated with relative ease and when it occurred it was capable of being detected by narrowband analysis.

5.10.6. Evaluation of the Relative Merits of Digital and Analogue Analysis

The simulated blade slap signals were also used to evaluate the relative merits of digital and analogue analysis. This study was considered necessary since doubt was expressed on the appropriateness of the analysis performed on the Spectral Dynamics Analogue Analyzer System described in section 2.2, although this type of analysis was being used by the majority of the helicopter manufacturers and investigators at that time.

The isolated impulse and simulated blade slap (helicopter noise + impulse) were analyzed on the Spectral Dynamics System and the ISVR Data Analysis Centre 'digital' analyzer which was based on a Myriad Computer. The frequency components of the impulse were also calculated by using basic Fourier analysis. Since the latter is of interest from the point of view of deriving the level of the 'maximum harmonic' relative to the peak level of the impulsive and the frequency of the 'maximum harmonic' this derivation is reproduced in Appendix 7.

The analogue analysis is shown in Figure 5.34 (bottom trace) and the digital result in Figure 5.37. With regard to this latter figure it will be noted that the 'base' noise on the tape recorder (as illustrated in the upper part of Figure 5.37) had a significant effect on the higher frequency components. The input was subsequently 'cleaned up' by making the digital input zero except in the region of the impulse and this resulted in, of course, a true representation of the mathematical solution being obtained.

From a comparison of the mathematical solution (dashed line on bottom trace of Figure 5.34) with the analogue analysis, it was evident that inherent errors are associated with the analogue approach. The accuracy decreased above 200 Hz although significant errors (greater than 1/2 dB) only occur above 400 Hz. These findings agree well with those of Quinn and Thomas [119] who discuss in detail the various parameters most likely to produce such errors. Even so from a general practical point of view analogue analysis can be considered adequate since errors in the main range of interest (100 to 300 Hz) are less than 2 dB and above 300 Hz the signal on a real helicopter and/or rotor is dominated by noise from other sources.

As indicated in figure 5.34 (bottom trace) the difference between the 'peak' of the impulse and the rms SPL of the maximum harmonic is 22 dB. This is representative of real blade slap and must be taken into account when recording/analyzing blade slap signals. Also as indicated in Appendix 7, although as a rough guide the maximum harmonic can be considered to occur at the same frequency as that of the 'impulse sine wave' (200 Hz which in this case corresponds with the 13th harmonic since the blade passing interval is equivalent to 15 Hz) this is not the case since it occurs at a slightly lower frequency (165 Hz, 11th harmonic).

5.10.7. Rating of Blade Slap

Rotor noise, and hence helicopter noise, is essentially impulsive in nature and measurements indicate that the crest factor (peak-to-overall rms) level is typically 10 to 15 dB. On a helicopter subjected to severe blade slap, however, this value can exceed 25 dB. Helicopter noise is normally rated in terms of either the perceived noise level (PNL) or the dB(A) value. The former is based on the method developed for aircraft and is used extensively within the aircraft industry. When comparing helicopter noise with traffic and/or community noise levels it is more usual to adopt the dB(A) unit. There is a fairly well established relationship between these two units for helicopters, as for many other noise sources, and hence there appears little to choose between the PNL and dB(A) methods for general use. The PNL is, however, slightly more sensitive to changes in spectrum shape and the recently introduced effective perceived noise levels (EPNL) method allows 'tone' and 'duration' correction to be applied. The general trends obtained from PNL (PNdB) analysis would, however, be similar to those from the EPNL concept.

The problem of rating helicopter noise can be best illustrated by reference to Figure 5.38 which shows oscillograms of two noise signals adjusted such that when measured in terms of dB(A)-rms SLOW - they give the same value. On a PNL (PNdB) analysis the 'banging' noise is about 1.8 PNdB higher than the non-banging Wessex noise and a study of the $\frac{1}{3}$ octave band spectra suggests that this is largely a result of the higher frequency components associated with the engine. It is obvious from these time histories that they will sound very different.

In order to assess in greater depth the rating problem a small programme was formulated in which 'simulated blade slap' signals were used. The aim was to establish the influence of the magnitude of the impulse and relative merits of using rms SLOW, rms FAST and IMPULSE. The possibility of using the 'peak' $\frac{1}{3}$ octave band level was also evaluated. For this study the simulated blade slap recordings described in section 5.10.4 were used. The range of test conditions is illustrated in Figure 5.39 for the impulse plus the Wessex external hover noise recording. The 'peak' levels were used as a reference and as indicated the 'impulse level' covered the range (relative to the typical peak of the real helicopter noise) from -5 dB to +20 dB. A similar set of recordings were developed by using a Wessex internal noise recording as a reference.

The narrowband analysis results for the conditions illustrated in Figure 5.39 are shown in Figure 5.40. It will be observed that for the impulse of +5 dB and above all the analyses exhibit the classic blade slap appearance with well defined blade passing harmonics in the 100 to 300 Hz frequency range.

Standard analysis was performed on the complete range of recordings using rms SLOW, rms FAST and IMPULSE detectors. The $\frac{1}{3}$ octave band spectra for the 'Wessex (external noise) + impulse' derived using rms SLOW are illustrated in Figure 5.41. The PNL values were calculated from $\frac{1}{3}$ octave band data and the results are illustrated for the complete range of signals in Figure 5.42. Similar analysis was performed in terms of dB(A) and the results are illustrated in Figure 5.43.

The result shows that although use of rms SLOW, rms FAST and IMPULSE give different absolute levels the trends are for all practical purposes identical. It follows that there is no advantage in using IMPULSE in place of rms SLOW. This is understandable if meter characteristics are taken into consideration since, although IMPULSE has a rise time constant of 35 ms compared to 500 ms for rms SLOW, the time constant

of the detector circuit is relatively long when compared to the 5 ms duration of the impulse. These aspects have been studied further at WHL [120, 121] . It also followed that all the methods were inadequate for rating blade slap since the subjective difference was considered to be more in the order of 10 to 12 dB over the range of test conditions.

In an attempt to see if any better agreement with the expected trend could be obtained if the 'peak' which occurs in the $\frac{1}{3}$ octave band was used in place of the rms value, a simple experimental study was performed. The $\frac{1}{3}$ octave band 'peak' values were only used if, after inspection on an oscilloscope, they showed clear evidence of the repetitive impulsive signal. When this was not the case the standard rms SLOW $\frac{1}{3}$ octave band value was used. It was also considered that rather than the absolute 'peak', the rms of the peak should be used; this was obtained by simply subtracting 3 dB from the 'peak' value determined from an oscilloscope trace. The results obtained by using this approach are illustrated in terms of the PNL values, together with the standard results obtained from rms SLOW levels, in Figure 5.44. It will be noted that, relative to the standard rms slow analysis, this gave a higher value for the higher impulsive signals. For the 'impulse +20 dB' the increase was 5 dB which was only just below the value expected if it was to give a good measure of impulsive noise. This method is, however, so complex since it requires knowledge of the basic non-impulsive noise before a decision can be made on whether to use the 'peak value - 3 dB' or the straightforward rms SLOW value. Also there is no scientific justification in using this approach since the PNL concept applies to $\frac{1}{3}$ octave band <u>rms</u> type analysis. It was, however, the view of the author that the 'crest factor' correlated fairly well with the subjective impression of such signals.

This work also highlighted another problem area since the very impulsive signals tended to 'ring' the filter and instead of the sine wave which was applied at the input, a multiple impulse (of 4 to 6 sine waves) was obtained at the output. This investigation also suggested that rather than attempt a correction based on such detailed analysis, a better approach to consider would be the use of a 'crest factor' based on a 'wide pass band' or dB(A) filter. Such an approach was subsequently evaluated at WHL for rating 'blade slap' [122].

Another problem, which came to light during the initial part of these studies, was that if the 'AC output' of a B & K Microphone Amplifier and B & K Level Recorder combination is used for the measurement of

impulsive signals then significant errors (up to 5 to 6 dB) will result in the measured value of the equipment as set up according to the ISO recommended value for rms SLOW [123]. This is due to the poor and non-linear response of the Level Recorder and has been confirmed by a number of other bodies including NPL. During the course of the time of this investigation this has, however, given rise to problems, since before it was recognised, a '12 dB correction' was considered necessary for a signal with a high level of blade slap. This value was a result of a '6 dB subjective correction' and another 6 dB arising from the fact that measured results were analyzed on a B & K Level Recorder. This difficulty can be overcome by taking meter readings (as was adopted for the investigations at ISVR reported in section 5.10.2) or by using a B & K Amplifier with a 'DC output' and fitting the level recorder with a DC potentiometer.

5.11. BLADE SLAP CRITERIA

5.11.1. Blade Slap Factors

The blade slap theory was developed on the assumption that the blade chord and spanwidth effect of the vortex were small. The BSF (outlined in section 5.9.2.6) is therefore more likely to be applicable to helicopters with relatively small chord blades. For large chord blades it would be necessary to treat the source as an array of dipoles and obtain the overall effect by a summation process. Although this would be relatively simple, it does not appear justified since the details of blade/vortex intersection likely on any helicopter are so vague.

A comparison between the subjective assessments and the values of BSF(P) and BSF(E) calculated for a range of helicopter is given in Table 5.2 and shown in Figures 5.45 and 5.46 respectively. The BSF has been plotted on a log scale, which is, of course, equivalent to using a dB scale. In addition to the helicopters referred to in section 5.5 the values for the Sikorsky S65 and Milhail (USSR) Mil 10 are shown. It will be observed that there is fairly good correlation between the BSF's and the subjective observation, particularly for the power solution (BSF(P), Figure 5.45).

The values for the Mil 10 are extremely large, while observations of the helicopter suggest it is very quiet and without blade slap [124]. At the time of this assessment of the Mil 10 the gross weight was only 85000 lbs in which case the BSF(P) and BSF(E) are reduced to 4540×10^7 and 20.8×10^7 respectively. These are, however, still well above those of the other helicopters considered.

Information on the S65 is sparse, but there are indications that blade slap is not a significant problem on this helicopter, even although the value of the BSF is relatively large.

As already mentioned the theory is not really suited to helicopters with large chord blades. The chord width of the Mil 10 is very large (39 inches) which could account for the fact that the BSF does not appear to agree with the subjective assessment in this case. The chord of the S65 blade is also relatively large (26 inches), but this is only slightly greater than the chord width of the UH-1D blade (21 inches). The UH-1D result, as shown in the figure, appears to agree well with the subjective assessments of the blade slap noise.

An examination of the limited number of results suggests that although the blade slap factor is appropriate for single rotor helicopters with a low number of blades (2 or 3) and tandem rotor helicopters it is not applicable to multi-bladed (5 or more) single rotor helicopters. It should be remembered that the factor assumes not only that blade/vortex interaction occurs, but that it occurs in the less favourable form. It could be that the wake distortion on single rotor helicopters with a large number of blades is considerably less than on those with, say, two blades, with the results that blade/vortex interaction is less likely to occur.

5.11.2. Blade Slap Factor Criterion

From the study of BSF in terms of power and energy, there appeared to be little to choose between the two approaches, although the power relationship, BSF(P), appeared to give a slightly better correlation. It was decided, therefore, to use this solution in the development of a blade slap factor criterion which could be used by a designer to evaluate the possible magnitude of 'blade slap' on a particular design.

The BSF(P) is given by the following formula:

$$BSF(P) = (V_T T/RB)^2 \qquad \text{(equation 5.26)}$$

where V_T = blade tip speed (ft/sec), T = total thrust = AUW (lbs), R = rotor radius (ft) and B = number of blades. This can be re-arranged as follows:

$$BSF(P) = V_T^2 . L_{BS}^2 \qquad (5.31)$$

where L_{BS} = blade span loading (lbs/ft)

By using data for a wide range of helicopters and the above relationship for BSF(P), an 'acceptability criterion' was established.

This is illustrated in Figure 5.47, but because of the scatter and range of results a 'band of values' has been chosen in preference to one specific value. As shown on the figure, this criterion implies that 'blade slap' would become very loud and unacceptable if the BSF(P) value exceeded the range 700-900 x 10^7. When using this approach it must, of course, be remembered that the BSF(P) predicts the less favourable condition (i.e. the maximum blade slap noise possible) and does not imply that blade slap will necessarily occur. The comments in section 5.11.1 relating to the Mil 10 and CH-53D (S65), which both have large BSF(P) values but do not produce significant blade slap, are equally applicable in this case. A study of possible blade vortex interaction patterns shows also that as the number of blades on a rotor is increased there is less likelihood of the theoretical case, considered in developing the BSF(P), being realised. From a simple study of possible blade/vortex interactions for a single rotor helicopter, it can also be seen that the magnitude of the lift fluctuation, and hence the noise, increases with increasing flight speed. Thus medium-high speed manoeuvres on conventional single rotor helicopters tend to produce louder blade slap than those associated with near hover conditions. This also explains why the level of blade slap associated with a whirl tower is lower than indicated by the BSF. In this case, the blade/vortex interaction is associated with the non-uniform flow induced by re-circulation and wind effects. Thus the BSF criterion can be expected to be over-restrictive for single rotor interactions which could occur in hover or slow forward flight.

5.11.3. Comparison of the BSF(P) and Boeing Vertol Criteria

The Boeing Vertol Company have established 'slap' and 'rotational noise' criteria for a single three bladed CH-47 rotor in hover [125, 126]. The blade slap criterion is reproduced, from these references in Figure 5.47. Although the original 'Boeing Vertol' data was presented on a linear scale graph, a 'log-log' format has been chosen for the figure since the criterion is then a straight line.

The Boeing Vertol criteria were established from the results of a listening jury who were presented with the noise of the rotor for a wide range of span loadings and tip speeds, and asked to rate the acceptability of the sounds. Very few details of the tests are available but it is stated that 80% of the subjects rated the noise unacceptable above the range shown on Figure 5.46.

The frequency range of the data was 200 Hz to 20 kHz, and hence the low frequency rotational noise was not included in the subjective evaluation. It is not possible to verify if this is a significant factor, but intuitively, it would be expected to affect, at least, the lower tip speed results. Analysis at ISVR, with specific reference to a Wessex, has shown that considerable energy occurs in the 200 Hz region and that the 'cut off' frequency should not be set above 120 Hz. Some analysis performed on the Chinook (2 x 3 blades) also revealed similar results, but since there is no further information available, on the CH-47 whirl tower test, it is not possible to investigate this aspect in any detail.

The 'slap criterion' obtained by Boeing Vertol takes the form $V_T^2 . L_{BS}$ (L_{BS}=blade span loading) and it is stated that this result is obtained from a simplified derivation for constant SPL from a blade vortex interaction. The BSF(P) discussed previously, however, results in a $V_T^2 L_{BS}^2$ law for a particular rotor. Details of the derivation of the relationship are not presented by Boeing Vertol and thus it is not possible to establish the reason for the difference.

The BSF(P) has been converted into the format used by Boeing Vertol. A direct comparison of the two criteria is given in Figure 5.47. It will be observed that, over the helicopter operating tip speed range shown, the difference in the slopes of the two curves is not a significant factor but the Boeing Vertol values are 2 to 3 times larger than the BSF(P) criteria.

It would be expected that any results obtained by using a whirl tower would suggest a higher criterion than the BSF factor given here, since the severe form of blade slap associated with the tandem rotor helicopters, and forward flight of single rotor helicopters, is unlikely to occur on a whirl tower. It is not known how Boeing Vertol carried out their tests, but it is thought that natural wake distortions, due to the presence of the whirl tower, and wind effects, were used to induce blade/vortex interaction. If this was the case, then the Boeing Vertol results would apply to low forward speed interaction effects, while the BSF criteria would be more appropriate to moderate and high speed flight conditions.

Values relating to a number of helicopters are included on Figure 5.47. The unrealistic nature of the Boeing Vertol criterion, for general application, is clearly illustrated in the case of the Bell

helicopters (UH-1B; UH-1D) and the Boeing Vertol Chinook (CH-47B) which all produce very loud blade slap. It should be noted, however, that the Boeing Vertol criterion is stated to apply only to a single rotor.

5.11.4. Use of the BS Criterion

The BSF criterion since its original development has been abbreviated for simplicity to 'blade slap criterion' or 'BS criterion'. This can be used in the design stage to give a 'feel' for the likely magnitude of blade slap. If the suggested limits are exceeded, then a detailed study should be made to determine the possibility of blade/vortex interaction. It should be remembered that the BSF will predict the least favourable case, and except in the case of tandem helicopters, the actual noise would most likely be lower than indicated. It may be extremely difficult to determine if blade/vortex interaction would occur since this is dependent on a large number of variables including cross-wind and blade/fuselage interference and, of course, the changes in rotor operating parameter necessary for control. In this latter context it is worth noting that on a conventional large multi-bladed single rotor helicopter, blade slap is usually induced only in 'low power descents' and manoeuvres. Theoretical methods are not yet available to allow the actual vortex paths to be predicted in detail and it is suggested, therefore, that the best approach would be to carry out flow visualization studies with a model rotor in a wind tunnel.

With the limitations of the BSF method taken into account, it agrees reasonably well with practical results, except possibly in the case of large multi-bladed single rotor helicopters. Even for this latter type of helicopter there does appear to be general agreement between the blade slap noise and the criterion if severe blade slap is induced.

5.12. CONTROL OF BLADE SLAP

5.12.1. Scope of Application

A detailed investigation (on a consultancy basis) was carried out on behalf of New York Airways and Pan Am Airways into the problems arising from the operation of helicopters, which generated high levels of blade slap, in New York City. From this study, and the 'back-up' *ad hoc* experiments and design reviews, a number of important guide lines for the control of 'blade slap noise' were established. Also, at other times during the course of the blade slap investigations reported in this thesis, the results were applied wherever possible to the real helicopter case. In some instances it was not possible to use the actual 'model

results', but the general trends and implications of the work were used in the development of design and operational rules. The most important of these noise control procedures are outlined in this section together with their effectiveness.

5.12.2. New York Airways Study

New York Airways operated Boeing Vertol V107 helicopters on to the Pan-Am building in downtown New York. This helicopter generates high levels of blade slap which, in addition to being subjectively unpleasant, tended to rattle windows and excite room resonances. This enhanced even further the subjective annoyance. The impulsive signals also reflected off the skyscrapers with the result that the position of the helicopter could not be located and some rooms, which at first glance were shielded from the helicopter, were subjected to high levels of blade slap. By careful flight path control it was found, however, that the impact of the noise could be minimized: flights were therefore scheduled so that they took place as far as possible over water (rivers) and avoided noise sensitive areas. In this latter context park areas appear to be less of a problem than residential areas and people appear content to 'look up' at helicopters flying over an otherwise quiet park. The subjective impression also appeared more favourable since reflection was a minimum and the helicopter position could be located from the noise. It is possible that the fear element, which is often present in the case of helicopters flying low over built up areas, was lower relative to that experienced in a high rise apartment.

5.12.3. Design Considerations

5.12.3.1. Tandem rotor helicopters

Tandem rotor helicopters can generate blade slap in all regimes of flight. A detailed comparison was made between the Boeing Vertol V107 and Bristol (later Westland) Belvedere helicopter, since unlike the V107 the Belvedere produced very little blade slap during normal operations. This review was supplemented by flow visualization studies using a model tandem rotor rig. It soon became clear that the most important parameters were blade separation and blade overlap. On the V107 the overlap was 68% (defined in terms of rotor radius) while on the Belvedere it was 30%. It followed that if the separation should be increased and the overlap reduced so that both in the hover and in forward flight the tandem configuration would effectively act as two individual main rotors then blade slap could largely be avoided. It was also considered that this

would reduce the level of the normal rotational noise which is also dependent on the interaction of one rotor with the wake shed by the other. This concept was eventually taken up by Boeing Vertol in their experimental Chinook designated the 'Boeing 347' [127]. On this helicopter blade slap was effectively non-existent and the general level of main rotor noise was very low. The parent Chinook 'C model' on the other hand generates high levels of blade slap.

It also follows from considerations of the interactions between one rotor and another, that the relative 'trim' (position) of the two rotors can be used to offset the effects of blade slap. In this context it is worth noting that although statically the rear rotor is normally situated above the front rotor, the disc plane tilt is such that in flight the 'front of the rear rotor' can be below the 'rear of the front rotor'. Use of 'trim' was exploited by Boeing Vertol on their V107 since on this helicopter the tilt of two rotor axes could be controlled (within limits) by the pilot. The results of tests analyzed by the author indicated that reductions in the level of blade slap by 5 to 7 dB were possible.

5.12.3.2. Single rotor helicopters

Helicopters with two bladed rotors are more prone to blade slap than those with a higher number of blades. This is fundamentally true from the point of view of blade/vortex interaction and appears to be equally true if 'blade thickness' is taken into account. The latter - which appears to be the main source in high speed flight - is, however, mainly a function of the high blade tip speed/large blade chord (and hence thickness) necessary on such a design to obtain the desired lift/performance characteristics. Blade tip speed and blade thickness can be used to control 'blade thickness' noise and blade tip speed is an important parameter in the case of blade/vortex interaction noise. The tip vortex strength is, however, essentially a function of the blade span loading and hence very high on such designs. It can also be shown that the interaction paths on a two bladed helicopter are such that the blade/vortex interaction (if it occurs) will be in a form which will result in a high level of blade slap noise. It would appear, therefore, that with such a design it is extremely difficult to reduce 'blade slap' to acceptable levels while at the same time obtaining a satisfactory performance. On a multi-bladed design (3 or more blades) the interaction (if it occurs) between a blade and a tip vortex will be less severe than on an equivalent 2 bladed rotor. The tip vortex strength will also tend to be lower and traditionally slightly lower rotor tip speeds are employed. Thus a

multi-bladed single rotor has obvious advantages from the blade slap point of view over both the 2 bladed and tandem rotor helicopters. It could also be argued that it is not possible to obtain a satisfactory design with a 2 bladed rotor if high speed and performance is also required.

5.12.3.3. Operational aspects

On helicopters which do not generate blade slap in the hover or steady forward flight (i.e., in general all helicopters excluding those with a two bladed main rotor or tandem rotors) blade slap can be generated during manoeuvres. Conditions associated with blade slap are bank turns (typically 40° or more for severe blade slap), shallow descents (500 to 900 ft/min appear to produce the worst conditions) and the 'flare' approaching a hover.

On the majority of helicopters blade slap can be detected by the pilots in the cockpit. This, however, is not the case on all helicopters and thus some pilots can fly in a blade slap regime such as low power descent without it being noticed on the helicopter. Blade slap is also often associated with changes in collective pitch (both positive and negative charges), high altitude, high temperature and high gross weight.

It follows from the above general comments that rapid manoeuvres should be avoided if possible. In this context 'bank turns' are the main problem and it is of interest to note that the current arrangements in London where helicopters have to turn (prior to landing) over the river, leads to blade slap and high noise which would not arise if such tight turns did not have to be employed. Flight path angle/descent rate during approach is also a critical factor and again with wise choice these parameters can be selected to ensure 'blade slap' is kept to a minimum. This concept has been exploited by Bell Helicopters and a 'fly neighbourly' flight profile is published for their civil helicopters [128, 129].

Ad hoc experiments carried out on the author's advice at WHL, and by the RAF using service helicopters, have indicated that 'blade slap' which normally occurs during a typical flight into a heliport/landing pad can easily be avoided and an effective reduction of 10 dB achieved in flight noise.

It is also important that if blade slap occurs, but is not detected in the cockpit, some form of 'blade slap' indicator, either direct or from knowledge of flight parameters such as velocity/descent rate etc., should be supplied to the pilot.

Helicopter vibrations often increase with the occurrence of blade slap, but there does not appear to be any direct correlation between blade slap and airframe vibrations.

5.13. CONCLUSIONS

1. Blade/tip vortex interaction is the most important mechanism for the generation of blade slap.
2. An additional blade slap mechanism appears to be associated with high tip speed rotors: this is likely to be due to shock wave formation and/or blade thickness effects.
3. The acoustic signature of 'high speed slap' is the same as that associated with blade/vortex interaction.
4. Blade stall, including periodic stall, will not generate impulsive blade slap type noise.
5. Helicopters with 2 bladed main rotors and tandem main rotors are most prone to blade slap.
6. Blade slap is generated on all helicopters during bank turns and on most helicopters during low power descent.
7. Blade slap is an impulsive signal repeating at the blade passing frequency which on narrowband analysis exhibits 'peaks' at blade passing harmonics which dominate the spectrum in the frequency range 150 to 400 Hz (10th to 20th harmonic).
8. The 'bang' approximates very closely to a single sine wave type impulse on the majority of helicopters; a multiple impulse of 2 or 3 impulses occurs on the Bell UH-1B and CH-46 helicopters.
9. The blade slap 'bang' energy occurs typically in the range around 250 Hz.
10. When 'blade slap' occurs on a helicopter the 'peak-to-peak' levels and SPL in the frequency range 200 to 400 Hz are increased by 10 dB. The OASPL and dB(A) are, however, only increased by 2 to 3 dB.
11. The severity of blade slap cannot be determined from OASPL, dB(A), PNL or $\frac{1}{3}$ octave band type of analysis - hence the subjective impression is underrated by conventional rating methods. This applies even if equipment with IMPULSE detectors is used.
12. Use of 'peak' $\frac{1}{3}$ octave band values in the PNL calculation improves the correlation with the subjective impression - the method is however impracticable. A crest factor approach is suggested.
13. Impulsive signals 'ring' $\frac{1}{3}$ octave band filters normally used for PNL type analysis; this needs further examination.
14. Information on the characteristics of the tip vortex is vague and confused and requires further study. Based on the limited data available it seems reasonable to assume that the vortex viscous core

is 10% of the blade chord and the 'peak' (tangential) velocity corresponds approximately to an induced angle (based on tip speed) of $\pm$ 20°.

15. Blade/tip vortex interaction is difficult to define in precise detail. The blade slap 'source' can however be estimated by the use of a simple potential flow (rigid) wake model.

16. On a real helicopter the blade slap is considered to be dependent on:

$$(V_T T/RB)^2 = (V_T L_{BS})^2,$$

where V_T = blade tip speed, T = total thrust (AUW), R = rotor radius, B = number of blades and L_{BS} = blade span loading. Thus the level of blade slap will increase with tip speed and blade loading as well as with all-up weight (AUW).

17. Blade slap is subjectively under-estimated on conventional analysis by 6 dB(A).

18. A helicopter which generates blade slap is 12 dB more annoying than one without blade slap (6 dB subjective correction + 6 dB increase in measured level).

19. The loudness of blade slap is independent (over the range considered) of pulse duration; thus on a real helicopter the influence of blade chord is expected to be small.

20. Blade slap can be simulated electrically by a sine signal wave (of frequency in the range 200 to 250 Hz) repeated at the required blade passing frequency (which is typically in the range 15 to 20 Hz).

21. Blade slap can be detected on narrowband analysis when it is just audible.

22. Analogue analyzers can be used for narrowband analysis of blade slap, but the accuracy decreases above 200 Hz.

23. A blade slap criterion (BS criterion) defined in terms of blade loading vs tip speed has been developed.

24. Flight path selection can be used to control blade slap. The layout of a tandem rotor can be chosen to minimize blade slap, but on a two bladed single rotor helicopter the reduction of blade slap does not appear possible without a loss in performance since tip speed is the most important parameter.

TABLE 5.1 - BLADE SLAP ENERGY LIMITS

Helicopter	FILTER FREQUENCY LIMITS		Envelope 'peak' freq from N/B Traces, Hz.
	Frequency Range Hz.	Centre Freq. Hz.	
Wessex	120 - 270	195	200
CH-46A	190 - 380	285	275
V107	120 - 480	300	230
Bell UH-1B	90 - 320	205	250
Belvedere	80 - 320	200	170
Sycamore	120 - 450	285	220
S61	120 - 480	300	-

TABLE 5.2: HELICOPTER BLADE SLAP ASSESSMENT

Helicopter		No.of Blades	Rotor Radius	Blade Chord Width	A.U.W.	Rotor R.P.M.	Tip Speed	Blade Slap Factor		Subjective Assessment
								B.S.F.(P)	B.S.F.(E)	
			ft.	ins.	lbs.		ft/s	(x 10^7)	(x 10^7)	
Bell:	UH-1B	2	22	21	8500	324	745	2050	5.05	Very loud
	UH-1D	2	24	21	9500	324	814	2500	5.25	Very loud
Sikorsky:	S58	4	28	16.4	13000	195	570	440	1.0	*
	S61	5	31	18.3	19000	203	660	650	1.48	*
	S65	6	36.1	26	35000	185	700	1290	4.05	*
Westland:	Wasp/Scout	4	16	10.5+	5500	400	670	330	0.44	Little slap at high altitude.
	Wessex 2 & 5	4	28	16.4	12600	221	650	625	1.25	Slight banging.
	Wessex 3	4	28	16.4	13500	228	670	655	1.27	Slight banging.
	Whirlwind	3	26.5	16.4	8000	218	600	370	0.80	No slap.
	Belvedere	2x4	24.5	15.5	19000	250	640	385	0.78	No slap.
Boeing Vertol:	V107	2x3	25	18	19650	264	690	820	1.78	Loud
	Chinook	2x3	30	25.3	33000	230	720	1740	5.02	Very loud
Hiller:	SL 4	2	17.7	14	3100	370	690	365	0.64	No slap
	FH-1100	2	17.7	10.2	2750	368	680	285	0.36	*
Hughes:	OH-6A	4	13.2	6.8	2400	470	650	87	0.08	*
	269 A	3	12.7	6.8	1600	483	650	78	0.069	*
Kaman:	K 20	4	22	21.6	8637	277	640	395	1.12	*
	K 600-3	4	23.5	15.7	5969	248	610	150	0.32	*
Lockheed:	XH-51A	4	17.5	12	4700	355	660	195	0.30	*
Milhail:	Mil 10	5	57.4	39	95790	120	720	5760	26.4	*

+ Value at blade tip.

*subjective information not available - blade slap unlikely.

PLATE 5·1 WESTLAND WESTMINSTER

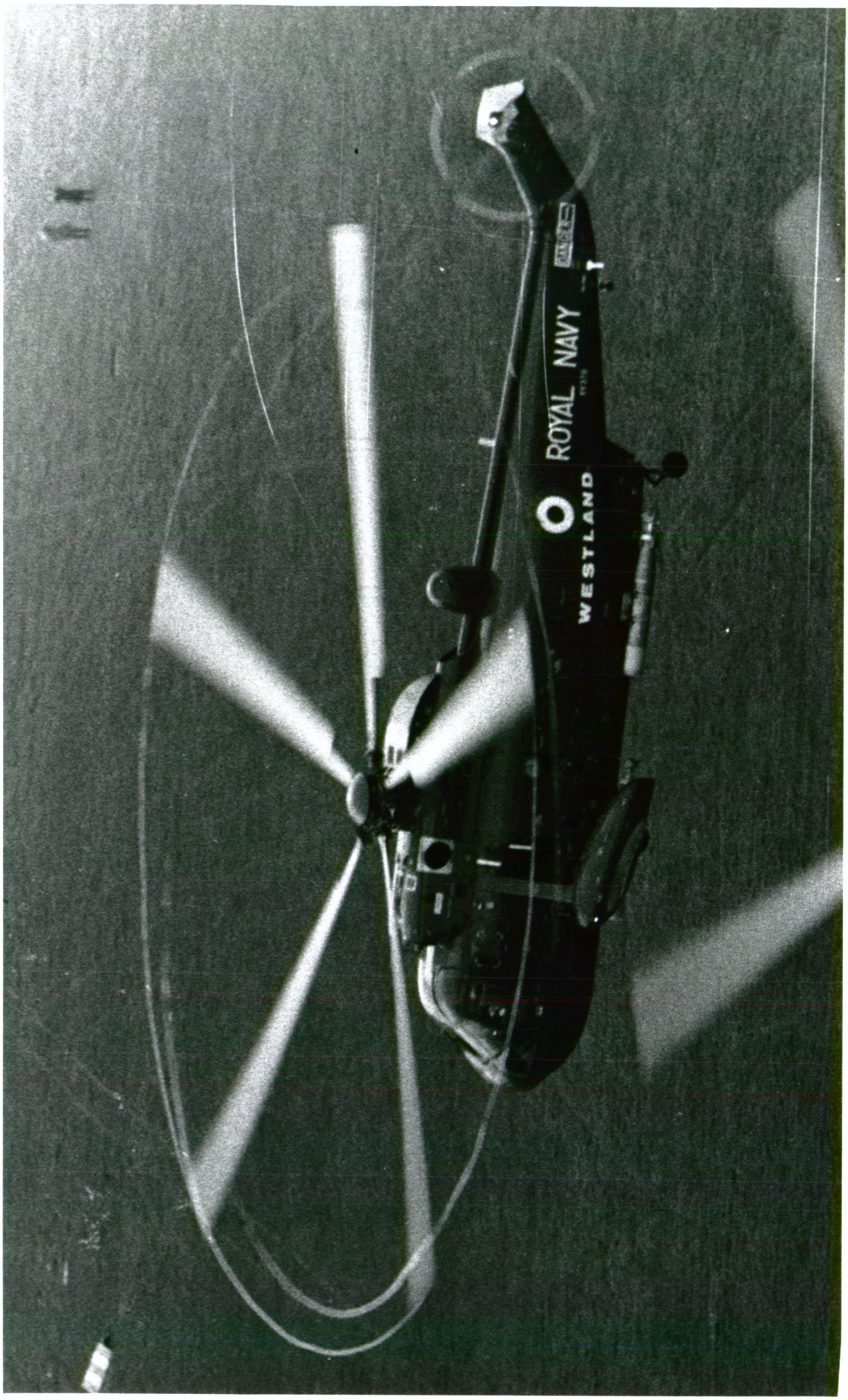

PLATE 5·2 HOVERING SEA KING

PLATE 5·3 HOVERING SEA KING

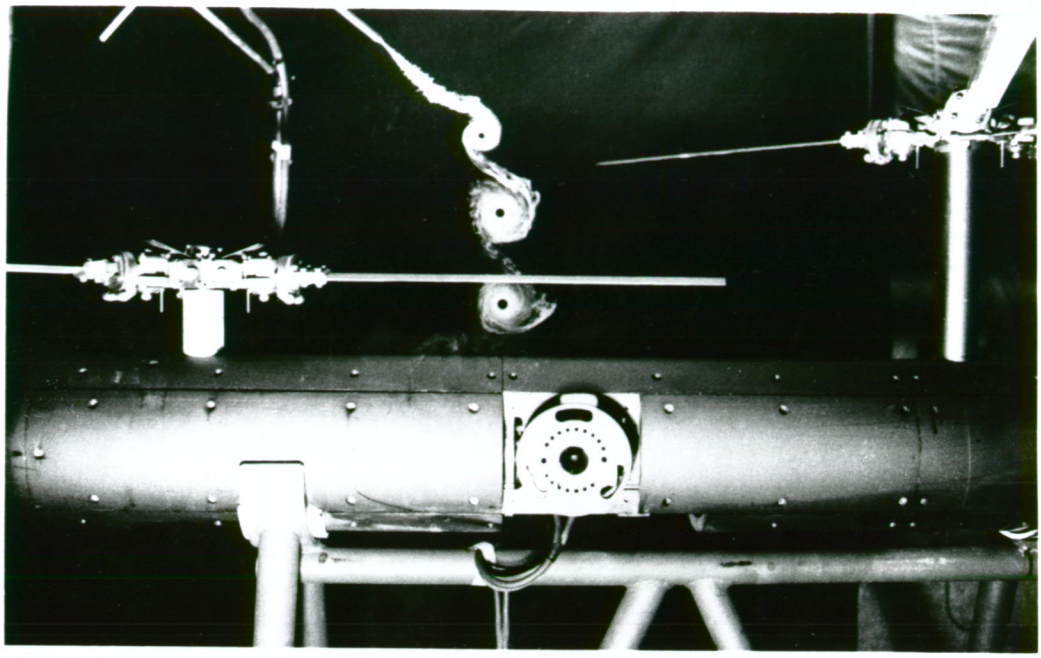

(PITCH 10° ~ TIP SPEED 400 ft/s)

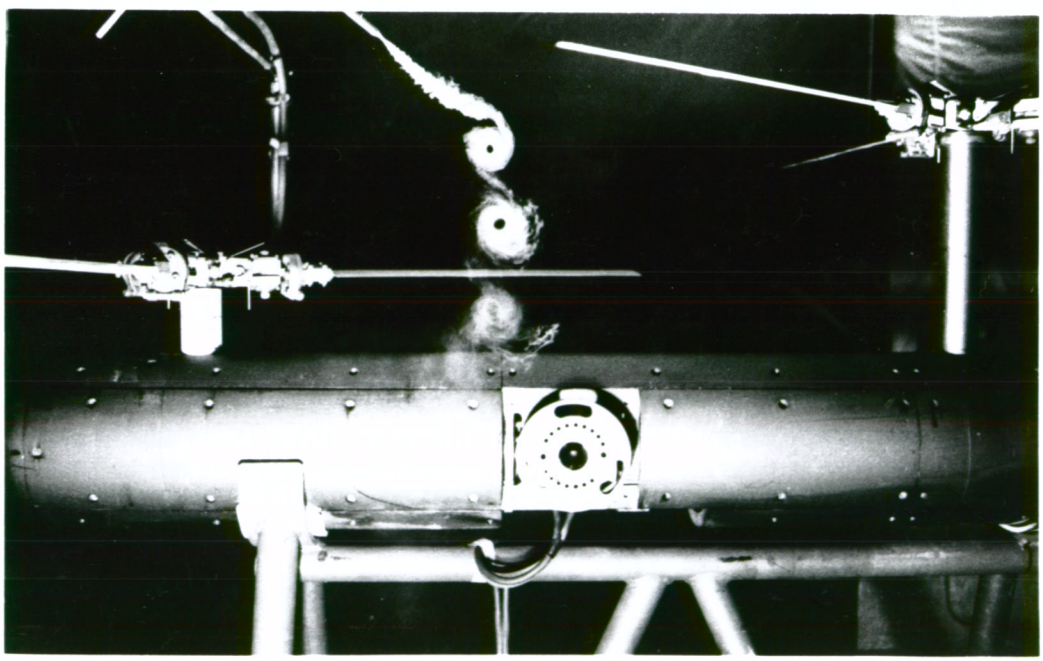

PLATE 5•4 TANDEM ROTOR RIG

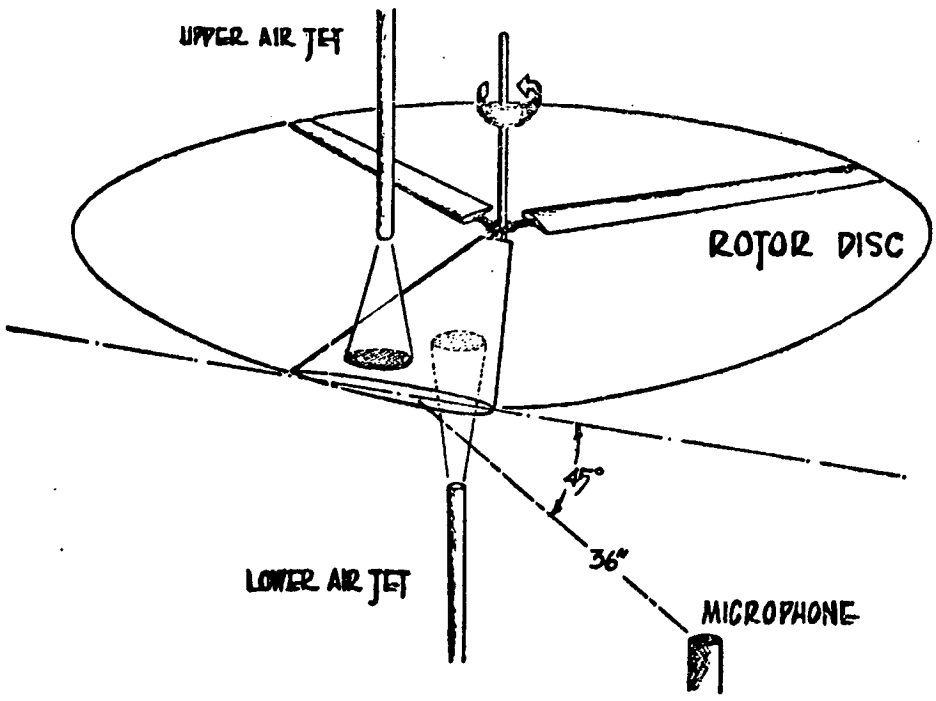

FIGURE 5.1. GENERAL TEST ARRANGEMENT

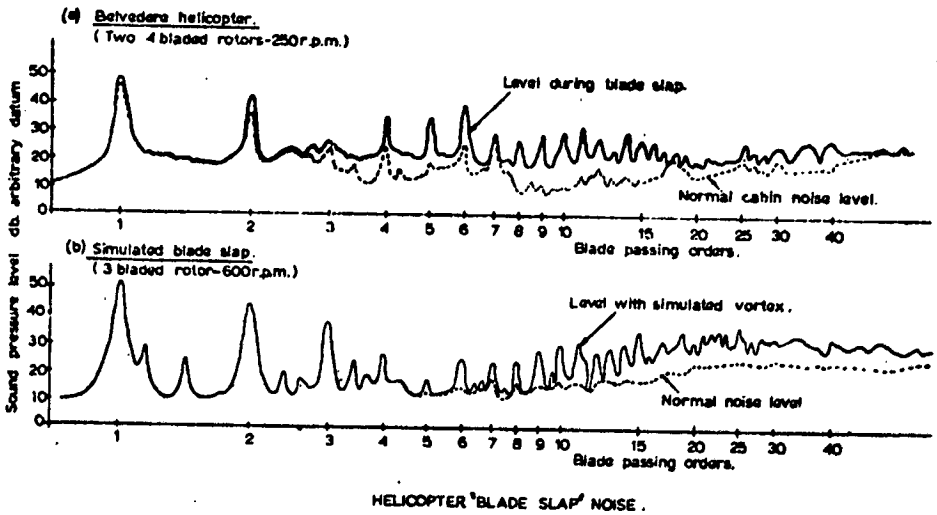

FIGURE 5.2. NARROWBAND ANALYSIS: BELVEDERE AND ROTOR RIG

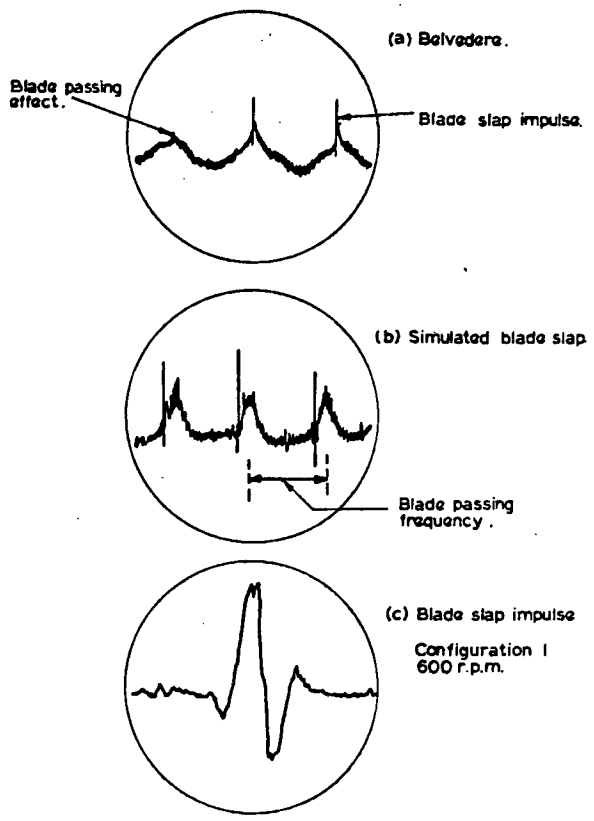

FIGURE 5.3. BLADE SLAP: OSCILLOGRAMS

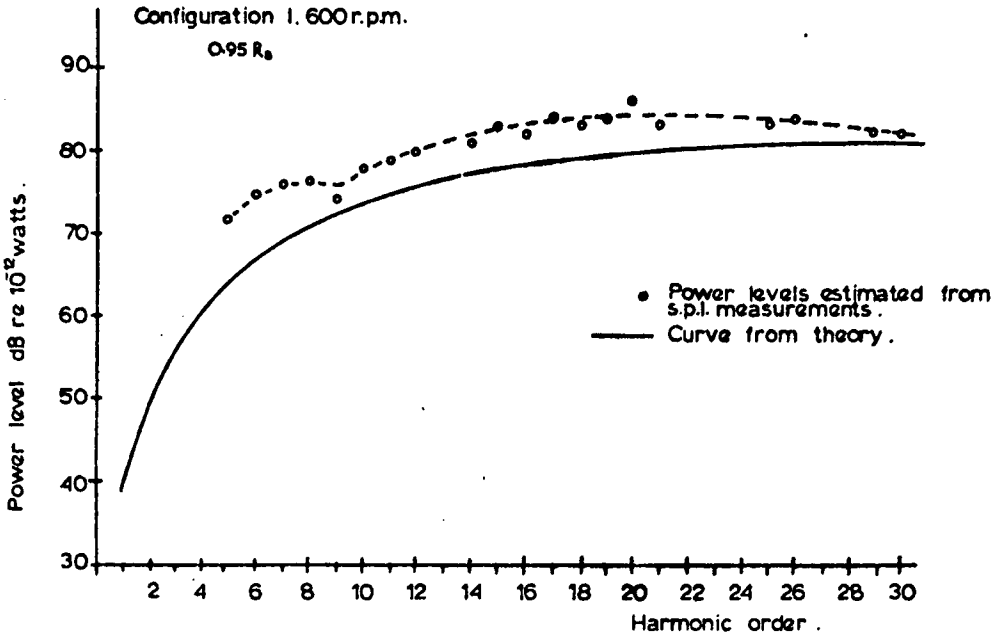

FIGURE 5.4. COMPARISON OF CALCULATED AND ESTIMATED SOURCE POWER

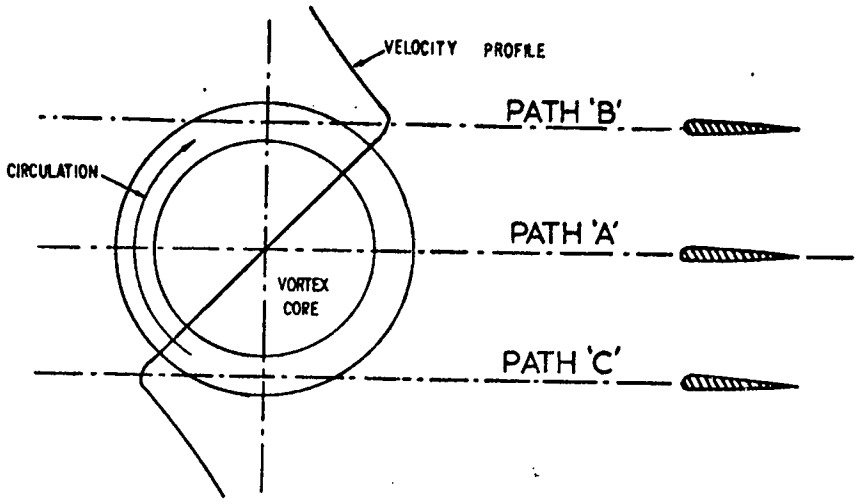

FIGURE 5.5. IDEALISED BLADE VORTEX INTERSECTION

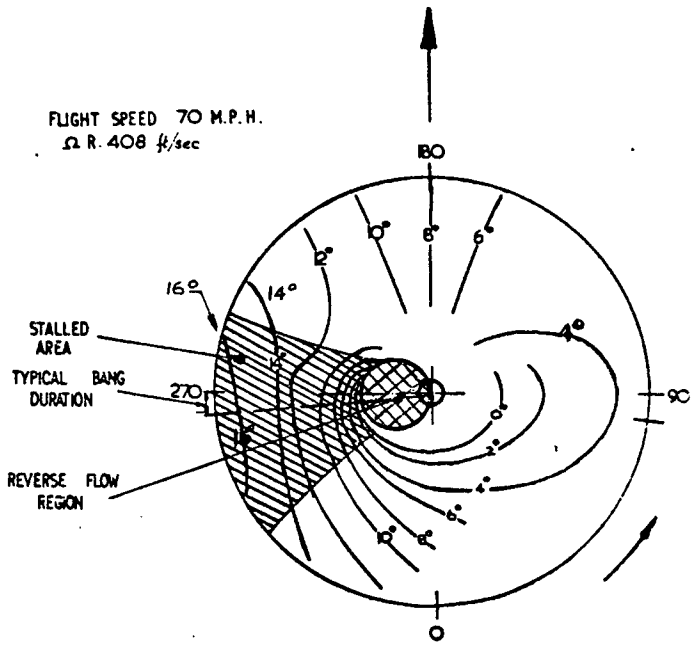

FIGURE 5.6. TYPICAL ANGLE OF ATTACK CONTOUR FOR SINGLE ROTOR HELICOPTER

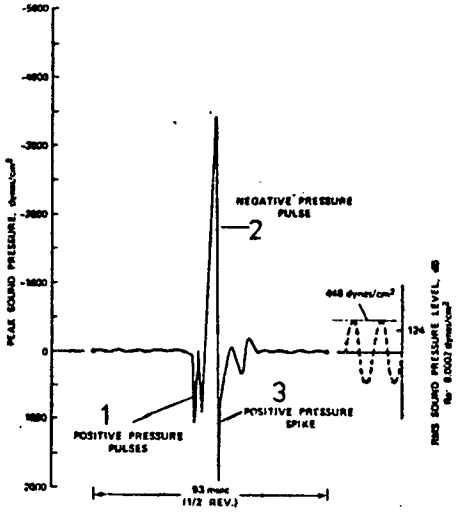

FIGURE 5.7. ACOUSTIC WAVEFORM - REFERENCE (87)

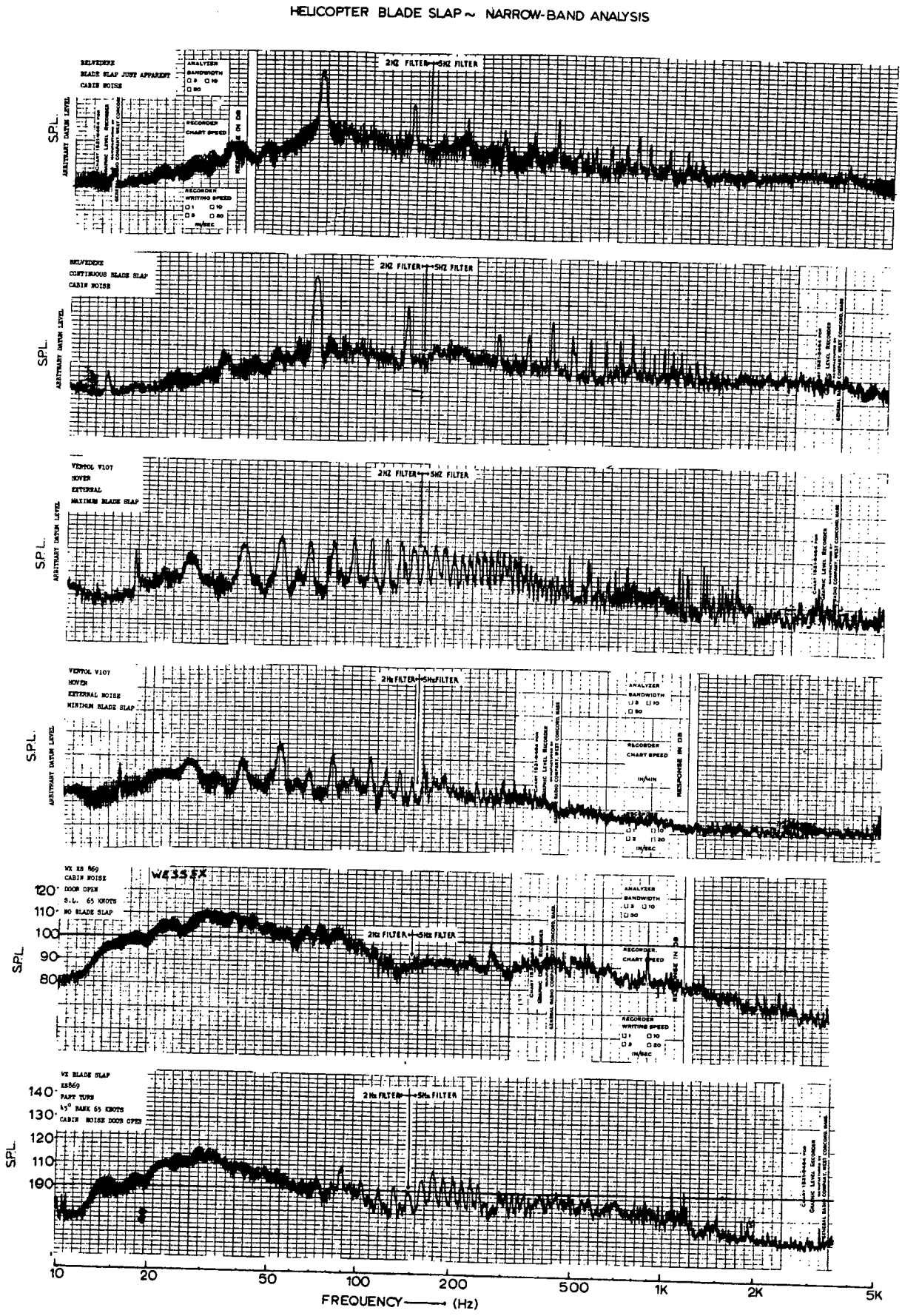

FIGURE 5.8. NARROWBAND ANALYSIS: BELVEDERE; VERTOL 107; WESSEX

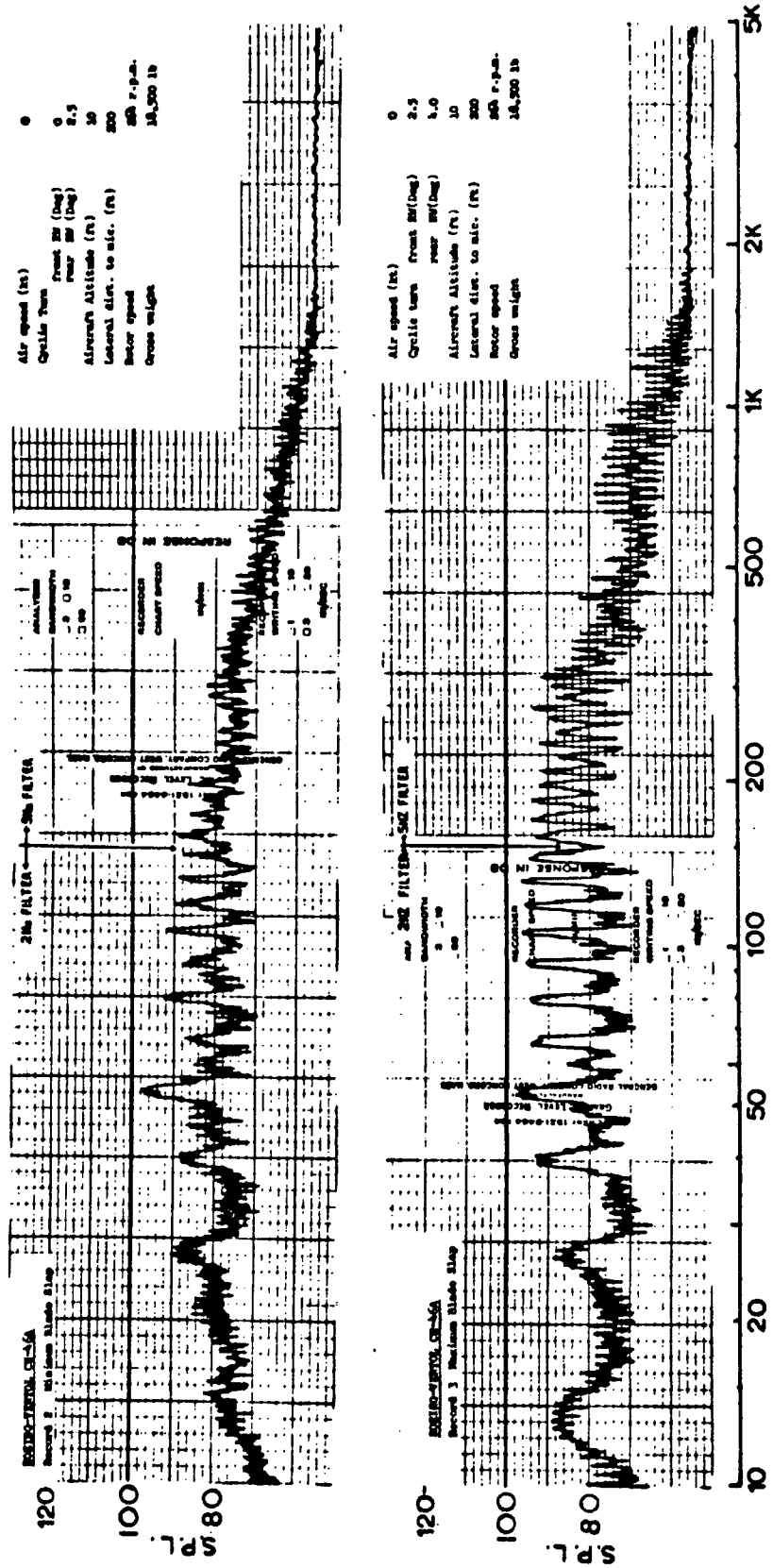

FIGURE 5.9(a). NARROWBAND ANALYSIS: BOEING VERTOL CH-46A (HOVER)

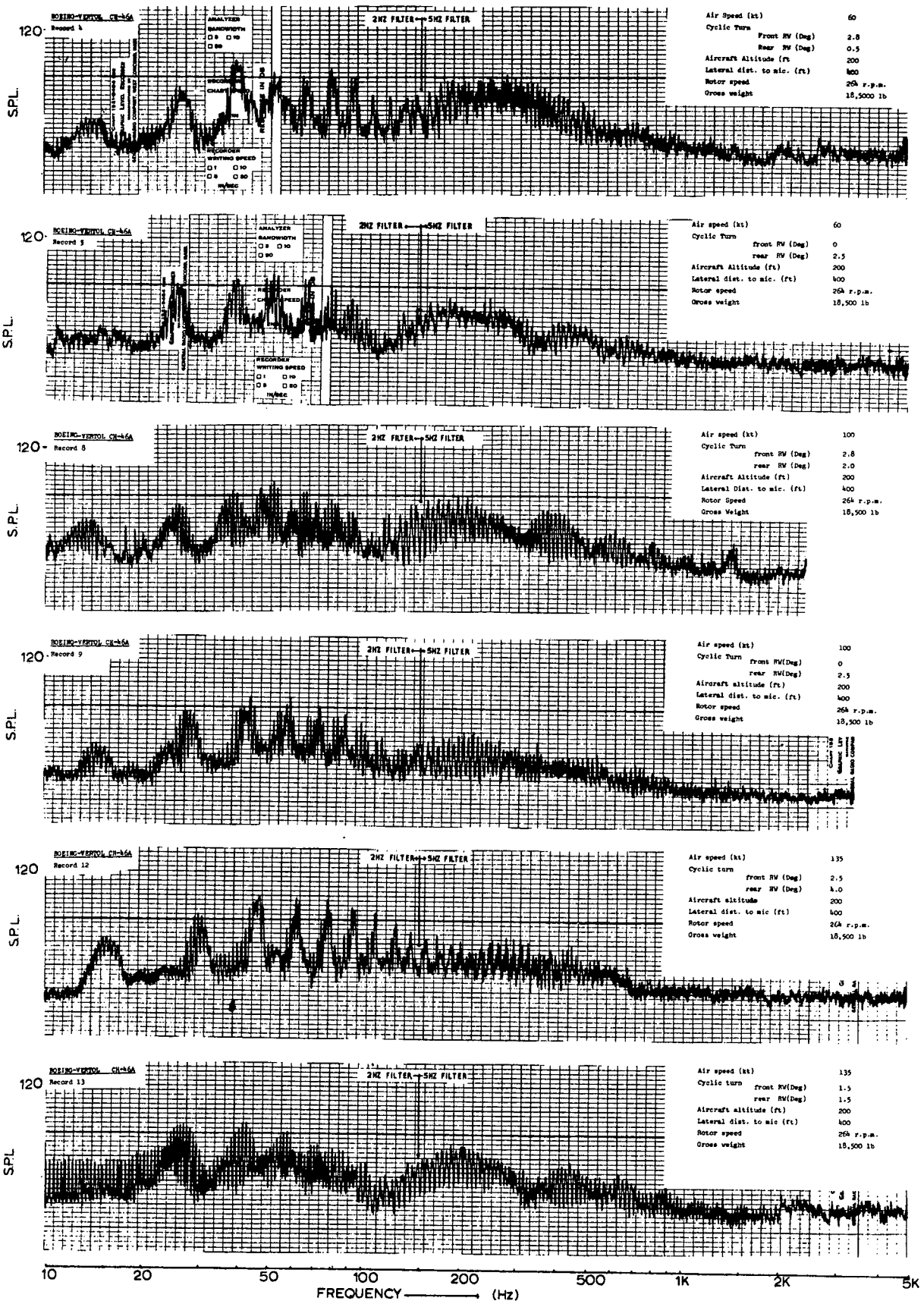

FIGURE 5.9(b). NARROWBAND ANALYSIS: BOEING VERTOL CH-46A (FORWARD FLIGHT)

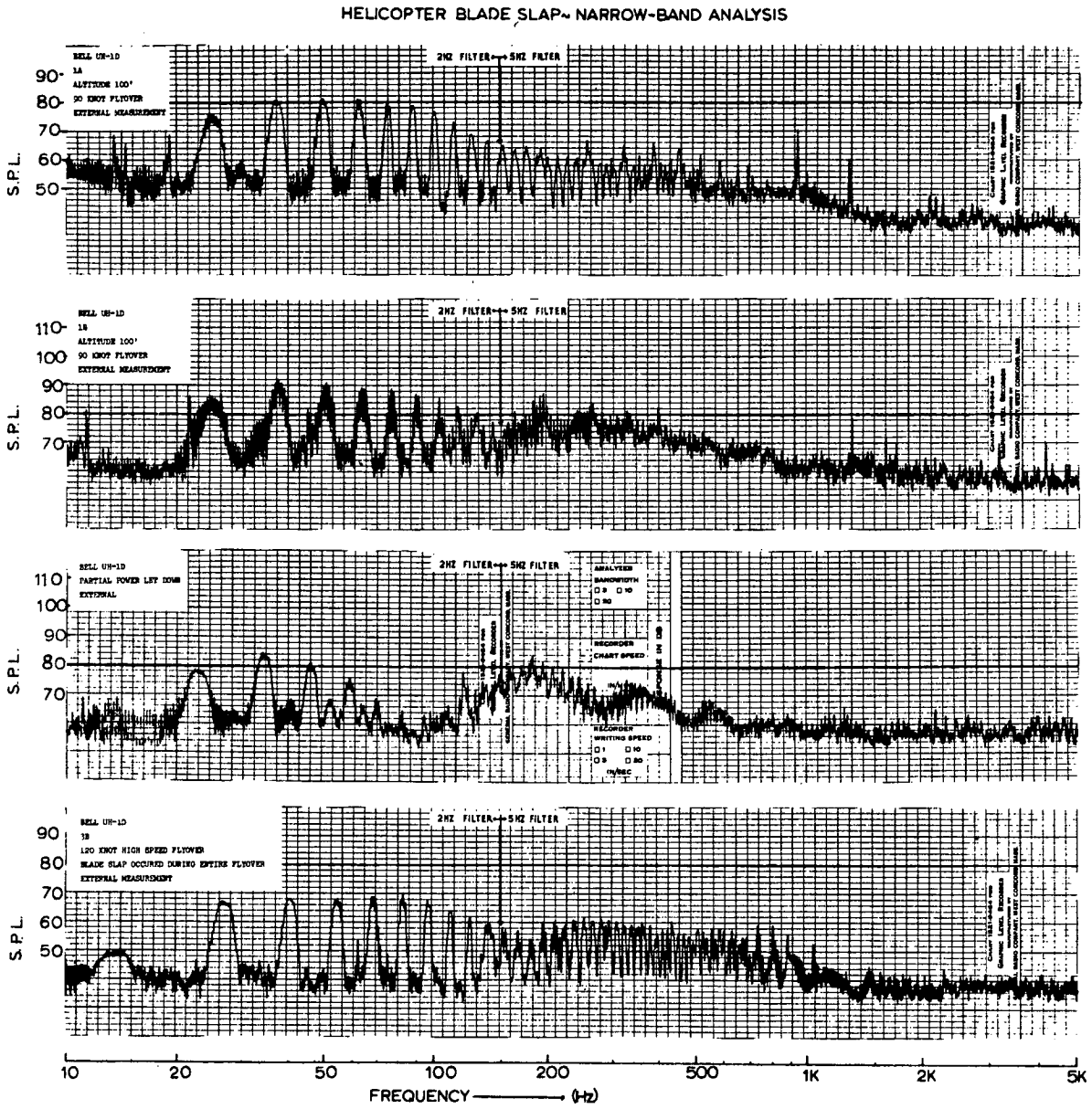

FIGURE 5.10. NARROWBAND ANALYSIS: BELL UH-1D

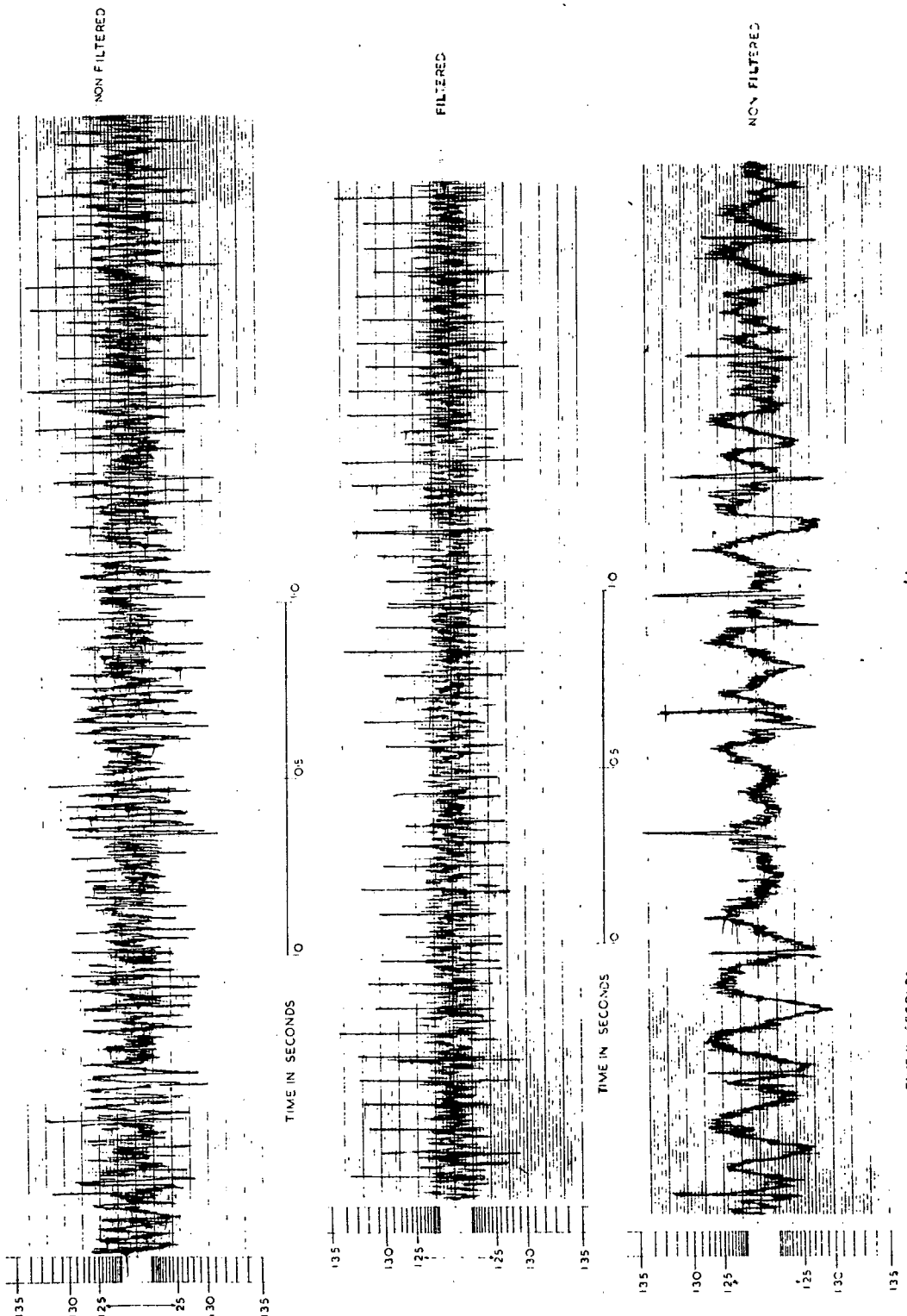

FIGURE 5.11(a). PRESSURE TIME HISTORIES: WESSEX MK.5

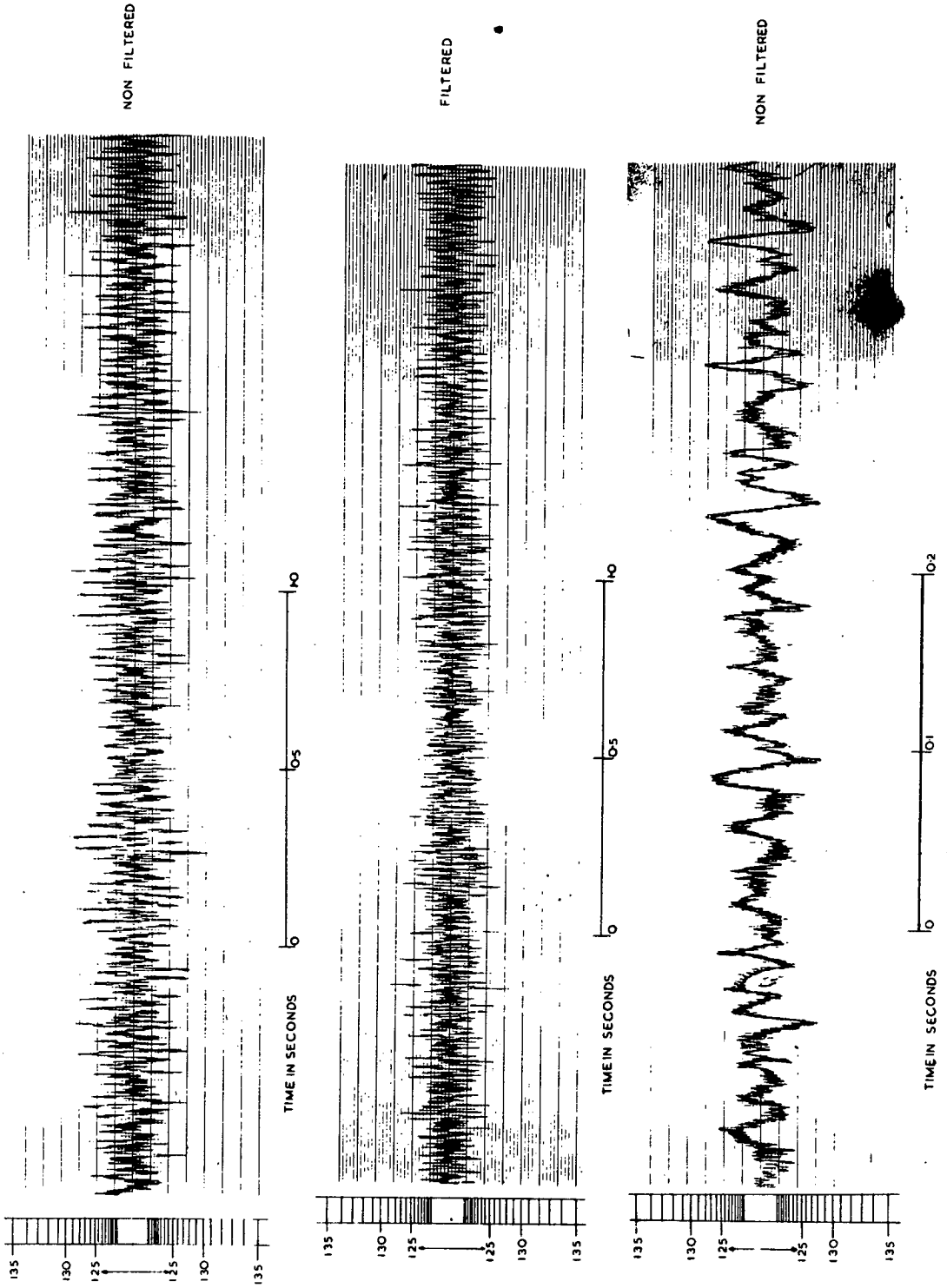

FIGURE 5.11(b). PRESSURE TIME HISTORIES: WESSEX - NO BLADE SLAP

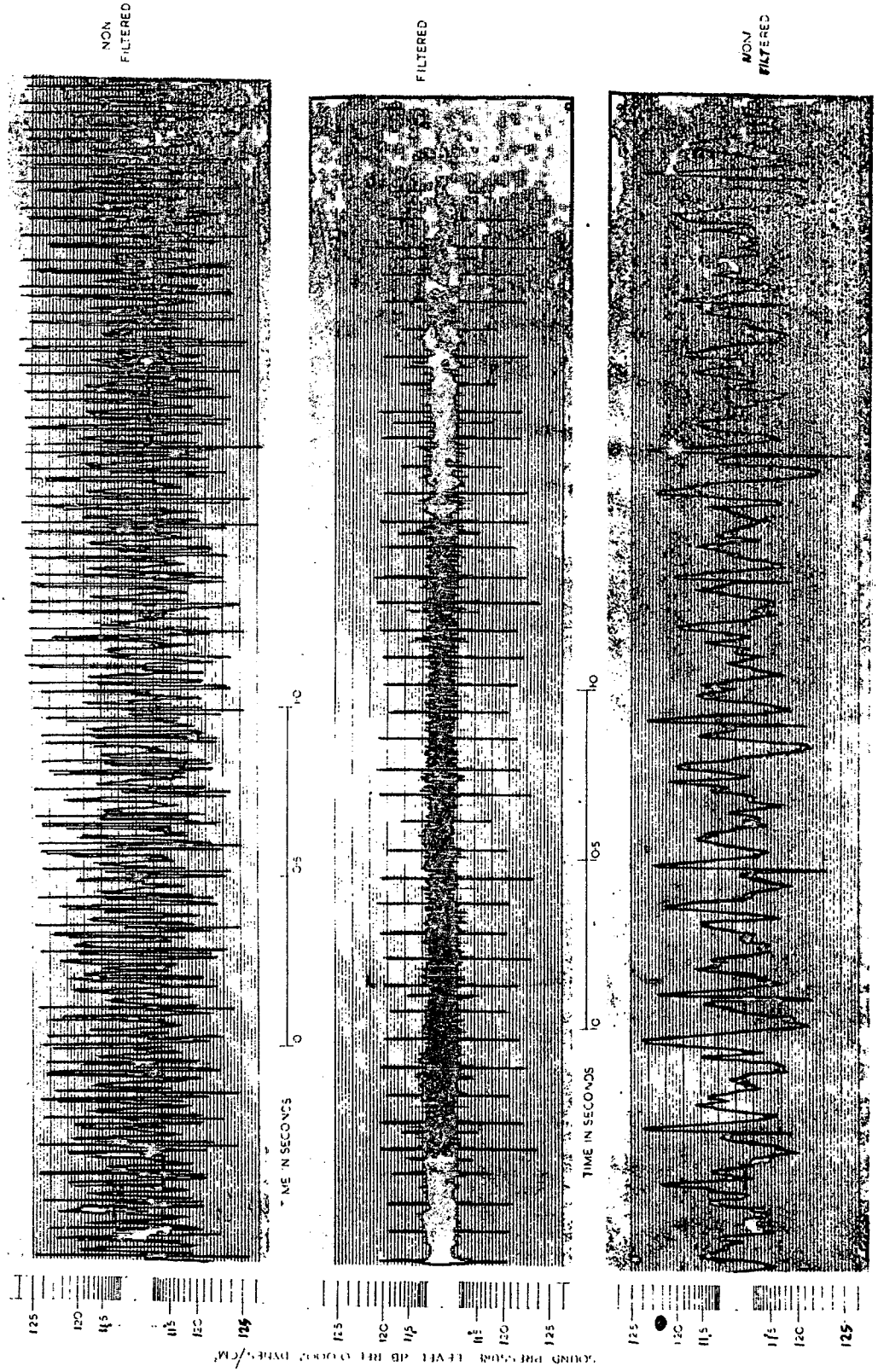

FIGURE 5.12(a). PRESSURE TIME HISTORIES: SYCAMORE WITH BLADE SLAP.

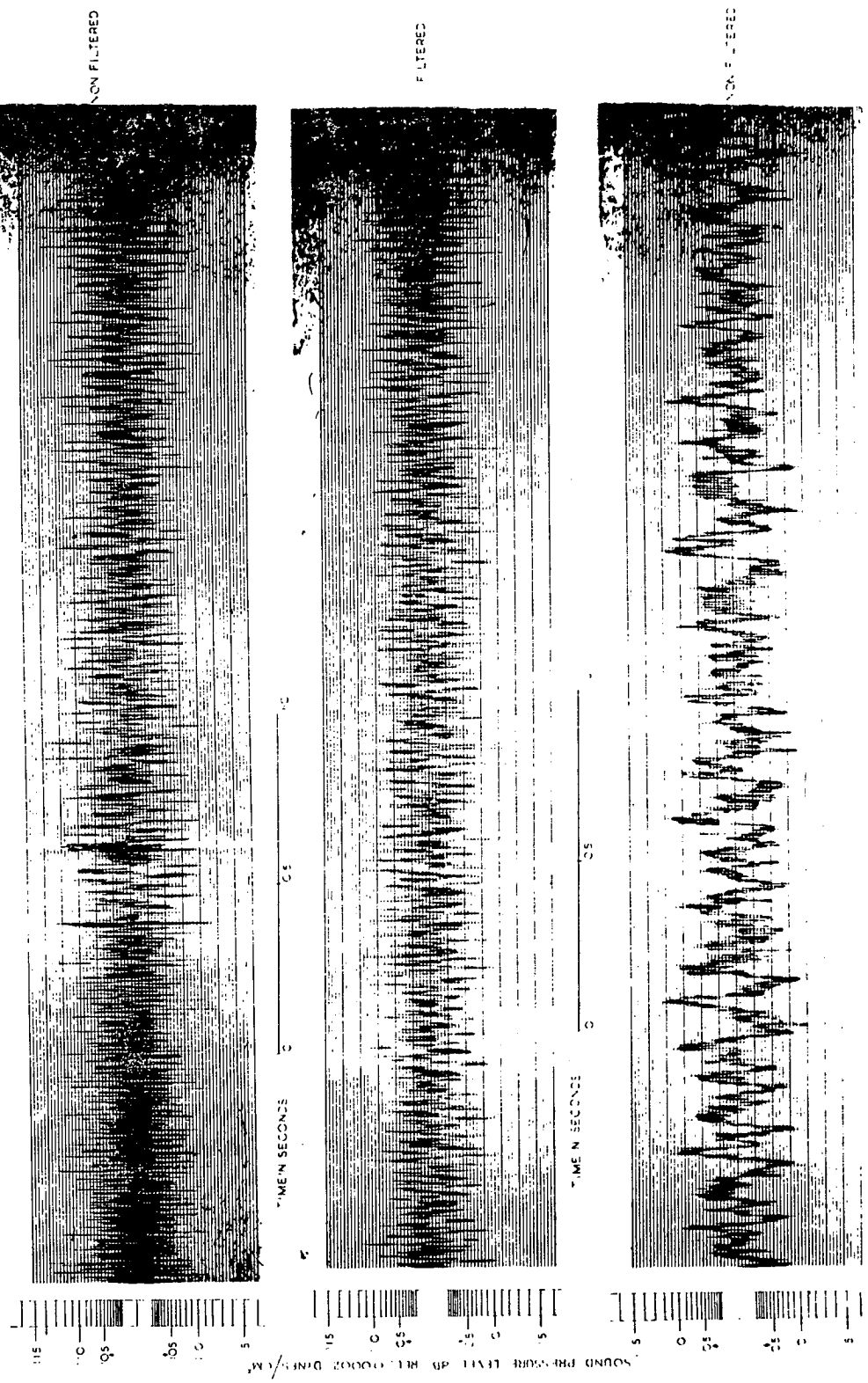

FIGURE 5.12(b): PRESSURE TIME HISTORIES: SYCAMORE - NO BLADE SLAP

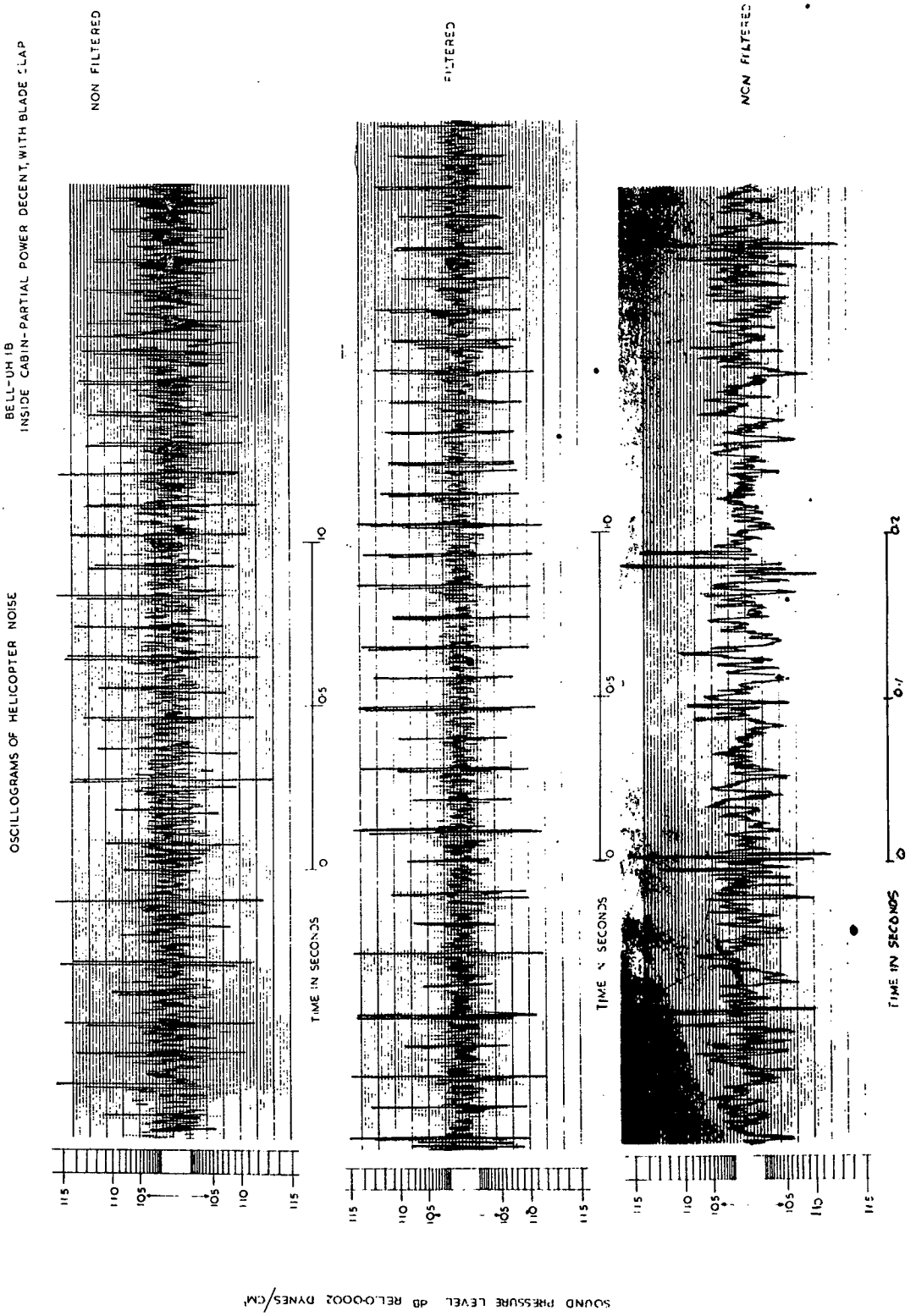

FIGURE 5.13(a). PRESSURE TIME HISTORIES: BELL UH-1B WITH BLADE SLAP

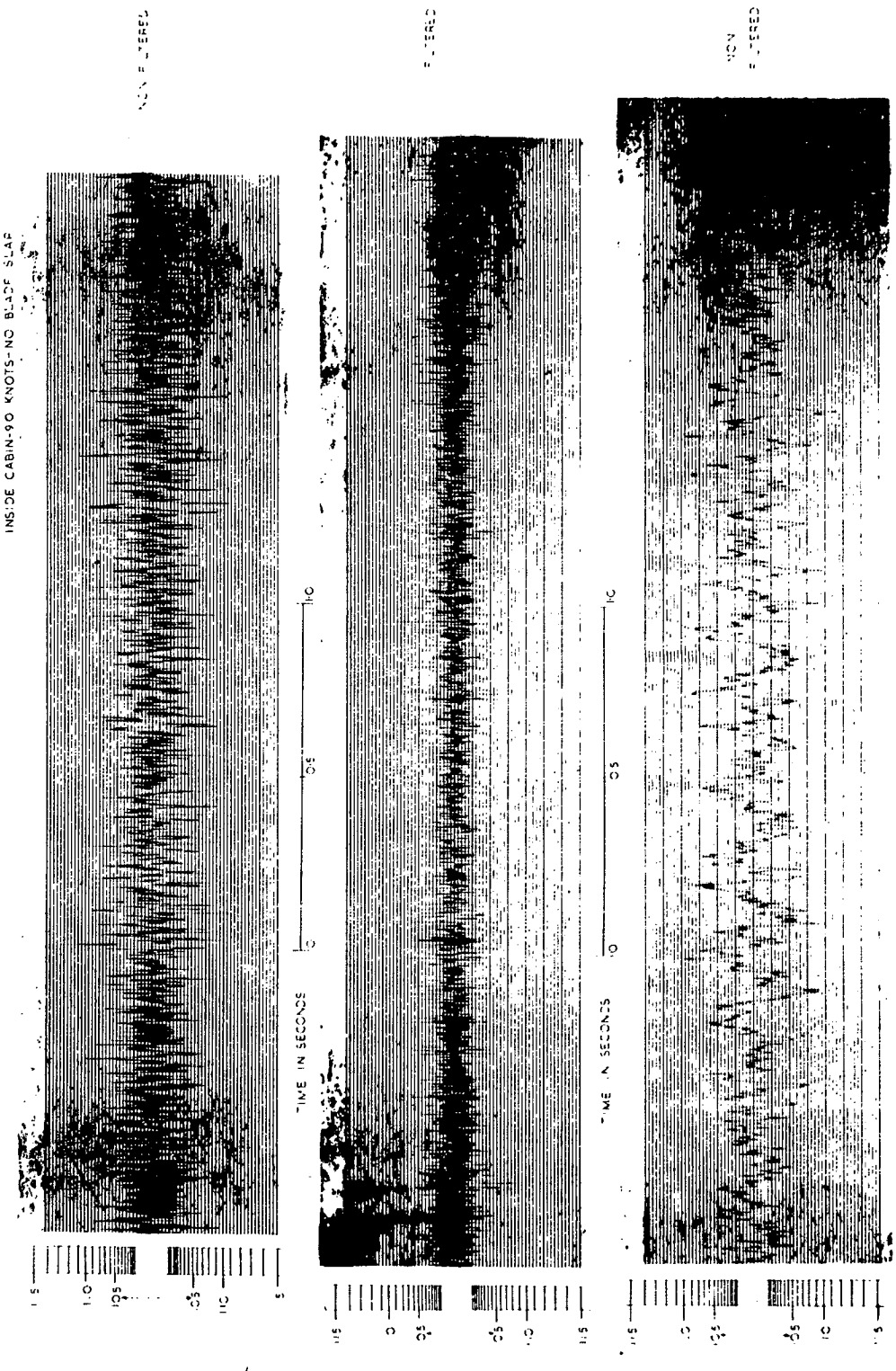

FIGURE 5.13(b). PRESSURE TIME HISTORIES: BELL UH-1B - NO BLADE SLAP

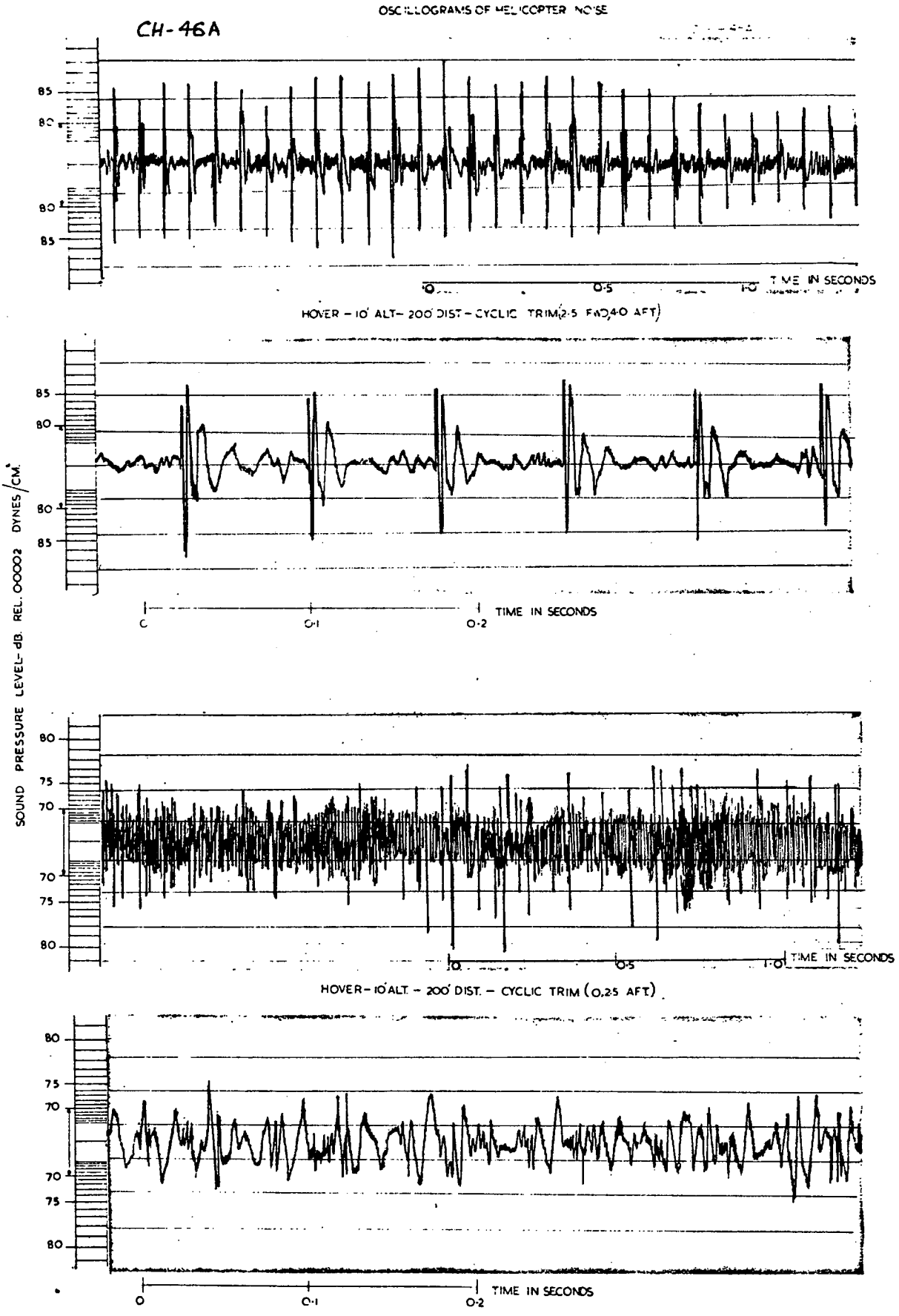

FIGURE 5.14. PRESSURE TIME HISTORIES: BOEING VERTOL CH-46A (HOVER)

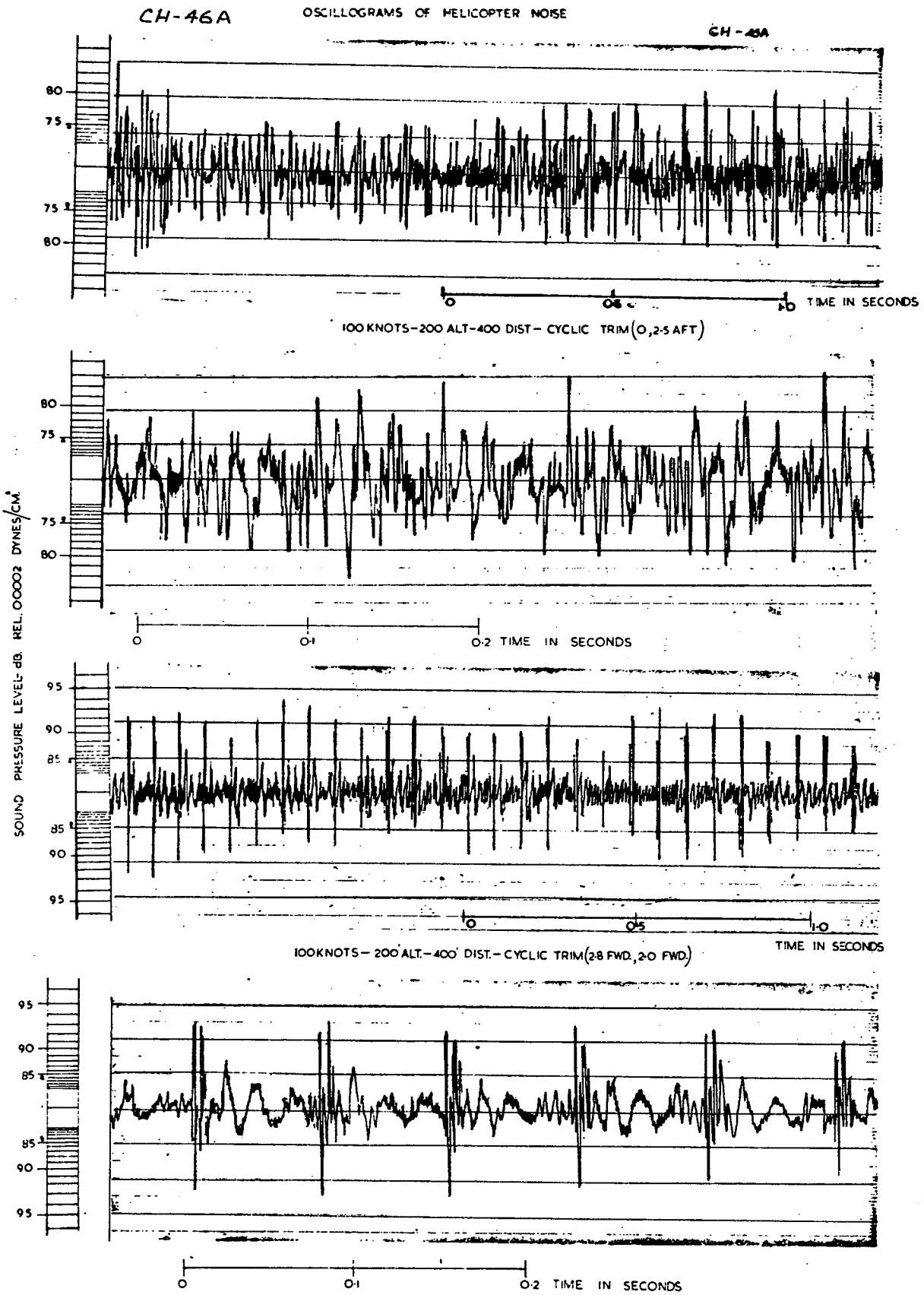

FIGURE 5.15. PRESSURE TIME HISTORIES: BOEING VERTOL CH-46A (FORWARD FLIGHT)

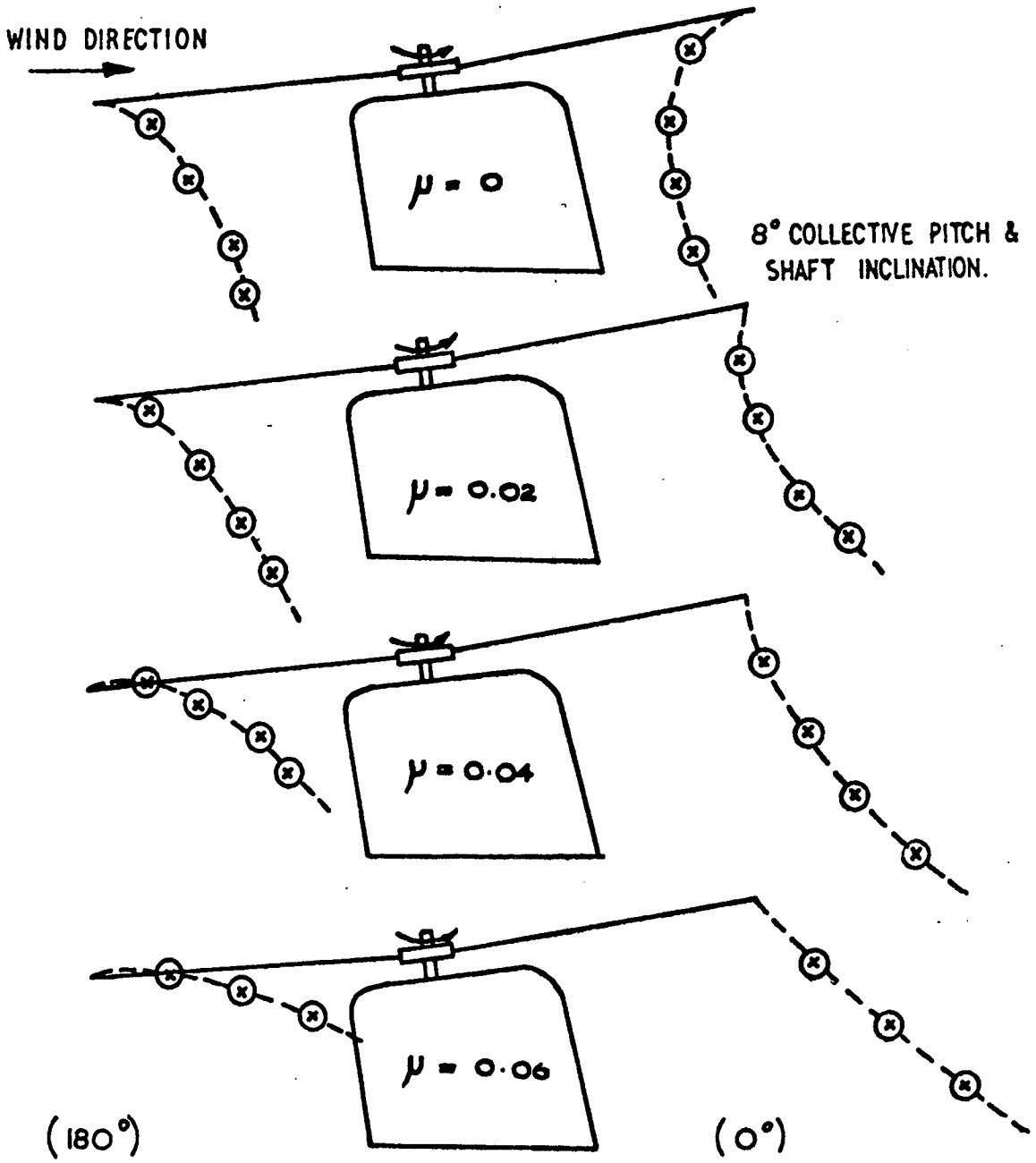

FIGURE 5.16. VORTEX PATHS IN THE FORE AND AFT PLANE - REFERENCE (92)

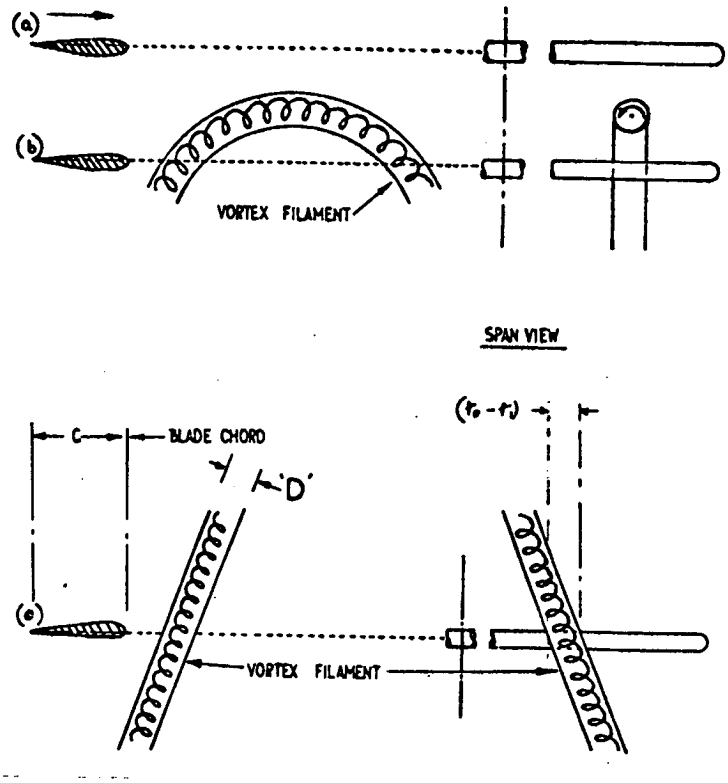

FIGURE 5.17. IDEALISED BLADE/VORTEX INTERSECTIONS

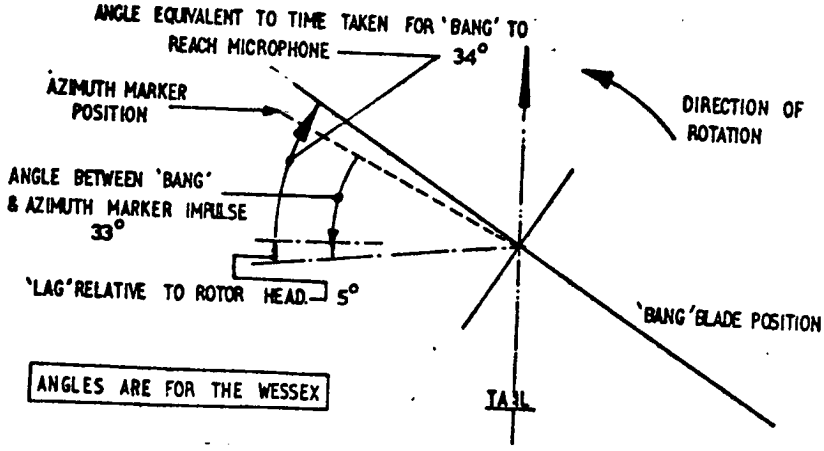

FIGURE 5.18. BLADE 'BANG' AZIMUTH LOCATION

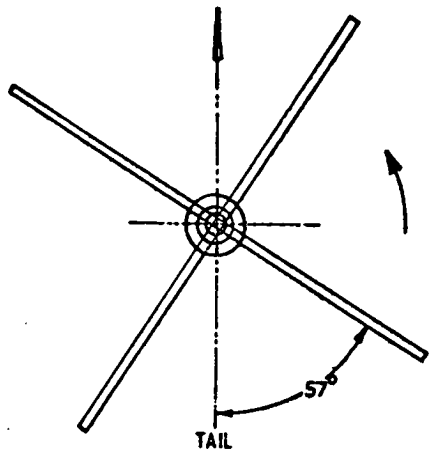

(a) Test Result

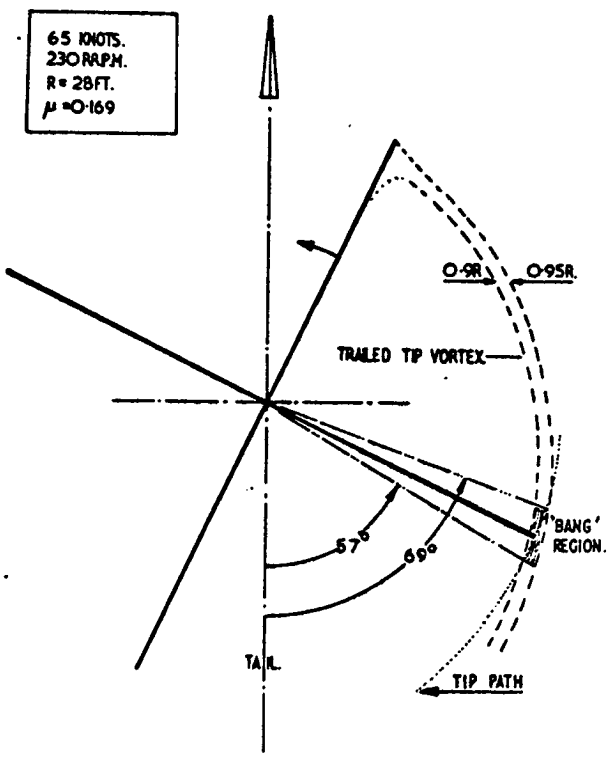

(b) Rigid Wake Model

FIGURE 5.19. BLADE SLAP SOURCE LOCATION - WESSEX RESULTS

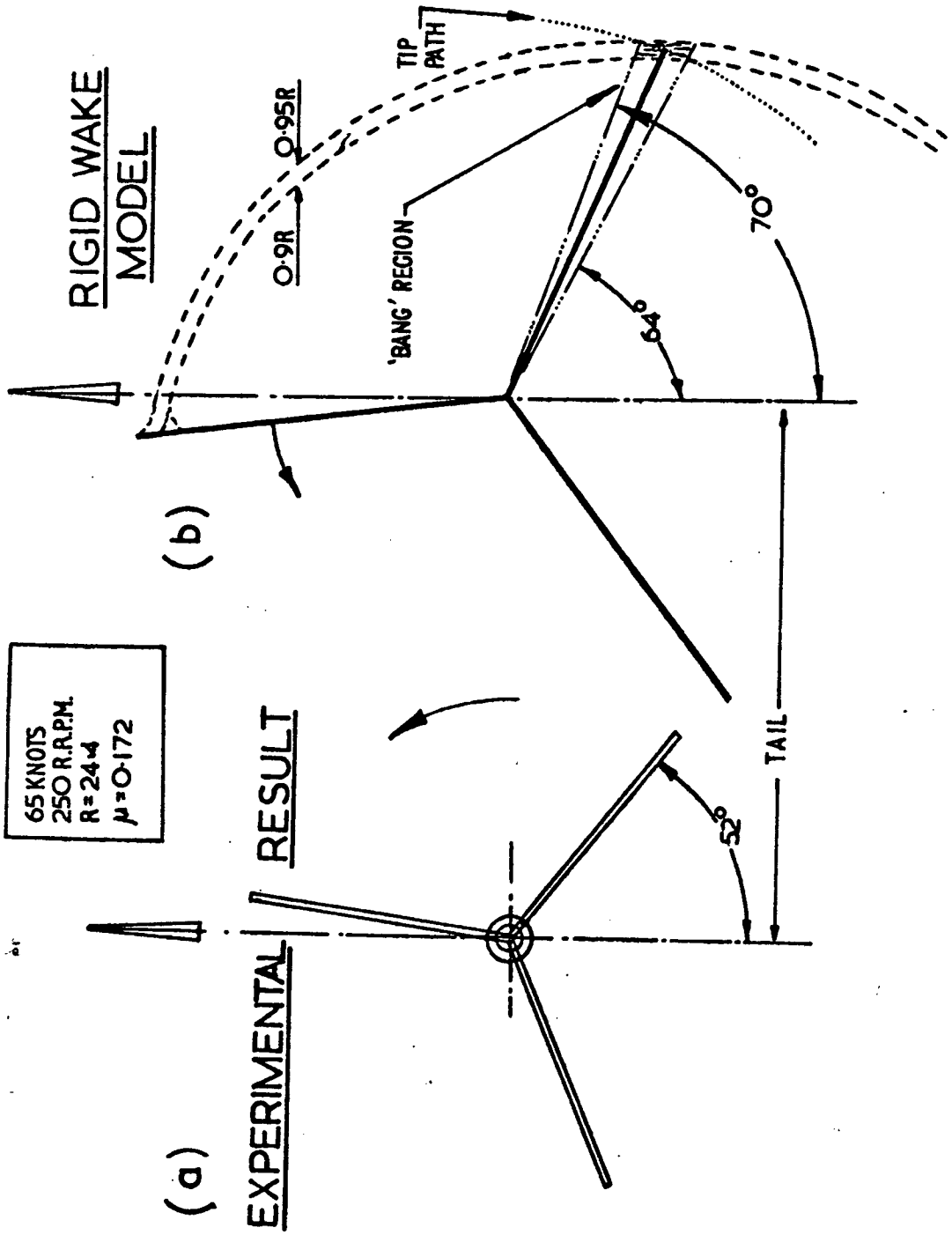

FIGURE 5.20. BLADE SLAP SOURCE LOCATION - SYCAMORE RESULTS

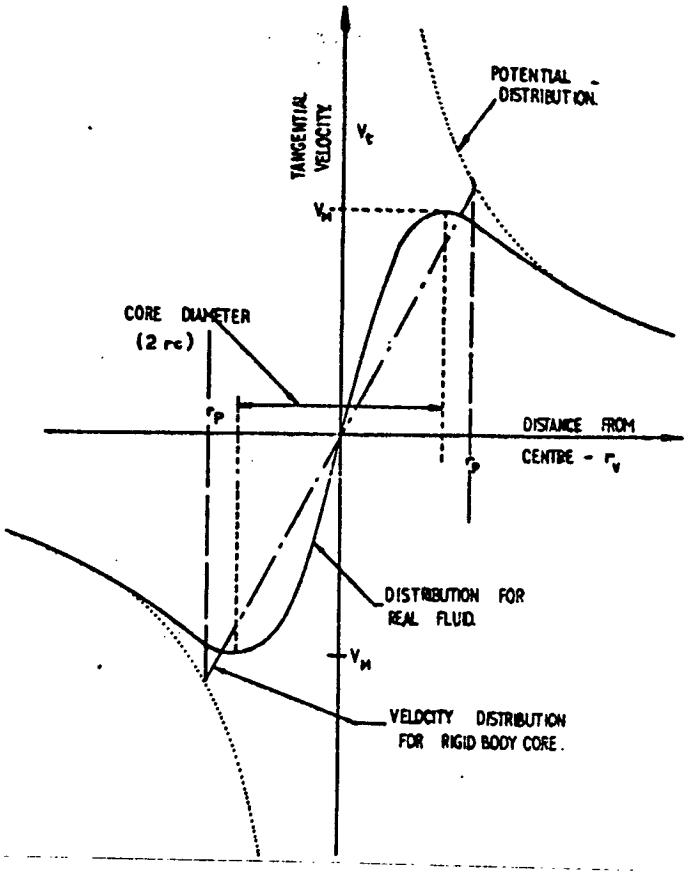

FIGURE 5.21. VELOCITY DISTRIBUTION THROUGH A TIP VORTEX

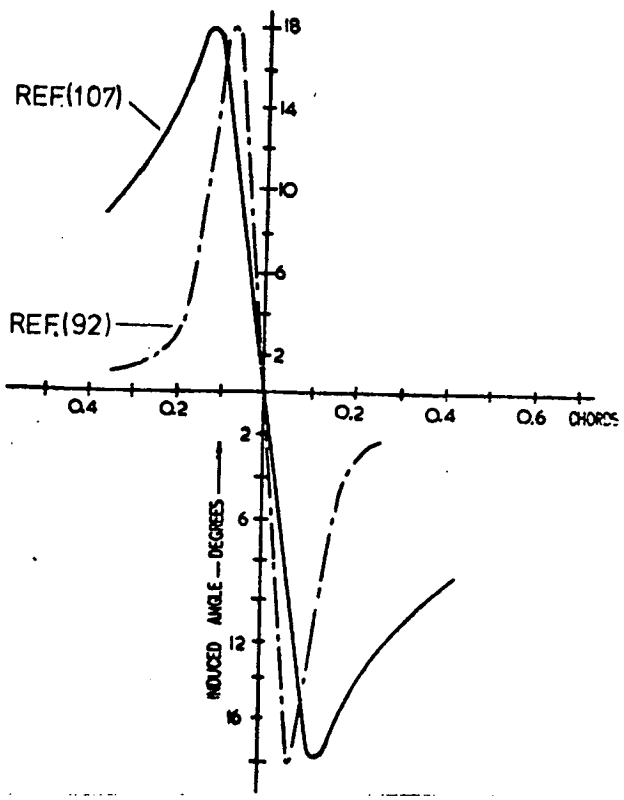

FIGURE 5.22. MEASURED VORTEX PROFILES

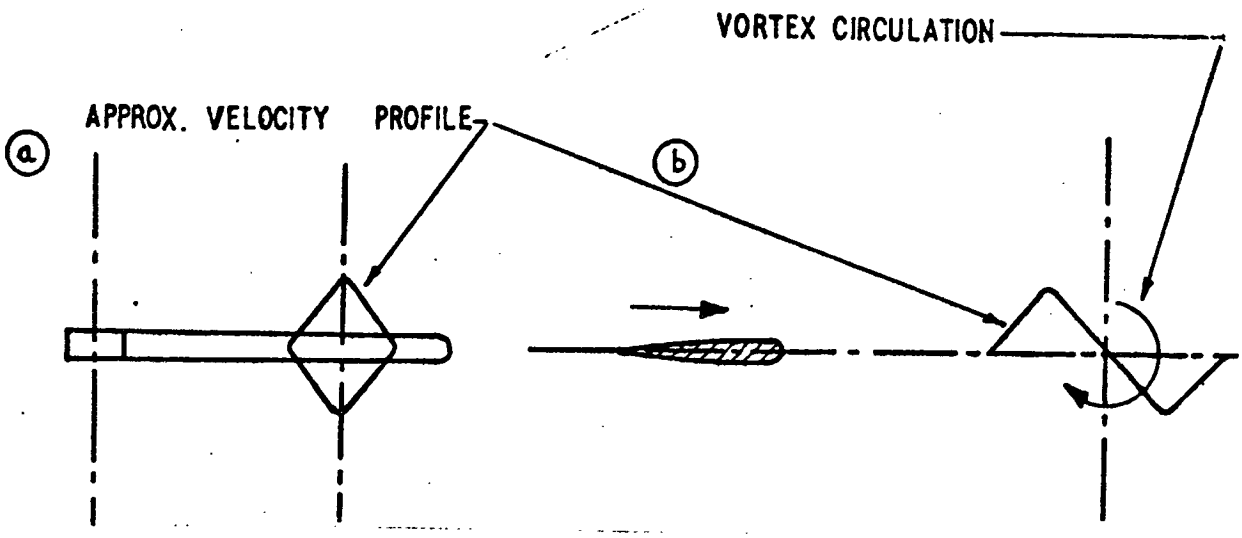

Figure 5.23.1. Vortex core axis parallel to span of blade.

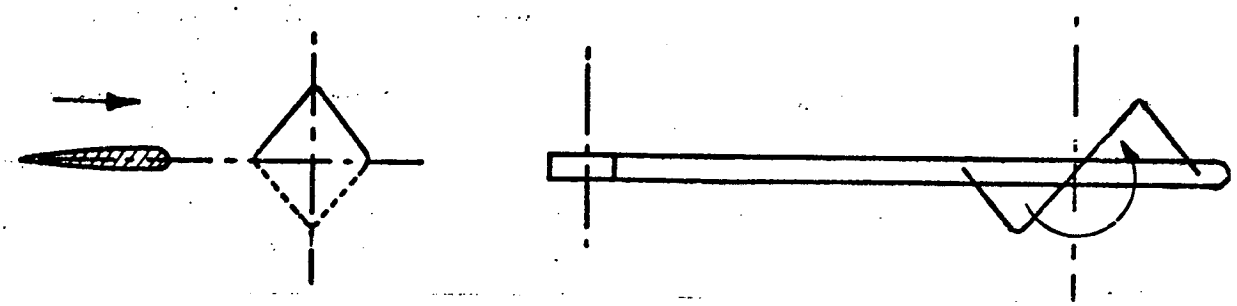

Figure 5.23.2. Vortex core axis parallel to direction of blade motion.

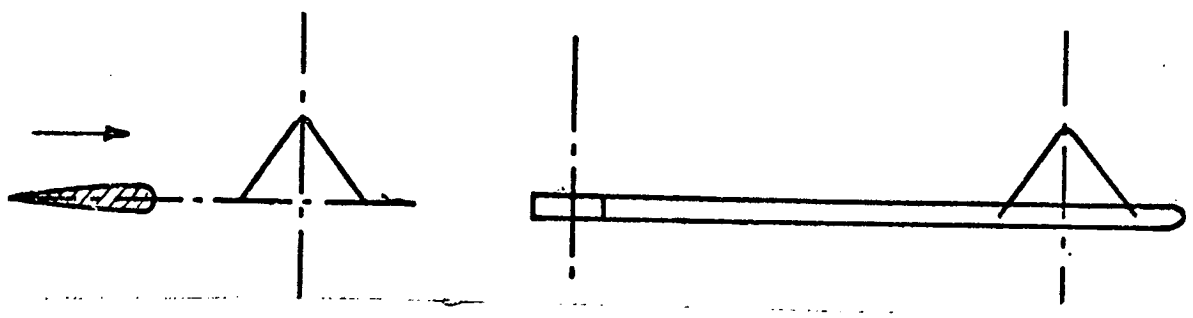

Figure 5.23.3. Theoretical model for case shown in Figure 5.23.2.

FIGURE 5.23. BLADE VORTEX INTERSECTIONS

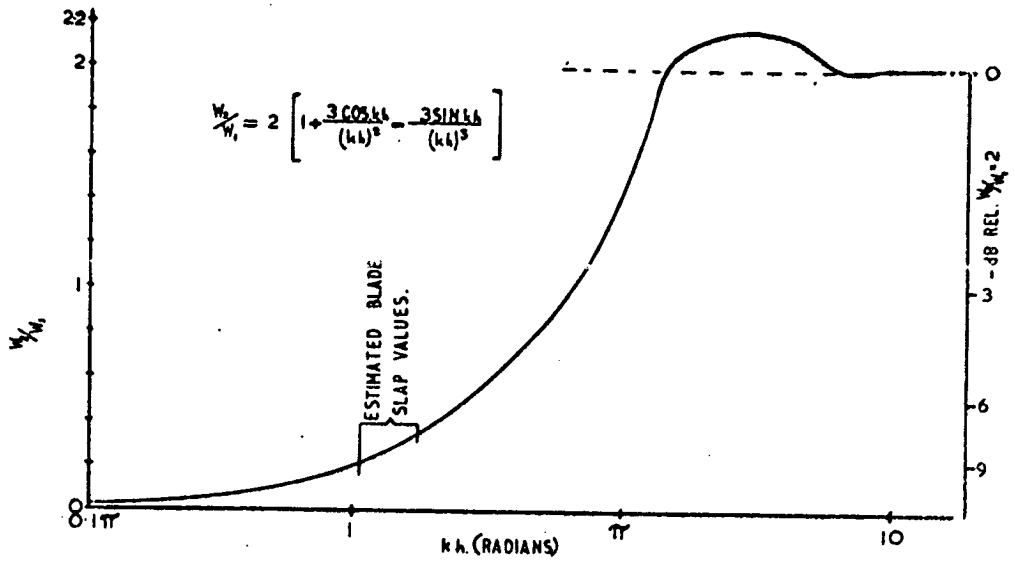

FIGURE 5.24. INFLUENCE OF DIPOLE SEPARATION DISTANCE ON ACCURACY OF PREDICTION METHOD

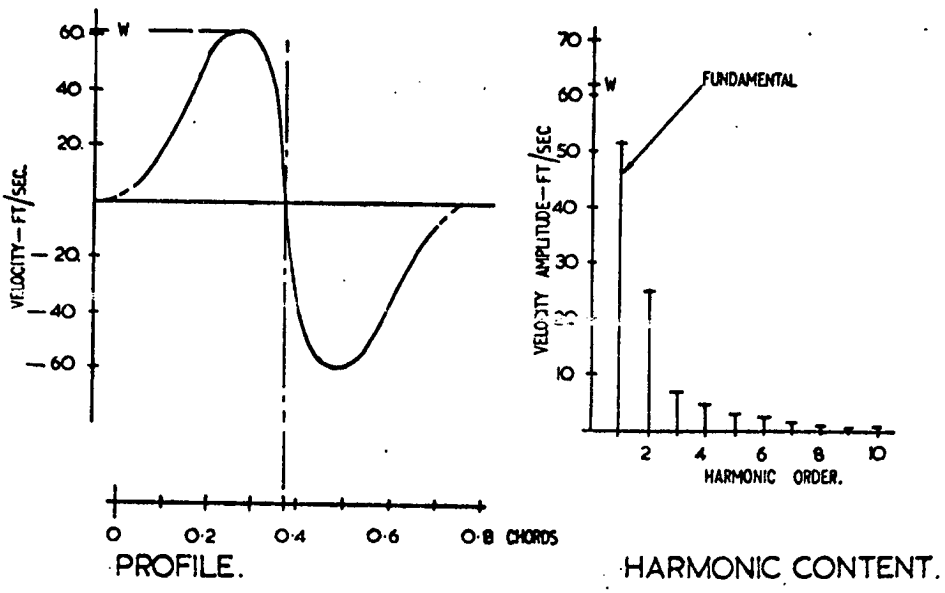

FIGURE 5.25. IDEALISED TIP VORTEX CHARACTERISTICS

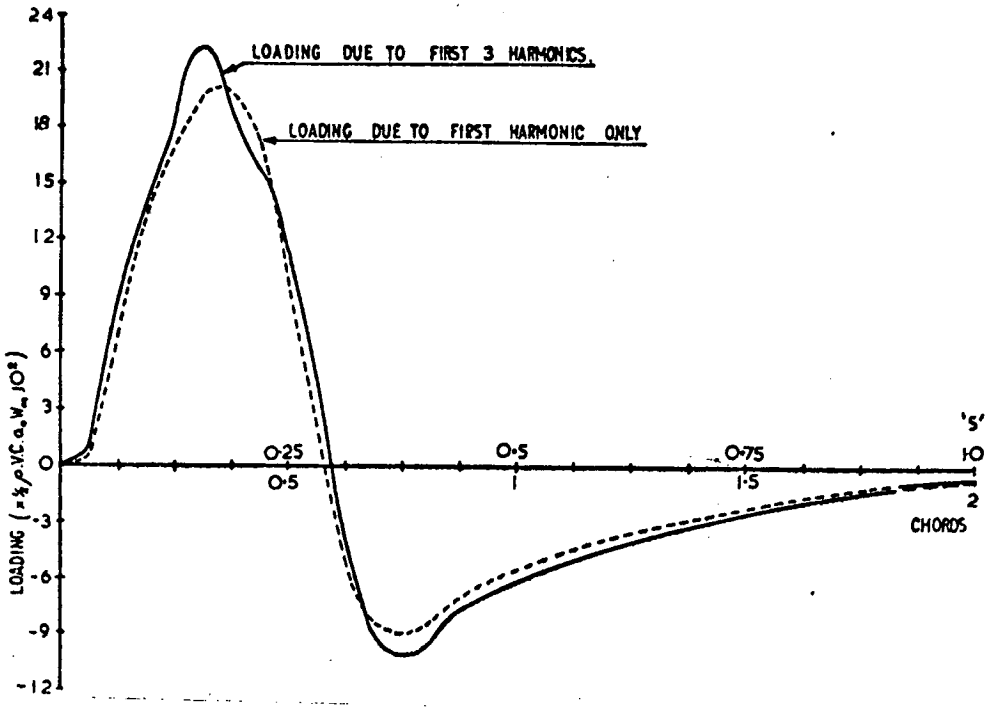

FIGURE 5.26. BLADE LOADING (FOR FIRST HARMONIC AND FIRST THREE HARMONICS)

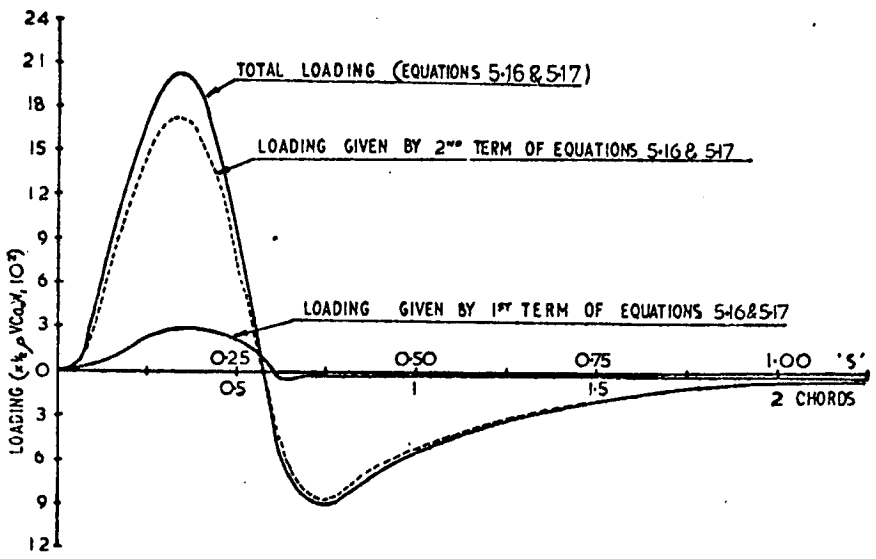

FIGURE 5.27. BLADE LOADING FOR FIRST HARMONIC

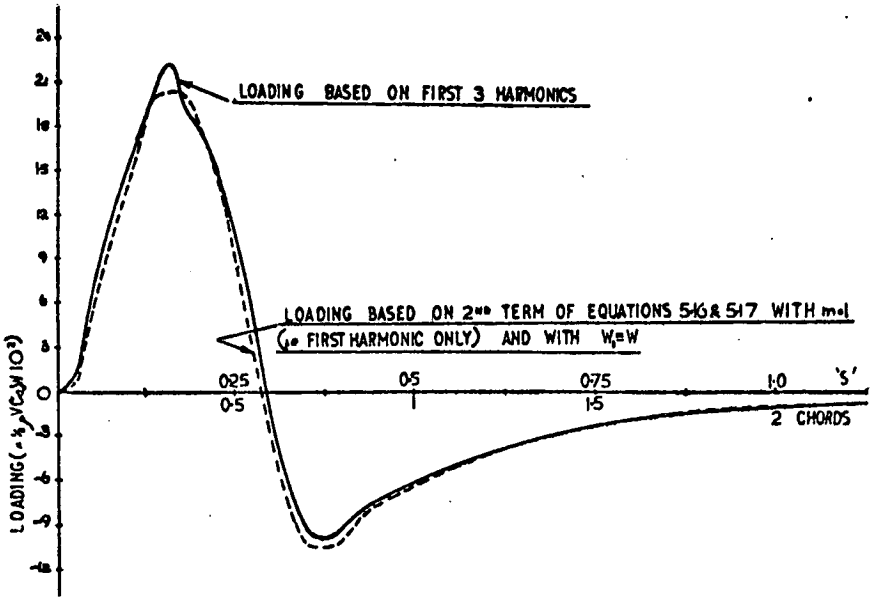

FIGURE 5.28. BLADE LOADING - COMPARISON OF FULL AND APPROXIMATE SOLUTIONS

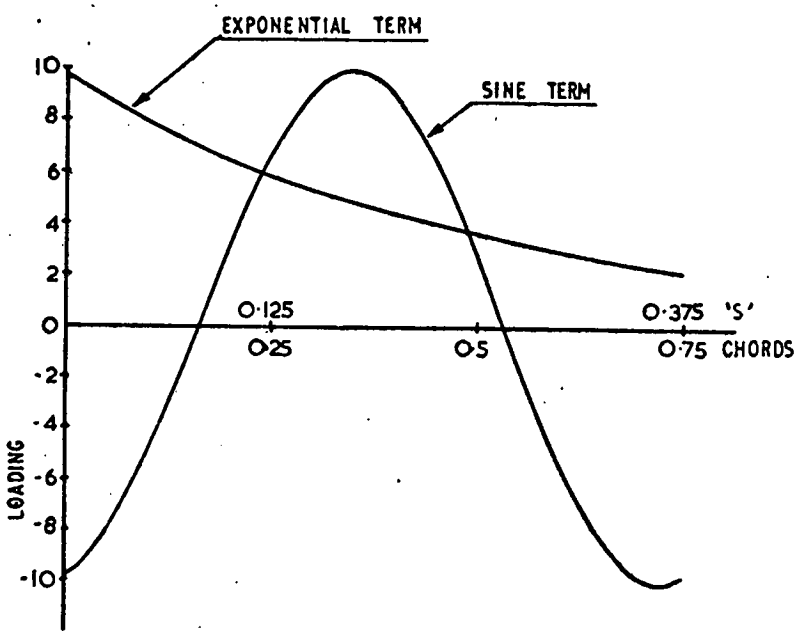

FIGURE 5.29. BLADE LOADING - COMPARISON OF EXPONENTIAL AND SINE COMPONENT

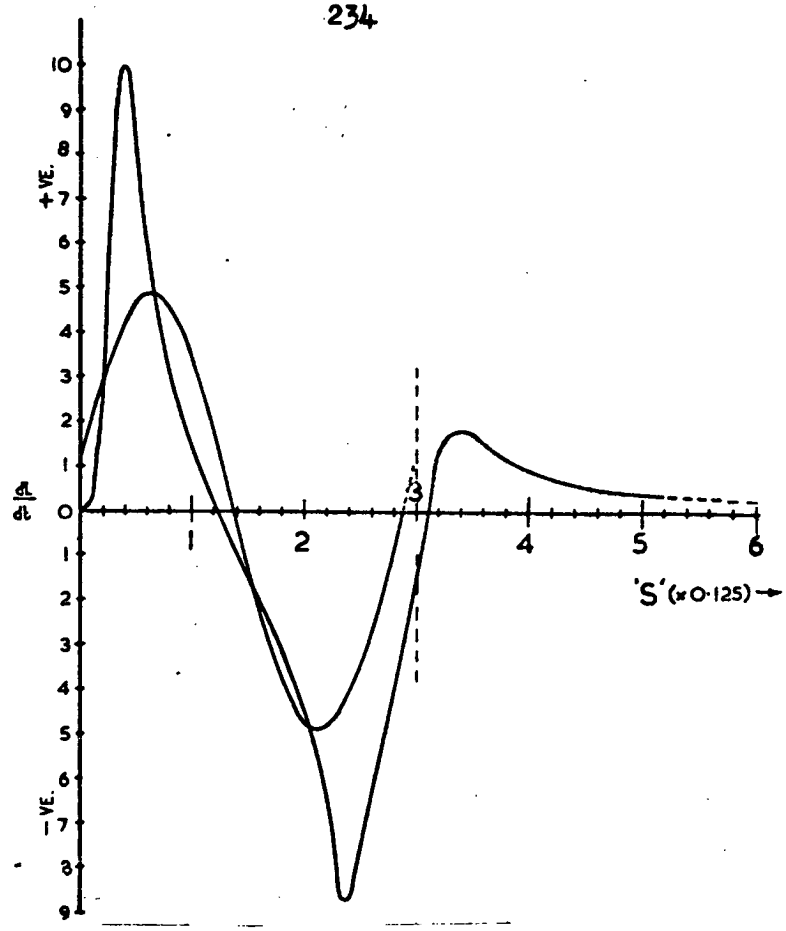

FIGURE 5.30. VARIATION OF dL/dt WITH DISTANCE

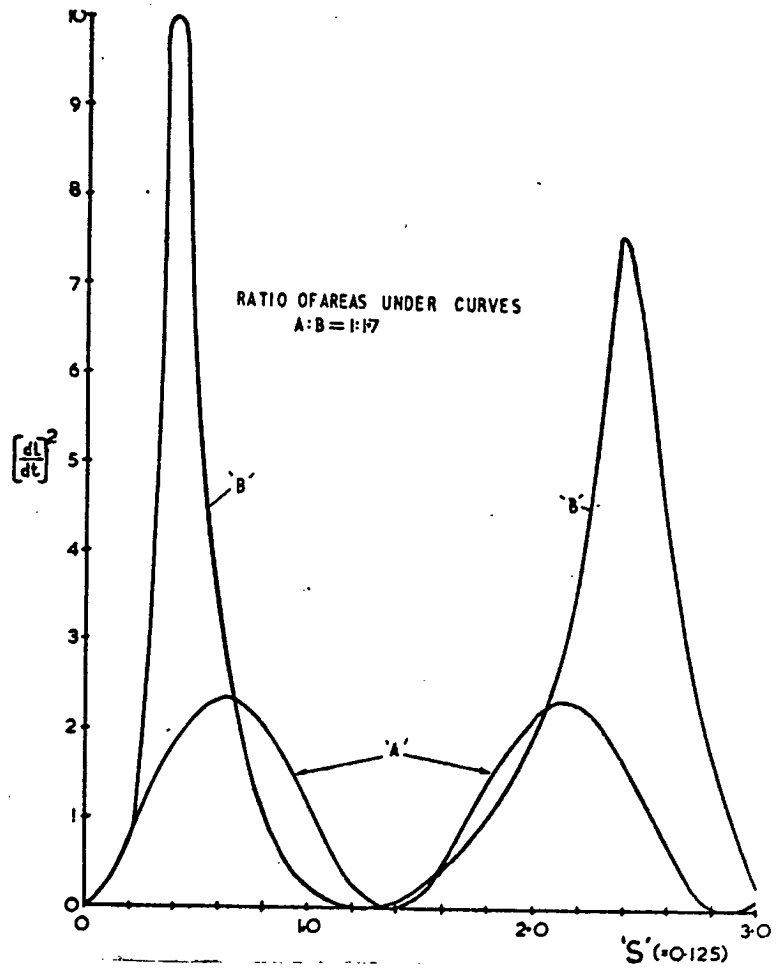

FIGURE 5.31. VARIATION OF $\left[dL/dt\right]^2$ WITH DISTANCE

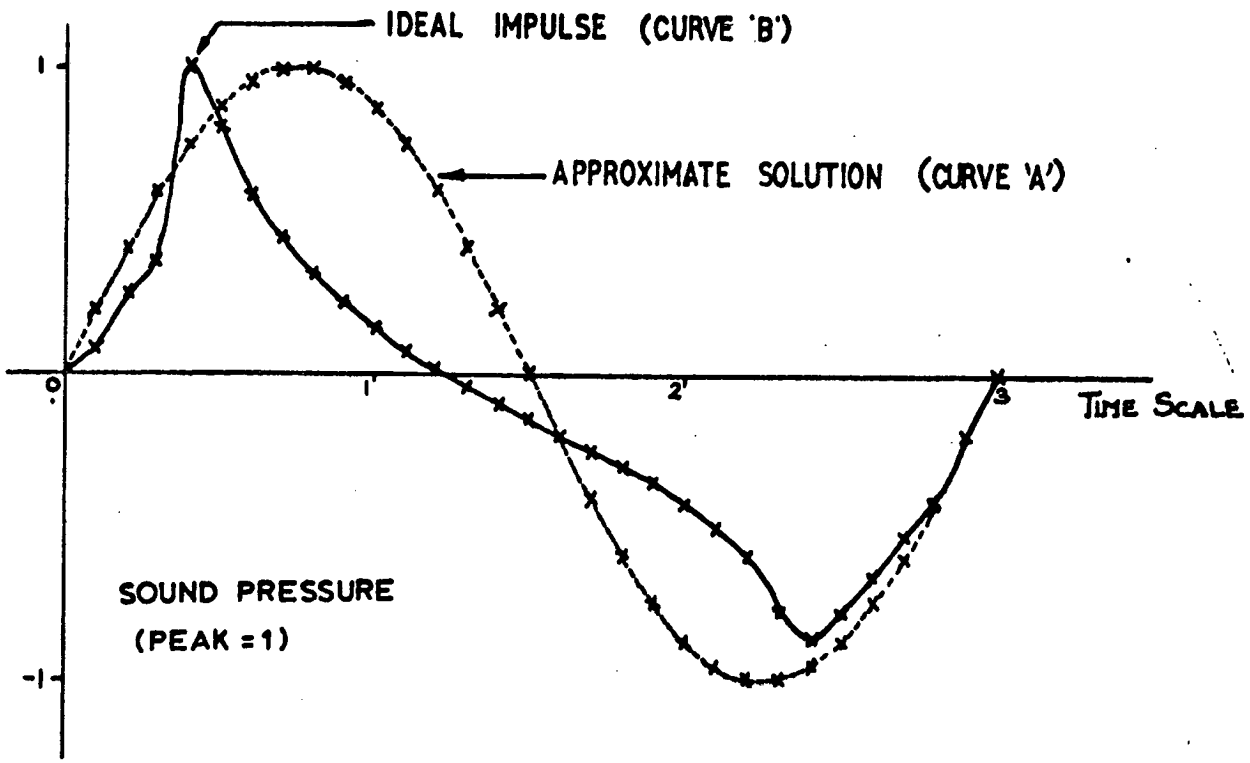

FIGURE 5.32. BLADE SLAP - IMPULSE CHARACTERISTICS

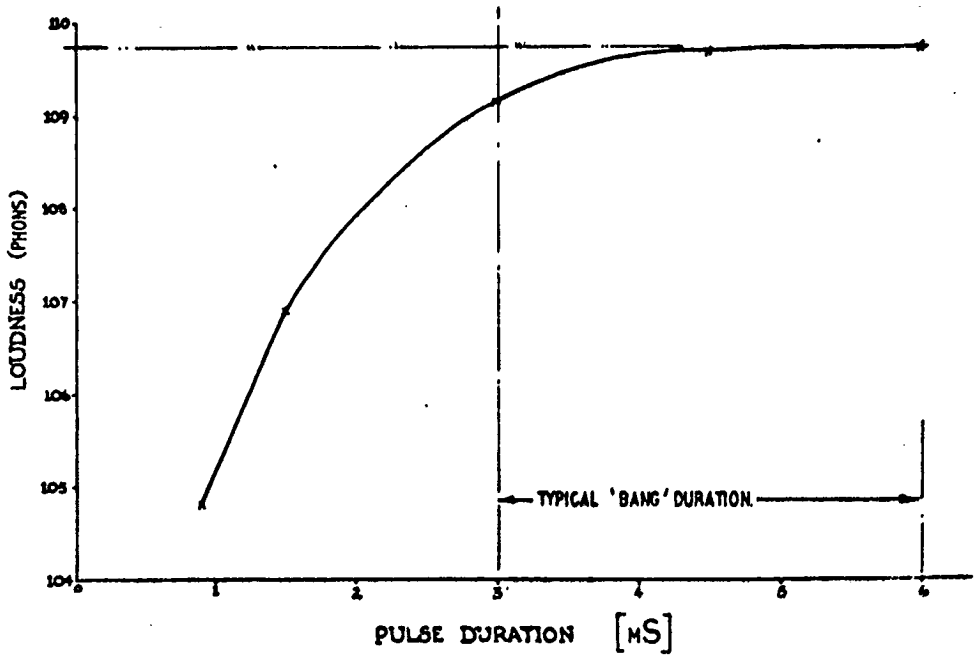

FIGURE 5.33. LOUDNESS vs PULSE DURATION

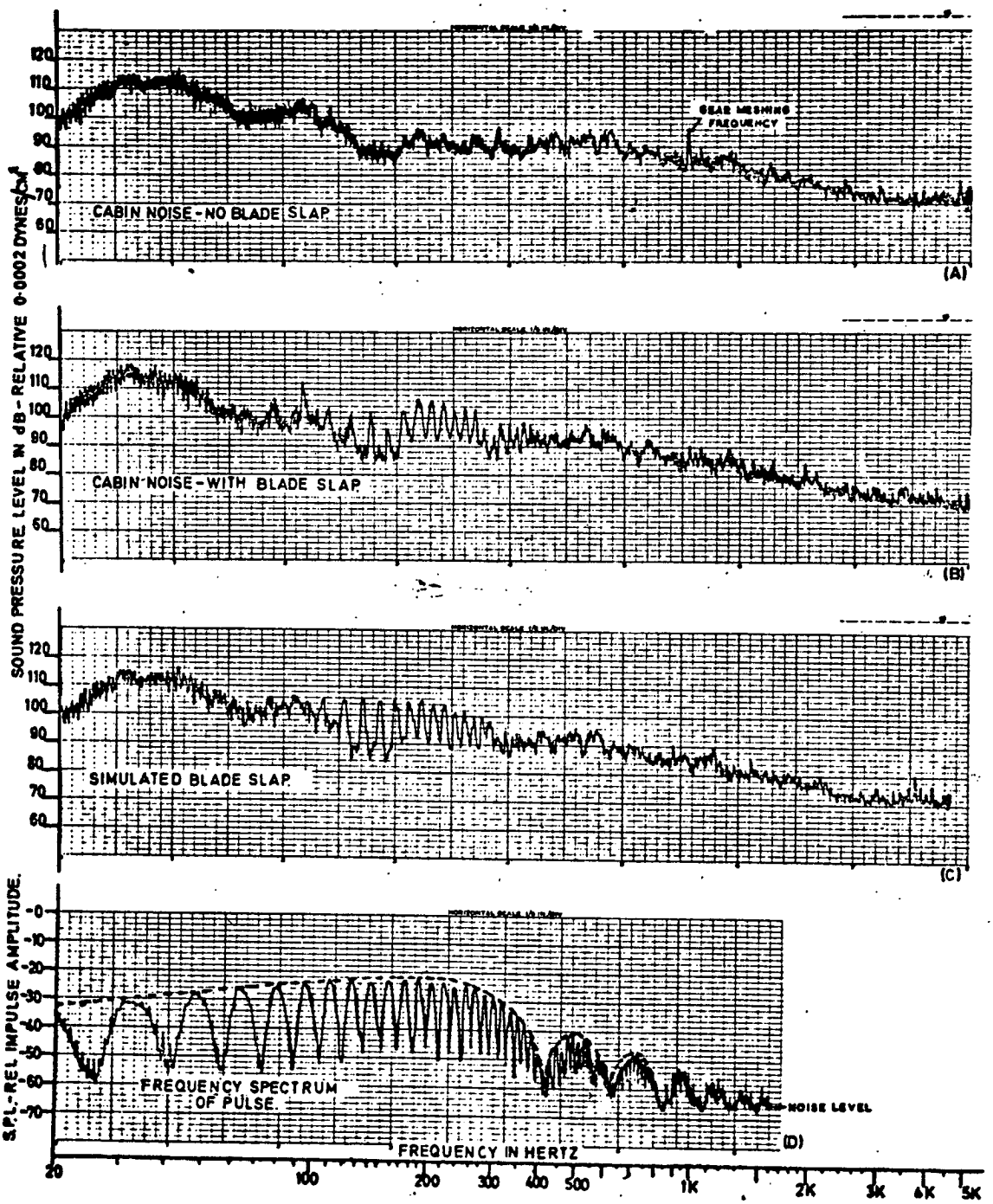

FIGURE 5.34. NARROWBAND ANALYSIS: SIMULATED AND REAL BLADE SLAP

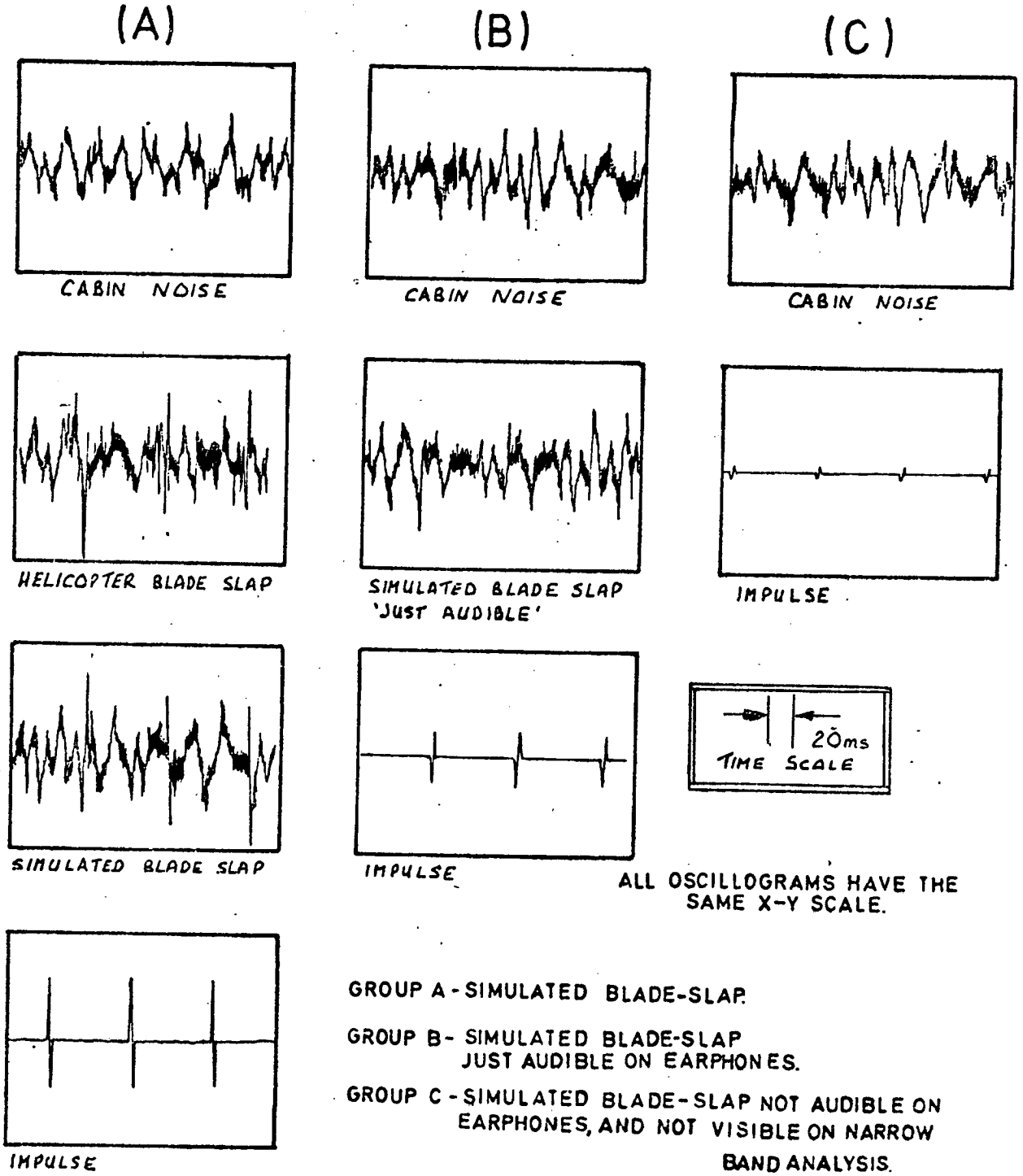

FIGURE 5.35. OSCILLOGRAMS OF SIMULATED BLADE SLAP

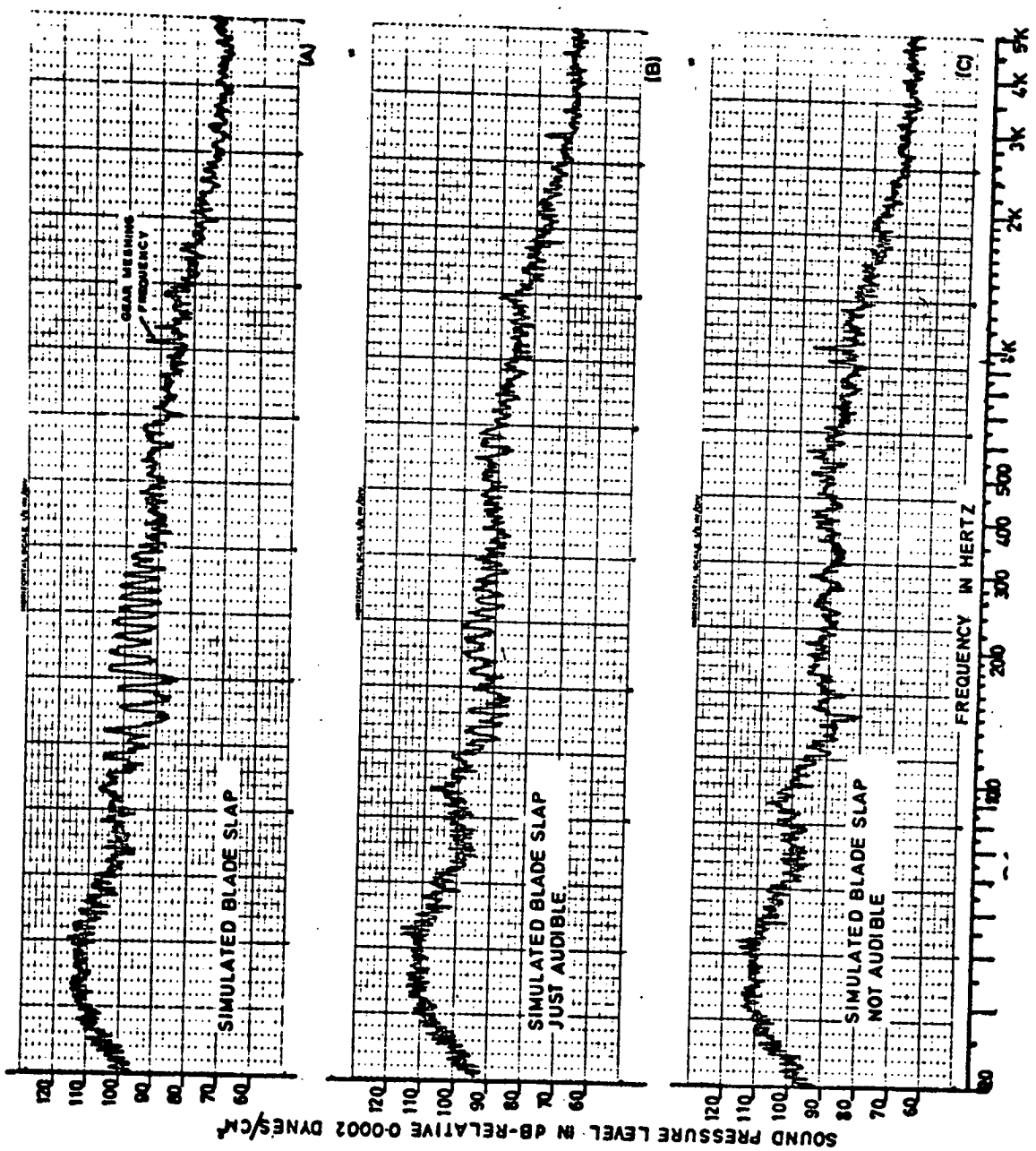

FIGURE 5.36. NARROWBAND ANALYSIS OF SIMULATED BLADE SLAP

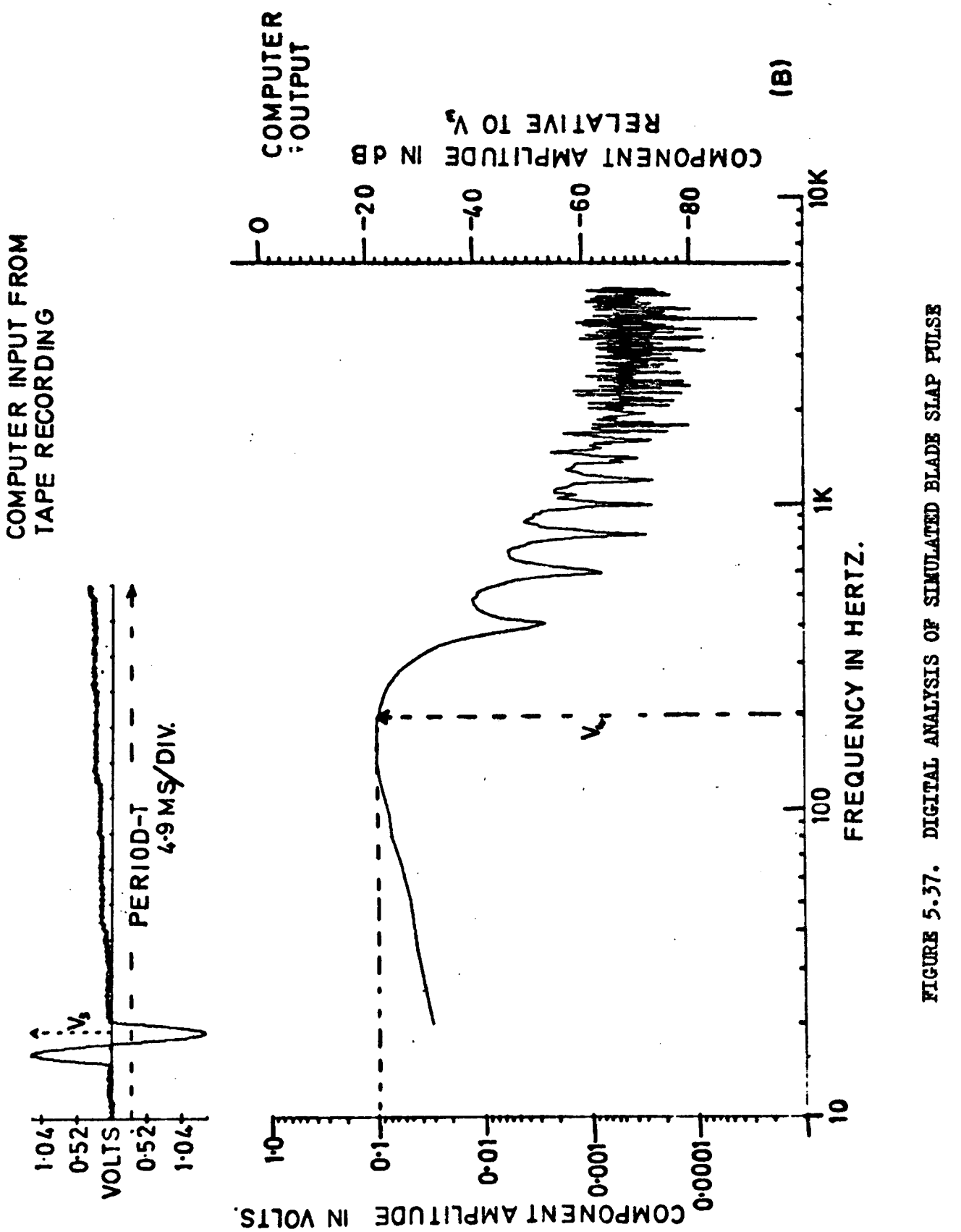

FIGURE 5.37. DIGITAL ANALYSIS OF SIMULATED BLADE SLAP PULSE

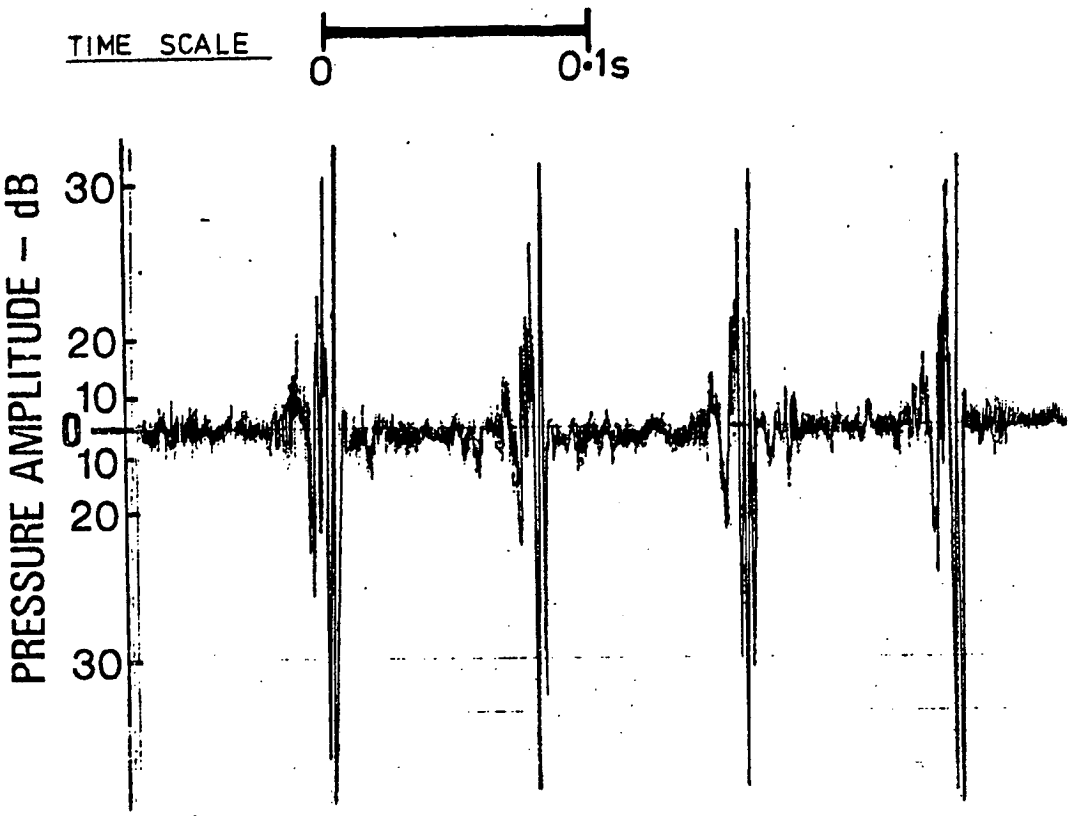

'Banging' Helicopter (large tandem rotor helicopter)

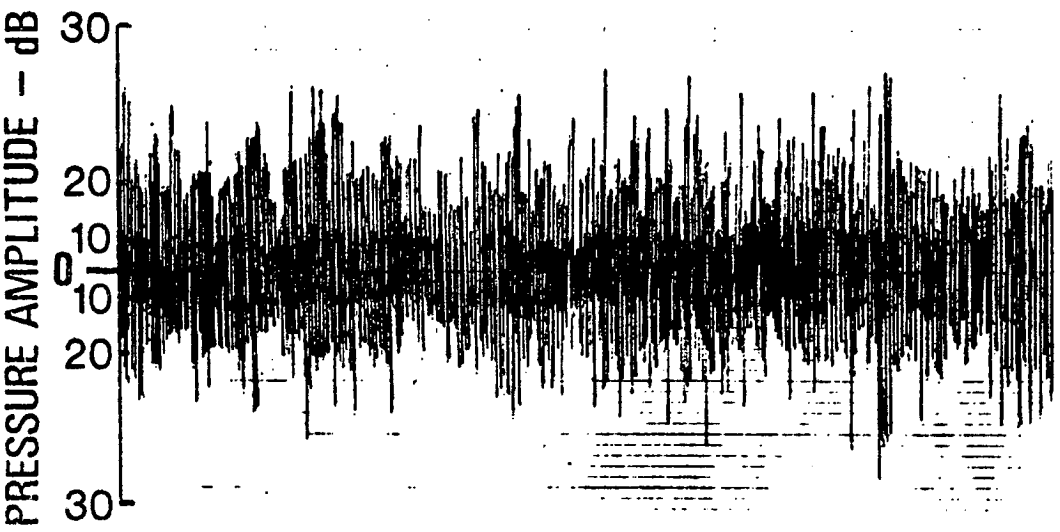

'Non-Banging' Helicopter (Wessex)

FIGURE 5.38. PRESSURE TIME HISTORIES: COMPARISON OF A 'BANGING' AND 'NON-BANGING' HELICOPTER

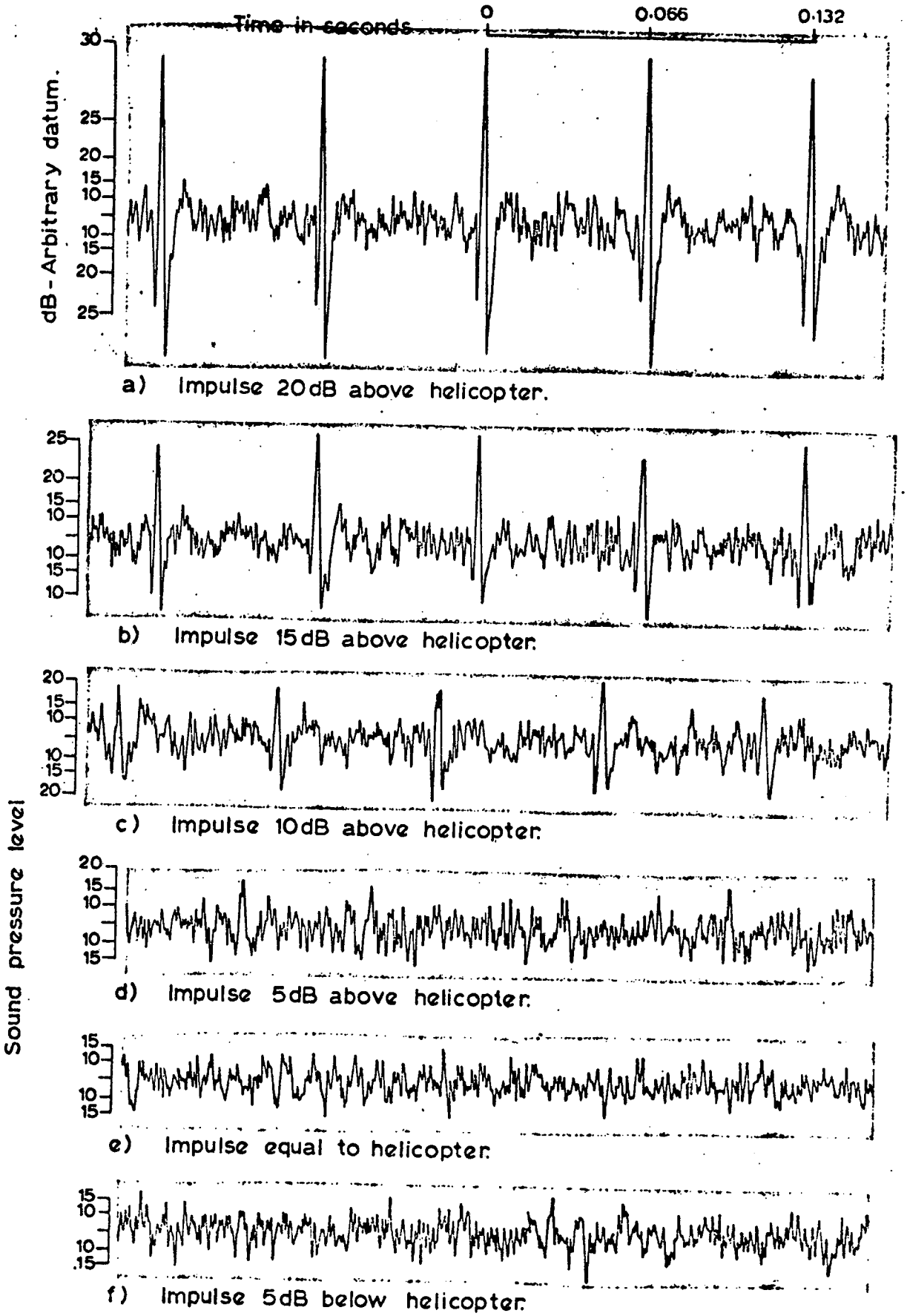

FIGURE 5.39. OSCILLOGRAMS OF SIMULATED BLADE SLAP (WESSEX EXTERNAL NOISE + IMPULSE)

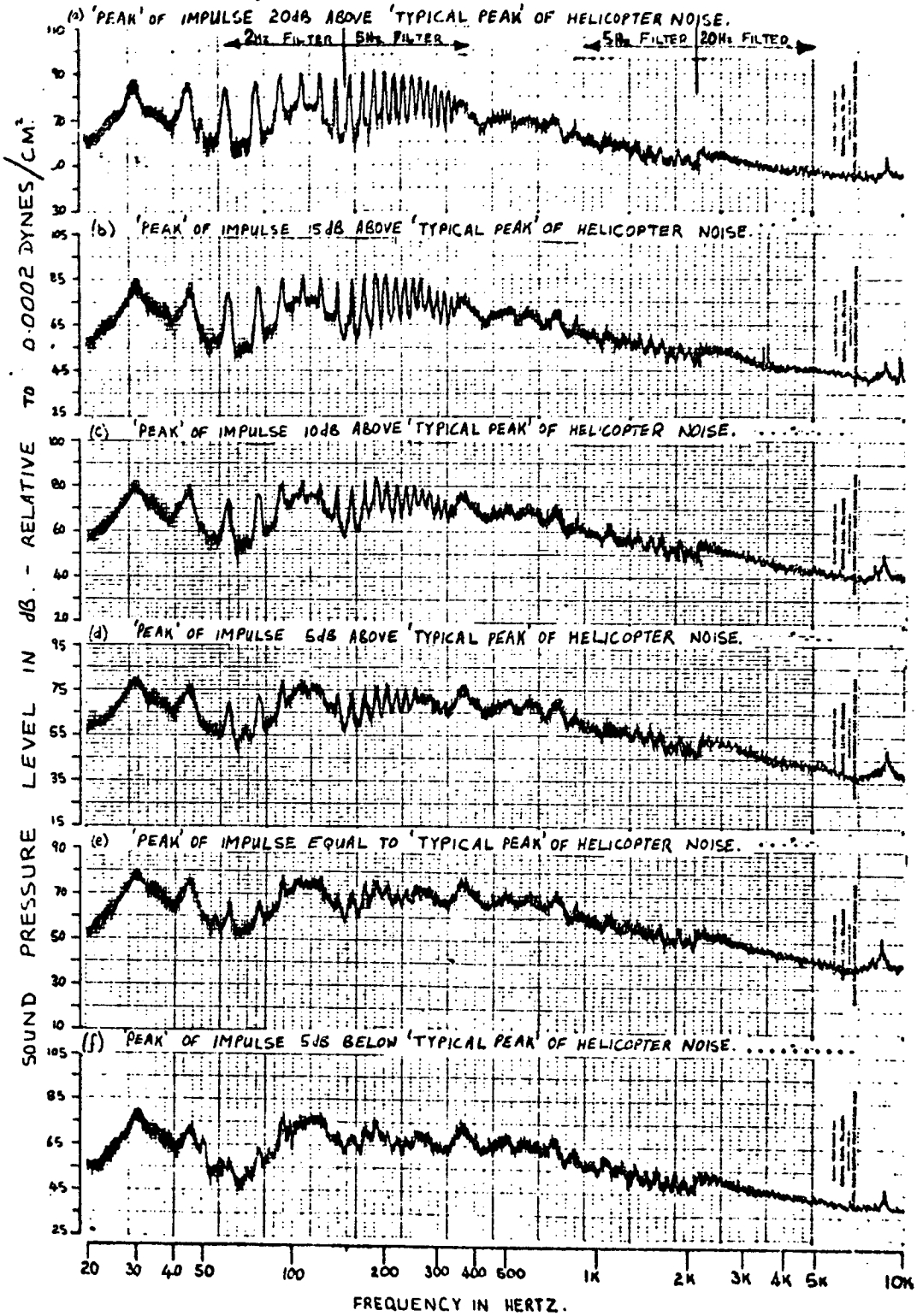

NARROW BAND ANALYSIS OF SIMULATED BLADE SLAP.

WESSEX EXTERNAL NOISE (HOVER) PLUS REPETATIVE IMPULSE SIGNAL.

FIGURE 5.40. NARROWBAND ANALYSIS OF SIMULATED BLADE SLAP

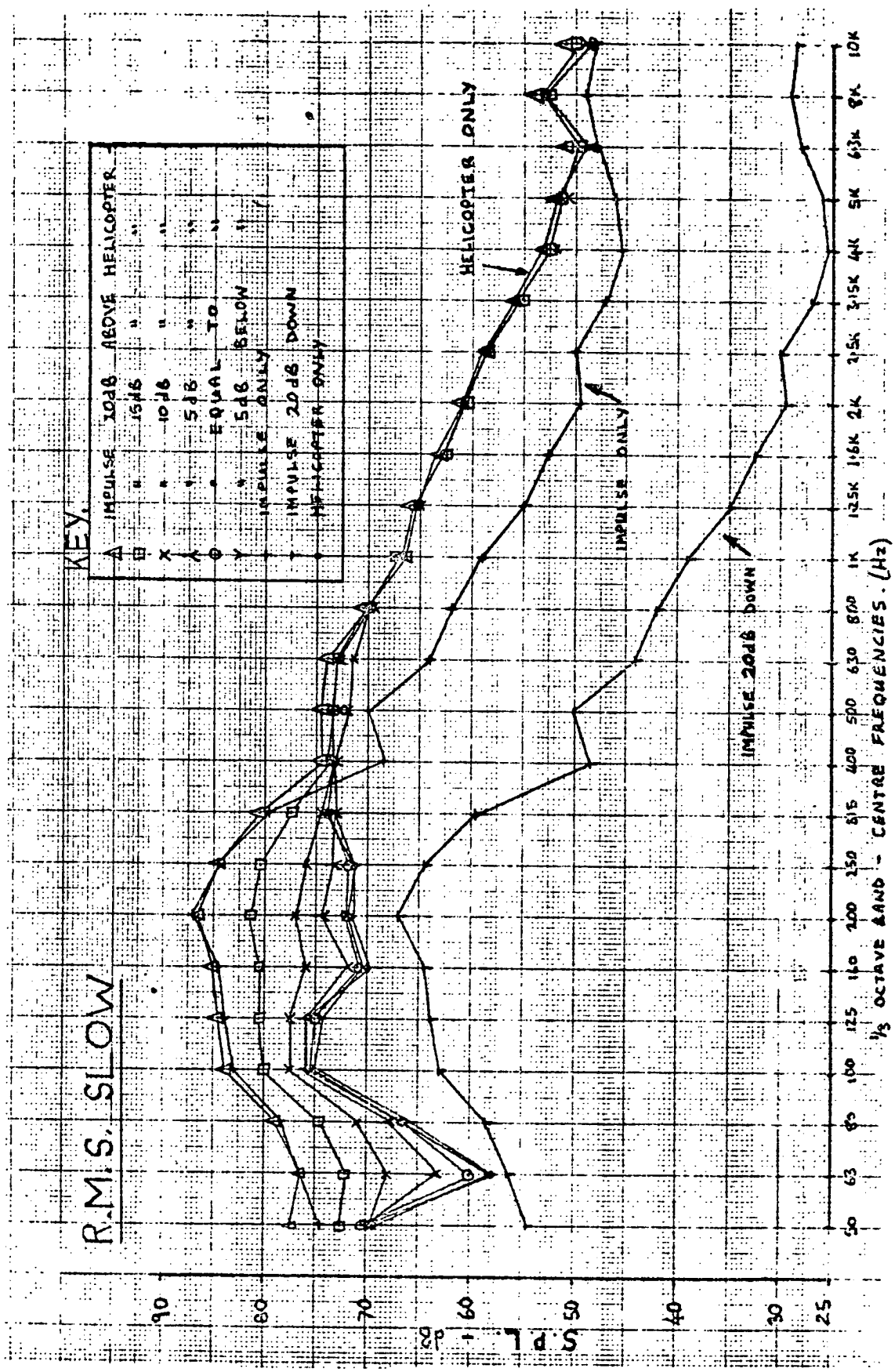

FIGURE 5.41. VARIATION OF $\frac{1}{3}$ OCTAVE BANDS WITH IMPULSE LEVEL

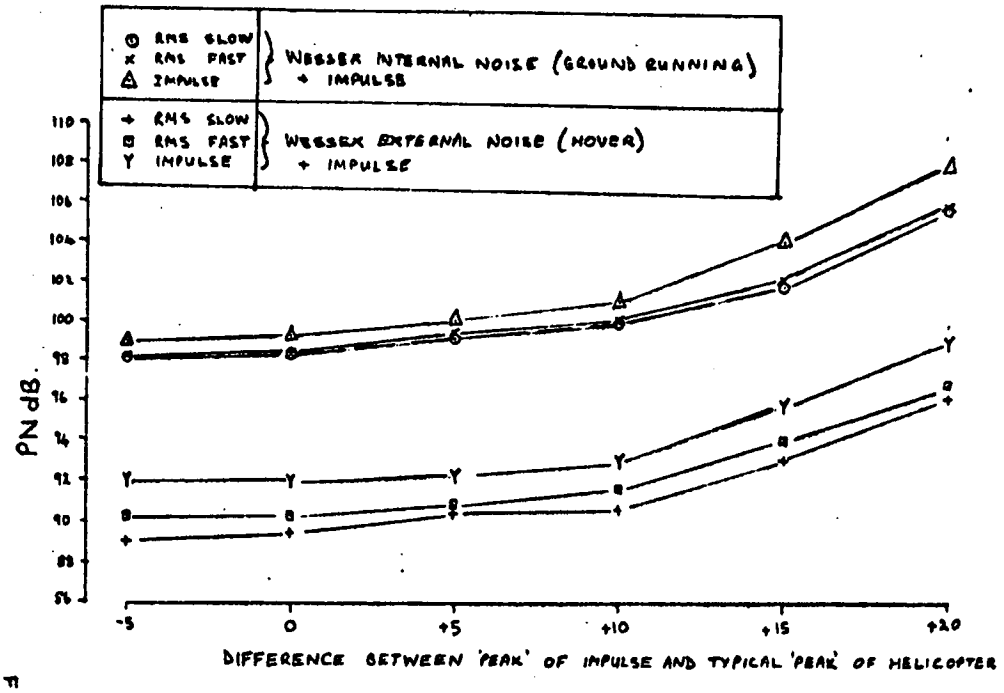

FIGURE 5.42. VARIATION OF PNL (PNdB) WITH IMPULSE LEVEL

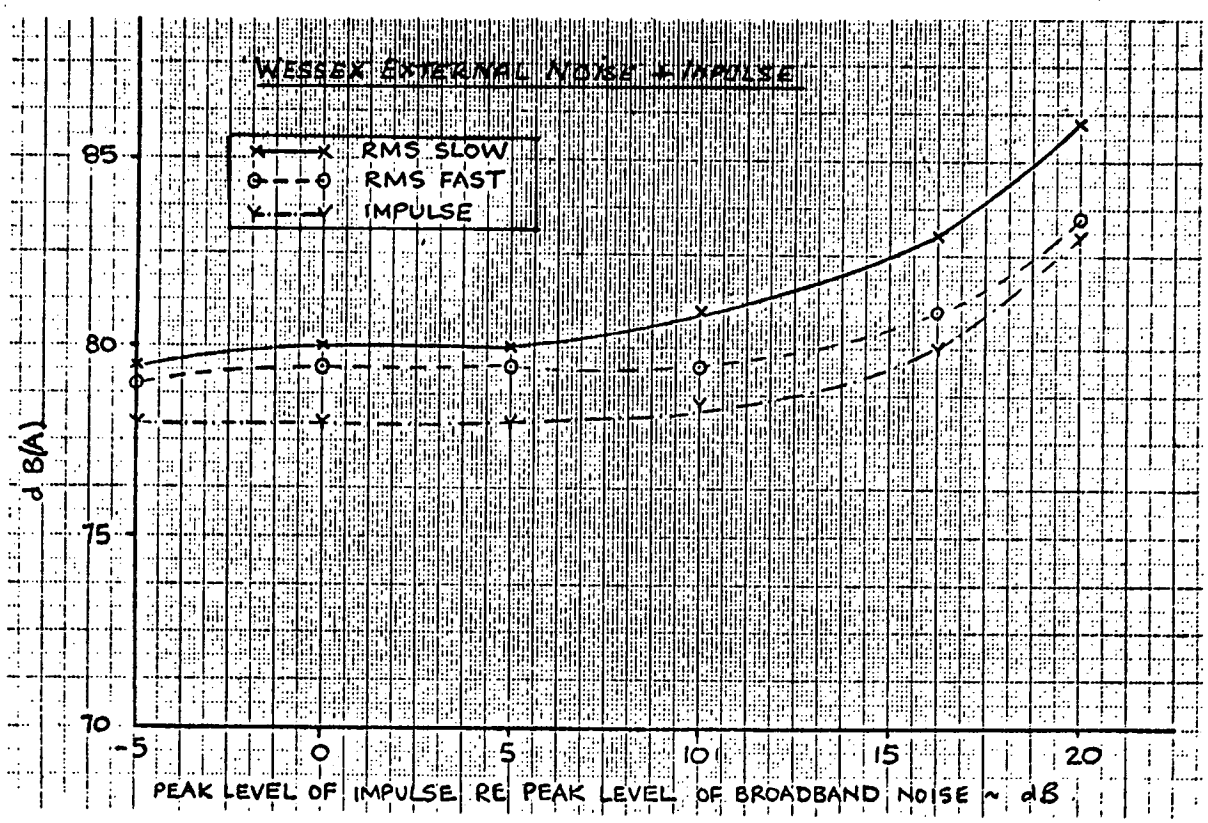

FIGURE 5.43. VARIATION OF dB(A) WITH IMPULSE LEVEL

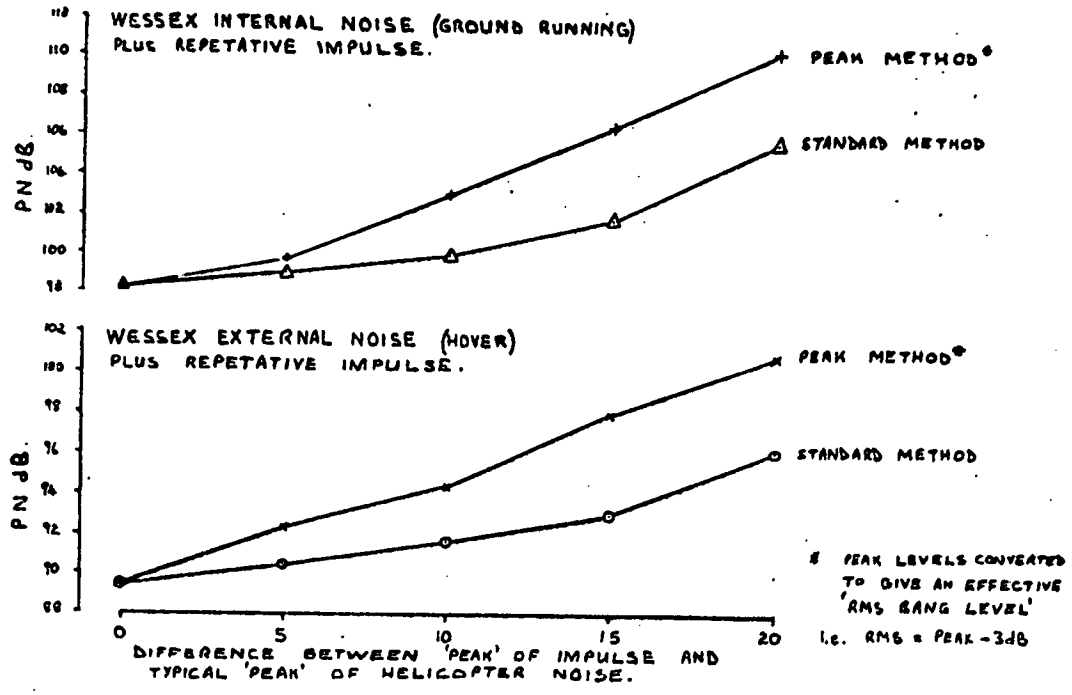

FIGURE 5.44. VARIATION OF PNL (PNdB) WITH IMPULSE LEVEL - COMPARISON OF STANDARD AND 'PEAK' METHOD

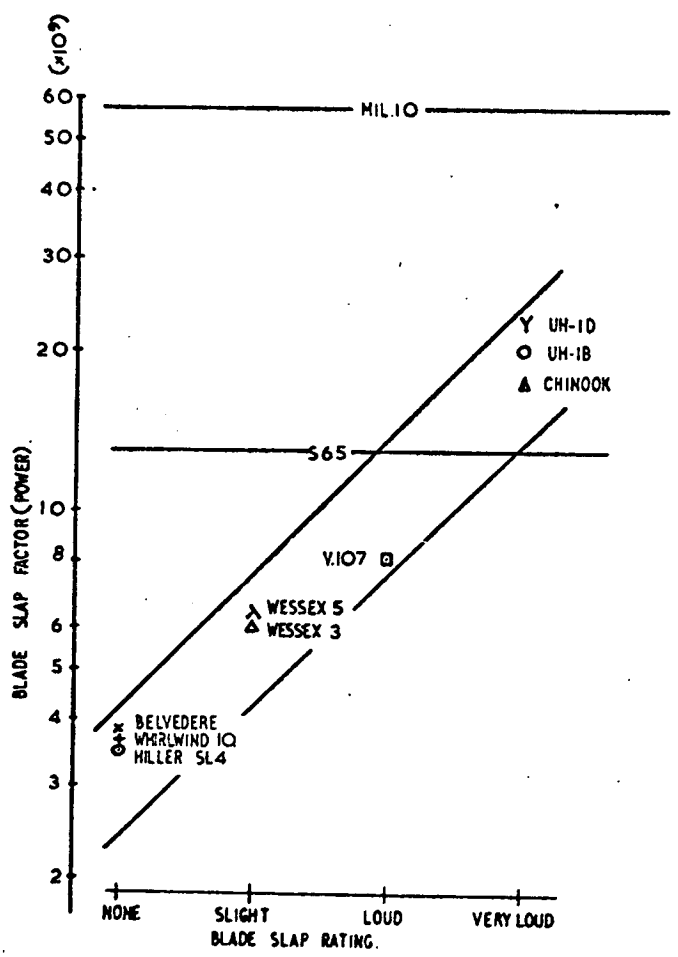

FIGURE 5.45. BLADE SLAP FACTOR (POWER) vs SUBJECTIVE ASSESSMENT

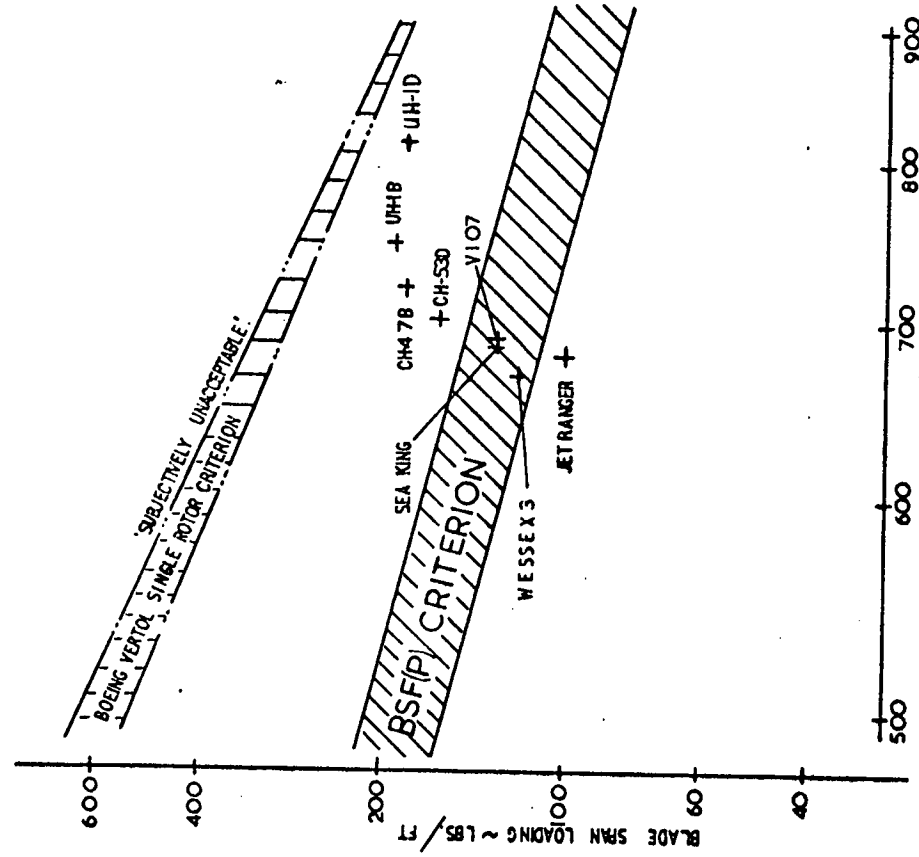

FIGURE 5.47. BLADE SLAP CRITERIA

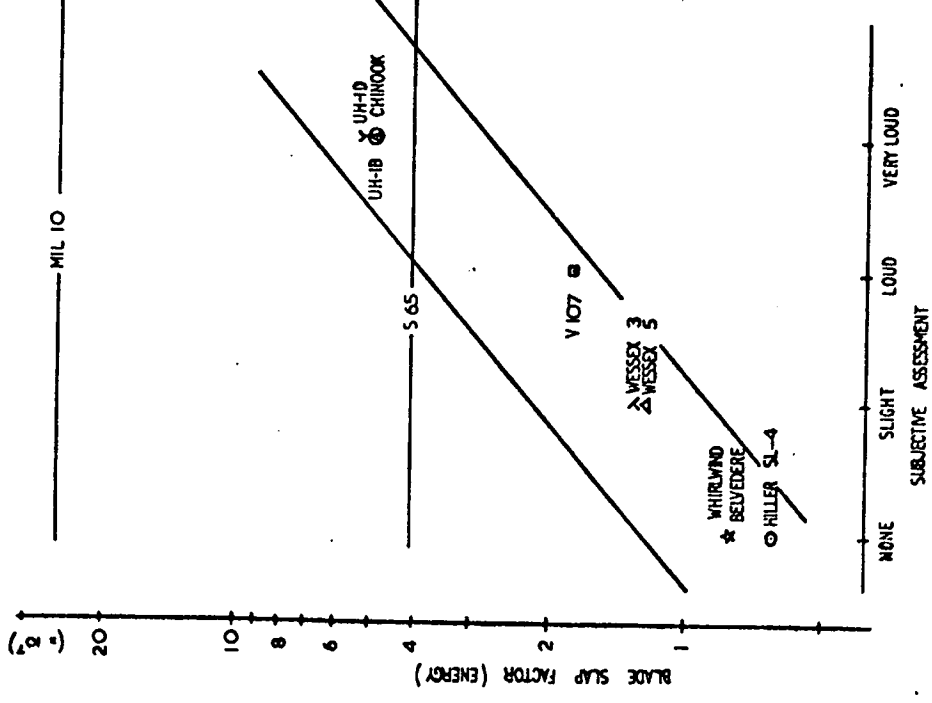

FIGURE 5.46. BLADE SLAP FACTOR (ENERGY) VS SUBJECTIVE ASSESSMENT

CHAPTER 6: BLADE STALL - BLADE/GUST INTERACTION

6.1. INTRODUCTION

The importance of transient gust loadings had been clearly illustrated by the 'blade slap' study (Chapter 5) and by ad hoc tests where the ISVR model was subjected to a distorted inflow induced by a fan or by 'blocking off' a part of the rotor disc area. In the case of a 'sharp gust' with gust length of the same order as the blade chord, it was expected that a similar effect to that arising from blade/tip vortex (blade slap) interaction would result. It was anticipated that the theoretical model developed for the 'blade slap' could be applied directly to this case. As the 'gust length' was increased, however, the point source acoustic model was expected to break down and hence a more refined approach taking into account the distribution of the source was required. For this the rotational (discrete frequency) noise model developed by Tanna [18] was used; a number of modifications were, however, necessary to make it compatible with the specific requirements of this study. In selecting the maximum 'gust length' to be employed consideration was given to the need to ensure that the blade would 'stall'. Based on aerodynamic data it appeared that providing the induced angle was sufficiently high (well above that associated with classic blade stall), then a gust length equivalent to 2 or 3 blade chords would be sufficient. Taking this into account and the fact that any gust disturbance on a real helicopter will in general be over a relatively small area, a maximum 'gust length of 7 chords' was selected - this being equivalent to approximately 18° of the rotor disc when mounted under the rotor at a position corresponding to 0.9 R where R is the rotor radius.

6.2. TEST FACILITIES

6.2.1. Rotor Rig

The ISVR rotor rig was fitted with a three bladed rigid rotor head; the standard 9 ft diameter rotor with blades of rectangular planform without twist having an NACA 0012 aerofoil section and a 4 inch chord was used.

In order to eliminate downwash and re-circulation effects and enable the influence of the 'gust' to be studied under as near as possible ideal conditions, the rotor rig was run with the blades set at zero pitch. The blades tips were tracked in the normal manner, with the aid of a stroboscopic light and mirror arrangement, so that the maximum 'spread'

between all three blades over the test range of 300 rpm to 900 rpm was no greater than 1.5 the individual blade thickness. To obtain this track it was found necessary, however, to apply 1° of positive pitch at the cuff of one of the blades. During this work it was noticed that, as in some of the blade slap studies, the blades were not equally spaced: one of the blades was displaced by $\frac{1}{2}$ chord which is equivalent to a 2° azimuthal displacement. Attempts to correct this minor error proved unsuccessful and hence testing was carried out with this setting. The final results suggested that this had some effect on the data obtained, whereby the cancellations of the high blade passing frequency rotor harmonics were slightly displaced (section 6.6.2).

The rotor speed measurement system was also calibrated since some previous tests had indicated that there was a slight error in the electronic monitoring system employed. Again a stroboscopic light source was used and the final results were double checked by examining the narrowband analysis results of the rotor noise. It was found an error of 3% over full range of speeds could result if the rotation speed (rpm value) was simply adjusted up to a certain value. This was partly a result of the electronic trigger device used and partly the sluggishness of the detection circuit. This was overcome by incorporating a more sensitive detector and following a procedure where the rotor speed was taken up to a speed just above the desired value and then adjusted down.

6.2.2. Air-jet Apparatus

Following the approach used in the original blade slap investigation [1] it was decided to use a simple air-jet arrangement to produce the controlled 'gusts'. A suitable air supply was available in the laboratory and it appeared to be simply a matter of feeding air into a 'master cylinder' and piping off a number of airlines to supply a number of air-jets. A study of the air-jets used during the blade slap investigation indicated that to keep the variations in velocity ('ripple') within acceptable limits along the full length of the gust (7 chords, 28 inches) a total of 24 air-jets would be required. A simple device based on this concept was duly constructed but this proved unsatisfactory because the velocity profile was far from uniform along the length of the gust. A second unit was built which took the form of a large cylinder with 24 outlets (accurately located on a fixed radius) at one end. After changing the 'air jets' and incorporating 'clamps' on the individual air-jet supply lines so the flow to each air-jet could be adjusted, an

acceptable velocity characteristic was obtained. Each nozzle was 6 inches long and had an internal diameter of $\frac{1}{4}$ inch; these were mounted in a curved support stand. The next stage involved selecting the appropriate rotor disc/nozzle separation distance. The air-jets were set in line (at 1 inch intervals). The complete test set up is illustrated diagrammatically in Figure 6.1.

The resulting velocity profile was measured by tracking a pitot tube (later replaced by a hot wire anemometer probe) over the nozzles. Some typical results are illustrated in Figure 6.2 and as will be noted the measurements were made over a range of distances and supply pressures. From these extensive tests it was found that an 8 inch separation gave an acceptable compromise between the need for a uniform velocity profile, a well defined gust and as high as possible gust velocity. With this setting the 'ripple' was typically in the order of 5%.

At this time an attempt was made to see if the final air-jet velocity profile could be predicted from knowledge of the velocity profile from a single air-jet, by simple vector addition. This did not give very good correlation and indicated a 20% 'ripple' about the mean whereas as mentioned previously a 5% value was obtained in practice. It was hoped that this method could have been used to 'tailor' any particular velocity profile, but since it proved unsatisfactory experimental techniques had to be used.

The influence of the number of nozzles is shown in Figure 6.3. This shows that there was a difference of 20 ft/s between the maximum air velocity from one nozzle and three nozzles, while the addition of more nozzles merely increased the length of the gust profile without increasing the amplitude. This applied at all supply pressures used and since it was desirable to have a constant 'maximum' velocity irrespective of gust length the shortest gust considered was that associated with 3 air-jets which corresponded to 1.25 chord/5 inch length. Also the supply pressure was restricted to a value which gave a maximum gust velocity of 125 ft/s, since at higher velocities there was a marked increase in air-jet noise and this tended to mask the rotor noise.

In addition to the air-jets used to obtain the 'linear profile' with gust lengths varying from 1.25 chords (5 inches) to 7 chords (28 inches), a second set of air-jets of 24 inches in length were manufactured. These were similar in all other respects to the six inch nozzles. Their length was such, however, that the rotor plane/air-jet separation between

the first and last nozzle could be increased sufficiently to enable a velocity profile with an amplitude which increased linearly with distance to be obtained. The nozzle arrangement is illustrated in diagrammatic form in Figure 6.4 and some typical results, which show the mean velocity, in Figure 6.5. As in the case with the constant velocity gust the 'ripple' was within 5%. The aim of this study was to determine the point at which the blade stalled, since as it entered the gust the induced angle would be increasing on a linear basis to a value well above the stall angle. Due to apparent non-stalling, in the classic sense, of the blade during the initial series of tests and time limitations, this aspect was not however pursued.

6.3. TEST PROGRAMME

6.3.1. Variation of Gust Length and Amplitude

The gust 'length' was varied between 1.25 and 7 chords and the gust amplitudes ranged from 45 ft/s to 125 ft/s as illustrated diagrammatically in Figure 6.3. The test conditions are detailed in Table 6.1 and corresponding blade tip speeds, blade velocity at centre of gust and induced angles for 300 rpm, 600 rpm and 900 rpm are detailed in Table 6.2.

6.3.2. Constant Induced Angle Tests

In addition to this main programme, a test format was formulated to evaluate the changes in noise with gust length at constant induced angle. It was hoped that it would be possible to choose induced angles below, as well as above, the classic stall value of approximately 14°. Small induced angles could not be generated in a well defined form with the air-jet arrangement used and tests could therefore only be made over the range from 15° to 30°. It was thought that at least at the higher induced angles/long gust lengths, the blade would stall and this would result in a dramatic increase in broadband noise. The complete test series for test study is detailed in Table 6.3 and the required angles were obtained by simply setting up the required supply pressure and rotor rpm. These tests proved, however, unsuccessful as discussed in section 6.6.7.

6.3.3. Noise Measurements

Noise measurements were taken initially at a number of positions illustrated in Figure 6.6. The recordings made directly above the rotor (position 7) sounded subjectively best and the impulsive 'bang' could be clearly heard above the basic rotor noise. When narrowband analysis results of these conditions were examined, the high order discrete

frequencies associated with the 'bang' were masked by the rotor (and possibly jet) broadband noise. Since the main object was to study the discrete frequency (rotational) noise components, it was desirable to obtain narrowband traces with 'clean clear peaks'. The analysis for position 6 (9 ft; 1 diameter) from the source region and at 45° to the horizontal (see Figure 6.6) showed clearly the individual discrete frequencies and thus this position was deemed the optimum location. The main programme was, therefore, subsequently carried out with the microphone at only this position as illustrated in Figure 6.1.

Recordings of the noise were taken for the complete range of conditions listed in Tables 6.2 and 6.3. In addition to the 'air on' (impulsive noise condition) measurements, 'air off' (normal rotor noise) measurements were also taken so that the level of 'impulse noise' could be determined. Ambient background and 'air-jet only' recordings were also made in order that the fact that the results examined were not influenced by these effects could be verified.

6.4. THEORETICAL STUDY

6.4.1. Aims

The main aims of this investigation were to predict the discrete frequency acoustic spectra of a rotor subjected to transient/impulsive gust loading and verify these results with measured values obtained from the experimental tests. As the blade passes through the gust it is subjected to a rapid change in lift, which in turn applies a fluctuating force on the surrounding air and thus generates noise. The actual noise generation was taken to be dipole in nature with the dipole axis being in the same direction as the line of action of the fluctuating force. Since the rotor was run in this case with the blades at zero pitch the dipole axis was vertical. It follows that, in addition to development of the acoustic theory, a method for calculating the blade loading as the blade passed through the gust had to be derived.

6.4.2. Theory: Blade Loading

The approach adopted followed that developed in connection with the blade slap investigation which is reproduced in Appendix 4. This approach makes use of Kussner's function [77] which is based on the lifting line theory as applied to a two-dimensional aerofoil. In the blade slap study emphasis was placed on short 'sine wave' type gusts and a simple manual solution was used to calculate the blade loading. This did not give the required accuracy for the 'longer gusts' and since an

extensive range of gust profile was involved a computer program was developed.

The discontinuity in the blade loading prediction (as described in Appendix 4) presented some major problems. It was originally planned to compute the complete time history of the loading, but this proved impracticable and the program was limited initially to calculating the blade lift inside the gust only. There is an exponential decay of loading as the blade passes out of the gust and the program was subsequently modified to 'add' this decay to the loading values calculated for 'inside gust' to give a complete time history of the lift fluctuation. A brief outline of this program is given in Appendix 8.

To check the program a 'sine wave' gust of the type used in the earlier blade slap investigation was employed. This is illustrated in Figure 6.7 and a comparison between the previous manual calculation and program results is illustrated in Figure 6.8. Computations for the complete range of profiles used in the study were made and some typical blade loading results for 1, 6 and 24 air-jets are reproduced in Figure 6.9.

6.4.3. Acoustic Theory

Initially the simple dipole theory which had been used in the 'blade slap' study was used to compute, from knowledge of the blade loading, the acoustic spectra of the noise during the passage of the blade through the gust. This theory is summarized in Appendix 6.

It was appreciated that this simple point dipole theory would not be applicable to the 'long gust' case. Hence a version of what at that time was an advanced computer program for the prediction of rotational noise due to fluctuating loadings on rotor blades, developed by Tanna [18] was modified for use in this study. A brief summary of this theory and the computer program is given in Appendices 9 and 10 respectively.

6.4.3.1. Use of 'effective blade chord' concept

In order to provide a cross check between the two methods, a sine wave (short gust) was used. It was found that large differences existed between the two sets of results, with the values given by the detailed rotational noise program being much lower than those given by the point dipole theory. It was also clear from examination of the results and the measured acoustic data that it was the more complex program which was in error. Since there was no apparent reason for this discrepancy, a somewhat detailed investigation had to be conducted in order to explain why they occurred since there were no program errors and

the method outlined by Wright and Tanna [29] had been followed to the letter. The details of this study, from which it was found that an 'effective chord' rather than the actual blade chord had to be used in the prediction, are discussed in Appendix 11. This overcomes the problem associated with this study, but it is not known what effect this approach has on the calculations of noise for blade loadings which contain both 'slow time varying components' and high frequency impulsive components, since according to Wright [28] the former requires use of the real chord in the program. Further investigations of these aspects were, however, outside the scope of this investigation.

6.4.3.2. Comparison of point dipole and rotational noise models

In addition to evaluation of the two methods carried out in determining the combination of the integration interval and effective chord values to be used (Appendix 11), the acoustic spectra given by the point dipole and the rotational noise theories were compared for a range of 'gust lengths'. The results for the two extreme cases, corresponding to 0.75 chord (1 air-jet) and 7 chords (24 air-jets) are shown in Figure 6.10. It was found that for the short gust (upper spectra on figure) the difference was less than 3 dB over the majority of the harmonic range. In the case of the long gust (lower spectra) there is a difference of at least 5 dB between the 'peaks' and a 'phase shift', although the 'fall-off rate' of the 'peak' levels show the same trend. These differences are due to the fact that whereas in the 'simple point dipole' method it is assumed that the lift fluctuations take place at a fixed point and a simple correction term is applied for the spanwise effect, in the full rotational noise theory the effect of the gust is integrated in both the azimuth and spanwise directions. Thus as expected the point dipole method becomes increasingly inaccurate as the length of the gust profile is increased and it departs further from the point source assumptions. The results also confirmed that the simple model could be used to a fair degree of accuracy for short disturbances and supports its use in the blade slap study, where precise details on the 'tip vortex' are often lacking.

6.5. RESULTS

Narrowband analysis results (using the Spectral Dynamic system described in section 2.2.4) were obtained for the conditions detailed in Table 6.2. Typical results are shown in Figures 6.11 to 6.14 inclusive. Figure 6.11 shows for one specific condition the acoustic spectra for the 'air-on' (impulsive) condition, 'air-off' (normal rotor noise) condition,

the corresponding 'air-jet' noise, ambient background noise and internal instrumentation (equipment) noise. From these traces it can be seen the influence of the 'gust' raises the level of the discrete frequencies to well above that associated with normal operation of the rotor rig. Figure 6.12 shows the effect of rotor speed (for a fixed gust length of 7 chords), Figure 6.13 the changes in noise associated with increasing the gust length from 1.25 chords (3 air-jets) to 7 chords (24 air-jets) at a fixed rotor speed and Figure 6.14 similar results for 900 rpm condition as the magnitude of the gust amplitude is increased from 45 ft/s (induced angle 6.7^{o}) to 125 ft/s (induced angle 18^{o}). From these and similar analyses the harmonic levels were extracted and plotted in a convenient form for comparison with the theoretical results which were derived from the rotational noise program.

6.6. DISCUSSION OF RESULTS

6.6.1. Components in Rotor Noise Recordings

Figure 6.11 shows spectra related to 600 rpm (282 ft/s tip speed). The 'air-jet noise' and rotor noise (rig on-air jets off) results show that these two generated the same order of broadband noise at a frequency above 2 kHz. When compared to the level generated by the rotor when subjected to the gust (rig on-air jets on) there is a good 10 dB difference and hence the results of interest were not in any way affected by the 'air-jet noise'.

The laboratory background (ambient) noise was in general 15 dB or more below the normal rotor noise and 30 dB below the rotor noise 'peak' produced by the passage of the blade through the gust. It will also be observed that except for mains frequency 'pick-up' at 50 Hz, 100 Hz and 150 Hz, the level of internal instrumentation noise was typically 20 dB and 50 dB below the background noise and 'rotor noise with gust' recordings respectively.

6.6.2. Comparison of Measured and Computed Spectra

The SPL's of the acoustic spectrum for harmonic orders, based on the blade passing frequency, up to the 30th were computed for a wide range of conditions and compared with the experimental results. A representative selection of these are produced as Figures 6.15 to 6.18 inclusive.

It can be seen that for the short gusts (3 air-jets, 1.25 chords - Figures 6.15 and 6.16) that, apart from experimental scatter (typical ± 3 about the mean) the measured values agree well with the theoretical

curves. It will also be observed, however, that some of the 'harmonics', particularly those in the harmonic range 18 to 26, differ by up to 8 dB from the theoretical value. This is considered to be due to cancellation and reinforcement of some of the harmonics arising from the fact that one of the blades was displaced by 2° from its ideal position and that the individual blades most likely responded in a slightly different manner to the gust impulse. The need to apply 1° of positive pitch at the cuff to one blade (section 6.2.1) also most likely influenced the response of the blades since although two blades were at zero pitch and hence zero lift, the third blade had small equal positive and negative forces on it.

The experimental results for the long gust (24 air-jets, 7 chords - Figures 6.17 and 6.18) show the same general characteristic as the theoretical predictions both in terms of the amplitude and the 'shape' of the spectrum. As will be noted, however, the experimental 'dips' and 'peaks' are displaced in frequency from the theoretical curves. These differences are again considered to be due to the non-uniformities and irregularities in the blade loading 'impulses'.

There was a discrepancy in all cases between the predicted and measured level of the fundamental. For the short gust the SPL value was in general under predicted and it was considered the measured value was that associated with the normal rotor noise. For long gusts, however, the predicted levels were higher by up to 16 dB (see Figure 6.18) than those measured. This tends to imply an 'error' in the mean or low harmonic component of the blade lift used in the calculations. Alternatively the measured value could have been influenced by room effects or the basic rotor noise. None of these could however account for the differences observed and although various ad hoc modifications were made to the 'blade loading data', the observed effects could not be simulated. In this context it is also of interest to note that although the level of the fundamental was independent of gust amplitude it was nevertheless dependent on the length of the gust. It appears, therefore, that the level of the fundamental is to some extent associated with the 'drag' of the rotor blades since this is expected to be a function of gust length. Even with the above discrepancy taken into account it seemed fair to conclude that the measured and predicted values showed good agreement over the full range of gust profiles investigated, particularly in the higher order harmonic range of interest, and that the theory was adequate.

6.6.3. Variation of SPL with Rotor Speed

The variation of SPL with rotor speed can be seen in Figure 6.12, which shows the narrowband analysis results, and in generalized form in Figures 6.15 to 6.18 inclusive. There is an increase in amplitude of each harmonic and an appearance of higher order harmonics with each increase in speed. Harmonic orders of up to 30 and above are clearly detectable and the discrete frequencies appear more distinctive at the higher rotor speeds.

As the speed of the rotor is increased a broadband 'hump' appears around 1 kHz to 1.5 kHz. At 300 rpm there is no 'hump' and the spectrum is 'flattish' in appearance, but at 600 rpm a 'hump' shape can be seen together with discrete frequencies. As the speed is increased to 900 rpm the 'hump' broadens and more discrete frequencies appear.

Theoretical and experimental results for a number of blade passing harmonics for a short gust (1.25 chords, 3 air-jets) are shown in Figure 6.19. Theoretically the predicted SPL of the low and high harmonic orders tend to be dependent on V^4 and V^6, respectively, where V is the blade tip speed for the short gust case shown, while for a long gust the variation of all harmonics is typically V^4. The experimental results show similar trends in terms of variation with velocity, but the absolute values tend to differ slightly from the theoretical predictions and appear to be all on the higher side at 300 rpm.

The variation in OASPL (dB Lin) with rotor speed is shown in Figure 6.20. There is as can be seen an increase in level with both rotor speed and gust amplitude. At 300 rpm there is a rise of 18 dB as the gust velocity is increased from 45 ft/s to 125 ft/s. For high speeds for the same increase in gust velocity the OASPL rises by 15 dB. The curves follow a V^2 law at the lower rotor speeds (300 to 500 rpm) and a V^6 law at higher speeds (700 to 900 rpm) as indicated on Figure 6.20.

6.6.4. Variation with Gust Amplitude (Gust Velocity)

The variation of SPL with gust amplitude for a short gust (1.25 chords, 3 air-jets) at a rotor speed of 900 rpm is shown in Figure 6.14. The fundamental or first harmonic (45 Hz) is clearly shown and as can be seen is essentially independent of the amplitude of the gust velocity. The second blade passing harmonic (at 90 Hz) and the higher order harmonics on the other hand increase dramatically with gust amplitude.

Figure 6.21 shows a comparison of a selection of the predicted and experimental harmonic levels; to avoid overlapping of the experimental

values they have been 'separated' and plotted to an arbitrary datum. The agreement between the two sets of data when plotted in this format is relatively poor. It will also be observed that whereas the theory suggests a steady increase in harmonic level with gust amplitude, the experimental results show a marked increase in level above a gust amplitude of 105 ft/s. It was fairly obvious that there was an additional factor which was not being accounted for in the theory, but the experimental results did not give any indication of its nature. The OASPL values showed a similar trend as illustrated in Figure 6.22. The results all lie within a 10/12 dB band and again a dramatic increase in level occurs as the gust velocity is varied from 105 ft/s to 125 ft/s.

6.6.5. Variation with Gust Length

The general effect of gust amplitude can be seen on Figure 6.13 and as will be noted the fundamental or first harmonic (frequency 30 Hz) increases dramatically as the gust is lengthened. Each increase in gust length also resulted in a slight increase in the number of high harmonics which could be detected. It can also be seen that there is an increase in the broadband noise 'hump' at 1 kHz with gust length.

It is extremely difficult to compare the theoretical prediction and experimental results as a function of gust length, because of significant changes which occur in the acoustic spectrum. This can be appreciated by reference to Figures 6.15 and 6.18. If, however, the low frequencies are ignored then it can be shown that the levels obtained in the mid-frequency region (15th harmonic) are for all practical purposes independent of the gust length. In other words the level associated with the 'envelope' of the 'peaks' on Figures 6.17 and 6.18 is similar in magnitude to the values shown respectively on Figures 6.15 and 6.16 in the mid frequency range of interest. These theoretical trends agreed well with the experimental results. This is not surprising since in general terms it is the initial change in lift as the blade enters the gust which is responsible for the majority of the noise and increasing the gust length simply increases the 'source size' and lowers the initial 'cancellation frequency'.

A plot of the OASPL level against gust length, for the various gust amplitudes, is reproduced as Figure 6.23. For the gust amplitude of 45 ft/s, the OASPL is for all practical purposes 'flat' (constant in amplitude) over the full gust range (1.25 to 7 chords) considered. At higher gust amplitudes, however, initially there was a slight increase

in level with gust length with the OASPL reaching a maximum at $5\frac{1}{2}$ chords (18 air-jets), after which it decreased to a minimum at $6\frac{1}{4}$ chords (24 air-jets). This effect occurred at all rotor speeds as can be seen from Figure 6.24 and the value for 7 chords (24 air-jets) tended to be of a similar order to that at $6\frac{1}{4}$ chords.

6.6.5.1. Blade stall study

It was thought that the trend described above may have been linked to blade stall and hence it was decided to study these results in more detail. An examination of their narrowband spectra did not reveal any clear trends and in the context of this evaluation the spectra were difficult to interpret. $\frac{1}{3}$ octave band analysis was, therefore, performed to enable the general characteristics to be established.

A representative set of $\frac{1}{3}$ octave band spectra are shown in Figure 6.25 for gust lengths corresponding to 3, 18 and 21 air-jets. Intermediate values follow the same general pattern, but have been omitted for clarity. The SPL above 2 kHz reached a maximum value at a gust length of $5\frac{1}{2}$ chords (18 air-jets), decreased as the gust was lengthened to $6\frac{1}{4}$ chords (21 air-jets) and then increased again as the gust was extended to 7 chords (24 air-jets). It was confirmed by studying the 'air-off' results that the effect was genuine and not influenced by 'air-jet' noise. Similar variations occurred below 150 Hz, but between 150 Hz and 2 kHz, particularly around 500 Hz, the 1.25 chord (3 air-jet) condition had the highest level. The narrowband results showed this to be due to the fact that with the short gusts some very high 'peaks' - up to 10 dB above the general mean - were obtained and that the $\frac{1}{3}$ octave band results were controlled by just a few high level discrete frequencies. This effect can be seen on Figures 6.15 and 6.16 and if this aspect is taken into account and the 'mean harmonic' value in the $\frac{1}{3}$ octave band considered, then these results tend to follow the same trends as the low and high frequency regions. In the case of the results for the longer gusts the variation in level between the individual discrete frequencies is small and hence the $\frac{1}{3}$ octave band values obtained by analysis are more representative of the 'average' level of the discrete frequencies.

The 10 kHz $\frac{1}{3}$ octave band values obtained from this analysis are illustrated as a function of gust length in Figure 6.26. This again showed a reduction in level at the $6\frac{1}{4}$ chord (21 air-jet) position, after which it increased again.

It was not possible to calculate accurately the $\frac{1}{3}$ octave band trends to be expected, but from a simple summation of the predicted harmonic spectrum it was estimated that the $\frac{1}{3}$ octave bands in the region of 1000 to 1250 Hz (and 100 to 125 Hz) would exhibit a 6 to 10 dB increase in level as the gust length was initially increased to 5 chords, followed by a further 1 to 2 dB increase as the gust was further extended to 7 chords. The results are in general agreement with this trend except for the reduction at $6\frac{1}{4}$ chords which was not predicted. Also the increase of broadband noise at high frequency (5 to 10 kHz) was not expected. It is considered that the reduction at $6\frac{1}{4}$ chords is most likely associated with some form of blade stall but this could not be verified. It was also surprising to find an increase in broadband noise at high frequency since when rotor blades stall they are expected to exhibit an increase in broadband noise over a wide frequency range and particularly in a region which on this rotor would correspond to a frequency of 1000 to 1250 Hz. An examination of the narrowband traces tended to suggest, however, that in this region (which is essentially controlled by discrete frequency noise) the broadband noise increased uniformly with gust length.

6.6.6. Subjective Study

During the tests, and afterwards upon playback on a hi-fi system, the subjective impression of the rotor noise was assessed. As the blade passed through the gust an impulsive blade slap type noise was generated. The 'sharpness' increased with rotor speed and gust amplitude, but there was little effect with changes in gust length although the character of the basic rotor rotational noise sounded slightly different at the long gust settings. This is not surprising since the sharpness, and hence subjective impression, would be controlled by the initial gust rise rate. Blade stall was expected to give rise to an increase in broadband noise, but there was no noticeable change in the characteristics of the noise.

6.6.7. Constant Induced Angle Tests

The recordings were subjectively assessed and analyzed in terms of $\frac{1}{3}$ octave bands and 1/1 octave bands. There was no significant change in noise characteristics with gust length and/or amplitude except of the type previously discussed. Since also there was no real indication of blade stall, it was decided that the results would not furnish any further information and this study was curtailed.

6.7. CONCLUSIONS

1. A well defined blade slap type impulse was generated by the rapid lift fluctuations of the blade as it passed through the gust.
2. Theoretical and experimental results showed good agreement both in amplitude and characteristics over the full range of gust profile used in the investigation. This implies that the simple blade loading (lift) model and the rotational noise program can be used to predict blade/gust interaction effects.
3. In the rotational noise theory it was necessary to replace the blade chord term with an 'effective chord', which had to be chosen so that the blade loading profile was fully represented. It is not known what effect this approach would have on the calculation of noise for blade loadings which contain both 'slow time varying components' and high frequency impulsive components since, according to available information, the former requires use of the real chord.
4. The 'cancellation dips' and 'reinforcement peaks' in the experimental results were slightly displaced in frequency from the theoretical values. This is thought to be due to non-uniform blade spacing and the fact that positive pitch had to be applied to the cuff of one blade to obtain the desired 'track'. The results are very sensitive to such effects.
5. Discrete gusts with induced angles of 45° and lengths of up to 7 chords, did not appear to give rise to any significant stall. In other words a rapid change of 'angle of attack' did not induce stall - this is in agreement with the results obtained by Ham [78].
6. The broadband noise increased slightly with rotor speed, gust amplitude and gust length. Although there was no well defined stall region, a change in noise characteristics (possibly linked with a form of stall) occurred at a gust length of $6\frac{1}{4}$ chords.
7. Theoretically the SPL of the lower harmonics for a short gust followed a V^4 law while the higher harmonics tended to be dependent on V^6. At greater gust lengths (above 3 chords) all the harmonics followed V^4. Thus on a real rotor where the broadband noise increases approximately with V^6 and rotational noise can exhibit characteristics of V^{10} (or higher) dependence, blade/gust interaction noise would be less significant as the rotor speed was increased. Subjectively, however, the impulse would still be important.

8. The OASPL followed a V^2 law at low rotor speeds (300 to 500 rpm) and V^6 at higher speeds (700 to 900 rpm). It increased with gust length and amplitude: at a gust length of $6\frac{1}{4}$ chords it exhibited a decrease in level.
9. At a gust velocity of 105 ft/s there was a dramatic increase in OASPL and it appeared if there was a source not accounted for by the theory or the blade loading model was inadequate - this needs further evaluation.
10. The level of the fundamental or first harmonic was dependent on gust length, but unaffected by changes in gust amplitude at a fixed gust length. Thus it appeared to correlate with 'drag'.
11. The predicted level of the fundamental was over predicted for all but 'short gusts' (where level is a function of normal rotor noise). At present there appears to be no reasonable explanation for the difference in level between the measured and predicted values.

TABLE 6.1: TEST CONDITIONS

No. of Air Jets	GUST LENGTH		GUST AMPLITUDE ft/s				
	inches	chords	0	47	77	105	125
1	3	0.75	X	X	X	X	X
3	5	1.25	0	0	0	0	0
6	10	2.50	X	X	X	X	X
9	13	3.25	0	0	0	0	0
12	16	4.00	X	X	X	X	X
15	19	4.75	0	0	0	0	0
18	22	5.50	X	X	X	X	X
21	25	6.25	X	X	X	X	X
24	28	7.00	0	0	0	0	0

EACH CONDITION WAS EXAMINED AT THE FOLLOWING ROTOR SPEEDS

RPM	300	400	500	600	700	800	900
Tip Speed ft/s	141.3	188.4	235.5	282.6	329.7	376.8	423.9
REC/ANAL.	0	X	X	0	X	X	0

X = CONDITION RECORDED ONLY: 0 = CONDITIONS ANALYZED

TABLE 6.2: INDUCED ANGLE OF INCIDENCE

Rotor Speed RPM (ft/s)	Blade Velocity at centre of gust ft/s	Gust Velocity ft/s	Induced Angle degrees
300 (141.3)	127.2	45	19.5
		77	31.1
		105	39.5
		125	44.5
600 (282.6)	255.4	45	10.0
		77	16.8
		105	22.4
		125	26.1
900 (423.9)	381.6	45	6.7
		77	11.4
		105	15.4
		125	18.0

TABLE 6.3: LIST OF CONDITIONS FOR PRODUCING INDUCED ANGLES

Induced Angle degrees	Gust Velocity ft/s	Supply Pressure p.s.i.	RRPM	Tip Speed ft/s
30	77	10	310	145
	105	15	430	200
	125	20	513	240
25	77	10	390	182
	105	15	530	248
	125	20	635	298
20	45	5	290	136
	77	10	500	235
	105	15	680	324
	125	20	805	378
15	45	5	395	185
	77	10	675	317
	105	15	925	435

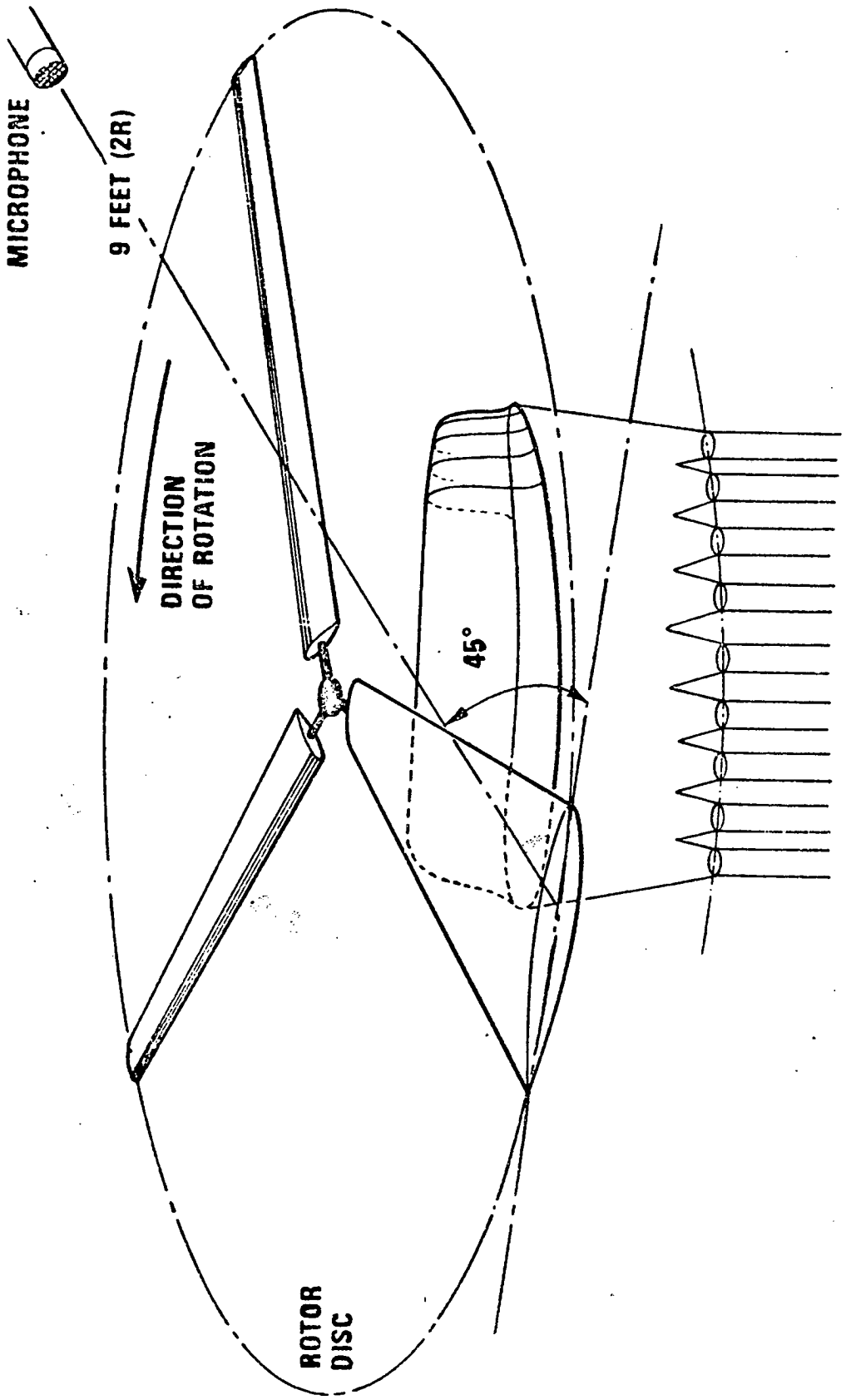

FIGURE 6.1. TEST ARRANGEMENT

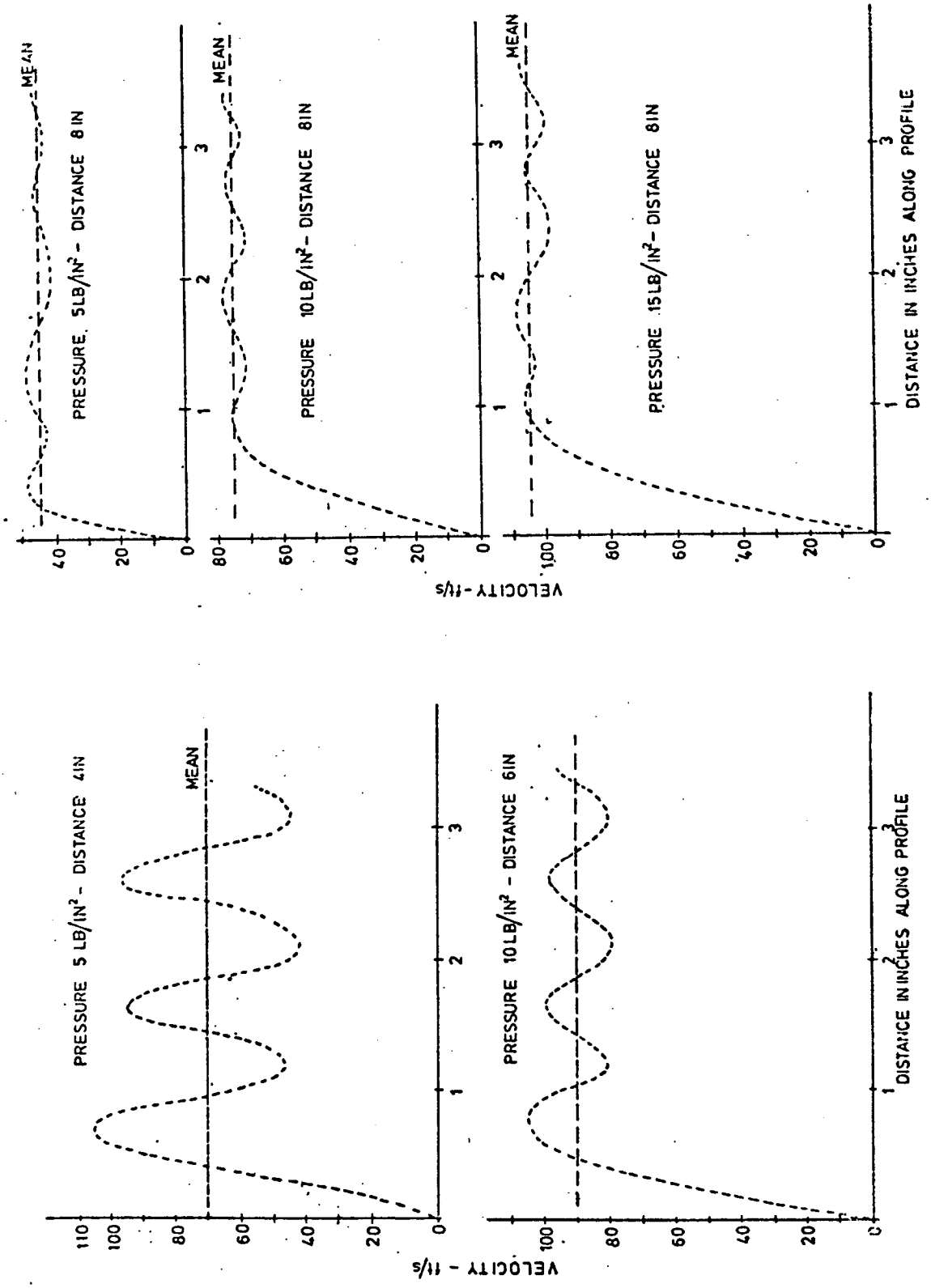

FIGURE 6.2. VELOCITY PROFILES

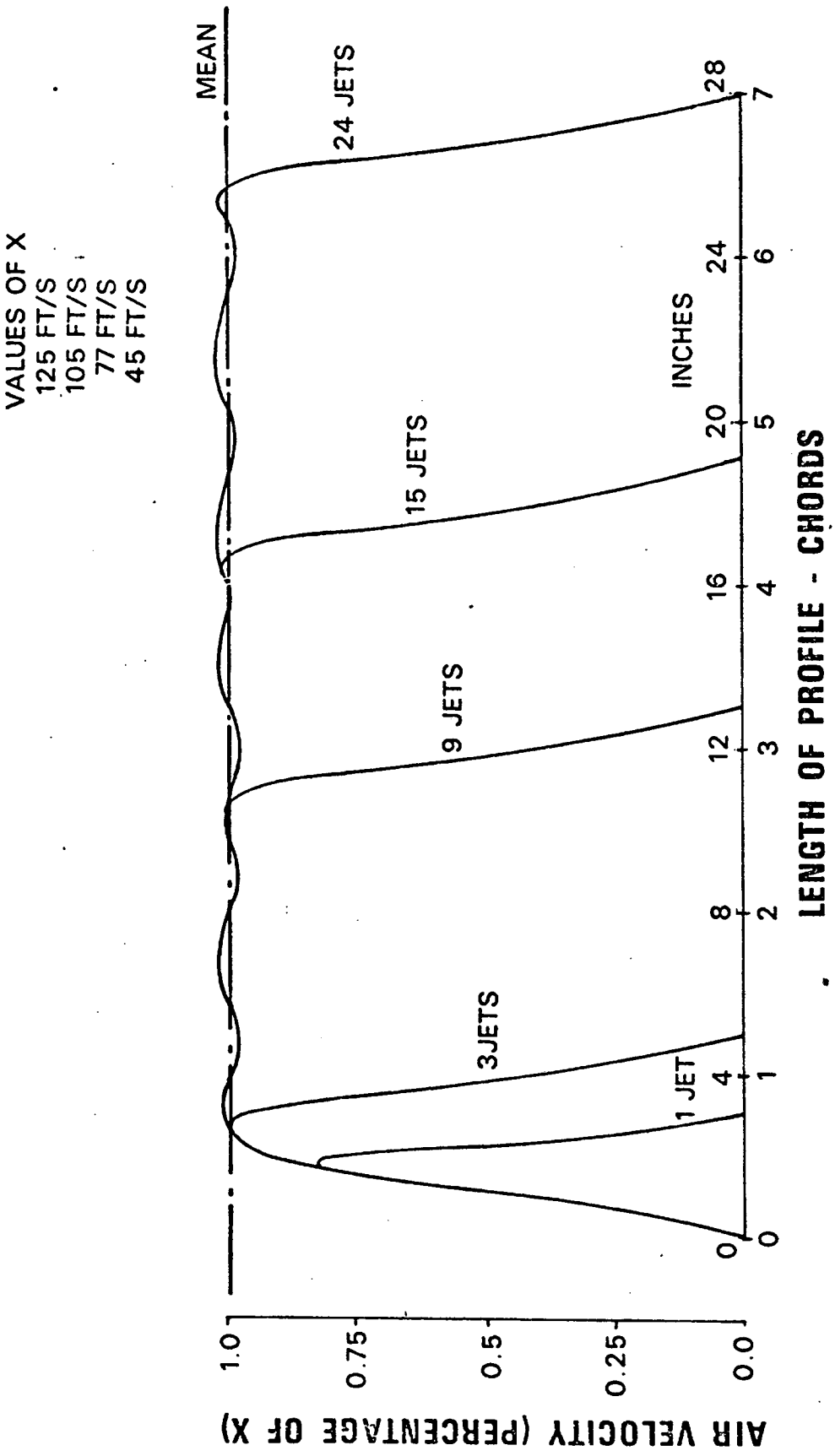

FIGURE 6.3. VELOCITY PROFILE: INFLUENCE OF NUMBER OF AIR-JETS

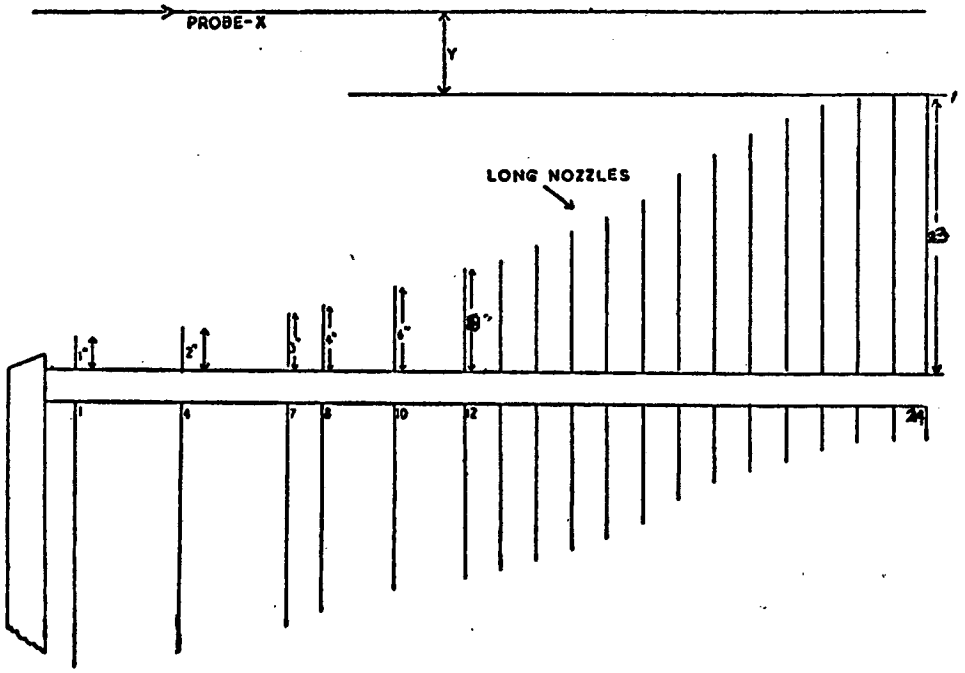

FIGURE 6.4. AIR-JET ARRANGEMENT FOR LINEARLY INCREASING VELOCITY PROFILE

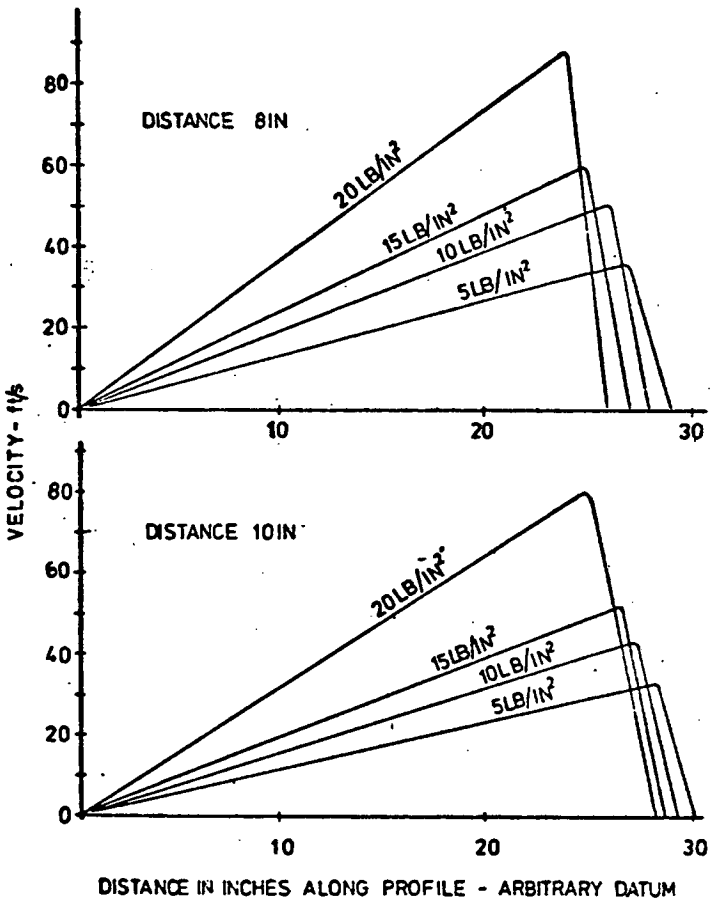

FIGURE 6.5. VELOCITY PROFILES: LINEARLY INCREASING WITH DISTANCE

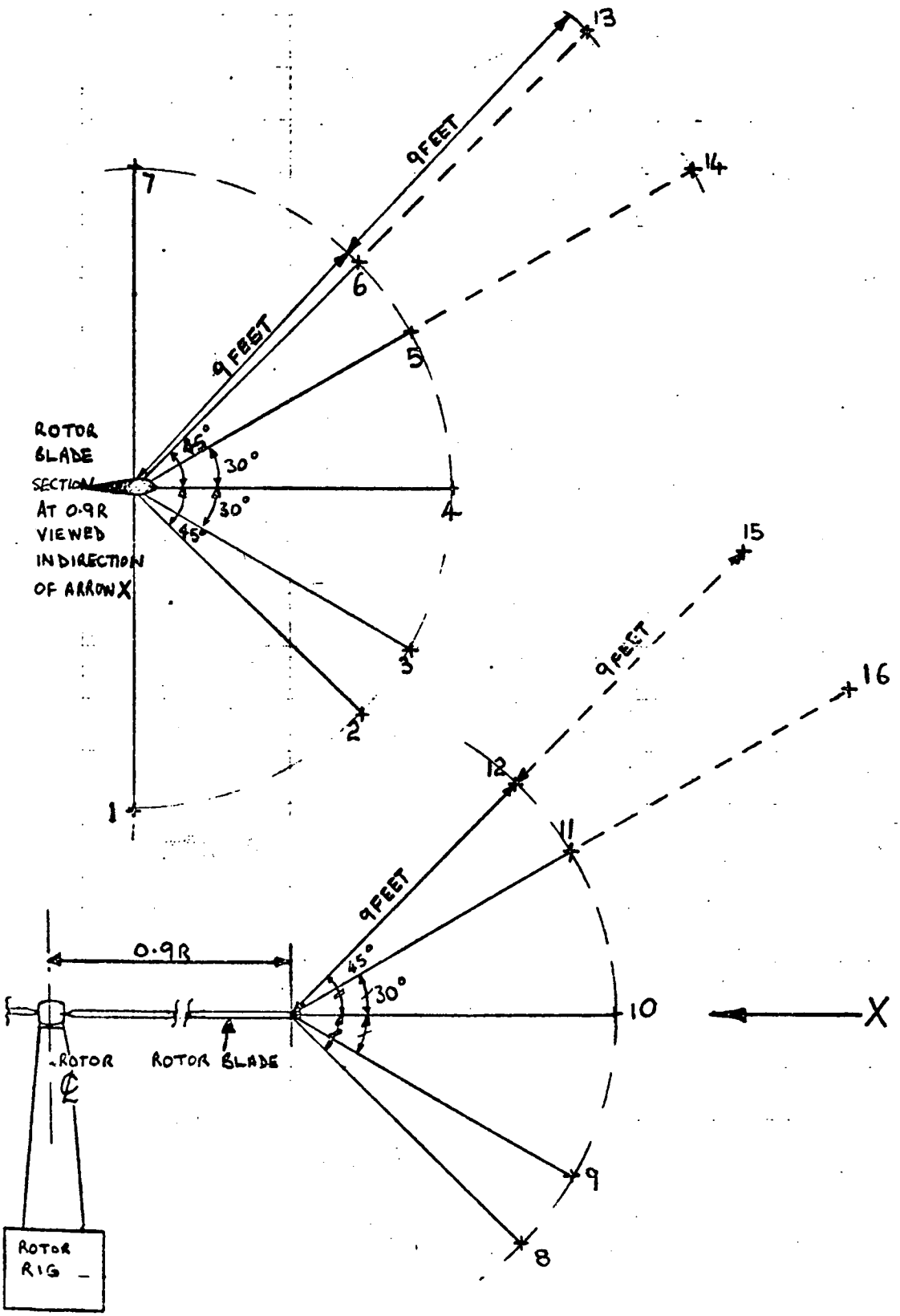

FIGURE 6.6. MICROPHONE POSITIONS - INITIAL TESTS

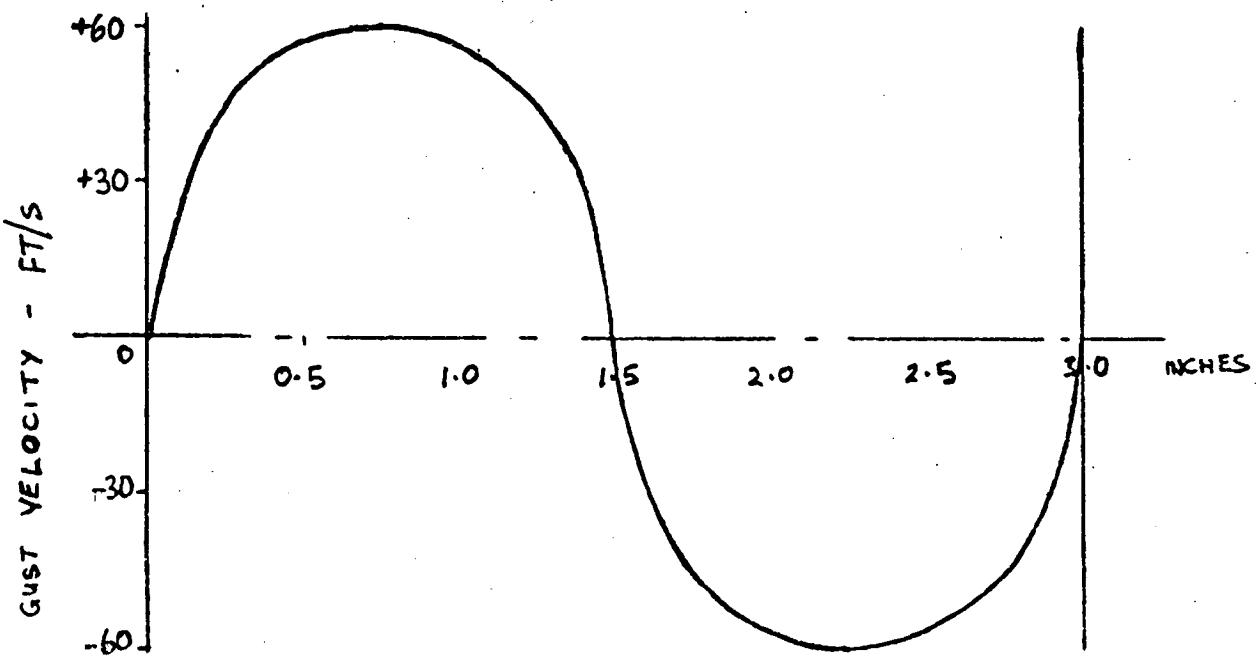

FIGURE 6.7. GUST PROFILE USED FOR EVALUATION OF BLADE LOADING PROGRAM

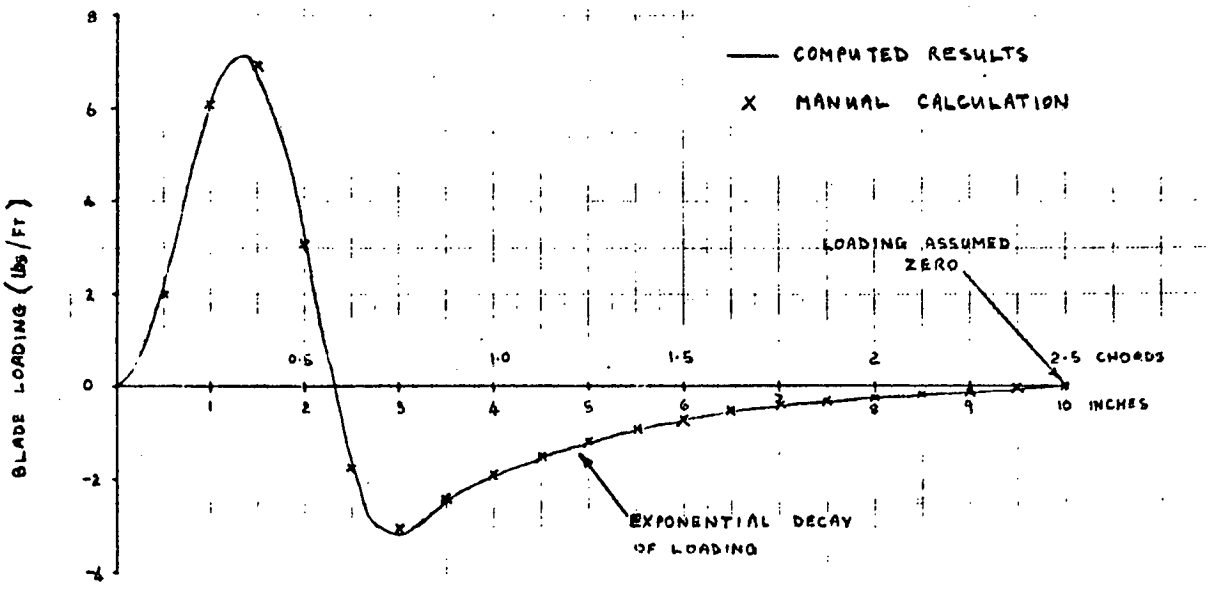

FIGURE 6.8. BLADE LOADING (SINUSODIAL GUST)

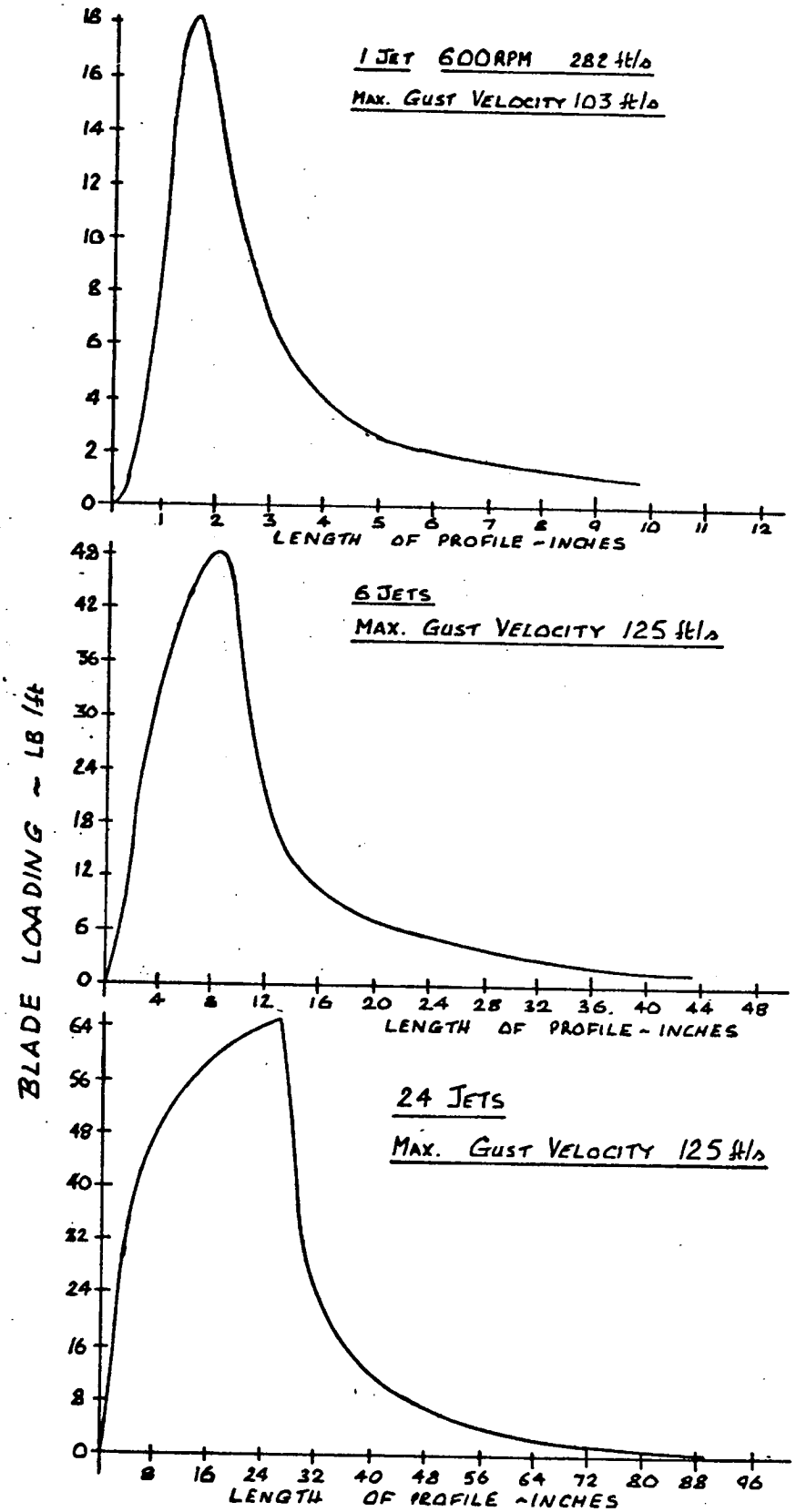

FIGURE 6.9. COMPUTED BLADE LOADINGS

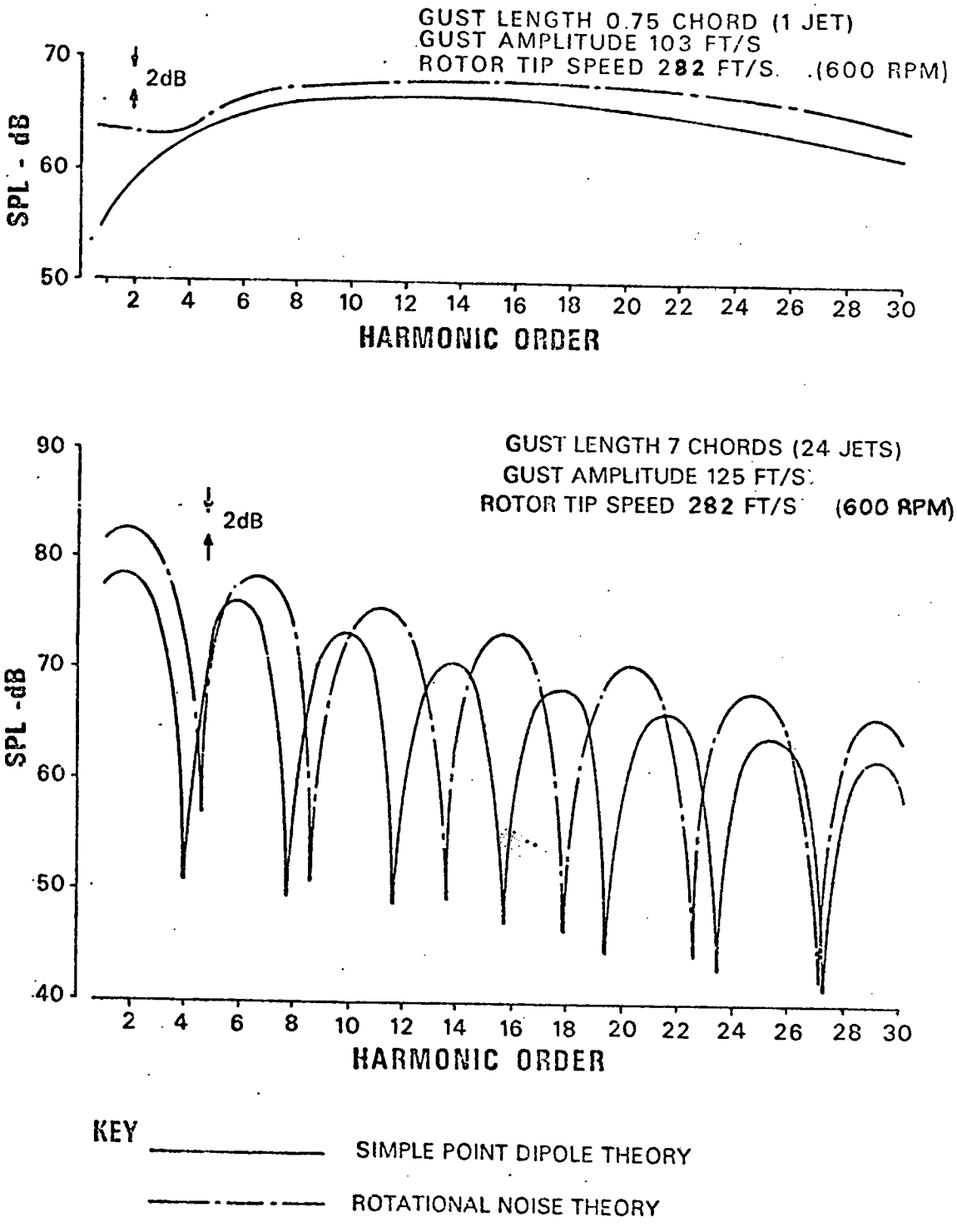

FIGURE 6.10. COMPARISON OF ACOUSTIC THEORIES

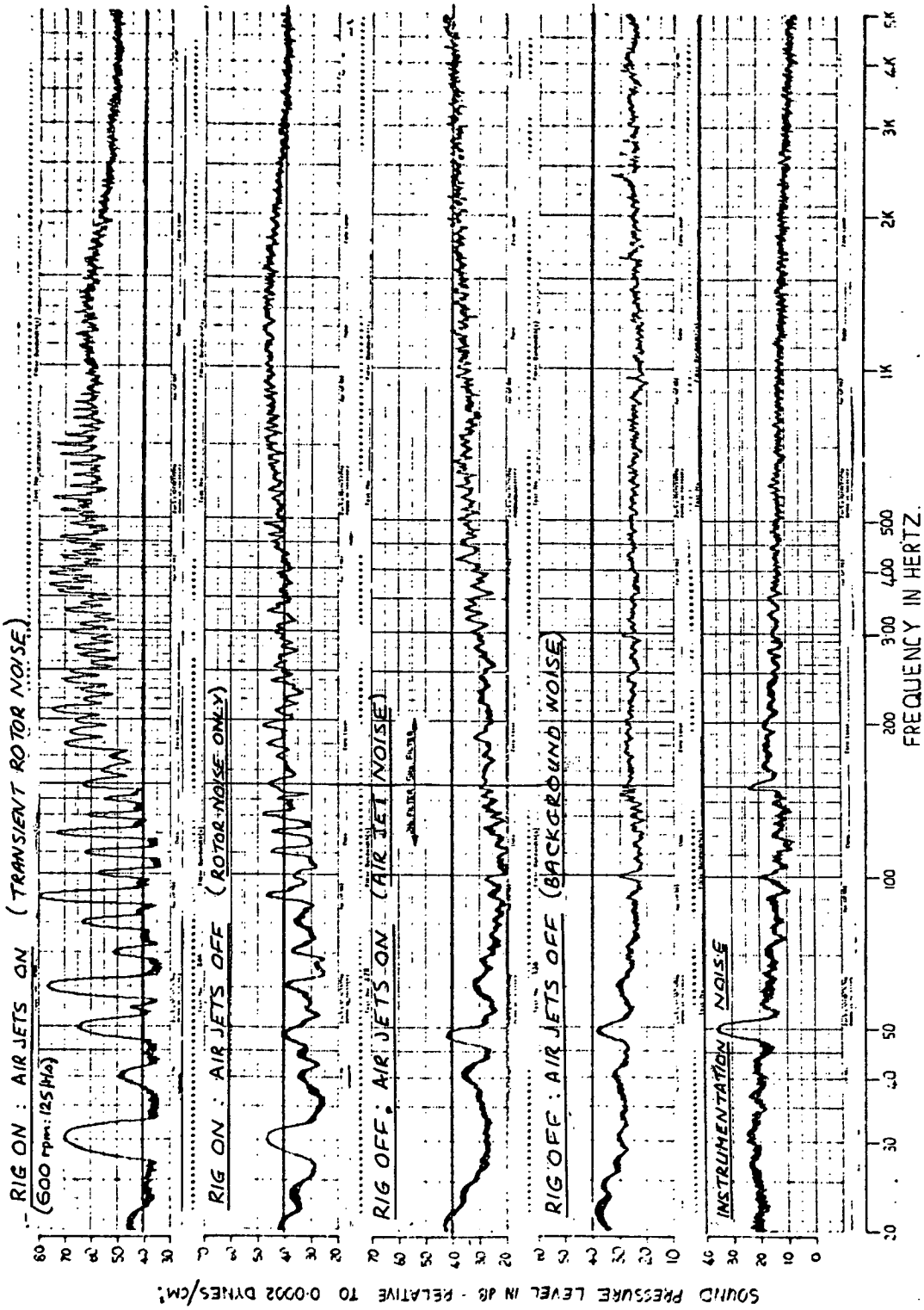

FIGURE 6.11. NARROWBAND ANALYSIS: ROTOR, RIG AND BACKGROUND NOISE

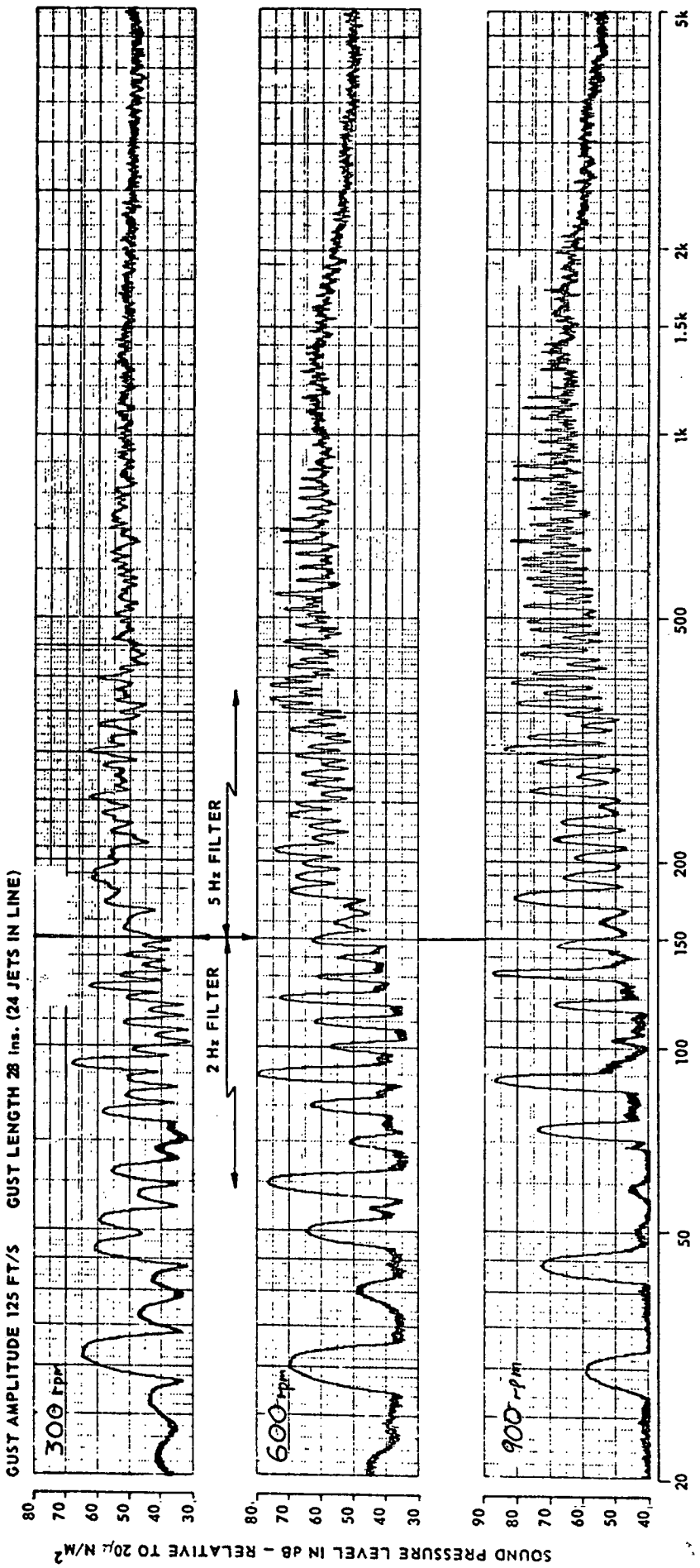

FIGURE 6.12. NARROWBAND ANALYSIS: VARIATION WITH ROTOR SPEED

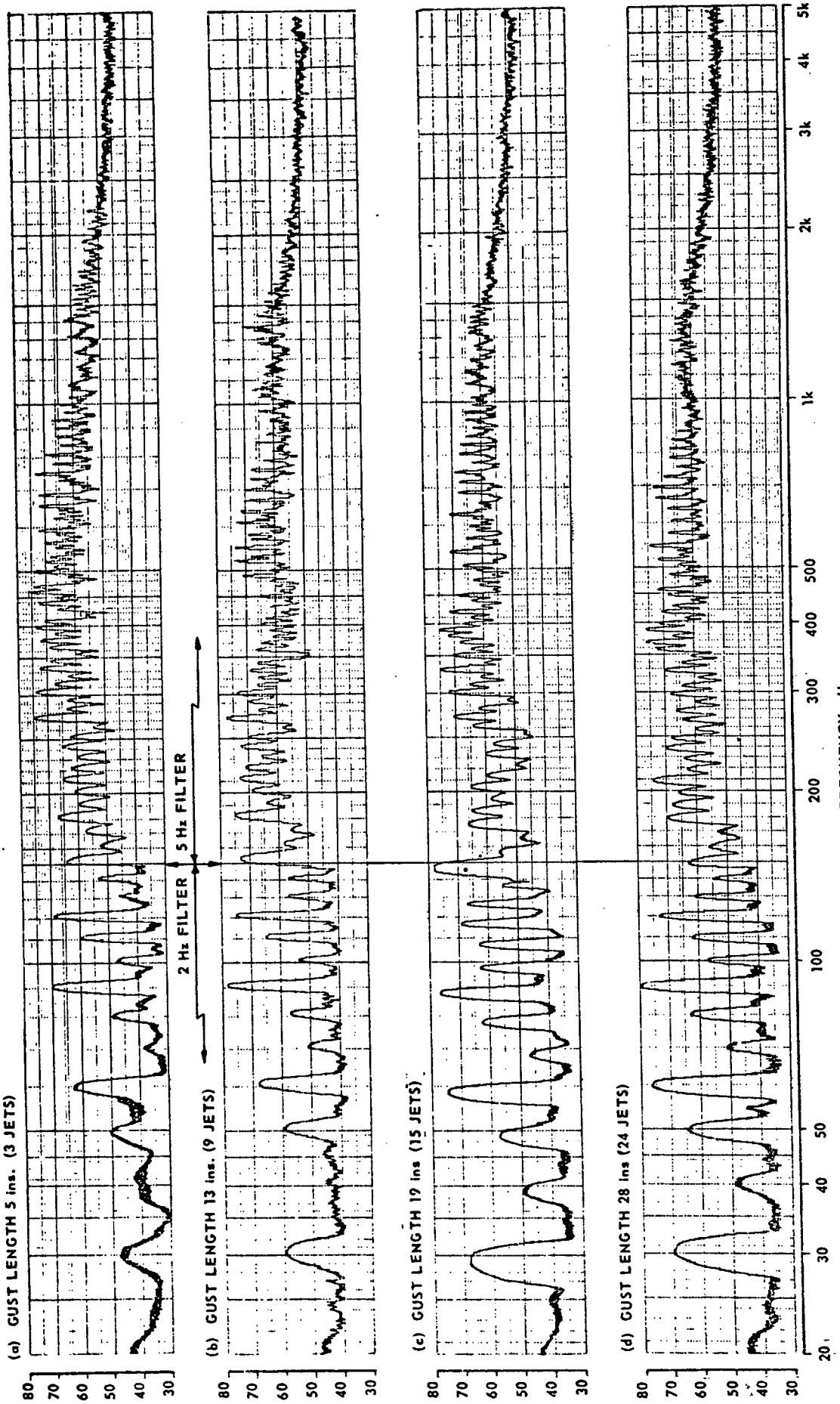

FIGURE 6.13. NARROWBAND ANALYSIS: VARIATION WITH GUST LENGTH

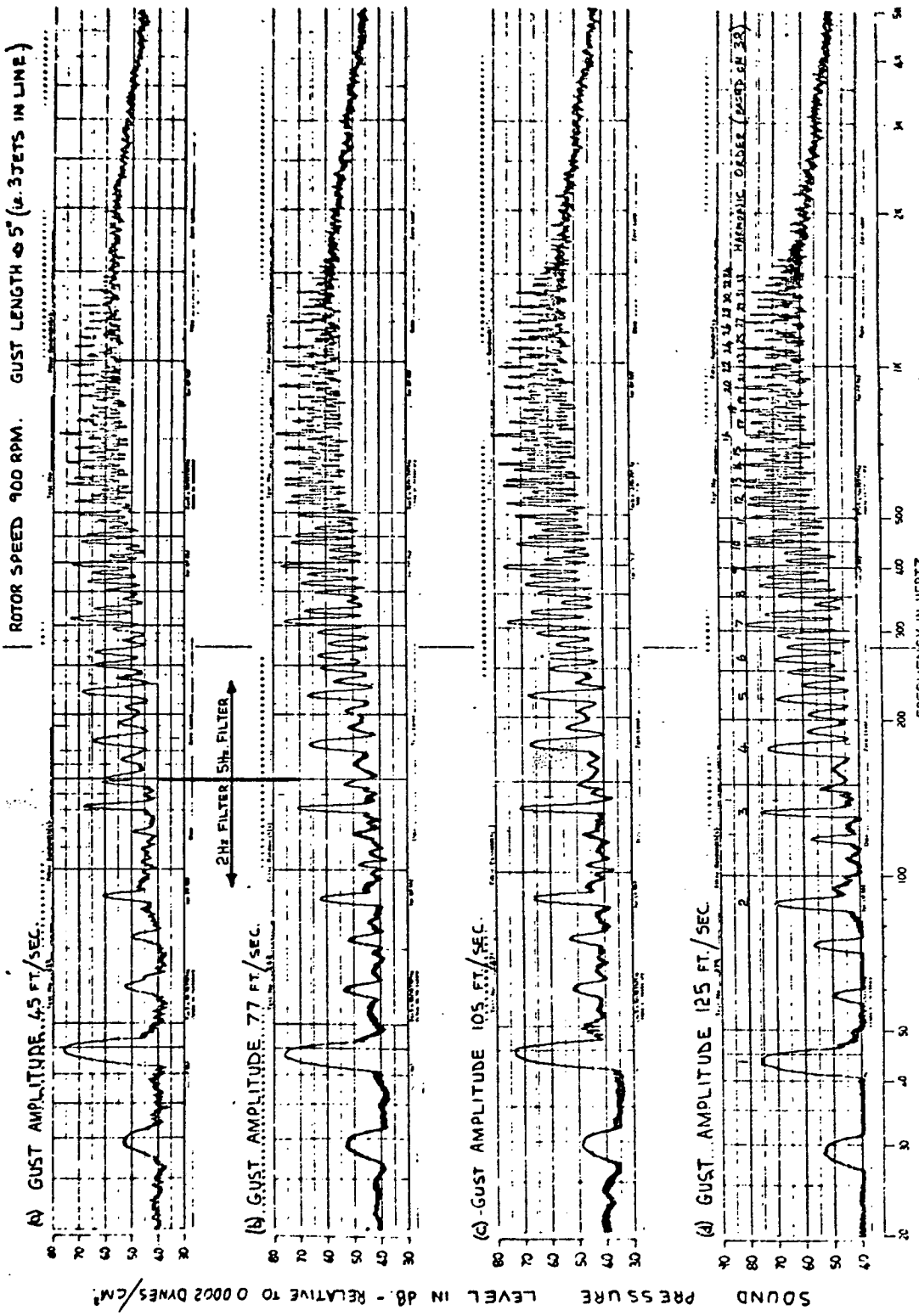

FIGURE 6.14. NARROWBAND ANALYSIS: VARIATION WITH GUST AMPLITUDE

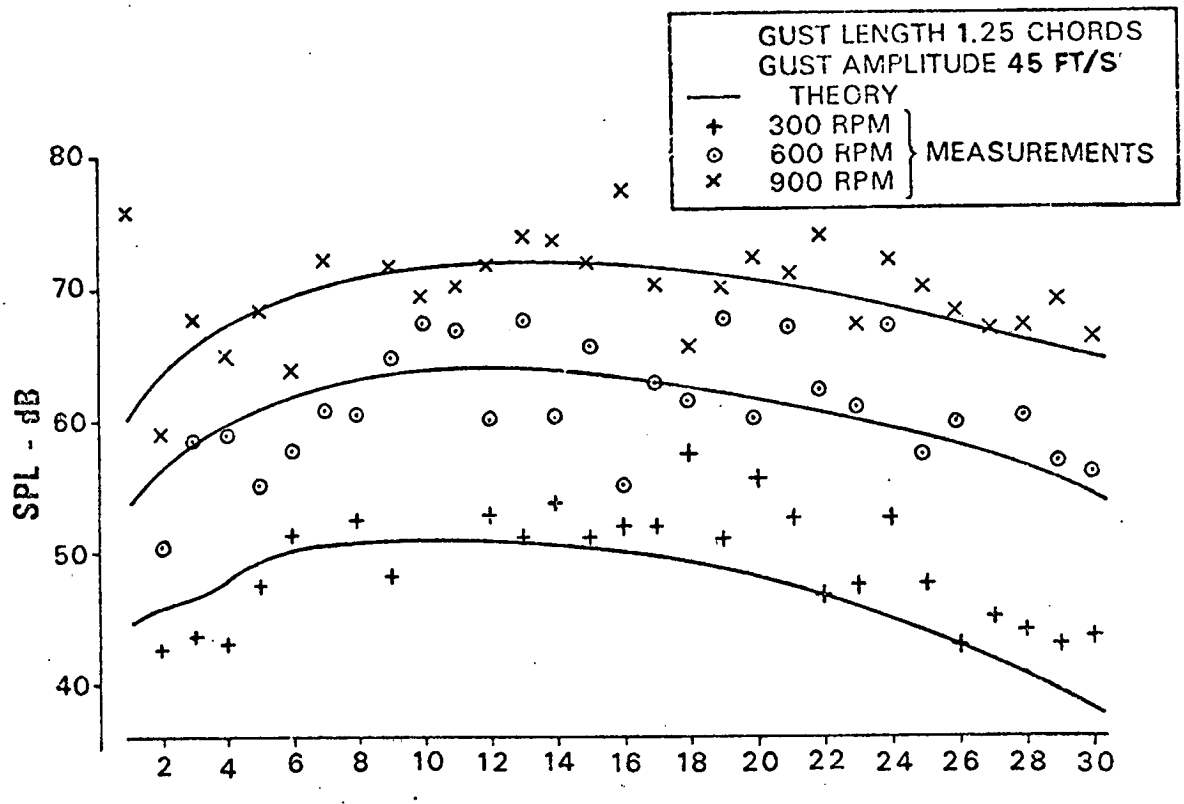

FIGURE 6.15. COMPARISON OF CALCULATED AND MEASURED SPL (SHORT GUST)

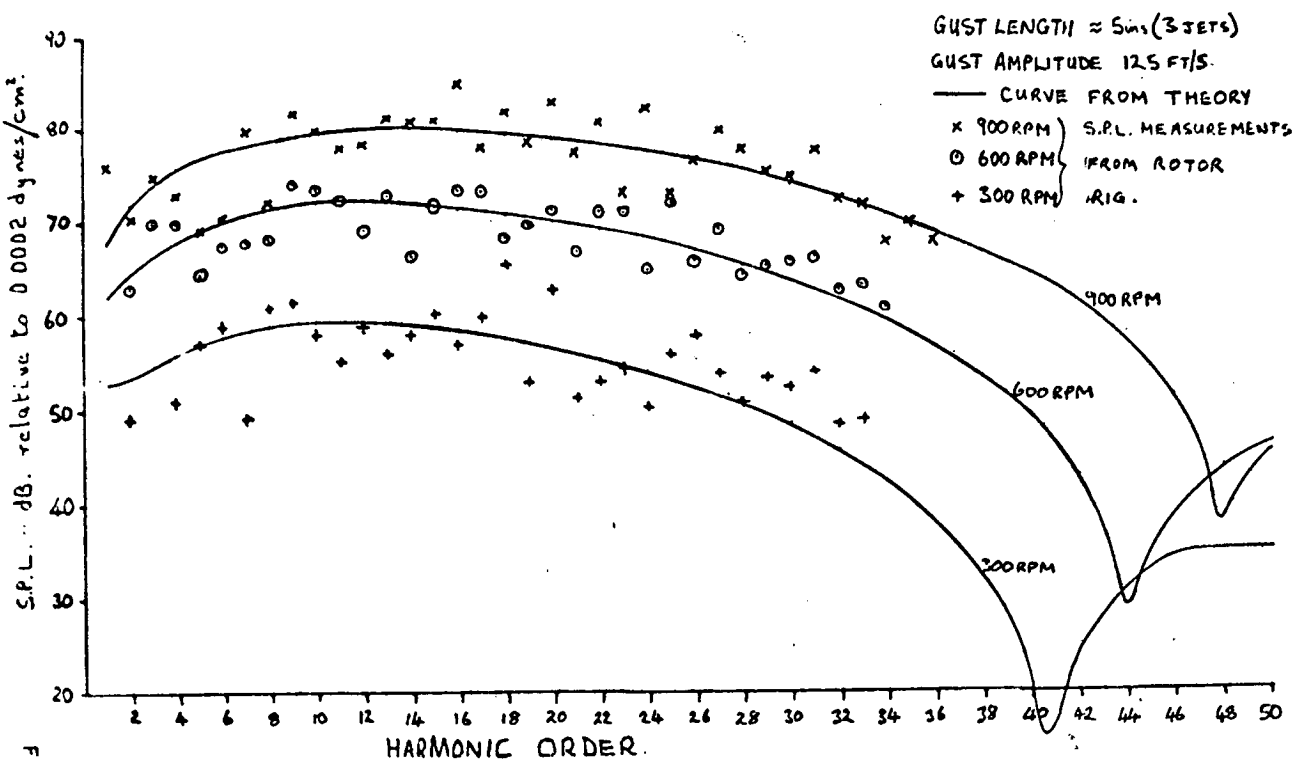

FIGURE 6.16. COMPARISON OF CALCULATED AND MEASURED SPL (SHORT GUST)

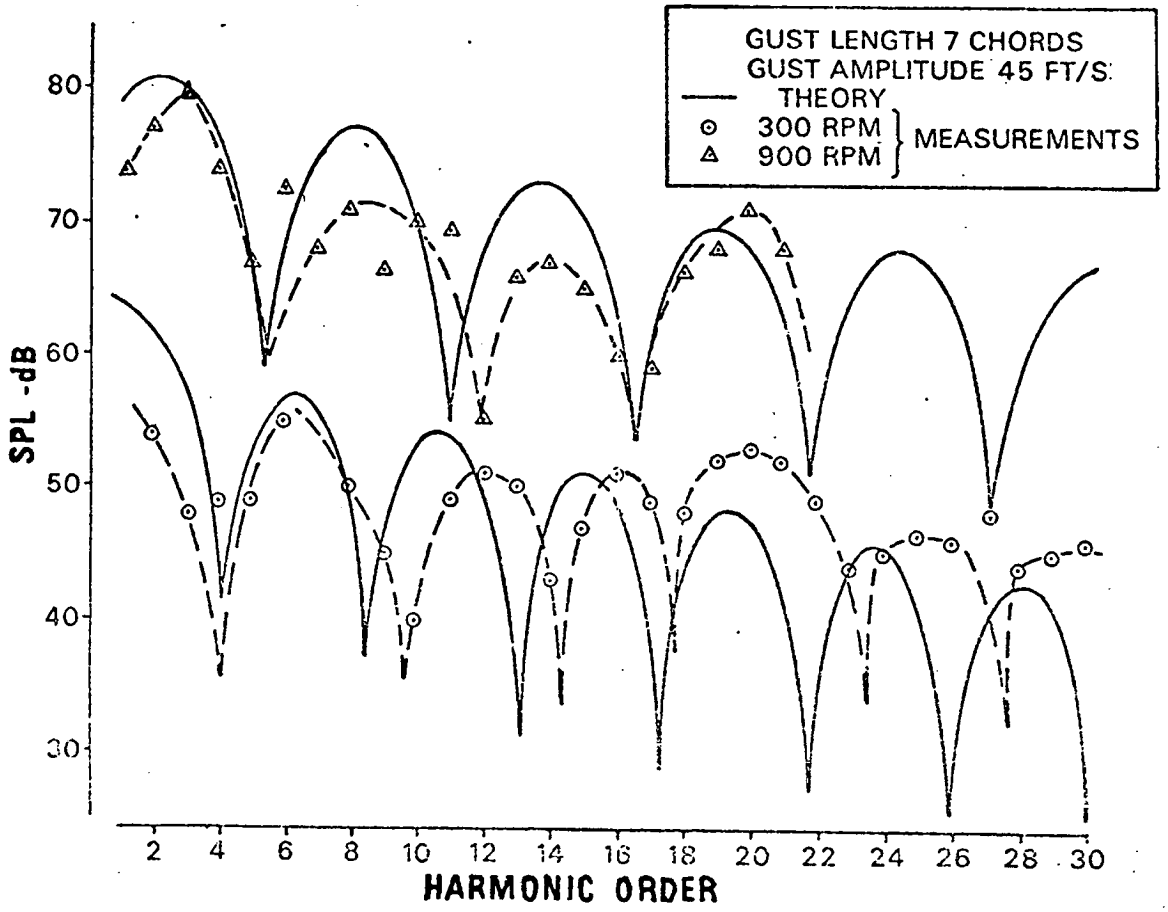

FIGURE 6.17. COMPARISON OF CALCULATED AND MEASURED SPL (LONG GUST)

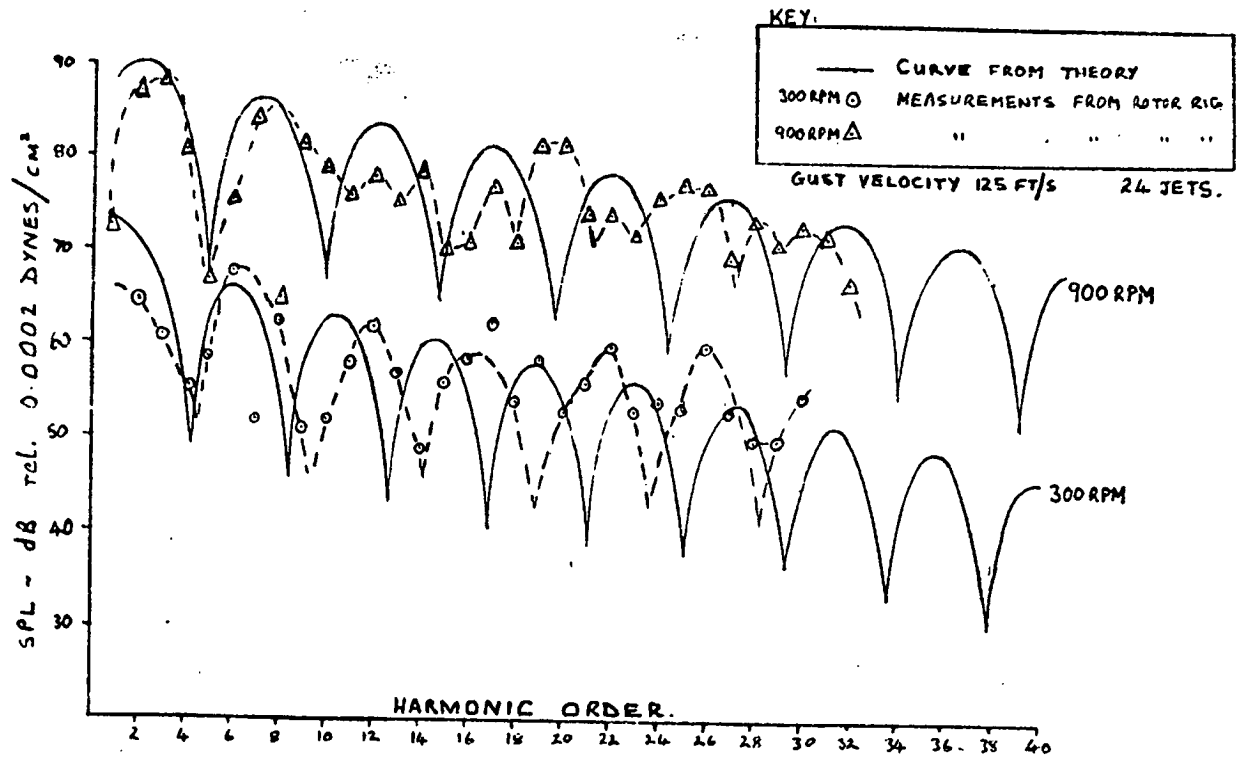

FIGURE 6.18. COMPARISON OF CALCULATED AND MEASURED SPL (LONG GUST)

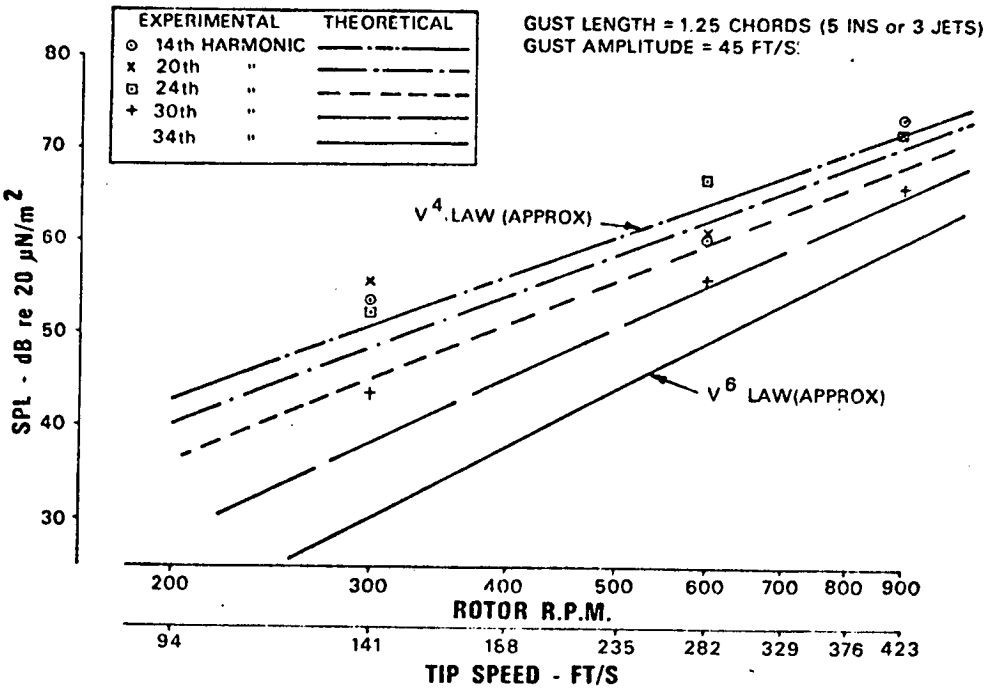

FIGURE 6.19. VARIATION OF HARMONIC SPL WITH ROTOR SPEED

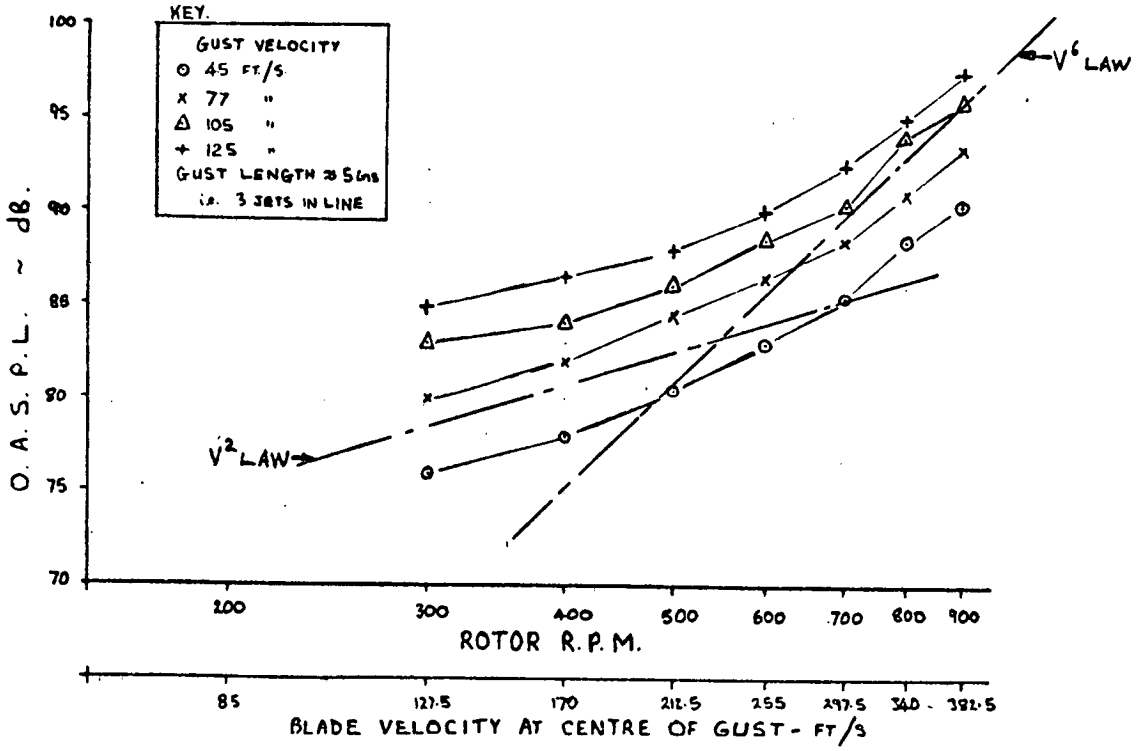

FIGURE 6.20. VARIATION OF OASPL WITH ROTOR SPEED AND GUST VELOCITY

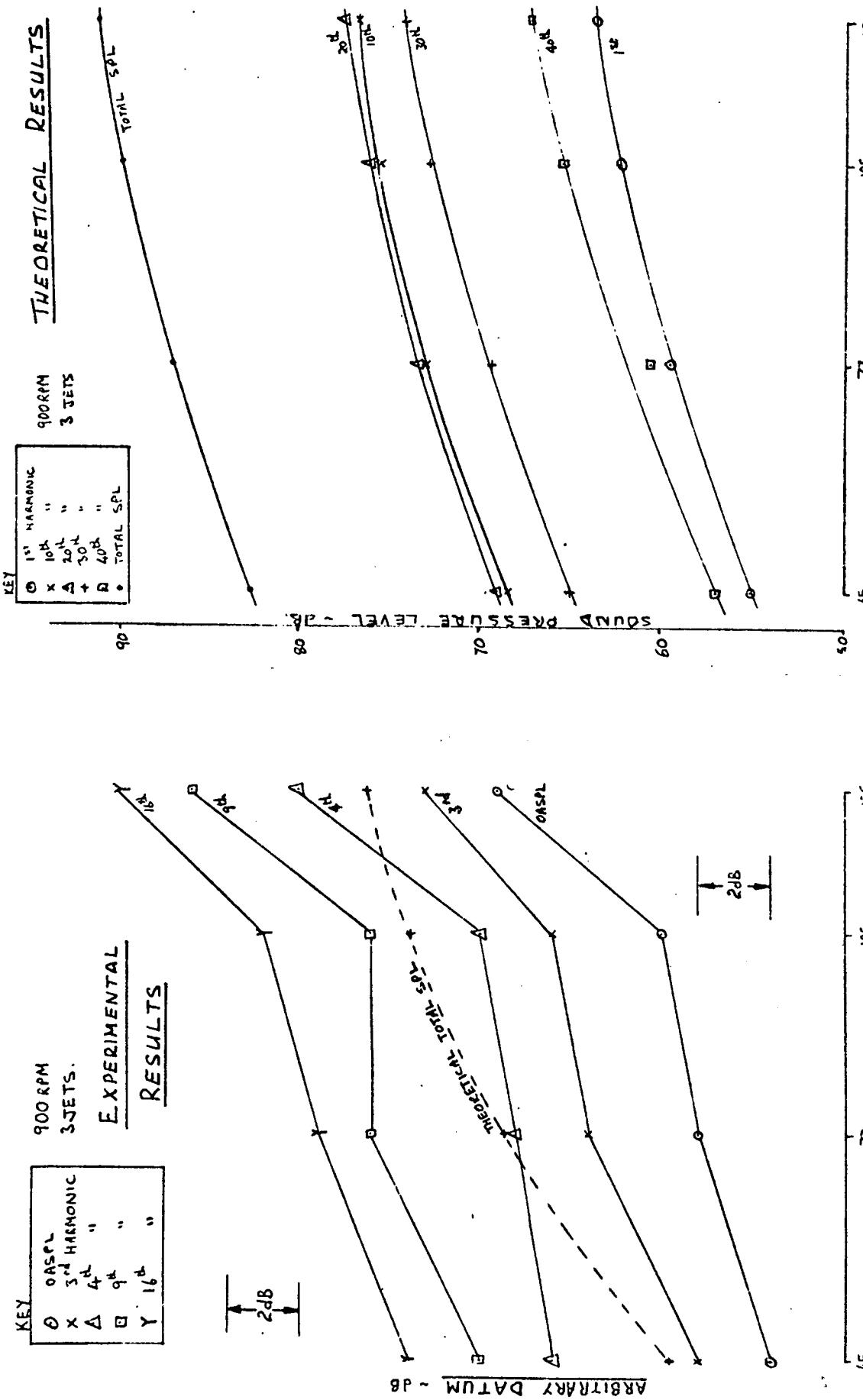

FIGURE 6.21. VARIATION OF HARMONIC SPL WITH GUST AMPLITUDE (THEORY AND EXPERIMENT)

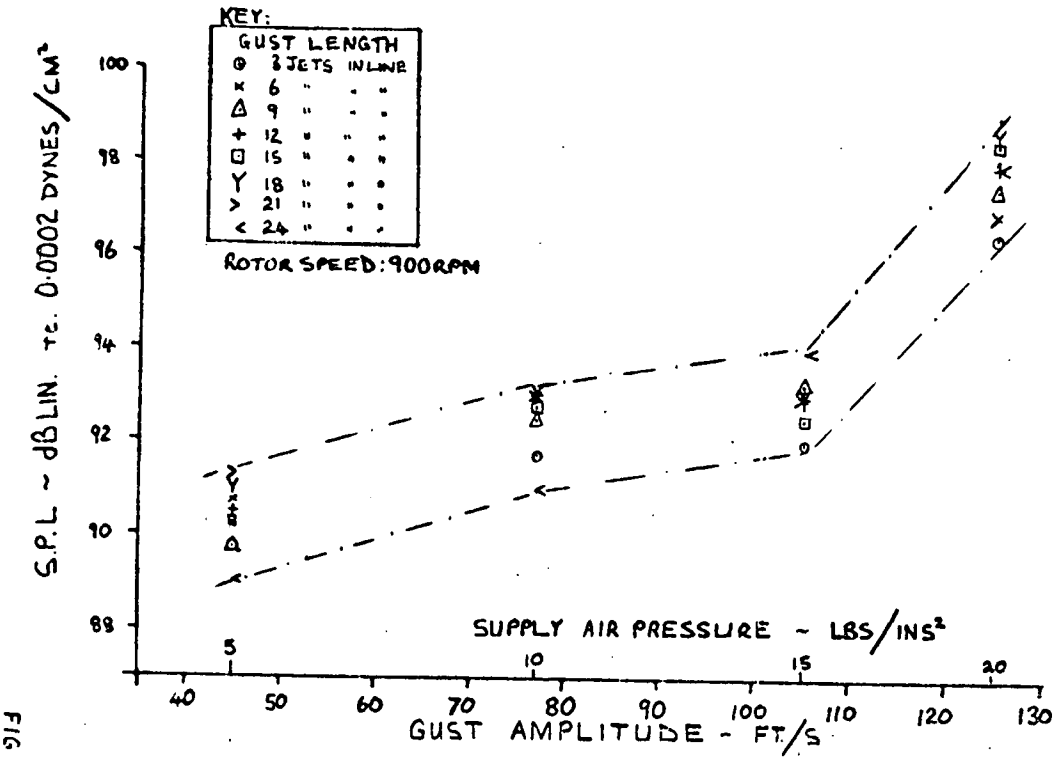

FIG

FIGURE 6.22. VARIATION OF OASPL WITH GUST AMPLITUDE

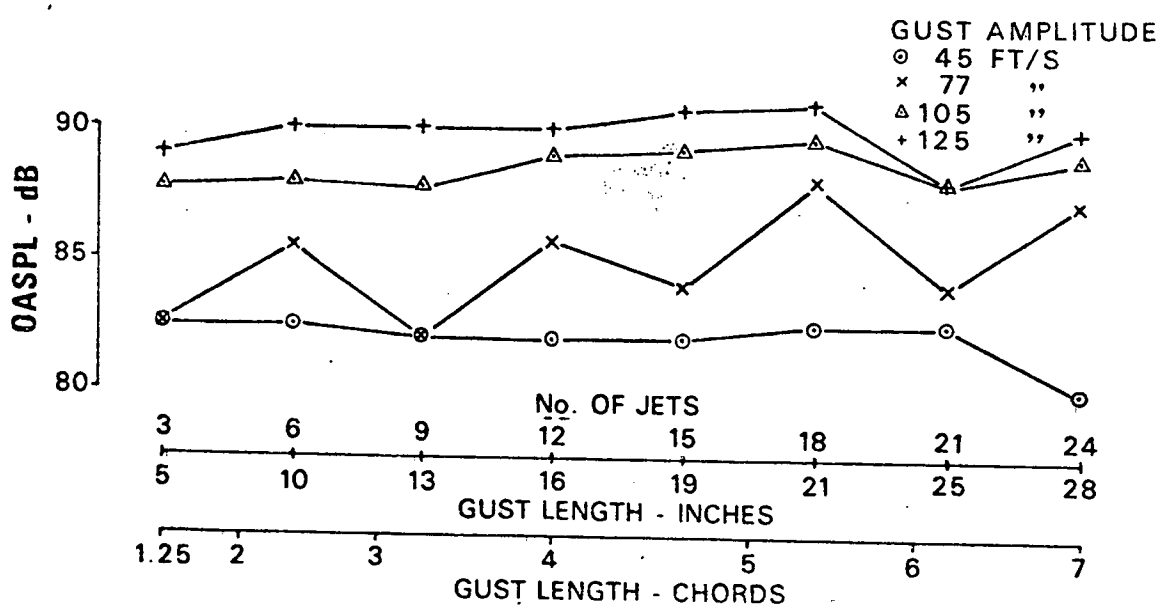

FIGURE 6.23. VARIATION OF OASPL (50 Hz to 10k Hz) WITH GUST LENGTH

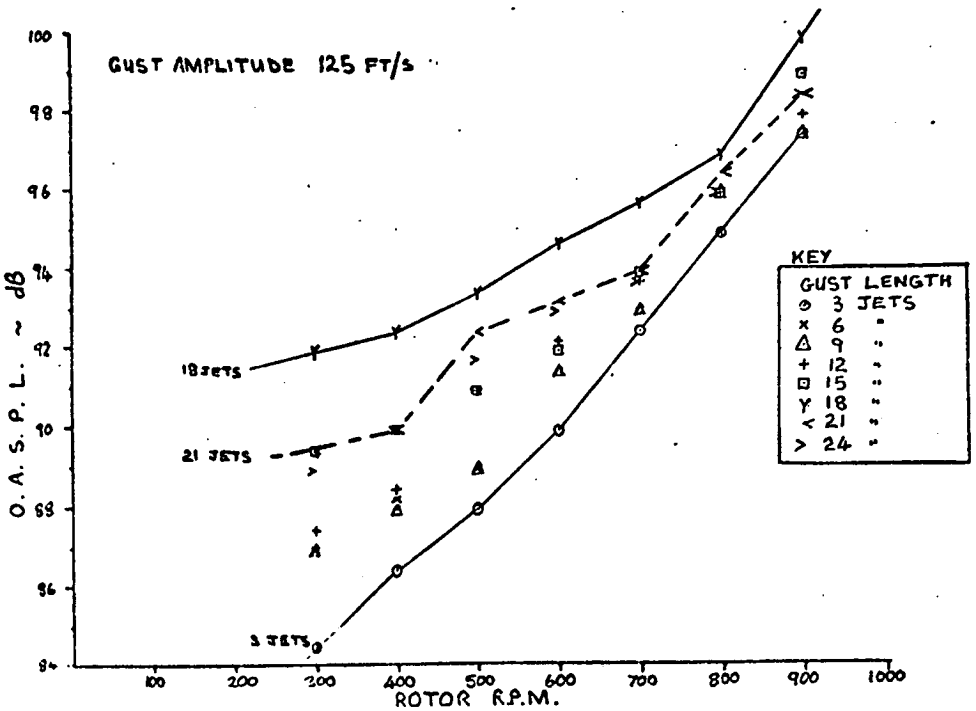

FIGURE 6.24. VARIATION OF OASPL WITH ROTOR SPEED AND GUST LENGTH

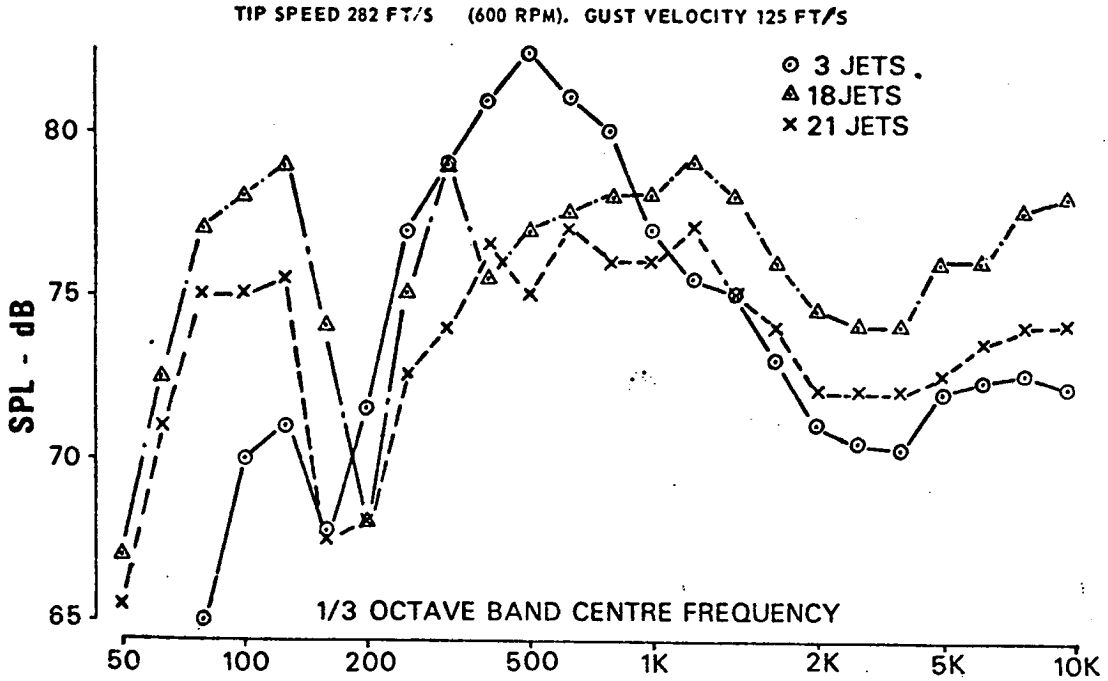

FIGURE 6.25. $\frac{1}{3}$ OCTAVE BAND SPECTRA: VARIATION WITH GUST LENGTH

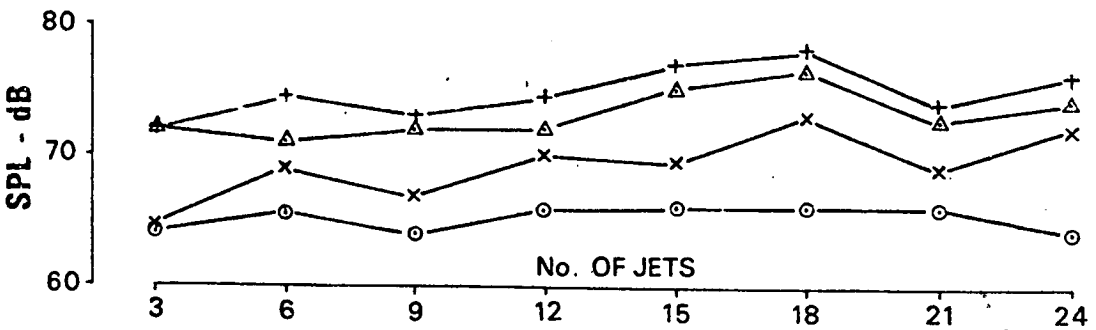

FIGURE 6.26. VARIATION OF 10k Hz $\frac{1}{3}$ OCTAVE BAND WITH GUST LENGTH

CHAPTER 7: BLADE/FUSELAGE INTERACTION

7.1. INTRODUCTION

Main rotor noise is more impulsive at the 'rear' (tail on) of a hovering helicopter than in the front (nose on) and this has been associated with the passage of the blade over the fuselage. The impulsiveness and high level of tail rotor noise is also believed to be to some extent dependent on the tail rotor/tail pylon interaction. These aspects had not been studied in detail, although they obviously had a significant effect on the level and subjective impression of helicopter noise. A programme was therefore formulated to enable these interaction effects to be investigated in detail on a model scale.

The fuselage/tail pylon was represented by a cylinder; this shape was chosen in preference to any other to ease the theoretical calculations. The cylinder (circular fuselage) was mounted under the ISVR 9 ft diameter rotor. The theoretical blade lift fluctuations resulting from the interactions were evaluated by using Bramwell and Johnston's theory [21] and the acoustic spectra was calculated using a rotational noise program developed from that derived by Tanna [18, 130]. The predicted values were compared with results obtained from narrowband analysis of noise measurements. Cylinder (fuselage) transient surface pressure measurements were obtained and compared with values derived from the aerodynamic theory.

7.2. TEST FACILITIES

7.2.1. Rotor Rig/Blade Pressure Transducers

The ISVR 9 ft diameter rotor rig was fitted with the three bladed rigid rotor head and the standard untwisted blades. A pair of Kulite LQL-125-5 miniature pressure transducers was fitted by WHL in a fourth blade, and it was intended to measure the blade pressure response. After calibration at WHL, and checks at ISVR, this blade was fitted to the rotor rig. At this stage it was discovered that the upper transducer had failed and that the lower gauge only responded to static pressures. The faults appeared to be associated with the detail installation and since WHL could not offer any assistance in this matter and expertise was not available at ISVR, it was decided to delete the measurement of blade pressure from the program.

The rotor thrust measurement device discussed in section 2.5 was incorporated into the rotor rig during the initial stages of this study.

7.2.2. Rotor/Fuselage Interaction Simulation

The 'fuselage' was a cylinder of 12 inches diameter and 30 inches long. It had three pressure tapping points on the surface 9 inches from one end plate at 30° separation - these were fitted with B & K type UA 0015 mountings to enable flush fitting of B & K ½ inch pressure microphones (type 4134). The cylinder was supported on a stand by using a simple 'V support' as illustrated in Figure 7.1. The cylinder was mounted under the rotor as shown in Plates 2.1 and 7.1 and the range of rotor/cylinder positions are shown in diagrammatic form in Figure 7.2. With this arrangement the pressure tapping could be positioned at any angle simply by rotating the cylinder and hence a circumferential distribution of pressure could be obtained. Similarly the radial position, within the limits indicated on Figure 7.2, could be set to any desired value.

7.3. TEST PROGRAMME

7.3.1. Scope

In the programme as originally envisaged it was intended to study the blade pressure, cylinder pressure and the noise output as a function of the variation of rotor speed, blade/cylinder separation distance, blade pitch and radial position, both theoretically and experimentally. The theory used was independent of the sign of the pitch, but in the case of the experimental results differences between positive pitch and negative pitch setting was expected. Blade pressure measurements were subsequently abandoned (see section 7.2.1) and due to time limitations the full programme was not completed. The items relating to the cylinder pressures selected for study and reported on in this report are indicated in Table 7.1. At first glance it may appear that the conditions studied could have been better selected; at the time however the aim was to give as wide a cover of the complete programme as possible and place the main emphasis on the noise results. Similar analysis as planned for the cylinder pressure was planned for the noise results. A major problem was, however, experienced with the rig 'thrust measurement' device which took considerable time to rectify. In addition a number of minor problems were encountered with the computer programs which set back the analysis/prediction schedule. It was decided therefore to place emphasis on the data collection with a view to completing the full analysis at a later stage. It was also anticipated that an extension would be granted to the contract supporting this programme to complete the

work as originally envisaged. Additional funding could not, however, be obtained and as a result a number of aspects of interest could not be examined in the full depth desired. Also as a result of curtailment of the programme the number of conditions analyzed were far less than ideally required. The result was that instead of being able to study the 'noise implication' as a function of a number of variables, it was only possible to conduct a comparison between theory and experiment at selected conditions. The cases chosen for this comparison do, however, indicate the general characteristics and the main areas of interest.

7.3.2. Noise Measurements

Tests were conducted for both downwash (positive blade pitch) and upwash (negative blade pitch) cases over a speed range varying from 400 rpm (188.5 ft/s tip speed) to the maximum possible for the particular pitch chosen. A list of the conditions, together with the rotor/fuselage separation distance tested, is given in Table 7.2. In order that the influence of the rotor/fuselage interaction could be assessed measurements at all the test conditions were repeated with the fuselage removed (normal rotor noise).

Noise measurements were made at the position illustrated in Figure 7.3 and as can be seen microphones 1 and 2 are approximately 1 and 2 rotor diameters from the 'tip region'.

7.3.3. Fuselage Pressure Measurements

Pressure measurements were obtained for a range of conditions with the blade set with both positive and negative pitch (downwash and upwash). The rotor blade to fuselage separation distance H, defined in Figure 7.4, was varied from 8 to 16 inches in the case of positive pitch and from 10 to 16 inches for the negative pitch case. These distances refer to the ideal 'stationary rotor' and take no account of 'coning effects' which result in an effective increase in rotor blade separation at the blade tip for positive pitch and a decrease for negative pitch. Coning results in a tip movement of 1 to 2 inches - this effect is discussed in section 7.6.1.

The separation notation (H) used refers to the distance from the cylinder (fuselage) centre as illustrated in Figure 7.4 and should not be confused with the rotor/cylinder clearance (S on Figure 7.4). Since the cylinder radius was 6 inches, the 8 inch and 16 inch separation distances imply (excluding coning effects) true separations of 2 inches and 10 inches respectively. It also follows that, since the coning in

the tip region was in the order of 2 inches, an '8 inch condition' was not possible when testing with negative pitch.

7.3.4. Steady Thrust Measurements

Rotor thrust measurements were made over the full range of test speeds and for pitch setting ranging from 0° to $\pm 10^{\circ}$ (in increments of 2°) with the cylinder removed. The positive and negative pitch setting gave, within the measurement accuracy, identical results. Tests were repeated with the fuselage in position, but unfortunately the thrust measurement system developed a fault which was not detected until after the programme had been completed. Accurate measurements are, therefore, not available of the steady (or mean) thrust with the cylinder in position; calculations suggest, however, that to a first order the mean thrust would not be changed from those obtained without the cylinder under the rotor.

7.4. THEORETICAL INVESTIGATION

7.4.1. Aims

The main aim was to predict the acoustic spectra of the rotor when subjected to transient loadings arising from rotor/fuselage, or more precisely rotor wake/fuselage, interaction. Since acoustic theories had already been relatively well established emphasis was placed on determination of the blade loading since a successful prediction obviously depended on being able to calculate the blade lift/time dependency accurately. A secondary aim was the determination of the pressure distribution over the surface of the cylinder.

7.4.2. Aerodynamic Model

The mathematical model developed by Bramwell and Johnston [21] was used as the basis for calculating the transient blade loading and cylinder (fuselage) pressure field. In this theory the flow field around the blade was substituted by a two-dimensional vortex flow field in a plane normal to the fuselage, the strength of the vortex K being taken as $\frac{1}{2}\pi$ of the circulation Γ around the aerofoil (blade), i.e. $K = \Gamma / 2\pi$. The treatment of the problem as a two-dimensional case enabled conformal transformation techniques to be used and the result was then approximated to the three-dimensional flow case by applying an 'end effect' correction term. This approach was developed as a part of this study by Devani [22] into a form which allowed the influence of the rotor/fuselage interference to be assessed. A summary of this theoretical development is given for the transient blade loading and cylinder surface pressure in Appendix 12 - since in both cases this is

based on estimations of the change in blade circulation due to the presence of the cylinder (fuselage) this development is also outlined in Appendix 12.

7.4.2.1. Transient blade lift

The theory is outlined in Appendix 12 and the blade lift is given by

$$L_T = \rho V a_o \times \frac{R_e\left[-2a_1 V \sin(\gamma_o - \nu) + \frac{2a_1 a^2 U}{(a_1 + \bar{z}')}\right]}{R_e\left[1 - \frac{2a}{a_1 + z'} + \frac{2a_1}{a_1 + z''}\right]} \qquad (7.1)$$

where ρ = density of air, V = blade velocity, ao = lift curve slope, γ_o = collective blade pitch, ν = induced angle at blade section, a = radius of fuselage, a_1 = radius of cylinder which transforms into flat plate of chord 4 a_1 under transformation

$$z = \zeta + a^2/\zeta = c/4 \qquad (Re \text{ indicates real part of equation - see Appendix 12 for further explanation of terms})$$

$$\zeta' = -x_o - i y_o; \quad \zeta'' = \zeta' - a^2/\zeta$$

The general concept is illustrated in diagrammatic form in Figure 7.4 and if ψ is taken as negative when the blade is approaching the fuselage and positive when receding from it, then xo = r Sin ψ, yo = H, the height = a + S where S and a is the rotor fuselage separation distance and radius of the fuselage respectively.

From Bramwell and Johnston [21] it appeared that an 'end correction' should be applied (in a similar manner to that described in section 7.4.2.2 in connection with the cylinder surface measurements) but in addition to being complex, it was not clear if the formula developed for calculating the lift could be modified. Correction factors of the type devised for the steady thrust calculations discussed in section 2.6 were therefore applied in this case.

A computer program was developed to enable the fluctuating blade lift as the blade passed over the cylinder to be calculated - this program is defined in Appendix 13. Calculations were made for a radial position of 0.95 R over an azimuth range (see Figure 7.4) of $\pm$ 40° for a series of blade tip speeds and rotor/cylinder separations. A typical result is reproduced in Table 7.3.

7.4.2.2. Cylinder surface pressure

It was shown (see Appendix 12) that the pressure at a point N (X_N, Y_N) on the cylinder was given by

$$p - p_o = P_1 + P_2 - P_3 \qquad (7.2)$$

where $P_1 = \frac{\rho KV}{Ao}\left\{\frac{(1-k^2)\sin\delta o - 2k\cos\delta o \sin(\delta-\delta o)}{1-2k\cos(\delta-\delta o)+k^2}\right\}$,

$P_2 = \frac{1}{2}\rho U^2$,

and $P_3 = 2\rho\left\{U\cos\delta - \frac{K}{Ao}\left[\frac{k-\cos(\delta-\delta o)}{1-2k\cos(\delta-\delta o)+k^2}\right]\right\}^2$.

The symbols Ao, δo and δ are illustrated on Figure 7.4, $k = a/Ao$, ρ = density of the air, p_o = atmospheric pressure and U = induced velocity.

$K = \Gamma/2\pi$ where Γ is the blade circulation. In the study carried out by Devani [22] the impact of taking account of slight variations in K and the inclusion of the resulting second order $(\partial K/\partial t)$ terms was assessed. It was shown that this was negligible, being less than 2% of the predicted pressure, and thus for the main calculations K was taken as being equal to $VcC_L/4$ as recommended in reference [21].

The 'end correction' formula devised by Bramwell and Johnston [21] was used in this study.

To enable the pressure/time characteristics to be calculated as the blade passed over the cylinder the computer program outlined in Appendix 14 was developed. Pressure measurements were calculated at a position corresponding to an 'overhead' blade radial position of 95% R. Calculations were made for blade movements of 2° over an azimuth range of $\pm 40^\circ$. Results were obtained for a range of rotor speed and blade/cylinder separations and a set of typical results, with 'end corrections' applied, is reproduced in Table 7.4.

7.4.3. Acoustic Theory

The rotational noise program developed by Tanna [18] and summarized in Appendix 9 was modified to enable the SPL of a range of noise harmonics to be calculated. This program was subsequently combined with the transient blade loading program summarized in Appendix 13 to give a complete program which allowed the SPL to be calculated directly from the input parameters required by the blade loading program: this is described in general terms in Appendix 15.

7.4.4. Limitations of Aerodynamic Theory

The Bramwell and Johnston theory [21] used as a basis of the theoretical study had been developed on the assumption that ideal flow conditions existed. If such conditions could be achieved in practice then it follows that the theory would be equally applicable to the 'downwash' (positive blade pitch) and the 'up wash' (negative blade

pitch) cases. In practice the conditions are far from ideal because the viscous forces affect the flow - this is illustrated in diagrammatic form in Figure 7.5. As can be seen the flow suffers from separation on the 'downstream' part of the fuselage (cylinder) whereas the 'upstream' is very nearly laminar. It follows that the theory is valid, streamline flow being assumed, on the 'upstream' side of the flow. On the 'downstream' side separation makes the flow turbulent and the velocity potential concept is no longer valid. It follows that in the 'downwash case' (positive pitch) the blades pass through the laminar 'upstream' part of the flow as indicated in Figure 7.5(a) and hence the theory of Bramwell and Johnston [21] would be expected to apply. In the 'upwash' flow (negative pitch) case the rotor passes through the turbulent part of the 'downstream' flow, Figure 7.5(b), and hence the theory is no longer applicable. This is, of course, a rather elementary simplification of the flow field; even so it does illustrate the general difference between the two conditions studied.

In the theoretcial study the Bramwell and Johnston approach [21] was, however, used for both the 'downwash' and 'upwash' cases since as far as could be determined there is no theory available for taking fully into account the 'upwash' (negative pitch case). Also it seems from a fundamental point of view sensible to establish the differences between the 'ideal theory' and the practical case. In the above simplification the 'pulsation effect' of the flow as the blade passes over the cylinder and any Reynolds number effects are ignored.

7.5. RESULTS

7.5.1. Transient Blade Lift

Since the blade pressure transducer work was not pursued due to difficulties with the pressure gauges, this aspect could only be studied from the theoretical point of view. A graphical representation of the results detailed in Table 7.3 is reproduced as Figure 7.6 which shows the transient lift per unit span (ΔL_T) as a function of azimuth angle Ψ.

The 'maximum' transient lift component ΔL_{TM} which occurs as the blade passes directly over the cylinder at $\Psi = 0$ (see Figure 7.6) was computed for a range of rotor speeds, blade/fuselage separations and blade pitch and typical results are given in Figures 7.7, 7.8 and 7.9. In addition to the absolute amplitude of ΔL_{TM}, the term $\Delta L_{TM}/L_S$, which is the ratio of the calculated transient lift to the calculated steady lift

(L_s) is shown - a 'log-log' plot has been used since this leads to 'straight lines' on the figures.

As can be seen from Figure 7.7, $\Delta L_m/L_s$ is independent of rotor speed and hence the transient component is directly related to the steady lift value. As the separation distance is increased the 'transient lift' component decreases as expected in amplitude. It will be noted that (for the case shown) the transient component is 57% of the steady value for the 8 inch results which corresponds to a 2 inch or $\frac{1}{2}$ chord rotor/cylinder separation. This reduces to 19% when the separation is increased to 2 chords (8 inches which is equivalent to a height H of 14 inches).

A rather interesting result is that as the blade pitch is increased (Figure 7.9), $\Delta L_m/L_s$ decreases from 80% at 2° pitch angle to 26% at 10° of pitch. This is due to the fact that the steady lift component (L_s) increases more rapidly with pitch than the transient lift component (L_m) - this can be seen on Figure 7.9. These results are, of course, theoretically independent of pitch direction, although in practice the comments made in section 7.4.4 will apply.

7.5.2. Cylinder (Fuselage) Surface Pressures

UV time-history traces of the measured cylinder surface pressure were obtained and two traces which illustrate the general characteristics are reproduced in Figure 7.10. It will be noted that the pressure pulses are essentially different in the two cases. For the 'positive pitch' condition (downwash case) the pulse is largely 'one sided', while in the case of 'negative pitch' (upwash condition) the pulse approaches a sine wave in character. The corresponding theoretical result is shown in Figure 7.11 (reproduced from the data given in Table 7.4) and it will be noted that it exhibits the character associated with the experimental 'positive pitch' results, Figure 7.10(b), although the negative portion (values below the datum) is more pronounced on the experimental results.

7.5.3. Acoustic Measurements

Narrowband analysis was performed on the majority of the conditions by using the Spectral Dynamics analyzer system (section 2.4) and a selection of the results for microphone position 1 and 2 are reproduced in Figure 7.12. The normal rotor noise spectrum (no cylinder) recorded at microphone 1 for +6° pitch is shown in trace 'a' and the result when the cylinder is positioned under the rotor is given in trace 'b'. Traces

'c' and 'd' illustrate the corresponding data for microphone 2 and traces 'e' and 'f' show results for -6° pitch. It is difficult to assess from such traces the impact of the rotor/cylinder interaction and thus it was necessary to obtain the level of the 'interaction noise', by subtracting the normal rotor noise from the spectra obtained with the cylinder under the rotor rig. In this it was considered that if the 'interaction effects' were 10 dB above the normal rotor noise then the level was that due to the interaction; if however the difference was between 2 and 10 dB the appropriate corrections were applied to obtain the actual interaction levels. For differences of 2 dB and below the result was ignored. Such spectra are reproduced in Figures 7.13 to 7.16.

Theoretical predictions were made for the full range of conditions and results for the test conditions are indicated on Figures 7.13 to 7.16. It will be noted that the theory gives a maximum at the 2nd/3rd blade passing harmonic and then there is a general decay in the level with increasing harmonic order. It will also be observed that in all cases the experimental results suggest a cancellation, which shows on the figures as a 'dip' around the 11/12th blade passing harmonic. Also as can be seen the theoretical levels (except for the first few harmonics) are in general below the experimental results.

7.6. DISCUSSION OF RESULTS

7.6.1. Influence of Coning Angle

When pitch, and hence lift, is applied to a rotor blade it takes up a position such that when the lift, drag and centrifugal forces are balanced, the 'tip path' plane is above the plane through the rotor hub normal to the rotor axis. In other words the blade 'cones up' and the tip is displaced relative to the static or zero pitch tip path plane. This applies both on a hinged (articulated) rotor and a rigid rotor, as used for the tests. In the case of a rigid rotor which is fixed at the root, the blade stiffness is such that under load it bends and on the model the blade tip took up a position at the tip which to a first order was similar to that on a 'hinged rotor'.

The theory is essentially a blade element (strip) theory and the calculations were made for specific rotor/cylinder separation distances. Over the spanwise element considered the influence of 'coning angle' is small and hence can be ignored. The theoretical results were, however, simply made in terms of a specified separation distance

referenced for convenience to the value at the tip. For the positive pitch case (+ve pitch) then the actual blade/cylinder separation distance H^1 is the defined value H (see Figure 7.4) plus the coning effect. For negative pitch (-ve pitch) results the opposite is true and the actual separation is less than the defined value H. Calculations were made for a series of separation (H) values from 8 inch to 16 inch (in 2 inch increments) and the experimental separation distances 'S' were defined in terms of the 'static separation'. It follows therefore that the '10 inch theoretical result' does not correspond directly to the '10 inch experimental result'. In this context it is worth noting that although statically the blade droops under gravity the height of the rotor hub centre (and hence ideal or true static blade position) was known and this was used for setting up the experimental conditions.

It follows, therefore, that difficulties occur when attempting to make a direct comparison between the calculated and experimental results. During the initial phase of the investigation a quick check suggested that the 'coning effect' was for all practical purposes 2 inches at the tip and hence it should have been possible to simply compare, say, the results by making the necessary adjustment. When, on comparison of the theoretical data, differences between the two sets of results were found, a more detailed investigation was carried out (by using a stroboscopic light and a mirror arrangement). This revealed that the tip displacement (relative to the static value) varied between 1 and 2 inches depending on the speed/pitch setting. It followed therefore that at the main radial position of interest (95% R), for a condition when the 'coning effect' was 1 inch, the actual separation distances S for the experimental '10 inch conditions' were in the order of 5 inch and 3 inch for the +ve pitch and -ve pitch cases, respectively, compared to the static value of 4 inch*. The corresponding H values to be used in the theory would be 11 inch and 9 inch - unfortunately this aspect was not fully appreciated at the time that the theoretical calculations were made and the values were simply calculated at a range of values nominally the same as the experimental reference value (i.e., 8 inch, 10 inch, 12 inch, etc). It was planned to re-run the programs, but this was not possible within the time constraints of the programme. Thus it has been necessary in the theoretical/experimental review to compare the test data with the nearest, or a range of, theoretical values.

*Note: Nominal value of S = H-radius of cylinder: i.e., S=H - 6 (inch) (see Figure 7.4)

7.6.2. Cylinder (Fuselage) Pressure

7.6.2.1. General characteristics

On comparing the experimental time history (Figure 7.10(b)) and the theoretical (Figure 7.11), general agreement in the character between the two was obtained. This was not, however, the case for negative pitch results as can be seen by comparing Figure 7.11 with Figure 7.10(a). This is considered to be due to the fact that the ideal flow conditions assumed in the derivation of Bramwell and Johnston's theory [21] do not exist and as discussed in section 7.4.4 flow separation takes place in the downstream part of the flow (see Figure 7.5).

7.6.2.2. Variation with speed

7.6.2.2.1. Positive pitch

Theoretical and experimental 'peak' pressure results are compared for $+6^{\circ}$ pitch in Figure 7.17 as a function of rotor speed (plotted to a log scale). Four curves are illustrated on this figure:

(a) experimental results for 10 inch static separation (H=10, S=4),
(b) the 'theoretical uncorrected 10 inch separation' results which take no account of coning angle or end effects,
(c) 'theoretical end-corrected' results for 10 inch separation, and
(d) theoretical curves for 12 inch separation - this corresponds approximately to the experimental result, with the coning angle taken into account.

Firstly it will be observed that the slopes of the curves are identical, following a V^2 law. Application of an 'end-correction' significantly reduces the estimation of the 'peak' pressure (by approximately 30%) and if a similar correction is applied to the 'theoretical 12 inch separation' curve, then the theoretical values would fall below those measured experimentally. The general agreement, when the type of experiment is taken into account, is considered to be good and it is anticipated that if precise 'coning angle' measurements had been taken even better agreement could have been obtained.

7.6.2.2.2. Negative pitch

Experimental data was not obtained; the theoretical curves would, however, be identical to those indicated on Figure 7.17.

7.6.2.3. Variation with separation distance

7.6.2.3.1. Negative pitch

A typical set of theoretical (uncorrected for end effects) and experimental 'peak' pressures are illustrated on Figure 7.18. It

will be noted there is a difference both in the general characteristics and absolute levels. If an allowance for 'end effects' had been made a better agreement would have been obtained at the lower separation distances. On the other hand taking coning into account would tend to increase the difference. In this context it is worth noting that for this case the negative pitch 10 inch experimental results would be expected to correspond approximately to the 8 inch theoretical value.

7.6.2.3.2. Positive pitch

This was not studied: the theoretical curve would, however, be identical to that indicated in Figure 7.18 and it is of interest to note that even for a 16 inch separation (actual theoretical blade/fuselage of 10 inch or 2.5 chords) the 'peak' pressure is still a significant factor.

7.6.2.4. Variation with blade pitch

This aspect was not examined.

7.6.2.5. Circumferential distribution of pressure

7.6.2.5.1. Positive pitch

A typical set of results are reproduced in Figure 7.19 and show the variation in pressure with angle around the cylinder. It will be noted that whereas the theoretical model suggests, as expected, a maximum directly under the blade ($\delta = 90^{\circ}$) measurements indicate a reduction in pressure at this point, i.e. a 'dip' in the curve. This was not examined in depth but if it is assumed that the flow is laminar outside the region bounded by $\delta = 60^{\circ}$ to $\delta = 120^{\circ}$ (i.e., 30° either side of the vertical), then it would appear that some form of flow separation takes place between 60° and 120°. This is difficult to understand, but it could be associated with the fact that the flow is transient in nature (pulsing with the blade passage) rather than uniform. Even so it would appear that outside the range 60° to 120° fairly good correlation between the theoretical and experimental results are obtained. In this case, however, better agreement was generally obtained if 'end corrections' and 'coning effects' were ignored. This is an aspect which obviously warrants further examination since the Bramwell and Johnston theory [21] is often used to predict fuselage pressures.

This relatively large difference between the 'theoretical' and experimental curves and the apparent 'dip' in the measurements at $\delta = 90^{\circ}$ must also be taken into account when evaluating the cylinder pressure results presented previously since they are quoted only for the $\delta = 90^{\circ}$ position. In other words the difference on Figure 7.17, which shows the variation with speed, would appear to be essentially due to the fact that circumferential distribution of pressure does not follow

the theoretical curves. This is another area which needs further examination.

7.6.2.5.2. Negative pitch

This aspect was not examined, although the theoretical curve would take the form illustrated on Figure 7.19. Considerable departure from the theoretical model would, however, be expected because of the flow distortion discussed previously.

7.6.2.6. Variation with position along the cylinder

7.6.2.6.1. Negative pitch

The 'radial' distribution is illustrated in Figure 7.20. The influence on the theoretical curve of the 'end correction' is clearly shown. The 'peak' predicted at 90% R agress fairly well with the experimental value; the 'fall-off' beyond this point is, however, more rapid than suggested by the theory and more akin to that associated with the 'fall-off' of the steady blade loading (section 2.6).

7.6.2.6.2. Positive pitch

This was not evaluated.

7.6.3. Rotational Noise

7.6.3.1. Theoretical considerations

Harmonic levels for $\Psi \pm 20^{\circ}$ and $\pm 40^{\circ}$ (relative to the centre of cylinder position) were investigated to study the effect of the azimuthal range on the predicted spectra. Outside these ranges the loading was assumed zero; this approach was adopted since the aim was to study the influence of blade/fuselage interaction only. Similar results were obtained with both ranges except that, as expected, use of data over a $\pm 40^{\circ}$ azimuth range gave slightly higher results at the higher harmonics (15th and above). Since the former, however, enabled a reduction in computer time, predictions based on a $\Psi \pm 20^{\circ}$ range were selected for detailed comparison with the experimental results.

7.6.3.2. Positive pitch (downwash) case

As can be seen from Figure 7.12, the overall rotor noise spectrum was not affected to any great extent by the blade/cylinder interaction. The maximum influence was in the frequency range 50 Hz to 500 Hz with increases in the harmonic levels of typically 1 to 5 dB. It was also observed that the interaction introduced 'sub harmonics' (rotor passing or rotor rotational harmonics) in the range 50 Hz to 250 Hz and that analysis of the level of some of these showed that they were increased to a level 10 dB above the previous 'broadband' noise level.

Comparison of the theoretical and experimental harmonic levels (Figure 7.13 and 7.14) showed that fair agreement was obtained for the

first 7 harmonics and that at higher harmonics the predicted SPL was significantly lower than the measured values. Consideration of the 'coning effects' would not significantly affect the correlation. The implication from this comparison is that the actual 'pulse' width is significantly sharper than predicted theoretically. This is also supported by the 'cancellations' in the experimental results which tends to suggest that a well-defined repetitive pulse is generated whose 'width' is less than indicated by the theory (this is discussed in Chapter 6). This is important and obviously needs clarification before the method can be applied to prediction of full scale blade/fuselage interaction effects.

7.6.3.3. Negative pitch (upwash) case

This configuration had a significant effect on the rotor noise with harmonic levels exhibiting on average increases by 2 dB to 10 dB in the frequency range 100 to 400 Hz with the highest increases in the 3rd to 12th harmonics. Typical results are reproduced in Figure 7.16 and show that even if 'coning' is taken into account the predicted values are well above those given by the theory. This is considered to be an underestimation of the 'sharpness' of the pulse and the influence of 'flow separation'.

7.6.3.4. Comparisons of positive (downwash) and negative (upwash) conditions

By studying the positive and negative pitch narrowband results (Figure 7.12) it can be seen that the 'upflow' case (negative pitch) generates higher noise levels than the equivalent 'downflow' case. It is difficult to make a precise comparison because of the influence of 'coning angle', but Figure 7.21 shows a comparison derived from consideration of a number of individual traces. Also indicated on the figure are the levels associated with the normal rotor noise on the rig. As can be seen the 'upflow' rotor noise is up to 10 dB higher than the corresponding 'downflow' rotor noise over a fairly wide frequency range. The trend occurred throughout the tests and in terms of dB(A) the difference was typically 10 dB. This is particularly important from the point of view of a real helicopter tail rotor, since they are often operated in 'hover' in a manner which corresponds to the 'upwash' (negative pitch) case. It will also be observed from Figure 7.21 that even the 'downwash'/positive pitch case still exhibits a significant increase in noise as compared to the level generated by the normal rotor.

7.7. CONCLUSIONS

1. Placing a cylinder (fuselage) under a rotor gives an increase in rotational noise: the effect is more pronounced in the case when the flow is drawn over the cylinder (negative pitch case) than when the flow is directed down over the cylinder. Even so there is still a marked increase in the noise level, and impulsiveness, in the positive pitch case.
2. Theory based on Bramwell and Johnston's work [21] shows fair agreement with the experimental results for the positive pitch (downflow) case; further refinement is, however, needed to take account of 'coning effects' and there is an indication that the 'end correction' is in error.
3. Comparison of theory and experiment suggests that the 'pulse' may be sharper than given by the Bramwell and Johnston theory [21].
4. The general trends associated wtth the 'peak pressure' on the cylinder as a function of blade/cylinder separation and velocity are very similar to those given by the theory.
5. The pressure on the cylinder departs from the theoretical characteristics at angles within $\pm 30^{\circ}$ of the vertical. At $\psi = 0^{\circ}$ the experimental results exhibit a dip, while the theoretical curve suggests a maximum. This is an important aspect and needs further examination.
6. The cylinder pressure measurements for positive pitch (upflow case) show a negative pressure prior to, and just after, the main pressure pulse. This is not predicted by the theory and thus the 'pulse' has effectively a higher frequency content than the corresponding smooth theoretical pressure curve.
7. The results suggest that on a real helicopter interference between the tail rotor and the tail pylon (or tail fin) is likely to be a significant factor, particularly since in many designs the flow in 'hover' and low speed flight is drawn over the pylon (positive pitch case). This also has implications on tail rotor design, but other aspects such as aerodynamic performance must be taken into account.
8. Although this programme was curtailed the trends are of sufficient interest to support the need for a further examination, since even with a blade/cylinder clearance of 2 chords increases in noise were detectable. Such clearances are used on real helicopters.

9. Although differences between the theory and experimental results were found, overall it seems fair to conclude that the theory is sufficiently accurate for it to be applied to the full scale positive pitch (downflow) conditions. Programs developed during this investigation could be applied directly to such cases.
10. A completely different theoretical approach will be necessary to take account of the apparent flow distortions associated with the negative pitch (upflow) case, since it appears that the noise is more a function of the wake shed by the cylinder. Theoretical models of the form developed in connection with the blade/gust interaction (Chapter 6) could form the basis for such a method.

TABLE 7.1: CYLINDER PRESSURE STUDY

Cylinder Pressure	Theory (+ve & -ve pitch)	Experiment	
		+ve pitch	-ve pitch
Variation with Rotor Speed (V)	✓	✓	X
Variation with Separation (H)	✓	X	✓
Variation with Blade Pitch ( )	X	X	X
Function of angle	✓	✓	X
Radial Distribution	✓	X	✓

✓ condition examined. X condition not investigated.

TABLE 7.2: TEST PROGRAMME

Blade Pitch (Degs)	Rotor/Cylinder Separation		Rotor Speed Range rpm	
	H (inches)	S (inches)	Min	Max
0	8, 10, 12, 14, 16	2, 4, 6, 8, 10	400	900
+2	8	2	400	890
+4	8	2	400	870
+6	8, 10, 12, 14, 16	2, 4, 6, 8, 10	400	820
+8	8	2	400	780
+10	8	2	400	745
+12	8, 10, 14, 16	2, 4, 6, 8	400	700
-2	10, 12, 14	4, 6, 8, 10	400	870
-4	10, 12, 16, 16	4, 6, 8, 10	400	800
-6	10, 12, 14, 16	4, 6, 8, 10	400	800
-8	14	8	600	
-10	14	8	600	
-12	14	8	600	

TABLE 7.3: TRANSIENT BLADE LIFT

ψ (DEG.)	TRANSIENT LIFT PER SPAN (LBS./INCH)
-40	-0.01219327
-36	-0.01380916
-32	-0.01575605
-28	-0.01800128
-24	-0.02029029
-20	-0.02170344
-16	-0.01942228
-12	-0.00568363
-10	0.01042067
- 8	0.03629335
- 4	0.11731388
0	0.17180791
4	0.11731388
8	0.03629335
10	0.01042067
12	-0.00568363
16	-0.01942228
20	-0.02170344
24	-0.02029029
28	-0.01800128
32	-0.01575605
36	-0.01380916

TABLE 7.4: CYLINDER PRESSURE RESULTS

(ROTOR SPEED; 600RPM; H= 10", δ=90° $r = 0.95R_T$).

ψ (DEG.)	TIME (SECS.)	PRESSURE, P (LBS/IN^2)
-40	-0.01111	-0.0002687
-36	-0.01000	-0.0002902
-32	-0.00888	-0.0003055
-28	-0.00777	-0.0002990
-24	-0.00666	-0.0002991
-20	-0.00555	0.0000202
-16	-0.00444	0.0007991
-12	-0.00333	0.0032766
- 8	-0.00222	0.0117735
- 4	-0.00111	0.0414837
0	0	0.0862634
4	0.00111	0.0414837
8	0.00222	0.0117735
12	0.00333	0.0032766
16	-0.00444	0.0007991
20	0.00666	-0.0002991
24	0.00777	-0.0002990
32	0.00888	-0.0003055
36	0.01000	-0.0002902
40	0.01111	-0.0002687

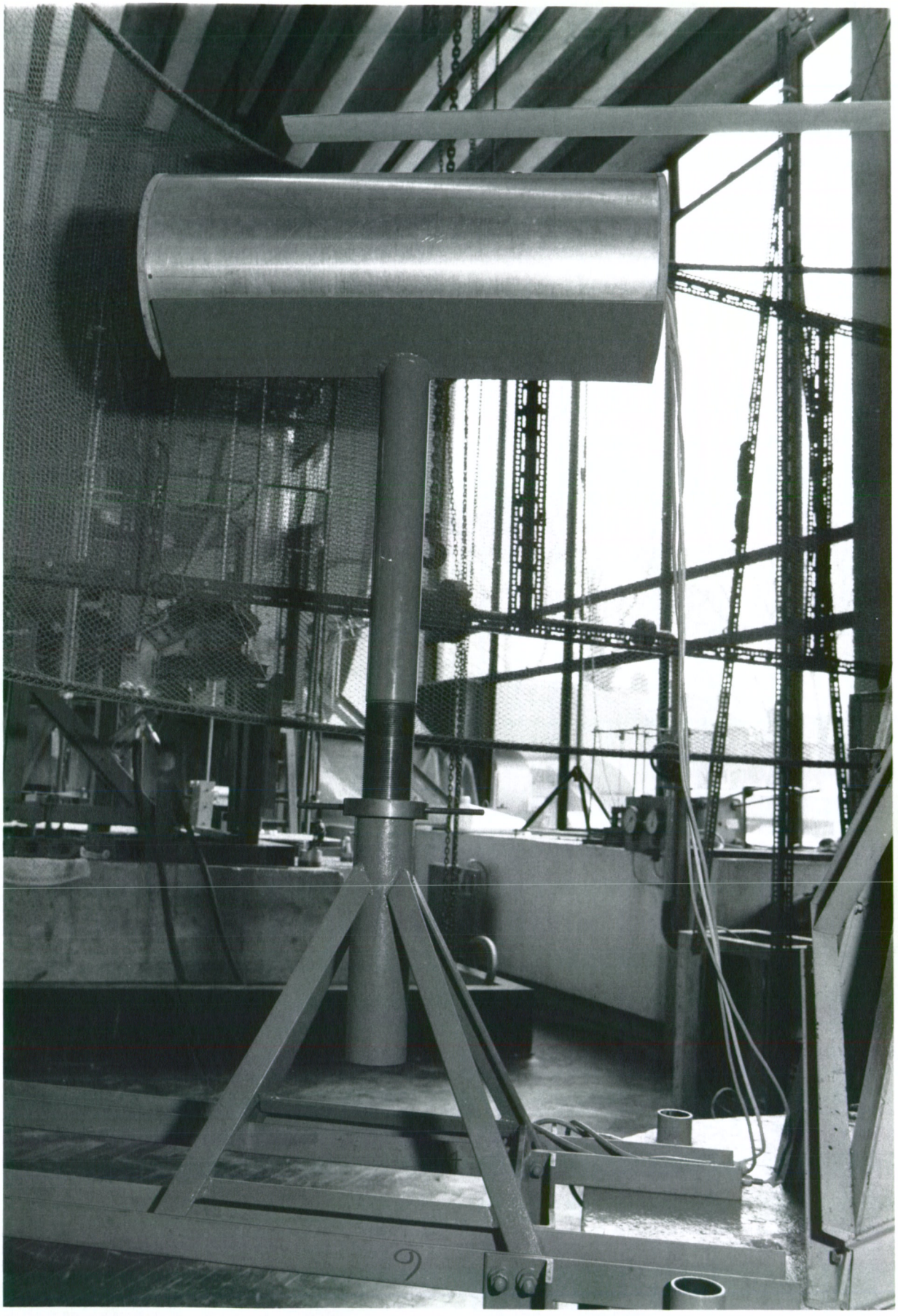

PLATE 7.1: ROTOR/FUSELAGE SIMULATION

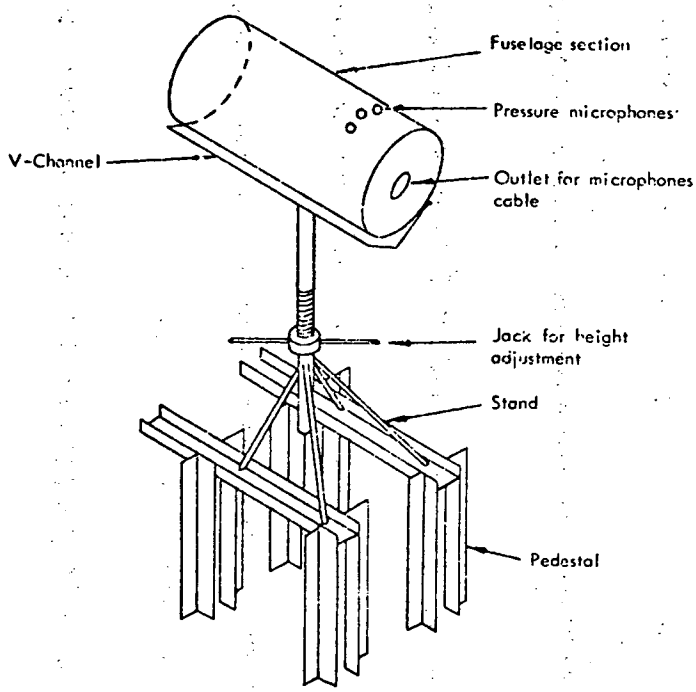

FIGURE 7.1. FUSELAGE MOUNTING FACILITY

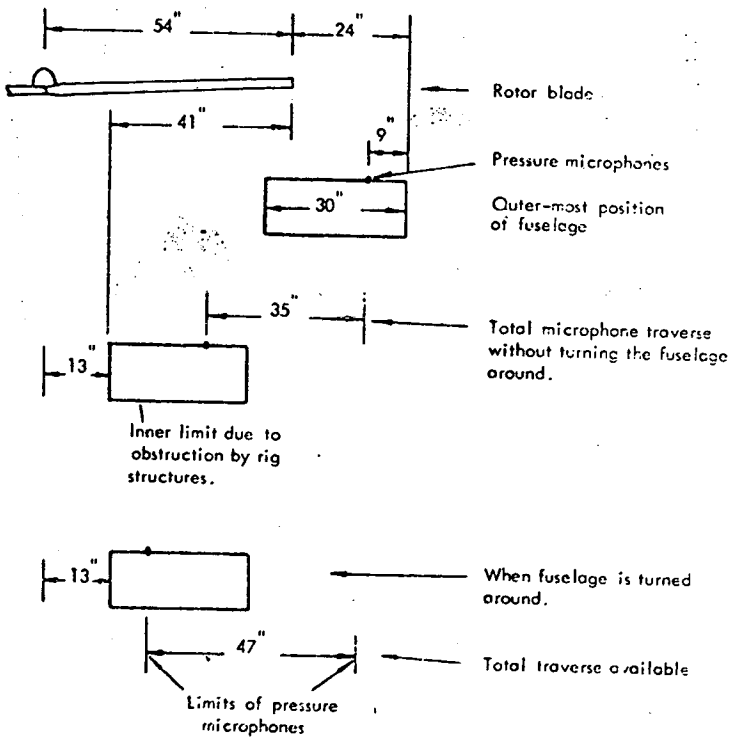

FIGURE 7.2. ROTOR/FUSELAGE (CYLINDER) ARRANGEMENT

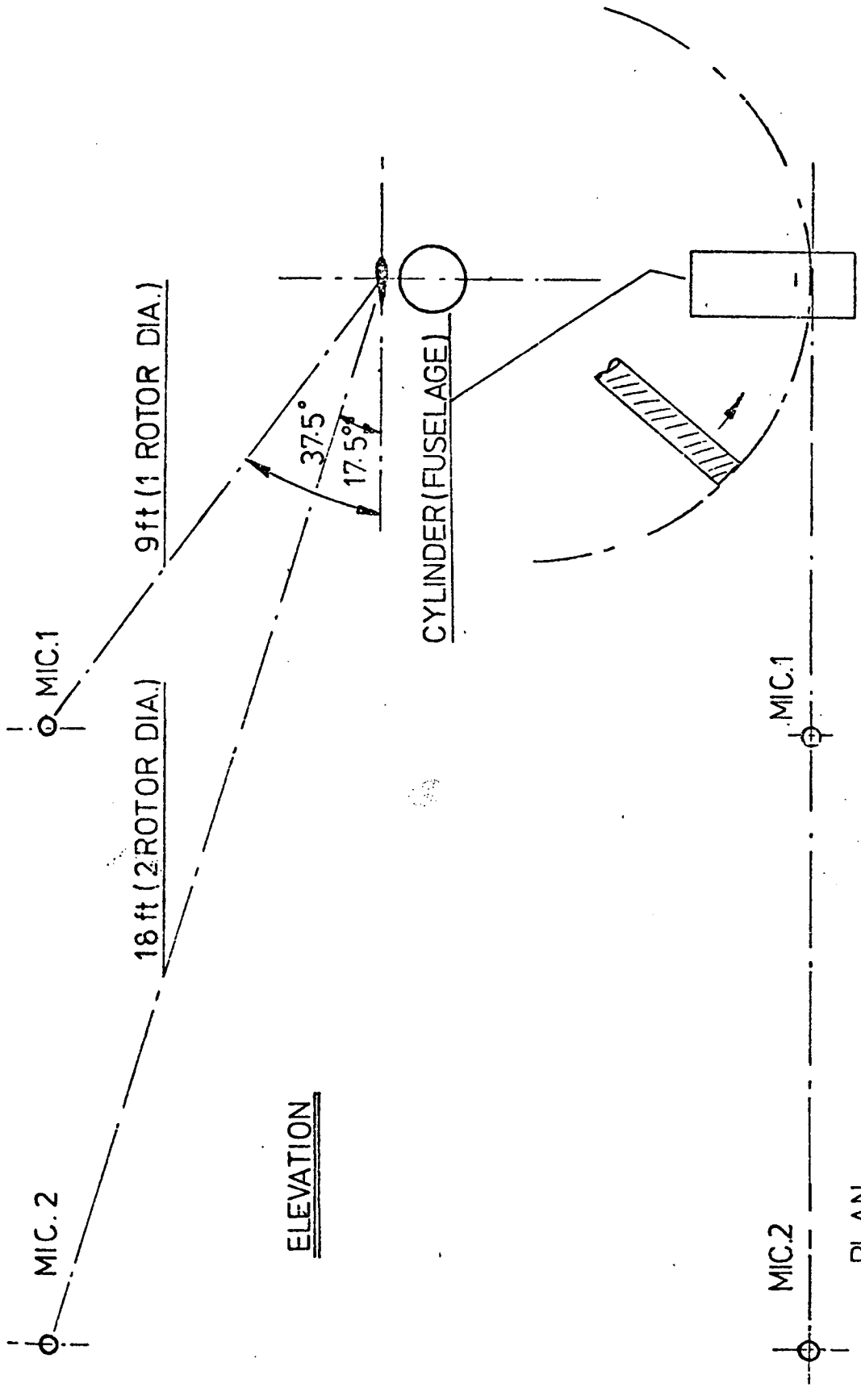

FIGURE 7.3. MICROPHONE POSITIONS

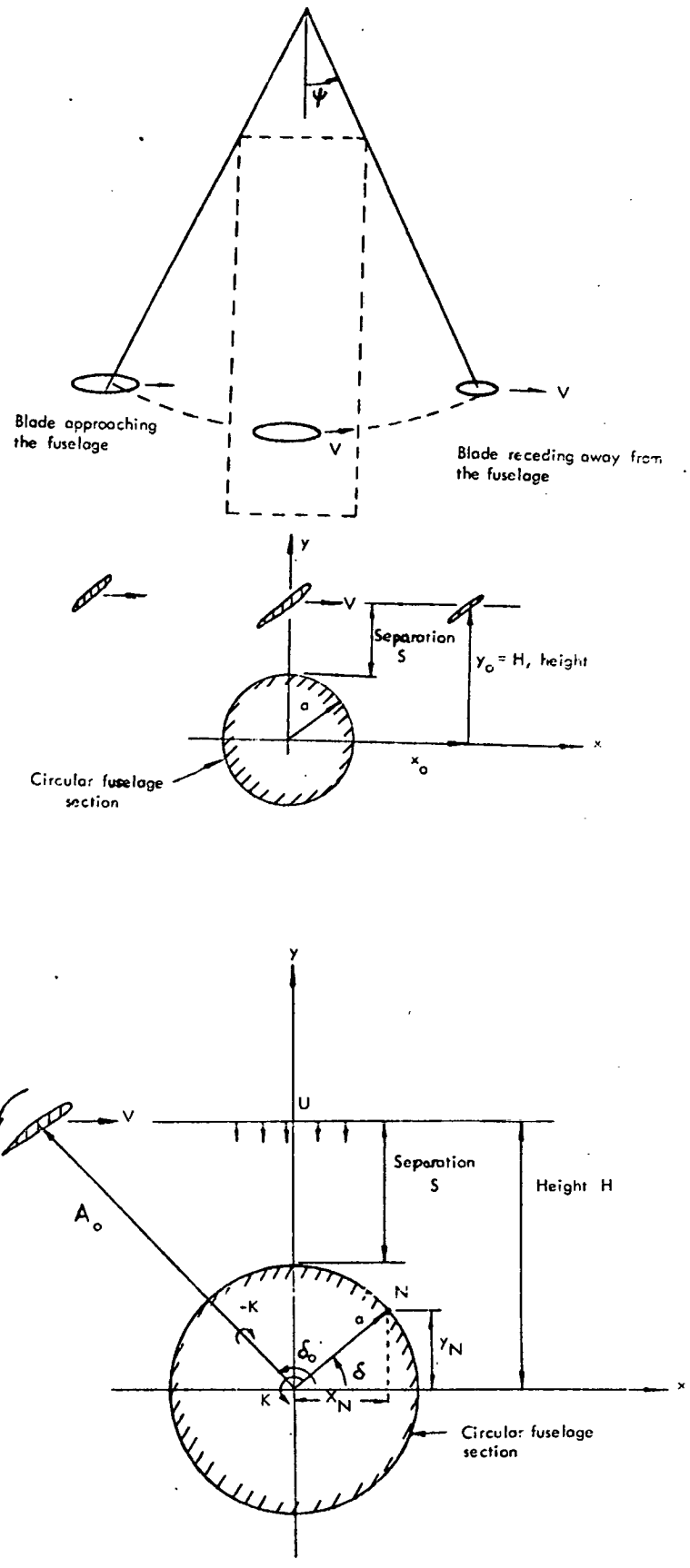

FIGURE 7.4. DIAGRAMMATIC REPRESENTATION OF PASSAGE OF BLADE OVER CYLINDER

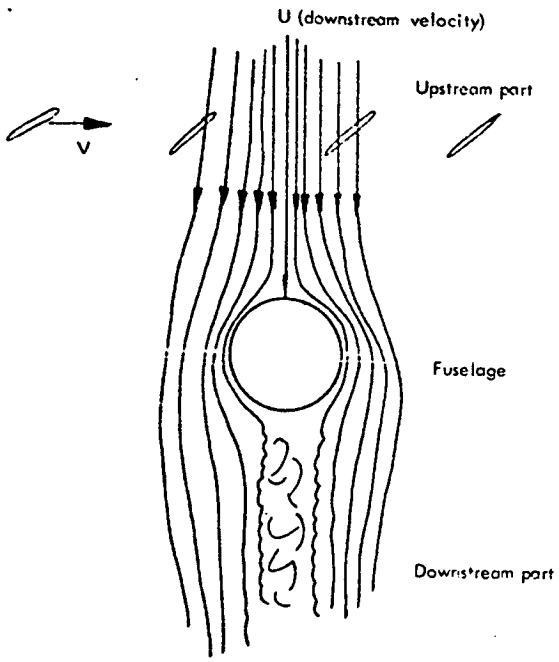

(a) Positive Pitch (Downwash) Case

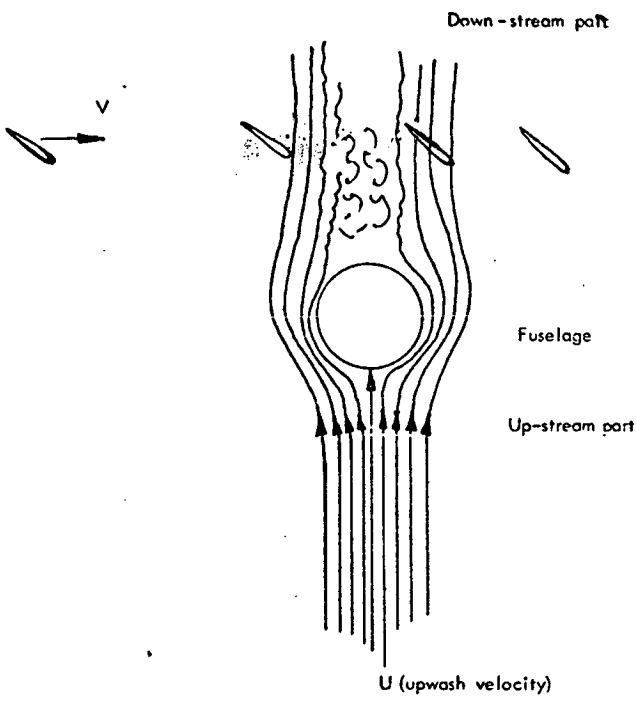

(b) Negative Pitch (Upwash) Case

FIGURE 7.5. DIAGRAMMATIC REPRESENTATION OF ROTOR/FUSELAGE FLOW FIELD

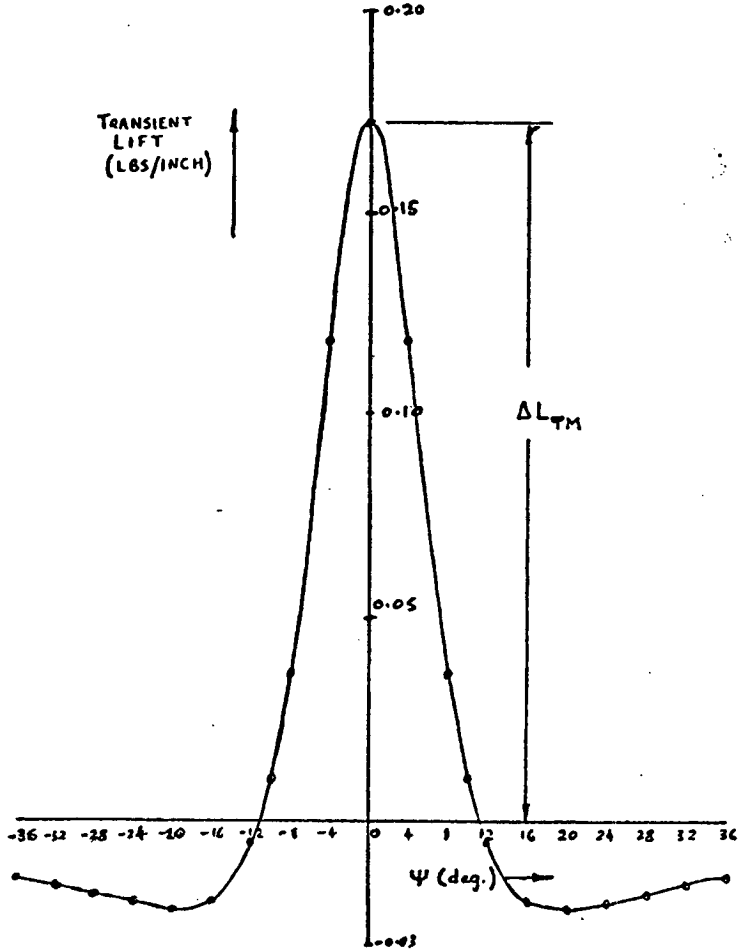

FIGURE 7.6. TRANSIENT BLADE LOADING

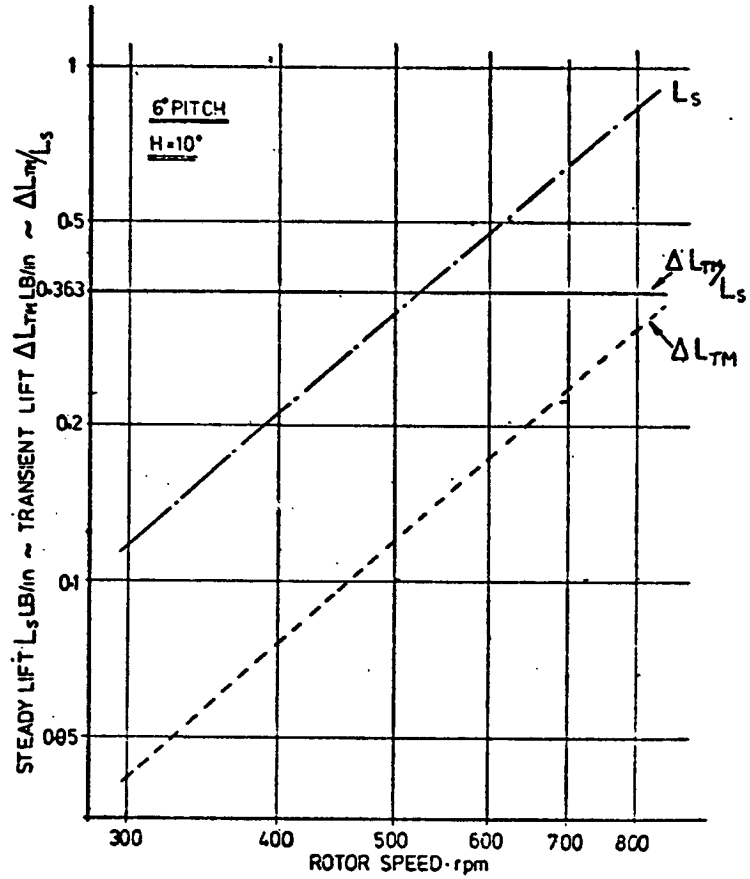

FIGURE 7.7. VARIATION OF BLADE LOADING WITH ROTOR SPEED

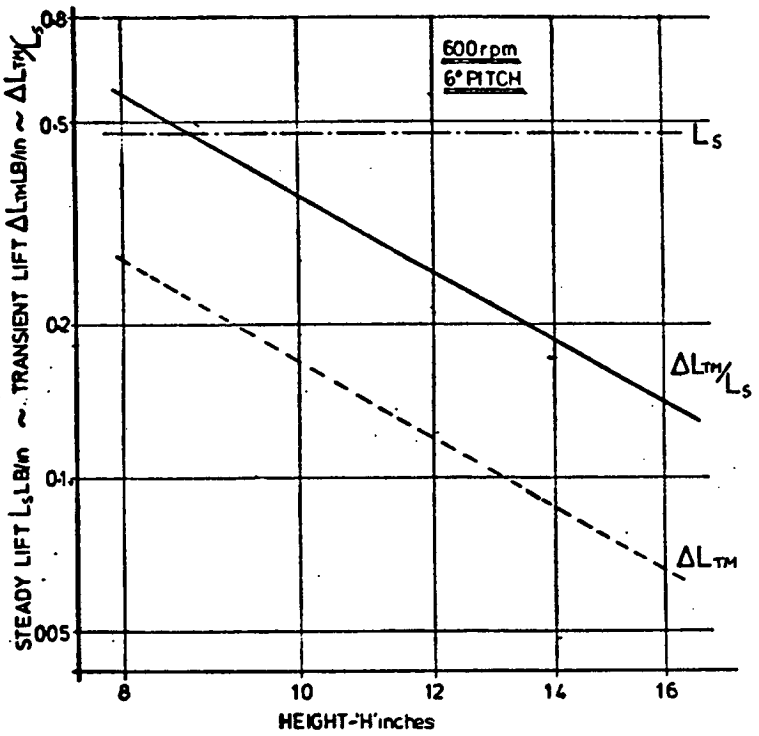

FIGURE 7.8. VARIATION OF BLADE LOADING WITH ROTOR/ CYLINDER SEPARATION

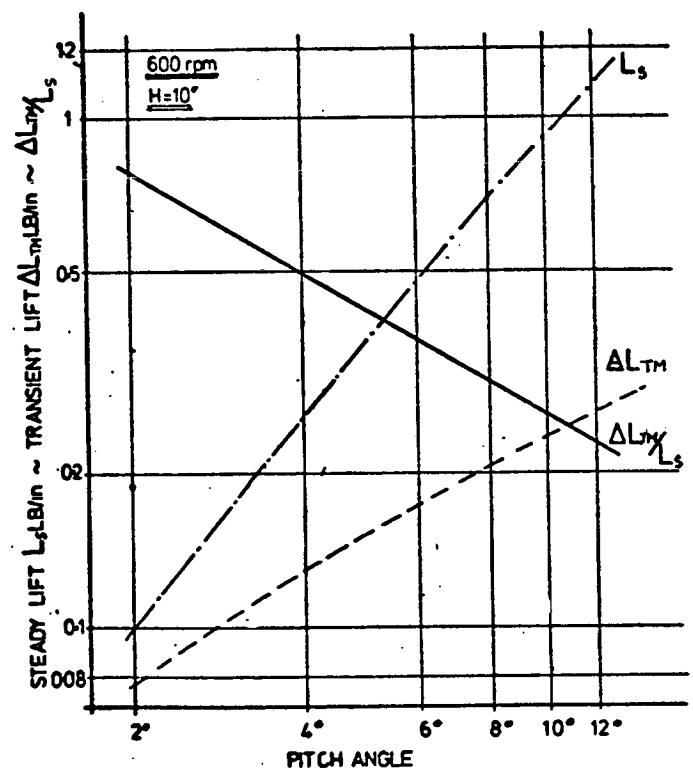

FIGURE 7.9. VARIATION OF BLADE LOADING WITH PITCH ANGLE

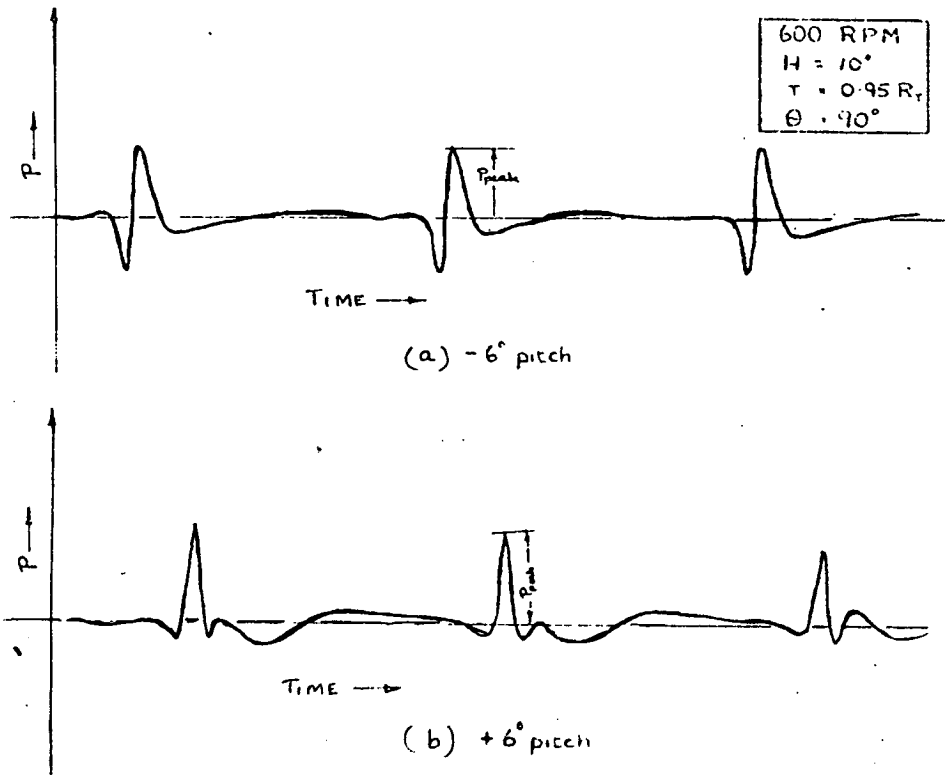

FIGURE 7.10. CYLINDER PRESSURE TIME HISTORY TRACES

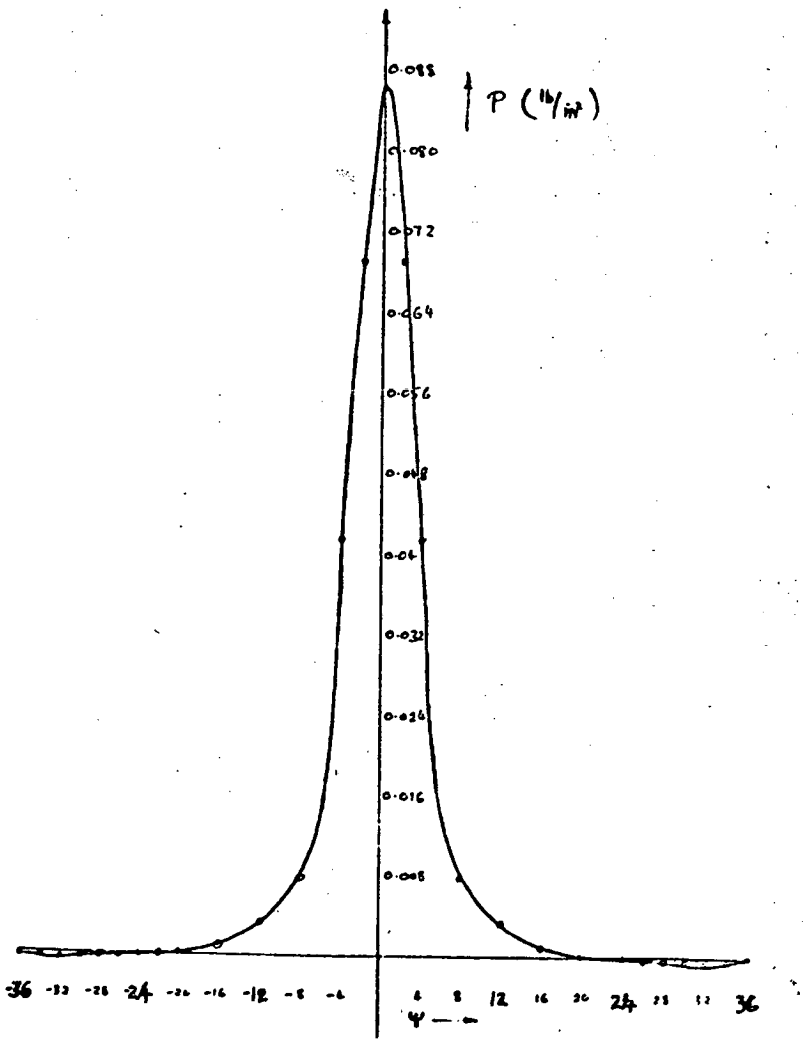

FIGURE 7.11. THEORETICAL CYLINDER PRESSURE - VARIATION WITH ANGLE

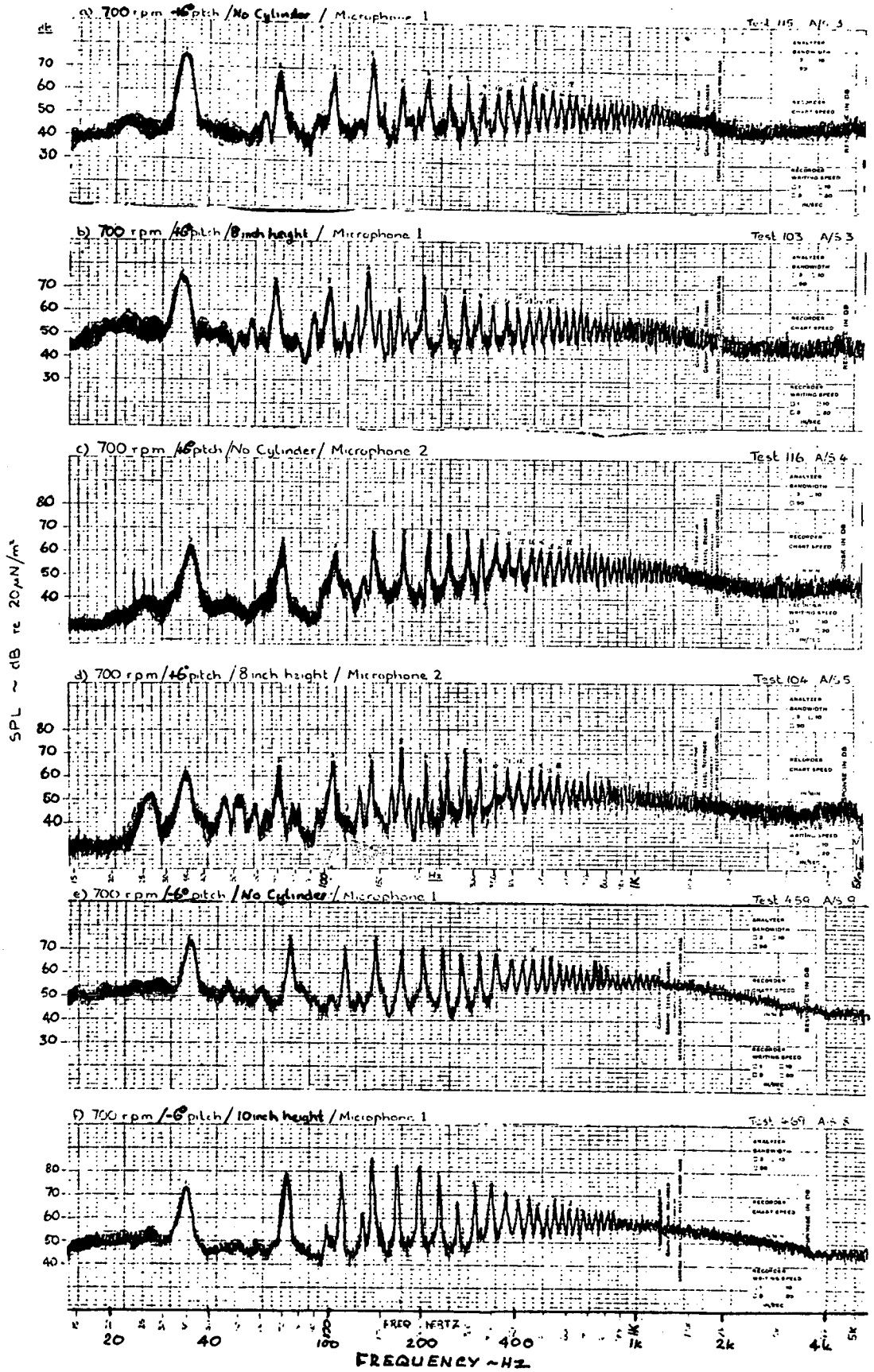

FIGURE 7.12. NARROWBAND ANALYSIS

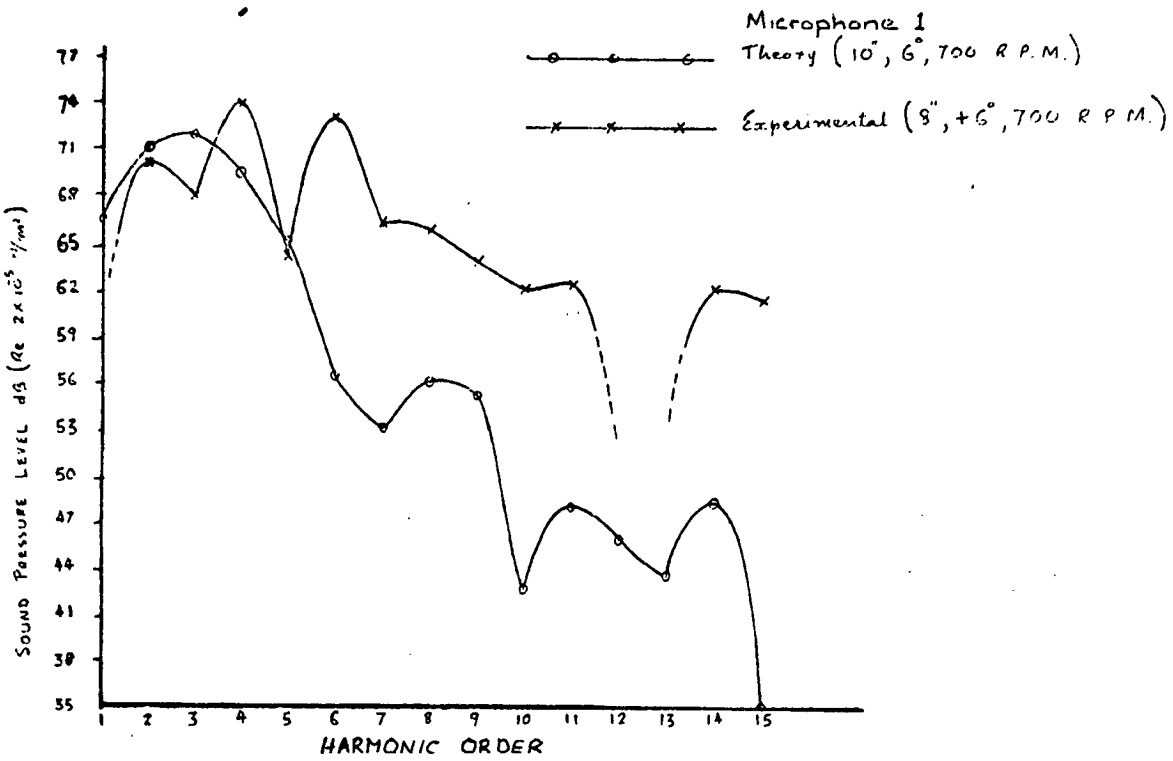

FIGURE 7.13. COMPARISON OF THEORETICAL AND EXPERIMENTAL RESULTS (POSITIVE PITCH CASE)

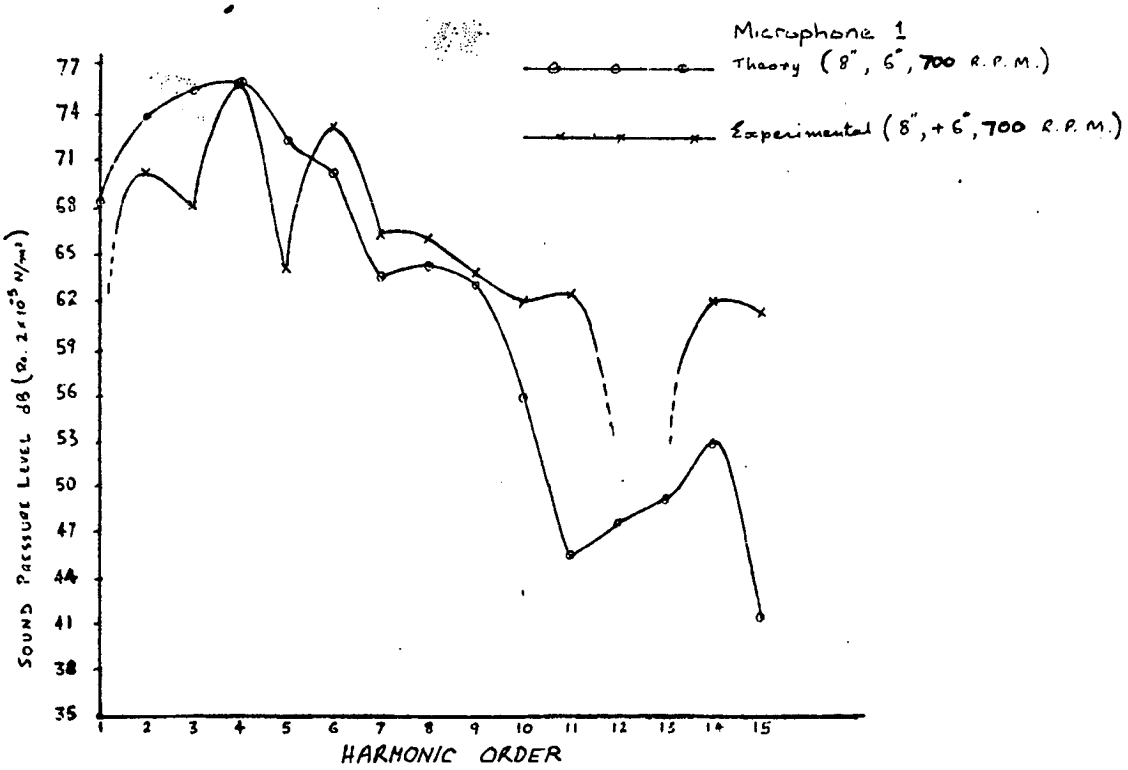

FIGURE 7.14. COMPARISON OF THEORETICAL AND EXPERIMENTAL RESULTS (POSITIVE PITCH CASE)

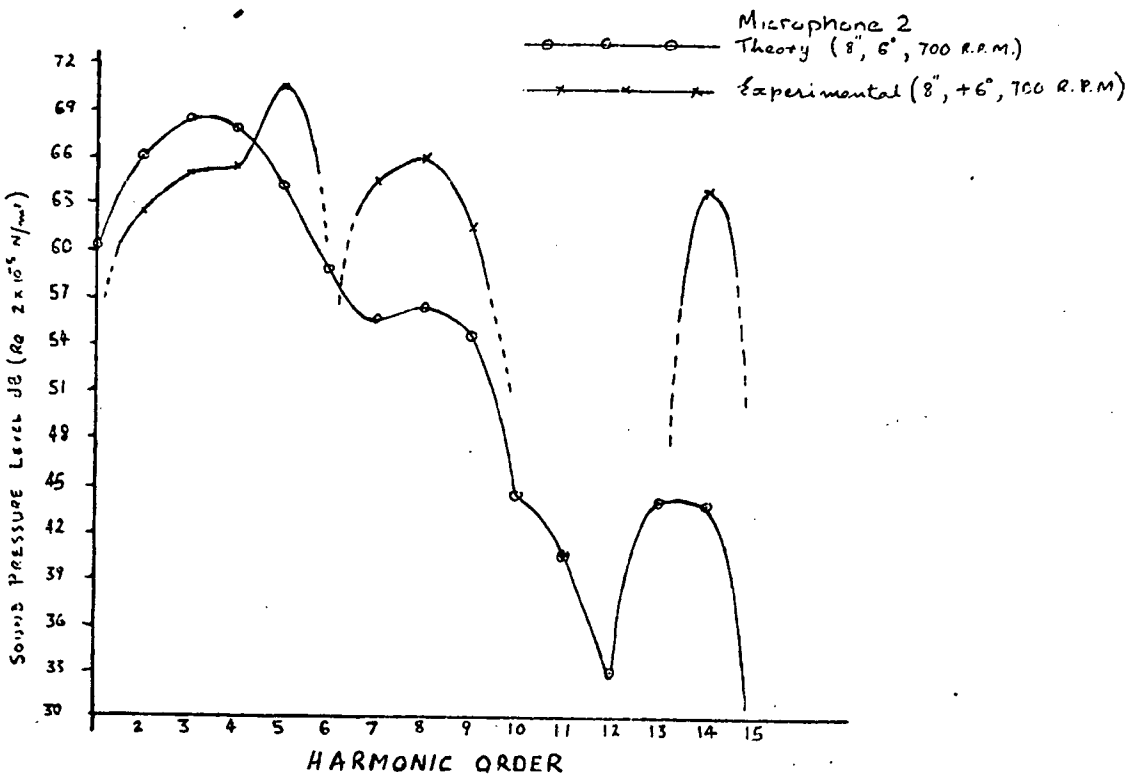

FIGURE 7.15. COMPARISON OF THEORETICAL AND EXPERIMENTAL RESULTS (NEGATIVE PITCH CASE)

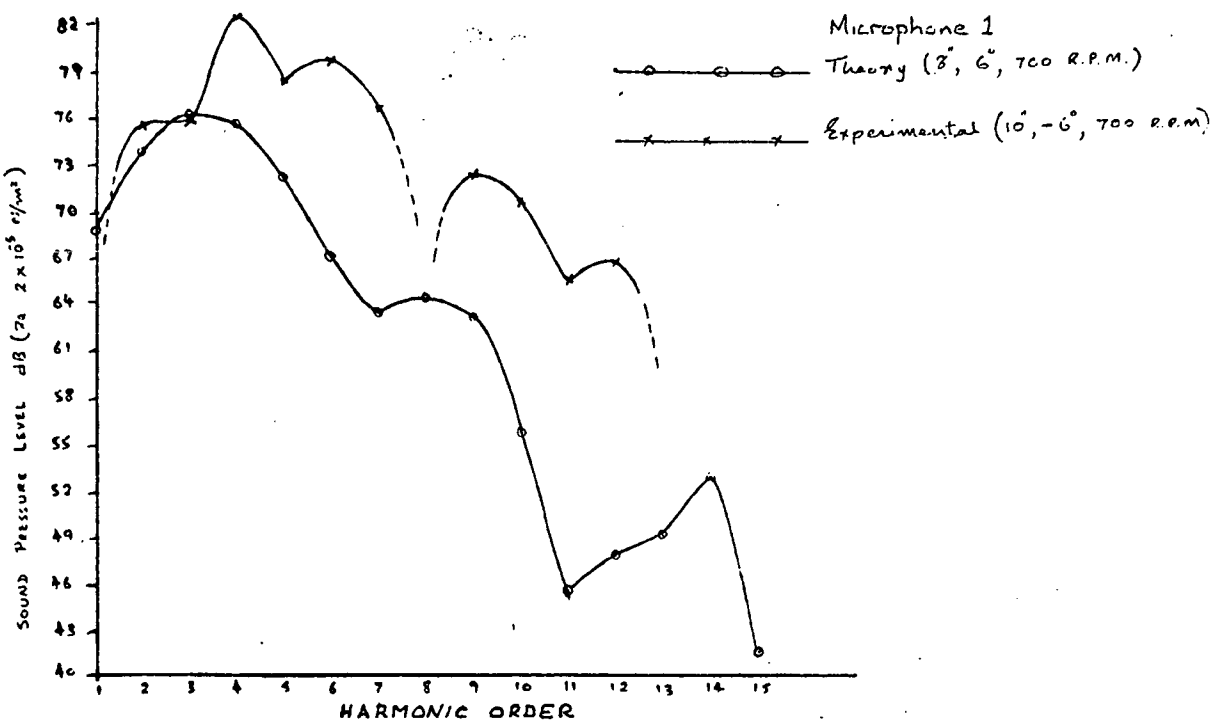

FIGURE 7.16. COMPARISON OF THEORETICAL AND EXPERIMENTAL RESULTS NEGATIVE PITCH CASE)

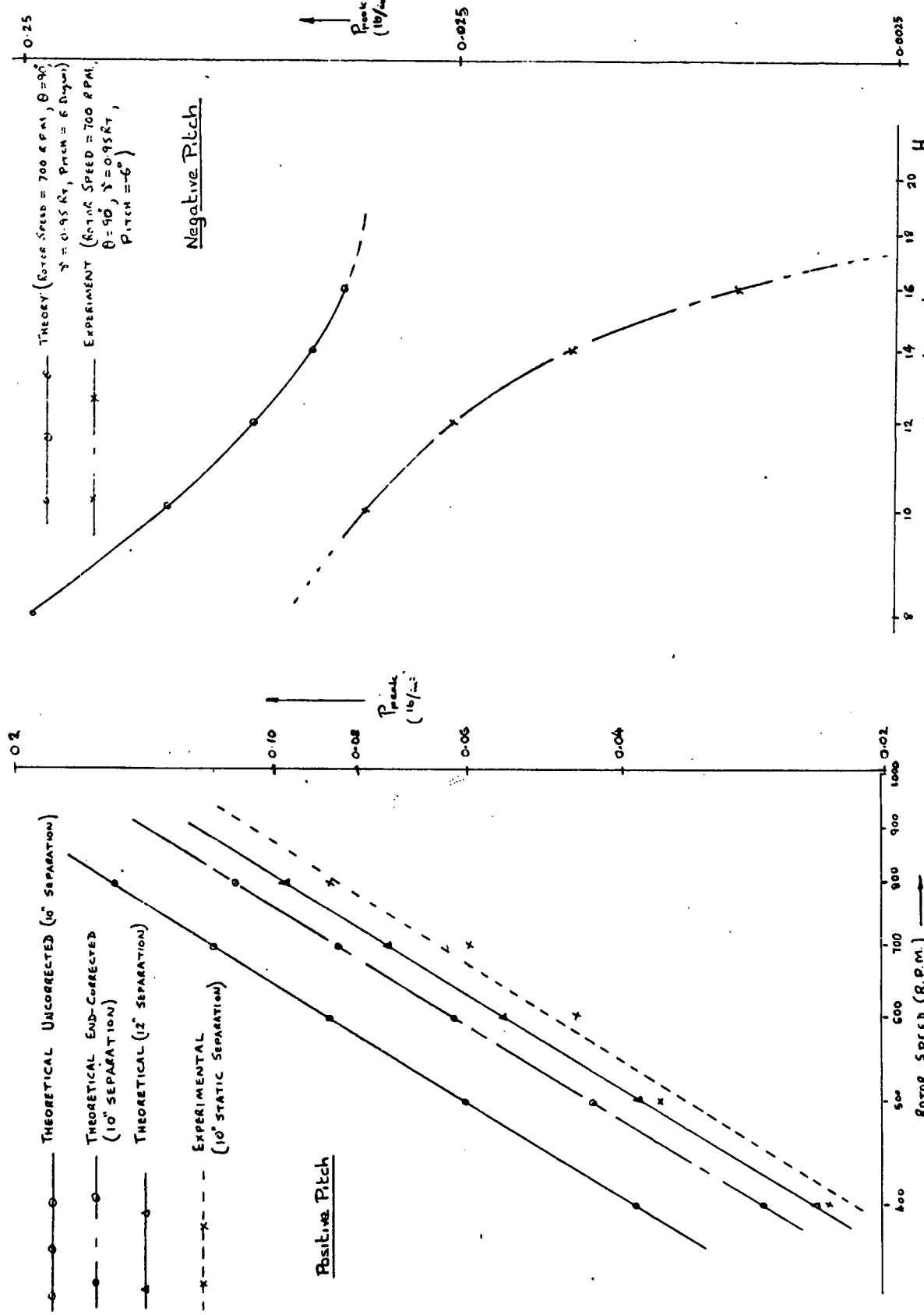

FIGURE 7.17. PEAK CYLINDER PRESSURE vs ROTOR SPEED (POSITIVE PITCH CASE)

FIGURE 7.18. PEAK CYLINDER PRESSURE vs SEPARATION DISTANCE.

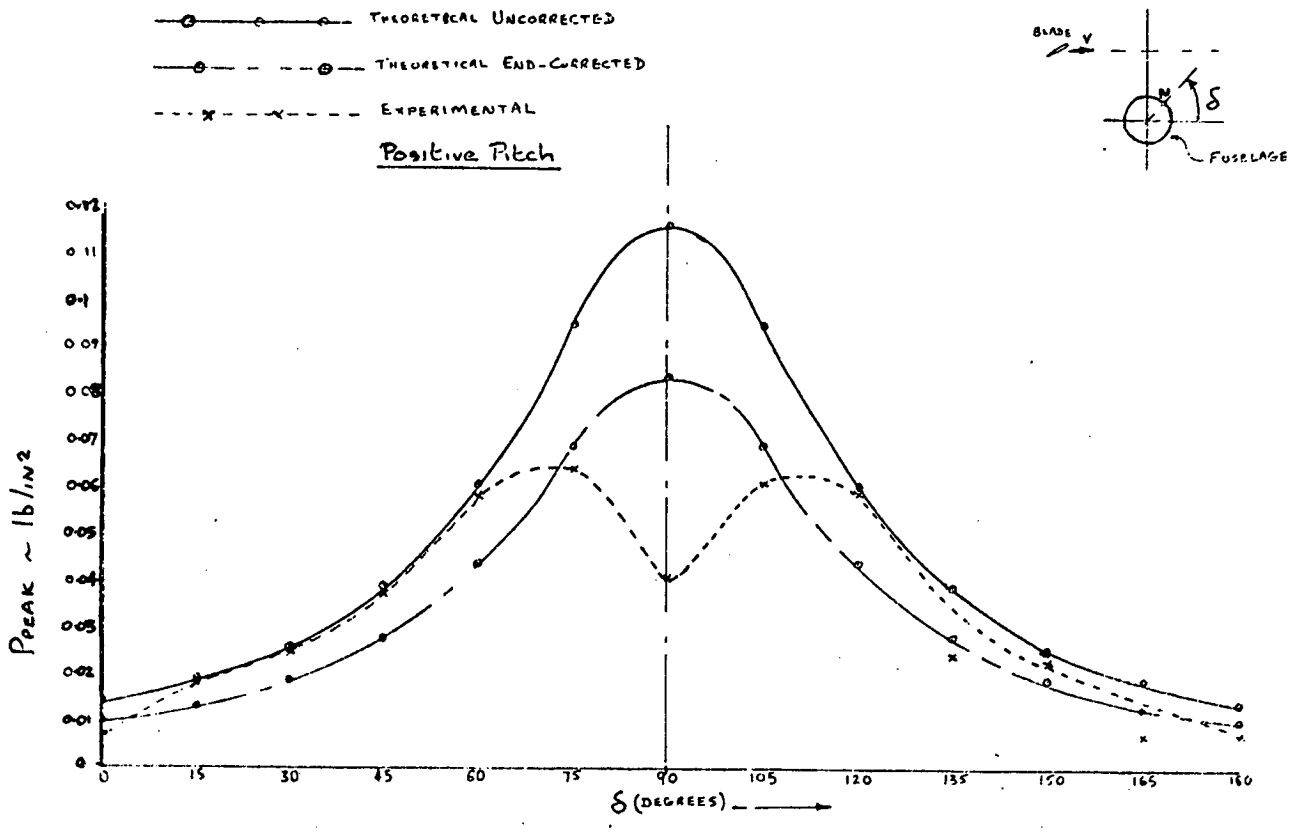

FIGURE 7.19. CIRCUMFERENTIAL PRESSURE DISTRIBUTION

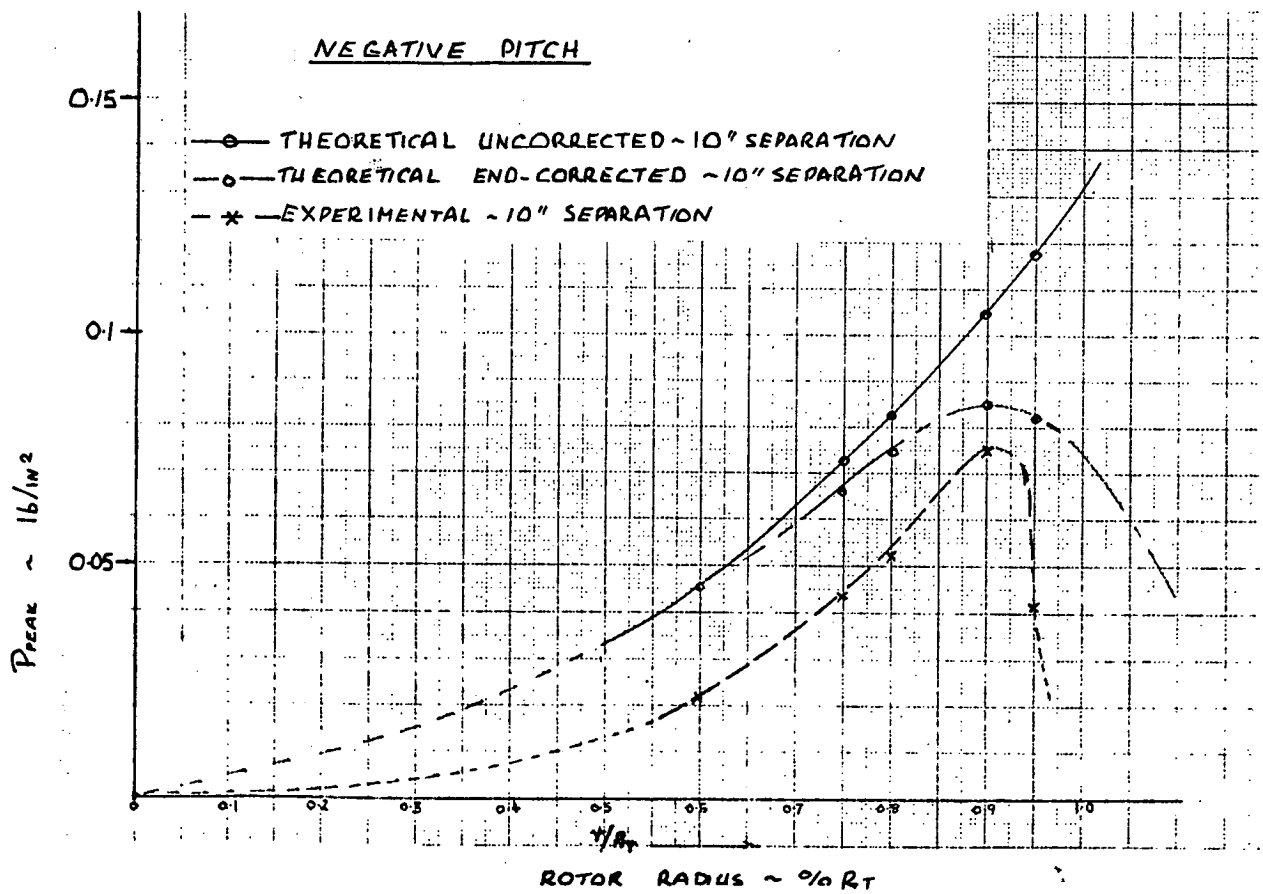

FIGURE 7.20. RADIAL (LENGTH) DISTRIBUTION OF PRESSURE.

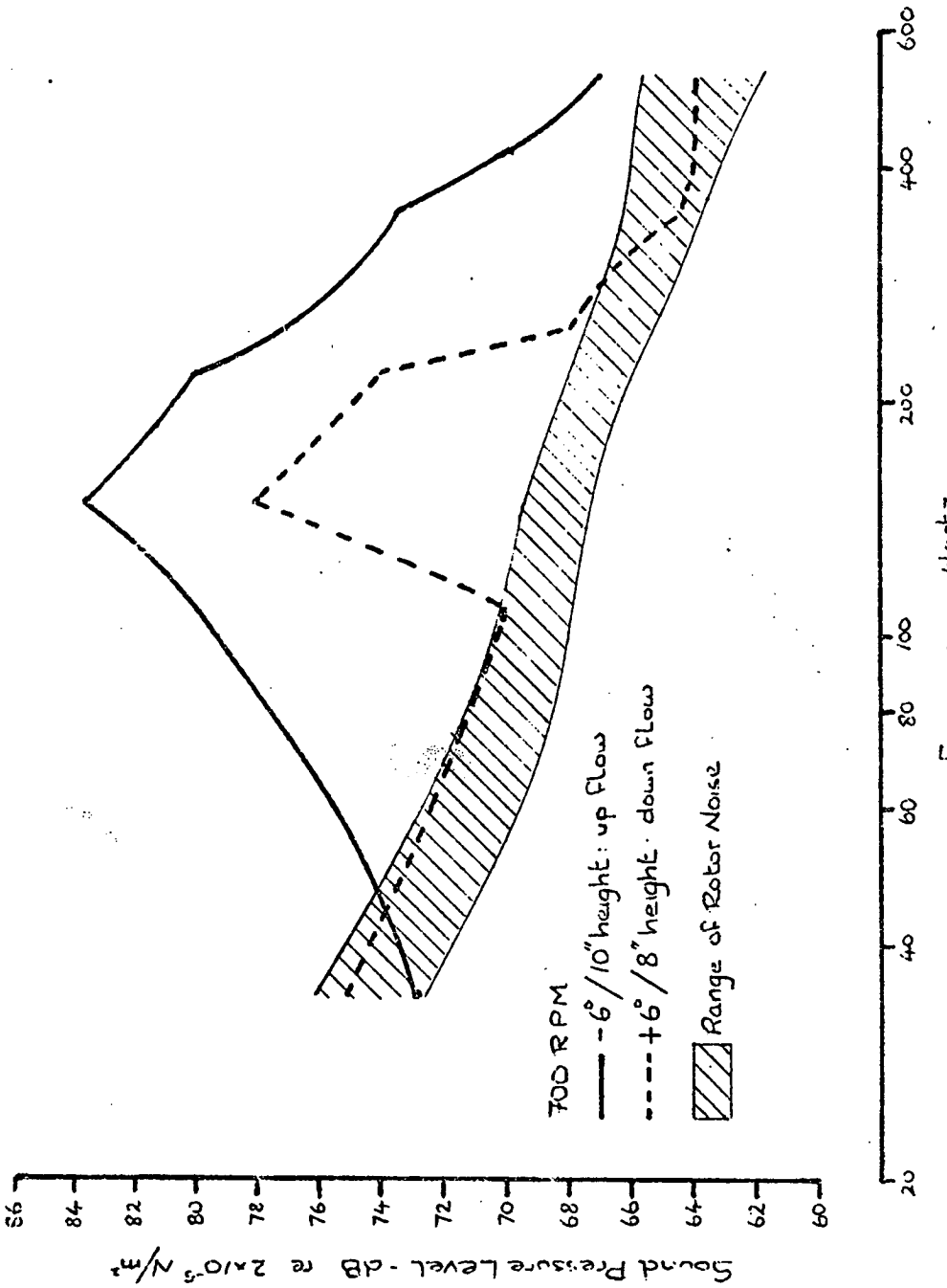

FIGURE 7.21. ROTATIONAL NOISE: COMPARISON OF POSITIVE AND NEGATIVE PITCH RESULTS.

CHAPTER 8: CONCLUSIONS

8.1. INTRODUCTION

The detailed specific conclusions relating to each topic studied as part of this programme are detailed at the end of the appropriate chapter. It is not proposed to repeat or summarize these detailed conclusions in this chapter, but rather to concentrate on the aspects which are of wider interest and highlight the commonality between the results of the various topics investigated. In addition the implications of the results obtained on the noise generated by a real helicopter, and the rotor design/configurations which can be used for its control, are reviewed. For convenience and clarity these general conclusions are discussed under specific headings although, of course, they are in many cases inter-related.

The acoustic theories used in the various investigations reported in this thesis were in the main based on the work of Lighthill [112]. In addition to the theoretical developments made by (and under the guidance of) the author, use was made of the theoretical models and computer programs devised by Wright [28, 31], Wright and Tanna [29] and Tanna [18, 130]. In these theories the mechanism is assumed to be dipole in nature and although in the early blade slap work the source was treated as a point dipole (compact source), distributed (non-compact) sources were considered in the case of the blade/gust and blade/fuselage interaction studies. In general it was assumed that these theories were applicable to the cases under investigation and hence any inadequacies of the theories from a fundamental point of view were not examined. It follows that no attempt was made to comment on the work of Ffowcs Williams and Hawkings [131] who have suggested that quadrupole sources may be explicitly identified as important in the generation of discrete (rotational) noise on a rotor. Such a mechanism, and any non-linear effects not accounted for in the theories would, however, only be expected to be distinctively significant on high speed rotors and hence the test programmes conducted as a part of this study are not suited to studying such aspects. It is also worth noting that any departure from the theories arising from refraction of the sound by the (air) flow field and any other flow effects on the rotor, are likely to be small since even in the case of a real helicopter the typical velocity of the 'downwash' (mean flow) is only 75 ft/s (23 m/s; Mach No. 0.07).

8.2. OVERALL PROGRAMME

The programme outlined in this thesis was aimed at furthering the understanding of helicopter rotor noise and in particular transient effects. As a natural consequence it has covered a large number of topics since helicopter noise is a complex combination of the noise generated from a number of sources each of which generates noise by several mechanisms. In general terms this programme has shown that although it would be difficult, if not impossible, to calculate the basic rotor noise characteristics because of the limitations of available aerodynamic models, the noise arising from well defined and specific interactions - transient effects - which give rise to excess noise can be successfully predicted. This is not meant to imply that every detail resulting from a blade/discrete flow field interaction can be established, but rather that the main controlling parameters can be estimated and that the available theoretical models are sufficiently accurate for general use.

8.3. IMPACT ON ROTOR NOISE OF TRANSIENT EFFECTS

Most transient effects or discrete interactions result in a dramatic increase in the rotational (discrete frequency) noise and in particular the higher harmonics. This is understandable since such disturbances act over a relatively small area of the complete rotor disc and, since this is small compared to the distance between the rotor blades, it generates frequencies well above that associated with the blade passing interval. The influence on the broadband noise is very much less marked and in many cases it would seem that the broadband noise is independent of such effects. As the length and/or area of the disturbance is increased, however, it would appear that the broadband noise exhibits a slight increase. This was clear in the case of the blade/gust interaction study when the gust length was extended to 7 chords. Even so the increase was small and at $6\frac{1}{4}$ chords a slight drop in the broadband noise level occurred. This was probably associated with some type of stalling effect or breakdown in the steady flow condition, but cannot at this time be fully explained.

8.4. ROTATIONAL NOISE

Rotational (discrete frequency) noise, in particular the higher harmonic content, is very sensitive to transient effects. Marked increases in the level of noise can be generated by even small flow disturbances and because of its impulsive nature it is usually subjectively

annoying. These effects become more marked as the rotor speed is increased and thus transient effects are very important on high tip speed rotors. It is generally considered that the 'base rotational noise' associated with a 'clean rotor' is a function of the inlet flow and/or self generated flow field disturbances. It follows, therefore, as found in practice, that rotational noise (relative to broadband noise) is also more significant on high speed rotors.

The transient effects, which can be considered to give rise to excess noise, can be relatively easily predicted provided the corresponding aerodynamic blade loads/lift fluctuations can be calculated. This was demonstrated in the case of blade/gust interaction, blade/fuselage interaction (downwash condition) and blade/vortex intersection studies since in each of these the flow characteristics could be defined. It follows by implication that the noise from other forms of flow disturbance, even if they act over a large area of the rotor, can be calculated if the aerodynamic blade response can be modelled. Thus in addition to being able to predict the transient effects it should ideally be possible to do the same, as suggested in a number of theoretical studies, for the complete 'base noise' of any rotor. The situation is, however, very much more complex since firstly it is not practicable at the present time to establish the 'base' inflow (or blade response) characteristics and secondly, even if these were known, the three dimensional effects which occur at the tip cannot be defined with any accuracy. The position on a real rotor is further complicated by the fact that in addition to the steady and fluctuating forces which arise, thickness effects have to be considered. Until recently the impact of blade thickness on noise was only considered to be important at blade tip speeds approaching Mach 1; evidence now suggests that it may be a significant parameter at much lower tip speeds and that the actual projected blade thickness has an impact on the noise level. It would appear that in addition to the levels the character of the basic rotational noise is also very dependent on the absolute tip speed and it is clear from the model and full scale results that a full understanding is not yet available. By implication on a real helicopter the situation relating to the main rotor becomes even more complex due to numerous, and unpredictable, flow disturbances and interactions which can occur. In the case of the tail rotor, noise prediction is even more difficult since it is subjected to the influence of the main rotor wake, the tail pylon and the discrete wake shed by the rotor head and fuselage itself.

In the above discussion it is assumed that the limitations are connected with the determination of the aerodynamic conditions in which the rotor is operating. Although this is in general true it is worth noting that in the acoustic theories available the importance or otherwise of the chordwise distribution and the relative merits of using the 'real chord' or an 'effective blade chord' in the calculations need clarification. This is a relatively important point since differences at high frequency from using the two approaches can be as large as 20 dB.

Analysis of the basic rotational noise on a 'clean full scale' rotor has indicated that it correlates reasonably well with the projected blade thickness based on the blade angle of attack. This suggests that the self generated flow field is likely to be more significant than the inflow conditions. If this is the case then the shed wake and the boundary layer would be important. Thus it would seem sensible to place some effort on examining this aspect since the self generated flow field should be quantifiable. Some credibility is given to this argument since results from a 'wide' range of 'clean rotors' show very similar spectrum characteristics even though the size of the rotors and test environments are very different. On the other hand the aerofoil parameters such as blade/chord ratio, blade/span ratio, etc., are very similar on the majority of helicopter rotors and it may be that the blade responds in a similar manner to a wide range of inflow conditions. It is well established that if a rotor is subjected to a large disturbance the higher harmonics increase significantly while some of the lower harmonics remain relatively constant. Thus in addition to the self generated wake effects, it is likely that the scale of rotor, relative to the inflow distortions, is important and thus on a 'dirty' rotor the inflow conditions would be likely to control the noise.

With these considerations taken into account it seems fair to conclude, therefore, that even though the transient effects which give rise to excess rotational noise can be readily predicted, it is likely to be a considerable time before the 'basic' rotor rotational noise can be estimated to the desired accuracy.

8.5. BROADBAND NOISE

The observation from the transient rotor noise studies that the broadband noise was insensitive to such changes agreed well with the general survey of the low frequency broadband rotor noise and the parallel investigation conducted with use of real helicopter results.

This showed that, unless the flow disturbance was very high, the level of low frequency broadband noise was essentially a function of the blade geometry and tip speed. More detailed studies revealed that it was dependent also on the effective blade thickness or angle of attack. At first glance this may appear to be a contradiction since the transient effects also give rise to variation in the angle of attack. In this case, however, the changes in the angle of attack occur over a relatively small area of the blade and for a relatively short period and there is insufficient time for the blade circulation characteristics to change. For this reason the blades do not stall, even if the angle of attack range for a short gust is several times above the classic stall angle value. It follows therefore that changes in the low frequency broadband noise would not be expected until a significant portion of the rotor disc was subjected to such effects. In this context wind would not be expected to have a marked effect since the 'gust size' is usually relatively small compared to the size of a real rotor and a uniform disturbance, such as in a wind tunnel, would be required before large changes in the level of low frequency broadband noise would be expected. The reverse is true in the case of rotational noise and the smaller the area of disturbance (in general terms) the higher the levels of rotational noise and more marked the transient or impulsive effects.

There is very little real understanding of the basic mechanisms involved in the generation of broadband noise although it does appear to be associated, in some way, with the shed (vortex) wake. As in the case of the rotational noise, the nature of boundary layer is therefore likely to be important, particularly since in this case it is clear that the noise is self generated and essentially independent of the inflow conditions. Yudin's proposal [59] that the noise varied with $C_D.S.V^6$ appears to explain the general trends, but except for the fact that at high lift the drag is proportional to the thrust there seems to be no direct evidence for the thrust dependency assumed by many investigators. Recent analysis indicating that the noise varies with the blade thickness based on the angle of attack (and hence indirectly thrust) again seems to suggest that the shed wake is important.

Differences in the spectral characteristics between the model rotor and helicopter results on the one hand and the full scale results on the other seem difficult to understand, but since other investigations on full scale rotors have shown similar trends to those of the author this requires further investigation since it may help in defining the mechanism involved.

From the observation of the insensitivity of low frequency broadband noise to gust effects, etc., it follows that empirical and semi-empirical formula can be developed and this observation also explains why the available prediction methods are so accurate on the particular family of rotors for which they were developed. It would seem that the main controlling parameters are V, S and α where V is the tip speed, S the blade area and α the angle of attack. Since on a helicopter the thrust T is directly related to S and α, it is clear why many of the predictions formula have a thrust dependency (usually T^2) term. It also follows, since in the majority of cases the empirical constant associated with such formulae have been derived from rotors operating at their design limit, that the formulae, which usually take the form of $V^x T^y$ or $V^x.T^y.S^z$, would be expected to break down when applied to a rotor which is operating well off its design condition or one of a very different type. This is the case in practice and hence the conventional formula cannot be used to predict, for example, the 'ground idle' case where the rotors are unloaded (zero thrust).

8.6. MODEL vs FULL SCALE

8.6.1. Rotational Noise

The 'basic' rotational noise characteristics determined from the model rotor and the full scale rotor exhibited a number of important differences which cannot be really explained. If on the other hand a well defined blade/flow field interaction is considered then the model rotor and full scale rotor give identical and predictable results. This was clearly illustrated in the case of the blade slap where real helicopter measurements agreed well with those derived by simulating blade/tip vortex interaction on a model rotor. These observations have a much wider implication since it is implied that although a model is well suited to studying transient effects, it is considerably less acceptable if used to investigate the basic rotational noise characteristics associated with a real helicopter rotor. Intuitively this is understandable since if the 'basic' rotational noise is dependent to some extent on the inflow characteristics then the ratio of the physical size of the rotor, say, to the size of the eddies in the flow would be expected to be important. Also the 'tip effects' may be very dependent on the actual Reynolds number. From the point of view of the study of tail rotor noise, however, use of a model has obvious advantages. Firstly the level of rotational noise to broadband noise is high as on a real tail rotor and secondly on a tail rotor the main mechanisms of interest arise

from interaction effects such as blade/pylon interference, main rotor tip vortex/tail rotor interaction, etc. Thus the problems associated with fully explaining the 'base' or datum noise characteristics are not encountered.

The above comments are based on the general observations made of the rotational noise characteristics. Some of these objections may, however, be overcome if the data is examined in a greater depth since, as explained in Chapter 3, the model rotor at the higher tip speeds tested appeared to a first order to give results which correlated with those of the full scale rotor measured at a similar (but low) tip speed. This obviously requires further study before definite conclusions can be reached; in the meantime it would seem prudent to adopt the approach outlined previously. In this context it is worth noting that the apparent differences in the rotational noise on the model rotor and the full scale rotor did not appear to correlate with any Reynolds number effect, since in each case there was relatively well defined and repeatable variation in the noise with tip speed and pitch and/or thrust. If the changes had been a function of the different flow characteristics, the model rotor results would have been expected to show a change as the tip speed was increased and the laminar/turbulent boundary at a Reynolds number of 10^6 exceeded.

8.6.2. Broadband Noise

Unlike rotational noise, the characteristics of which appear to be very dependent on the size of the rotor, broadband noise can in principle be studied on either a model rotor or full scale rotor. There is one disadvantage in using a model rotor, however, in that the level of the broadband noise, relative to the rotational noise, is lower than on a full scale rotor. This can obviously present difficulties in recording and analysis due to higher signal-to-noise ratio requirements. If this aspect is overcome then, provided care is taken with the analysis, a model rotor is suitable for investigating broadband noise. Since, however, the level of both rotational noise and broadband noise is a function of the number of blades, a 4 bladed rotor would seem preferable to a 2 bladed design because of the lower rotational noise content.

8.7. REAL HELICOPTER CASE

8.7.1. Main Rotor

8.7.1.1. Rotational noise

From the comments on the sensitivity of rotational noise to input flow conditions and operating environment, it would be expected that vastly different spectral characteristics would be obtained from different helicopters, rotors, etc. This is,however,not the case and it has been shown that the rotational noise levels associated with full scale rotors (on whirl towers and helicopters) give spectra which are not greatly different in terms of the harmonic decay rate. This suggested that the fluctuating forces generated are to a first order similar and linked in some manner to the steady or mean lift. This would be the case if they were controlled by the magnitude of the tip vortex or possibly the shed wake. This warrants further review since it may offer a method of overcoming the problem of predicting the 'basic aerodynamic forces' and enable a satisfactory rotational noise prediction method, even if semi-empirical, to be obtained. This could take the basic form suggested by the author in Chapter 4, but rather than such a simple solution the spectrum would be expected to be dependent on the rotor parameters including the number of blades.

8.7.1.2. Broadband noise

Since it has been fairly conclusively shown that broadband noise is dependent only on the rotor geometry, tip speed and operating angle of attack α, it should be possible to develop a reliable prediction method to cover all rotors. Wright [31] has taken up this concept but this obviously requires further refinement to overcome the limitations imposed by his assumptions that the noise varies according to a fixed velocity law, irrespective of the absolute value, and the somewhat arbitrary selection of the 'α term'. Clearly, however, absolute thrust has little direct effect on the level of broadband noise, although its influence is taken into account in the 'α term'.

8.7.2. Tail Rotor

The impact on rotor noise of the flow distortions for the case when the flow is drawn over the fuselage is much more significant than due to the simple blockage effect when the downwash is directed over the pylon. Thus fuselage, or rather pylon (tail fin), effects are more important in the case of the tail rotor than the main rotor. This is particularly true in the case of many helicopters since in the 'hover'

or low speed flight case the flow is drawn over the tail pylon. Also there is a tendency to increase the tail pylon (tail fin) size, to provide improved stability and 'unload' the tail rotor in cruise flight. This has obvious disadvantages from the noise point of view. Also in this 'upwash' case the current theory developed by Bramwell and Johnston [21] is inappropriate. Even so ideally if the flow field could be determined the noise could be calculated from available fluctuating force theories. This area, however, requires further study since it is far from clear if the flow environment in which a tail rotor operates could be predicted. This is likely to be difficult because of the complex geometry of the conventional tail pylon (tail fin) and the general lack of knowledge on main rotor and tail rotor flow fields on a real helicopter.

8.8. QUIET HELICOPTER DESIGN

Over the typical operating range of a real helicopter, rotational noise varies approximately as V^{10} and the (low frequency) broadband noise as V^{6}. Rotational noise, relative to the broadband level, is more significant as the number of blades is decreased and the tip speed increased. It follows that to obtain a quiet rotor, it should be multi-bladed (5 or 6 blades being a practical limit) and operated at as low a tip speed as possible. A helicopter can be really designed to meet the lift (hover) requirements but if the tip speed is too low the upper flight speed and general performance would be severely limited. It is necessary to make a compromise and a 4 or 5 bladed rotor with a tip speed of the order of 650 ft/s would be desirable for a helicopter in the range of 10,000 lb to 30,000 lb AUW. The actual tip speed of blade parameters can be calculated to the accuracy required in project designs by using the generalised methods outlined in chapter 4.

Tail rotor noise is usually of a relatively high level and difficult to reduce. A tandem rotor configuration is therefore preferable to a 'Sikorsky type' layout with a main rotor and tail rotor. This assumes, of course, little or no main rotor/main rotor interaction since if it occurs very high levels of blade slap can be generated. The original Boeing Vertol V107 (CH-46) and Chinook (CH-47A) helicopters both suffered from this problem. The tandem rotor Belvedere on the other hand did not generate blade slap except in high banked turns. Boeing Vertol subsequently re-configured their Chinook (CH-47C) helicopter to give the Boeing 347. This had a raised rear pylon which

separated the two rotors and an extra blade was added to each rotor to reduce the tip vortex strength. This resulted in a design which had effectively two isolated main rotors and the noise level was very low, being no more than that associated with the small (3000 lb) Bell Jet Ranger, even though the AUW of the 347 was 34,500 lb [132].

Alternatively the same low noise levels could be produced by a side-by-side configuration as employed on the MIL MI-12 (USSR). This has two large 5 bladed rotors and the noise is mainly broadband in nature on this 200,000 lb AUW rotorcraft. In the smaller category of helicopter the tandem rotor concept has been employed a number of times on prototype helicopters in the USA such as the Filper BETA 200 (2 seat, 1700 lb), Filper BETA 400 (4 seat, 2530 lb) and the McCullock 4E (4 seat, 2400 lb), but these have never been produced for general use. Such designs do, however, illustrate that the tandem rotor principle can be applied across the complete helicopter size spectrum.

The need for a tail rotor can also be overcome by the use of co-axial contra-rotating arrangements where two rotors are run in opposite directions on the same shaft. This concept has been successfully employed by Kamov (USSR) on the 'Ka' range of helicopters. Recently Sikorsky (USA) have also taken up this concept in connection with their ABC design. Kaman (USA) adopted a slightly different arrangement on their Huskie helicopter in which the two rotors were on separate rotor shafts slightly displaced from one another such that the rotors operated like an 'egg beater'. On such designs, unlike on the tandem rotor and side-by-side configurations, interaction between the wake of the upper rotor and the blades of the lower rotor will occur. The severe 'blade slap' type interactions are unlikely to occur except at very high forward speed, due to the wake geometry. Thus the 'interaction noise' is likely to be more akin to rotational noise. There is no generally available theory but Lowson [133] has proposed a method, which suggests that for typical helicopter rotors the level of interaction noise will be well below the normal rotational noise. This is supported by test results from the Kaman Huskie [134] and a Servotex (UK) contra-rotating rotor [135] developed for the Canadair CL-84. There is, however, an indication from the data that, as expected, the harmonic content is similar to that associated with a 'dirty rotor' and thus the spectrum follows closely the 'upper curve' of the envelope discussed in section 4.7.1. From these observations, and a comparison of noise data for the Kaman Huskie with that derived from 'Sikorsky type' helicopters, it

seems fair to conclude that a contra-rotating rotor design is preferable (for the same tip speeds) to a main rotor/tail rotor configuration.

On a 'Sikorsky type' configuration with a main rotor and tail rotor, use of multi-bladed rotors is essential if the noise is to be kept to a minimum. Blade slap is very severe on a 2 bladed main rotor design because of high tip speed/high blade loading employed and the fact that in flight blade/tip vortex interaction in the less favourable form can easily occur; on the other hand it rarely occurs on a 4 bladed design. A similar situation arises in the case of the tail rotor which on many small helicopters is the most annoying source. Two bladed tail rotors are commonly chosen for weight reasons and if such designs are replaced by a four bladed rotor, preferably at lower tip speed, then significant reduction can be obtained as demonstrated by Hughes [136].

The case relating to the tail rotor is, however, generally more complex and the direction of rotation and position relative to the main rotor has also to be considered. Obviously it is not possible to remove completely the tail rotor from the flow field of the main rotor. In principle the tail rotor could be positioned such that the complete rotor was above, in flight, the wake shed by the main rotor. In this case the rotational direction should be 'top of blade forward' so that the lower blade, if it interacts with the main rotor wake, would be at the mimimum combined 'tip + forward' speed. Such a layout, due to offset forces, etc., is impracticable and hence the rotor should be positioned below the influence of the main rotor or as low as possible. In this case the rotation direction should be 'top blade rearwards'. This layout may result in the tail rotor being positioned mid way up the tail pylon (tail fin) rather than, as conventionally adopted, at the top. This solution is considered to be preferential even though the 'blockage' will be increased, since it is estimated that any main rotor wake, and hence main rotor tip vortex, interactions with the tail rotor will be likely to be more severe than the pylon blockage effects. This will be particularly true under cruise and high speed flight conditions. Ideally, of course, the blockage should also be kept to a minimum and hence the rotor/pylon clearance should be as large as practicable.

Once the layout, etc, has been chosen to reduce the rotor interactions to a minimum, the overall aim should be, in the case of a 'Sikorsky type' design, to match the noise from the two rotors to obtain a balanced noise solution where subjectively the levels from two rotors

are the same. This will result in the tail rotor tip speed being lower than that of the main rotor, whereas traditionally they are the same. Attempts, by choice of the number of blades, etc., should also be made to lower the rotational noise even if this results in an increase in the level of the broadband noise. This is because broadband noise is subjectively less objectionable than rotational noise and on any 'clean' design minor distortion in the flow could result in an increase in 'excess' rotational noise which, on a dirty design, would not be noticed. Also broadband noise is to a first order independent of such effects.

If high tip speed rotors are used on helicopters then compressibility effects and blade thickness both become important. This is particularly true in the case of helicopters with 2 bladed main rotors which have large chord (and hence thick) blades. Thus again a multibladed rotor is preferred since smaller chord (thinner) blades can be employed. These effects can be reduced by thinning the blade in the tip region from the conventional 12% to, say, 6% which is an absolute minimum for structural reasons. Tip shapes also offer advantages in offsetting the drag rise and formation of 'shock waves' and according to some evidence change the structure of the generated tip vortex. There is, however, a practical limit to tip modifications and thickness reductions and because of the dynamic and aero-elastic constraints 'thin tip blades' are difficult and expensive to develop. Also at the present time there is no reliable theory, except those based on thickness effects which apply only to the high speed flight case, to guide the design. Thus control of noise on a high speed/high performance helicopter is difficult since the aerodynamic requirements are incompatible with the needs of a quiet helicopter. Even so a viable and acceptable helicopter from both the operational and noise point of view can be designed providing the rotor (main and, if applicable, tail rotor) tip speeds are maintained below about 675 ft/s and care is taken to minimise the interaction effects and keep the level of rotational noise, relative to the broadband noise, as low as possible.

REFERENCES

1. J.W. LEVERTON 1966 M.Sc thesis, University of Southampton. Helicopter Blade Slap.
2. J.W. LEVERTON 1968 NASA Contractor Report. NASA CR-1221. Helicopter Noise - Blade Slap; Part 1: Review and Theoretical Study.
3. J.W. LEVERTON 1972 NASA Contractor Report. NASA CR-1983. Helicopter Noise - Blade Slap; Part 2: Experimental Results.
4. J.W. LEVERTON 1966 ISVR Consultation Report No.1032. Investigation of Complaints arising from the operation of a helicopter service on to the Pan-Am Building, New York, USA.
5. J.W. LEVERTON 1967 ISVR Memorandum 197 - Selection of an Automatic Narrowband Analyzer for the Study of Helicopter Rotor Noise.
6. T.R. IVES and J.W. LEVERTON 1971 Westland Research Paper RP 407 Measurement and Analysis of Rotor/Propeller Noise. (Abridged version: 1972 J.B.C.S.A. Conference Proceedings - The Recording and Interpretation of Engineering Measurements)
7. J.W. LEVERTON 1968 Proceedings of AGARD Conference on Helicopter Propulsion Systems, Ottawa, Canada, Paper 20. Helicopter Noise.
8. J.W. LEVERTON 1972 Proceedings AGARD Specialists' Meeting on Aerodynamics of rotary wings, Marseille, France. The noise characteristics of a large clean rotor.
9. J.W. LEVERTON and J.S. POLLARD 1972. Proceedings of American Helicopter Society Mideast Region Symposium on Status of Testing and Modeling Techniques for V/STOL Aircraft, Essington, Penn, USA. Paper 17. A Comparison of the Noise Characteristics of Full Scale and Model Helicopter Rotors.
   Also 1973 J. Sound Vib 30(2), 135 - 152
10. M. NOAK 1967 Proposal - Department of Aeronautics and Astronautics, University of Southampton. An experimental investigation on the effect of blade tip planform on the aerodynamics of a helicopter rotor.
11. J.S. POLLARD and J.W. LEVERTON 1972 Westland Research Paper RP 414. Effect of Blade Tip Planform on the Noise and Aerodynamics of a Helicopter Rotor.
12. A.R. WHATMORE 1969 M.Sc thesis, University of Southampton. A Study of Transient Noise from Helicopter Rotor Blades.

13. J.W. LEVERTON 1973 Journal of the American Helicopter Society, Technical Notes. Helicopter Noise - Are Existing Methods Adequate for Rating Annoyance or Loudness?

14. J.W. LEVERTON 1975 Proceedings First European Rotorcraft and Powered Lift Aircraft Form, Southampton, England. Helicopter Noise Assessment.

15. J.W. LEVERTON 1975 Journal of Sound and Vibration, 43(2). Helicopter Noise: Can it be adequately rated?

16. A.D. DODSON 1969 M.Sc thesis, University of Southampton. An investigation into Rotor Rotational Noise of Helicopters in the Single and Tandem Rotor Configuration.

17. J.W. LEVERTON 1971 J. Royal Aeronautical Society, Vol 75 No.726, 385-397. The Sound of Rotorcraft.
Also 1970 Westland Research Paper, RP 390

18. H.K. TANNA 1968 ISVR Technical Report No.12. Computer program for the prediction of rotational noise due to fluctuating loading on rotor blades.

19. C.B. AMOR 1972 ISVR Contract Report 72/73. Transient Rotor Noise Study (Phase 1 Final Report)

20. C.B. AMOR and J.W. LEVERTON 1972 Proceedings of American Helicopter Society Mideast Region Symposium on Status of Testing and Modeling Techniques for V/STOL Aircraft, Essington, Penn, USA. Paper 16. An investigation of Impulsive Rotor Noise using a Model Rotor.
Also 1973 J. Sound Vib 28(1), 55-71

21. A.R.S. BRAMWELL and J.B.B. JOHNSTON 1965 RAE Technical Report No.65127. A theory of the aerodynamic interference between a helicopter rotor blade and a fuselage and wing in hovering and forward flight.
Also 1965 ARC Memoranda No.3514.

22. S.H. DEVANI 1974 ISVR Contract Report 74/15. Transient Rotor Noise Study, Phase II - Final Report.

23. S.E. WRIGHT and J.W. LEVERTON 1969 Proceedings of the Third CAL/AVLABS Symposium on Aerodynamics of Rotary Wing and V/STOL Aircraft, Buffalo, NY, USA. Helicopter Rotor Noise Generation.

24. J.W. LEVERTON 1975 Proceedings AIAA 2nd Aero Acoustics Conference, Hampton, Va, USA, Paper 75-451. Discrete Frequency Rotor Noise.

25. J.W. LEVERTON 1972 Westland Research Paper, RP 419. The Noise Characteristics of a large 'clean' rotor.

26. A.S. HALLIDAY and D.K. COX 1960 NPL Technical Report. Wind Tunnel Experiments on a Model of a Tandem Rotor Helicopter.

27. N.J. STAINER 1969 M.Sc.thesis, University of Southampton. An Experimental Investigation into Rotational Noise for a low Solidity Rotor.

28. S.E. WRIGHT 1968 ISVR Technical Report No.5. Sound Radiation from a Lifting Rotor Generated by Asymmetric Disc Loadings.

29. S.E. WRIGHT and H.K. TANNA 1969 ISVR Technical Report No.15. A computional study of rotational noise.

30. J.B. OLLERHEAD and M.V. LOWSON 1969 USAAVLABS Technical Report 68-60. Studies of Helicopter Rotor Noise.

31. S.E. WRIGHT 1971 J. Sound Vib. 17, 437 - 498. Discrete radiation from rotating periodic sources.

32. J.W. LEVERTON and R.E. COUSER 1967 ISVR Memorandum No.169. Helicopter rotor noise - single bladed rotor results.

33. J.W. LEVERTON 1973 Westland Research Paper. RP 438 (3 Parts). A Further Investigation of Rotor Noise (Final Report)

34. J.W. LEVERTON, B.J. SOUTHWOOD, A.C. PIKE and M.C. WOODWARD 1976. Proceedings of the Second European Rotorcraft and Powered Lift Aircraft Forum, Paper No.17. A revaluation of Helicopter Main Rotor Noise.

35. J.W. LEVERTON 1967 ISVR Memorandum, No.194. Helicopter Noise (Report for the period 1 Dec. '66 to 30 May '67).

36. J.W. LEVERTON 1969 ISVR Memorandum, No.311. Helicopter Rotor Noise, Final Report: Part II - Experimental Study of Rotor Noise.

37. A.C. PIKE, B.J. SOUTHWOOD, M.C. WOODWARD and J.W. LEVERTON 1975 Westland Research Paper RP 521 (3 Parts). Helicopter Rotor Noise Research - Analysis of Recorded Data.

38. L.Y. GUTIN 1936 Physikalische Zeitschrift det sowjetunion, Vol.9 No.1. Translated 1948 NACA Technical Memorandum, TM-1195. On the Sound Field of a Rotating Propeller.

39. J.O. GODDARD and T.J. STUCKEY 1964 Westland Report No.AAD 4/1. Investigation and Prediction of Helicopter Rotor Noise. Also 1967 J. Sound Vib. 5(1), 50-80.

40. I.M. DAVIDSON and T.J. HARGEST 1965 J. Royal Aeronautical Society Vol.69. Helicopter Noise.

41. R. SCHLEGEL, R. KING and H. MULL 1966 USAAVLABS Technical Report 66-4. Helicopter Noise Generation and Propagation.

42. S.E. WIDNALL 1966 AIAA Journal. Vol 6. A Correlation of Vortex Noise Data from Helicopter Main Rotors.

43. L.H. WILKES 1968 Westland Research Paper, RP 349. Noise Research on Helicopter Rotors.

44. M.V. LOWSON, A.R. WHATMORE and C.E. WHITFIELD, 1972 Loughborough University of Technology Report TT 7202. Source mechanisms for rotor noise radiation.

45. C.R. COX 1969 Proceedings of 3rd CAL/AVLAB Symposium on V/STOL Aerodynamics, Buffalo, NY, USA. Rotor Noise Measurements in Wind Tunnels.

46. R.G. SCHLEGEL 1971 Proceedings US Army Helicopter Symposium, Durham, N.Carolina, USA. Summary Session Report.

47. R.H. SPENCER, H.STERNFELD and B.W. McCORMICK 1966 USAAVLABS Technical Report, 66-1. Tip vortex core thickening for application tc helicopter rotor noise reduction.

48. P.N. GODDARD 1971 Westland Research Memorandum, 92. An investigation into the effect of Blade Tip Planform on the Noise Generated by a Helicopter Rotor.

49. W.A. SPIVEY and G.G. MOREHOUSE 1970 Proceedings of 26th Annual National Forum of American Helicopter Society. New insights into the design of swept-tip rotor blades.

50. C.W. HICK and H.H. HUBBARD 1947 NACA Technical Note, No.1354, Comparison of Sound Emission from Two-blade, Four-blade and Seven-blade Propellers.

51. R.G. LOEWY and L.R. SUTTON 1966 Journal of Sound and Vibration 4(3). A theory for predicting the rotational noise of lifting rotors in forward flight, including a comparison with experiment.

52. P.J. NOAD 1963 Westland Aircraft, Fairey Aviation Division Report T.H.G. Note No.5/63. Theoretical Prediction of Helicopter Rotor Noise.

53. K.N. DODD and G.M. ROPER 1961 RAE Technical Note, M.S.45. A Deuce Programme for Propeller Noise Calculations.

54. B.A.M. PIGGOTT 1962 RAE Technical Note M.S.317. A Mercury Autocode Programme for Propeller Noise Integrals.

55. D.L. HAWKINGS and M.V. LOWSON 1976 Proceedings of AIAA 2nd Aero Acoustics Conference, Hampton, Va, USA. p.539. Tone Noise of High-Speed Rotors.

56. F. FARASSAT, R.J. PEGG and D.A. HILTON 1976 Proceedings of AIAA 2nd Aero Acoustics Conference, Hampton, Va, USA, p.601. Thickness Noise of Helicopter Rotors at High Tip Speeds.

57. H.K. TANNA 1968 Note prepared for Westland Helicopter Ltd. Helicopter Rotor Noise.

58. E.J. RICHARDS and D.J. MEAD (Editors), 1968 Noise and Acoustic Fatigue in Aeronautics. John Wiley and Sons Ltd.

59. E.Y. YUDIN 1944 Zhurnal Teknicheskoi Fiziki, Vol 14 No.9. Translation: 1947 NACA Technical Memorandum No.1136. On the Vortex Sound from Rotating Rods.

60. H.H. HUBBARD 1953 NACA Technical Note 2968. Propeller-Noise Charts for Transport Airplanes.

61. H.H. HUBBARD and A.A. REGIER 1947 NACA Technical Note 1358. Propeller-Loudness Charts for Light Airplanes.

62. J.W. LEVERTON and H.K. TANNA 1968 ISVR Consultation Report. SRN4 Hovercraft. Internal and external noise survey - preliminary report.

63. H. STERNFELD, R.H. SPENCER and J.O. SCHAIRER 1971 Boeing Vertol Report Prepared for U.S. Army Research Office, Ref.D210-10229-1. An investigation of noise generated on a hovering rotor.

64. J.D. SHILLADAY 1970 Westland Helicopter Research Paper, No.387. Helicopter and Convertible Rotorcraft Noise Estimation.

65. (WILSON REPORT) 1963 H.M.S.O. publication Cmnd 2056. Noise, Final Report.

66. 1967, British Standards Institution, BS.4142, Method of Rating Industrial Noise Affecting Mixed Residential and Industrial Areas.

67. F.B. BURPO and R.R. LYNN 1962 TCREC Technical Report 62-42. Measurement of Dynamic Airloads on a Full Scale Semi-Rigid Rotor.

68. J.A. SCHEIMEN 1964 NASA Technical Memorandum TMX-952. A Tabulation of Helicopter Rotor Blade Differential Pressures, Stress and Motions as measured in Flight.

69. R.G. SCHLEGEL and W.E. BAUSCH 1968 Sikorsky Aircraft Report (issued as USAAVLAB Technical Report 70-1B). Helicopter Rotor Rotational Noise Prediction and Correlation.

70. S.E. WRIGHT 1969 ISVR Technical Report No.14. Theoretical Study of Rotational Noise.

71. J.T. HOWLETT, S.A. CLEVENSON, J.A. RUPF and W.J. SNYDER 1977. NASA Technical Note, TD D-8477. Internal noise reduction in a large civil helicopter.

72. J.S. POLLARD and J.W. LEVERTON 1976 Proceedings Second European Rotorcraft and Powered Lift Aircraft Forum, Paper 19. Cabin Noise Reduction - Use of Isolated Inner Cabins.

73. BELL HELICOPTER CO. 1962 TCREC Technical Report No.62-73. A study of the origin and means of reducing helicopter noise.

74. F.W. TAYLOR 1965 M.Sc thesis University of Southampton. Helicopter Blade Slap.

75. J.W. LEVERTON and F.W. TAYLOR 1966 J. Sound Vib. 4(3), 345-357. Helicopter Blade Slap.

76. F.W. TAYLOR and J.W. LEVERTON 1966 Proceedings: U.S. Army Scientific Symposium. Helicopter Blade Slap.

77. R.L. BISPLINGHOFF, H. ASHLEY and R.L. HALFMAN 1957 Aeroelasticity. Addison Wesley Publishing Co, New York.

78. N.D. HAM 1967 Proceedings: American Helicopter Society 23rd Annual National Forum, Washington, USA. Stall flutter of helicopter rotor blades: A special case of the Dynamic Stall phenomenon.

79. F.O. CARTA 1967 AAIA Paper 67-18. The unsteady normal force response of an airfoil in a periodically distorted inlet flow including stalling effects.

80. F.D. HARRIS and R.R. PRUYN 1967 Proceedings: American Helicopter Society 23rd Annual Forum, Washington, USA. Blade Stall - Half Fact, Half Fiction.

81. N.D. Ham and M.I. YOUNG 1966 J. Sound Vib 4(3), 431-444. Limit Cycle Torsional Motion of Helicopter Blades due to Stall.

82. A.R. IVES 1967 Private Communications from Westland Helicopters Ltd.

83. H. STERNFELD 1967 AGARD Conference Proceedings, Paper No.22. Influence of the tip vortex on helicopter rotor noise.

84. Modern Developments in Fluid Dynamics - High speed Flow, Vol 11. Clarendon Press.

85. H.H. PEARCEY 1960 Proceedings of the 2nd International Congress in the Aeronautical Sciences, Zurich. The aerodynamic design of section shapes for swept wings.

86. F. TAMKI 1957 Proceedings IXth Congress International de Mecanique Applique, Bruxelles. Experimental studies on the stability of the transonic flow past airfoils.

87. F.H. SCHMITZ and D.A. BOXWELL 1975 Proceedings of First European Rotorcraft and Powered Lift Aircraft Forum, University of Southampton. In-flight Far Field Acoustic Measurements of Helicopter Impulsive Noise.

88. D. HAWKINGS 1975 Westland Research Memorandum, 299A. A prediction method for thickness noise.

89. C.R. VAUSE, F.H. SCHMITZ and D.S. BOXWELL 1976 Proceedings of 32nd Annual National V/STOL Forum of the American Helicopter Society, Washington DC, USA. High-Speed Helicopter Impulsive Noise.

90. H. STERNFELD and J.O. SCHAIRER 1969 Boeing Vertol Document D8-2464-1A. Study of Rotor Blade Tip Vortex Geometry for Noise and Airfoil Applications.

91. C.R. COX 1967 Bell Helicopter Company Report 576-099-052. Full scale helicopter rotor noise measurements in AMES 40 by 80 foot wind tunnel.

92. I.A. SIMONS and R.E. PACIFICO 1966 ISVR Internal Report. Flow visualization studies on a two blade model rotor.

93. N.D. HAM 1963 Proceedings CAL/TRECOM Symposium on Dynamic Load Problems associated with helicopters and V/STOL aircraft, Vol.1. An experimental investigation of the effect of a non-rigid wake on rotor blade airloads in transonic flight.

94. S. TARAINE 1963 Proceedings CAL/TRECOM Symposium on Dynamic Load Problems associated with helicopters and V/STOL aircraft, Vol.1. Experimental and theoretical study of local induced velocities over a rotor disc.

95. P. CRIMI 1966 CAL/USAAVLABS Symposium Proceedings, Vol.1. Prediction of rotor wake flows.

96. A.P. WHITE 1966 J. Sound Vib.4(3), 282-304. Vtol Periodic Aerodynamic loadings: The problems, what is being done and what needs to be done.

97. M. SULLY 1965 Paper presented at symposium on Noise and Loading actions of helicopters, V/STOL aircraft and ground effect machines, Southampton University.

98. G.N. ADAMS 1966 CAL/USAAVLABS Symposium proceedings, Vol.1. Propeller Research at Canadair Ltd.

99. B.W. McCORMICK and J.L. TANGLER 1965 Report: Department of Aeronautical Engineering, The Pennsylvania State University, USA. A study of the vortex sheet immediately behind an aircraft wing.

100. I.A. SIMONS, R.E. PACIFICO and J.P. JONES 1966 CAL/USAAVLABS Symposium Proceedings, Vol.1. The movement, structure and breakdown of trailing vortices from a rotor blade.

101. I.A. SIMONS 1965 ISVR Memorandum No.126. Blade-Vortex interaction on helicopter rotors in forward flight.

102. A.F. LEHMAN 1968 Proceedings American Helicopter Society 24th Annual National Forum. Model studies of helicopter rotor flow patterns in a water tunnel.

103. R.G. SCHLEGEL 1965 Sikorsky Aircraft Report. Helicopter Noise Generation.

104. H. LAMB 1932 Hydrodynamics. Cambridge University Press.

105. N.A.V. PIERCY 1947 Aerodynamics 2nd Edition. E.U.P.

106. SPREITER and SACKS 1951 J.Aeronautical Society. The rolling up of the trailing vortex sheet and its effect on the downwash behind a wing.

107. B.W. McCORMICK 1963 Report: The Boeing Vertol Company (Unpublished) A study of the vortex system of the Vertol V107 II rotor.

108. J.B. RORKE and R.C. MOFFITT 1973 Sikorsky Aircraft Report (Ref.Contract NASA-10446). Wind tunnel simulation of full scale vortices.

109. C.V. COOK 1972 Proceedings AGARD Specialist Meeting on Aerodynamics of rotary wings, Marseille, France. The Structure of the Rotor Blade Tip Vortex.

110. J.W. LEVERTON 1968 Westland Research Proposal Brochure, B.433. A further investigation of rotor noise.

111. J.P. JONES 1967 University of Southampton - Private Communications.

112. M.J. LIGHTHILL 1961 Proceedings of the Royal Society, The Bakerian Lecture. On sound generated aerodynamically.

113. C.L. MORFEY 1968 University of Southampton - Private Communications.

114. E.E. ZEPLER and J.R.P. HAREL 1965 J.Sound Vib.2(3)249. The loudness of sonic booms and other impulsive sounds.

115. C.G. RICE and E.E. ZEPLER 1967 J.Sound Vib 5(2). 285-289. Loudness and pitch sensation of an impulsive sound of very short duration.

116. R.R.A. COLES, G.R. GARINTHER, D.C. HODGE and C.G. RICE 1966. ISAV Memorandum No.162. Hazardous exposure to impulsive noise.

117. C.G. RICE 1967 ISAV Memorandum No.184. The hazards to hearing of impulsive noise.

118. C.G. RICE 1968 University of Southampton - Private Communications.

119. J.S. QUINN and C.E. THOMAS 1964 U.S. Air Force Institute of Technology Report AD 607117. Application of Heterodyne Analyzers to Pulse Analysis.

120. B.J. SOUTHWOOD and A.C. PIKE 1976 Westland Helicopter Ltd Report AA1147. The rating and subjective assessment of helicopter blade slap.

121. A.C. PIKE and J.W. LEVERTON 1977 Proceedings Inter-Noise Control Conference, Zurich, Switzerland. An analogue method for quantifying impulsive noise.

122. J.W. LEVERTON 1977 Proceedings of 9 International Congress on Acoustics, Paper A23. Subjective Assessment of Blade Slap.

123. 1971 ISO Recommendation R1996. Assessment of noise with respect to community response.

124. C.E.P. JACKSON 1967 Westland Helicopter Ltd Test Report, 4701 HN. Noise Measurements on Mi 10.

125. C.W. ELLIS 1969 Proceedings Third CAL/AVLABS Symposium, Buffalo, USA: Panel Discussion.

126. H. STERNFELD and R.H. SPENCER 1969 S.A.E. Report, No.690684. Recent Research in Rotor Noise Reduction.

127. W.E. HOOPER 1971 Boeing Vertol Report. The Boeing Mode 347 Flying Qualities Demonstrator Program.

128. C.R. COX Bell Helicopter Report. How to operate the light helicopter more quietly.

129. C.R. COX Bell Helicopter Report. How to operate the medium helicopter more quietly.

130. H.K. TANNA 1970 Ph.D. thesis, University of Southampton.

131. J.E. FFOWCS WILLIAMS and D.L. HAWKINGS 1969 Journal of Sound and Vibration, 10(1). Theory relating to the noise of rotating machinery.

132. 1970 Boeing-Vertol Division News, Oct Edition.

133. M.V. LOWSON 1970 Note Prepared for Westland Helicopters Ltd. Predicted noise levels for conventional and ABC rotors.

134. K.A. WINSPEAR and J.S. POLLARD 1974 Westland Helicopters Ltd Research Memorandum 252. External Noise Measurements on Two Helicopters; Comparison of measured and predicted Kaman Huskie Noise Levels.

135. G.R. TAYLOR 1972 Westland Helicopters Ltd, Applied Acoustics Note AA 1026. Noise Characteristics of the Servotex Limited Canadair (CL-84) Contra-Rotating Rotor.

136. N.B. HIRSH 1972 Proceeding 28th Annual National Forum of the American Helicopter Society, Paper 604. Design Requirements for a Quiet Helicopter.

137. R.H. WHEELOCK 1972 Bell Helicopter Company. An introduction to the Helicopter.

138. G. SISSINGH 1939 NACA Technical Memorandum, 929. Contribution to the Aerodynamics of Rotating-Wing Aircraft.

139. J.P. ROBBOTT 1956 NACA Technical Note 3688. Static thrust measurement of the aerodynamic loading on a helicopter rotor blade.

140. R. VON MISES 1959 Theory of Flight. Dover Edition

141. S.F. HOERNER 1958 Fluid Dynamic Drag. Hoerner

142. A.A. NIKORLSKY 1951 Helicopter Analysis. Wiley

143. L.M. MILNE-THOMSON 1948 Theoretical Aerodynamics, Macmillan and Co. Ltd.

144. P.E. HEMKE 1947 Elementary Applied Aerodynamics

APPENDIX 1: SELECTION OF FILTER CHARACTERISTICS

A.1.1. FILTER CHARACTERISTICS

The characteristics of a filter are defined in terms of bandwidth, shape factor and the maximum attenuation of 'off tuned' frequencies; this is illustrated in Figure A.1.1.

The bandwidth is usually quoted in terms of width of the filter at the -3 dB attenuation point. This is commonly referred to simply as the 3 dB point. Some manufacturers, however, use the 1 dB point and thus quote a smaller value than if the 3 dB point was used. This should be checked when comparing filters.

The shape factor, which is the ratio of the bandwidth of the 60 dB point, to the 3 dB point gives a measurement of the discrimination ability of the filter at 'off-tune' frequencies.

The maximum attenuation must also be taken into consideration, since this also affects the discrimination against 'off tune' frequencies.

A 'shape factor' is used in general to describe constant bandwidth filters which have fairly straight sided skirts. For constant percentage filters a description of skirt characteristics can also be made using the shape factor, provided the 'maximum attenuation' is also quoted. This is illustrated in Figure A.1.1, where the two filter types have the same bandwidth and shape factor. At frequencies less than $\left(\frac{B' \times S.F.}{2}\right)$ away from the tuned frequency the constant percentage filter would give slightly better discrimination, while for frequency greater than $(B' \times S.F./2)$ the opposite is true. The attenuation differences between the two types of filter can be considerable at a frequency, say, an octave away from the tuned frequency. Where, as with a constant bandwidth filter, the attenuation of 'off-tuned' frequencies increases with the difference between off tune frequency and the 'tuned frequency', on a 'constant bandwidth' filter it will most likely flatten out to a constant value (see Figure A.1.1.). The above comments are based on the filter alone, and without regard to the practical limitations imposed by the dynamic range of the system.

A.1.2. RELATIONSHIPS OF FILTER PARAMETERS

Although the following is only directly applicable to straight sided 'constant bandwidth' filters, it can be applied to 'constant percentage' filters provided the aspects outlined in the previous paragraph are taken into account. Suppose it is required to attenuate a frequency 'f' from the tuned frequency by XdB (see Figure A.1.2.).

Assuming the filter is straight sided (as shown) from the 3 dB point, with a shape factor S.F., then the positions O, P, Q, R, S and T are fixed by definition: this is reasonable since it is only the shape of the filter above the 3 dB point between P, O and Q which has not been defined.

Then $\Delta f = (O"P") + (TP")$ and $O"P" = B'/2$,

$$\Delta f = \frac{B'}{2} + \frac{B'(S.F. -1)}{2}\left[\frac{X}{57} - 3\right], \text{ if } \Delta f \geqslant \frac{B'}{2} \qquad (A.1.1)$$

In addition to giving the necessary attenuation to the adjacent frequency, the filter must be capable of giving a signal where the 'peak' can be detected. This is illustrated in Figure A.1.3. It would be impossible to know for certain if a peak existed unless an output as shown in Figure A.1.3 (c) could be obtained.

Figure A.1.4 illustrates the problem and shows the cross-over point 'e' at V above the datum (which for practical purposes will be the 'system' noise level). The actual output will be the sum of the two single outputs (shown by continuous lines), with the result that the combined output near the cross-over point 'e' will take the form indicated by the dotted line. Since at 'e' the levels of the two signals are the same they will add to give a 3 dB increase to the output. To allow the lower peak (f_2) to be located (V + 3)dB should be a few dB below the level (Z) of the lower peak. V = (Z - 10)dB would be ideal. Using the notation on Figure A.1.4 it can be shown by considering the filter characteristics and making the assumption outlined previously that

$$\Delta f = B' + \frac{B'(S.F. -1)}{2}\left[\frac{Y + Z - 2V - 6}{57}\right]; \quad \Delta f \geqslant B'/2 ,$$

or putting V + (Z - 10)dB

$$\Delta f = B' + \frac{B'(S.F. -1)}{2}\left[\frac{Y - Z + 14}{57}\right] \text{ Hz.} \qquad (A.1.2)$$

X in equation A.1.1 and Y and Z in equation A.1.2 are obviously dependent on the dynamic range of the system - this is discussed in the next section.

Equation A.1.2 is the more exacting and if the conditions specified by it are met, then equation A.1.1 will also be satisfied. If the frequencies of the harmonics are known and only the levels at these known frequencies are required, then equation A.1.1 can be used; if, however, the frequencies are not known accurately or if the levels are to be obtained from a paper trace, equation A.1.2 should be used to determine the optimum filter characteristics.

If these equations are examined, it will be noted that for small values of Δf (< 10 Hz) the solutions are practically identical. As Δf increases, the difference between the two solutions also increases. For large values of Δf, equation A.1.1 will give the larger value for bandwidth and/or shape factor, since as mentioned previously it is less exacting.

A.1.3. EFFECT OF DYNAMIC RANGE

Before the equations given in A.1.2 can be applied it is necessary to establish the relationship between the signal and the dynamic range of the system at the particular bandwidth and gain settings being use. Any calculation should be based on the least favourable set of conditions. Assume that the spectra consists of two discrete frequencies f_1 and f_2 with $(f_1 - f_2) = \Delta f$ and that f_1 is at the maximum allowable level and f_2 is at the minimum reliable level. For the level of 'f_2' to be unaffected by the 'system noise' it will have to be 10 dB above it. This assumes that the random system noise is a constant level (see Figure A.1.5).

Also if 'f_1' is to be attenuated such that it has no effect at all on the f_2 level it must be at least 10 dB below the system noise level. Thus 'X', the attenuation required, is given by $X = (Y + 10)$dB.

A.1.4. DETERMINATION OF THE FILTER CHARACTERISTICS FOR HELICOPTER ROTOR NOISE STUDIES

In the helicopter work the blade passing harmonics will be located by detecting 'peaks' in the noise spectrum: thus equation A.1.2 is applicable. The minimum separation of two adjacent harmonics or peaks will be 5 Hz. If Y is taken as 55 dB and Z = 10, then from equation A.1.2

$$10 = 2B' + B'(S.F. - 1). \quad (1.035) \qquad (A.1.3)$$

A compromise between bandwidth and shape factor is now necessary; a shape factor of 4 has become almost a standard. If S.F. is taken as 4, the above equation gives B = 1.96. Since the most demanding case has been taken, a filter with an S.F. of 4 and a bandwidth of 2 Hz would appear to just meet the requirements. The maximum bandwidth (when S.F. = 1) is 5 Hz.

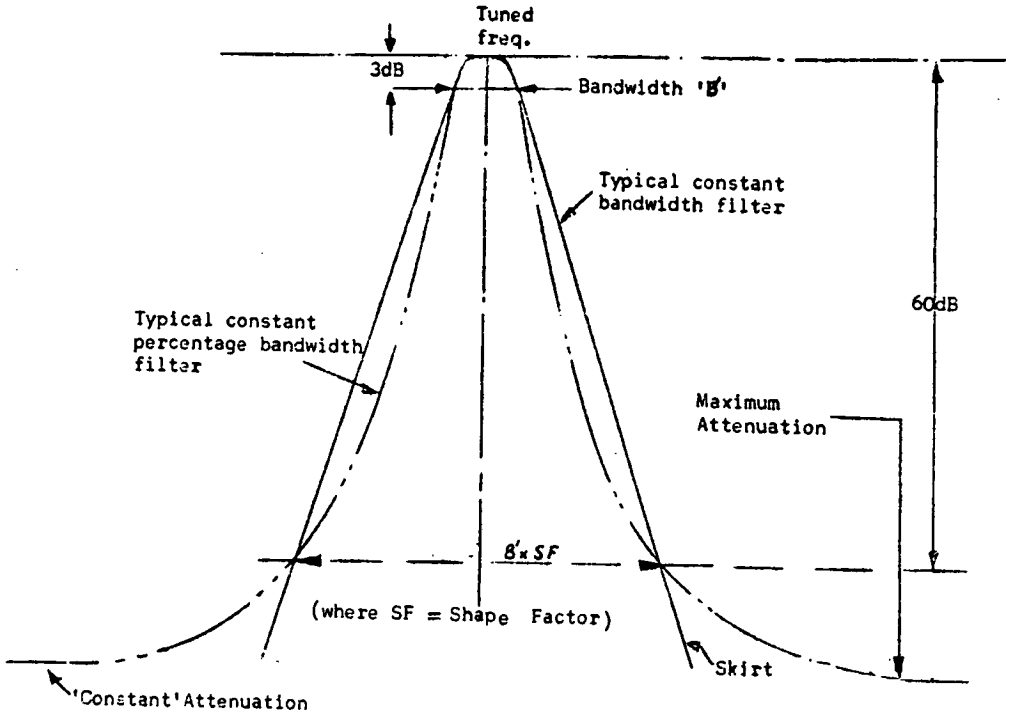

FIGURE A.1.1. FILTER CHARACTERISTICS

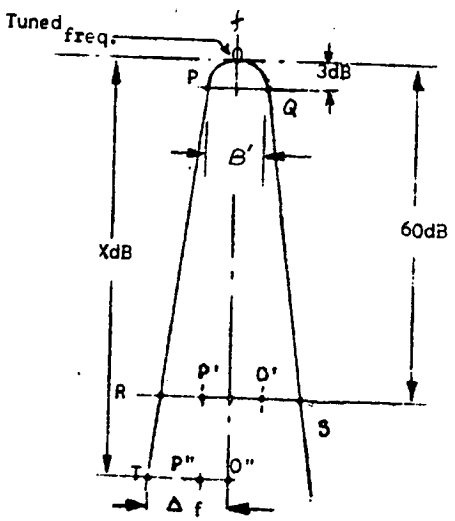

FIGURE A.1.2. ATTENUATION OF A FILTER

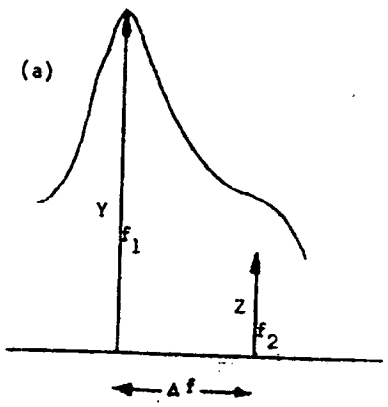

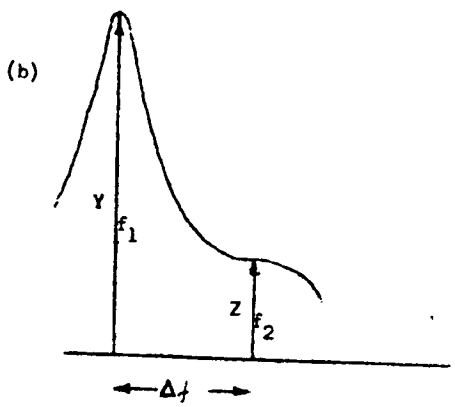

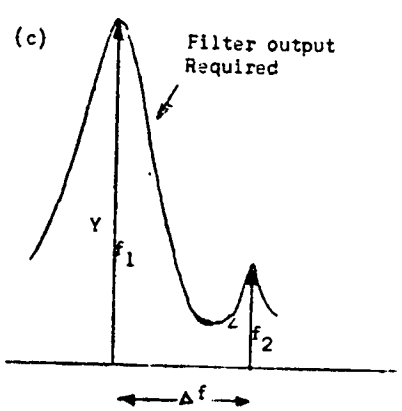

FIGURE A.1.3. FILTER OUTPUT FOR TWO DISCRETE FREQUENCIES

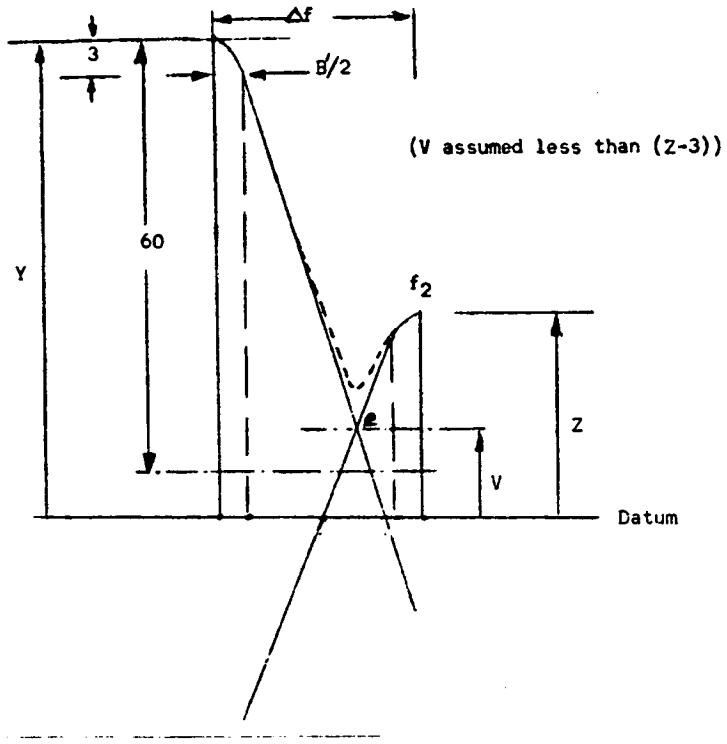

FIGURE A.1.4. RELATIONSHIP OF FILTER PARAMETERS AND 'PEAK' SEPARATION

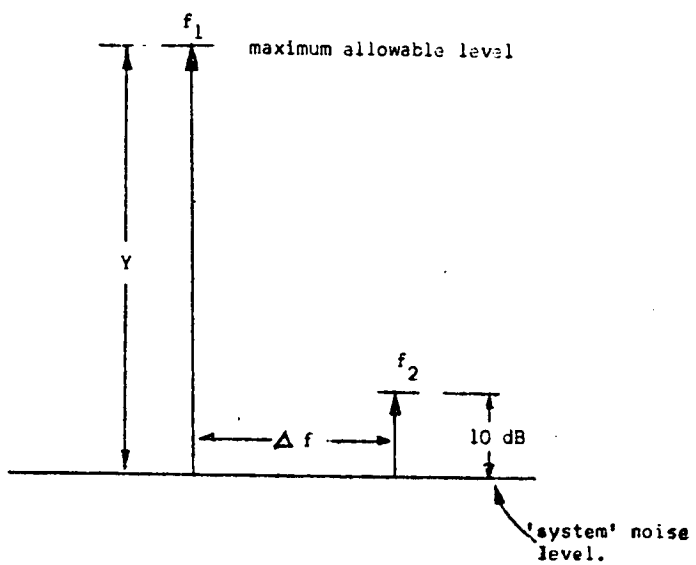

FIGURE A.1.5. RELATIONSHIP BETWEEN DYNAMIC RANGE AND SIGNAL LEVELS

APPENDIX 2: AERODYNAMIC THEORY

A.2.1. CALCULATION OF LIFT

Consider an elemental section of the blade - then the lift on the section is given by:-

$$dL = \tfrac{1}{2}\rho\, c\, V_r^2\, C_L.dr \qquad (A.2.1)$$

where ρ = density, c = blade chord, V_r = velocity at r, r = radius, C_L = lift coefficient.

Replacing V_r by ωr, where ω = angular velocity (rotational speed in rad/s) and considering elemental lift due to B blades, then:

$$dL_B = \tfrac{1}{2}\rho\, c.B\, (\omega r)^2\, C_L.dr \qquad (A.2.2)$$

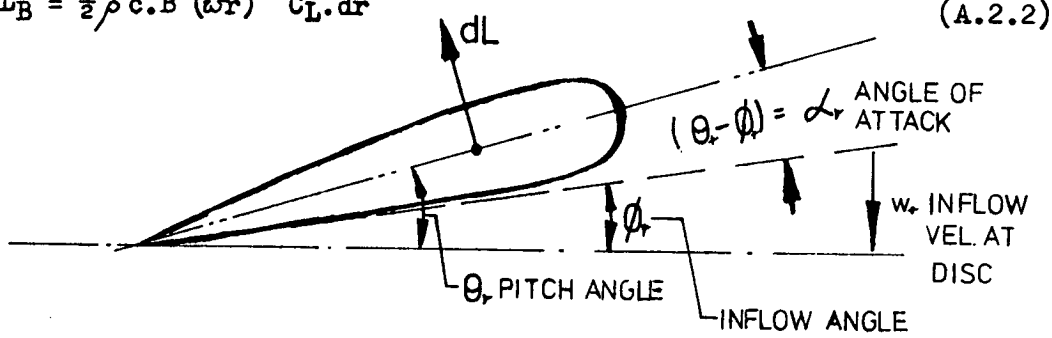

Assuming simple momentum theory, then lift is the rate of change of momentum through the disc, i.e.

$$dL = 2w_r \times (\text{mass}) = 2w_r\,(\rho\, 2\pi r\, dr w_r) = 4\pi r w_r^2 \rho\, dr \qquad (A.2.3)$$

Now $C_{L_r} = a_0(\theta_r - \phi_r)$ where a_0 = lift curve slope and $\phi_r = \frac{w_r}{V_r} = \frac{w_r}{\omega r}$.
From these relationships and by equating A.2.2 and A.2.3 above it can be shown that

$$w_r^2 + \left[\frac{Bc\omega a_0}{8\pi}\right] w_r - \left[\frac{Bc\omega^2 a_0 \theta_r}{8\pi}\right] = 0 \qquad (A.2.4)$$

Let $\lambda_r = \frac{w_r}{\omega R_T}$, from which it follows that $\phi_r = \lambda_r \frac{R_T}{r}$, then

$$\lambda_r^2 + \left[\frac{Bca_0}{8\pi r}\right] \lambda_r - \frac{Bca_0\theta_r}{8\pi r^2} = 0 \qquad (A.2.5)$$

For a non-twisted rotor blade, such as used on the ISVR model rotor, θ_r in equation A.2.5 is a constant and can be replaced by θ. In the case of a twisted rotor blade, as used on a real helicopter, the actual value at each radial position must be used. Traditionally, partly due to manufacturing reasons, helicopter rotors have a uniform twist as illustrated over.

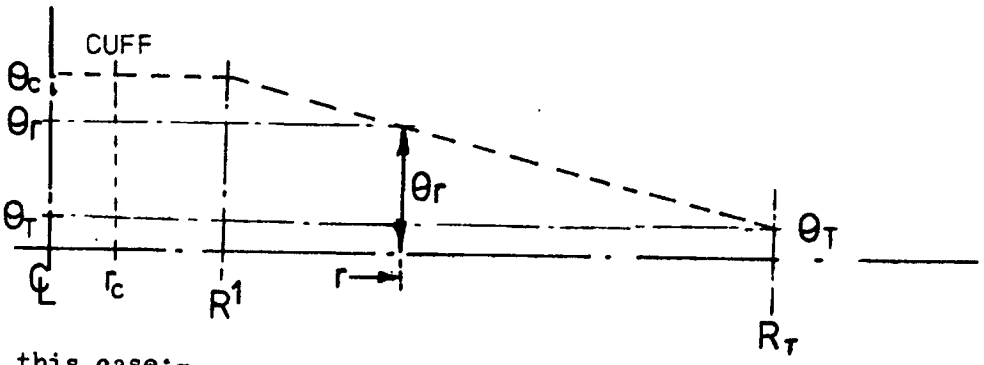

In this case:-

$$\theta r = \theta c - \theta_T \left[\frac{r - R^1}{R_T - R^1} \right] \quad r > R^1 \qquad (A.2.6)$$

where θc = pitch angle at cuff, θ_T = pitch angle at tip and R^1 = radius at which twist starts (see figure above) and this can be substituted in equation (A.2.5).

Equation A.2.5 can be solved for λ_r, from which ϕ_r (and α_r) can be obtained.

$$\text{Now } dL/_{dr} = \underbrace{\tfrac{1}{2}\rho c a_0}_{\text{constant}} \times \underbrace{r^2 (\theta_r - \phi_r)}_{\text{variable depending on r \& }\theta} \times \underbrace{\omega^2}_{\text{speed term}} \qquad (A.2.7)$$

where dL refers to the lift per blade.

Once ϕ_r has been calculated, dL/dr can be found and the total lift derived from

$$L_T = B \int_{rc}^{R_T} dL/_{dr} = \tfrac{1}{2}\rho c a_0 B \omega^2 \times \int_{rc}^{R_T} r^2 (\theta_r - \phi_r) dr \qquad (A.2.8)$$

A.2.2. THRUST/DRAG RELATIONSHIPS

Consider the rotor illustrated in diagrammatic form below.

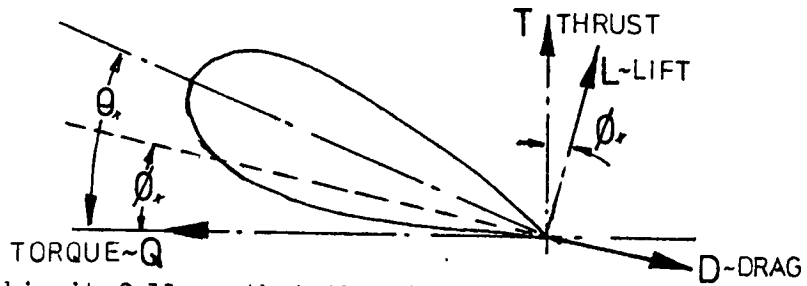

From this it follows that the elemental thrust is given by

$$dT/_{dr} = dL/_{dr} \cos\phi_r - dD/_{dr} \sin\phi_r \qquad (A.2.9)$$

In a similar manner it follows that the elemental torque (dQ/dr) is given by:

$$dQ/_{dr} = dL/_{dr} \cdot r \sin\phi_r - dD/_{dr} \cdot r \cos\phi_r \qquad (A.2.10)$$

It follows that the total thrust (T) and torque (Q) can be written as:

$$T = \int_{rc}^{R_T} dL/_{dr} \cos\phi_r \cdot dr - \int_{rc}^{R_T} dD/_{dr} \cdot \sin\phi_r \cdot dr \qquad (A.2.11)$$

$$Q = \int_{rc}^{R_T} dL/_{dr} \cdot r \sin\phi_r dr - \int_{rc}^{R_T} dD/_{dr}\, r \cos\phi_r dr. \qquad (A.2.12)$$

It will be noted that these equations contain a 'lift term' + a 'drag term'. The drag is defined in terms of the drag coefficient C_{Do}:

$$dD/_{dr} = \tfrac{1}{2}\rho c\, C_{Do}(\omega r)^2 \qquad (A.2.13)$$

C_{Do} can be determined (on a non-twisted rotor) from the measured torque when running at zero pitch. Ideally this constant is independent of rotor speed (Reynolds number effect) and constant along the span.

It can be shown that in equation A.2.11 the 'lift term' is considerably larger than the 'drag term' and thus for all practical purposes, since ϕ_r is small $\cos\phi_r \simeq 1$, and

$$T = \int_{rc}^{R_T} dL/_{dr} \cdot \cos\phi_r = L \qquad (A.2.14)$$

In the determination of the torque (equation A.2.12), however, both the 'lift term' and the 'drag term' are of importance.

It can be shown that equation A.2.12 can be written in the form

$$Q = \tfrac{1}{2}\rho c\omega^2 \cdot B \underbrace{\int_{rc}^{R_T} r^3 \left[a_o(\theta_r - \phi_r) \cdot \sin\phi_r + C_{Do} \cos\phi_r \right] dr}_{\text{Independent of speed: } (\theta_r - \phi_r) \text{ and } \phi_r \text{ function of r.}} \qquad (A.2.15)$$

Since ϕ_r is small (for the model rotor ϕ_r varies between 1.7° and 11.2°) equation A.2.15 can be re-written as:

$$Q = \tfrac{1}{2}\rho\, c\omega^2 \cdot B \cdot \int_{rc}^{R_T} r^3 \left[a_o(\theta_r - \phi_r)\cdot\phi_r + C_{Do} \right] dr \qquad (A.2.16)$$

- this again can be really calculated.

A.2.3. TIP EFFECTS

In the above calculation no allowance has been made for 'tip losses', the solutions which contain the 'lift term' are therefore an over-estimate due to the 'fall-off' in lift in the rotor tip region. A number of empirical relationships have been developed within the helicopter industry [137] and the two solutions commonly employed are:

$$T^1 = T\left(1 - \sqrt{\frac{2\,C_T}{B}}\right) \qquad (A.2.17)$$

$$T^1 = T\left(1 - \frac{\text{tip chord}}{2R_T}\right) \qquad (A.2.18)$$

where T^1 = true thrust, T = calculated thrust, C_T = thrust coefficient $= \dfrac{T}{\pi R_T^2 \rho (\omega R_T)^2}$

These two solutions yield basically the same results; equation A.2.17 was derived by Sissingh [138] from experimental considerations and equation A.2.18 simply assumes that a spanwise length at the tip equivalent to $\frac{1}{2}$ blade chord develops no thrust. Neither of these solutions appears to agree very well with the measured data for a non-twisted rotor given in reference (139). It was decided, therefore, that since the model rotor used in these studies was similar to the ISVR model rotor, a more realistic approach would be to use the test data to devise an empirical correction factor. This also had the advantage that rather than a simple correction on the total lift, corrections could be applied as a function of radial position.

Such an approach was adopted by the author and from a study of the data in reference (139) it was concluded that the correction terms could be independent of pitch and tip speed over the test range. The correction factors devised were, as a function of radial position, as indicated below.

Radial Position %R	0-40	50	60	70	80	85	90	92	95	100
Correction Factor k_L	1.0	0.9	0.9	0.8	0.8	0.8	0.85	0.85	0.65	0

The maximum lift was taken to occur at 92%R. An example which illustrates the application of this approach is given in Figure A.2.1 which shows results for a 3 bladed rotor operating at 6° pitch/600 rpm.

A.2.3.1. Lift/Thrust Relationship

If the 'correction factor' k_L is taken into account then equation A.2.8 becomes

$$L_T = B\int_{rc}^{R_T} dL/dr = \tfrac{1}{2}\rho c a_o B.\omega^2 \int_{rc}^{R_T} r^2 k_{L_r}(\theta_r - \phi)\,dr \qquad (A.2.19)$$

where k_{L_r} is a function of the radius r.

A.2.3.2. Torque/Drag Relationship

In a similar manner to above the 'thrust/lift' term in the torque equation is modified and equation A.1.16 becomes

$$Q = \tfrac{1}{2}\rho c\omega^2 B \int_{rc}^{R_T} r^3 \left[ao.k_L(\Theta_r - \phi_r).\phi_r + C_{Do} \right] dr \qquad (A.2.20)$$

The 'profile drag' term (C_{Do}) is, as indicated, unchanged.

A.2.4. APPLICATION OF THEORY

A.2.4.1. Lift/Thrust

Lift values were calculated for the complete model rotor test range, 0^o-12^o pitch, 400-1000 rpm and 1 to 4 blades. As part of this calculation the angle of attack as a function of radial position and pitch was derived: a set of results for the three bladed rotor is produced in Figure A.2.2. In these calculations the 'tip corrections' discussed above have not been applied. The corresponding generalised lift term, $r^2 k_L(\Theta - \phi)$, is shown in Figure A.2.3 - in this case as can be seen the 'correction factors' have been taken into account. The values are independent of tip speed and it will be noted that the curves are identical in shape for all pitch settings. The total lift can be obtained from these curves by use of the following relationship:

Total Lift = $\tfrac{1}{2}\rho c a_o.B\omega^2 \times$[Area under $r^2 k_L(\Theta - \phi)$ curve] (A.2.21)

A.2.4.2. Torque

The torque solution for the 3 bladed rotor as shown is illustrated in Figure A.2.4. Here both the 'lift term' and the 'drag terms' have been considered. The profile drag which increases with rotor radius over the complete rotor results is practically independent of pitch and then added to this is the induced drag (lift term). The result is that, as indicated, the torque for 2^o is very similar to that of the zero pitch case and not until high pitch angles is the torque dominated by the lift component. In a similar manner to that described above for the lift, the torque can be calculated from:

$$\text{Torque, } Q = \tfrac{1}{2}\rho c \times B \times \omega^2 \times \left\{ \begin{matrix} \text{area under the curve} \\ r^3\left[a_o k_L(\Theta - \phi)\phi + C_{Do}\right] \end{matrix} \right\} \qquad (A.2.22)$$

In this derivation it is assumed that C_{Do} is independent of lift/thrust (pitch) and tip speed. This is not the case and it has been shown by a number of investigators that C_{Do} varies with both lift coefficient (C_L) and Reynold number (speed). The former is considered to be more important

and Von Mises [140] suggested that for symmetrical sections:-

$$C_{Do} = C_{Do}\,\text{min} + \tilde{k}\, C_L^{\,2} \qquad \text{(A.2.23)}$$

where C_{Do} min is the value at zero pitch and $\tilde{k}$ a constant.

Hoerner [141] proposed a similar solution, while Nikolsky [141] gave the following expression:-

$$C_D = C_D\ \text{min} + K_1\alpha + K_2\alpha^2 + K_3\alpha^3 + \ldots \qquad \text{(A.2.24)}$$

From reference (142) it seems that, except when non-symmetrical aerofoil sections and/or large angle of attack are involved and the blade is in the stalled region, it is necessary only to consider K_1 and K_2. This approach was followed and resulted in the following equation:-

$$C_{Do} = C_{Do}\,\text{min} - 5.13 \times 10^{-4}\alpha_1 + 4.5 \times 10^{-4}\alpha_1^2 \qquad \text{(A.2.25)}$$

where C_{Do} min $= 1.46 \times 10^{-2}$

and α_1 = the theoretical value at 0.9R.

Use of this equation (as discussed in Chapter 2, section 2.6) gave reasonable agreement with experiment.

C_{Do} min was obtained from test data using the relationship (derived from equation A.2.13)

$$C_{Do}\,\text{min} = \frac{HP \times 4400}{B\omega^2 \rho\, cR_T^4} \qquad \text{(A.2.26)}$$

where HP = Horse power absorbed by the rotor.

Over the test range (300 to 1000 rpm) the variation about the mean for 'C_{Do} min' was only 4%.

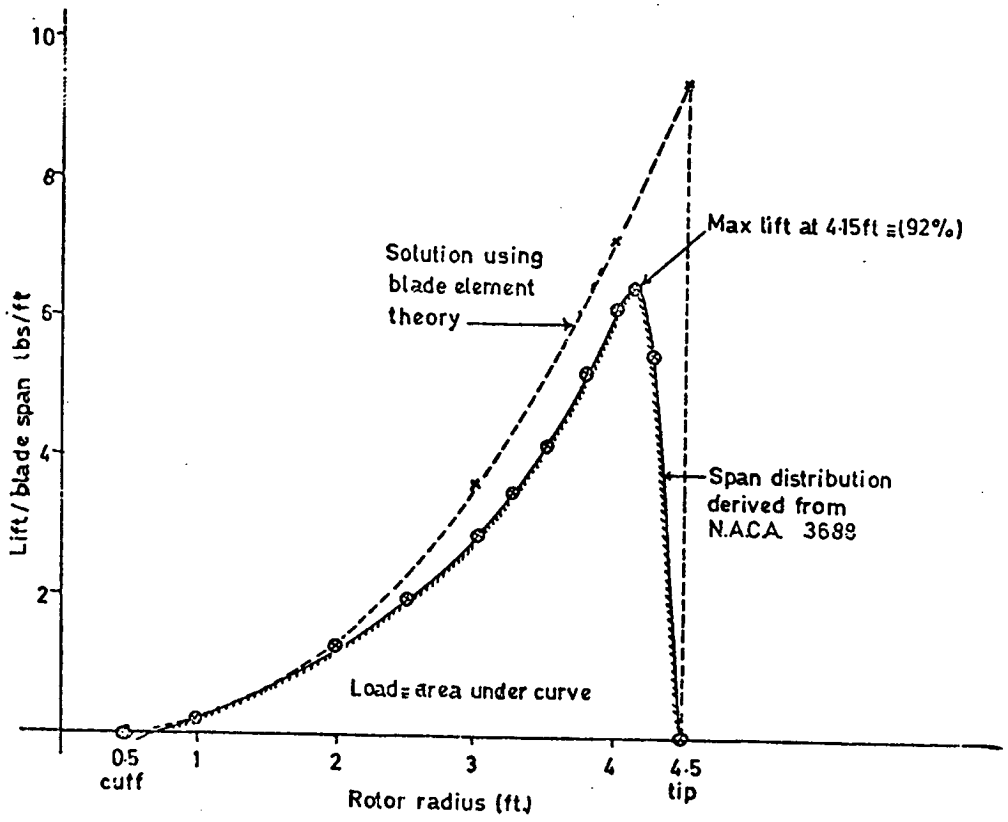

Comparison of spanwise loading calculated using blade element theory and estimated from N.A.C.A.3688 (method of obtaining empirical correction for calculating blade lift). [139]
Case illustrated: 3 blades - 6° pitch - 600 r.p.m.

FIGURE A.2.1. RADIAL BLADE LOADING

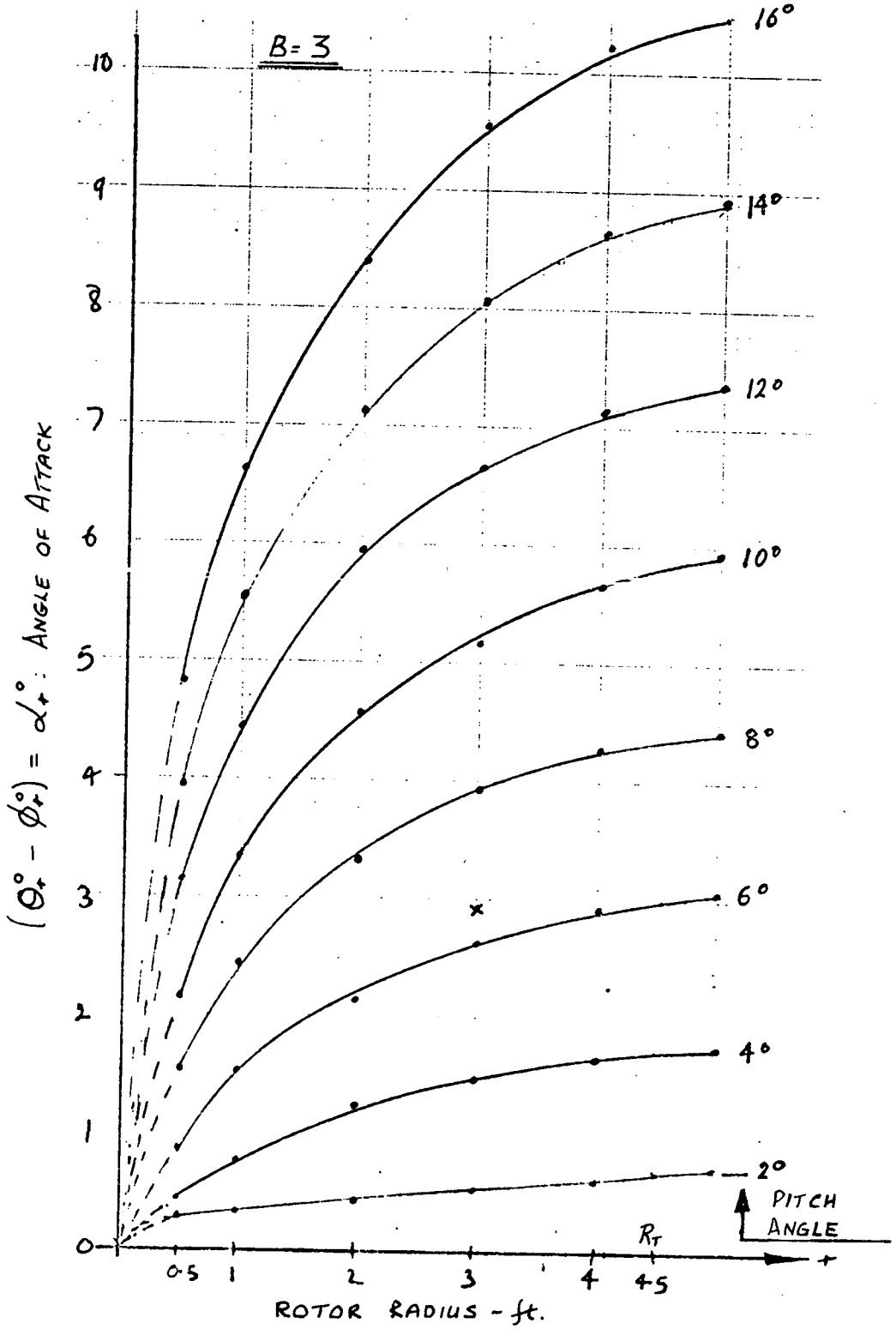

FIGURE A.2.2. VARIATION OF 'ANGLE OF ATTACK' WITH ROTOR RADIUS

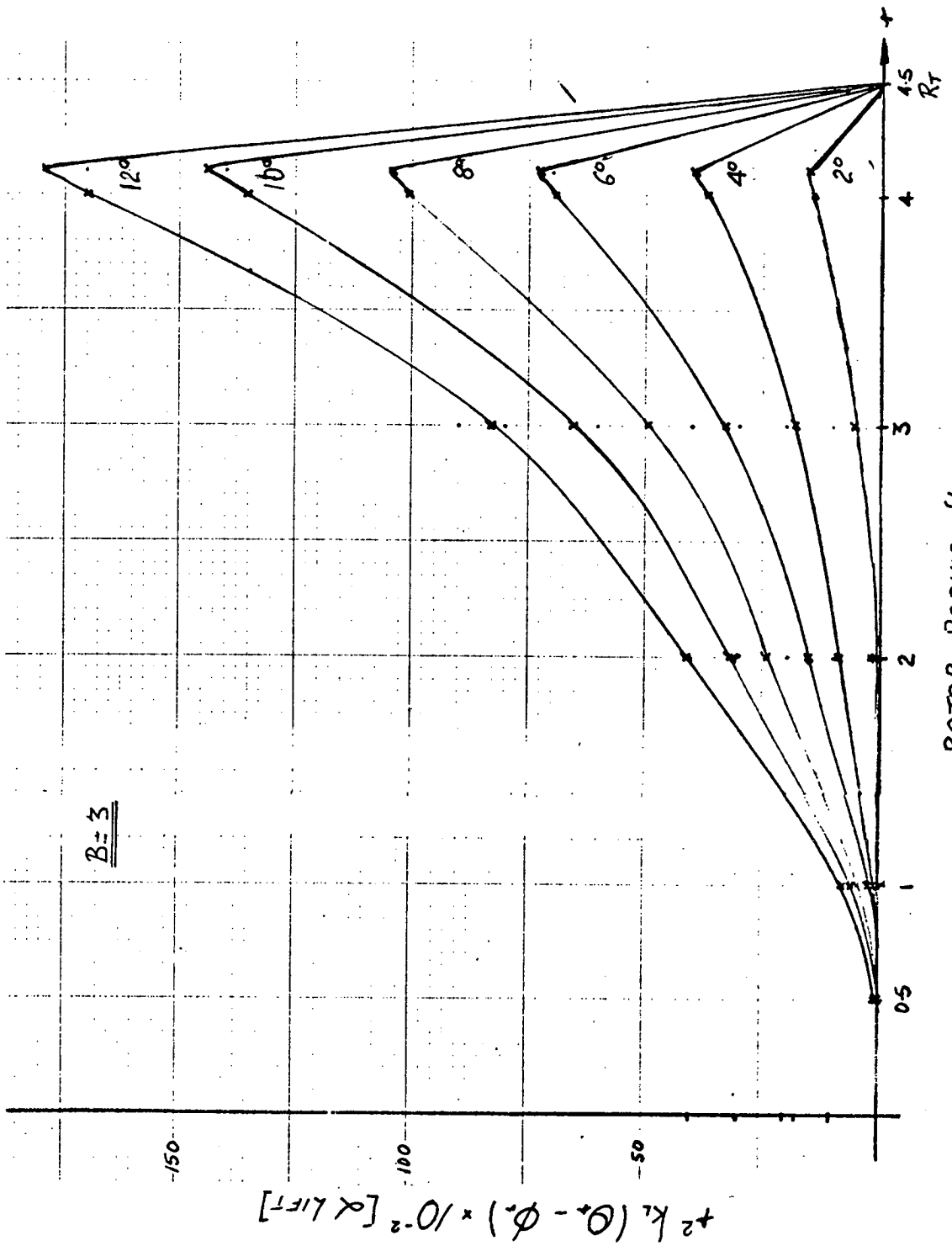

FIGURE A.2.3. VARIATION OF LIFT WITH BLADE PITCH

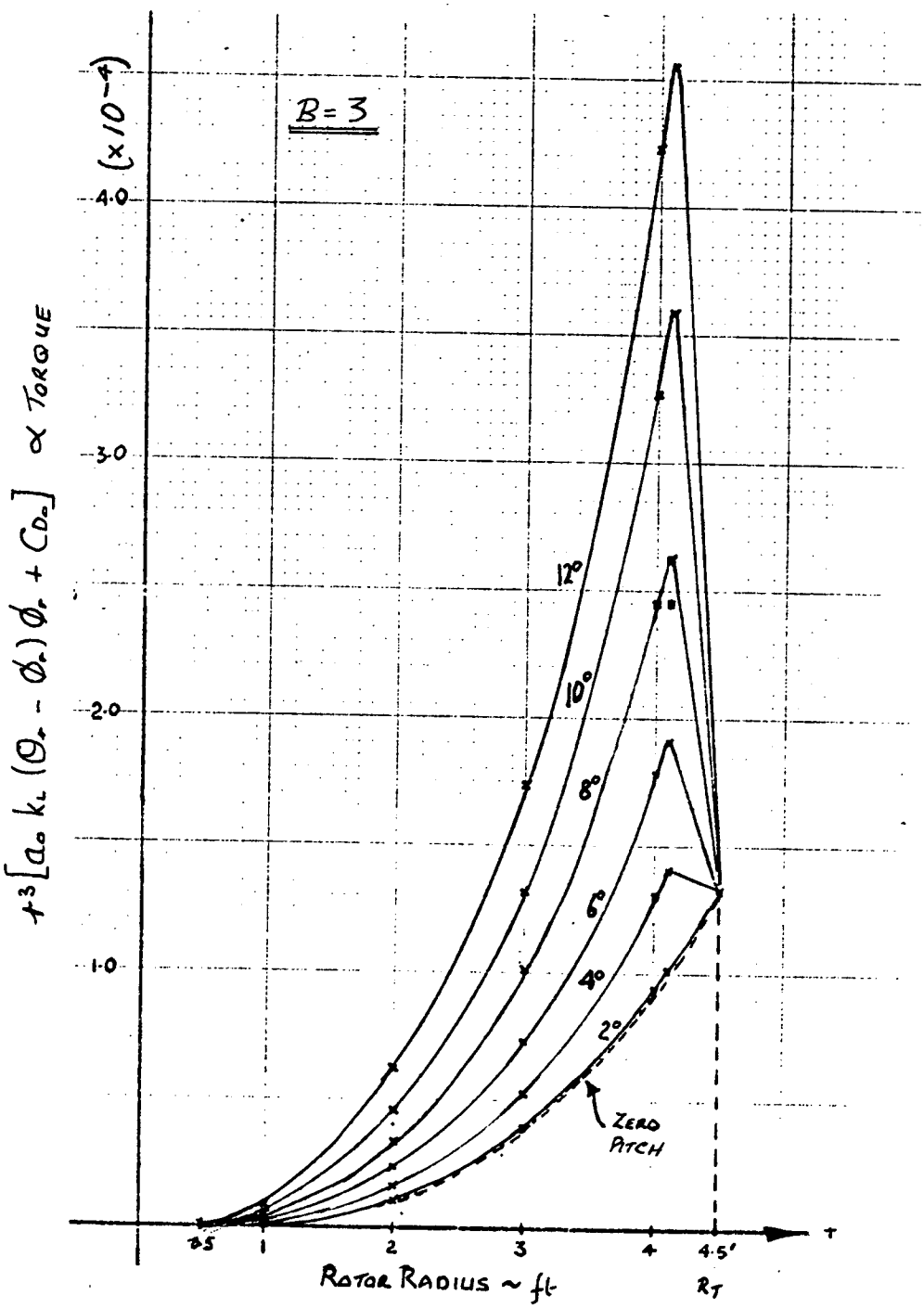

FIGURE A.2.4. VARIATION OF TORQUE WITH ROTOR RADIUS

APPENDIX 3: BROADBAND NOISE PREDICTION METHODS

A.3.1. DAVIDSON AND HARGEST FORMULA [40]

Davidson and Hargest used actual helicopter results measurements and data from the work of Goddard and Stuckey [39] to develop the following relationship for the SPL at 500 ft:

$$SPL\ (500) = 60 \log V_T + 20 \log C_{LT} + 10 \log S + f1 + f2 + f3 - 84\ dB \quad (A.3.1)$$

where C_{LT} = lift coefficient referred to the blade tip = $T/\frac{1}{2}\rho V_T 2.S$, f1 = forward speed correction, f2 = correction for atmospheric turbulence and f3 = directivity term. S = total blade area. V_T = tip speed.

For the hover case in still air and with the directivity factor proposed by Davidson and Hargest this can be re-written as:

$$SPL\ (500) = 20 \log V_T + 20 \log T - 10 \log S - 25.6 - 20 \log \sec \Phi\ dB, \quad (A.3.2)$$

where Φ is the angle relative to the vertical axis. Thus directly under the rotor ($\Phi = 0^\circ$):

$$SPL\ (500/0^\circ) = 20 \log V_T + 20 \log T - 10 \log S - 25.6 \quad (A.3.3)$$

With Φ taken as 75° (15° below the rotor disc plane) equation (A.3.2) becomes:

$$SPL\ (500/75^\circ) = 20 \log V_T + 20 \log T - 10 \log S - 37\ dB \quad (A.3.4)$$

A.3.2. GODDARD AND STUCKEY [39]

Goddard and Stuckey obtained a relationship from full scale whirl tower tests using Wessex (S.58) blades. From this they obtained a semi-empirical formula for calculating the overall SPL of 'vortex' noise - this can be reduced to:

$$SPL = 16.6 \log T_B + 26.8 \log V_T - 20 \log r - 20 \log \sec \beta + 2.8\ dB \quad (A.3.5)$$

where T_B = thrust/blade lbs (not total thrust T), r = distance from the source and β = angle between the tip located dipole axis and the observer.

With the assumption $\beta = \Phi$ as used before, this can be modified to give the SPL at 500 ft/0° to the axis as follows:

$$SPL\ (500) = 16.6 \log T_B + 26.8 \log V_T - 81\ dB, \quad (A.3.6)$$

or in the terms of the total thrust T ($T = T_B \times B$)

$$SPL\ (500) = 16.6 \log T + 26.8 \log V_T - 16.6 \log B - 81\ dB \quad (A.3.7)$$

where B is the number of blades. The Goddard and Stuckey formula,

because thrust per blade is used instead of the more conventional total thrust T, has often been mis-applied and/or misquoted in the literature.

It also follows that if 500 ft/75° is considered then the formula can be re-written as

$$SPL\ (500) = 16.6 \log T + 26.8 \log V_T - 16.6 \log B - 70\ dB \qquad (A.3.8)$$

A.3.3. HUBBARD [60]

Hubbard developed a relationship for propellers, based on the work of Yudin [59], which indicated that the 'vortex-noise' was proportional to V^6 and the first power of the propeller blade area A_B, his final formula being

$$\bar{I}_V = (SPL) = 10 \log_{10} kA_B(V_{0.7})^6/10^{-16} \qquad (A.3.9)$$

where $V_{0.7}$ = velocity at 70% propeller radius.

Hubbard's measurements were made at a distance of 300 ft and an angle 105° from the axis of rotation. The constant k was determined empirically for the measurement position; this gave k as 3.8×10^{-27}. It follows that the above equation can be re-written as

$$SPL\ (300) = 60 \log V_T + 10 \log A_B - 117.9\ dB \qquad (A.3.10)$$

Converting to 500 ft gives

$$SPL\ (500) = 60 \log V_T + 10 \log S - 115.8\ dB \qquad (A.3.11)$$

This formula has been applied in a number of ways - Sikorsky [41] and Boeing Vertol [64] substituted the actual blade area for the 'effective blade area A_B' and in doing so removed the influence of thrust. Hubbard states, however, that the equation is based on C_L values of 0.4 and that other values can be obtained by use of the 'effective blade area' term A_B which is defined as

$$A_B = 2T/\rho C_L(V_{0.7})^2 \qquad (A.3.12)$$

Clearly then the SPL is dependent on the thrust T. A number of other interpretations have also been implied by other investigators. In general, however, it would appear that in most investigations equation (A.3.11) has been used when calculating noise according to Hubbard's formula.

It will be noted that the basic Hubbard formula (Equation (A.3.11)) has the same parameters as the original relationship devised by the author - section 4.8.1 equation (4.2) - with the exception of the constant which results in an absolute level change of approximately 16 dB.

A.3.4. SIKORSKY [41]

Sikorsky (Schlegel, King and Munch) used whirl tower data in a similar manner to Goddard and Stuckey. Tests were conducted using a CH-3C rotor fitted with five blades and a CH-53A rotor system with six blades. They modified the approach developed by Hubbard [60] mentioned in section A.3.3 to take into account C_L variations and the difference in 'k' for helicopter rotors. From this they obtained the following:

$$\text{SPL (300 ft/75°)} = 20 \log V_{0.7} + 20 \log T - 10 \log S - 35.7 \text{ dB} \quad \text{(A.3.13)}$$

where $V_{0.7}$ = velocity at 70% radius (ft/sec). Converting to 500 ft and using V_T gives

$$\text{SPL (500 ft/75°)} = 20 \log V_T + 20 \log T - 10 \log S - 43 \text{ dB} \quad \text{(A.3.14)}$$

This solution is identical to that of Davidson and Hargest at 75° (section A.3.1) with a 6 dB difference in the constant term.

APPENDIX 4: DETERMINATION OF BLADE LOADING

The approach employed, originally adapted in reference (1) uses Kussner's Function [77] for the determination of the loading. Kussner's Function is based on the lifting line theory applied to a two dimensional aerofoil.

The rotor blade is assumed to be moving as a wing through a gust at a velocity equal to that of the blade section at the centre of the gust. The load at any point, L(s), in terms of an arbitrary gust profile, $w(\sigma)$, illustrated in Figure A4.1, is given by:

$$L(s) = \tfrac{1}{2}\rho . V . c . a_o \int_0^s w(\sigma) . K_f'(s - \sigma) d\sigma \qquad (A4.1)$$

where

s = any point measured from start of gust - a dimensionaless variable given by $s = \frac{Vt}{b}$ where V = velocity of wing at centre of gust

b = half chord

σ = point at which load is being considered

K_f = Kussner's Function.

A suitable approximation for $K_f(s - \sigma)$ is given in reference (77) and takes the form :

$$(s - \sigma) \simeq 1 - \tfrac{1}{2} e^{-0.13(s - \sigma)} - \tfrac{1}{2} e^{-(s - \sigma)} \qquad (A4.2)$$

From this it follows that

$$K_f'(s - \sigma) = 0.065 e^{-0.13(s - \sigma)} + 0.5 e^{-(s - \sigma)} \qquad (A4.3)$$

Hence equation (A4.1) can be rewritten as :

$$L(s) = \tfrac{1}{2}\rho . V . c . a_o \int_0^s w(\sigma) \left\{ 0.065 e^{-0.13(s - \sigma)} + 0.5 e^{-(s - \sigma)} \right\} d\sigma \qquad (A4.4)$$

For convenience let $\chi_1 = \frac{1}{2}.\rho.V.c.a_o$ 0.065

$\chi_2 = \frac{1}{2}.\rho.V.c.a_o$ 0.5

$g = 0.13$

Then equation (A4.4) becomes

$$L(s) = \chi_1 e^{-gs} \int_o^s w(\sigma).e^{g\sigma}.d\sigma + \chi_2 e^{-s} \int_o^s w(\sigma).e^{\sigma}.d\sigma \quad (A4.5)$$

Consider now a gust of arbitrary profile. While the blade is in the gust (i.e. $s < Y$ where Y is the non-dimensional gust length), then the loading L(s) will be given by equation (A4.5). After the blade passes out of the gust, $w(\sigma)$ becomes zero and cannot directly affect the loading. This does not imply that the blade load is zero, since a distribution of shed vorticity would be left in the wake by the aerofoil as it passed through the gust. This would affect the aerofoil even when outside the original gust, and the loading would therefore take a finite time to decay.

Hence the loading for the blade outside the direct effect of the gust ($s \geq Y$) is given by :

$$L(s) = \chi_1 e^{-gs} \int_o^Y w(\sigma).e^{g\sigma}.d\sigma + \chi_2 e^{-s} \int_o^Y w(\sigma).e^{\sigma}.d\sigma \quad (A4.6)$$

Since Y is constant the value of the integral will be a constant, and the loading decay will take on an exponential form with increasing s.

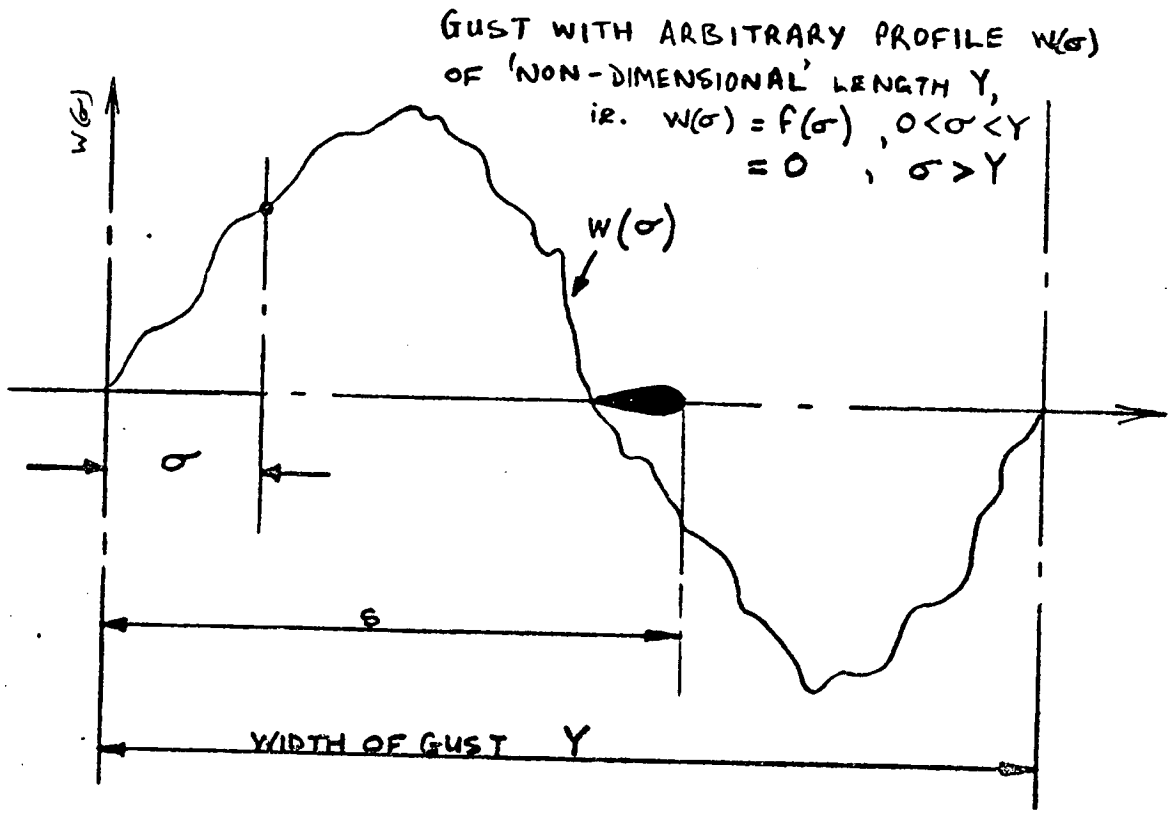

FIGURE A.4.1. GUST CHARACTERISTICS

APPENDIX 5: ACOUSTIC THEORY

SOUND POWER RELATIONSHIP

A theory has been developed for the noise produced when a blade passes through an impulse or gust of known form and profile (Appendix 4). The rotor blade is assumed to be rigid and not to deflect when passing through the gust. For the noise calculations it is treated as a thin plate.

Lighthill [112] has shown that the pressure at a point whose position relative to a point dipole has co-ordinates x_i (i = 1,2,3) takes the form

$$p - p_o = \frac{x_i}{4\pi r^2}\left[\frac{1}{c_o}\cdot\frac{\partial F_i}{\partial t}\left(t - \frac{r}{c_o}\right) + \frac{1}{r}\cdot F_i\left(t - \frac{r}{c_o}\right)\right] \qquad (A5.1)$$

where F_i is the fluctuating force and r the distance of the observation point from the source.

The second term in the prior equation becomes small when the distance from the point to the source r is much larger than a typical wavelength of the sound radiated. Thus, for the 'far field',

$$p - p_o = \frac{x_i}{4\pi r^2}\cdot\frac{1}{c_o}\cdot\frac{\partial F_i}{\partial t}\left(t - \frac{r}{c_o}\right). \qquad (A5.2)$$

The loading per unit span L_s, on each small area of blade can be assumed to act as a point dipole acoustic source, provided the chord is small compared with a wavelength. Thus for a small element of span

$$(p - p_o) = \frac{x_n}{4\pi r^2}\cdot\frac{1}{c_o}\cdot\frac{\partial L_s}{\partial t}\left(t - \frac{r}{c_o}\right) dx \qquad (A5.3)$$

so that the total radiated noise is

$$p - p_o = \int_{\text{span}} \frac{1}{4\pi r}\cdot\frac{x_n}{r}\cdot\frac{1}{c_o}\cdot\frac{\partial L_s}{\partial t}\left(t - \frac{r}{c_o}\right) dx \qquad (A5.4)$$

In addition, if the span length over which the gust acts, $(r_o - r_1)$, is small compared with the acoustic wavelength, and if L_s is assumed constant over $(r_o - r_1)$, then

$$\int_{\text{span}} \frac{\partial L_s}{\partial t}\left(t - \frac{r}{c_o}\right) d_x = \left[\frac{\partial L_s}{\partial t}\right](r_o - r_o) \qquad (A5.5)$$

and the factor $(1/4\pi r)\ (x_n/r)$ in equation (A5.4) can be replaced by $(1/4\pi \bar{r})\ (\bar{x}_n/\bar{r})$ where $\bar{r}$ is the distance of the observation point from the mid-point of the span length and $\bar{x}_n$ is the co-ordinate normal to the span at this mid-point.

The mean radiated intensity, I in the 'far field', is

$$I = \frac{\overline{(p - p_o)}^2}{\rho_o c_o} \qquad (A5.6)$$

and the total radiated energy W_s is the surface integral of the intensity over the surface of a large sphere. It therefore follows that

$$W_s = \frac{1}{12\pi\rho_o c_o^3} \cdot \overline{\left[\frac{\partial L_s}{\partial t}\right]^2} \cdot (r_o - r_1)^2 \qquad (A5.7)$$

APPENDIX 6: ACOUSTIC THEORY
SIMPLE POINT DIPOLE MODEL

The pressure at a point in the far field whose position relative to the dipole has co-ordinates x_i $(i = 1,2,3 \ldots.)$ is given by the Lighthill equation [112]

$$p - p_o = \frac{x_i}{4\pi r^2} \left\{ \frac{1}{c_o} \frac{\partial F_i}{\partial t} (t - r/c_o) \right\} \qquad (A6.1)$$

where F_i is the fluctuation force

r is the distance of the observation point from the source

$(t - r/c_o)$ is referred to as the 'retarded time' and is the instance when a wave travelling at the speed of sound (c_o) has to leave the source in order to reach the point of observation in time t.

Considering a blade loading per unit span (L_s) perpendicular to the plane of rotation such that:-

$$\delta F_i \equiv \delta F_n = L_s . \delta x$$

where δx is a small increment of span over which L_s acts.

$$\delta(p - p_o) = \frac{x_n}{4\pi r^2} \cdot \frac{1}{c_o} \cdot \frac{\delta L_s}{\delta t} \cdot (t - r/c_o) \cdot \delta x \qquad (A6.2)$$

Integrating over the blade span region of interest $(r_o - r_1)$ and taking the mean square of pressure one obtains:-

$$\overline{(p - p_o)^2} = \left(\frac{1}{4\pi \bar{r}} \cdot \frac{\bar{x}_n}{\bar{r}} \cdot \frac{1}{c_o} \cdot (r_o - r_1) \cdot S' \right)^2 \overline{\left[\frac{\partial L(t)}{\partial t} \right]^2} \qquad (A6.3)$$

where S' is a constant dependent upon the spanwise load distribution

e.g. for a half sine wave distribution $S' = \frac{2}{\pi}$

$\bar{r}$ is the observer distance from the centre of the elemental blade area.

$\bar{x}_n$ is the normal coordinate from the mid-point of the area under consideration.

and $S'\left[\frac{\partial L(t)}{\partial t}\right] = \left\langle \frac{\partial L_s}{\partial t} \right\rangle_{(r_o - r_1)}$

Note: When the elemental span length $(r_o - r_1)$ is small compared with the acoustic wavelength then the 'retarded time' $(t - r/c_o)$ is unimportant.

The blade loading, L, is represented by the following fourier equation which is based on the "blade spacing interval":-

$$L = \tfrac{1}{2}x_c + \sum_{n=1}^{\infty} a_n \mathrm{Sin}(n\omega t) + \sum_{n=1}^{\infty} b_n \mathrm{Cos}(n\omega t). \qquad (A6.4)$$

where a_n, b_n are constants

$\omega = 2nf$ where f = blade passing frequency

n = 1,2,3,.... harmonic number,

from which is obtained, for the nth harmonic:-

$$\overline{\left[\frac{\partial L(t)_n}{\partial t}\right]^2} = C_n{}^2 n^2 \frac{4\pi^2}{\tau^2} \cdot \frac{1}{2} \qquad (A6.5)$$

where

$C_n{}^2 = a_n{}^2 + b_n{}^2$

τ = blade passing interval

Hence substituting in equation (A6.3) gives:-

$$\overline{(p - p_o)^2} = \left\{ \frac{1}{2\sqrt{2}} \cdot \frac{1}{r} \cdot \frac{\bar{x}n}{\bar{r}} \cdot \frac{1}{c_o} (r_o - r_1)\, S' \frac{C_n \cdot n}{\tau} \right\}^2 \qquad (A6.6)$$

Therefore SPL for the nth harmonic is given by

$$SPL_n = 20\ \mathrm{Log} \left\{ \frac{1}{2\sqrt{2}} \cdot \frac{1}{r} \cdot \frac{\mathrm{Cos}\,\phi}{c_o} r'S' \cdot \frac{C_n \cdot n}{\tau} \right\} - 20\mathrm{Log}\, P_{ref} \qquad (A6.7)$$

where $r' = r_o - r_1$

and $\mathrm{Cos}\,\phi = \frac{\bar{x}n}{\bar{r}}$ where ϕ is the angle subtended between the dipole axis and the source-observer line.

APPENDIX 7: FOURIER ANALYSIS OF IMPULSE

A7.1. IMPULSE MODEL

Assume (a) the 'Noise' signal is a sine wave due to a gust, refer to Figure A7.1, (b) this signal can be derived from a blade loading of the form given in Figure A7.2, i.e. a displaced cosine wave.

From simple point dipole theory

$$SPL_n \propto L_n.n \qquad (A7.1)$$

where SPL_n = SPL of the n^{th} noise harmonic (the desired result)
L_n = n^{th} harmonic of lift signal
n = harmonic number
SPL_n = n^{th} harmonic of the assumed sine wave noise signal.

A7.2. FOURIER ANALYSIS OF NOISE SIGNAL

The peak amplitude is I , and if $f(t)$ defines the wave form then

$$f(t) = 0 \qquad \text{for} \qquad 0 \leq t < b$$
$$= I.\sin\pi\left(\frac{t-b}{d-b}\right) \quad \text{for} \quad b \leq t \leq d \qquad (A7.2)$$

The origin was chosen so as to make the periodic function odd which gives the coefficients A_n in the Fourier series equal to zero.

The Fourier representation of $f(t)$ is:

$$f(t) = \frac{A_o}{2} + \sum_{n=1}^{\infty} A_n \cos w_n t + B_n \sin w_n t \qquad (A7.3)$$

where

$$A_o = \frac{1}{T}\int_{-T}^{T} f(t).dt$$

$$A_n = \frac{1}{T}\int_{-T}^{T} f(t) \cos w_n t.dt$$

$$B_n = \frac{1}{T}\int_{-T}^{T} f(t) \sin w_n t.dt$$

Since A_n is zero for the odd function, we have:

$$f(t) = \sum_{n=1}^{\infty} B_n \sin \frac{n\pi t}{d}$$

i.e. $$B_n = \frac{2}{d} \int_0^c f(t) \sin \frac{n\pi t}{d} .dt \qquad (A7.4)$$

$$= \frac{2I}{d} \int_b^c \sin \frac{n\pi t}{d} \sin \pi\left(\frac{t-b}{d-b}\right).dt$$

Since $f(t)$ is zero from $t = 0$ to $t = b$, the integration goes from $t = n$ to $t = d$

Hence

$$B_n = -\frac{2Id}{\pi}(d-b) \sin \frac{n\pi b}{d} \left[\frac{1}{n^2(d-b)^2 - d^2}\right] \qquad (A7.5)$$

A7.3. FOURIER ANALYSIS OF BLADE/LOADING SIGNAL

The wave form is defined by

$$f(t) = 0 \qquad \text{for } 0 \leq t < b$$

$$= I\{1 - \cos\pi\left(\frac{t-b}{c-b}\right)\} \qquad \text{for } b \leq t \leq d$$

Now $$f(t) = \frac{A_o}{2} + \sum_{n=1}^{\infty} A_n \cos w_n t + B_n \sin w_n t$$

where $$A_o = \frac{1}{T} \int_{-T}^{T} f(t).dt$$

$$A_n = \frac{1}{T} \int_{-T}^{T} f(t) \cos w_n t\, dt$$

$$B_n = \frac{1}{T} \int_{-T}^{T} f(t) \sin w_n t.dt$$

Since the function is even, the B_n coefficients are zero. Hence

$$f(t) = \frac{A_o}{2} + \sum_{n=1}^{\infty} A_n \cos \frac{n\pi t}{d} \qquad (A7.6)$$

i.e.

$$A_n = \frac{2}{d} \int_o^d f(t) \cos n\pi t.dt$$

$$= \frac{2a}{d} \int_b^d \cos \frac{n\pi t}{d} - \cos \frac{n\pi t}{d} \cos \pi(\frac{t-b}{d-b}).dt \qquad (A7.7)$$

Since $f(t)$ is zero from $t = 0$ to $t = b$, the integration goes from $t = b$ to $t = d$. Hence

$$A_n = \frac{2Id^2}{n\pi} \left[\frac{1}{n^2(d-b)^2 - d^2} \right] \sin \frac{n\pi b}{c} \qquad (A7.8)$$

Now consider the equation of each signal:

Noise signal

$$N = \frac{dL}{dt} = I \sin \pi(\frac{t-b}{d-b})$$

$$\therefore L = I(\frac{d-b}{\pi})\left[1 - \cos\pi(\frac{t-b}{d-b})\right]$$

Blade loading signal

$$L = I\left[1 - \cos(\frac{t-b}{d-b})\right]$$

$$\therefore N = \frac{dL}{dt} = I \sin \pi(\frac{t-b}{d-b}).\frac{\pi}{d-b} \qquad (A7.9)$$

As shown above, the two (N) noise equations differ only by a constant $\pi/(d-b)$ so that the A_n and B_n coefficients differ by some constant ratio.

In the Fourier equations

$$L(n) = \sum A_n \cos \frac{n\pi t}{d}$$

$$\frac{\partial L}{\partial t} = A_n \sin \frac{n\pi t}{d} . \frac{n\pi}{d}$$

$$N(n) \propto \overline{\left[\frac{\partial L}{\partial t}\right]^2} \propto A_n^2 . n^2 . \tfrac{1}{2}(\frac{\pi}{d})^2 \qquad (A7.10)$$

and

$$N(n) = \frac{\partial L}{\partial t} = \sum B_n \sin \frac{n\pi t}{d} .(\frac{\pi}{d-b})$$

$$N(n) \propto \overline{\left[\frac{\partial L}{\partial t}\right]^2} \propto B_n^2 \cdot \tfrac{1}{2}\left(\frac{\pi}{d-b}\right)^2 \qquad \text{(A7.11)}$$

Hence $A_n^2 . n^2 . K_1 = B_n^2 . K_2$ (A7.12)

where $K_1 = \left(\frac{\pi}{d}\right)^2$

and $K_2 = \left(\frac{\pi}{d-b}\right)^2$.

Equations (A7.5) and (A7.8) were computed and the corrections K_1 and K_2 made to the coefficients and the results compared in Figure A7.3.

It was intuitively expected that the maximum would be at the 13th harmonic (n = 13) or 200 Hz. Figure A7.3 clearly shows this is not true in this case, in fact the maximum occurs at the 11th harmonic (n=11).

The reason for this difference was not understood and so a manual calculation was executed. The two major terms in the Fourier analysis of the noise signal, namely

$$\sin \frac{n\pi b}{d} \quad \text{and} \quad \frac{1}{n^2(d-b)^2 - d^2}$$

were plotted for n = 1 → 25 and are shown in Figure A7.4. The curve for the sine $\frac{n\pi b}{d}$ term is shown to be symmetrical and goes to zero at n = 13. The curve for the other term is not symmetrical but has an infinite value at n = 13. For n = 13 the denominator of the term $1/(n^2(d-b)^2-d^2)$ becomes zero so the calculation has to be repeated for this special case when determining the coefficients. As the curve for this second term is not symmetrical this could explain why the computations show a maximum at n = 11.

Referring to Figure A7.3 it shows that the harmonics of n = 8 to n = 14 all lie within 0.75 dB of the maximum. When reduced to the same scale as on the narrowband analysis trace of the impulse the curve will appear flat between n = 8 and n = 14, as shown in Figure 5.34. In the past it has been assumed that the peak occurs at the frequency of the original noise signal. As shown above this assumption is not strictly true, although as a quick mental check it is a reasonable assumption.

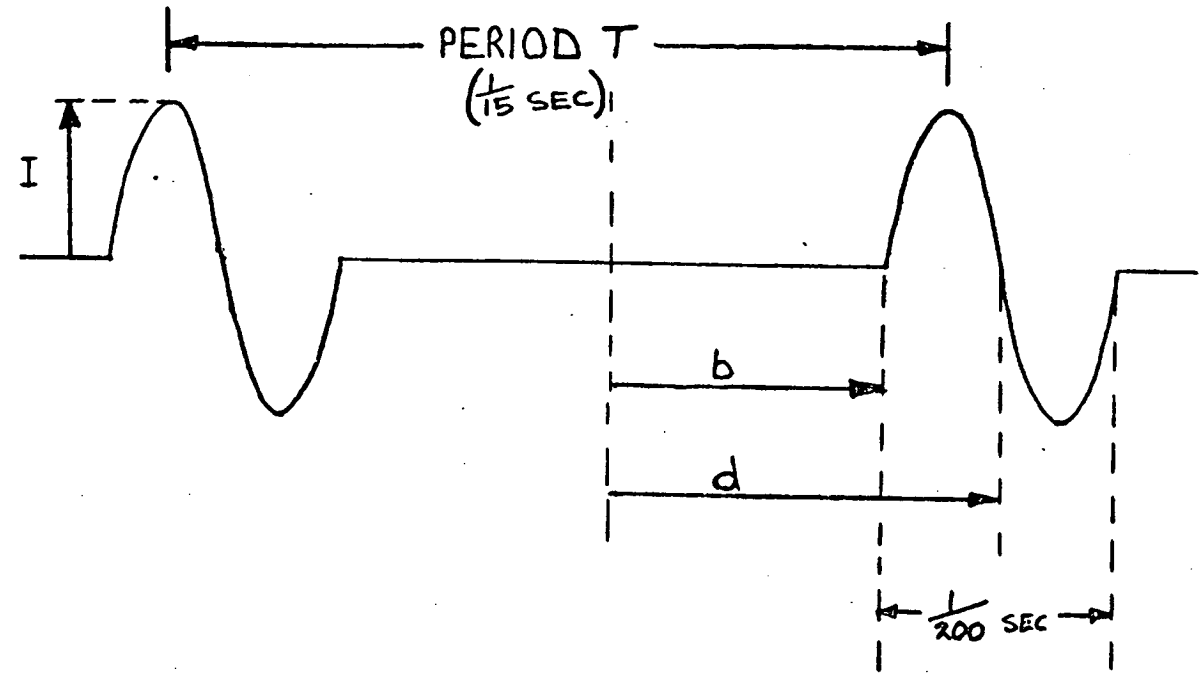

FIGURE A.7.1. IMPULSE (NOISE) WAVEFORM

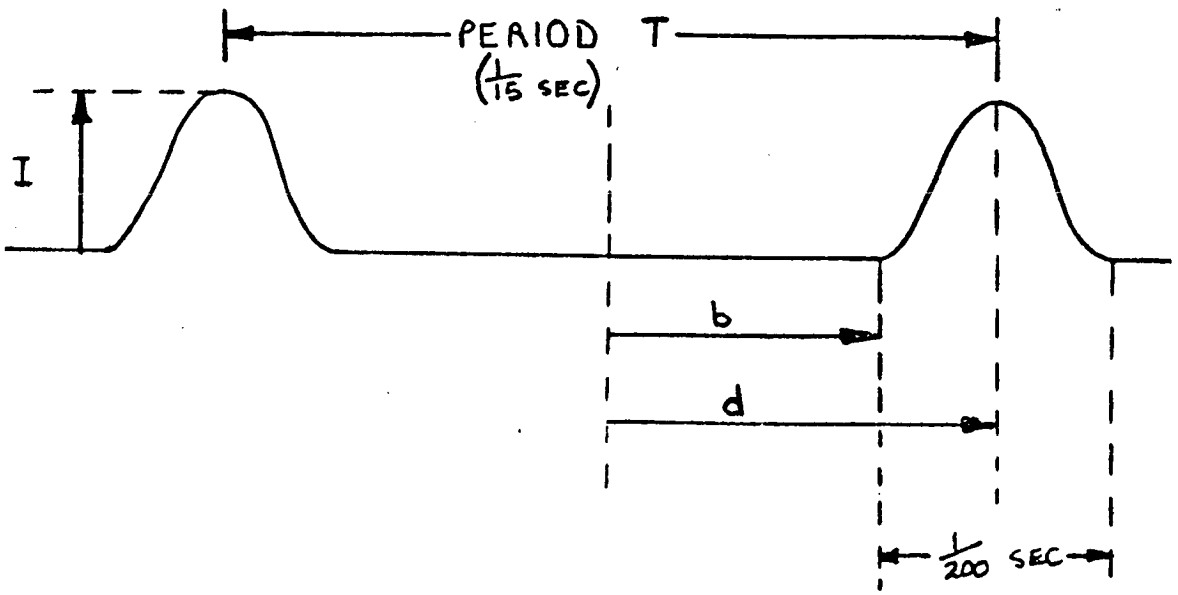

FIGURE A.7.2. BLADE LOADING

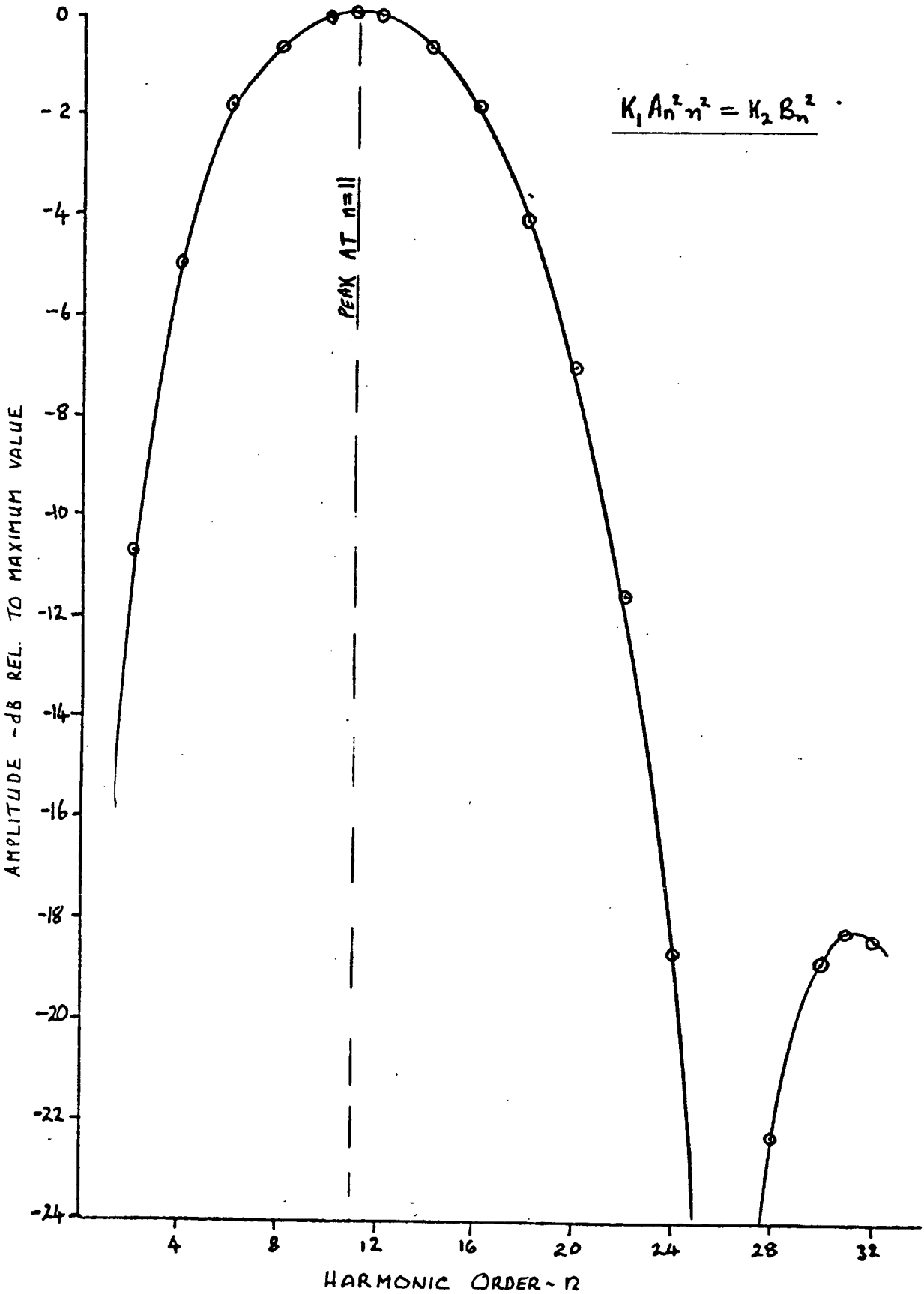

FIGURE A.7.3. SPECTRUM OF COEFFICIENTS $K_1 A_n^2 n = K_2 B_n^2$

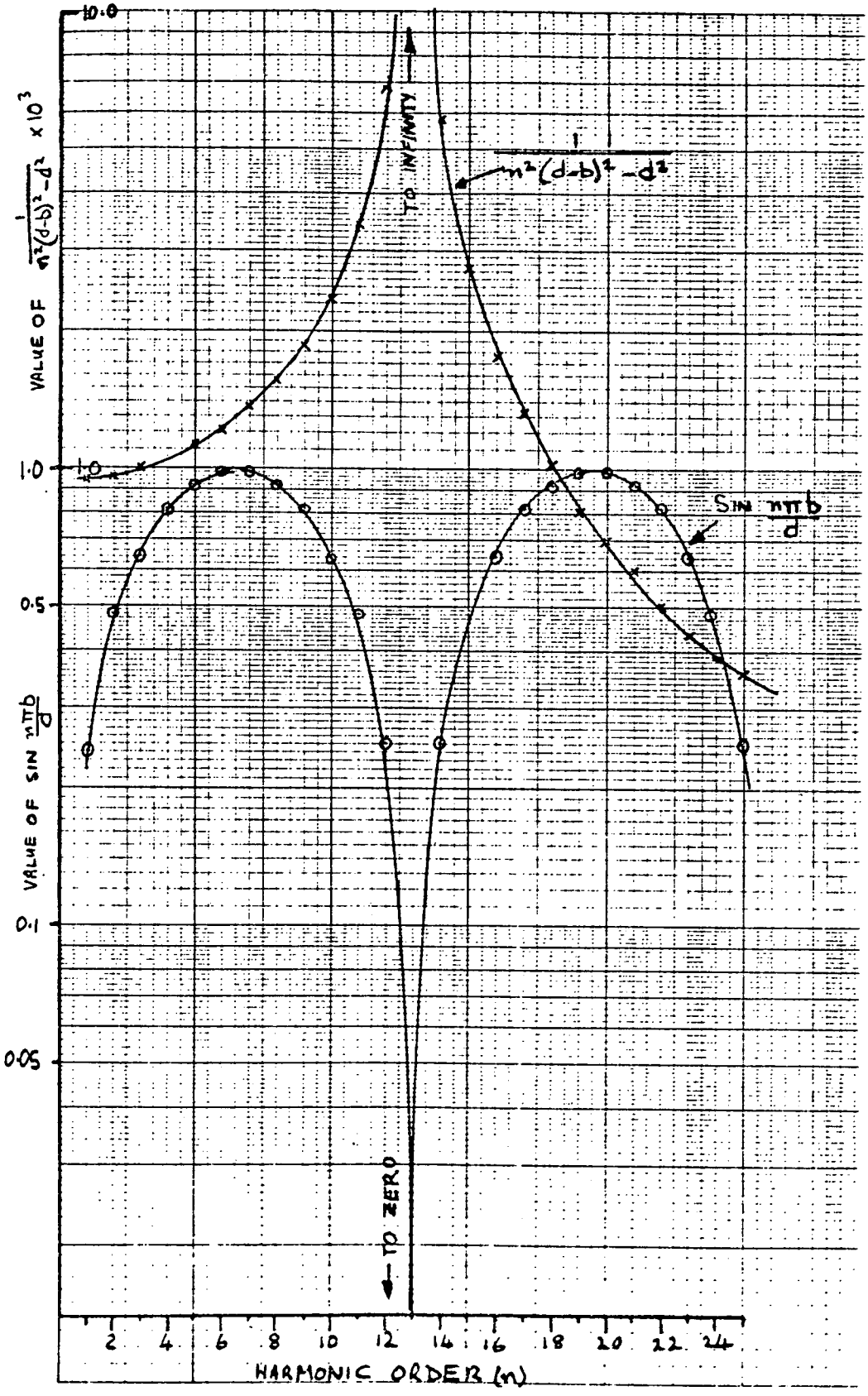

FIGURE A.7.4. SPECTRUM OF THE TERMS SIN $\frac{n\pi b}{d}$ AND $\frac{1}{n^2(d-b)^2-d^2}$

APPENDIX 8: BLADE LOADING PROGRAM

A8.1. CALCULATION PROCEDURE

The lift on the blade as it passed through the gust is given by the equation:

$$L(s) = Ae^{-as}\int_0^s w(\sigma)e^{a\sigma}.d\sigma + Be^{-s}\int_0^s w(\sigma)e^{\sigma}.d\sigma$$

The theory involved is explained in Appendix 4.

The above equation was programmed in Fortran IV Language for use on the 1907 ICT computer at the University of Southampton. The integration was achieved by the trapezoidal rule.

A flow diagram is shown in Figure A8.1 and the complete program is given in section A8.4.

A8.2. PROGRAM NOMENCLATURE (in order of appearance)

Name	Meaning
W	Maximum gust velocity, ft/s
X	Any point measured from start of gust, ins.
S	Any point measured from start of gust, dimensionless variable
WA	Variable given by $w(\sigma)e^{a\sigma}$
WB	Variable given by $w(\sigma)e^{\sigma}$
AA	Value under integral at each station $\int_0^s w(\sigma)e^{a\sigma}$
AB	Value under integral at each station $\int_0^s w(\sigma)e^{\sigma}$
EA	Variable given by e^{-as}
EB	Variable given by e^{-s}
XL	Lift on the blade, lbs/ft.
TITLE	Any desired title
RPM	Rotor rotational speed in revolutions per minute
WW	Gust velocity at each station, ft/s
PK	Number of air jets producing gust
N	Number of stations in gust
P	Integration interval, inches

V Blade velocity at centre of gust, ft/sec.

B Constant given by $B = \frac{1}{2}\rho V c a_o$ 0.065

A Constant given by $A = \frac{1}{2}\rho V c a_o$ 0.5

H Integration interval in trapezoidal rule

NN Number of stations outside of gust given by N x 5

J End code

= 0 if last case

= 1 if cases to follow

A8.3. PROGRAM INPUT PARAMETERS

The parameters which must be known to use the program are listed below.

Ω angular velocity of blade, r.p.m.

R diameter of rotor, feet

$w(\sigma)$ gust velocity, ft/s

Y gust length, ins.

c Blade chord, ins.

a_o lift curve slope

ρ density of air.

A8.4. COMPUTER PROGRAM

```
0008                    MASTER LIFT
0009                    DIMENSION W(500),X(500),S(500),WA(500),WB(500),AA(500),AB(500),EA(
0010                   1500),EB(500),XL(500),TITLE(12)
0011                    DIMENSION RPM(7)
0012                 22 CONTINUE
0013                    READ(1,6)TITLE
0014                 6  FORMAT(12A6)
0015                    READ(1,8)(RPM(K),K=1,7)
0016                 8   FORMAT(7F0.0)
0017                    READ(1,1)WW
0018                 1  FORMAT(F0.0)
0019                    READ(1,1)PK
0020                    READ(1,3)N
0021                 3  FORMAT(I3)
0022                    READ(1,4)(W(I),I=1,N)
0023                 4  FORMAT(8F0.0)
0024                    READ(1,1)P
0025                    DO 99 K=1,7
0026                    V=RPM(K)*3.14159265*0.135
0027                    B=0.002378*V*5.73/12.0
0028                    A=B*0.065*2.0
0029                    H=P*0.5
0030                    X(1)=0.0
0031                    DO 100 I=2,N
0032                100 X(I)=X(I-1)+P
0033                    DO 104 I=1,N
0034                    S(I)=X(I)/2.0
0035                     WA(I)=W(I)*EXP(0.13*S(I))
0036                104 WB(I)=W(I)*EXP(S(I))
0037                    XA=0.0
0038                    XB=0.0
0039                    DO 105 I=1,N-1
0040                    AA(I)=0.5*H*(WA(I)+WA(I+1))
0041                    AB(I)=0.5*H*(WB(I)+WB(I+1))
0042                    EA(I)=EXP(-0.13*S(I+1))
0043                    EB(I)=EXP(-S(I+1))
0044                    XA=XA+AA(I)
0045                    XB=XB+AB(I)
0046                105 XL(I)=A*EA(I)*XA+B*EB(I)*XB
0047                    NN=5*N
0048                    DO 101 I=N+1,NN+1
0049                101 X(I)=X(I-1)+P
0050                     DO 102 I=N,NN+1
0051                102 S(I)=X(I)/2.0
0052                    DO 106 I=N,NN
0053                    EA(I)=EXP(-0.13*S(I+1))
```

```
0054                    EB(I)=EXP(-S(I+1))
0055                106 XL(I)=A*EA(I)*XA+B*EB(I)*XB
0056                    WRITE(2,6)TITLE
0057                    WRITE(2,7)RPM(K),V,WW,PK
0058                 7  FORMAT(8HURPM(K)=,F7.3,2X,15HBLADE VELOCITY=,F7.3,3X,20HMAX. GUST
0059                   .VELOCITY =,F7.3,13HNO. OF JETS =,F3.1,/5X,6HX(INS),5X,8HL(LB/FT),5
0060                   2X,6HX(INS),5X,8HL(LB/FT),5X,6HX(INS),5X,8HL(LB/FT),5X,6HX(INS),5X,
0061                   38HL(LB/FT)///)
0062                    WRITE(2,2)(X(I+1),XL(I),I=1,NN)
0063                 2  FORMAT(5X,F7.4,5X,F7.3,5X,F7.3,5X,F7.3,5X,F7.3,5X,F7.3,5X,F7.3,5X,
0064                   1F7.3)
0065                 99  CONTINUE
0066                    READ(1,5)J
0067                 5  FORMAT(I2)
0068                    IF (J) 21,21,22
0069                 21  CONTINUE
0070                    STOP
0071                    END

END OF SEGMENT, LENGTH   422, NAME  LIFT
```

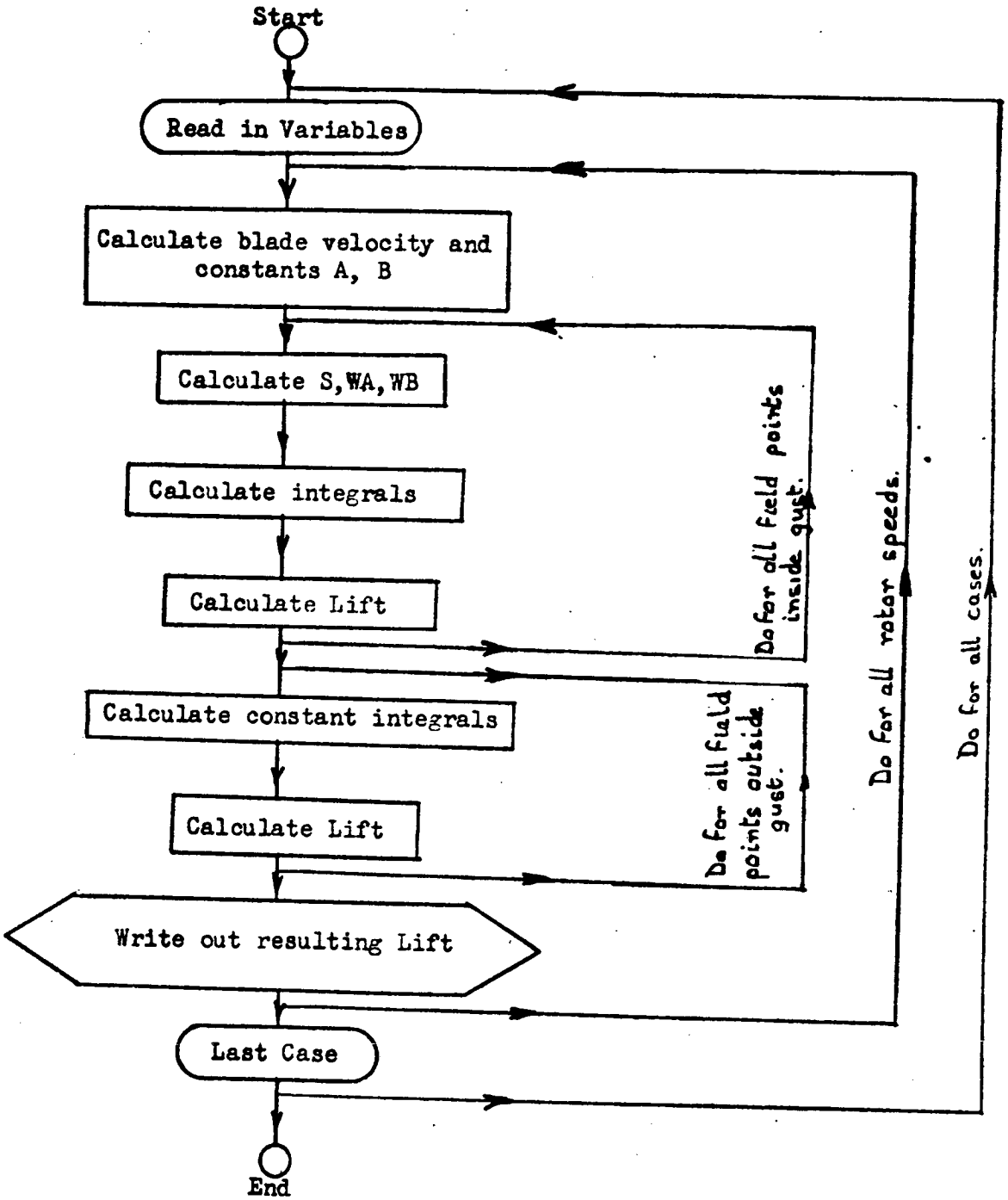

FIGURE A.8.1. PROGRAM FLOW DIAGRAM

APPENDIX 9: ROTATIONAL NOISE THEORY

A9.1. LIST OF SYMBOLS

B	rotor blade number
c	blade chord, inches
c_o	speed of sound, feet per second
D	distance from source point on rotor disc to field point inches
$L(r,\psi)$	total blade section loading at point (r,ψ) on the rotor disc, pounds per inch
m	harmonic number
p_{re}'	real component of sound pressure, pounds per in^2
p_{im}'	imaginary component of sound pressure, pounds per in^2
r	distance from centre of rotor head to source point on the rotor disc, inches
R_T	tip radius, inches
R_f	distance from centre of rotor head to field point, inches
SP_{mB}	root-mean square sound pressure at a field point, pounds per $inch^2$
Ω	rotor rotational speed, radians per second
β	blade pitch angle, degrees
ψ	azimuth angle in rotor plane, degrees (0^o at tail, positive in direction of rotation)
θ	field point azimuth angle, degrees
σ	angle between rotor plane and field point, degrees (positive upwards)

A9.2. ROTATIONAL NOISE PROGRAM

A modified version of the computer program for the prediction of rotational noise due to fluctuating loading on rotor blades, developed by Tanna [18] was used to calculate the rotational noise.

A9.3. SUMMARY OF ROTATIONAL NOISE PROGRAM

With reference to the rotor and field point geometry shown in Figure A9.1, the r.m.s. value of the m^{th} harmonic of sound pressure, SP_{mB}, at a field point (R, θ, σ) due to a B-bladed rotor rotating at Ω radians per second is given by:-

$$SP_{mB} = \frac{R_T}{2\sqrt{2}\pi c}\left[(p_{re}')^2 + (p_{im}')^2\right]^{\frac{1}{2}} \qquad (A9.1)$$

where

$$p_{re}' = \int_0^{R_T}\int_0^{2\pi} \frac{L(r,\psi)}{mD^2}\sin\left(\frac{mcB}{2r}\right).\left[\frac{mB\Omega}{c_o}\sin U + \frac{\cos U}{D}\right].$$

$$\left[\sin\beta.\cos\sigma.\sin(\psi-\theta) + \cos\beta.\sin\sigma\right] r\,dr\,d\psi \qquad (A9.2)$$

and

$$p_{im}' = \int_0^{R_T}\int_0^{2\pi} \frac{L(r,\psi)}{mD^2}\sin\left(\frac{mcB}{2r}\right).\left[\frac{mB\Omega}{c_o}\cos U - \frac{\sin U}{D}\right].$$

$$\left[\sin\beta.\cos\sigma.\sin(\psi-\theta) + \cos\beta.\sin\sigma\right] r\,dr\,d\psi \qquad (A9.3)$$

for which

$$U = mB\left[\frac{\Omega D}{c_o} + \frac{c}{2r} + \psi\right] \qquad (A9.4)$$

$$D = \left[R_T^2 + r^2 - 2R_T r\cos\sigma\cos(\psi-\theta)\right]^{\frac{1}{2}} \qquad (A9.5)$$

The method used repeatedly evaluated the basic sound pressure equations (A9.1), (A9.2) and (9.3). This includes a double integration. One integration is around the rotor disc with the sample points (azimuth angles) chosen at constant intervals. The other integration is along the radius where sample radial stations are unevenly spaced. A subroutine called SIMCOR is included to perform the integration by the trapezoidal rule.

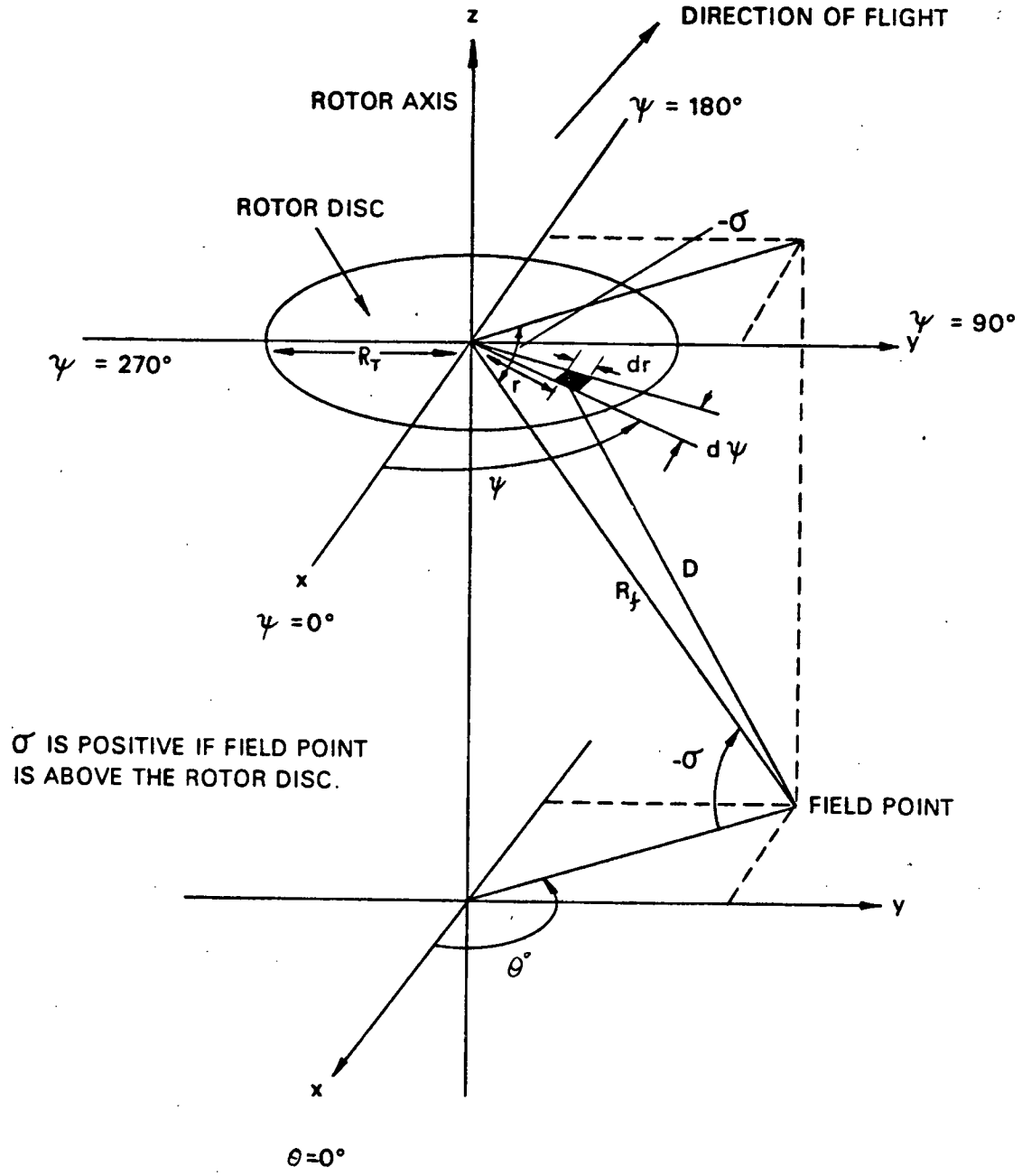

FIGURE A.9.1. ROTOR GEOMETRY AND FIELD POINT LOCATION

APPENDIX 10: ROTATIONAL NOISE PROGRAM

A10.1. PROGRAM MODEL

The computer program for the prediction of rotational noise due to fluctuating loading on rotor blades was modified for use in this investigation of transient rotor noise.

The working of the program is fully explained in reference (18) and the theory summarised in Appendix 9.

The flow diagram is shown in Figure A10.1 and a copy of the program printout is shown in section A10.2.

The modifications made to the program given in reference (18) are as follows:

(a) the lift on the blade is read in as direct blade loading in lbs/ft instead of steady and harmonic components,

(b) the lift is only read in over the blade loading profile length; the program takes the lift on the remainder of the rotor disc to be zero,

(c) the chord length used is an 'effective chord' and must be small in relation to the azimuth integration interval.

```
LINE                                ATLAS  FORTRAN                    12/12/71        VERSION 7
NUMBER                          SOURCE ROUTINE LISTING                 16.39.41    COUNTER*      11
                                                                                  LABEL FIELD
    1          DIMENSION D(1222,7),R(7),V8(7),V8I(7),TITLE(12),V2S(1222),V2SI(122
              15),PSI(1222),PRAD(1222),XL(7,1222)
    2          DIMENSION XXL(1222)
    3          RAD=1./57.2957795
          C    READ FLT. COND. PARAMETERS AND BLADE SECTION LOADING. PRINT SAME.
    4        111 READ 2,TITLE
    5          2 FORMAT(12A6)
    6            READ 3,NEND,NFP,RBN,CHG,CM,SOS,R0,B01,B1,B11,Q
    7          3 FORMAT(2I2,9F8.2)
    8            READ 31,NHAR,NRAD,ANG
    9         31 FORMAT(2I2,F10.7)
   10            NP=IFIX((360.0/ANG)+1.001)
   11            NT=NP-1
   12            PSI(1)=0.
   13            PRAD(1)=0.
   14            DO 4 I=2,NP
   15            PSI(I)=PSI(I-1)+ANG
   16          4 PRAD(I)=PSI(I)*RAD
   17            READ 7,(R(I),I=1,NRAD)
   18            READ 66,NPG
   19         66 FORMAT(I3)
   20            READ 7,(XXL(J),J=1,NPG)
   21          7 FORMAT(7F-5.2)
   22            ABC=0.0
   23            CBA=3.14159265/6.0
   24            DO 9 I=1,NRAD
   25            DO 10 J=1,NPG
   26         10 XL(I,J)=XXL(J)*SINF(ABC)
   27          9 ABC=ABC+CBA
   28            DO 77 I=1,NRAD
   29            DO 77 J=1,NPG
   30         77 D(J,I)=XL(I,J)/12.0
   31            DO 777 I=1,NRAD
   32            DO 777 J=NPG,NP
   33        777 D(J,I)=0.0
   34         88 PRINT 2,TITLE
   35            PRINT 8,B01,B1,B11,CM,OMG,RBN,R0,(R(I),I=1,NRAD)
   36          8 FORMAT(4HOB01,E15.6,4H  B1,E15.6,5H  B11,E15.6,7H  CHORD,E15.6,7H
                 1 OMEGA,E15.6,8H  BLADES,F7.0,//25H RADIUS AT START OF TWIST,F15.6,
                 2////30X,21HBLADE SECTION LOADING,///7H RADIUS,10X,1H1,14X,1H2,14X,
                 31H3,14X,1H4,14X,1H5,14X,1H6,14X,1H7,/8H AZIMUTH,2X,7F15.6//)
   37            PRINT 2,TITLE
   38            OMG=3.14159265*OMG/30.
   39            SOS=12.*SOS
   40            B01=B01*RAD
   41            B1=B1*RAD
   42            B11=B11*RAD
   43            Q=Q*RAD
          C    BEGIN MAJOR LOOP ON FIELD POINTS
   44            DO 999 II=1,NFP
   45            READ 11,CAPR,THETA,ALFA
   46         11 FORMAT(3F12.4)
   47            PRINT 12,CAPR,THETA,ALFA
   48         12 FORMAT(12H0FIELD POINT,10X,6HRADIUS,E15.6,5X,7HAZIMUTH,E15.6,5X,9H
                 1ELEVATION,E15.6,//20X,8HHARMONIC,10X,14HSOUND PRESSURE,15X,3HSPL)
```

A10.2: COMPUTER PROGRAM (CONTD)

```
      CAPR=12.*CAPR
      ALFA=RAD*ALFA
      THETA=RAD*THETA
      DO 999 M=1,NHAR
      DO 990 KK=1,NRAD
      DO 99 JJ=1,NT
      CAPS=SQRTF(CAPR*CAPR+R(KK)*R(KK)-2.*CAPR*R(KK)*COSF(ALFA)*COSF(PRA
     1D(JJ)-THETA))
      BETA=B01-G*(R(KK)-R0)+B1*COSF(PRAD(JJ))+B11*SINF(PRAD(JJ))
      SBTA=SINF(BETA)
      CBTA=COSF(BETA)
      V=M
      V=V*(RBN*OMG*CAPS/SOS+.5*CH*RBN/R(KK)+RBN*PRAD(JJ))
      TEMP=M
      V25(JJ)=(Q(JJ,KK)*SINF(.5*TEMP*RBN*CH/R(KK))*(COSF(V)/CAPS+(TEMP*R
     1BN*OMG/SOS)*SINF(V))*(SBTA*COSF(ALFA)*SINF(PRAD(JJ)-THETA)+SINF(AL
     2FA)*CBTA)*R(KK))/(TEMP*CAPS*CAPS)
      V25I(JJ)=(Q(JJ,KK)*SINF(.5*TEMP*RBN*CH/R(KK))*(COSF(V)*TEMP*RBN*OM
     1G/SOS-SINF(V)/CAPS)*(SBTA*COSF(ALFA)*SINF(PRAD(JJ)-THETA)+SINF(ALF
     2A)*CBTA)*R(KK))/(TEMP*CAPS*CAPS)
   99 CONTINUE
      V25(NP)=V25(1)
      V25I(NP)=V25I(1)
      MN=NP
      CALL SIMCOR (NP,PRAD,V25,AR,MN)
      V8(KK)=AR
      CALL SIMCOR (NP,PRAD,V25I,AR,MN)
      V8I(KK)=AR
  990 CONTINUE
      MN=NRAD
      CALL SIMCOR (NRAD,R,V8,PRTAR,MN)
      CALL SIMCOR (NRAD,R,V8I,PRTAI,MN)
      PRTA=(.03582245*CAPR/CH)*SQRTF(PRTAR**2+PRTAI**2)
      SPL=20.*0.4353*ALOGF(ABSF(PRTA/2.9E-9))
      PRINT 997,M,PRTA,SPL
  997 FORMAT(25X,I2,5X,2E20.8)
  999 CONTINUE
      IF(NEND) 9999,9999,111
 9999 GO TO EXIT
      END
```

```
LINE                        ATLAS  FORTRAN                 12/12/71        VERSION 7
NUMBER               SOURCE ROUTINE LISTING                16.30.52     COUNTER.     578
                                                                     LABEL FIELD
      SUBROUTINE SIMCOR (N,A,X,R,MN)
      DIMENSION A(MN),X(MN)
      R=0.
      DO 159 MM=2,N
  159 R=R+(X(MM-1)+X(MM))*(A(MM)-A(MM-1))/2
      RETURN
      END
```

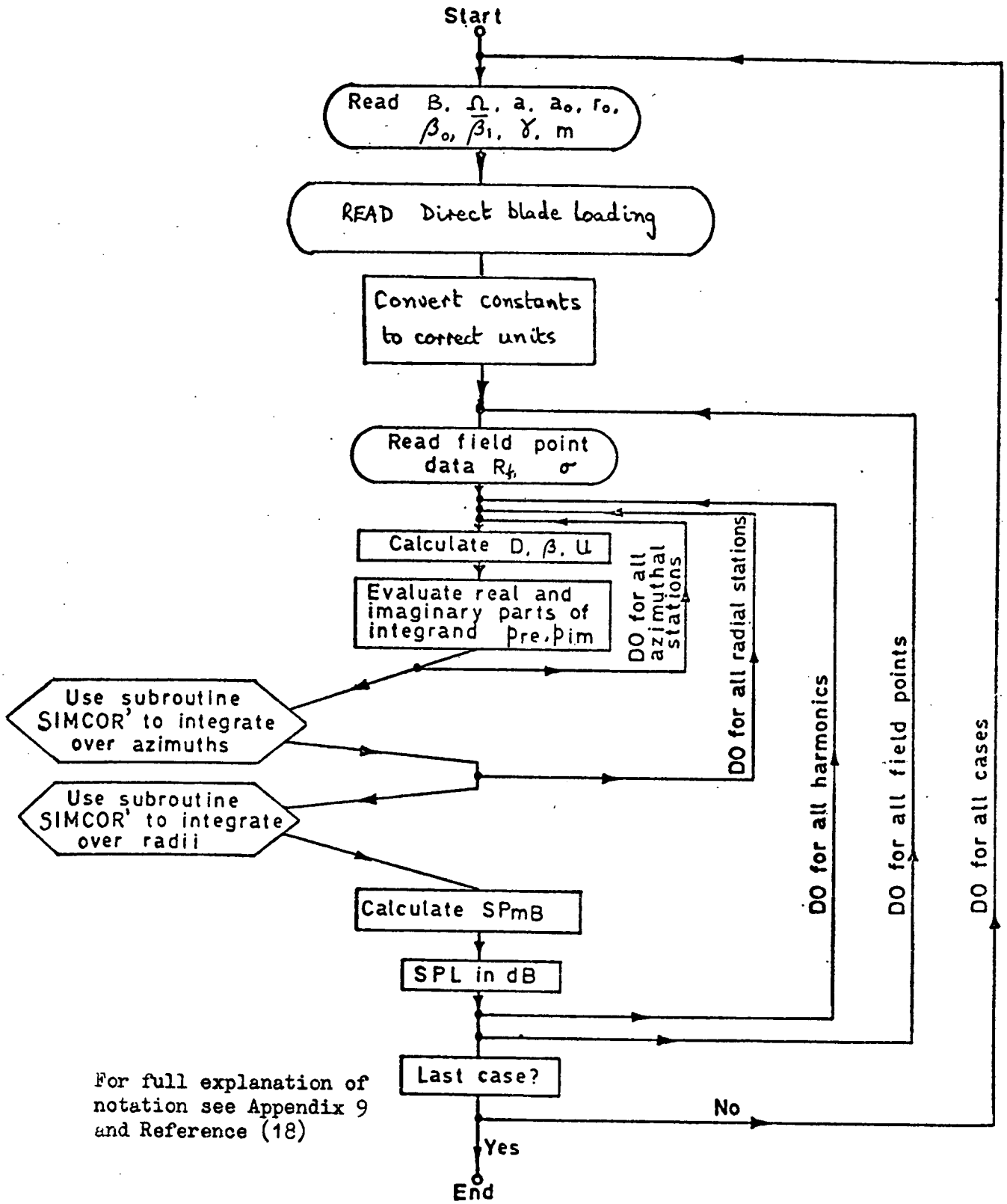

FIGURE A.10.1. PROGRAM FLOW DIAGRAM

APPENDIX 11: INVESTIGATION OF ERRORS IN INITIAL ROTATIONAL NOISE PROGRAM

A11.1. INTRODUCTION

As mentioned in the main text (Chapter 6 - section 6.4.3.1) the rotational noise program when originally used gave levels for the discrete frequency rotational noise which were very low (when compared to the simple dipole model and acoustic measurements) and appeared in error. This prediction method - which is outlined in Appendix 10 - was based on a program developed by Tanna [18] as a part of a theoretical investigation into the generation of rotor noise by Wright and Tanna [29]. In this appendix the investigation aimed at clarifying this situation and the results obtained are outlined. Since the program is complex and the arguments somewhat involved, they are presented in a descriptive and diagrammatic form rather than in mathematical terms. In this discussion all other aspects relating to the program are ignored and it is assumed that the basis of the rotational noise program is correct.

A11.2. STANDARD PROCEDURE

To enable the degree of accuracy required in predicting the sound pressure level (SPL) of the rotational noise harmonics to be obtained, azimuth integration intervals chosen were 0.25" or 0.5" (corresponding to approximately 0.3° and 0.6°) depending on the 'sharpness of the gust' under consideration. These values were selected after discussion with Tanna and are more demanding than the general recommendations for the choice of integration interval which implies that if 40 harmonics on a 3 blade rotor are of interest (i.e. if maximum mB = 120), then the 'maximum tolerable' integration interval would be 1°. In Tanna's final report [130] it is, however, stressed that it is advisable to leave a safety margin whenever possible in order to ensure a valid computation.

In the rotational noise program the chordwise distribution is assumed to be rectangular in shape; in other words at each azimuth station considered, the blade loading is assumed to be uniform over the blade chord width as indicated in Figure A11.1. When studying the characteristics of full scale rotors the azimuth integration is usually taken to be of the same order as the blade chord and therefore the 'rectangular loading profile' interpretation is a good approximation to a slowly varying profile as illustrated in Figure A11.2.

A11.3. TRANSIENT LOADING CASE

Consider now the case relating to a transient loading profile. As mentioned above the azimuth integration interval has to be small to enable the required accuracy, particularly in the case of the high harmonics, to be obtained. For the sharp gusts the 'integration step' was taken as 0.25 inch (0.3^{o}). The program assumes that at each 'station' the loading is uniformly distributed (rectangular) over the complete chord. This is shown diagrammatically in Figure A11.3 and it is obvious that the program is falsely interpreting the loading profile. It can be seen from this figure that the impulse is to some extent 'smoothed out' but more important it is extended or elongated. The result of this is that the high harmonics given by the Fourier analysis are reduced. This can be seen by reference to Figure A11.4 which shows, in a simplified form, the Fourier analysis of 'single pulse' whose duration is increased (elongated).

A11.4. USE OF 'EFFECTIVE CHORD'

It seemed clear from this review that use of the real blade chord in the program was giving rise to the problems encountered and following further discussions with Tanna it was agreed to investigate this aspect in some depth. A study was therefore made of the effect of varying the 'chord length' and azimuth integration interval. The chord, termed for convenience 'effective chord', was varied between 0.1 and the true value of 4 inches and the integration (azimuth) interval between 0.25 and 0.5 inches for three different idealised profiles.

The comparisons made are set out in Figures A11.5 to A11.7, together with the blade loading profiles considered. As can be seen from these figures the larger the 'effective chord' the lower the predicted SPL values. As the 'effective chord' approaches a value equal to the integration (azimuth) interval, then the case is reached where the final value is independent of the 'effective chord' length. It was also shown for a short gust that providing the integration interval was sufficiently small, then (with the 'effective chord' set at a value equal or less than the integration interval) the results of the rotational noise program agreed with those obtained analytically and by use of the simple dipole model. A typical set of results which shows the SPL values given by the rotational noise program, used in the manner described above, and the point dipole program are given in Figure A11.8. The differences between the two programs are plotted on Figure A11.9

and as can be seen are less than 1 dB over a large portion of the harmonic range considered. The difference at the first and second harmonics is somewhat large and this is considered to be due to errors arising from the fact that although a 'sharp gust' is considered, it is still of a significant size when compared with the 'point dipole' concept.

It followed from this study that in calculating the SPL values using the rotational noise program both a small integration (azimuth) interval and an 'effective chord' was used. Normal procedure was to set these to the same value, with the final selection being based on an inspection of the 'input gust'.

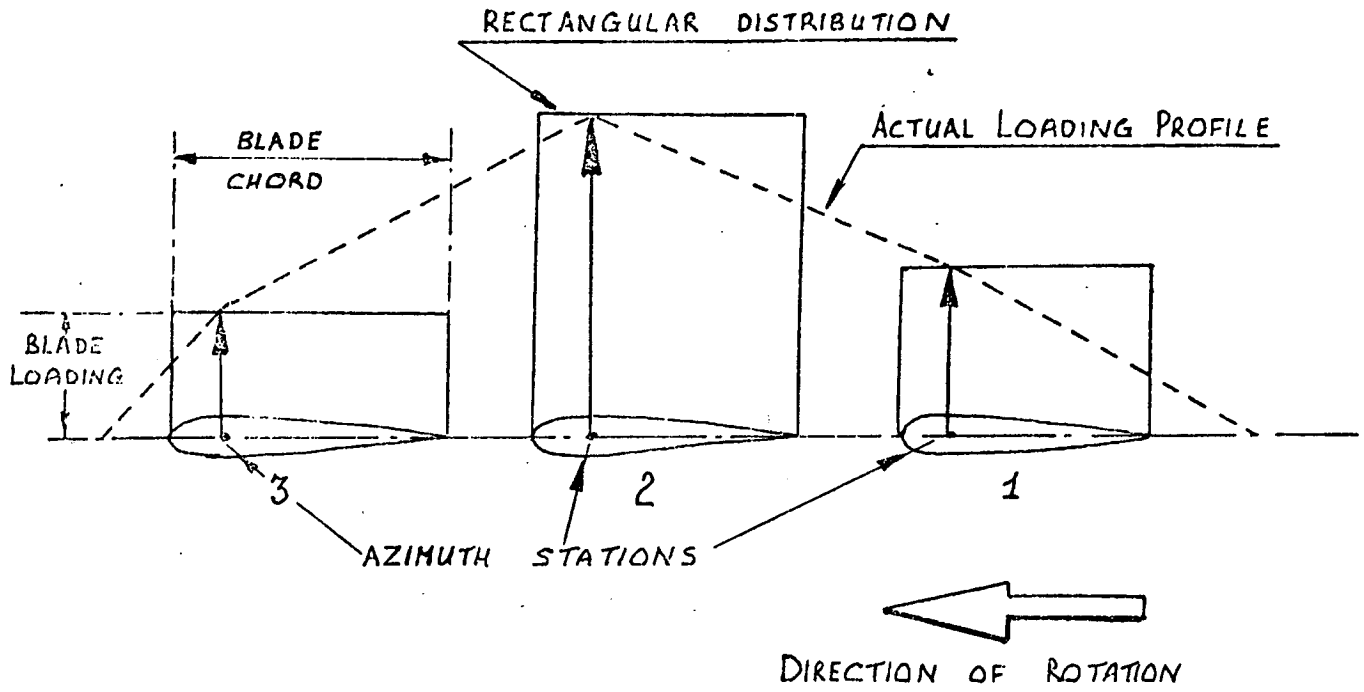

FIGURE A.11.1. RECTANGULAR BLADE LOADING MODEL

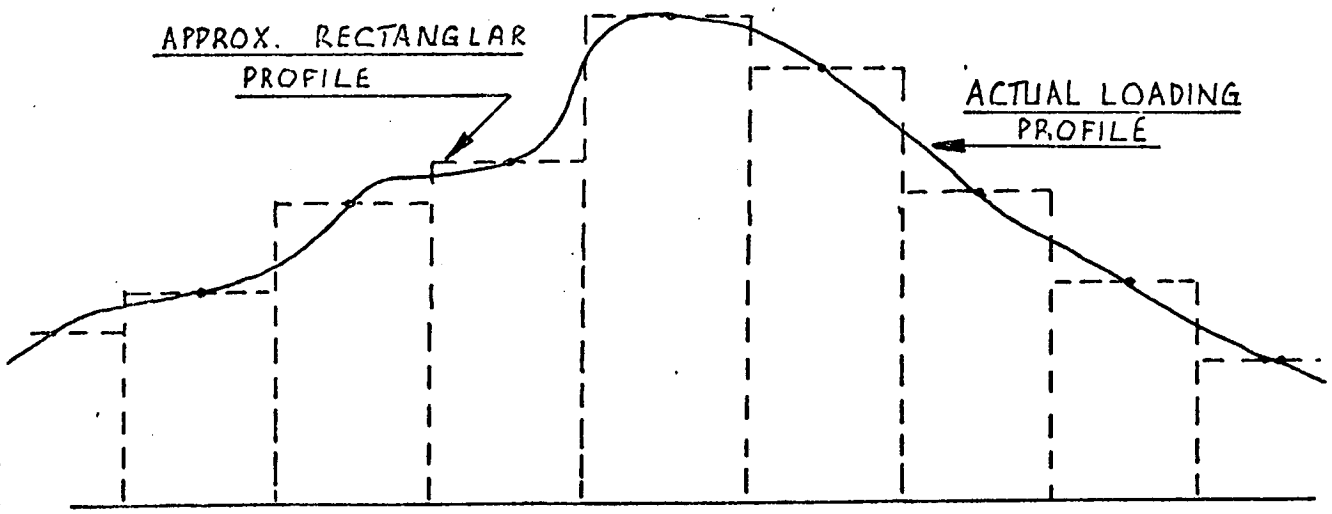

FIGURE A.11.2. SLOWLY VARYING LOADING PROFILE

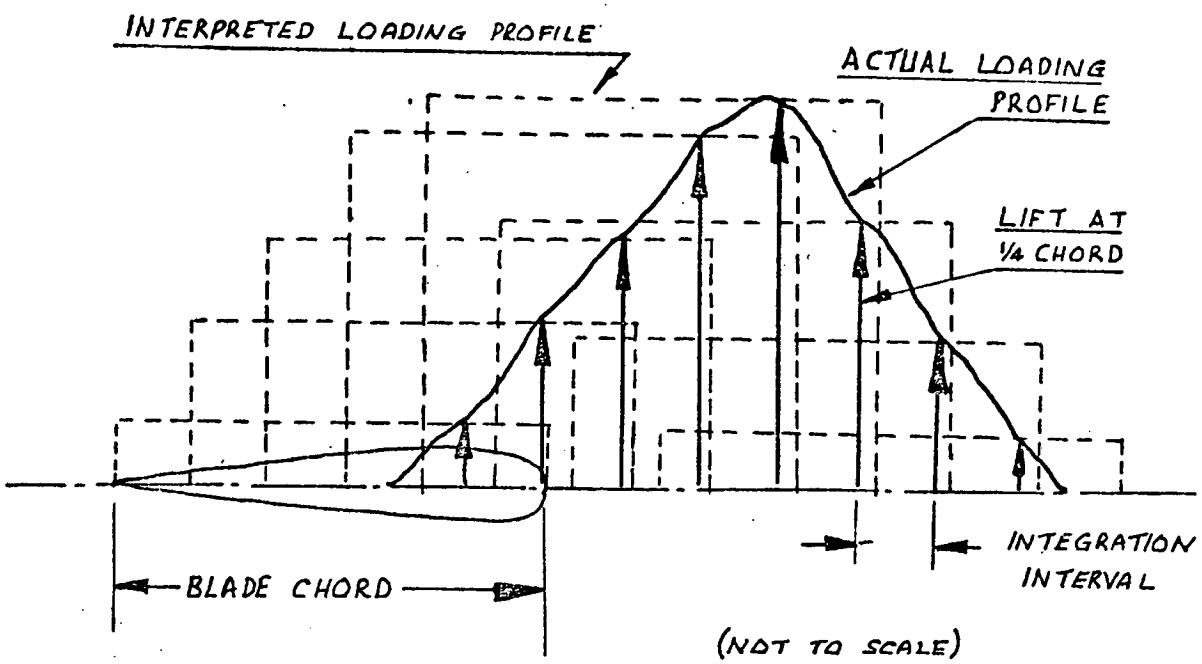

FIGURE A.11.3. RAPIDLY VARYING LOADING PROFILE

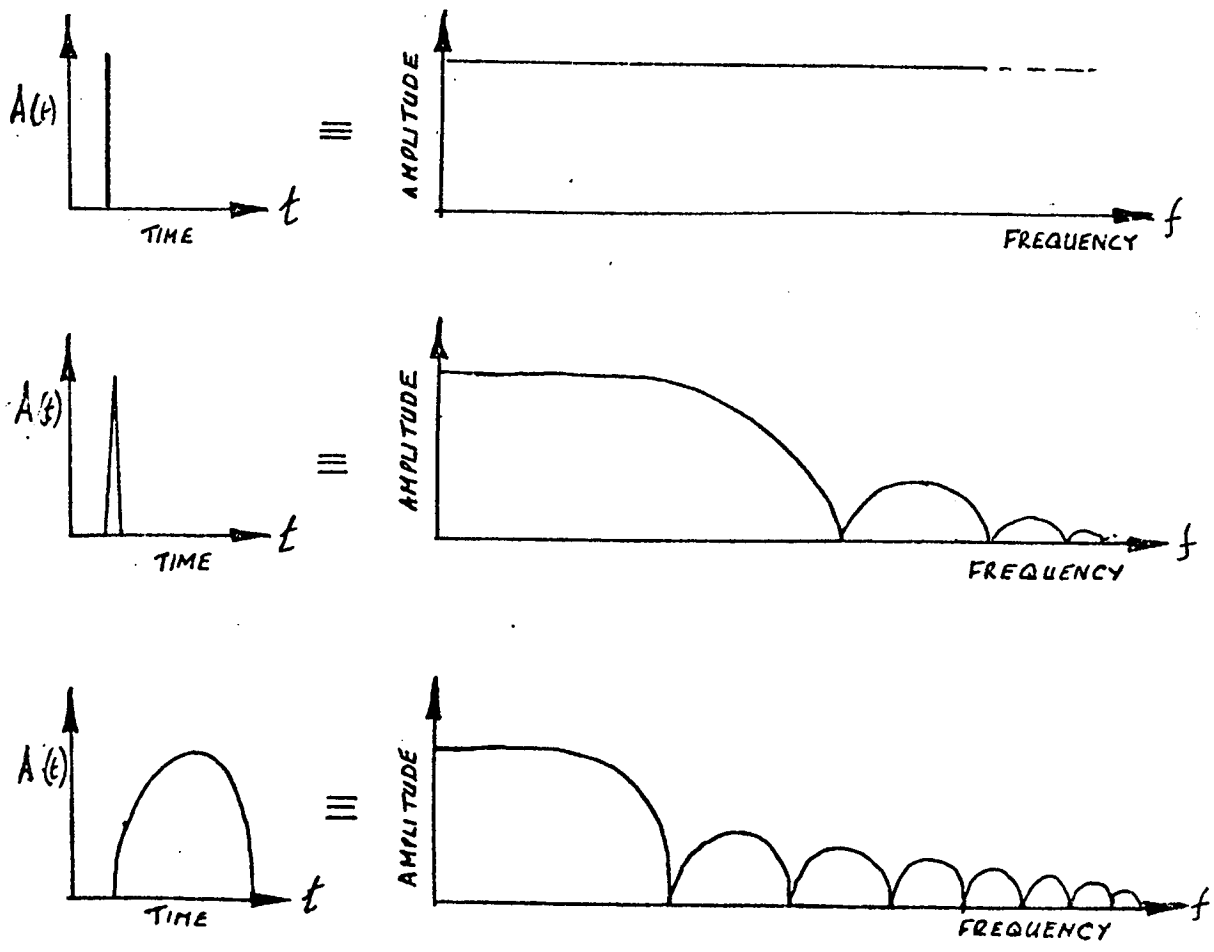

FIGURE A.11.4. DIAGRAMMATIC REPRESENTATION OF FOURIER ANALYSIS

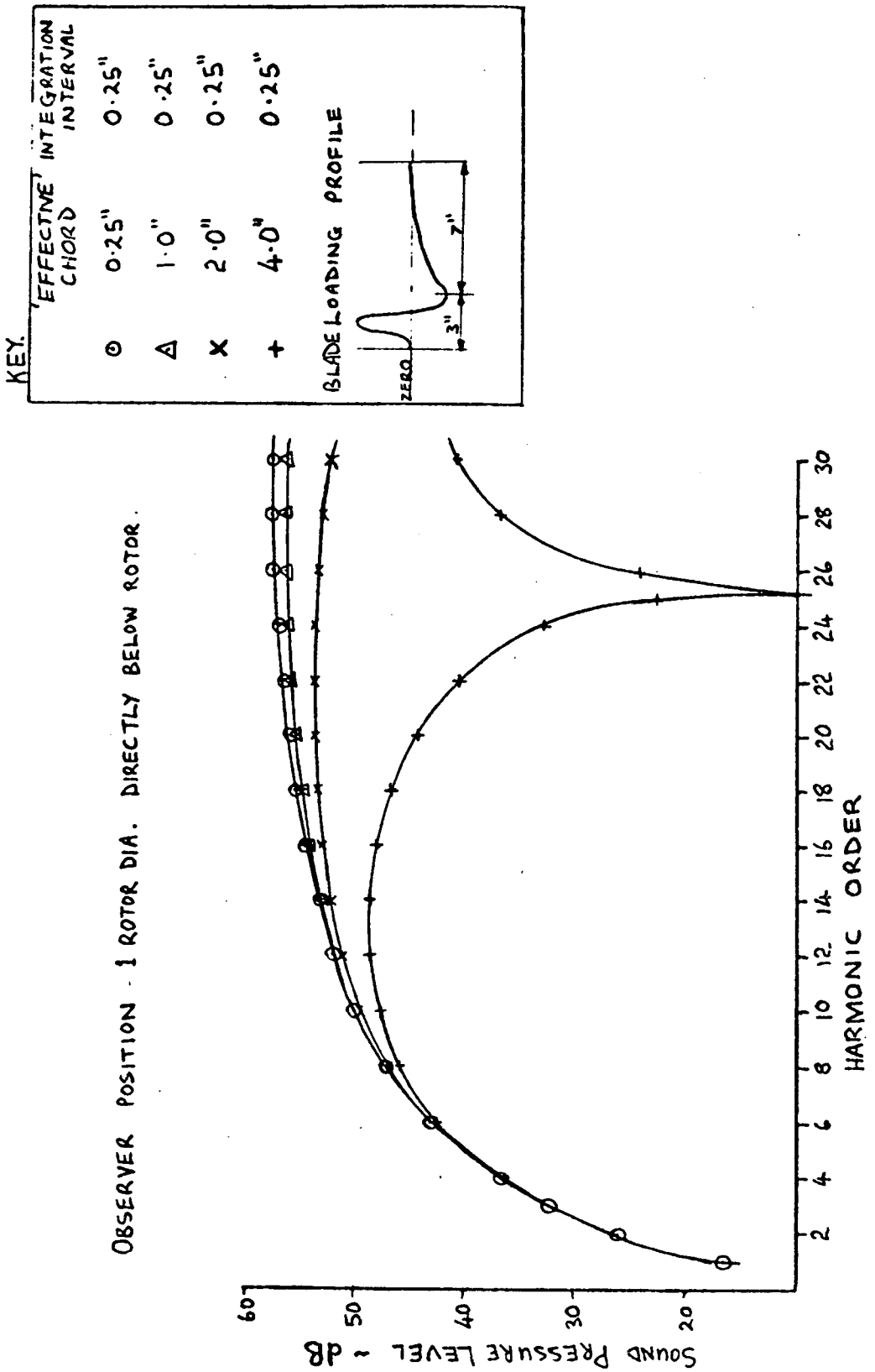

FIGURE A.11.5. COMPUTED SPL - SINE WAVE TYPE GUST

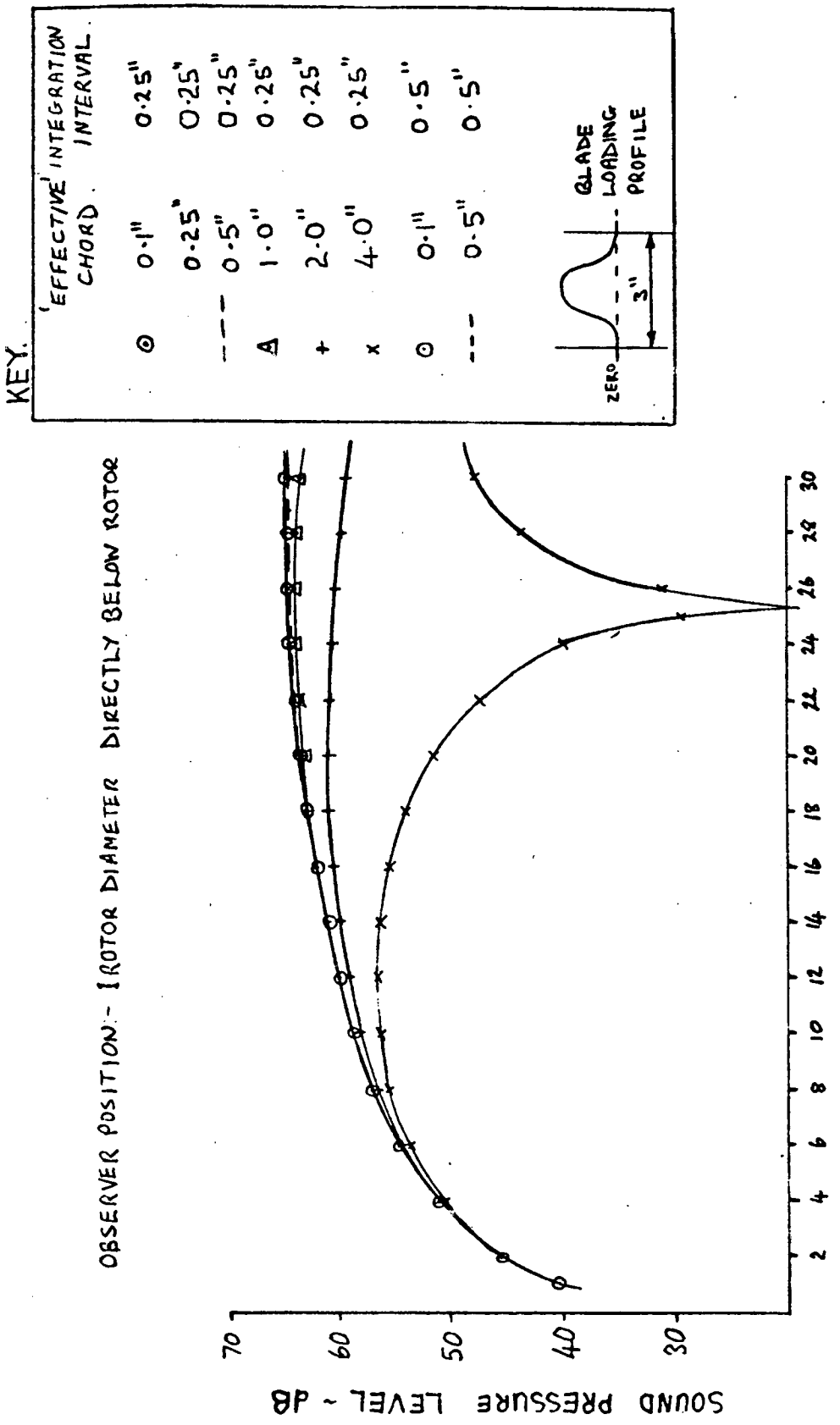

FIGURE A.11.6. COMPUTED SPL - COSINE WAVE TYPE GUST

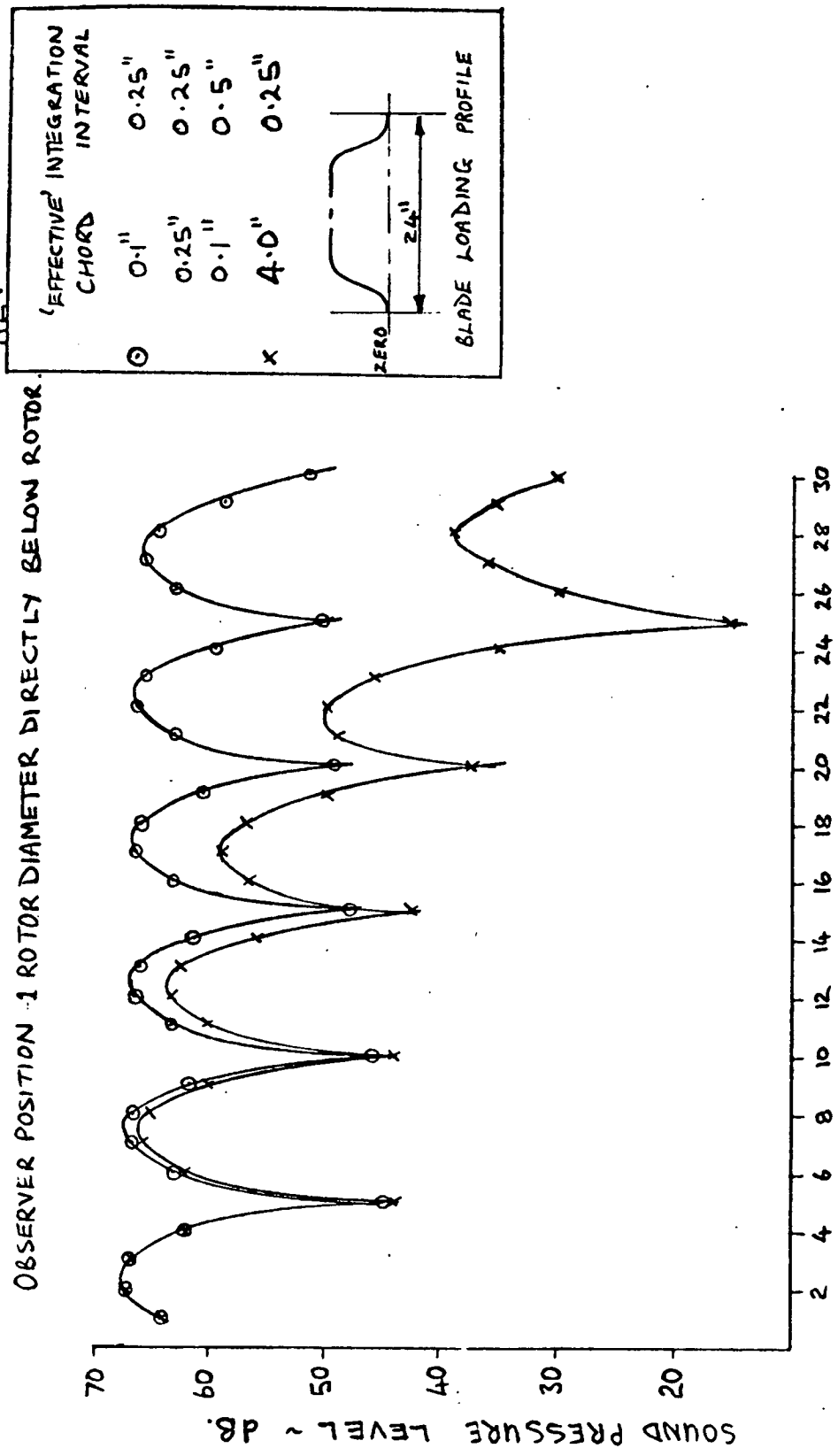

FIGURE A.11.7. COMPUTED SPL - EXTENDED COSINE WAVE TYPE GUST

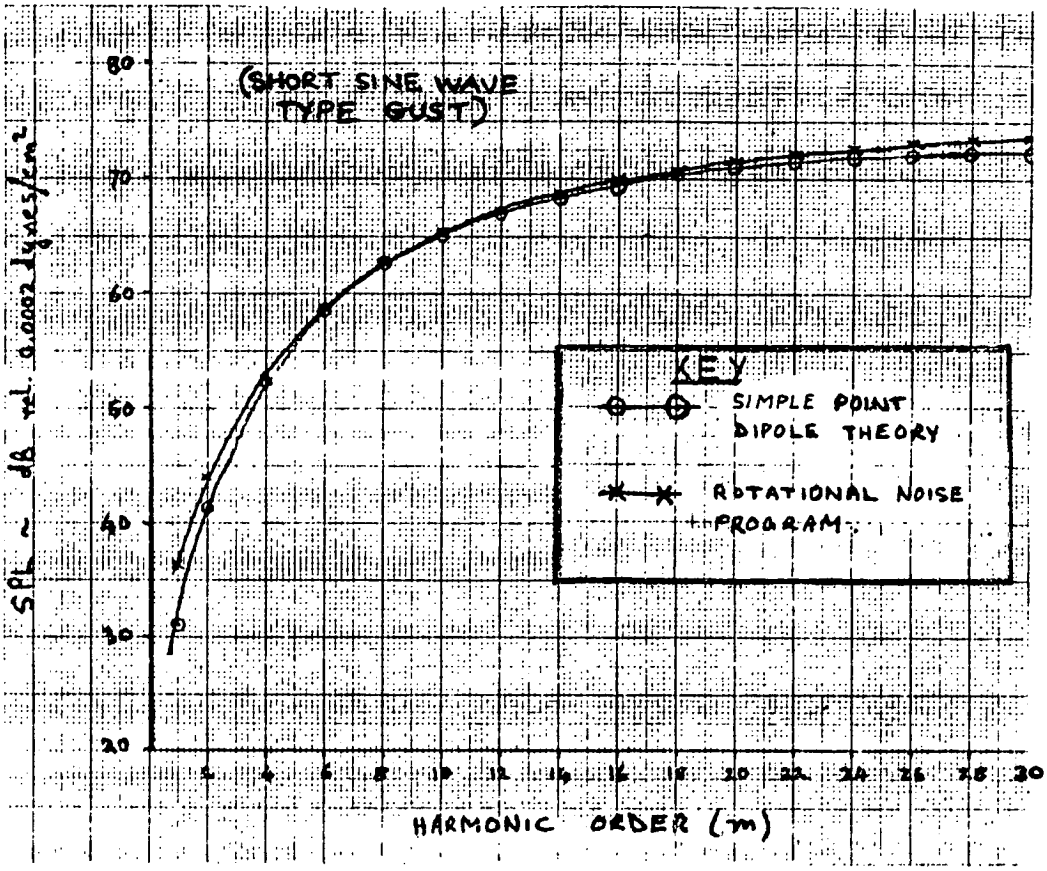

FIGURE A.11.8. COMPARISON OF SIMPLE POINT DIPOLE AND ROTATIONAL NOISE PROGRAM PREDICTIONS

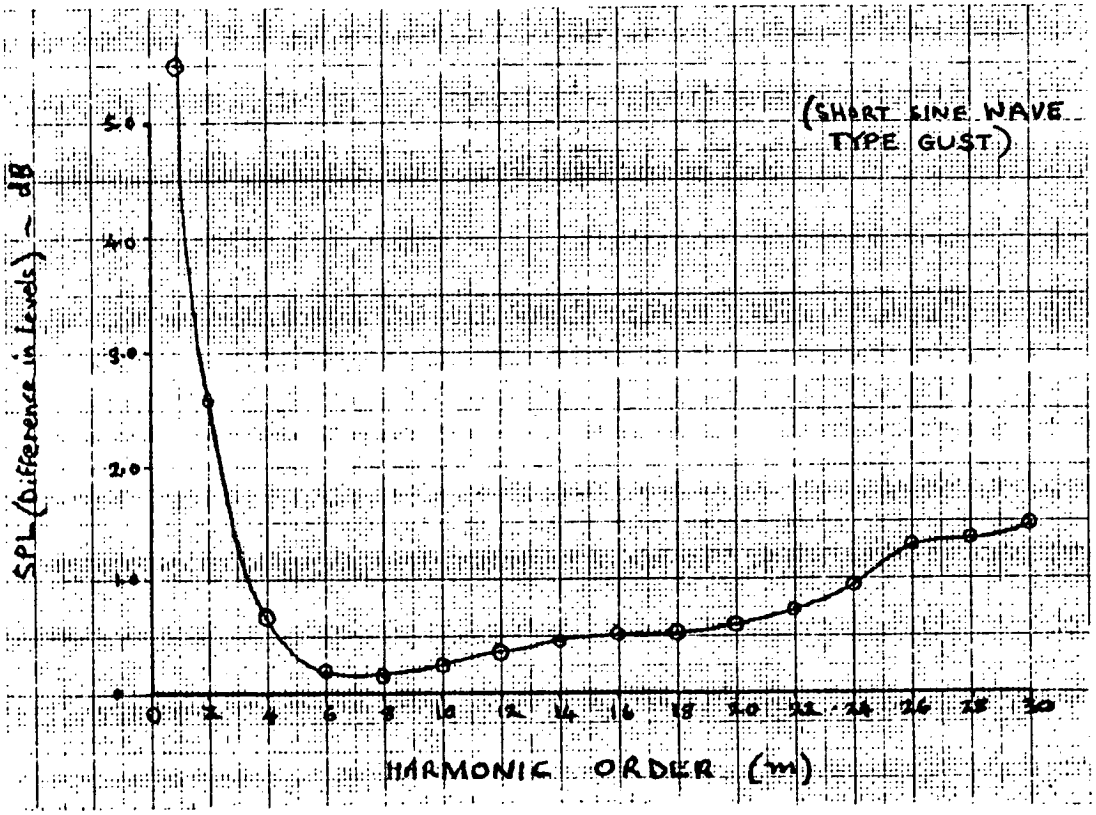

FIGURE A.11.9. DIFFERENCE BETWEEN SIMPLE POINT DIPOLE AND ROTATIONAL NOISE PROGRAM PREDICTIONS

APPENDIX 12: BLADE/FUSELAGE INTERACTION THEORETICAL DEVELOPMENT*

A12.1. CALCULATION OF THE CHANGE IN BLADE CIRCULATION DUE TO THE PRESENCE OF THE FUSELAGE

To calculate the change in blade circulation due to the presence of a fuselage, use is made of a Milne-Thomson theorem [143] since an exact method is not known. This theorem allows the circulation around a circular cylinder to be written down if the position of the stagnation point on the cylinder is known. The theorem states that if a point z_s is to be a stagnation point on the cylinder, and if the cylinder is placed in a flow field whose complex potential is $f(z)$, then the circulation around the cylinder is given by:

$\Gamma = 2\pi K = 2\pi \times$ Real part of $2i z_s f'(z_s)$.

In the case under consideration the cylinder is in fact the transformed circle of radius $a_1 = c/4$ which would transform into a flat plate of chord 'C' under the transformation $\bar{z} = z + a_1^2/z$. The external flow field is obtained by finding the effect on the flow field due to the presence of the circular fuselage. This is achieved by locating the image system of the vortex K in the fuselage. Referring to Figure A12.1, the image system of vortex of strength K at a point $\bar{z}_o$ in the presence of a circular fuselage of radius 'a', consists of a vortex of strength K at the centre of the fuselage and another of strength -K at the inverse point, $\bar{z} = a^2/\bar{z}_o$

As discussed in reference [21] the approximation $\bar{z} = z$ is a good one even at a distance of 1 chord from the centre of the aerofoil. Therefore, in the succeeding sections, it is justified to take the position of the image vortices in the physical and transformed planes as the same.

A12.1.1. Circulation for Downwash Case (+ve Blade Pitch)

When deriving the external flow potential, the relative velocity at the blade is split, for convenience, into components U and V, i.e. normal to and in the direction of blade motion respectively. If the blade chord makes an angle $+\nu_o$, taking the convention that for the downwash case (positive lift) the blade pitch is positive and is negative for the upwash case, then the flow potential for the downwash case is given by

$$f(z) = Vz\,e^{i\nu_o} - iUze^{i\nu_o} + \frac{ia^2Ue^{-i\nu_o}}{z - \bar{z}'} + iK\log(z - z') - iK\log(z - \bar{z}') \qquad \text{(A12.1)}$$

*Note: This theoretical development was derived from the work of Bramwell and Johnston [21].

where $f(z)$ is referred to axes fixed in the transformed aerofoil circle; as shown in Figure A12.1, z' is the position of the centre of the fuselage circle and $z'' = z' - a^2/z'$.

Now, since U is small compared with V, $U^2+V^2=V^2$ and, assuming ν_0 to be a small angle, the second term of equation (A12.1) can be absorbed into the first term and

$$f(z) = Vze^{i(\nu_0-\nu)} + \frac{ia^2U}{z-\bar{z}'} + iK\log(z-\bar{z}') - iK\log(z-z'') \tag{A12.2}$$

where $\nu = U/V$ (the induced angle at the blade)

then $$f'(z) = Ve^{i(\nu_0-\nu)} + \frac{ia^2U}{(z-\bar{z}')^2} + \frac{iK}{z-z'} - \frac{iK}{z-z''} \tag{A12.3}$$

where $f'(z)$ is obtained by differentiating $f(z)$ with respect to z.

Now, for the transformed circle of radius a, the stagnation point is at $z = z_s = -a_1$, so that

$$K = \Gamma/2\pi = \text{Real part of } 2iz_s f'(z_s)$$

$$= Re\left[-2ia_1 f'(-a_1)\right]$$

$$= Re\left[-2ia_1 Ve^{i(\nu_0-\nu)} - \frac{2a_1a^2U}{(a_1+\bar{z}')^2} - \frac{2a_1K}{a_1+z'} + \frac{2a_1K}{a_1+z''}\right] \tag{A12.4}$$

The above expression for K reduces to

$$K = \frac{Re\left[-2ia_1 Ve^{i(\nu_0-\nu)} - \frac{2a_1a^2U}{(a_1+\bar{z}')^2}\right]}{Re\left[1 + \frac{2a_1}{a_1+z'} + \frac{2a_1}{a_1+z''}\right]} \tag{A12.5}$$

$$= \frac{Re\left[2a_1V\sin(\nu_0-\nu) - \frac{2a_1a^2U}{(a_1+\bar{z}')^2}\right]}{Re\left[1 + \frac{2a_1}{a_1+z'} + \frac{2a_1}{a_1+z''}\right]} \tag{A12.6}$$

A12.1.2. Circulation for Upwash Case (-ve Blade Pitch)

The flow potential in this case becomes

$$f(z) = \left\{ V z e^{-i\nu_0} + i U z e^{-i\nu_0} - \frac{i a^2 U e^{i\nu_0}}{z - \bar{z}'} - i K \log(z - z') - i K \log(z - z'') \right\} \quad \text{(A12.7)}$$

Going through the same process of algebra as for the downwash case, the circulation expression is obtained as

$$\Gamma = 2\pi K$$

$$= 2\pi \frac{Re\left[-2a_1 V \sin(\nu_0 - \upsilon) + \frac{2a_1 a^2 U}{(a_1 + \bar{z}')^2}\right]}{Re\left[1 + \frac{2a_1}{a_1 + z'} + \frac{2a_1}{a_1 + z''}\right]} \quad \text{(A12.8)}$$

A12.2. TRANSIENT LIFT EQUATION

From the substitution vortex strength, K, the circulation is obtained as

$$\Gamma = 2\pi K \quad \text{(A12.9)}$$

Kutta-Joukouski theorem gives the lift as

$$L = \rho V \Gamma = \rho V (2\pi K) \quad \text{(A12.10)}$$

If $\bar{L}_0$ is the steady undisturbed lift, then

$$L_0 = \rho V (2\pi K_0) \quad \text{(A12.11)}$$

where K_0 is the steady undistributed vortex strength.

$\bar{L}_0$ is also given in terms of coefficient of lift as

$$\bar{L}_0 = C_L \tfrac{1}{2} \rho c V^2$$

$$= 2a_1 C_L \rho V^2 \quad \text{(A12.12)}$$

From reference (144)

$$C_L = 2\pi(\nu_0 - \upsilon) \quad \text{(A12.13)}$$

Where ν_0 and υ are collective pitch and induced angles respectively, in radians.

K_0 is obtained from equations (A12.11), (A.12.12), and (A12.13) as

$$K_0 = 2a_1 V(\nu_0 - \upsilon) \quad \text{(A12.14)}$$

Also $\frac{L}{\bar{L}_0} = \frac{K}{K_0}$

$$\therefore L = K \cdot \frac{\bar{L}_0}{K_0} \quad \text{(A12.15)}$$

Now, if a_o is the lift curve slope for the blade section,

then $$\overline{L}_o = 2a_1 \rho V^2 a_o (\nu_o - \nu) \qquad \text{(A12.16)}$$

Thus from (A12.14) and (A12.16)

$$\frac{\overline{L_o}}{K_o} = \rho V a_o$$

Equation (A12.15) thus becomes

$$L = \rho V a_o K \qquad \text{(A12.17)}$$

Using the expression for K as given by equation (A12.8), the transient lift equation becomes:

$$L_T = \rho V a_o \frac{Re\left[-2a_1 V \sin(\nu_o - \nu) + \frac{2a_1 a^2 U}{(a_1 + \bar{\zeta}')^2}\right]}{Re\left[1 - \frac{2a_1}{a_1 + \zeta'} + \frac{2a_1}{a_1 + \zeta''}\right]} \qquad \text{(A12.18)}$$

where ζ' denotes the position of the centre of the fuselage in the ζ- plane and $\zeta'' = \zeta' - a^2/\zeta'$ (see Figure A12.1) The position of the blade, i.e. of the centre of the transformed circle, is given in the z- plane - the physical plane - as $z_o = x_o + i y_o$. However, as pointed out in section A12.1.1, the co-ordinates z and ζ are approximately the same.

Therefore,

$$\zeta' = -x_o - i y_o$$

where, from the geometry illustrated in Figure A12.2 it can be seen that if ψ is taken as negative when the blade is approaching the fuselage and positive when receding from it then

$x_o = r \sin\psi$ and y_o = H, the height = a + S, where S and a are the rotor fuselage separation distance and radius of the fuselage respectively.

Making the above substitutions in equation (A12.18) gives the transient lift as a function of velocity, r, H, and ψ.

A12.3. FUSELAGE PRESSURE FORMULAE

A12.3.1. Deviation of Cylinder Pressure Formula

Using the transformation $z = \zeta + a^2/\zeta$ and taking the centre of the circular fuselage as origin of co-ordinates (Figure A12.3), the complex potential for the system is given, in terms of induced velocity U, as

$$W = -iUz + iUa^2/z + iK \text{ Log } (z - z_o) - iK \text{ Log } \left(z - \frac{a^2}{z_o}\right) + iK \log z \qquad \text{(A12.19)}$$

The velocity components u and v, relative to x and y are given by $-u + iv = dW/dz$

$$= -iU - i\frac{Ua^2}{z^2} + i\frac{K}{z} + \frac{iK}{z - z_0} - i\frac{K}{z - a^2/\bar{z}_0} \quad \text{(A12.20)}$$

Putting $z = ae^{i\delta}$ and $\bar{z}_0 = A_0 e^{-i\delta_0}$ the velocity components at a point $N(a, \delta)$ on the cylinder surface are given by

$$-u + iv = -i\left\{U(1 + e^{-2i\delta}) - \frac{K}{a}e^{-i\delta}\left[1 + \frac{1}{1 - \frac{1}{k}e^{i(\delta - \delta_0)}} - \frac{1}{1 - ke^{-i(\delta - \delta_0)}}\right]\right\} \quad \text{(A12.21)}$$

where $k = a/A_0$ and

$$-u + iV = -i\left\{U(1 + e^{2i\delta}) - \frac{K}{a}e^{i\delta}\left[1 + \frac{1}{1 + \frac{1}{k}e^{i(\delta - \delta_0)}} - \frac{1}{1 - ke^{i(\delta - \delta_0)}}\right]\right\} \quad \text{(A12.22)}$$

The velocity, q, at any point on the cylinder is given by

$$q^2 = (u - iv)(u + iv) \quad \text{(A12.23)}$$

which after simplification becomes

$$q^2 = 4\left\{U\cos\delta - \frac{K}{A_0}\frac{k - \cos(\delta - \delta_0)}{[1 - 2k\cos(\delta - \delta_0) + k^2]}\right\}^2 \quad \text{(A12.24)}$$

Since the flow is unsteady, the appropriate form of Bernoulli's equation is

$$P + \tfrac{1}{2}\rho q^2 - \frac{\partial \Phi}{\partial t} = P_0 + \tfrac{1}{2}\rho U^2 \quad \text{(A12.25)}$$

where P_0 is the atmospheric pressure.

To find $\partial\Phi/\partial t$ we must calculate the real part of $\partial W/\partial t$

Differentiating (A12.19) with respect to t and putting $z = ae^{i\delta}$ and $z_0 = a_0 e^{i\delta_0}$ gives the real part as

$$\frac{\partial \Phi}{\partial t} = \frac{KV}{A_0\{1 - 2k\cos(\delta - \delta_0) + k^2\}}\left[(1 - k^2)\sin\delta_0 - 2k\cos\delta_0\sin(\delta - \delta_0)\right] \quad \text{(A12.26)}$$

If Ω is the angular velocity of the rotor and r is the radial distance of the section under consideration, $V = \Omega r$ is the speed with which the blade section passes the fuselage.

Thus the pressure at a point on the cylinder is

$$P - P_o = \rho \frac{\partial \phi}{\partial t} + \frac{1}{2}\rho U^2 - \frac{1}{2}\rho q^2$$

$$= \frac{\rho K V}{A_o}\left[\frac{(1-k^2)\sin\delta_o - 2k\cos\delta_o \sin(\delta-\delta_o)}{1 - 2k\cos(\delta-\delta_o) + k^2}\right]$$

$$+ \frac{1}{2}\rho U^2 - 2\rho\left\{U\cos\delta - \frac{K}{A_o}\frac{[k - \cos(\delta-\delta_o)]}{[1 - 2k\cos(\delta-\delta_o) + k^2]}\right\}^2 \quad \text{(A12.27)}$$

Subtracting the steady pressure $\frac{1}{2}\rho U^2(1-4\cos^2\delta)$ on the cylinder due to downwash from (A12.27), the pressure increment is obtained as

$$P - P_o' = \frac{\rho K V}{A_o}\left[\frac{(1-k^2)\sin\delta_o - 2k\cos\delta_o \sin(\delta-\delta_o)}{1 - 2k\cos(\delta-\delta_o) + k^2}\right]$$

$$+ \frac{2\rho K}{A_o}\cdot\frac{k - \cos(\delta-\delta_o)}{1 - 2k\cos(\delta-\delta_o) + k^2}\left\{2U\cos\delta + \frac{K}{A_o}\frac{k - \cos(\delta-\delta_o)}{(1 - 2k\cos(\delta-\delta_o) + k^2)}\right\} \quad \text{(A12.28)}$$

where P'_o is the undisturbed pressure at the point of interest on the cylinder. If the blade is directly above the fuselage,

$\delta_o = \pi/2$ and

$$P - P_o' = \frac{\rho K V}{A_o}\frac{1-k^2}{1 - 2k\sin\delta + k^2} + \frac{2\rho K}{A_o}\cdot\frac{k - \sin\delta}{1 - 2k\sin\delta + k^2}$$

$$\times\left\{2U\cos\delta - \frac{K}{A_o}\frac{k - \sin\delta}{1 - 2k\sin\delta + k^2}\right\} \quad \text{(A12.29)}$$

In terms of the local blade C_L (equation (A12.29)) can be written as

$$P - P_o = \frac{\rho V^2 c\, C_L}{4\pi A_o (1 - 2k\sin\delta + k^2)}\left\{1 - k^2 + 2(k - \sin\delta)(2\nu\cos\delta\right.$$

$$\left. - \frac{c\,C_L}{4\pi A_o}\left(\frac{k - \sin\delta}{1 - 2k\sin\delta + k^2}\right)\right\} \quad \text{(A12.30)}$$

since $4\pi K = VcC_L$ and where $\nu = U/V$

The pressures on the circular fuselage can be calculated using equation (A12.30).

A12.3.2. <u>Constant Circulation Case</u>

The pressure at a point $N(x_N, y_N)$ on the fuselage is given by equation (A12.28), this can be written as

$$p - p_o = \rho \frac{\partial \phi}{\partial t} + \frac{1}{2}\rho U^2 + \frac{1}{2}\rho q^2$$

$$= P_1 + P_2 + P_3$$

where

$$P_1 = \frac{\rho KV}{A_o}\left\{\frac{(1-k^2)\sin\delta_o - 2k\cos\delta_o\sin(\delta-\delta_o)}{1-2k\cos(\delta-\delta_o)+k^2}\right\}$$

$$P_2 = \tfrac{1}{2}\rho U^2$$

$$P_3 = 2\rho\left\{U\cos\delta - \frac{K}{A_o}\left[\frac{k-\cos(\delta-\delta_o)}{1-2k\cos(\delta-\delta_o)+k^2}\right]\right\}^2 \qquad \text{(A12.31)}$$

where the symbols A_o, δ_o, and δ are as illustrated on Figure A12.4 and $K = \frac{a}{A_o}\cdot p_o$ is the atmospheric pressure.

If the blade co-ordinates are (x_o, y_o) with respect to the centre of the fuselage then $Ao = x_o^2 + y_o^2$. Referring to Figure A12.2 $y_o = H$, the height and $x_o = r\sin\psi$. Thus the pressure distribution around the fuselage circumference can be obtained as a function of blade speed, r, ψ and height H.

A12.3.3. Effect of the Variation in Circulation

When deriving the pressure formula quoted in section A12.3.2 the P_1 term in the unsteady Bernoull's equation was determined by differentiating W, the flow potential, with respect to time. Using the image of the vortex in the fuselage, the flow potential was obtained as:

$$W = -iU\bar{z} - \frac{iUa^2}{\bar{z}} - iK(\bar{z}-\bar{z}_o) - iK\log\left(\bar{z} - \frac{a^2}{\bar{z}_o}\right) + iK\log\bar{z} \qquad \text{(A12.32)}$$

However, when differentiating W to get $\partial\phi/\partial t$ (it being the real part of $\partial W/\partial t$) K was taken as a constant. To take the effect of the variation in K into account an additional term has to be added to the P_1 term. This is given by

$$\text{'Add'} = i\left\{\log(\bar{z}-\bar{z}_o) - i\log\left(\bar{z} - \frac{A^2}{\bar{z}_o}\right) + i\log\bar{z}\right\}\frac{\partial K}{\partial t} \qquad \text{(A12.33)}$$

where, referring to Figures A12.1 and A12.4

$\bar{z} = x_n + i\,y_n = a\cos\delta + ia\sin\delta$ and $\bar{z}_o = x_o + i\,y_o = r\sin\psi + iH$

Using the expression for K given in equation (A12.8) and denoting the numerator and the denominator of the expression by N and D respectively, $\partial K/\partial t$ becomes

$$\partial K/\partial t = \frac{D\,\partial N/\partial t - N\,\partial D/\partial t}{D^2} \qquad \text{(A12.34)}$$

where $N = Re\left\{-2a_1 V\sin(\nu_o - \nu) + \frac{2a_1 a^2 U}{(a_1 + \bar{z}_1)^2}\right\}$

$$\partial N/\partial t = Re\left\{\frac{-2a_1a^2U}{(a_1+\bar{z}')^3}\cdot\frac{\partial\bar{z}'}{\partial t}\right\} \qquad \text{(A12.35)}$$

where $z' = -x_0 - iy_0 \quad ; \quad \bar{z}' = -x_0 + iy_0$

$$\frac{\partial\bar{z}'}{\partial t} = \frac{\partial z'}{\partial t} = -\frac{\partial x_0}{\partial t} = -V$$

and $$\partial N/\partial t = Re\left\{\frac{2a_1a^2UV}{(a_1+\bar{z}')^3}\right\}$$

$$\partial D/\partial t = \frac{-2a_1}{(a_1+z'')^2}\cdot\partial z''/\partial t + \frac{2a_1}{(a_1+z')^2}\cdot\frac{\partial z'}{\partial t} \qquad \text{(A12.36)}$$

now $$z'' = z' - a^2/z' \qquad \text{(A12.37)}$$

$$\partial z''/\partial t = \frac{\partial z''}{\partial z'}\cdot\frac{\partial z'}{\partial t} = -V\left\{1+\left(\frac{a}{z'}\right)^2\right\} \qquad \text{(A12.38)}$$

Substituting equations (A12.37) and (A12.38) in equation (A12.36) gives $\partial D/\partial t$ as:

$$\partial D/\partial t = \frac{2a_1V}{(a_1+z'')^2}\left\{1+\left(\frac{a}{z'}\right)^2\right\} - \frac{2a_1V}{(a_1+z')^2} \qquad \text{(A12.39)}$$

A12.3.4. <u>End-Correction Formulae</u>

An approximation to three-dimensional flow is obtained by calculating an 'end effect' and applying it to the calculations for two-dimensional flow assumed in the derivation of the formula.

A factor f_e, derived by Bramwell and Johnston [21] to apply to the two-dimensional calculations, is:

$$f_e = \frac{\text{SINH}^{-1}\left(\frac{1-\varepsilon}{\gamma}\right) + \text{SINH}\left(\frac{\varepsilon}{\gamma}\right) - \frac{\left(1-\frac{\varepsilon^2}{\gamma^2}\right)+\varepsilon\left(1-\frac{\varepsilon^2}{\gamma^2}\right)}{\left\{(1-\varepsilon)^2+\gamma^2\right\}^{1/2}}}{2\,\varepsilon^2/\gamma^2} \qquad \text{(A12.40)}$$

where $\varepsilon = t/R_T$ and $\gamma = d'/R_T$. d' is the vertical distance of point N, on the cylinder, below the rotor disc and from the geometry of Figure A12.1 $d' = S + a\,(1-\sin\delta)$.

The above 'end correction' factor, f_e, was used in the investigation for the cylinder pressure calculations. It was anticipated that a similar approach would have been used in the steady blade lift calculation, but it was not clear how the above formula could be modified for this case. It was decided, therefore, to use the same correction factors as used in the steady thrust calculations as mentioned in section 2.6 of the main report.

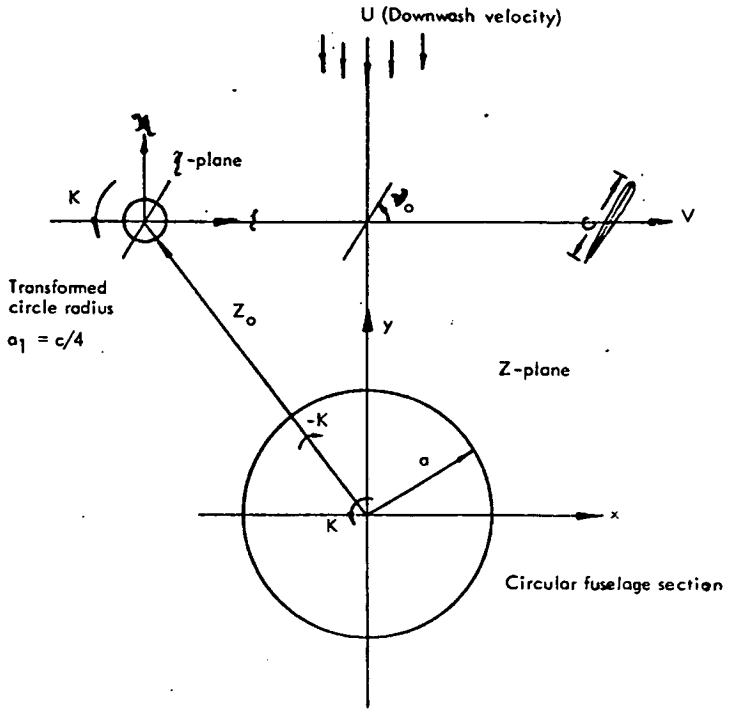

FIGURE A.12.1. BLADE VORTEX IMAGE SYSTEM

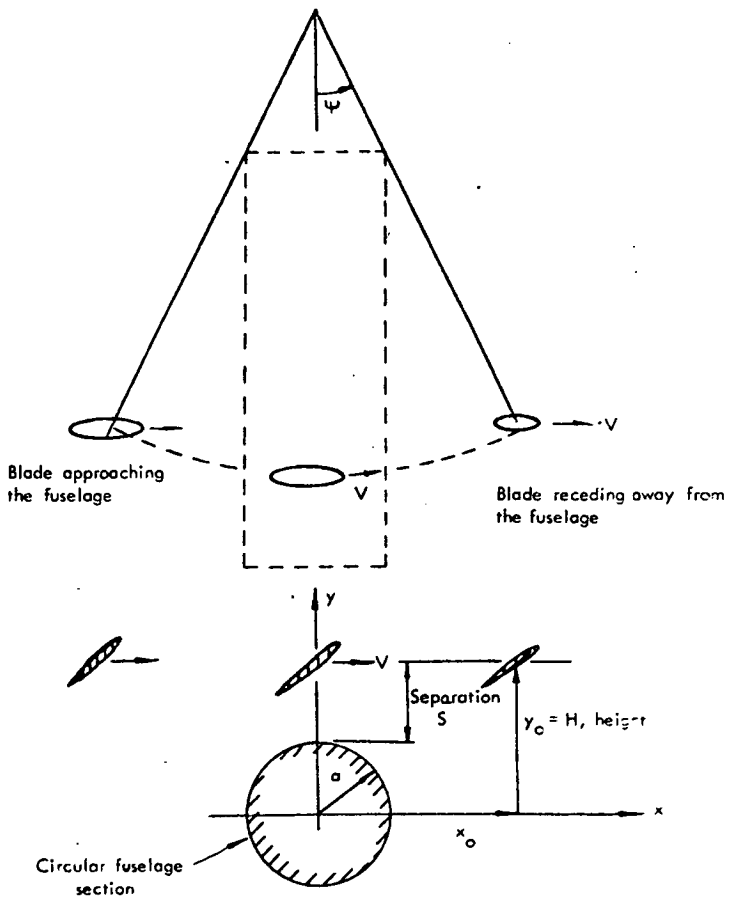

FIGURE A.12.2. PASSAGE OF BLADE OVER FUSELAGE

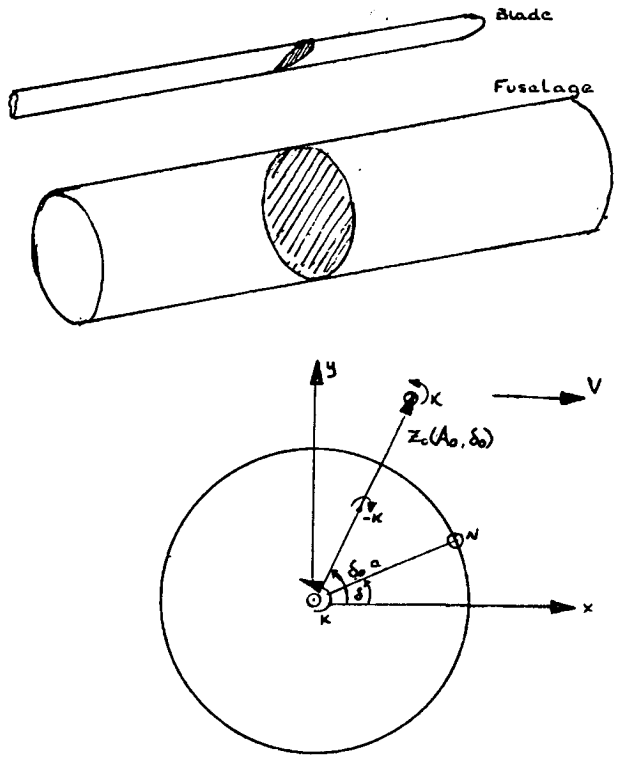

FIGURE A.12.3. IMAGE SYSTEM FOR VORTEX IN PRESENCE OF CIRCULAR SYSTEM

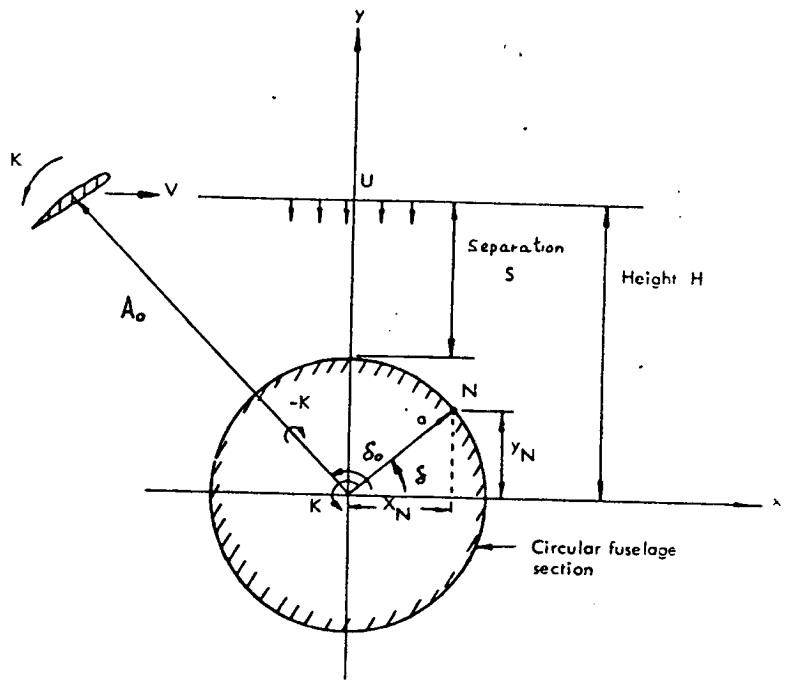

FIGURE A.12.4. FUSELAGE/BLADE GEOMETRY

APPENDIX 13: TRANSIENT BLADE LIFT COMPUTER PROGRAM

A13.1. CALCULATION PROCEDURE

The transient lift of the blade, as it passes over the fuselage, is given by the equation:

$$L = \rho V a_0 \frac{Re\left[-2a_1 V \sin(\nu_0 - \nu) + \frac{2a_1 a^2 U}{(a_1 + \bar{\zeta}')^2} \right]}{Re\left[1 - \frac{2a_1}{a_1 + \zeta'} + \frac{2a_1}{a_1 + \zeta''} \right]}$$ Equation (12.18)

where $\zeta' = -x_0 - i y_0$

$= -r \sin\psi - iH$ (see Appendix 12)

and $\zeta'' = \zeta' - \frac{a^2}{\zeta'}$

and $\nu = \frac{U}{V}$

$$= \frac{-\frac{Bc a_0}{8\pi r} + \sqrt{\left(\frac{Bc a_0}{8\pi r}\right)^2 + \frac{4Bc a_0 \nu_0}{8\pi r}}}{2}$$

The above equations are evaluated in the computer program MASTER UNSTEADY in the order as required. The program computes the steady blade lift and the unsteady (transient lift), in lbs/inch, at specified values of azimuthal co-ordinate ψ for each blade radial station.

The program reads in the parameters NRAD, NUNO, RANGE, OMG, LCS, CYRAD, HITE, ANG, RHO, RADIUS and computes the transient blade lift for a number of radial and azimuthal stations as mentioned above.

The input parameters mentioned above have been listed over with their units.

A13.2. INPUT PARAMETERS

The parameters required to use the program are:

NRAD	number of radial stations
NUNO	collective blade pitch angle ν_o , degrees
RBN	rotor blade number, B
OMG	rotor speed Ω R.P.M.
CH	blade chord c, inches
CYRAD	fuselage radius a, inches
HITE	height H, inches
ANG	the azimuthal interval, $d\psi$, at which the lift value is to be calculated, degrees
RHO	density of air,
RADIUS	rotor blade tip radius R_T, feet
RANGE	range is $2\psi_o$ degrees where $\pm\psi_o$ degrees is the range of azimuth for which blade lift is required.
R(I)	array for rotor radii values, inches
SCAL(I)	correction factors for lift, at corresponding radii values, as obtained from reference (138).

```
0007                MASTER UNSTEADY
0008                REAL LCB,K,NUNO
0009                COMPLEX ZD,ZDD,CZD
0010                DIMENSION Q(161,8),R(8),PRAD(161),BCAL(8),TITLE(9)
0011            111 READ(5,2) TITLE
0012            2   FORMAT(9A8)
0013                READ(5,3)NRAD,NUNO,RANGE,RBN,OMG,CH,LCB,CYRAD,HITE,ANG,RHO,RADIUS
0014              3 FORMAT(I0,11F0.0)
0015                PI=3.1415926536
0016                RAD=PI/180.0
0017                RHO=RHO/20736.0
0018                QQ=RBN*CH*LCB/(8.0*PI)
0019                WRITE(6,TITLE)
0020                TIP=PI*OMG*RADIUS/30.0
0021                RNUU=NUNO*RAD
0022                READ(5,5)(R(I),I=1,NRAD)
0023                WRITE(6,7)HITE,NUNO,OMG,TIP,RADIUS,R(1)
0024            7     FORMAT(8H HEIGHT=,F5.1,7H INCHES,8H  PITCH=,F5.1,4H DEG,8H  SPEED=
0025               1,F6.1,12H  TIP SPEED=,F6.1,7H FT/SEC/15H  ROTOR RADIUS=,F6.2,3H FT
0026               1,18H  RADIAL POSITION=,F6.1,7H INCHES//)
0027                READ(5,5)(BCAL(I),I=1,NRAD)
0028              5 FORMAT(9F0.0)
0029                NP=RANGE/ANG+1.001
0030                ANG=ANG*RAD
0031                PRAD(1)=-RANGE*RAD/2.0
0032                DO 4 I=2,NP
0033              4 PRAD(I)=PRAD(I-1)+ANG
0034                DO 223 I=1,NRAD
0035                VEL=PI*OMG*R(I)/30.0
0036                QR=QQ/R(I)
0037                PHI=(-QR+SQRT(QR*QR+4.0*QR*RNUU))/2.0
0038                RNU=RNUU-PHI
0039                RHOV=RHO*VEL*LCB*CH/2.0
0040                STEADY=RHOV*VEL*RNU*BCAL(I)
0041                DWV=PHI*VEL
0042                WRITE(6,6) R(I),STEADY
0043              6 FORMAT(10X,7HRADIUS=,F5.1,7H INCHES,25H   STEADY LIFT(LBS/INCH)=,F
0044               114.8//)
0045                WRITE(6,8)
0046              8 FORMAT(5H  PSI,2X,23HUNSTEADY LIFT(LBS/INCH)//)
0047                DO 223 J=1,NP
0048                PSI=PRAD(J)/RAD
0049                XCORD=R(I)*SIN(PRAD(J))
0050                ZD=CMPLX(-XCORD,-HITE)
0051                CZD=CONJG(ZD)
0052                ZDD=ZD-CYRAD*CYRAD/ZD
0053                K=REAL(VEL*SIN(RNU)-CYRAD*CYRAD*DWV/((A1*CZD)**2))/REAL(1.0*2.0*A1

0054               1/(A1*ZDD)-2.0*A1/(A1*ZD))
0055                Q(J,I)=RHOV*(K-VEL*RNU)*BCAL(I)
0056                WRITE(6,9)PSI,Q(J,I)
0057              9 FORMAT(1X,F5.1,6X,F14.8)
0058            223 CONTINUE
0059                END

END OF SEGMENT, LENGTH   375, NAME  UNSTEADY
```

APPENDIX 14: COMPUTATION OF FUSELAGE PRESSURE

A14.1. CALCULATION PROCEDURE

The equations to be computed for obtaining fuselage pressure are as follows:

Without $\frac{\partial K}{\partial t}$ term the fuselage pressure is given by:

$$p - p_0 = p_1 + p_2 - p_3$$

and with $\frac{\partial K}{\partial t}$ term the pressure equation becomes:

$$p - p_0 = p_1 + Add + p_2 - p_3$$

where,

$$p_1 = \frac{\rho K V}{A_0}\left[\frac{(1-k^2)\sin\delta_0 - 2k\cos\delta_0 \cdot \sin(\delta-\delta_0)}{1-2k\cos(\delta-\delta_0)+k^2}\right]$$

$$p_2 = \frac{1}{2}\rho U^2$$

$$p_3 = \left[i\log(z-z_0) - i\log\left(z-\frac{a^2}{\bar{z}_0}\right) - i\log z\right]\frac{\partial K}{\partial t}$$

and $Add, p_0, K, k, A_0, \delta_0, \delta, \rho, U, z, z_0$, and $\frac{\partial K}{\partial t}$ are as defined in Appendix 12.

The computer program MASTER PRESSURE computes fuselage pressure for K constant and/or variable, with and/or without $\frac{\partial K}{\partial t}$ term, or any combination of these. (The constant value of K being taken as $K = \frac{V_c C_L}{4\pi}$ [21] and the variable value being as defined in Appendix 12). The desired combination is obtained by choosing the right values of the input parameters KEY 1, KEY 2, and KEY 3; where KEY 1, KEY 2 and KEY 3 represent presence or absence of constant K, variable K and $\frac{\partial K}{\partial t}$ term respectively - the presence being denoted by 1 and the absence by 0. The program evaluated fuselage pressure for a range of rotor speeds from starting speed OMG to maximum rotor speed MRS (at intervals of 100 R.P.M.) and for a range of collective blade pitch values starting with NUNO to a maximum blade pitch MNN (at intervals of 2 degrees). For each blade pitch and rotor speed value it evaluates the pressure as function of blade azimuth

angle ψ.

A14.2. INPUT PARAMETERS REQUIRED

The input parameters (and their units) required to use the program are:

RIN	radial station r inches.
THETA	angle δ, degrees
CH	blade chord c, inches
Hite	height H, inches
LCS	lift curve slope a_o,
RADIUS	rotor blade tip radius R_T, inches
RHO	density of air, lbf-sec^2(slugs/ft^3)
OMG	initial value of rotor speed for 'speed D_o loop'
NUNO	initial value of collective blade pitch angle ν_o 'for pitch D_o loop' degrees
INT	blade azimuthal interval, $d\psi$, at which fuselage pressures are to be computed, degrees
IRANGE	the total range $2\psi_o$ degrees where $\pm\psi_o$ degrees is the range of azimuth for which blade lift is required; being an integer quantity
MRS	the maximum rotor speed for 'speed D_o loop' R.P.M., (must be an integer quantity)
MNN	the maximum blade pitch angle for 'pitch D_o loop' degrees (must be an integer quantity)

Pressures are calculated in lbs/in^2 units.

```
0008                MASTER PRESSURE
0009                COMPLEX Z,ZD,CZD,ZDD,IMAG
0010                REAL LCS,KAPPA,K
0011                READ(5,1)RIN,THETA,CH,CYRAD,HITE,LCS,RADIUS,RHO,OMG,NUNO,INT,
0012               1IRANGE
0013           1    FORMAT(9F0.0,3I0)
0014                READ(5,100)KEY1,KEY2,KEY3
0015          100   FORMAT(3I0)
0016                PI=3.1415926536
0017                Q=LCS*RHO*CH/(8.0*PI)
0018                RADIUS=RADIUS/12.0
0019                TIP=RADIUS*PI*OMG/30.0
0020                RHO=RHO/2070.0
0021                RAD=PI/180.0
0022                IMAG=(0.0,1.0)
0023                NRPM=OMG
0024                WRITE(6,2)NRPM,RADIUS,TIP
0025           2    FORMAT(10X,7HR.P.M.=,I4,10X,13HROTOR RADIUS=,F9.1,3H FT,
0026               110X,10HTIP SPEED=,F6.1,7H FT/SEC)
0027                WRITE(6,3)NUNO,HITE,RIN
0028           3    FORMAT(10X,6HPITCH=,I2,2X,3HDEG,10X,7HHEIGHT=,F5.2,6H  INCHES,10X,
0029               17HRADIUS=,F4.1,2X,6HINCHES)
0030                RNUNO=NUNO*RAD
0031                WRITE(6,9)THETA
0032           9    FORMAT(10X,6HTHETA=,F6.1,4H DEG)
0033                THRAD=RAD*THETA
0034                WRITE(6,4)
0035           4    FORMAT(30X,22HPRESSURES IN LB/SQ.IN.///)
0036                WRITE(6,6)
0037           6    FORMAT(1X,5HPSI,1X,5HTHNOT,5X,10HTIME(SEC.),11X,4HPRES,10X,
0038               15HPRESK,11X,4HPKAP,10X,5HPKAPK)
0039                VEL=PI*OMG*RIN/30.0
0040                QR=Q/RIN
0041                PHI=(-QR+SQRT(QR*QR+4.0*QR*RNUNO))/2.0
0042                RNU=RNUNO-PHI
0043                COFL=LCS*RNU
0044                KAPPA=VEL*CH*COFL/(4.0*PI)
0045                U=PHI*VEL
0046                IHR=IRANGE/2
0047                DO 10 NPSI=0,IRANGE,INT
0048                IPS=NPSI-IHR
0049                PSI=IPS*RAD
0050                TIME=(PSI*60.0)/(OMG*2.0*PI)
0051                XCORD=RIN*SIN(PSI)
0052                ANOT=SQRT(HITE**2+XCORD**2)
0053                RK=CYRAD/ANOT
0054                THNOT=ATAN2(HITE,XCORD)
```

```
      THDEG=THNOT/RAD
      IF (KEY3.EQ.1) GO TO 21
      IF(KEY2.EQ.0) GO TO 22
   21 CONTINUE
      Z=CMPLX(CYRAD*COS(THRAD),CYRAD*SIN(THRAD))
      ZD=CMPLX(-XCORD,-WITE)
      CZD=CONJG(ZD)
      ZDD=ZD-CYRAD*CYRAD/ZD
      DEN=REAL(1.0*CH/(2.0*(CH/4.0*ZDD))-CH/(2.0*(CH/4.0*ZD)))
      RNUM=REAL(VEL*CH*SIN(RNU)/2.0-CH*CYRAD*CYRAD*U/(2.0*((CH/4.0*CZD)
     1**2)))
      K=RNUM/DEN
      IF(KEY3.EQ.0) GO TO 23
      DNDT=-REAL((CH*CYRAD*CYRAD*U*VEL)/((CH/4.0*CZD)**3))
      DDDT=CH*VEL/2.0*REAL((1.0+(CYRAD/ZD)**2)/((CH/4.0*ZDD)**2)-1.0/
     1((CH/4.0*ZD)**2))
      DKDT=(DEN*DNDT-RNUM*DDDT)/(DEN**2)
      ADD=-RHO*REAL(IMAG*(CLOG(Z*ZD)-CLOG(Z-CYRAD*CYRAD/CZD)+CLOG(Z)))
      IF(KEY2.EQ.0) GO TO 24
      PR1K=(K*VEL/ANOT)*(((1.0-RK*RK)*SIN(THNOT)-2.0*RK*COS(THNOT)*SIN
     1(THRAD-THNOT))/(1.0-2.0*RK*COS(THRAD-THNOT)+RK*RK))
      PR2=U*U/2.0
      PR3K=2.0*(U*COS(THRAD)-(K*(RK-COS(THRAD-THNOT)))/(ANOT*(1.0-2*RK*
     1COS(THRAD-THNOT)+RK*RK)))**2
      PRES=RHO*(PR1K*PR2-PR3K)
      PRESK=PRES+DKDT*ADD
      IF (KEY1.EQ.1) GO TO 24
      WRITE(6,13)IPS,THDEG,TIME,PRES,PRESK
   13 FORMAT(I4,F6.1,3F15.10)
      GO TO 10
   24 CONTINUE
      PR1=(KAPPA*VEL/ANOT)*(((1-RK*RK)*SIN(THNOT)-2*RK*COS(THNOT)*SIN
     1(THRAD-THNOT))/(1-2*RK*COS(THRAD-THNOT)+RK*RK))
      PR2=U*U/2.0
      PR3=2.0*(U*COS(THRAD)-(KAPPA*(RK-COS(THRAD-THNOT)))/(ANOT*(1-2*RK*
     1COS(THRAD-THNOT)+RK*RK)))**2
      PKAP=RHO*(PR1*PR2-PR3)
      PKAPK=PKAP+DKDT*ADD
      IF (KEY2.EQ.1) GO TO 25
      WRITE(6,14)IPS,THDEG,TIME,PKAP,PKAPK
   14 FORMAT(I4,F6.1,F15.10,3UX,2F15.10)
      GO TO 10
   25 CONTINUE
    7 FORMAT(I4,F6.1,5F15.10)
      WRITE(6,7)IPS,THDEG,TIME,PRES,PRESK,PKAP,PKAPK
      GO TO 10
   22 CONTINUE
```

A14.3: COMPUTER PROGRAM (CONTD)

```
      PR1=(KAPPA*VEL/ANOT)*(((1-RK*RK)*SIN(THNOT)-2*RK*COS(THNOT)*SIN
     1(THRAD-THNOT)))/(1-2*RK*COS(THRAD-THNOT)*RK*RK))
        PR2=U*U/2.0
        PR3=2.0-(U*COS(THRAD)+(KAPPA*(RK-COS(THRAD-THNOT)))/(ANOT*(1-2*RK*
     1COS(THRAD-THNOT)*RK*RK)))**2
        PKAP=RHO*(PR1*PR2*PR3)
        WRITE(6,16)IPS,THDEG,TIME,PRES,PKAP
16      FORMAT(I4,F6.1,2F15.10,15X,F15.10)
        GO TO 10
23      CONTINUE
        PR1K=(K*VEL/ANOT)*(((1.0-RK*RK)*SIN(THNOT)-2.0*RK*COS(THNOT)*SIN
     1(THRAD-THNOT)))/(1.0-2.0*RK*COS(THRAD-THNOT)*RK*RK))
        PR2=U*U/2.0
        PR3K=2.0-(U*COS(THRAD)-(K+(RK-COS(THRAD-THNOT))))/(ANOT*(1.0-2.0*RK*
     1COS(THRAD-THNOT)*RK*RK)))**2
        PRES=RHO*(PR1K*PR2*PR3K)
        IF(KEY.EQ.1) GO TO 26
        WRITE(6,15)IPS,THDEG,TIME,PRES
15      FORMAT(I4,F6.1,2F15.10)
        GO TO 10
26      CONTINUE
        PR1=(KAPPA*VEL/ANOT)*(((1-RK*RK)*SIN(THNOT)-2*RK*COS(THNOT)*SIN
     1(THRAD-THNOT)))/(1-2*RK*COS(THRAD-THNOT)*RK*RK))
        PR2=U*U/2.U
        PR3=2.0-(U*COS(THRAD)+(KAPPA*(RK-COS(THRAD-THNOT))))/(ANOT*(1-2*RK*
     1COS(THRAD-THNOT)*RK*RK)))**2
        PKAP=RHO*(PR1*PR2*PR3)
        WRITE(6,12)IPS,THDEG,TIME,PKAP
12      FORMAT(I4,F6.1,F15.10,30X,F15.10)
10    CONTINUE
      STOP
      END

END OF SEGMENT, LENGTH  1050, NAME  PRESSURE
```

APPENDIX 15: TRANSIENT LIFT ROTATIONAL NOISE PROGRAM

A15.1. ROTATIONAL NOISE MODEL

The rotational noise harmonics for rotor/fuselage interaction were computed using a modified version of Tanna's Rotational Noise Program [18] - see Appendix 9.

A15.2. CALCULATION PROCEDURE

The modified rotational program MASTER ROTATIONAL used the rotational noise equations given in Appendix 9 (section A9.3) and the transient lift solution given in Appendix 12 (section A12.2). The method used repeatedly evaluates the basic sound pressure equations which included a double integration. One integration is around the rotor disc with the sample points (azimuth angles) chosen, at constant intervals. The other integration is along the radius.

A15.3. INPUT PARAMETERS

The input parameters (and their units), required to use the program are:

NEND	end code = 0 if last case = 1 if cases to follow
NFP	number of field points
NUNO	collective blade pitch angle ν_o, degrees
RBN	rotor blade number B
CH	blade chord C, inches
SOS	speed of sound, ft/sec.
LCS	Lift curve slope
CYRAD	fuselage radius a, inches
RHO	density of air ρ
HITE	height H, inches
RANGE	$2\psi_o$ degrees where $\pm \psi_o$ degrees is the range of azimuth for which blade lift is to be used to complete the rotational harmonics
RADIUS	rotor blade tip radius R_T, feet.
NHAR	number of harmonics, m, required
ANG	the azimuthal interval, $d\psi$, at which the left value is to be calculated, degrees
KEY 1, KEY 2) = 00 and KEY 3) = 99	if intermidiate output not desired if imtermediate output desired.

A15.4. COMPUTER PROGRAM

```
0008                MASTER ROTATIONAL
0009                REAL LCS,K,NUNO
0010                COMPLEX ZD,ZDD,CZD
0011                DIMENSION Q(321,8),R(8),V8(8),V8I(8),TITLE(9),V25(161),V25I(161),
0012               1PRAD(161),SCAL(8)
0013                RAD=1.0/57.2957795
0014                PI=3.14159265358
0015              111 READ(5,2)TITLE
0016              2   FORMAT(9A8)
0017                READ(5,3)NEND,NFP,NUNO,RBN,OMG,CH,SOS,LCS,CYRAD,RHO,MITE,RANGE,
0018               1RADIUS
0019                TIP=PI*OMG*RADIUS/30.0
0020                WRITE(6,7)MITE,NUNO,OMG,TIP,RADIUS
0021              7   FORMAT(8H HEIGHT=,F5.1,7H INCHES,8H  PITCH=,F5.1,4H DEG,8H  R.P.M=
0022               1,F6.1,12H  TIP SPEED=,F6.1,/H FT/SEC/13H  ROTOR RADIUS=,F6.2,3H FT
0023               1//)
0024                READ(5,3)NMAX,NRAD
0025              3 FORMAT(2I0,11F0.0)
0026                READ(5,11)ANG
0027                READ(5,33)KEY1,KEY2,KEY3
0028             33 FORMAT(3I2)
0029                RHO=RHO/2.0/32.0
0030                A1=CH/4.0
0031                QQ=RBN*CH*LCS/(8.0*PI)
0032                RNUO=NUNO*RAD


0033                NP=(RANGE/ANG)+1.001
0034                ANG=ANG*RAD
0035                PRAD(1)=-RANGE*RAD/2.0
0036                DO 4 I=2,NP
0037              4 PRAD(I)=PRAD(I-1)+ANG
0038                READ(5,5)(R(I),I=1,NRAD)
0039                READ(5,5)(SCAL(I),I=1,NRAD)
0040              5 FORMAT(8F0.0)
0041                DO 223 I=1,NRAD
0042                VEL=PI*OMG*R(I)/30.0
0043                QR=QQ/R(I)
0044                PHI=(-QR+SQRT(QR*QR+4.0*QR*RNUO))/2.0
0045                RNU=RNUO-PHI
0046                RHOV=RHO*VEL*LCS*CH/2.0
0047                DWV=PHI*VEL
0048                DO 223 J=1,NP
0049                XCORD=R(I)*SIN(PRAD(J))
0050                ZD=CMPLX(-XCORD,-MITE)
0051                CZD=CONJG(ZD)
```

A15.4. COMPUTER PROGRAM (CONT'D)

```
0051                ZZD=LONJG(ZD)
0052                ZDD=ZD*CYRAD*CYRAD/ZD
0053                K=REAL(VEL*SIN(RNU)*CYRAD*CYRAD*DWV/((A1*ZZD)**2))/REAL(1.0*2.0*A1
0054               1/(A1*ZDD)*2.0*A1/(A1*ZD))
0055                U(J,I)=RHOV*(K*VEL*RNU)*SCAL(I)
0056             225 CONTINUE
0057                WRITE(6,TITLE)
0058                SOS=SOS*12.0
0059                OMG=OMG*PI/30.0
0060                DO 999 II=1,NFP
0061                READ(5,11)CAPR,THETA,ALFA
0062             11 FORMAT(3F0.0)
0063                WRITE(6,12)CAPR,THETA,ALFA
0064              12 FORMAT(12HOFIELD POINT,10X,6HRADIUS,E15.6,5X,/HAZIMUTH,E15.6,5X,
0065               1/HELEVATION,E15.6,/20X,8HHARMONIC,10X,14HSOUND PRESSURE,15X,
0066               2/3HSPL)
0067                CAPR=12.0*CAPR
0068                ALFA=ALFA*RAD
0069                THETA=THETA*RAD
0070                SBTA=SIN(RNUU)
0071                CBTA=COS(RNUU)
0072                DO 999 M=1,NHAR
0073                DO 990 KK=1,NRAD
0074                DO 99 JJ=1,NP
0075                CAPS=SQRT(CAPR*CAPR*R(KK)*R(KK)-2.0*CAPR*R(KK)*COS(ALFA)
0076               1*COS(PRAD(JJ)-THETA))
0077                V=M
0078                V=V*RBN*(OMG*CAPS/SOS*0.5*CH/R(KK)*PRAD(JJ))
0079                TEMP=M
0080                V25(JJ)=(Q(JJ,KK)*BIN(0.5*TEMP*RBN*CH/R(KK))*(COS(V)/CAPS*(TEMP*
0081               1RBN*OMG/SOS)*SIN(V))*(SBTA*COS(ALFA)*SIN(PRAD(JJ)-THETA)*
0082               2SIN(ALFA)*CBTA)*K(KK))/(TEMP*CAPS*CAPS)
0083                V251(JJ)=(Q(JJ,KK)*SIN(0.5*TEMP*RBN*CH/R(KK))*(COS(V)*TEMP*RBN*
0084               1OMG/SOS-SIN(V)/CAPS)*(SBTA*COS(ALFA)*SIN(PRAD(JJ)-THETA)*BIN
0085               2(ALFA)*CBTA)*R(KK))/(TEMP*CAPS*CAPS)
0086              99 CONTINUE
0087                MN=NP
0088                CALL SIMCOM(NP,PRAD,V25,AR,MN)
0089                V8(KK)=AR
0090                CALL SIMCOM(NP,PRAD,V251,AR,MN)
0091                VBI(KK)=AR
0092                MN=NRAD
0093             990 CONTINUE
0094                CALL SIMCOM(NRAD,R,V8,PRTAR,MN)
0095                CALL SIMCOM(NRAD,R,V8I,PRTAI,MN)
0096                PRTA=(0.5962245*CAPR/CH)*SQRT(PRTAR**2+PRTAI**2)
0097                SPL=20.0*ALOG(ABS(PRTA/2.0E-9))
0098                WRITE(6,997)M,PRTA,SPL
0099             997 FORMAT(25X,I2,5X,2E20.8)
0100             999 CONTINUE
0101                IF(NEND)9999,9999,111
0102            9999 STOP
0103                END
```